

**An Astrobiological Study of High
Latitude Martian Analogue
Environments**

A thesis submitted for the Degree of Doctor of
Philosophy

By

Claire Rachel Cousins

University College London
Department of Earth Sciences

April 2010

I, Claire Rachel Cousins confirm that the work presented in this thesis is my own. Where information has been derived from other sources, I confirm that this has been indicated in the thesis.

ABSTRACT

The search for life on Mars is in part reliant on the understanding of Martian environments, both past and present, in terms of what life may inhabit these environments, how this life may be preserved in the rock record, and how this rock record may be detected during future missions to Mars. In particular, the upcoming European Space Agency mission ‘ExoMars’ has the primary aim to identify evidence of past or present life on Mars, and the work presented here is carried out within this context.

Volcanism is a geological process common to both Earth and Mars, and this work sought to conduct a multidisciplinary astrobiological study of terrestrial volcanic and associated hydrothermal environments that exist geographically at high latitudes. Specifically, subglacial basaltic volcanic environments were explored in terms of phylogenetic diversity, preservation of biosignatures, and habitability under Martian conditions. Additionally, these and other volcanic environments were utilised in the development and testing of the Panoramic Camera – an instrument that will form an integral component of the ExoMars rover instrument suite.

Results presented within this thesis demonstrate that subglacially erupted lavas provide a habitat for a diverse bacterial community, and that when such a community is subject to present-day Martian analogue conditions, survivability is significantly enhanced when a simulated subglacial volcanic system (i.e. heat and ice) is present. However, the generation of bioalteration textures – a biosignature common to glassy basaltic lavas – appears to be less common in subglacially-erupted lavas than their oceanic counterparts. Lastly, this work demonstrates the ability of the ExoMars PanCam in the detection of astrobiological targets, and shows the importance of utilising Martian analogue terrains both for biological studies, and also for testing rover instrumentation in preparation for upcoming missions.

ACKNOWLEDGEMENTS

First and foremost I would like to thank my supervisor Dr. Ian Crawford for his constant advice and enthusiasm throughout the past three years, and to my other supervisors Prof. John Ward, whose generosity and keen interest has made this work possible, and Dr. Adrian Jones for allowing me the freedom to take this project where I wanted. Additionally, I am completely indebted to Dr. Stephanie Hunter for patiently answering my numerous biology-related questions, and for managing (I hope!) to teach a geologist how to conduct microbiology research.

Much of the work in this thesis would not have been possible without the many collaborations with other researchers both in the UK and further afield. In particular I thank Dr. Andrew Griffiths and Prof. Andrew Coates for involving me in the development of the ExoMars PanCam instrument, and for sending me to the Arctic; Prof. John Smellie for providing Antarctic samples; Dr. Martin Towner for enabling me conduct the Mars chamber experiments; and Dr. Mike Storrie-Lombardi. Additionally I extend my thanks to the AMASE team and crew for making it a fantastic experience I shall never forget.

A big thanks to everyone in the planetary office for making it such a fun and friendly place to work, and to the usual suspects for the often much-needed Friday evening drinks – in particular Caja, Kate, Lottie, Ceri and Katie for many civilised (and uncivilised..) nights out. I also thank Phil especially for being a constant source of entertainment during the past 3 years.

I cannot possibly give enough thanks to Bry for always supporting me throughout, especially for enduring the bad moods and listening to excited rabbitings on relating to this work.

Lastly, one final enormous thanks to my family for their continual support and interest in my work, and for always sustaining me with well-fed breaks away from London and work whenever they were needed.

CONTENTS

| | |
|---|-----------|
| Abstract | 2 |
| Acknowledgements | 3 |
| List of Figures | 9 |
| List of Tables | 13 |
| List of Abbreviations | 15 |
| | |
| 1 Introduction | 16 |
| 1.1 Astrobiology..... | 17 |
| 1.1.1 The science of astrobiology..... | 17 |
| 1.1.2 Mars habitability past and present..... | 18 |
| 1.1.2.1 Phyllosilicates..... | 19 |
| 1.1.2.2 Sulphates..... | 20 |
| 1.1.2.3 Opaline Silica and Carbonate..... | 21 |
| 1.1.3 Martian analogue environments on Earth..... | 21 |
| 1.2 Volcanism and Associated Environments..... | 24 |
| 1.2.1 Subglacial volcanism on Earth..... | 25 |
| 1.2.2 Subglacial volcanism on Mars..... | 27 |
| 1.2.3 Hydrothermal environments on Earth and Mars..... | 31 |
| 1.3 High Latitude Martian Analogue Localities..... | 32 |
| 1.3.1 Iceland..... | 32 |
| 1.3.2 Antarctica..... | 34 |
| 1.3.3 Svalbard..... | 36 |
| 1.4 Geomicrobiology..... | 38 |
| 1.4.1 Assessment and identification of microbial communities..... | 38 |
| 1.4.2 Microcosms and environmental simulations..... | 40 |
| 1.4.3 Biosignatures..... | 42 |
| 1.5 Detection of Astrobiological Targets on Mars..... | 45 |
| 1.5.1 Rover instrumentation for Mars..... | 45 |
| 1.5.2 The ExoMars PanCam instrument..... | 48 |
| 1.6 Thesis summary..... | 50 |
| 1.6.1 Motivation for this work..... | 50 |
| 1.6.2 Aims and summary of chapters..... | 51 |
| | |
| 2 Materials and Methods | 54 |
| 2.1 Laboratory Materials..... | 55 |
| 2.1.1 Sterilization..... | 55 |
| 2.1.2 Solutions and Reagents..... | 55 |
| 2.1.3 Bacterial strains and plasmids..... | 56 |
| 2.2 Sampling of Environments..... | 57 |
| 2.2.1 Sampling protocols and field techniques..... | 57 |

| | |
|--|-----------|
| 2.2.2 Sampling locations..... | 58 |
| 2.2.2.1 Iceland..... | 58 |
| 2.2.2.2 Svalbard..... | 65 |
| 2.3 Cultivation and Identification of Microorganisms..... | 67 |
| 2.3.1 Media for isolation of microorganisms..... | 67 |
| 2.3.2 Preparation of chemically competent cells..... | 68 |
| 2.3.3 Microbial isolation from Icelandic samples..... | 68 |
| 2.3.4 Extraction of genomic DNA from cultivated isolates..... | 69 |
| 2.3.5 Polymerase chain reaction (PCR) amplification..... | 69 |
| 2.3.6 Purification and cloning of PCR products..... | 70 |
| 2.3.7 Sequencing of the 16s rDNA gene..... | 71 |
| 2.4 Phylogenetic Analysis of the Microbial Community..... | 72 |
| 2.4.1 Genomic DNA extraction from environmental samples..... | 72 |
| 2.4.2 PCR amplification..... | 73 |
| 2.4.3 16S Clone library construction and analysis..... | 75 |
| 2.5 Analytical Techniques..... | 76 |
| 2.5.1 Thin section and petrographic analysis..... | 76 |
| 2.5.2 Scanning Electron Microscope (SEM)..... | 76 |
| 2.5.3 Raman spectroscopy..... | 76 |
| 2.5.4 Inductively coupled plasma atomic emission spectroscopy (ICP-AES)..... | 77 |
| 3 Bacterial Diversity of Basaltic Lavas from Central Iceland..... | 78 |
| 3.1 Colonisation of Basaltic Lavas..... | 79 |
| 3.2 The Basaltic Subglacial Lava Environment..... | 80 |
| 3.2.1 Pillow lava (ASK9)..... | 84 |
| 3.2.2 Hyaloclastite lava (ASK4)..... | 85 |
| 3.3 Physical and Chemical Analysis..... | 86 |
| 3.3.1 Macro texture..... | 86 |
| 3.3.2 Micro structure..... | 87 |
| 3.3.2.1 Thin section analysis..... | 87 |
| 3.3.2.2 Porosity..... | 88 |
| 3.3.3 Geochemistry..... | 90 |
| 3.4 Phylogenetic Analysis..... | 92 |
| 3.4.1 Bacterial diversity of ASK4 hyaloclastite..... | 94 |
| 3.4.2 Bacterial diversity of ASK9 pillow basalt..... | 100 |
| 3.4.2.1 ASK9 Pillow Basalt ‘glass’ (ASK9G)..... | 101 |
| 3.4.2.2 ASK9 Pillow Basalt ‘interpillow’ (ASK9IP)..... | 105 |
| 3.4.3 Actinobacteria in the Askja lavas..... | 109 |
| 3.5 Variation in Community Composition and Diversity..... | 111 |
| 3.5.1 Phylum composition within the lavas..... | 111 |
| 3.5.2 Comparison of communities between the different lava lithologies..... | 113 |
| 3.5.3 Lithological controls on colonisation..... | 118 |
| 3.6 Conclusions..... | 120 |

| | |
|--|------------|
| 4 Bioalteration in Continental Antarctic Basaltic Lava..... | 121 |
| 4.1 Bioalteration and Detection of Life on Mars..... | 122 |
| 4.1.1 Controls on the formation of bioalteration..... | 122 |
| 4.1.2 Utilising a transitional subglacial – marine environment..... | 123 |
| 4.2 Description of Bioalteration in James Ross Island Hyaloclastites..... | 124 |
| 4.2.1 Morphology and ichnotaxonomy..... | 124 |
| 4.2.2 Biogenicity..... | 129 |
| 4.3 Bioalteration vs. Environment..... | 130 |
| 4.3.1 Bioalteration vs. aqueous environment..... | 131 |
| 4.3.2 Bioalteration vs. elevation and age..... | 134 |
| 4.4 Implications for Using Bioalteration as a Martian Biosignature..... | 140 |
| 4.5 Conclusions and Future work..... | 140 |
| | |
| 5 The Viability of a Subglacial Volcanic Habitat on Mars: An Experimental and Culture-Based Test..... | 142 |
| 5.1 Testing a Martian Analogue Environment..... | 143 |
| 5.2 Experimental Set up and Sample Processing..... | 144 |
| 5.2.1 Experimental set-up..... | 144 |
| 5.2.2 Sample processing and test for survivability..... | 147 |
| 5.3 Physical and Chemical Properties..... | 149 |
| 5.3.1 Temperature..... | 150 |
| 5.3.2 Chemistry..... | 151 |
| 5.4 Simulated Martian Conditions and Survivability..... | 153 |
| 5.4.1 Isolates from untreated lava..... | 157 |
| 5.4.2 Isolates from the subglacial volcanic microcosm (SVM)..... | 159 |
| 5.4.3 Isolates from the exposed Martian environment..... | 159 |
| 5.5 Identification of Cultures..... | 160 |
| 5.5.1 Untreated lava isolates..... | 161 |
| 5.5.2 Isolates from the subglacial volcanic microcosm (SVM)..... | 164 |
| 5.5.3 Isolates from the negative control..... | 166 |
| 5.6 Factors Affecting Survivability..... | 170 |
| 5.6.1 Survivability vs. phylotype..... | 170 |
| 5.6.2 Survivability and the lava environment..... | 172 |
| 5.7 Conclusions and future work..... | 173 |
| | |
| 6 Development and Testing of the Geological Filters on the ExoMars PanCam Instrument..... | 175 |
| 6.1 Formulating a New Geological Filter set for the ExoMars PanCam Instrument..... | 176 |
| 6.1.1 An astrobiological objective..... | 176 |
| 6.1.2 Selection of new geological filter wavelengths..... | 176 |
| 6.1.2 Description of the new geological filter sets..... | 181 |
| 6.2 Detection of Astrobiological Targets in Martian Analogue Samples..... | 184 |
| 6.2.1 Martian analogue rocks..... | 185 |
| 6.2.2 Multispectral imaging..... | 186 |

| | |
|---|------------|
| 6.2.3 Martian analogue PanCam reflectance spectra..... | 189 |
| 6.3 UV detection of Astrobiological Targets..... | 203 |
| 6.3.1 Detection of gypsum..... | 204 |
| 6.3.2 Detection of photosynthetic communities..... | 208 |
| 6.4 Conclusions and Future Work..... | 210 |
| 7 Testing Filter Set ‘F2-12’ On Martian Analogue Targets in Svalbard..... | 213 |
| 7.1 Instrument Specifications and Operation..... | 214 |
| 7.2 PanCam Analysis of Astrobiological Targets..... | 217 |
| 7.2.1 Sverrefjell: lithological diversity and past habitability..... | 219 |
| 7.2.2 Jotun and Troll Springs: detection of biosignatures..... | 234 |
| 7.2.3 Wahlenbergfjord: detection of iron oxide deposits..... | 241 |
| 7.3 Conclusions and Future Work..... | 246 |
| 8 Discussion..... | 248 |
| 8.1 High Latitude Volcanic Environments..... | 249 |
| 8.2 Subglacial Volcanic Environments on Mars..... | 251 |
| 8.2.1 Availability of liquid meltwater..... | 251 |
| 8.2.2 Initial colonisation..... | 252 |
| 8.2.3 Potential for photosynthesis and chemosynthesis..... | 253 |
| 8.2.4 Habitat duration..... | 254 |
| 8.2.5 Biosignatures..... | 254 |
| 8.3 Implications for the ExoMars Mission..... | 256 |
| 8.3.1 Developing PanCam for an astrobiology mission..... | 256 |
| 8.3.2 Application to future astrobiology missions..... | 260 |
| 8.4 Future work..... | 260 |
| 8.4.1 The Kverkfjoll subglacial caldera..... | 261 |
| 8.4.2 Hveradalur..... | 262 |
| 8.4.3 Hveratagl..... | 263 |
| 8.4.4 Initial Environmental Data..... | 263 |
| 8.5 Final Conclusions..... | 265 |
| REFERENCES..... | 267 |
| APPENDIX..... | 296 |
| A) Data Tables..... | 296 |
| Table 1. EDS measurements (as oxide wt.%) from glassy regions of ASK004 hyaloclastite and ASK009 pillow basalt..... | 296 |
| Table 2. Exhaustive list of all closest novel relatives and species relatives for the ASK4B environmental clones based on BLASTn 16s rDNA similarity..... | 297 |
| Table 3. Exhaustive list of all closest novel relatives and species relatives for the ASK9G environmental clones based on BLASTn 16s rDNA similarity..... | 298 |
| Table 4. Exhaustive list of all closest novel relatives and species relatives for the ASK9IP environmental clones based on BLASTn 16s rDNA similarity..... | 299 |

| | |
|---|-----|
| B) Equations | 300 |
| Equation 1. Porosity..... | 300 |
| Equation 2. Shannon’s Diversity Index..... | 300 |
| Equation 3. Simpson’s Diversity index..... | 300 |
| | |
| C) PanCam sample & mineral spectra | 301 |
| | |
| D) Publications | 302 |

LIST OF FIGURES

Chapter 1: Introduction

| | |
|---|----|
| 1.1 Total Alkali-Silica (TAS) plot for in-situ and orbital Martian rock elemental oxide measurements..... | 24 |
| 1.2 Subglacial volcanic processes, products, and environments..... | 26 |
| 1.3 Putative glaciovolcanic features on Mars..... | 30 |
| 1.4 Map of Mars showing sites of putative endogenic hydrothermal activity..... | 31 |
| 1.5 Map of Iceland showing the location of central volcanoes..... | 33 |
| 1.6 A simplified cross section through east - central Iceland..... | 34 |
| 1.7 Map of James Ross Island, northern Antarctic Peninsula..... | 35 |
| 1.8 Physical map showing the location of the Svalbard Archipelago..... | 36 |
| 1.9 Map of the Svalbard archipelago..... | 37 |
| 1.10 Bioalteration texture morphologies in basaltic volcanic glass..... | 43 |
| 1.11 Artists impression of the ExoMars Rover and technical drawing of one of the PanCam Wide Angle Cameras..... | 48 |

Chapter 2: Materials and Methods

| | |
|---|----|
| 2.1 Satellite map of Iceland..... | 59 |
| 2.2 Map showing localities a) Krysuvik, Helgafell, and Geysir; b) Kverkfjoll, Askja, and Namafjall..... | 60 |
| 2.3 Photographs of Icelandic localities where sampling took place..... | 63 |
| 2.4 Field sites in Bockfjord, Svalbard..... | 66 |

Chapter 3: Bacterial Diversity of Basaltic Lavas from Central Iceland

| | |
|--|-----|
| 3.1 Aerial view of the Askja caldera eastern rim..... | 82 |
| 3.2 Map of mean maximum and minimum temperature..... | 83 |
| 3.3 a) Pillow basalt outcrop; b) typical pillow morphology; c) alteration between pillows..... | 84 |
| 3.4 Context photograph of the hyaloclastite outcrop at Askja..... | 85 |
| 3.5 a) ASK4 hyaloclastite; b) ASK9 Pillow Lava 'Glass'; c) ASK9 Pillow Lava 'Interpillow'..... | 86 |
| 3.6 Digital microscope images of all three lava environments..... | 87 |
| 3.7 Thin section images of lavas ASK4 and ASK9..... | 88 |
| 3.8 TAS classification diagram of ASK4 and ASK9 lavas..... | 91 |
| 3.9 Phylogenetic tree of all clones from all three lava environments..... | 93 |
| 3.10 Representative environments of BLASTn closest relatives to the ASK4B Hyaloclastite bacterial clones..... | 95 |
| 3.11 Phylogenetic tree of ASK4 hyaloclastite bacterial clones (ASK4B)..... | 98 |
| 3.12 Phylogenetic tree of the 12 archaeal clones from ASK4 hyaloclastite..... | 100 |
| 3.13 Representative environments of BLASTn closest relatives to the ASK9 Pillow Basalt 'glass' bacterial clones..... | 102 |

| | |
|---|-----|
| 3.14 Phylogenetic tree of ASK9 pillow basalt ‘glass’ clones (ASK9G)..... | 105 |
| 3.15 Representative environments of BLASTn closest relatives to the ASK9 Pillow basalt ‘interpillow material’ bacterial clones..... | 106 |
| 3.16 Phylogenetic tree of ASK9 pillow basalt ‘interpillow’ clones (ASK9IP)..... | 109 |
| 3.17 Phylogenetic tree of clones within the Actinobacteria..... | 110 |
| 3.18 Stacked bar charts showing the distribution of Bacterial phylotypes..... | 113 |
| 3.19 Rarefaction curves for the three lava environments..... | 116 |

Chapter 4: Bioalteration in Continental Antarctic Basaltic Lavas

| | |
|---|-----|
| 4.1 Examples of bioalteration textures and abiotic alteration..... | 125 |
| 4.2 Bioalteration ‘pitting’ and ‘etching’ into glass boundaries under SEM..... | 126 |
| 4.3 Ichnofossil taxonomic classifications identified in the hyaloclastites..... | 128 |
| 4.4 K-means clustering of the mean bioalteration values..... | 133 |
| 4.5 Plot showing sample elevation and bioalteration values..... | 135 |
| 4.6 Plot of bioalteration values against hyaloclastite age..... | 136 |
| 4.7 Diagram of a simplified James Ross Island subglacial lava sequence showing different stages of fluid alteration and microboring production..... | 138 |

Chapter 5: The Viability of a Subglacial Volcanic Habitat on Mars: An Experimental and Culture-Based Test

| | |
|---|-----|
| 5.1 Experimental set up of the SVM within the Mars environmental chamber..... | 146 |
| 5.2 Photograph of the Mars chamber, showing the Mars gas source, -30°C freezer, UV light input and atmospheric pressure pump..... | 146 |
| 5.3 Experimental set-up inside the sterile container a) before; and b) after 6 days of incubation..... | 147 |
| 5.4 Real-time temperature graph of the meltwater layer within the subglacial volcanic simulation..... | 151 |
| 5.5 Dissolved element composition of the dH_2O ‘glacial’ water, SVM meltwater, and Skaftá and Grimsvotn caldera lake..... | 153 |
| 5.6 CFU’s plotted against number of lava fragments..... | 154 |
| 5.7 Mean (n=5) CFUs from each of the untreated lava, simulated subglacial volcanic microcosm (SVM), and negative control..... | 156 |
| 5.8 Untreated lava colonies on PBA after 40 days growth..... | 157 |
| 5.9 Pure isolates from untreated lava ASK9 plates..... | 158 |
| 5.10 Cultures from subglacial pillow basalt from the SVM..... | 159 |
| 5.11 Pillow agar inoculated with negative control pillow basalt..... | 160 |
| 5.12 Phylogenetic tree for all isolates, along with their closest relatives..... | 169 |
| 5.13 Stacked bar chart showing a) the isolate phyla; and b) the isolate genus..... | 171 |

Chapter 6: Development and Testing of the Geological Filters on the ExoMars PanCam Instrument

| | |
|--|-----|
| 6.1 Filter wavelengths used in the Beagle camera..... | 177 |
| 6.2 a) Spectra of montmorillonite (CM20 – CM27), opal, and gypsum (SU2202 and HS333) with OH and H ₂ O absorption bands at 950 and 1000nm respectively; b) USGS | |

| | |
|--|-----|
| spectra of the minerals used to statistically calculate new filter selections for ‘F1-12’ and ‘F2-12’ | 181 |
| 6.3 Plot of filters and estimated filter bandpasses for Beagle2 and new filter sets, together with the absorption bands for ferric or ferrous iron and water, and also the emission peaks for nontronite and jarosite..... | 183 |
| 6.4 Reflectance spectra of nontronite (SWa-1.a) and jarosite (JR2501) showing the effect of the different filter sets on diagnostic features..... | 184 |
| 6.5 Martian analogue samples used for testing different filter sets..... | 185 |
| 6.6 Experimental set up for PanCam – style multispectral imaging..... | 187 |
| 6.7 Experimental set up for UV illumination using a) LED+Foculus+B2 filter wheel; b) Laser+Digital camera..... | 188 |
| 6.8 Example image of sample NBO as seen with a 590nm filter..... | 188 |
| 6.9 Martian analogue sample spectra modelled for: column (A) Beagle2; (B) F1-12; (C) F2-12; (D) F3-12 filter sets..... | 190 |
| 6.10 SEM image of the hyaloclastite..... | 192 |
| 6.11 BSE images of a) mineral-filled vesicle and b) botryoidal amorphous silica deposits in sample NAL..... | 193 |
| 6.12 Raman spectrum of the orange deposits on sample NBO and jarosite for comparison..... | 194 |
| 6.13 Raman spectra for GY1 R3 and GY1 R4 showing the presence of haematite and sulphur respectively..... | 195 |
| 6.14 F2-12 spectra for GY1 regions ‘Red’ and ‘Yellow’, which have a Raman spectrum of haematite and sulphur respectively..... | 196 |
| 6.15 BSE image of GY2 silica sinters, showing preserved biological and cellular structures within the silica matrix..... | 196 |
| 6.16 Spectral parameter plot of 900nm band depth vs. 440 – 700nm slope for the Martian analogue rock spectra..... | 199 |
| 6.17 Spectral parameter plot of 920 – 1000nm slope vs. 440 – 700nm slope for the Martian analogue rock spectra..... | 200 |
| 6.18 Spectral parameter plot of 470nm band depth vs. 900nm band depth for the Martian analogue rock spectra..... | 201 |
| 6.19 Digital camera captured image of sample KV007 under natural light and showing the native epifluorescence emitted from gypsum deposits..... | 205 |
| 6.20 Magnified Foculus captured image of KV007 epifluorescence at a distance of 2m through the green filter..... | 205 |
| 6.21 KV007 gypsum epifluorescence..... | 206 |
| 6.22 Raman spectrum of KV007 vesicle deposits using 785nm laser excitation..... | 206 |
| 6.23 KH chasmolithic lichens illuminated with a) solar lamp and b) 365nm fluorescence, both seen through a 560nm filter..... | 208 |
| 6.24 Epilithic lichen UV fluorescence..... | 210 |
| Chapter 7: Testing Filter Set ‘F2-12’ on Martian Analogue Targets in Svalbard | |
| 7.1 The PanCam instrument used for field testing in Svalbard..... | 214 |
| 7.2 Position of the PanCam Calibration Target (PCT)..... | 217 |

| | |
|--|-----|
| 7.3 Sverrefjell Volcano in Bockfjord..... | 219 |
| 7.4 Digital photograph of rock targets at BOCK01..... | 221 |
| 7.5 Left WAC RGB colour composite image of the BOCK01 rock targets at a distance of 4.70m from the WAC optical axis..... | 222 |
| 7.6 PanCam spectra of all the target and control rocks from the scene..... | 223 |
| 7.7 PanCam spectra of BOCK01 targets ‘X’ and ‘S’, plus library spectra re-sampled to PanCam filter wavelengths..... | 224 |
| 7.8 Partial PanCam spectra of BOCK01 targets ‘S’ and ‘X’ that match mineral library spectra..... | 225 |
| 7.9 WAC RGB colour composite of the outcrop at Sverrefjell volcano..... | 227 |
| 7.10 ‘Marianne’ HRC image of layering structures within the outcrop..... | 228 |
| 7.11 HRC target images showing two different lithologies..... | 229 |
| 7.12 PanCam spectra of SV01 targets..... | 230 |
| 7.13 440 – 660nm slope vs. 880nm band depth spectral parameter plot for PanCam targets for BOCK01 and SV01 at Sverrefjell volcano..... | 232 |
| 7.14 Right WAC RGB colour composite image of Jotun Springs..... | 235 |
| 7.15 PanCam spectra from Jotun Springs..... | 237 |
| 7.16 Spectral mapping of targets at Jotun Springs..... | 238 |
| 7.17 Troll Spring carbonate terraces..... | 239 |
| 7.18 Right WAC RGB composite of the outcrop..... | 242 |
| 7.19 HRC image of Target 3..... | 242 |
| 7.20 PanCam spectra of targets shown in Figure 7.18..... | 243 |
| 7.21 440 – 660nm slope vs. 880nm band depth spectral parameter plot for geological targets..... | 244 |
| 7.22 Stratigraphic section through the outcrop at Wahlenbergfjord..... | 246 |
| Chapter 8: Discussion | |
| 8.1 Google Earth areal view of the different environments sampled..... | 250 |
| 8.2 PanCam spectra of Precambrian stromatolites..... | 258 |
| 8.3 Map showing the locations of Kverkfjoll sample sites..... | 261 |
| 8.4 Contextual photograph of the area around Hveradalur..... | 262 |
| 8.5 Hydrothermal pools at Hveratagl..... | 264 |

LIST OF TABLES

Chapter 1: Introduction

| | |
|---|----|
| 1.1 Potential lines of enquiry associated with Martian analogue research..... | 22 |
| 1.2 DNA extraction pitfalls from volcanic environments..... | 39 |
| 1.3 Biogenicity criteria for endolithic microborings..... | 45 |
| 1.4 Overview of past and future planned rover/lander instrumentation..... | 47 |

Chapter 2: Materials and Methods

| | |
|---|----|
| 2.1 Table of all samples collected from Iceland..... | 64 |
| 2.2 Table of sites in Svalbard..... | 66 |
| 2.3 Oligonucleotide primer pairs used for the amplification of bacterial and Archaeal 16S rDNA genes from environmental and isolate DNA..... | 74 |

Chapter 3: Bacterial Diversity of Basaltic Lavas from Central Iceland

| | |
|---|-----|
| 3.1 Porosity estimates..... | 90 |
| 3.2 Closest relatives with the ASK4B Hyaloclastite clones..... | 96 |
| 3.3 Archaeal community members from ASK4 hyaloclastite..... | 99 |
| 3.4 Closest relatives with the ASK9 Pillow Lava ‘glass’ clones..... | 103 |
| 3.5 Closest relatives with the ASK9 Pillow Lava ‘interpillow’ clones..... | 107 |
| 3.6 Phylogenetic distribution of Bacterial genotypes..... | 114 |

Chapter 4: Bioalteration in Continental Antarctic Basaltic Lavas

| | |
|--|-----|
| 4.1 Example bioalteration values used to determine the extent of bioalteration within the JRIVG hyaloclastites..... | 131 |
| 4.2 Mean bioalteration values for hyaloclastites from James Ross Island..... | 139 |

Chapter 5: The Viability of a Subglacial Volcanic Habitat on Mars: An Experimental and Culture-Based Test

| | |
|--|-----|
| 5.1 Environmental conditions in the Mars chamber and on the surface of present day Mars..... | 147 |
| 5.2 Measured pH, temperature, and dissolved element concentration from the dH_2O ‘glacial’ water and meltwater after 1 week incubation..... | 153 |
| 5.3 Colony growths on media plates inoculated with lava or meltwater after 30 days incubation at 20°C..... | 155 |
| 5.4 Quantification of colony growth expressed as a % of growth per 100 lava fragments or 100µl of meltwater..... | 156 |
| 5.5 Identification of isolates as determined by RDP..... | 161 |
| 5.6 BLAST database closest environmental isolate relatives and closest cultured species based on 16s rDNA similarity (%) with the ASK009 and Mars Chamber isolates..... | 168 |

Chapter 6: Development and Testing of the Geological Filters on the ExoMars PanCam Instrument

6.1 Hydrated mineral reflectance spectra used for PanCam filter selection.....179
6.2 Filter centre wavelengths for B2 and the proposed filter sets.....182
6.3 Description and original location of the samples used in this study.....186
6.4 Ability of the Beagle2 and new filter sets to detect specific spectral features in the Martian analogue rock spectra.....197
6.5 Spectral parameters used to assess the different filter sets.....198

Chapter 7: Testing Filter Set ‘F2-12’ on Martian Analogue Targets in Svalbard

7.1 Filter characteristics for the AMASE camera filters.....215
7.2 AMASE PanCam WAC and HRC demonstrator specifications.....216
7.3 Summary of the four PanCam test sites during AMASE field deployment.....218

Chapter 8: Discussion

8.1 All minerals and biosignatures used to aid design and testing of the ExoMars PanCam instrument.....257

LIST OF ABBREVIATIONS

| | |
|---------------|---|
| AMASE | Arctic Mars Analog Svalbard Expedition |
| BLAST | Basic Local Alignment Search Tool |
| BSA | Bovine serum albumin |
| BSE | Back Scatter Electron |
| CCD | Charge Coupled Device |
| CFU | Colony Forming Units |
| CRISM | Compact Reconnaissance Imaging Spectrometer for Mars |
| CTAB | Hexadecyltrimethyl ammonium bromide |
| CZD | Czapek-Dox |
| DMSO | Dimethylsulphoxide |
| DNA | Deoxyribonucleic acid |
| EDS | Energy Dispersive X-Ray Spectrometer |
| ESA | European Space Agency |
| FWHM | Full Width Half Maximum |
| HRC | High Resolution Camera |
| IMP | Imager for Mars Pathfinder |
| IPTG | Isopropyl β -D-1-thiogalactopyranoside |
| IR | Infrared |
| LB | Luria Bertani |
| LCTF | Liquid Crystal Tunable Filters |
| LED | Light Emitting Diode |
| LIBS | Laser Induced Breakdown Spectroscopy |
| MATLAB | Matrix Laboratory |
| MER | Mars Exploration Rover |
| MIMA | Mars Infrared Mapper |
| NASA | National Aeronautics and Space Administration |
| NB | Nutrient Broth (microbial growth medium) |
| NBAF | NERC Biomolecular Analysis Facility |
| NCBI | National Centre for Biotechnology Information |
| NERC | Natural Environment Research Council |
| OMEGA | Observatoire pour la Minéralogie, l'Eau, les Glaces et l'Activité |
| PanCam | Panoramic Camera |
| PCR | Polymerase Chain Reaction |
| PCT | PanCam Calibration Target |
| PSSRI | Planetary and Space Sciences Research Institute |
| rDNA | Ribosomal DNA |
| RDP | Ribosomal Database Project |
| RGB | Red Green Blue |
| SDS | Sodium Lauryl Sulphate |
| SEM | Scanning Electron Microscopy |
| USGS | United States Geological Survey |
| UV | Ultraviolet |
| WAC | Wide Angle Camera |

CHAPTER 1

INTRODUCTION

This thesis is focused upon a central theme of utilising terrestrial environments as analogues of those environments believed to have existed on Mars, either in the past or at this present day. This is done with the aim of furthering our understanding of the theoretical habitability of Martian environments based on experimental and observational geomicrobiology, and of helping to develop and test actual Martian rover instrumentation that will be used to search for evidence of life on Mars. This work therefore is strongly multi-disciplinary, and this chapter will introduce the key concepts, techniques, and existing work that are relevant to this thesis.

Astrobiology as a subject in its own right is discussed first within the context of Mars, and this section will review the scientific understanding of why Mars in particular is of such significant interest in astrobiological exploration. This includes the similarity between the Earth and Mars, existence of liquid water, and the potential range of habitable environments where Martian life could survive. The environments studied in this work are specifically associated with volcanism, a process widespread across Earth and Mars, and indeed many other locations in the Solar System. As such, volcanic environments of relevance to Mars are reviewed here in the depth.

1.1. Astrobiology

1.1.1 The Science of Astrobiology

The field of astrobiology aims to determine the origin, evolution, and distribution of life throughout the Universe. As a result of this considerably broad scope, it is an inherently interdisciplinary subject, drawing from the well-established sciences of biology, geology, chemistry, planetary science and astronomy. Research at the interface of these scientific fields provides the astronomical and planetary context in which habitable conditions form, the geological conditions that allow life to arise, and the ecological and biological interactions that make survival and evolution possible. Despite our advancing understanding of the planetary bodies both within, and outside, our solar system, to our knowledge the existence of life remains an entirely unique feature of Earth, and will remain so until the unambiguous detection of either extinct or extant life on another planetary body. One of the main drivers for recent astrobiological research has been the discovery of life thriving in environments previously considered entirely hostile to life, and that these so-called ‘extreme’ environments are analogous to those identified on other planetary bodies. Mars in particular is notable in its apparent similarity to some of these extreme environments on Earth, and as a result has been of considerable astrobiological focus. Habitable environments that are hypothesised to have existed on Mars include impact-induced hydrothermal systems (Newsom *et al.* 2001); deep subsurface volcanic environments (Boston *et al.* 1992); endolithic environments (Walker & Pace 2007); subglacial volcanoes (Chapman 2003); saline lakes (Mancinelli *et al.* 2004), and permafrost (Gilichinsky *et al.* 2007).

Until human space exploration becomes widely feasible, rover-based exploration of Mars will remain the most important activity for understanding the detailed geological and biological history of the planet. Some of the most significant and conclusive discoveries in planetary exploration have resulted from in-situ analysis using instrumentation onboard landers. The very first successful lander mission to Mars was the USSR Mars 3 mission (landed 1971). This was swiftly followed by the NASA Viking landers (landed 1976), which were famous for their on-board biological experiments. The NASA Pathfinder mission followed (landed 1997), and this pioneered the use of rover technology. Missions since have, like Viking, had an underlying astrobiological objective. The NASA Mars Exploration

Rovers (MER) Spirit and Opportunity (landed 2004) are one of the most successful missions to date, and have revealed a great deal about the planet's geological history and potential for past habitability. Rather than carrying out direct biological experiments as Viking did, these rovers were designed to be 'geologists', and through gathering geological evidence of the planets environmental history, they provide data to assess the potential for life on Mars through the identification of habitable conditions. Likewise, the recent NASA Phoenix polar lander (landed 2008) was sent to detect and analyse water ice in situ at the Martian surface, and to assess whether Mars contains the essential ingredients for life, but not to directly search for evidence of life itself. The ESA Beagle2 lander (launched 2003) was a UK-led mission which aimed to carry out the next direct search for life since the Viking mission. Sadly this mission was lost, and the search for life on Mars now lies with the next two missions planned for Mars within the coming decade: The NASA Mars Science Laboratory (planned launch 2011), and the ESA ExoMars mission (planned launch 2018). Both these missions have life detection as part of their key scientific objectives.

1.1.2 Mars habitability past and present

One of the primary reasons why Mars is of particular astrobiological interest is the widespread evidence suggesting past, or even present, habitable conditions. Water in particular is widely regarded to be the most significant factor regarding the habitability of any given environment, and there is a large amount of data that appears to show water was both widespread and plentiful on Mars in the past, leading to the formation of huge fluvial networks within the most ancient (Noachian) Martian terrains (Baker *et al.* 1991; Carr 1996, Carr 1987). This water is now absent from the Martian surface, giving rise to the dry and dusty surface environment that we see today. Presently, most water is locked away as ice at the poles, although a considerable quantity is believed to also exist within the subsurface, forming an extensive global cryosphere (Mitrofanov 2005, and references therein; Hiesinger *et al.* 2000; Carr 1987). In particular, the Phoenix lander sent back images showing polygonal ground, highly characteristic of permafrost terrains (Smith *et al.* 2009; Mellon *et al.* 2008a,b), and also close up images of ice deposits just several centimetres below the surface (Smith *et al.* 2009).

In addition to geomorphological evidence of past liquid water, the results of the hyperspectrometers OMEGA (on board the ESA Mars Express orbiter) and CRISM (on board the NASA Mars Reconnaissance Orbiter) currently orbiting Mars have revealed a large diversity in surface mineralogy and lithology (Mustard *et al.* 2008; Bibring *et al.* 2005). Hydrated minerals on Mars have now been defined into three distinct hydrated mineral terrains. First and oldest are the phyllosilicates, which are found in early Noachian terrains (Mustard *et al.* 2008; Bibring *et al.* 2006). These are predominantly Fe, Mg and Al- rich phyllosilicates that often occur as alternating lithologies (Loizeau *et al.* 2007). Secondly are the sulphates, notably gypsum and kieserite amongst others (Gendrin *et al.* 2005; Bibring *et al.* 2005). These span the Late Noachian and early Hesperian terrains, and it has been suggested they indicate a change from neutral pH conditions to more acidic environments (Bibring *et al.* 2006). In contrast are the recently discovered deposits of hydrated silica on Mars, thought to be the youngest of the three hydrated mineral lithologies and potentially indicative of non-acidic conditions (Milliken *et al.* 2008). Likewise, small isolated deposits of carbonates in the Nili Fossae region have been detected (Ehlmann *et al.* 2008a). These carbonates, believed specifically to be magnesite, are thought to have formed via hydrothermal alteration of olivine rich ultramafic rocks (Ehlmann *et al.* 2008a). These mineral terrains are discussed in further detail in the following sections.

1.1.2.1 Phyllosilicates

The oldest of these hydrated mineral terrains, the phyllosilicates, are layer silicates, which commonly form from the hydrous alteration of volcanic material (Stroncik & Schmincke 2002). The OMEGA instrument aboard Mars Express has detected mineralogically diverse phyllosilicates on the Martian surface in association with Noachian terrains (Poulet *et al.* 2005; Bibring *et al.* 2006). Here, Fe/Mg smectites and montmorillonite-type minerals have been identified (Bibring, *et al.* 2007; Poulet *et al.* 2005), and nontronite is particularly common (Bibring *et al.* 2006). In the Mawrth Vallis region, smectites including montmorillonite and nontronite have been identified, and are thought to form part of a large phyllosilicate rich geological unit (Loizeau *et al.* 2007). These phyllosilicates have been described in detail, and reveal a complex aqueous history of early Mars that may be indicative of long-term aqueous alteration of

basaltic/igneous material (Bishop *et al.* 2008; Poulet *et al.* 2005). It has also been noted that the formation of these clay minerals could have occurred within the subsurface, through hydrothermal alteration, a scenario which would not require a warm and wet early Mars to have existed over long time-scales (Bibring *et al.* 2006). Such subsurface aqueous alteration is commonly seen within basaltic lava edifices and hyaloclastite lavas that were erupted beneath an overlying glacier or ice cap, resulting in low temperature hydrothermal circulation and widespread phyllosilicate formation beneath the ice (Smellie 2007).

1.1.2.2 Sulphates

Sulphates have been identified in layered terrains on Mars by OMEGA and are thought to either be evaporates, forming from Fe and Mg- rich brine lakes, or the result of hydrothermal sulphur rich fluids circulating through volcanic ash deposits (Gendrin *et al.* 2005). Analysis by the Mars Exploration Rovers (MER) at Meridiani Planum and Gusev crater have yielded a great deal of information on the nature of sulphates on Mars. In particular, Jarosite was identified at Meridiani (Klingelhofer *et al.* 2004) and subsequent work suggests other iron sulphate minerals may also be present (Lane *et al.* 2004). Additionally, kieserite and gypsum have been identified by the OMEGA instrument at several locations on Mars (Bibring *et al.* 2005; Gendrin *et al.* 2005). Sulphates are found across Earth and are commonly formed through volcanic activity (such as alteration of volcanic rocks by acidic fumaroles) or evaporitic processes (Martinez-Frias *et al.* 2006). In acidic environments, sulphates can be precipitated abiotically, but microbes are often involved in the process, as is seen in hydrothermal settings and acid mine drainage environments (Bishop *et al.* 2004a). Additionally, sulphate minerals such as gypsum have been found to act as a microhabitat on Earth, particularly for photosynthetic organisms that exploit its translucent nature. Cyanobacterial communities have been found to be living within evaporitic sediments of the Abu Dhabi Sabkha, where the algae mats present within gypsum and halite contribute to the reflectance spectra observed (Howari 2006). Sulphate formation however is more common in acidic water conditions, and doesn't necessarily require a long term presence of liquid water, as clays do (Poulet *et al.* 2005).

1.1.2.3 Opaline Silica and Carbonate

The most recently discovered of these hydrated minerals is opaline hydrated silica, detected by CRISM (Milliken *et al.* 2008), and also identified by the MER Spirit at Gusev Crater (Rice *et al.* 2010; Squyres *et al.* 2008). Opaline silica commonly forms in hot spring systems, where the eruption of silica supersaturated hot spring fluids at the surface gradually produces siliceous sinters over time. Additionally to this, opaline silica can form via hydrothermal weathering of basaltic rock, stripping the mafic minerals away leaving behind a silica-rich crust (Schiffman *et al.* 2006). Silica sinters are known to be excellent bio-preservers on Earth, and the discovery of hydrated silica on Mars could have important implications for the detection of Martian biosignatures potentially similar to those commonly found in hot spring sinters on Earth (Preston *et al.* 2008; Goryniuk *et al.* 2004). Likewise the discovery of carbonates holds promise for the detection of microfossils within putative hydrothermal carbonate deposits (e.g. Allen *et al.* 2000).

1.1.3 Martian analogue environments on Earth

There are many terrestrial environments that are considered plausible analogues of potentially habitable environments on other planetary bodies, either in the past or at the present day (e.g. Cavicchioli 2002). These terrestrial environments provide us with a working model of potential astrobiological targets. The astrobiological study of any analogue environment needs to encompass several interdisciplinary lines of research. Firstly, it is important to understand how the environment is created and sustained – that is, what geological processes and climatic conditions have produced the observed conditions, and crucially, what makes this particular environment habitable. Secondly, and perhaps of most interest, is discovering what lives in these environments, and identifying any evidence that this life leaves behind in the geological record (biosignatures). Lastly, in order to achieve this identification, it is necessary to be able to detect evidence of these environments on the planetary surface itself.

Table 1.1 outlines several potential lines of enquiry when researching any given Martian analogue environment, focusing principally on what lives there, how it lives there, and how it may be detected. It is noted that such lines of enquiry,

together with the vast majority of Martian analogue research (including that described in this thesis), relies upon the assumption that Martian life would be based upon the same biochemical structures and pathways that are fundamental to terrestrial life. Whilst this may seem to be an overly Earth-centric viewpoint, there is reason to believe this is likely to be the case. During the first ~1 billion years of Solar System history, impacts were commonplace, and as such any developing or developed life forms could feasibly be transported between Earth and Mars (in both directions), a process known as lithopanspermia (Mileikowsky *et al.* 2000). Even without any early cross contamination between the two planets, the early environments of both planets (within which life had originated at least on Earth) may have been similar enough to lead to the generation of life based on the same biomolecular template (McKay & Stoker 1989). Lastly, the search for life on another planet cannot be purely serendipitous, instruments and techniques need to be designed and tested to look for specific biosignatures, a process which is reliant upon the only example of life currently available, that on Earth.

Table 1.1. Potential lines of enquiry associated with Martian analogue research. Those subjects that are underlined are explored in this thesis.

| Line of enquiry | Description or example |
|---------------------------------------|---|
| <u>Environmental characterisation</u> | Geological formation, physiochemical properties, local climatic factors and processes, (bio)geochemical cycling |
| <u>Phylogenetic diversity</u> | Identification of bacterial and archaeal community (e.g. diversity and composition) indigenous to the environment, microbial ecology |
| <u>Isolation of microorganisms</u> | Cultivation of microorganisms to understand their physiology and survival in extreme environments and under Martian conditions |
| Metabolic pathways | Identification of chemosynthetic pathways that could be sustained on Mars |
| <u>Biosignatures</u> | Formation, identification, and interpretation of isotopic, molecular, morphological, and spectroscopic indicators of life or biological processes |
| <u>Environment simulations</u> | Simulated microcosms under Martian conditions to test the viability of analogue life and habitats |

Table 1.1 Continued

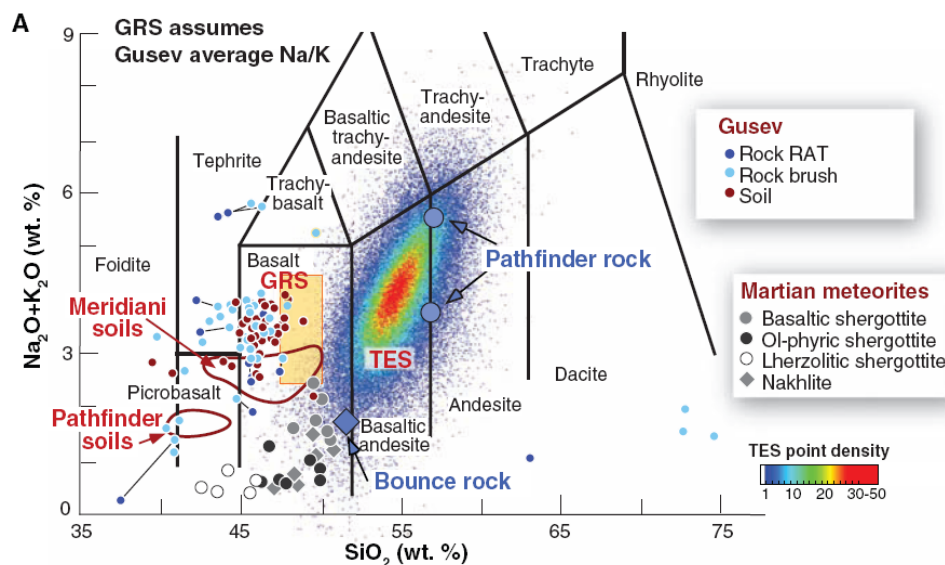
| Line of enquiry | Description or example |
|--|--|
| <u>Rover-based detection of habitable environments</u> | Using rover instrumentation to identify targets within which to look for signs of past or present life |
| Rover-based detection of life | Using rover instrumentation to detect evidence of past or present life, such as organic biomolecules |
| Orbiter-based detection of habitable environments | Using orbital images, mapping, and spectroscopic data to identify regions on Mars that may have been/may still be able to support life |

The surface of Mars today is characterised by conditions that are highly unfavourable to life. The lack of liquid water, high solar UV radiation and presence of chemical oxidants in the Martian soil render the surface unsuitable for even the most extreme forms of life that we know of. As a result, if life were to survive on present day Mars, it would presumably reside within the Martian subsurface, protected from the surface extremes. Terrestrial environments that have received considerable attention as proxies for past or present Martian habitats include the Antarctic Dry Valleys (Walker & Pace 2007; Wierzchos *et al.* 2005; Nienow *et al.* 1988), the Atacama Desert (Navarro-Gonzalez *et al.* 2003), evaporite environments (Edwards *et al.* 2006; Rothschild 1990), acid mine drainage systems (Amils *et al.* 2007), the deep subsurface (Chapelle *et al.* 2002; Stevens & McKinley 1995), and hydrothermal/hot spring systems (Varnes *et al.* 2003; Rathbun & Squyres 2002). These environments have shown a promising array of resilient microbial communities that thrive under harsh environmental conditions, and this encourages the idea that life may have resided on Mars in the past. In particular, a large percentage of Mars is considered to be volcanic in nature. As a result, it is important to identify and understand volcanic environments in terms of their habitability and potential for microbial colonisation. Volcanic environments on Earth have been explored extensively in terms of biodiversity and chemical cycling, such as hydrothermal vents (Harmsen *et al.* 1997), hot springs (Kvist *et al.* 2007; Ellis *et al.* 2005), and deep sea lava flows (Edwards *et al.* 2003).

1.2 Volcanism and Associated Environments

Volcanism provides a way for a planet to release internal heat, which has been left over from its formation, generated by radioactive elements, and tidal stresses, and as such is a process seen throughout the Solar System (Wilson 2009). Volcanism on Earth is exceptionally varied, with volcanic activity accompanying regions of tectonic plate movement, be it where plates converge at subduction zones, or at mid-ocean ridges where new crust is formed. Plate tectonic activity has resulted in volcanism that is diverse both in its setting, and particularly in its chemistry and resulting mineralogy. Mars on the other hand lacks any similar plate tectonic system, and volcanism is limited to localised regions of significantly high heat flow, comparable to hot-spot volcanism seen at Hawai'i or Iceland for example. As a consequence, volcanism on Mars is largely unevolved chemically, dominated by ultramafic – basaltic – basaltic andesite lavas (McSween *et al.* 2009; Wyatt *et al.* 2003). Figure 1.1 shows on a Total Alkali-Silica (TAS) plot (Le Bas *et al.* 1986) of the broad classification of Martian rocks, based on in-situ data from the MER and Pathfinder rover missions, orbital data from the Gamma-Ray Spectrometer (GRS) and Thermal Emission Spectrometer (TES) on the Mars Odyssey and Mars Global Surveyor orbiters respectively, and laboratory data from Martian meteorites. The plot shows that the composition of the Martian crust is largely basaltic, ranging between unevolved picritic compositions to basaltic andesites.

Figure 1.1. Total Alkali-Silica (TAS) plot for in-situ (MER, Pathfinder) and orbital (GRS, TES) Martian rock elemental oxide measurements (McSween *et al.* 2009).



Volcanic environments on Earth that are used as Martian analogues in this work are restricted to firstly terrestrial volcanoes that are considered similar to those believed to exist on Mars, and secondly to volcanically-driven hydrothermal environments. Subglacial basaltic volcanoes and associated lava flows are focused on in particular, and are described in further detail below. Hydrothermal systems are widespread on Earth, and those that are associated with basaltic volcanism were of particular interest.

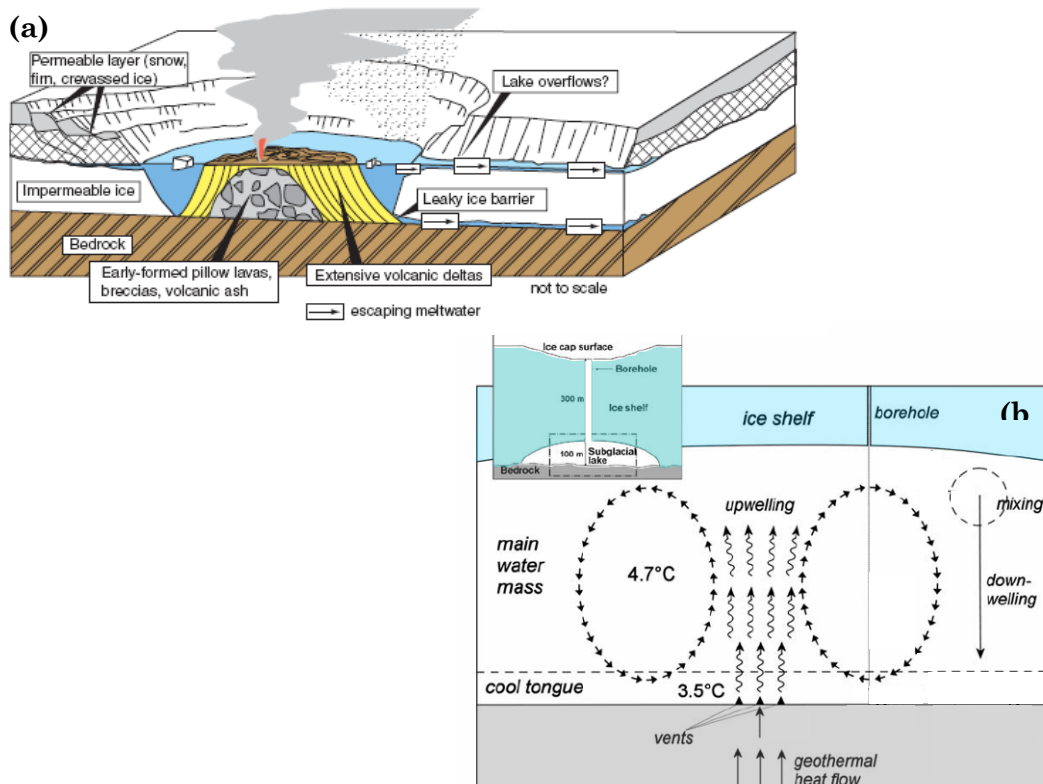
1.2.1 Subglacial volcanism on Earth

Subglacial volcanism results from the interaction between intrusive magma and an overlying glacier. On Earth it is a common feature of volcanically active high latitude terrains, but also sporadically at low latitudes coupled with high elevation. Examples of widespread volcano – ice interaction today include those found in Iceland (Bourgeois *et al.* 1998), British Columbia (Edwards *et al.* 2002), and Antarctica (Smellie & Skilling 1994). Geomorphological products indicative of basaltic subglacial volcanism include tuyas and moberg ridges. Tuyas form as a result of central vent eruptions into an overlying thick ice sheet (Bourgeois *et al.* 1998), whilst moberg ridges result from a series of fissure eruptions beneath the ice, forming long ridges following the strike of the rift. These eruptive features display a distinctive elevated topography in contrast to the surrounding terrain due to the restrictive role of the ice into which the lava was erupted, preventing the lateral flow of lava away from the eruptive centre. Subsequent retreat of ice reveals these distinctive volcanic landforms. The importance of subglacial volcanoes in astrobiology principally lies in the fact that subglacial eruptions on Earth often generate large volumes of meltwater that can be stored and transported beneath the overlying glacier (Wilson & Head 2002), and therefore may have provided a haven for life on Mars.

The birth of subglacial volcanic environments begins with the initial eruption of basaltic magma into an overlying glacier or ice cap. The eruption of this magma can be in the form of a sill, dyke or large voluminous intrusion. Quite often, the force of this eruption will fracture the ice before any melting has taken place (Wilson & Head 2002), but eventually about two thirds of the heat content of a subglacial lava flow will be used to melt the surrounding glacial ice (Head & Wilson 2007). After this initial intrusion of magma, conductive heat flow will

melt surrounding ice, whilst the low temperatures of the ice will begin solidifying the magma, eventually forming a solid, glassy crust as part of pillow lava formation. Convection plays a large role in the transfer of heat from the magma body to the overlying ice (Höskuldsson & Sparks 1997). As the magma flow diminishes, the growth of the lava edifice ceases but the overlying ice continues to melt due to the convective transfer of heat through the liquid water interface between the magma and the ice (Head & Wilson 2002). Additionally, subglacial hydrothermal systems in between eruptions may continually melt the base of the glacier, sustaining a subglacial caldera lake (Björnsson 2002). Over time, a subglacial edifice can grow within this subglacial lake during eruptions, consisting of pillow basalts, hyaloclastite beds and palagonite tuffs (Smellie & Skilling 1994). Figure 1.2 below summarises these environments. If the edifice becomes large enough to break through the ice, a cap rock of horizontal subaerial lava is deposited. Alternatively, if the eruption is smaller, perhaps the result of a fissure, entirely subglacial hyaloclastite ridges or pillow mounds will form. These edifices will then remain beneath the glacier until exposed and eroded.

Figure 1.2. Subglacial volcanic processes, products, and environments; a) cartoon of an emergent subglacial volcanic eruption that becomes subaqueous as the eruption progresses and meltwater is produced (from Smellie 2007); b) Subglacial volcanic meltwater environment at Skafá caldera (adapted from Johanesson *et al.* 2007) whereby geothermal heat from the dormant subglacial volcano maintains a subglacial lake.



1.2.2 Subglacial volcanism on Mars

It is generally observed that due to the existence of large quantities of water ice at the poles and within the global cryosphere, coupled with widespread active volcanism, interaction between the two is inevitable throughout the history of the planet. The likely processes of volcano – ice interactions on Mars have been described and discussed in depth by Head & Wilson (2002), and involve the emplacement of sills, dykes, lava flows and large magma bodies into cryospheric/permafrost like ground or into an existing ice cap, with the process thought to be much the same on Mars as that observed on Earth.

Whilst volcanism in itself is not necessarily conducive to life, sites of volcano – ice interaction are favourable for life on Mars for several reasons. Firstly, being located within the subsurface, localised environments are protected from the hostile surface conditions. Secondly, the interaction between geothermal heat flow and an overlying cryosphere or ice cap is highly conducive to the generation of hydrothermal systems. Squyres *et al.* (1987) have modelled the effect of lava intruding into ice-rich ground, and found that such subsurface heat can generate a significant source of liquid water. Similarly Wilson & Head (2007) have calculated that during a subglacial eruption on Earth the resulting melted ice thickness is 6-7 times that of the magma layer thickness. This liquid water can then cycle via convection through the emplaced lava pile, and into the overlying ice-rich ground or ice cap, provided that meltwater temperature exceeds 4°C (Höskuldsson & Sparks 1997). Such geothermally heated convection systems have been modelled by Travis *et al.* (2001). Volcanism/cryospheric interaction and subsequent meltwater generation has been proposed several times as an alternative explanation to the early ‘warm and wet’ Mars scenario thought to create the numerous channels and valleys apparently carved by liquid water (Fassett & Head 2007; Carr & Head 2003). As illustrated by Gulick (1998), much of the fluvial erosion on Mars is spatially and temporally related to volcanic activity, further demonstrating the potential importance of volcanic activity on Mars in the generation of liquid water available to life.

The proposed time-scale for the occurrence of subglacial volcanism on Mars ranges from the early Noachian, producing the extensive fluvial channels seen in the ancient cratered terrain (Carr & Head 2003), to as recent as <20 Ka (Hovius

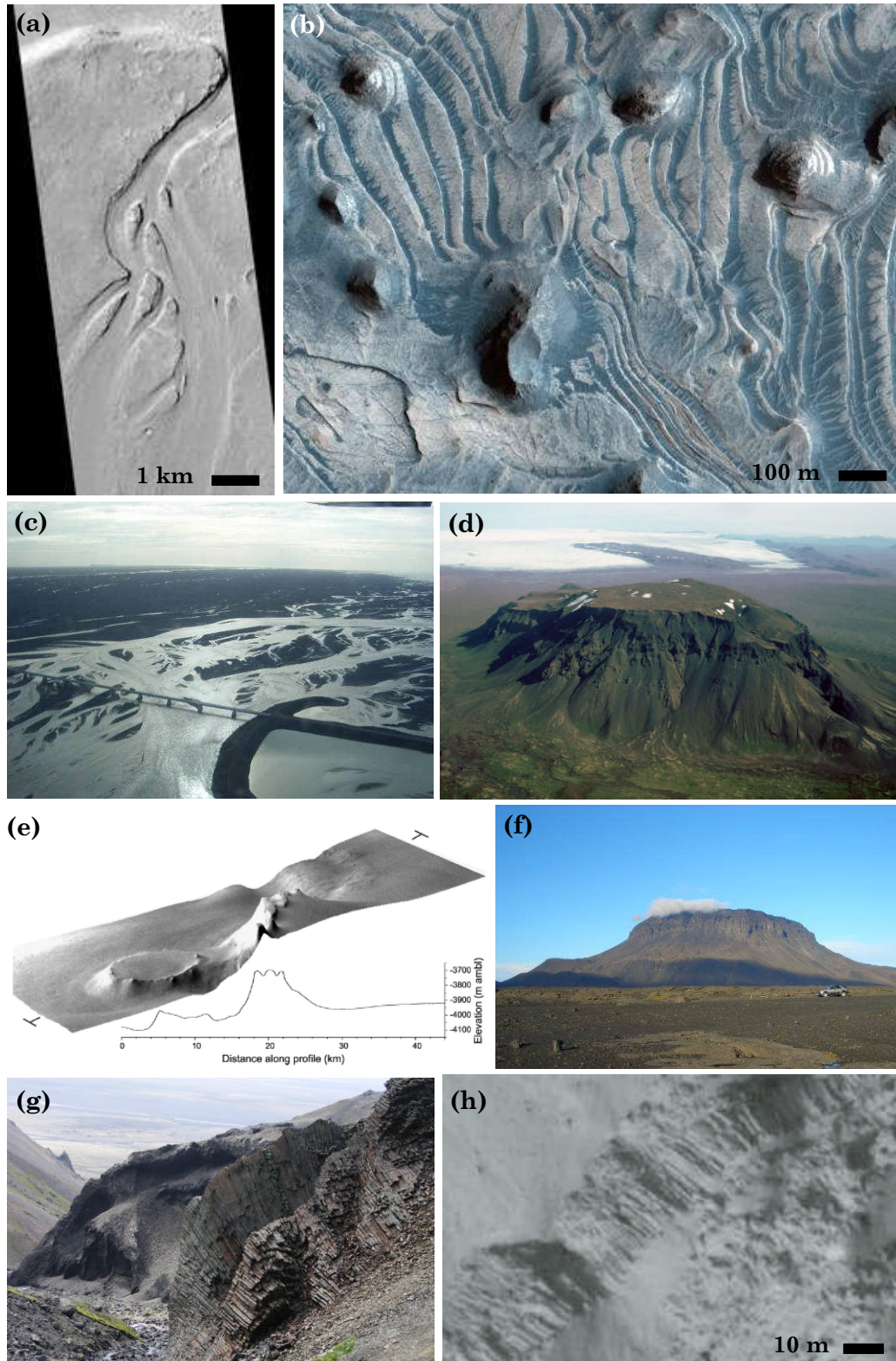
et al. 2008). Additionally to this are the numerous examples throughout the Hesperian terrains (e.g. Fassett & Head 2007; Ghatan & Head 2001). Magma-ice interaction on Mars is thought to be responsible for forming regional topographic features such as large-scale ground collapse and chaotic terrain, major outflow channels, mega-lahars, tuyas, and pseudocraters (Head & Wilson 2002). Examples of Martian terrains that are considered analogous to subglacial volcanic features on Earth are shown in Figure 1.3. Whilst it is impossible to determine the exact nature of an eruption purely by remote sensing observation, topographical features have been identified which bear striking similarities to magma – ice interactions on Earth. These include flat topped tuyas (Head & Wilson 2007; Ghatan & Head 2002), lava ridges (Ghatan *et al.* 2003) and related sedimentary deposits typical of glacial outburst floods caused by geothermally melted ice (Jökulhlaups). Allen (1979) identified many analogues of terrestrial subglacial volcanoes in both the northern plains and near the south polar cap of Mars. Since then, more candidate subglacial volcanoes and regions of volcano – ice interaction have been identified. Such features include tuyas and moberg ridges, both of which are commonly seen in Iceland. Many notable examples of volcano – ice interaction are located close to the South polar ice cap, within the Dorsa Argentea Formation. Here, certain features have been interpreted as subglacial volcanoes that potentially erupted into the Hesperian south polar ice cap (Ghatan & Head 2001). These features are based on their distinct morphological similarity to terrestrial subglacial eruptions, as well as the existence of basal meltwater drainage channels extending away from the volcanoes (Ghatan & Head 2001). Likewise, interior layered deposits (ILD) in the Vallis Marianas region on Mars, originally proposed to be the result of lacustrine/fluvial activity, show abundant evidence for a glaciovolcanic origin (Chapman & Smellie 2007).

More recently, subglacial volcanism has been used to describe larger features, notably those depicting a fluvial/flood outburst induced morphology. At Abalos Colles near the north polar ice cap, there is evidence of more recent subglacial volcanism, possibly within the last 20,000 years, as indicated by the presence of flat topped ridges and a large, water incised chasm (Hovius *et al.* 2008). The formation of the chasm in particular has been compared to Icelandic Jökulhlaups, with the described analogue for this area being the 1996 Gjalp

subglacial eruption (Hovius *et al.* 2008). Importantly, in terms of habitable environments, it is proposed that a ponding of meltwater would have occurred here prior to its catastrophic release (Hovius *et al.* 2008).

Lastly, high Martian obliquity has most likely led to extensive periodic growth of polar ice caps, increasing the geographical range where subglacial volcanic environments can develop. Kadish *et al.* (2008) document the evidence for tropical mountain glaciation around the Tharsis region, in the form of what has been interpreted to be terminal moraines, subglacially erupted dykes, sills and tuya morphologies. Additionally there are other equatorial features, including the Aromatum Chaos depression, interpreted as a site of cryospheric disruption caused by the intrusion of a volcanic sill and subsequent melting of the surrounding ice (Leask *et al.* 2006), and the catastrophic flood deposits in the Juventae Chasma region and associated outflow channel Maja Valles, which are inferred to be a result of sub-ice volcanism (Chapman *et al.* 2003). Likewise Squyres *et al.* (1987) have described Icelandic moberg-like morphology in the Aeolis Mensae region. Importantly, in terms of environmental habitability, this means that subglacial volcanic environments are not just restricted to high latitudes on Mars, increasing the geographical extent of possible habitats.

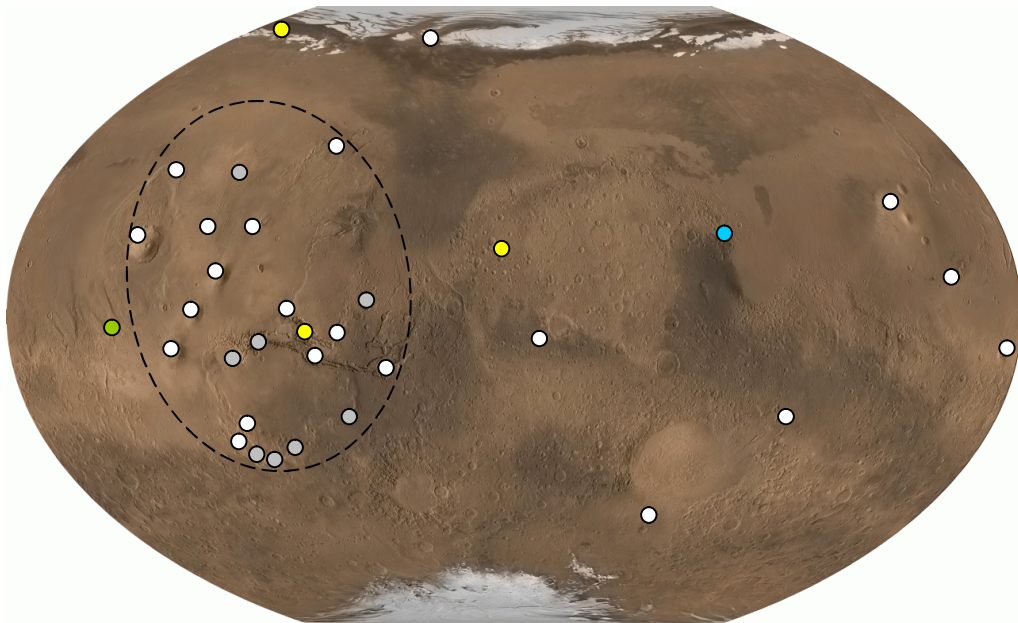
Figure 1.3. Putative glaciovolcanic features on Mars (a, b, e, h) and Icelandic examples (c, d, f, g); a) Fluvial channel at Cerberus Rupes (MOC, M2101914); b) Tuya-like terrain in Candor Chasma (HIRISE, PSP_003540_1735); c) Skeiðarársandur glacial outwash plain (road bridge for scale); d) Hlodufell basaltic tuya, ~5km long (Credit: Prof. John Smellie, 2006); e) Flat-topped volcano at Abalos Colles, (THEMIS, V10551038; Hovius *et al.* 2008); f) Herðubreið flat-topped volcano, ~5km long; g) Jointed lava flow (Credit: Dr. Dave McGarvie, 2006); h) Columnar jointing near Marte Vallis (HIRISE, PSP_005917_2020; Milazzo *et al.* 2009).



1.2.3 Hydrothermal environments on Earth and Mars

In addition to subglacial volcanism, regions of subaerial hydrothermal activity are also utilised as a Martian analogue. Hydrothermal environments exist through the interaction between geothermal heat and water, and are typified by steep redox gradients, chemical and physical weathering of bedrock, and the deposition of mineral deposits (Pirajno & Van Kranendonk 2005). Such processes are controlled largely by the nature of the bedrock (e.g. composition, permeability), temperature gradients, and availability of water. As such, these are highly dynamic systems that are exploited by a variety of chemosynthetic and photosynthetic life, and are a strong contender for the location of early evolution of life on Earth (Martin *et al.* 2008; Nisbet & Sleep 2001). This, coupled with the characteristic mineral deposits that are often preserved in the rock record, means hydrothermal systems are primary targets for astrobiological exploration of Mars. Geomorphological evidence for hydrothermal activity on Mars is typically associated with volcanism (Gulick 1998). Mineral deposits such as opaline silica (Rice *et al.* 2010), magnesite (Ehlmann *et al.* 2008a) and sulphates (Gendrin *et al.* 2005) strengthen the case for the existence of hydrothermal systems. Recently, Schulze-Makuch *et al.* (2007) reviewed potential endogenic (tectono-magmatic) hydrothermal activity and its distribution on Mars (Figure 1.4).

Figure 1.4. MOLA- and MOC map of Mars showing sites of putative endogenic hydrothermal activity (adapted from Schulze-Makuch *et al.* 2007). White = dominantly magmatic; grey = dominantly tectonic; yellow = sulphate deposition; blue = phyllosilicate deposition; green = chloride rich. Dashed line incorporates Tharsis-related activity. (Image Credit: National Geographic Society, MOLA Science Team, MSS, JPL, NASA).



This hydrothermal activity is typically associated with magmatic heating of subsurface ground ice and/or snow, and the plume-driven Tharsis region is thought to be of particular significance regarding long-lived hydrothermal activity associated with both tectonic rifting and magmatic episodes (Schulze-Makuch *et al.* 2007). This broad area is highlighted on the map in Figure 1.4.

1.3 High Latitude Martian Analogue Localities

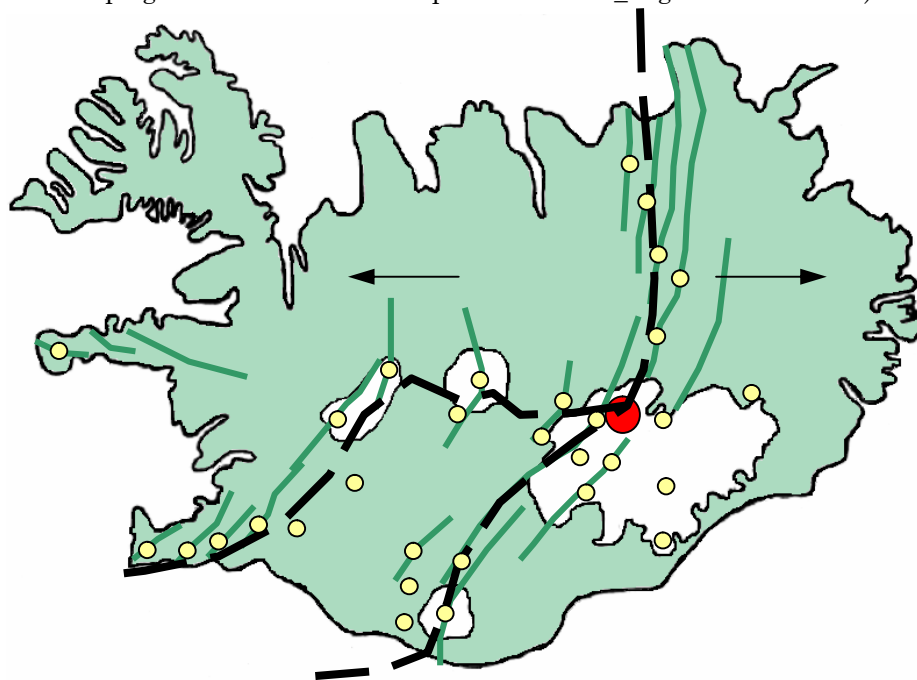
For this research, environments and their associated deposits were explored from three high latitude localities: Iceland (65°N), Svalbard (79°N), and James Ross Island, Antarctica (65°S). These three localities were chosen due to their high similarity to Mars, either in terms of present day environment, geology, or both. Samples for biological and geological laboratory analysis came predominantly from Iceland, whilst in-situ field testing and analysis was conducted in Svalbard during the joint NASA/ESA funded Arctic Mars Analogue Svalbard Expedition (AMASE). Samples from James Ross Island were kindly loaned by Prof. John Smellie from the British Antarctic Survey. High latitude environments are particularly advantageous for Martian analogue research due to their often extensive geological outcrops, lack of vegetation, lack of anthropogenic disturbance, and their present day exposure to cold, often sub-zero temperatures and lack of precipitation. Details of these three principle locations are described briefly below. Specific sites and samples are detailed further in Chapter 2.

1.3.1 Iceland

The island of Iceland is entirely volcanic, formed by the surface expression of the Mid Atlantic Ridge and an underlying mantle plume - the Icelandic Hot spot (Korenga 2004; Sigvaldason *et al.* 1974). It formed as a result of the rifting episode that led to the opening of the North Atlantic ~ 60 Ma, with the oldest rocks in Iceland dating to ~15 Ma (Sigmundsson & Sæmundsson 2008). The presence of such high levels of volcanism coupled with the high latitude of Iceland (64 – 66°N) mean many of Iceland's active volcanoes are overlain by glaciers. There are numerous examples of past (mostly Pleistocene) and current subglacial volcanic activity dominating the surroundings, now surrounded by later Holocene subaerial lava flows. Figure 1.5 shows the position of the main volcanic systems – note the correlation with the position of the glaciers.

Geologically, Iceland bears many similarities to proposed Martian volcanism. It is dominated by basaltic volcanism that is a result of fissure eruptions and mantle plume activity (Wilson 2009). Many volcanic features identified on Mars are also seen in Iceland, notably widespread basaltic flows (Keszthelyi *et al.* 2004) and shield volcanoes. The terrestrial analogues of some features on Mars, such as pseudocraters (rootless cones), are found predominantly in Iceland (Fagents & Thordarson 2007), and comparisons have been made between Martian and Icelandic glaciovolcanism (Chapman & Smellie 2007). Due to the cold climate of Iceland, weathering is slow, particularly in the interior and NE of Iceland where rainfall is lower, as little as $< 400\text{mm/yr}$ (Einarsson 1984). Therefore, Iceland is considered here as an ideal analogue for volcanic environments that have existed on Mars in the past.

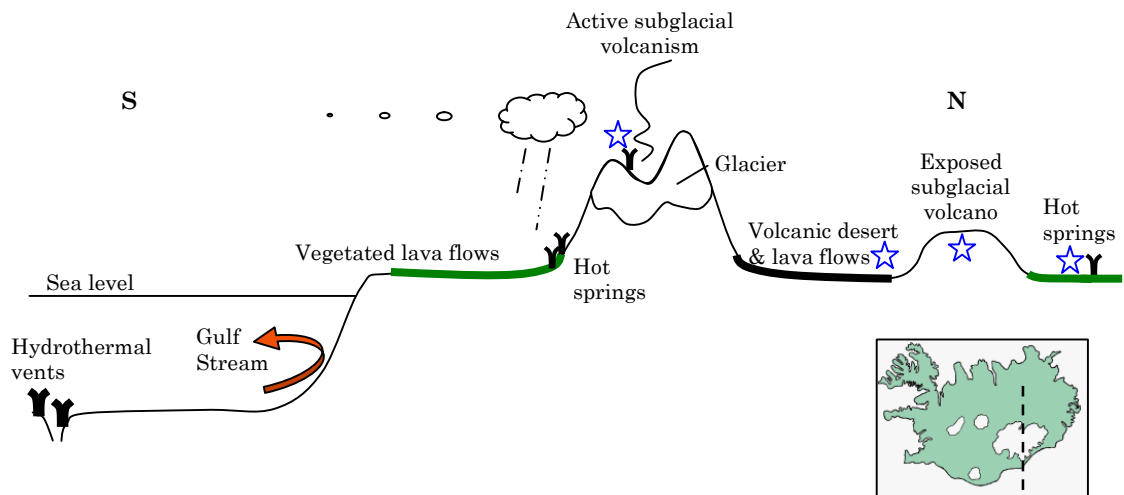
Figure 1.5. Map of Iceland showing the location of central volcanoes (yellow) and fissure systems (green) which together lie in the Icelandic Rift Zone (dashed line). The current location of the Icelandic hot spot is indicated by the red circle. Arrows show direction of plate movement. (Adapted from http://gullhver.os.is/website/hpf/orkustofnun_english/viewer.htm).



A simplified cross section through volcanic environments in Iceland is shown in Figure 1.6. Environments that were sampled in Iceland for this study fall broadly into one of two categories, and more details on specific localities and samples are given in the following chapter (Chapter 2, section 2.2.2). Samples

were either from subglacial volcanic environments, including both active subglacial volcanic hydrothermal systems, and older, now exposed subglacial volcanic lavas, or from subaerial hydrothermal environments, including hot spring mineral deposits and basaltic subaerial lavas that have been extensively altered by recent hydrothermal activity.

Figure 1.6. A simplified cross section through east - central Iceland (approximate transect shown inset) highlighting different volcanic environments (adapted from Herrera & Cockell 2007). Blue stars represent the subglacial volcanic and hot spring environments from this region of Iceland that are used for the work in this PhD.

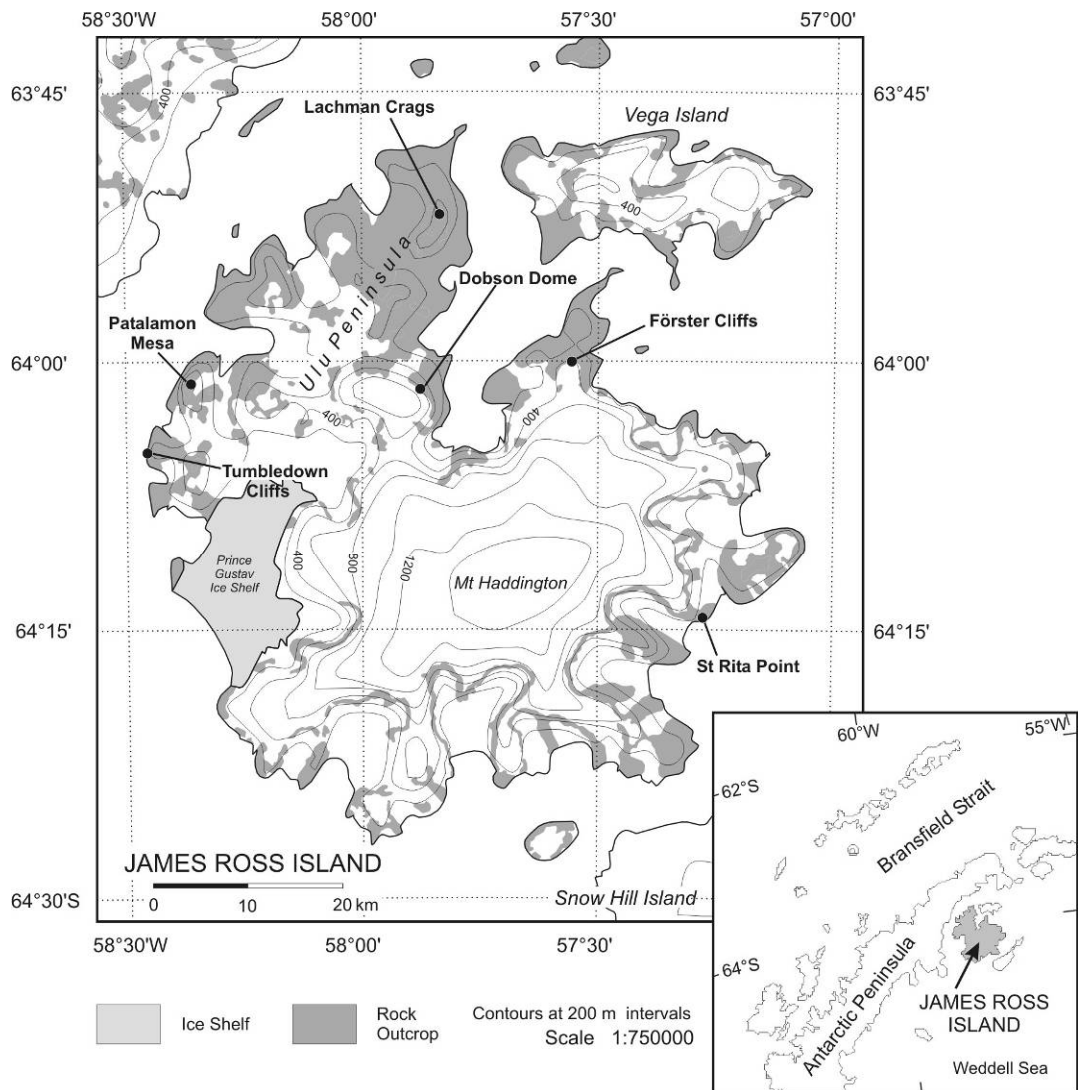


1.3.2 Antarctica

Antarctic environments experience some of the harshest conditions on Earth, with continually cold polar temperatures, desiccating winds and seasonal darkness. Extensive ice sheets exist here, and as such a significant amount of basaltic volcanism during the Pleistocene has been subglacial (Smellie *et al.* 2008). James Ross Island, which lies just off the coast of the Antarctic peninsular (Figure 1.7), consists of such subglacial volcanic sequences, named the James Ross Island Volcanic Group (JRIVG) – a large Neogene alkaline basaltic volcanic province that crops out extensively (Smellie 1999; Nelson 1975). The island is a polygenetic stratovolcano 40–60 km in basal diameter rising to about 1600m. The island was surrounded by at least seasonally ice-free conditions during multiple interglacial periods, when seawater was apparently able to percolate into the lava-fed deltas (Johnson & Smellie 2007). The sequences are also well dated by the $^{40}\text{Ar}/^{39}\text{Ar}$ method (Smellie *et al.* 2008; 2006). Most of the >50

eruptions documented were subglacial, producing multiple, voluminous and geographically extensive lava-fed delta sequences, each composed of subaqueous hyaloclastite foreset units and subaerial capping lavas (Smellie 2006; Skilling 2002). Samples of these hyaloclastite lavas were kindly provided by Prof. John Smellie for the analysis of biosignatures in Antarctic subglacially-erupted basaltic lavas (Chapter 4).

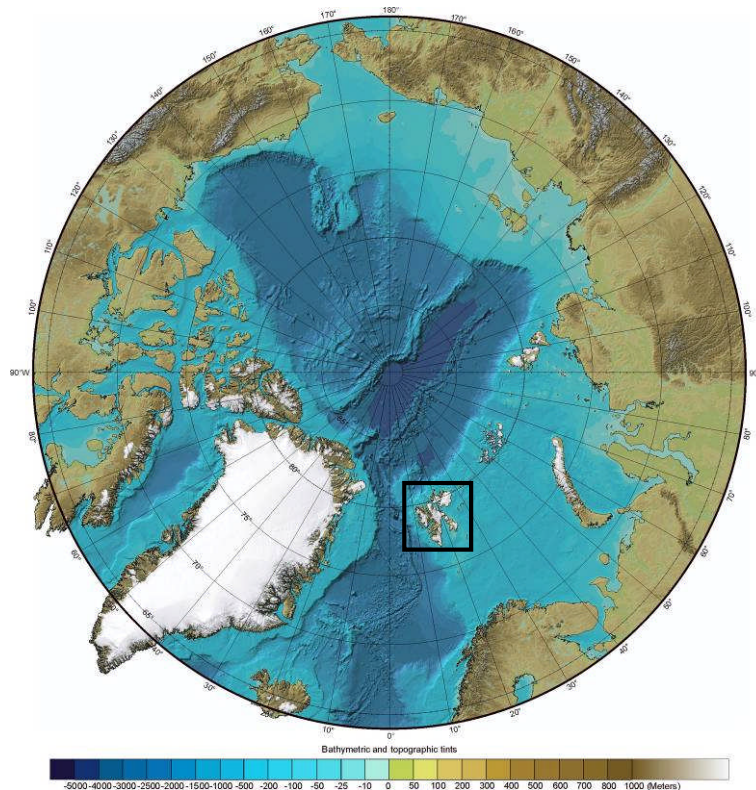
Figure 1.7. Map of James Ross Island, northern Antarctic Peninsula (inset), showing the locations of the six hyaloclastite deltas selected for study (Johnson & Smellie 2007).



1.3.3 Svalbard

The archipelago of Svalbard ($\sim 77 - 81^\circ\text{N}$) lies roughly equidistant from the North Pole and the northernmost coast of Norway (Figure 1.8), and is the most polar of the Martian analogue environments studied for this PhD. Unlike Iceland, which is largely volcanic, the islands that make up Svalbard contain a diverse and complex geological stratigraphy, with representative strata and lithologies from nearly every geological period, and from a variety of depositional environments. However, basaltic volcanism has more recently also played a significant role here, some of which, like Iceland, has been subglacial in nature (Skjelkvale *et al.* 1989).

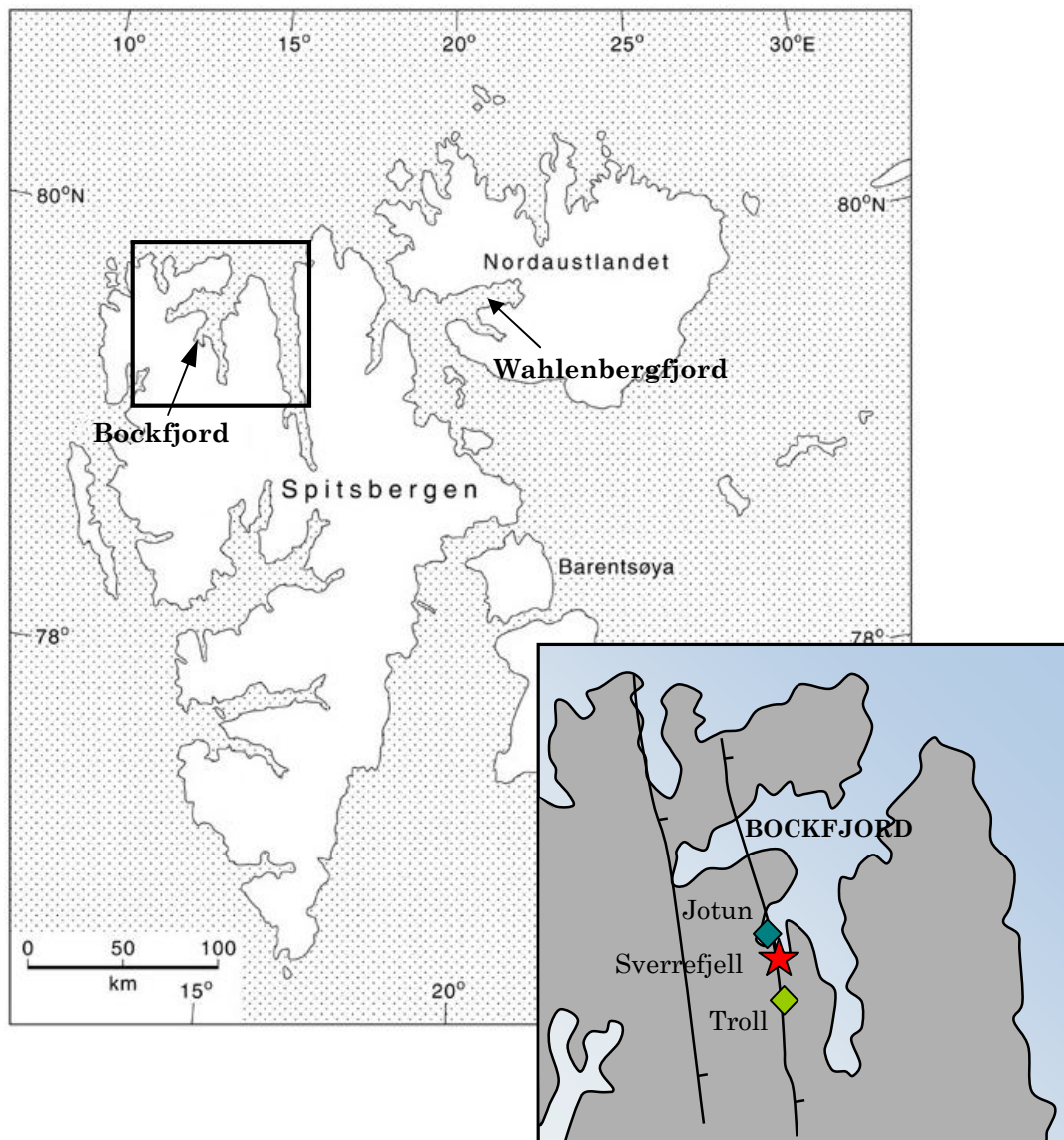
Figure 1.8. Physical map (polar projection) showing the location of the Svalbard Archipelago which lies just south of the polar circle at 80°N (Credit: NOAA). Iceland can also be seen at the edge of the bottom western corner of the map.



Svalbard was used solely for in situ field testing of the PanCam instrument (Chapter 7), and this field work was possible through the Arctic Mars Analogue Svalbard Expedition (AMASE) run by Hans Amundsen (Earth and Planetary Exploration Services, Expedition Lead) and Andrew Steele (Carnegie Institute, Science Lead). Localities within Svalbard were selected principally by the AMASE organisers, whilst PanCam testing was carried out in collaboration with

Nicole Schmidt (Deutsches Zentrum für Luft- und Raumfahrt), Arnold Bauer (Joanneum Research), and Francis Westall (Centre national de la recherche scientifique). The specific localities for field testing were the Bockfjord Volcanic Complex, and Wahlenbergfjorden. The sites visited within the Bockfjord Volcanic Complex include Sverrefjell volcano, Jotun Springs, and Troll Springs (Figure 1.9). As for Iceland, details on these specific localities are given in the following chapter.

Figure 1.9. Map of the Svalbard archipelago showing the localities of the in situ field tests carried out with the PanCam instrument. Three separate sites in Bockfjord were visited: Sverrefjell volcano, Jotun Springs, and Troll Springs. These are shown on the map inset (Diamonds = Spring sites; Star = volcano), and all lie along a major fault line (tick on downthrow side). Inset map adapted from Banks *et al.* (1999).



1.4 Geomicrobiology

Geomicrobiology encompasses research at the interface of the geosphere and biosphere, where microbial metabolism and cell surface interactions are intimately related to the rocks and minerals in their environment (Konhauser 2007). This thesis is focused on the prokaryotic inhabitants of volcanic environments and the potential biosignatures this life may produce that can be preserved in the volcanic rock record for future detection.

1.4.1 Assessment and identification of microbial communities

The prevalence of microbial communities in terrestrial environments has only come to light during the last few decades (Wintzingerode *et al.* 1997). The development of molecular-based assessments of communities has shown there to be an enormous and still largely unexplored microbial biosphere present on Earth (Pace 1997). Microbial communities have been shown to inhabit almost every conceivable environmental niche, utilising a wide array of metabolic pathways and survival strategies. These communities are typically explored using two principle methods: culture-based and culture-independent techniques.

It is well known that there is a large inconsistency between studies of microbial diversity based on culture-based and culture-independent techniques, and it has been estimated that only ~1% of microorganisms observable in nature can be isolated using standard techniques (Tringe & Rubin 2005; Kirk *et al.* 2004; Torsvik *et al.*, 1990). As a result, ecology studies based entirely on culture-based techniques lead to biased data, producing a highly incomplete picture of the microbial community in question (Amann *et al.* 1995). However, due to molecular phylogenetic techniques now widely available, ecological studies through cultivation have become superseded by recombinant DNA-based approaches. That is not to say they have become redundant – isolated microbes provide a wealth of information regarding morphology, metabolism, and ecological function (Joseph *et al.* 2003) but for the purpose of establishing microbial diversity within an environment, molecular phylogenetic analysis is typically the favoured approach, and ideally a combination of biomolecular and culture-based techniques should be employed. One of the most successful and widely used methods for establishing bacterial and archaeal diversity in any given environment is the comparable sequence analysis of the 16S rRNA gene (or the

18S gene for Eukaryotic genomics) – a small subunit of ribosomal DNA that contains both highly conserved sequence regions and also highly variable regions, and crucially is present within all living organisms. This combination makes it ideal for assessing microbial diversity based solely upon genetic data. The value of such information lies in the ability to objectively assess and quantify the identification of microorganisms at a variety of taxonomic levels (typically down to genus level), and also to determine how related microorganisms are within a specific environment and the broader biosphere.

Whilst the use of 16S rDNA allows a culture-independent assessment of microbial communities, it relies heavily on the successful and unbiased extraction of genomic DNA from the environment in question. This however is no trivial task, and at every stage of the DNA extraction process there is the opportunity to lose DNA, from the initial collection of the sample, to sample processing, and during the chemical extraction process itself. In addition, DNA extraction is often particularly difficult from ‘extreme’ environment samples. Several pitfalls specific to volcanic environments have been identified by Herrera & Cockell (2007). These, together with others, are summarised in Table 1.2, and demonstrate the need for careful consideration when planning a 16S rDNA study. Problems associated with specific techniques in 16S rDNA analysis are detailed in Chapter 2, section 2.4).

Table 1.2 DNA extraction pitfalls from volcanic environments (Herrera & Cockell 2007; Henneberger *et al.* 2006; Burlage *et al.* 1998).

| | Properties hindering DNA extraction | | Potential solution |
|-------------------------------|--|--|---|
| | Property | Problem | |
| Basaltic Lava | Low biomass | Unworkable levels of DNA extracted | Increase sample quantity, multiple sample extractions |
| | | Significant contamination obscures genuine diversity | Limit number of sample processing stages, carefully controlled sampling and processing |
| | Solid matrix | Microorganisms attached to, or deep inside rock matrix | Homogenisation and/or sonication of the sample to release cells |
| Hot spring soil/ fluid | Acidic pH <4 | Protonisation of purine and pyrimidine bases, increased adsorption of DNA to clay particles (see below). | Buffer sample immediately after collection (ideally >pH 6), prevention of cell lysis (e.g. by not freezing after collection). |
| | Clay content | Adsorption of DNA to smectite clay particles | Addition of skim milk powder to extraction solution |
| | High Fe and/or Al oxide | Adsorption of phosphate in the sugar-phosphate backbone of nucleic acids | Addition of phosphates to the extraction solution to compete with DNA phosphate. |

1.4.2 Microcosms and environmental simulations

Microcosms aim to recreate the natural environmental conditions and biogeochemical cycles within a small, confined, observable system. Microcosms can be purposefully biased towards certain metabolic and functional groups, for example by controlling the pH, temperature, light availability and nutrient flux. They are different to culture-based techniques which aim to eventually isolate the culturable portion of the microbial community, either through direct plating or through enrichment (e.g. Winogradsky columns). Controlled microcosms can reveal information regarding the ecological roles of different microorganisms, and their interaction with the environment they inhabit, such as changes in geochemical gradients and environment composition. Of particular interest to astrobiology research is the simulation of environments under Martian conditions. Testing proxy Martian conditions and environments is a key process to better understanding the potential of habitable environments on Mars in the past and the present day. Such Martian microcosms have demonstrated the potential for terrestrial microorganisms and communities to survive near the Martian surface, although many have shown full exposure to present day Martian conditions is rapidly detrimental to the viability of terrestrial life.

The majority of previous studies on the survivability of microorganisms under controlled Martian conditions have focused on pure strains of microorganisms. One of the first was carried out in the early 1960's. In that work, Hawrylewicz *et al.* (1962) tested the survivability and virulence of pathogenic microorganisms under vacuum and alternating temperature, and demonstrated that spores and certain anaerobic organisms can survive under these conditions for a few months. More recently, Diaz and Schulze-Makuch (2006) devised a method of establishing the viability of *Escherichia coli* and *Deinococcus radiodurans* after exposure to low temperature, low pressure and UV irradiation, whilst suspended in a variety of saltwater and freshwater Martian analogue soils and liquids of varying depths. The number of bacterial colonies that grew afterwards was used to calculate the viability of the different soils and liquids. Unsurprisingly *D. Radiodurans* fared much better to Martian conditions than *E. Coli*, but the survivability rates of both bacteria were greatly increased when protected inside a microhabitat 5cm below the surface or inside liquid water. However, the pressure conditions used in these experiments (83.3 kPa) did not match the low

pressure conditions on Mars (~0.6 mbar) and the authors predict that under such conditions the bacteria would have to be significantly deeper into the subsurface to survive. Morozova *et al.* (2007) exposed methanogenic Archaea to simulated Martian thermal conditions to establish their survivability (based on cell counts and methane production). They tested methanogens isolated from Siberian permafrost and reference methanogens isolated from non-permafrost habitats, and found a remarkable survivability rate for those isolated from Siberian permafrost. In contrast, the Martian thermal conditions killed ~99% of the reference methanogens. These results demonstrate the importance of using microorganisms from Martian analogue environments for survivability tests and, as before, suggested greater survivability of microorganisms on Mars below the surface. Microorganisms isolated from Siberian permafrost have been used in other survival tests since, and appear to be suitable model organisms for such experiments.

A recent paper by Smith *et al.* (2009) utilised *Psychrobacter cryohalolentis*, isolated from a subsurface hypersaline cryopeg in Siberian permafrost. These authors demonstrated that although psychrophilic microorganisms have been considered to be a major problem regarding planetary contamination, they showed no tolerance to the Martian environment, even during simulated 'dust storm' scenarios, and identified UV radiation and desiccation to be the primary lethal factors. However, they noted that if suitable UV shielding was provided, the chance of survivability would be greater, even more so if the desiccation factor could be overcome. This has been demonstrated by a previous experiment on the UV resistance of Antarctic cyanobacteria, that showed if under just 1mm of rock, cyanobacteria survived for at least 1 day under high Martian UV flux, and suggests organisms could survive within lithic habitats on Mars providing there were sufficient water and nutrient supplies (Cockell *et al.* 2005).

As well as these monoculture studies, there have also been experimental studies using complex and diverse soil communities. In the spirit of planetary protection, Foster *et al.* (1978) used soil samples collected from Cape Canaveral and found reduced atmospheric pressure had a significant effect in reducing growth of microbial populations, as determined by colony forming unit (CFU) counts, and that psychrotolerant microbes showed the greatest resistance. Likewise, Green *et*

al. (1971) showed psychrophilic and spore forming microbes could survive if within a subsurface environment. Far more recently, studies by Hansen *et al.* (2009; 2005) presented one of the first studies on whole natural soil communities to test for survivability, again advocating the use of Siberian permafrost communities. In particular, their most recent study (Hansen *et al.* 2009) highlights the advantage of using whole communities to identify those species that do and don't survive the environmental simulation.

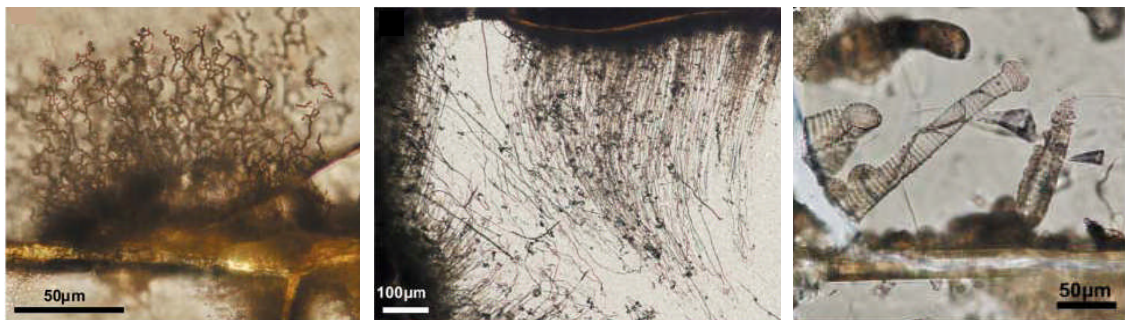
1.4.3 Biosignatures

A biosignature is a physical or chemical change to an environment, which is a direct consequence of biological activity within that environment. Biosignatures can be of any scale, ranging from atomic (such as isotope fractionation) to global (such as the presence of oxygen in Earth's atmosphere). Due to the diversity and ubiquitous nature of life on Earth, knowledge of biosignatures can be built up based on observable cause and consequence. This knowledge can then be extrapolated for searching for life on other planets. Biosignatures can be the remains of the microorganism itself, identified perhaps by the presence of organic carbon (such as kerogen), specific organic molecules (such as lipids), or unique spectroscopic signatures (e.g. those caused by photosynthetic pigments), or they can be the by-product of the microorganism's existence, such as trace and morphological fossils, and localised chemical changes in an environment (e.g. isotope fractionation). Biosignatures have been recognised as a powerful tool in the study of planetary biospheres and have since been characterised in terms of their reliability, or 'biogenicity'. Most importantly, it is essential to understand and recognise such biosignatures if they are to be used as positive evidence for the presence of life elsewhere.

Whilst the potential range of biosignatures within Martian analogue environments is enormous, one of these is particularly relevant to basaltic volcanic environments. This is the formation of so-called 'bioalteration textures' within basaltic volcanic glass, thought to be the direct result of microbial colonisation and reworking of these lavas, often down to depths of 500m into the basaltic oceanic crust (Furnes and Staudigel 1999). This colonisation produces distinctive tubules, etching and pitting along hydrous alteration fronts in the volcanic glass, easily identifiable in thin section. The first description of this

alteration was described by Ross and Fisher (1986), and since then, similar characteristic textures have been found in oceanic basalts at numerous locations, including the East Pacific Rise, Mid Atlantic Ridge, Juan de Fuca ridge and Ontong Java plateau (Fisk *et al.* 1998; Fisk *et al.* 2003; Furnes *et al.* 1996; Furnes *et al.* 2007; 2002; 2001; Thorseth *et al.* 1995; 1992; 2001a; 2003; Torsvik *et al.* 1998; McLoughlin *et al.* 2007; 2009). In these studies, biotic and abiotic alteration fronts were shown to be distinguishable. Abiotic alteration consists of palagonitization induced by hydrous alteration, and forms smooth alteration fronts of yellow palagonite that are continuous along, and parallel to, glass boundaries. By contrast, biologically mediated dissolution of glass is characterised by complex, irregularly distributed features (Figure 1.10).

Figure 1.10. Examples of bioalteration texture morphologies in basaltic volcanic glass (McLoughlin *et al.* 2009)



In previous studies, the biotic textures have been divided into ‘granular’ and ‘tubular’ types (Furnes *et al.* 2007). Granular textures consist of micron-sized coalesced spherical bodies that form irregularly distributed alteration fronts along glass boundaries and fractures. They are generally the most abundant type of bioalteration seen in oceanic basaltic lavas (Furnes and Staudigel 1999). Tubular textures are less common, and form long hair-like or tufted tubules protruding from fractures or other boundaries (e.g. vesicles) in the glass. Like the granular texture, the tubules are irregularly distributed, but consist of long narrow tubes with constant width. The tubes often display branching patterns, segmentation and irregular swellings (Furnes *et al.* 2007). Similar textures have also been identified in ancient oceanic crust sequences spanning the Phanerozoic, Proterozoic, and Archean (Furnes *et al.* 2007; 2005; 2004; 2002b; 2001b). More recently, these advances in the identification and description of bioalteration textures in seafloor lavas has led to the development of a systematic taxonomic

nomenclature to allow unambiguous comparisons between bioalteration textures found in spatially and temporally different lavas (McLoughlin *et al.* 2009). This taxonomic system is intended for the identification of trace fossils within volcanic glass, specifically in oceanic crust lavas, ophiolites, and greenstone belts only. However, this limitation largely reflects the current bias of bioalteration studies towards marine environments, and so it is assumed here that such a taxonomic system may be used to characterise identical bioalteration trace fossils that occur in volcanic glass from non-marine environments (i.e. subglacially-erupted lavas). McLoughlin *et al.* (2009) have identified five ichnospecies that occur in volcanic glasses. These species are split across two ichnogenera: *Granulohyalichnus* (granular bioalteration), and *Tubulohyalichnus* (tubular bioalteration) and represent the different bioalteration morphologies identified to date. *Granulohyalichnus vulgaris* is used to identify pitted granular textures widely seen along glass – palagonite alteration boundaries, and is the only ichnospecies in the *Granulohyalichnus* genera. Within the *Tubulohyalichnus* genera, ichnospecies have been assigned to identify simple tubular morphologies (*Tubulohyalichnus simplus*), branched behaviour (*Tubulohyalichnus stipes*), ornamented/segmented morphologies (*Tubulohyalichnus annularis*) and spiral/helicoidal bioalteration features (*Tubulohyalichnus spiralis*).

Bioalteration is potentially a good morphological biosignature for Mars exploration, either through analysis of meteorite samples or future Mars sample return missions. Firstly, despite the ubiquity of aqueous alteration in basalt, there is, so far, no known abiotic mechanism that can reproduce these textures (Fisk *et al.* 2006; Walton 2008). Secondly, the textures are distinctive in themselves (e.g. segmentation, invariant tubule widths, and tubule bifurcation) and indicative of biological activity through geochemical biosignatures, in particular negative $\delta^{13}\text{C}$ signatures (Izawa *et al.* 2009; McLoughlin *et al.* 2007; Staudigel *et al.* 2006). Thirdly, the identification of DNA lining the inner surfaces of microborings in fresh lavas provides perhaps the most convincing support for a biological origin (Furnes *et al.* 2001a; Torsvik *et al.* 1998; Giovanoni *et al.* 1996). Biogenicity criteria such as these, and others, are given in Table 1.3. Lastly, the fact that these biosignatures have been found in Archaean rocks on Earth (Furnes *et al.* 2004), demonstrates that they can survive the dynamic tectonic environment on Earth for periods of billions of years. This holds promise

for their survivability on Mars. The presence of basaltic volcanism on Mars, coupled with the evidence for aqueous alteration, is permissive for such biosignatures to form there (Izawa *et al.* 2009). Phyllosilicates, the major constituent of palagonite, have also been identified on Mars by the OMEGA instrument (Poulet *et al.* 2005). These are indicative of aqueous alteration of basalt, and there is possibly a high potential for endolithic microorganisms to alter subaqueous basalt in an early wet Martian environment (Banerjee *et al.* 2004a,b; 2006; Fisk and Giovannoni 1999a,b). Recent studies have hinted that this may be the case with the discovery of alteration textures in Martian meteorites that, in some cases, bear a striking similarity to microborings in seafloor lavas (Fisk *et al.* 2006).

Table 1.3. Biogenicity criteria for endolithic microborings from McLoughlin *et al.* 2007)

| Category | Description | Example |
|----------|---|--|
| 1 | A geological context that demonstrates the syngenicity and antiquity of the putative biological remains | a) Microtubes radiate from early re-healed fractures, but are cross cut by and pre-date late stage fractures and mineral growth. b) Endoliths colonise fluid inclusion trails |
| 2 | Evidence of biogenic morphology and behaviour | a) Fracture with granular alteration front of spheroidal microborings. b) Ambient inclusion trails. c) Etch pits d) Microtubes with simple branching. |
| 3 | Geochemical evidence for biological processing | a) Microtubes filled with 'biogenic' clays or with C, N, S or P deposits. b) Carbon isotope fractionation c) Ca, Fe, Mg or Na depletions in the matrix surrounding tubules |

1.5 Detection of Astrobiological Targets on Mars

Whilst exploring extremophilic communities and their biosignatures in Martian analogue environments on Earth is fundamental to the search for life on Mars, such work can only be put to practical use if relevant rock targets can actually be identified using Mars rovers and their on board instrumentation. As such, this Martian analogue research must be put into context regarding the current technological and financial capabilities of upcoming astrobiology missions. As it stands, the exploration of the Martian surface is still entirely restricted to robotic exploration. However, future plans for Mars sample return missions, and even more ambitious manned missions, will enable us to analyse Martian rocks using

sophisticated instrumentation and techniques, as is currently done using the limited number of Mars samples available through meteoritic in-fall. However, until such exploration becomes feasible, the search for Martian life will, for at least the next decade (Mars Science Laboratory in 2013, ExoMars in 2018), be entirely reliant on robotic exploration. As such, part of this PhD research investigates optimising the rover's ability to conduct astrobiological research, focusing on the detection of geological targets that will be of relevance to the ExoMars mission specifically.

1.5.1 Rover instrumentation for Mars

Rover-based instrumentation currently remains the most technologically suitable method for the in-situ exploration of planetary bodies within our Solar System, and for Mars specifically has so far been the only source of in-situ data acquisition. Instrumentation onboard rovers needs to be selected and designed to fulfil the mission aims and objectives, and a broad multi-instrument approach is typically undertaken with which to analyse a particular sample or in-situ surface outcrop. Such instruments from past missions that are specific to geological/astrobiological investigation are summarised in Table 1.4. These instruments are designed to complement each other, and are predominantly focused on identifying mineralogical and chemical species present, and performing micro – macro imaging to identify lithofacies and potential biogenic textures. It is noted that the stereoscopic camera (highlighted in grey, Table 1.4) has been, and still is, an integral part of all missions, providing the initial view of the surrounding terrain and local geology for both navigational and scientific objectives. This initial data set is then followed by detailed analysis and investigation of particular outcrops. Live biological experiments have not been part of lander instrumentation since the Viking experiments. Instead, the detailed evaluation of the geology of the terrain is used to reveal the presence of past or present habitable environments, within which to identify biosignatures.

Table 1.4. Overview of past and future planned rover/lander instrumentation specific to geological and astrobiological analysis. (NB: Mission-specific instrument names/acronyms have been omitted for simplicity).

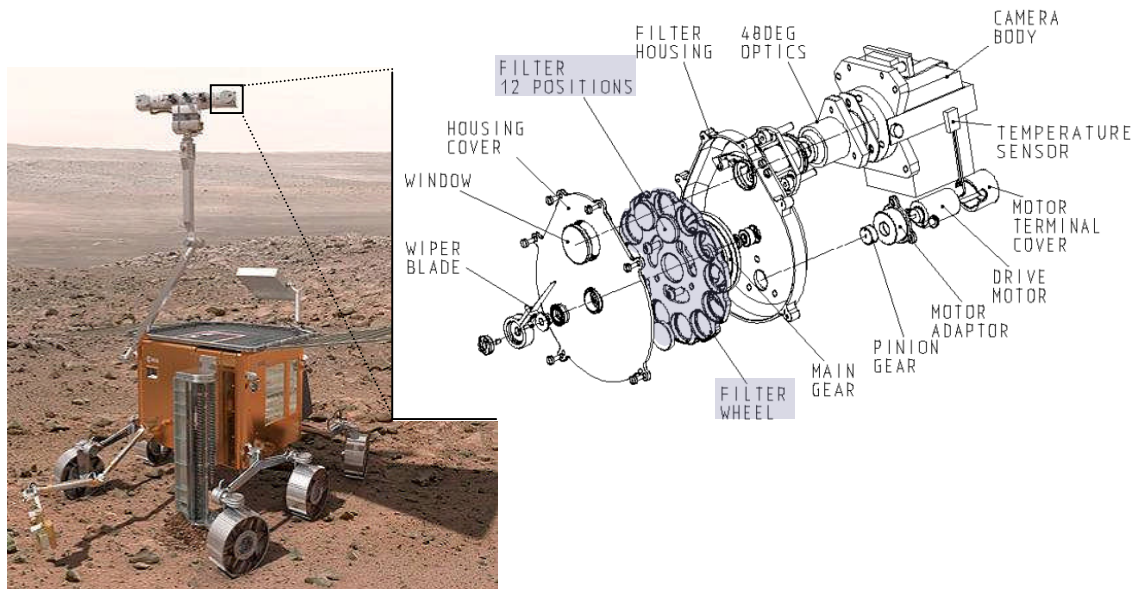
| Instrument | Objective | Mission |
|--|--|--|
| Three biological experiments utilising carbon assimilation, radiorespirometry and gas chromatography | Detection of photosynthetic life, organic compounds, respiration, gas release from biological activity | Viking |
| Alpha Proton X-Ray Spectrometer | Elemental chemistry of rocks and soils | Mars Pathfinder Beagle2 MER Mars Science Laboratory (MSL) |
| Mass Spectrometer | Gas analysis and isotopic analysis of rocks and soils and detection of organics | Viking Beagle2 Phoenix ExoMars |
| Stereoscopic camera + multispectral filter wheels | Visual analysis of surrounding terrain, multispectral analysis of rocks and soils | Viking Mars Pathfinder MER Beagle2 Phoenix ExoMars MSL |
| Mössbauer Spectrometer | Study of iron-bearing minerals | Beagle2 MER ExoMars |
| Miniature Thermal Emission Spectrometer / Infrared- Mapper | Mineralogy of rocks and soils | MER ExoMars* |
| Optical microscope | Small-scale features of rocks and soils | MER ExoMars* Phoenix MSL |
| Raman Spectrometer | Mineralogy of rocks and soils | ExoMars |
| Laser Induced Breakdown Spectrometer (LIBS) | Elemental chemistry of rocks and soils | ExoMars* MSL |
| X-ray Diffractometer | Mineralogy and elemental chemistry of rocks and soils | ExoMars MSL |
| Life Marker Chip | Antibody micro-array to directly detect life | ExoMars* |
| Wet Chemistry Lab | pH, redox potential and conductivity of soil | Phoenix |
| Atomic-force microscope | >10nm imaging of soil particulates | Phoenix |

*ExoMars instruments that were originally part of the payload but have since recently been de-scoped (pending further assessment).

1.5.2 The ExoMars PanCam instrument

The ExoMars rover will be equipped with a multi-purpose Panoramic Camera (PanCam) instrument, and will provide wide angle multi-spectral stereoscopic images of the rover's surroundings (for a detailed description see Griffiths *et al.* 2006). The instrument as a whole consists of three individual cameras: two Wide Angle Cameras (WAC) and one High Resolution Camera (HRC). The WACs enable stereo colour imaging of the surrounding scene, as well as multispectral imaging via the integration of a filter wheel (see Figure 1.11), whilst the HRC allows high resolution imaging of targets identified in WAC images. As currently implemented, multispectral imaging works by utilising a set of glass filters, manufactured at specific wavelengths and bandwidths, to record images from the field of view, from which reflectance values can be obtained. One filter yields one reflectance value, and the spread of filters produces a spectral profile at each image pixel. Therefore, the more filters available (currently 12), the more detailed the spectra will be.

Figure 1.11. Artists impression of the ExoMars Rover (Credit: ESA) together with a technical drawing of one of the PanCam Wide Angle Camera (WAC) 'eyes', based on Beagle2 heritage (Griffiths *et al.* 2005). The position of the filter wheel is highlighted.



Two of the main scientific objectives of the PanCam that will utilise this multi-spectral imaging capability, are firstly the acquisition of geological information proximal to the rover, and secondly identification of the most suitable locations for astrobiological investigation. It is noted that the PanCam is not designed to

be a life-detection instrument in itself, but provides the initial step in identifying suitable lithologies for further multi-level analysis with the aim to detect evidence of biological activity (Vago *et al.* 2005). This site identification will be heavily dependant upon the surrounding geological terrain and mineralogy identified by the PanCam, and as a result, the PanCam needs to be carefully designed to achieve this goal. As the PanCam multispectral imaging capability is, in part, dependant upon a suitable set of filters, the wavelengths of these individual filters needs to be optimised to fit the objectives of the ExoMars mission. The geological filter wavelengths for the PanCam are required to fall in the 440 – 1000nm range, with a minimum of 12 (and possibly up to 14) filter spaces available (Andrew Griffiths, *pers. Comm.*). A notional set of filter wavelengths has already been allocated for this PanCam, however this filter set was inherited from Beagle 2, which in turn was adopted from Mars Pathfinder. Filters for the Imager for Mars Pathfinder (IMP) device were selected with two main objectives in mind. Firstly, to identify ferric oxides and oxyhydroxides, and secondly to determine silicate mineralogy present, particularly pyroxenes (Smith *et al.* 1997). More recently, this filter set has been largely adopted for the MER PanCam, again focusing on the detection of iron-bearing silicates, iron oxides and oxyhydroxides, and also to provide a direct comparison to the IMP results (Bell *et al.* 2003). ExoMars on the other hand has a distinct astrobiological focus, and may encounter an extensive range of hydrated mineral-bearing lithologies. The result of this is that the notional filter set for the PanCam needs to be updated, and this is the focus of Chapter 6 of this thesis.

Whilst multispectral imaging at optical wavelengths to near-infrared (400 – 1000nm), can tell us a lot about mineralogy and chemistry, the majority of distinguishing spectral features occur in the infra-red, with many minerals exhibiting fairly featureless spectra between 440 – 1000nm. As a result, the combination of reflectance spectra with other instrumental analysis can provide a much clearer picture. A multi-instrument approach to astrobiological research has been shown to greatly improve interpretation, particularly of in-situ analysis of planetary material (Bishop *et al.* 2004b; Pullan *et al.* 2007). The addition of Raman spectroscopy in particular has been widely advocated for astrobiological research (Storrie-Lombardi *et al.* 2001; Wang *et al.* 1995), as its ability to detect and discriminate between geological and biological material at the micrometer

scale has made it a valuable tool (e.g. Sharma *et al.* 2007; Jorge Villar *et al.* 2005; Bishop *et al.* 2004b; Ellery & Wynn-Williams 2003). As a result it is one of the instruments planned to be part of ExoMars (Bazalgette *et al.* 2007; Rull Perez & Martinez Frias 2006). However, it is limited for ExoMars by its current confinement to a contact instrument, and therefore cannot be used for remote target selection, and this is where PanCam reflectance spectroscopy has an advantage. The combination of being able to detect regions or outcrops of interest from a distance, and then analyse them with a higher degree of confidence close-up, is a fundamental aspect of planetary rover exploration.

An additional feature that is proposed to be an integral part of the PanCam instrument is UV laser illumination to produce a native fluorescence response of organic and geological material (Storrie-Lombardi *et al.* 2009; 2008; Muller *et al.* 2009; Griffiths *et al.* 2008). Likewise, a 365nm LED illumination source is to be included on the Mars Science Laboratory Mars Hand Lens Imager (Edgett *et al.* 2009). UV epifluorescence works very simply by illuminating a sample with a near-UV light source, and recording the wavelength and intensity of the fluorescence that is emitted back. Many organic molecules exhibit this native fluorescence, including those created biologically (such as photosynthetic pigments) and those that exist abiotically, such as polycyclic aromatic hydrocarbons (PAH). This technique has been shown to easily highlight the presence of microbial communities within Antarctic sandstones and on the surface of terrestrial rocks (Storrie-Lombardi 2005), and also the presence of PAH at low concentrations (Storrie-Lombardi *et al.* 2008). UV illumination of minerals can also stimulate a fluorescent response, that although is not diagnostic *per se*, can rapidly reveal or highlight the presence of a deposit that may of interest.

1.6 Thesis summary

1.6.1 Motivation for this work

Astrobiology is, and will remain, an area of science that fascinates both scientists and the wider community. It aims to tackle some of the most fundamental questions regarding the existence of life in the Universe, and also the origins of life on Earth. As such, interest in astrobiology will continue to grow and gather momentum over the coming decade. Perhaps one of the most important, and

certainly most achievable, aspects of current astrobiological research is focused on the in situ detection of Martian life. In order to achieve this goal, much ground work is still needed to understand not only if and when life existed on Mars, but also where and how to detect it. The use of Martian analogue environments and terrains on Earth plays an essential role in answering these questions, and as a result forms the basic concept around which this thesis is structured. The potential environments that may have existed on Mars throughout its history are vast, consequently this work is focused on purely basaltic environments, specifically those that exist at high latitudes. This geographical selection means many of these basaltic environments experience interaction with ice, both during their formation and/or temporally as a result of seasonal extremes. Despite their applicability to Martian analogue research, these environments are largely unexplored, providing numerous avenues of research.

1.6.2 Aims and summary of chapters

The primary aim of this thesis was to utilise terrestrial volcanic environments on Earth as a basis for astrobiologically-focused Martian analogue research. Specifically, subaerial hydrothermal systems and subglacial basaltic volcanism in Iceland and Antarctica were used to assess microbial communities and develop techniques for the detection of astrobiological targets on Mars using ExoMars instrumentation. For this work, subglacial volcanism in particular is explored as a habitable environment on Mars, through the identification of microbial communities, testing the viability of Martian subglacial volcanic environments, and lastly assessing the feasibility of biosignatures. Additionally, subaerial volcanism is used in the development of ground-truthing techniques applicable to the development of the ExoMars PanCam instrument. The following is a brief summary outlining the contents of this thesis.

Chapter 2 details the core methodologies used throughout this research. This includes standard analytical techniques and methods that are common to more than one chapter. A fundamental component of this research was the successful sampling of geological and environmental samples from Iceland. Sampling methods and field descriptions of specific sampling locations are described here.

Chapter 3 details the identification and analysis of the Prokaryotic community residing within subglacially erupted pillow basalts and hyaloclastites situated within the cold and dry volcanic highlands of central Iceland. 16S rDNA clone libraries of the bacterial and archaeal communities present within these lavas were constructed, and the relationship between the community diversity and environmental parameters is assessed. Specifically, there is a clear difference in bacterial diversity between different lava lithologies, with hyaloclastite supporting a significantly more diverse community than pillow lava.

Chapter 4 focuses on the identification and occurrence of biosignatures within subglacially erupted lavas from Antarctica. Specifically bioalteration textures are assessed, and the large scale environmental controls on their formation are described. Such biosignatures are thought to be ideal for Martian exploration, where basaltic lavas, including some that have undergone past aqueous alteration, are widespread. The results of this work challenge that idea by showing the formation of bioalteration textures is sensitive to the local aqueous alteration environment, and the presence of basalt and aqueous conditions does not necessarily result in the production of bioalteration. The work in this chapter is published in the *International Journal of Astrobiology* 8 (1), 37 – 49 (2009), entitled “A Comparative Study of Endolithic Microborings from a Transitional Subglacial – Marine Environment”.

Chapter 5 details the experimental assessment of the habitability of subglacial volcanic environments exposed to present day surface Martian conditions. This was a culture-based test of viability, focused on the in-situ microbial community within subglacially erupted pillow lava. It is noted that this lava is from the sample outcrop as that used for 16S rDNA analysis described in Chapter 3, and so provides a direct comparison between the culturable, and non-culturable microbial community. It is shown that simulated subglacial volcanic environments provide adequate shielding from the external surface extremes, and viability within these systems is high.

Chapter 6 details work using both subglacial and subaerial lavas, as well as hydrothermal samples, to assess the potential of multispectral imaging and UV illumination in the detection of astrobiological targets on Mars. Astrobiological

targets include hydrated minerals, and fossilised and extant biological material present in volcanic environments. In relation to this analysis, a new set of geological filters for the ExoMars PanCam instrument is devised and tested, with the aim to improve the astrobiological capability of the PanCam for the mission objectives of ExoMars – to uncover evidence of past or present life within the Martian subsurface. The bulk of this work has been submitted to *Astrobiology*, entitled “Astrobiological Considerations for the Selection of Geological Filters on the ExoMars PanCam Instrument”. Additionally, the UV component of this work is published in *Astrobiology* 9 (10), 953 – 964 (2010), entitled “Laser Induced Fluorescence Emission (L.I.F.E.): Searching for Mars Organics with a UV-Enhanced PanCam”.

Chapter 7 develops the work detailed in Chapter 6, and presents results from testing the new geological filters in situ at Martian analogue field localities in Svalbard, as part of AMASE. Martian analogue terrain imaged using a replica of the ExoMars PanCam included ultramafic volcanics, hot spring carbonates, and iron oxide rich lithologies. Through such field testing it is shown that PanCam image and spectral data can identify past habitable terrains based on their mineralogy and lithological characteristics, but both fossil and extant life biosignatures largely remain undetected.

Chapter 8 integrates the results from the preceding chapters, demonstrating the essential role that interdisciplinary studies can play in helping to answer the fundamental questions in science, in this case, the question of whether life exists, or did once exist, on Mars. In particular, the importance of Martian analogue studies is discussed, based on the results of this work, with subglacial volcanic environments being explored specifically. Lastly, future work is proposed, as a natural progression of the work conducted for this PhD.

A list of all published conference abstracts and journal publications is given in Appendix D.

CHAPTER 2

MATERIALS AND METHODS

Astrobiology is a highly multidisciplinary field, and as such it requires the use of a wide variety of laboratory methods, exploiting well developed techniques from the fields of microbiology, geology, and chemistry. This chapter provides a description of the sampling localities, general methods, and analytical techniques used throughout the course of this research. Novel methods and experimentation devised specifically for this PhD are described in the relevant chapters. The following techniques described in this chapter were used to implement the following:

1) Aseptically obtain geological samples for biological analysis: microbiological techniques employed such as culturing, and particularly direct extraction and amplification of DNA, are sensitive to potential contaminants from the sampling equipment, surrounding environment, the person sampling, and the laboratory itself, and as such precautions to avoid such contamination are described.

2) Identification of the culturable and unculturable prokaryotic communities within basaltic lava: culturing techniques were used to isolate microorganisms, whilst DNA-based techniques were used to characterise the uncultured component of the prokaryotic community, particularly in relation to how different basaltic lithologies affect community composition and diversity.

3) Basic characterisation of mineralogy and lithology of geological samples: to provide context for geological samples used in more detailed experimentation and in particular the development and testing of the PanCam instrument. For this, a combination of transmission light and Scanning Electron Microscopy, Raman spectroscopy, and Energy Dispersive X-ray analysis were used.

2.1 Laboratory Materials

2.1.1 Sterilization

All glassware, reagents, culture media, water, and solutions were sterilised by autoclaving at 121°C for 20 minutes, or by filtration through a 0.22µm Millipore filter connected to a syringe. Geological equipment such as hammers and chisels were sterilised with Vircon prior to fieldwork, and subsequently flame sterilised immediately before sample collecting in the field with 70% ethanol. Any remaining equipment and labware (e.g. plastic 96-well plates, cryogenic vials) were purchased pre-sterilised.

2.1.2 Solutions and Reagents

The following solutions and reagents were used in the various protocols specific to the isolation of microorganisms and their subsequent genetic identification, and the DNA-based assessment of prokaryotic communities through the extraction of environmental genomic DNA and construction of clone libraries. Unless stated, all solutions were made using deionised and distilled water (dH_2O).

A) Isolation of microorganisms on Pillow Basalt Agar:

- Pillow basalt solution: finely crushed pillow basalt was suspended in distilled and deionised water at a concentration of 0.25g rock ml⁻¹. This solution was sterilized by autoclaving prior to addition to agar.

B) Genomic DNA extraction from microbial isolates:

- TE Buffer 10mM Tris HCl (pH 8)
 1mM EDTA (pH 8)
- 10% Sodium Lauyl Sulphate (SDS)
- 70% Ethanol
- CTAB Solution 0.7M NaCl
 10% Hexadecyltrimethyl ammonium bromide
 (CTAB)
- 5M NaCl

C) Production of chemically competent *E.coli*

- 1M Calcium Chloride (CaCl₂)

- 75mM Calcium Chloride plus 15% Glycerol (CaCl₂, 15% glycerol)
- 0.5M Magnesium Chloride (MgCl₂)

D) Screening recombinant bacterial colonies for cloning

- X-gal (5-bromo-4-chloro-3-indoyl-β-D-galactopyranoside): X-gal dry powder was dissolved in dimethyl sulphoxide (DMSO) to create a 40mg/ml stock solution, which was then added to molten, autoclaved agar media (~50°C) to a final concentration of 80µg/ml. Both X-gal and DMSO were purchased from Sigma.
- IPTG (Isopropyl β-D-1-thiogalactopyranoside: A 200mM stock solution (Sigma) was added to molten, autoclaved agar media (~50°C) to a final concentration of 0.5mM.
- Ampicillin: Ampicillin dry powder was dissolved in dH₂O to produce a stock solution of 50mg/ml, which was filter sterilized through 0.22µm Millipore filters, and stored at -20°C. This was added to molten, autoclaved agar media (~50°C), and to autoclaved LB broth, to a final concentration of 100µg/ml.

E) Agarose gel electrophoresis

- 10 X TBE
108.0 g l⁻¹ Tris (hydroxymethyl) methylamine
50 g l⁻¹ Orthoboric Acid
7.4 g l⁻¹ EDTA
- Hyperladder I (Bioline)
- Ethidium Bromide (used at a concentration of 0.1µl/ml)

2.1.3 Bacterial strains and plasmids

- *E. coli* strain JM107 was used to make chemically competent cells suitable for the transformation step in cloning.
- pGEM T-Easy plasmid vector (Promega) was used for ligation reactions
- pUC19 plasmid used as a control for transformation

2.2 Sampling of Environments

Samples from Icelandic environments formed the bulk of the work detailed in this thesis, and therefore sampling techniques and conditions are described in this section in detail. Field sampling took place on four separate trips between September 2006 and February 2008. Sample types included basaltic lavas, hydrothermal soil and mud, hydrothermal spring fluids, silica sinter deposits, and biomats. A list of Icelandic samples used for the research documented in this thesis is given in Table 2.1. Samples were collected for one of two objectives. Firstly to produce a representative set of geological Martian analogue or astrobiologically relevant material (e.g. basaltic lavas and hot spring deposits respectively), and secondly to conduct a microbiological study into an extreme volcanic environment that could be utilised as a Martian analogue. These Icelandic samples were used for the work detailed in Chapters 3 and 5 (both microbiological based study), and Chapter 6 (geological based study).

In addition to those chapters, Chapters 4 and 7 utilised non-Icelandic samples or localities, and the relevant details are briefly described here. For Chapter 4, basaltic hyaloclastite lava samples from Antarctica were kindly provided by Prof. John Smellie, who collected the samples during three field seasons led by the British Antarctic Survey. These samples had not been collected under any particularly notable conditions, and have since remained in storage at the BAS main headquarters in Cambridge, UK. Chapter 7 describes work conducted on location in Svalbard, and as such there are no specific sampling details that need be described here. However, details on specific Svalbard sites themselves that were used for PanCam testing are given further on in this section.

2.2.1 Sampling protocols and field techniques

The main issue when collecting, transporting, and storing samples was eliminating contamination, especially in the field. Contaminants can be from a number of sources, including wind blown material from other parts of the environment, humans, animals, equipment, and in the laboratory. Two methods were used to sample geological and hydrothermal material aseptically from different environments:

- Hammering: using a sterile hammer, specific sections of rock could be broken off whilst minimising contamination. These were then immediately transferred to sterile Whirlpak bags and sealed.
- Falcon tubes: soft sediments and fluids were either scooped into 50ml Falcon tubes using a flame-ethanol sterilised metal spatula, or transferred via sterile 10ml pipette.

All samples were kept as cold as possible and were untouched during the trip and transport. They were transported in the hold of the airplane back from Keflavik to London, where they were then stored at either -20C or 4°C at UCL until use.

2.2.2 Sampling Locations

2.2.2.1 Iceland

Sampling and fieldwork sites in Iceland were selected based on their relevance to the scientific objective of this PhD, and also in terms of logistics. Two main regions of Iceland were selected, the first in the Southwest on the Reykjanes Peninsular, and secondly the northern branch of the Icelandic Rift Zone. Whilst the Reykjanes Peninsular is advantageous in terms of logistical accessibility, the relatively warm and wet climate of this region caused by the Gulf Stream was not regarded here as a suitable ‘extreme’ environment from which to conduct a microbiological study. Therefore samples from this region of Iceland were collected for geological analyses only (see Table 2.1). In contrast, the northern branch of the Icelandic Rift Zone lies in the cold and dry Icelandic interior. The existence of this volcanic desert is largely due to frequent volcanic activity during the last ice age, which resulted in numerous high elevation subglacially-erupted volcanic edifices, and since then, laterally widespread subaerial lava flows. The high elevation terrain produced by past, and currently active volcanism, coupled with the high latitude geographic position of Iceland, has resulted in the growth of substantial glaciers on top of these volcanoes. The overall effect of these factors is a rain shadow that extends northwards across the Icelandic interior (see Figure 1.6 in Chapter 1). This area therefore was deemed as a suitable locality within which to research microbial life with relevance to past volcanic habitats that may have existed on Mars.

As noted in the Introduction chapter of this thesis, subglacial basaltic volcanism was an environment of particular interest. As such subglacial volcanoes, both active and extinct, were sampled. In total, six areas in Iceland were selected for sampling: Askja, Geysir, Helgafell, Namafjall, Krysuvik and Kverkfjoll, which are described below. In general, three of these sites were selected for the sampling of subglacial basaltic lavas (Askja, Helgafell, Kverkfjoll), whilst the remaining three are hydrothermal fields where samples collected included lavas that had undergone extensive hydrothermal alteration (Namafjall and Krysuvik), and mineral deposits (Geysir). Hydrothermal samples were also collected from Kverkfjoll, but due to time constraints this site was ear-marked for potential future investigation, and plans for this are detailed at the end of this thesis in the Discussion (Chapter 8).

Figure 2.1. Satellite map of Iceland showing the approximate position of the Icelandic Rift Zone (black dashed line) and sampling locations (red stars) in the two principle regions: the Southwest peninsular and the Neo-volcanic zone, indicated by the blue boxes which are shown in Figures 2.2a and b respectively.

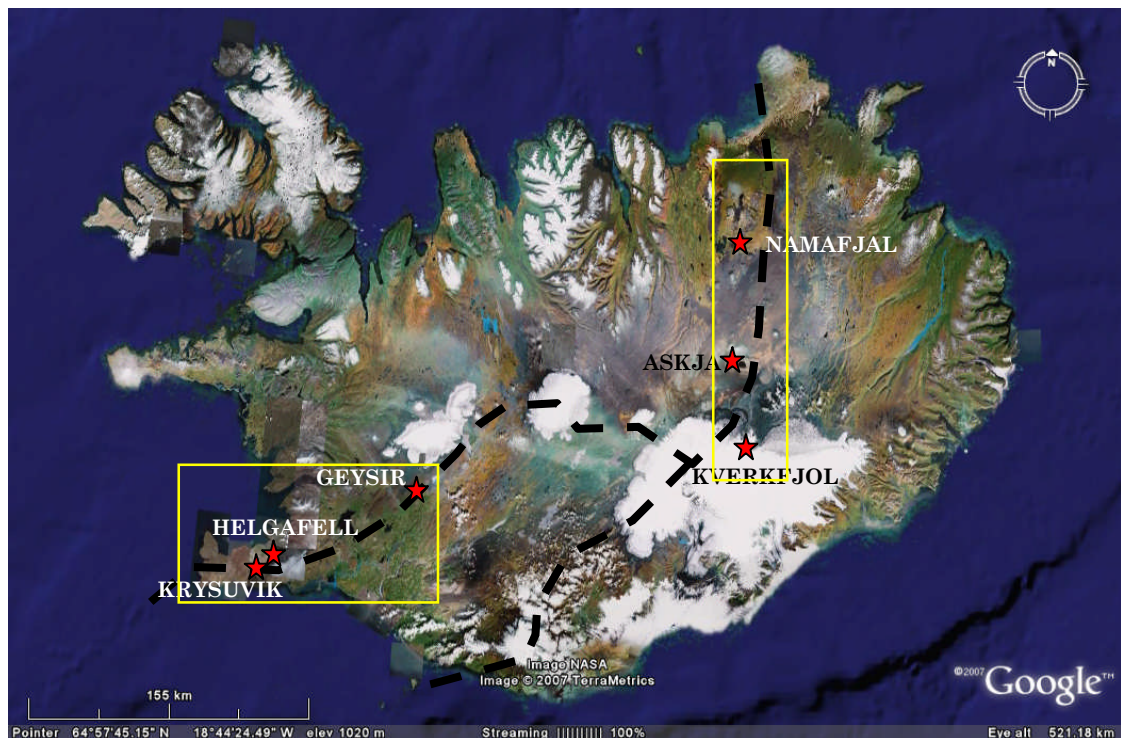
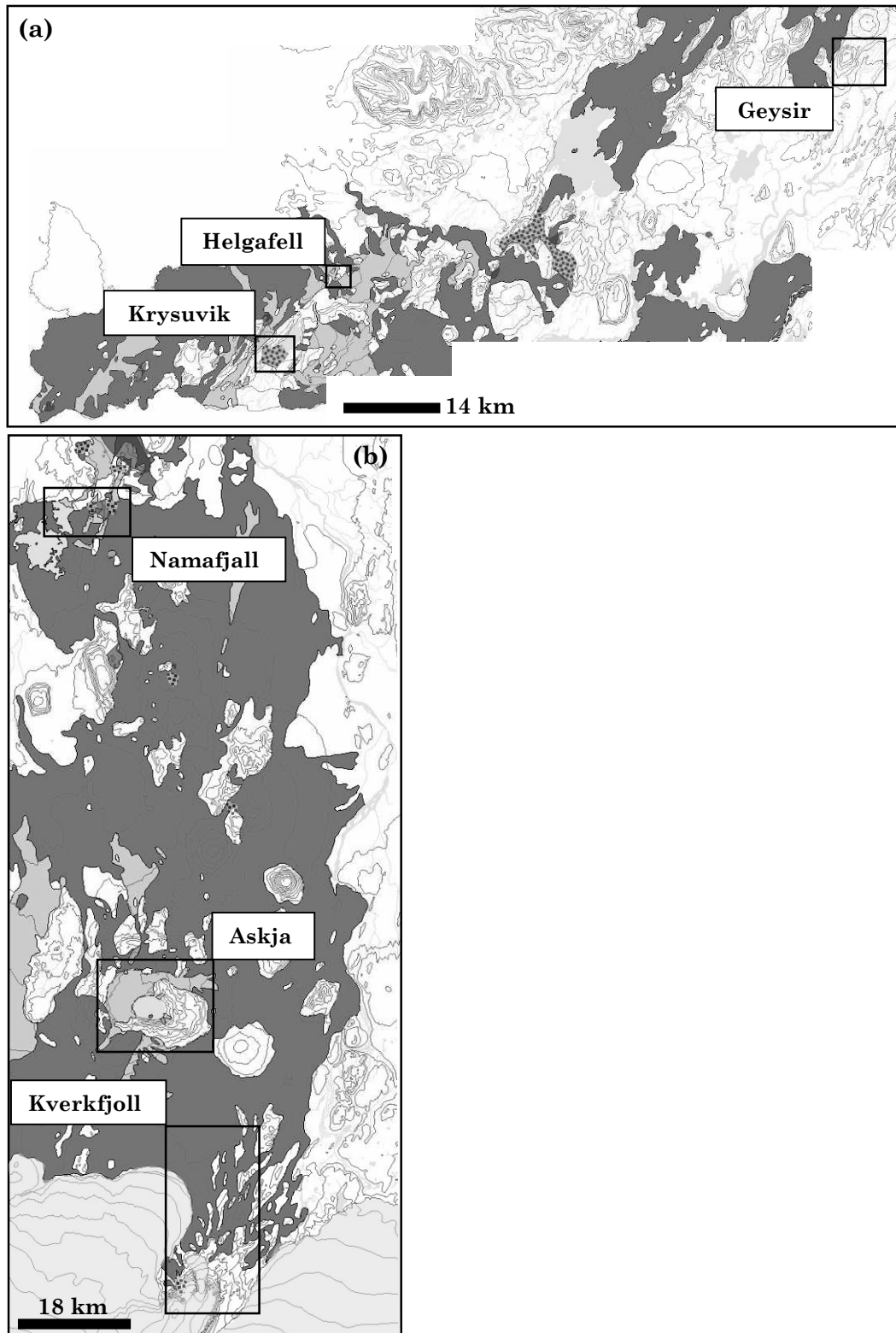


Figure 2.2. a) Map showing localities Krysuvik, Helgafell, and Geysir; and b) localities along the Neo-volcanic zone: Kverkfjoll, Askja, and Namafjall. White areas are largely Pleistocene subglacial lava flows; dark and mid-grey regions depict Holocene lava flows, with the mid-grey flows being the most recent; and spotted regions show areas of high geothermal heat. Light grey shows lakes, rivers and glaciers. Contour lines are on a scale of 1:500 000. (Adapted from http://gullhver.os.is/website/hpf/orkustofnun_english/viewer.htm).



A) Askja

Askja is a large caldera 45 km² in area, and forms part of the Dyngjufjoll volcanic complex which lies on the Neo-volcanic zone. The oldest parts of the complex were produced predominantly by basaltic magmatism, much of which was subglacial, forming an elevated topography of hyaloclastite and pillow basaltic lavas (Sigvaldason 1968), with an aerial extent of ~400km², and a maximum elevation of 1516m (Sigvaldason 2002). There is a main 8km diameter caldera, thought to be the result of ring and linear fissure subglacial eruptions towards the end of the last glaciation. Additionally a smaller inner 4.5km diameter caldera was formed during a rhyolitic 1875 Plinian eruption (Brown *et al.* 1991), and is now filled with water (Figure 2.3a). Askja was sampled due to the extensive exposures of largely unweathered subglacial basaltic lava flows, including both pillow basalt piles and hyaloclastite ridges.

B) Geysir

The Geysir geothermal area lies east of the western volcanic rift zone in Haukadalur, located in South Iceland. Numerous hot springs exist here, including the Geysir hot spring (now no longer erupting) and the famous Strokkur geysir. Volcanic activity in this region has been absent in the last 10,000 years, and it is thought the geothermal system is driven by volcanic intrusions from a now extinct central volcano (Pasvanoglu *et al.* 2000). All the boiling hot springs and fumaroles in the area are located within highly altered basalts, and springs and mud pots are found within the main hot spring area (Figure 2.3b). Extensive deposits of silica sinter exist around most of the alkaline hot springs, both as silica crusts around active springs or geysirs, and also as loose, broken deposits on hillsides. It is these loose samples of sinter that were collected for study.

C) Helgafell

Helgafell is a monogenetic subglacial fissure eruption (a 'tindar') which formed during the last glaciation in the Pleistocene. It is thought to have erupted beneath ~500m of overlying ice, and consists predominantly of hyaloclastite along with occasional pillow basalts and feeder dykes (Schopka *et al.* 2006). It is now surrounded by extensive Holocene subaerial basaltic lava flows (Figure 2.3c).

D) Krysuvik

Krysuvik, located on the Reykjanes Peninsular, is a small hot spring field with hot spring streams, fumaroles and mud pots, surrounded by subglacially erupted lava ridges. Hydrothermal activity is high, with high temperature fumaroles rapidly weathering surrounding lavas (Figure 2.3d). In addition, the springs themselves are saturated with silica, and opaline silica crusts can be found coating most lavas close to the streams generated by the springs.

E) Namafjall

The Namafjall geothermal field is ~3–4 km² in size (Saemundsson 1991) and lies on the Krafla fault swarm 9km south of the Krafla caldera (Larsen et al. 1979). Namafjall is a high temperature solfatara field, consisting of numerous sulphur depositing hot springs and fumaroles, boiling mud pots and hydrothermally altered lava and soil. Intercalated hyaloclastites and lava flows predominate the lithology in this area (Gudmundsson & Arnorsson 2002), many of which have experienced significant levels of weathering and alteration by acid fog (sulphur dioxide). Such lavas were sampled at this site due to their extensive sulphate deposits.

F) Kverkfjoll

Kverkfjoll is a partially subglacial central volcano, on the northern margin of Vatnajokull. It consists of two calderas, positioned geographically at right angles to each other, of which the northernmost caldera is only partially covered by the glacier (Hoskuldsson *et al.* 2006). This central volcano is also located almost directly above the Icelandic hot spot (Sigvaldason *et al.* 1974), which coupled with its position in the neo-volcanic zone, results in very high heat flow and intensive thermal activity (Olafsson *et al.* 2000). Extensive volcanism during the Pleistocene has resulted in numerous NE trending pillow basalt and hyaloclastite ridges (Figure 2.3e), formed during subglacial fissure eruptions. The retreating of Vatnajokull since the last ice age has since exposed these ridges, making them available for sampling.

Figure 2.3. Photographs of Icelandic localities where sampling took place. Localities where lava samples were collected are on the left, localities where hydrothermal samples were collected are on the right. a) Askja caldera looking west. In the foreground the small explosion crater ‘Viti’ can be seen. The main lake is the crater lake Öskjuvatn (formed during a 1875 Plinian eruption; b) A typical silica rich spring at Geysir, surrounded by sinter deposits; c) Helgafell viewed looking NW, surrounded by post-glacial Holocene lava flows; d) Krysuvik hydrothermal field looking NW; e) Subglacial basaltic lava flows outcropping north of Kverkfjöll; f) Frozen hydrothermal field at Namafjall.

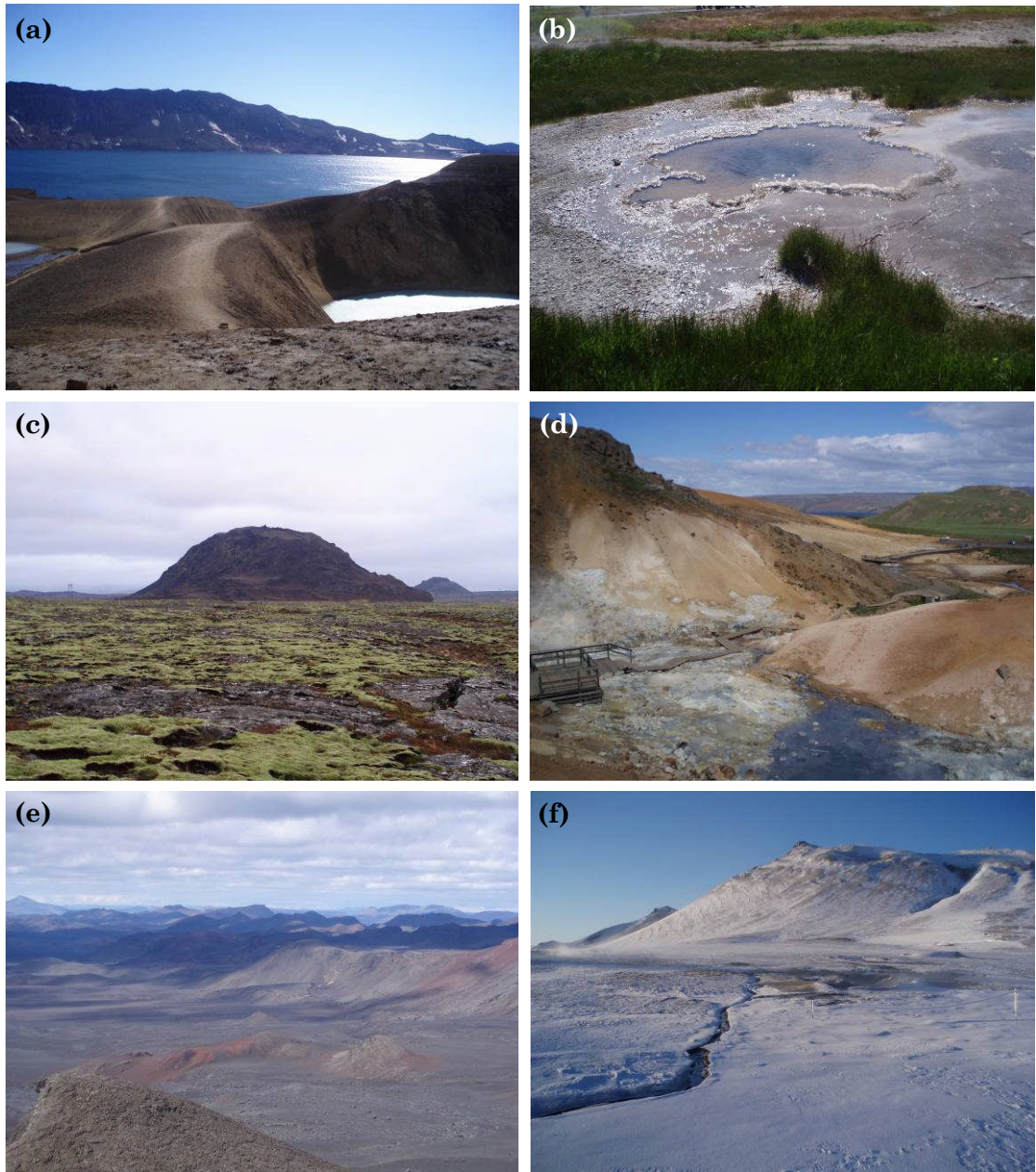


Table 2.1. Table of all samples collected from Iceland used in the work for this PhD (NB: Elevation not available for some sites)

| Name | GPS/Elevation | Month | Site Description | Sample type | Chapter |
|-------------------|---|-------|---|--|--|
| Askja | | | | | |
| ASK004 | 65° 03.264' N 016° 39.635' W 960m | July | Small hyaloclastite ridge | Medium-grained hyaloclastite | 3. Bacterial diversity of lavas |
| ASK009 | 65° 92.528' N 016° 36.207' W 805m | July | Pillow basalt pile between basal hyaloclastite and a jointed lava flow above. | Multiple samples of glassy, largely unweathered pillow basalt lava | 3. Bacterial diversity of lavas 5. Viability of a subglacial volcanic habitat on Mars |
| Geysir | | | | | |
| GY1 | 64° 18.825'N 20° 18.178'W | Sept. | Silica supersaturated hot spring system, numerous deposits of silica sinter | Sinter deposit with 1mm thick pink, black and yellow bands | 6. Development of geological filters on ExoMars PanCam |
| GY2 | | | | Silicified biomat with fibrous mat structure preserved | |
| Helgafell | | | | | |
| HF003 | 64° 0.349'N 21° 51.478'W 149m | Nov. | Monogenetic hyaloclastite edifice | Fine grained hyaloclastite | 6. Development of geological filters on ExoMars PanCam |
| Krysuvik | | | | | |
| KR003 | 63° 53.630'N 22° 4.123'W | Nov. | Solfatara field with fumaroles, hot springs and silica sinter deposits | Hyaloclastite with a surface layer of opaline silica | 6. Development of geological filters on ExoMars PanCam |
| Kverkfjöll | | | | | |
| KV2 | 64° 51.245'N 16° 26.941'W 734m | July | Subglacially erupted basalt pillow lava mounds | Vesicular pillow basalt | 6. Development of geological filters on ExoMars PanCam |
| KV4/6 | 64° 41.122'N 16° 40.562'W 1691m | July | Glacial solfatara and hot springs associated with active subglacial volcanism | Hot spring sediment and hydrothermal glacial meltwater | 8. Discussion – future work |
| Namafjall | | | | | |
| NAL | 65° 38.441'N 16° 49.056'W | Feb. | Solfatara field with numerous fumaroles and heavily altered lava | Extensively altered basaltic lava | 6. Development of geological filters on ExoMars PanCam |

2.2.2.2. Svalbard

Whilst all samples were acquired from Icelandic environments, in-situ field testing was conducted on site in Svalbard, and the specific sites where this was carried out are detailed here. As mentioned in Chapter 1 (section 1.3.3) sites were located firstly in Bockfjord (Figure 2.4), and secondly at Wahlenbergfjord (see Table 2.2). Bockfjord is home to the Bockfjord volcanic complex, and contains several Quaternary eruptive centers and hot spring activity, all located along a fault thought to represent the opening of the Arctic Basin and the Greenland Sea (Skjelkvåle *et al.* 1989). These volcanoes are composed of primitive alkali basaltic lavas, including abundant xenoliths from the upper mantle and lower crust. In particular, Sverrefjell volcano (Figure 2.4a) is unique in that it is exceptionally rich in these xenoliths, the vast majority of which are lherzolitic, and comprise 15 – 20% of the lava. In addition, the formation of Sverrefjell is thought to have been affected, at least in part, by glacial interaction, signified by outcrops of well formed pillow lavas and an abundance of volcanoclastic material (Skjelkvåle *et al.* 1989). The presence of the upper mantle xenoliths means that in terms of mineralogy, the Sverrefjell lavas are particularly rich in olivine. In addition, hydrothermally-deposited carbonates are also abundant, deposited in lava fractures and vesicles, and have been previously documented as a suitable analogue for the carbonate globules in Martian meteorite ALH84001 (Treiman *et al.* 2002), particularly in their zonation of ankerite, siderite, and magnesite.

Sverrefjell is located between two calcareous springs: Troll Springs to the south and Jotun Springs to the north (Figures 2.4b and c respectively). These springs are the northernmost documented continental hot springs in the world (Jamtveit *et al.* 2006; Banks *et al.* 1999). Troll Springs in particular is surrounded by large carbonate terraces, which extend over an area of 50 x 100m (Skjelkvåle *et al.* 1989), and are believed to be sourced entirely by sub-permafrost glacial meltwater, with the underlying Marble Formation being the likely source of spring Ca and CO₂ contents (Jamtveit *et al.* 2006). In contrast, Jotun Springs is significantly smaller, consisting of convex upwards mounds of carbonate instead of the large terraces seen at Troll.

Lastly, Wahlenbergfjord lies on the island of Nordaustlandet, the second largest island in the Svalbard archipelago. Little work has been conducted regarding the

geology of this island, and the vast majority of it is permanently ice covered. However, a brief geological overview of the area shows it to consist largely of sand and siltstones (Harland *et al.* 1998).

Figure 2.4. a) Field sites in Bockfjord (photo credit: Kjell Ove), looking west; b) Aerial view of Troll springs, main spring highlighted (Hammer *et al.* 2005); c) Jotun Springs



Table 2.2. Table of sites in Svalbard where in-situ field testing of the PanCam instrument was conducted in August 2009 (Chapter 7).

| Name | | GPS and Elevation | Description |
|-------------------|----------------------|--------------------------------------|---|
| Bockfjord | Sverrefjell (BOCK01) | 79° 26.247'N 13° 20.473'E 63m | Outwash plain of a steep river-cut valley on the eastern flank of Sverrefjell volcano |
| | Sverrefjell (SV01) | 79° 26.047'N 13° 19.494'E 182m | Volcaniclastic breccia outcrop on the northeastern flank of Sverrefjell volcano |
| | Jotun Springs (JS02) | 79° 27.358'N 13° 17.255'E 55m | Warm carbonate depositing hot springs with small, shallow terraces |
| | Troll Springs | 79° 23.316'N 13° 26.461'E 33m | Warm carbonate depositing hot springs with large, well developed terraces containing colour banding |
| Wahlenbergfjorden | | 79° 41.647'N 21° 0.651'E 9m | Iron oxide rich highly friable quartz sandstones and siltstones within a narrow river-cut gorge |

2.3 Cultivation and Identification of Microorganisms

Isolation of microorganisms *in vitro* is essential to provide the physiological and metabolic information required to place those microorganisms identified purely through molecular techniques into context. In addition, and with relevance to this work, microbial cultivation also allows the identification of those microorganisms that are presently viable. Cultivation of the microbial community from some natural environments typically has a low success rate. As such, growth media need to be carefully selected, firstly to encourage high levels of growth, and secondly to maximise diversity, particularly amongst the slower growing organisms that can be easily out-competed. Therefore a balance needs to be struck whereby enough nutrients are supplied to enable the growth of sufficient biomass, but also not in such high supply that only a small number of different phylotypes are isolated. Here, two different types of media were used for the isolation of bacteria from Icelandic pillow basalt (Chapter 5), one which attempts to emulate the basaltic lava environment, utilising a method modified from that typically used for soil extract agar (Burlage *et al.* 1998), and the other which is more universal to the isolation of environmental bacteria, but at quarter strength due to the oligotrophic nature of the basaltic lava environment. Additionally, standard laboratory media specific to the growth of *E.coli* were also used for recombinant-based molecular techniques.

2.3.1 Media for isolation of microorganisms

The following media were used for the isolation of microbial communities from basaltic lava samples:

- Half strength Czapek-Dox Agar (CZD): 12.5g l⁻¹ CZD broth (Difco)
2% agar
(CZD broth ingredients: Saccharose 30 g l⁻¹
 Sodium nitrate 3.0 g l⁻¹
 Dipotassium phosphate 1 g l⁻¹
 Magnesium Sulphate 0.5 g l⁻¹
 Potassium chloride 0.5 g l⁻¹
 Ferrous sulphate 0.01 g l⁻¹)
- Pillow Basalt Agar (PBA): 50µl ml⁻¹ of pillow basalt solution
 2% agar

Media for growth of *E.coli*:

- Luria Bertani (LB) Miller modification broth and agar (2%) were used for the growth of newly transformed and recombinant *E.coli* cells.

| | | |
|------------------------------|-----------------|------------------------|
| (Difco LB broth ingredients: | Tryptone | 10 g l ⁻¹ |
| | Yeast Extract | 5 g l ⁻¹ |
| | Sodium Chloride | 10 g l ⁻¹) |

- Nutrient Broth (NB) was used for the preparation of chemically competent cells

| | | |
|------------------------|--------------|-----------------------|
| (Difco NB ingredients: | Beef Extract | 3 g l ⁻¹ |
| | Peptone | 5 g l ⁻¹) |

Addition of other reagents:

Following autoclaving media were cooled to ~55°C before selective reagents (such as pillow basalt solution, see section 2.1.2) were added. For preventing fungal growth, Nystatin (Sigma) was used at a final concentration of 20µg/ml.

2.3.2 Preparation of chemically competent cells

Chemically competent *E.coli* were prepared for transformation reactions, and are so-called due to their ability to take up extracellular DNA from the surrounding environment. An overnight culture of *E.coli* was made by inoculating 5ml nutrient broth (NB) with *E.coli* strain JM107 and incubating overnight at 37°C shaking at 180 rpm. The following morning, this 5ml culture was poured into 20ml NB media pre-warmed to 37°C, which also contained 20mM MgCl₂. This was incubated for 1 hour at 37°C shaking at 180rpm. The culture was chilled on ice until cold and centrifuged for 10 minutes at 5000rpm at 4°C. The resulting pellet was kept on ice, and resuspended in 2ml ice cold sterile 75mM CaCl₂ containing 15% glycerol. This suspension was split into 100µl aliquots into pre-chilled 1.5ml vials, followed by storage at -80°C.

2.3.3 Microbial isolation from Icelandic samples

Pillow basalt agar (PBA) plates were inoculated by sprinkling crushed pillow basalt (<3mm particulate size) onto the surface of the set agar plate. The plates were incubated at 20°C. Plates were spiked with Nystatin, to limit fungal growth. Sterile control plates were made for the pillow basalt solution

supplemented agar, and stored amongst the experimental plates to check for any sources of laboratory airborne contamination. Pure isolates were obtained by sub-culturing individual colonies two or three times on fresh media.

For storage, pure isolate colonies were removed from the surface of the agar plate with a sterile loop and suspended in 1ml 70% glycerol in sterile cryogenic vials, and stored at -80°C.

2.3.4 Extraction of genomic DNA from cultivated isolates

Identification of the isolates cultivated from Iceland pillow basalt was achieved through characterisation of the 16S rDNA gene from genomic DNA extracted from each isolate. The method is adapted from Bailey (1995) and was used to obtain DNA from ~20mg cultured cells. The pure culture was taken straight from the agar plate and placed into a sterile 1.5ml Eppendorf tube. The cells were resuspended in 500µl lysis buffer (20 µg/ml proteinase K in 0.5% SDS) and incubated at 55°C for 30 minutes, with gentle inversions every 10 minutes. 100µl 5M NaCl and 80µl CTAB (pre-warmed to 65°C) were added and the solution incubated at 65°C for 10 minutes. Following incubation the tube was removed to room temperature and 680µl of isoamyl alcohol: chloroform (1:24) added (shaking vigorously). This was centrifuged at 13000 x g for 10 minutes, and the top aqueous layer removed into a fresh tube. DNA was then precipitated by adding 0.6 volumes of isopropanol and incubating at 4°C overnight. The solution was centrifuged at 13000 x g for 10 minutes to pellet DNA, which was then washed twice with 70% ethanol. DNA was then resuspended in 200µl TE buffer and stored at -20°C.

DNA fragments were separated by gel electrophoresis in 1% (w/v) TBE agarose gel containing Ethidium Bromide at a concentration of 1µl/100ml. DNA bands were visualised and photographed under UV light. For quantification, DNA concentration was measured using a Nanodrop Spectrophotometer.

2.3.5 Polymerase chain reaction (PCR) amplification

PCR allows the exponential replication of a particular gene sequence, in this case the 16S rDNA gene. The genomic DNA double helix is effectively ‘unravelling’ (melted) into two single strands, which provide the template from which to

replicate the DNA. Primers (short, single strand DNA sequences) specific to this region of DNA attach to conserved regions at both ends of the 16S rDNA gene, and serve as the starting point from which the polymerase enzyme can build the remaining complimentary strand of DNA through the addition of nucleotides, eventually producing a duplicate set of DNA (Steffan & Atlas 1991). This process is performed repeatedly, exponentially increasing with every cycle. PCR amplification was performed in a Techne TC-512 thermo-cycler. All reactions were carried out as 50µl reactions, each containing 5µl PCR Buffer (10x stock), 0.5µl each of dNTP mix (10mM stock), Taq DNA Polymerase, forward and reverse primers (10nmole stock) and Bovine Serum Albumin (10mg/ml stock), 42µl molecular grade water, and 1µl sample template DNA. Bovine Serum Albumin (BSA) was added to stabilise *taq* DNA polymerase in the PCR reaction, and was found to produce a significantly greater yield of PCR product. Bacterial primer pairs 27F and UN1492R were used, the sequences of which are given in Table 2.3 further on in this chapter.

The PCR program was as follows: initial denaturation step of 95°C for 4 minutes, then 25 cycles of 94°C for 30 seconds, 55°C for 30 seconds, 72°C for 1 minute, a final extension of 4 minutes at 72°C with a final hold at 10°C.

2.3.6 Purification and cloning of PCR products

16S rDNA PCR products (total 40µl) were loaded into a 1% agarose gel stained with Ethidium bromide, the correct bands excised with a clean scalpel, and extracted using the QIAquick Gel Extraction Kit (Qiagen) according to the manufacturers instructions. Purified PCR products were eluted in 50µl of sterile *dH*₂O.

Sequencing of the purified PCR products directly using primers 27F and UN1492R proved unsuccessful, and so the PCR products from each isolate were ligated into the pGEM plasmid vector supplied with the pGEM T-easy vector kit (Promega) for cloning and subsequent sequencing. Ligation was carried out following manufacturers instructions as follows: a ratio of 2µl PCR product was ligated to 1µl plasmid (pGEM) with the addition of 5µl Buffer, 1µl T4 ligase and 1µl molecular grade water (final volume 10µl). This was incubated at 4°C overnight and stored at -20°C if not being used for transformation immediately.

For transformation, 2µl ligation was added to 50µl JM107 chemically competent cells and incubated on ice for 30 minutes. The cells were heat shocked at 42°C for 45 seconds, incubated on ice for 2 minutes, then 450µl LB broth added. The transformation reactions were incubated at 37°C shaking sideways at 180rpm for 1.5 hours. After incubation 50µl and 100µl were spread onto pre-prepared LB agar plates supplemented with 100µg/ml ampicillin, 80mg x-gal and 0.5mM IPTG for blue/white screening of recombinants. Control fresh competent cells were also plated out as a negative control, and pUC19 plasmid DNA was used as a positive control. The plates were incubated at 37°C overnight. A single randomly selected white recombinant colony was picked with a sterile pipette tip and transferred to 5ml LB broth supplemented with 100µg/ml ampicillin. This was incubated overnight with shaking at 180rpm at 37°C. Growth was verified by visual identification of turbidity, and 1.5ml of culture was centrifuged at 13,000rpm in a microcentrifuge to pellet cells. The plasmid was purified from the cells using the Qiaquick mini-prep kit, following the manufacturers instructions, and the resulting plasmid DNA was eluted in 50µl sterile dH₂O.

2.3.7 Sequencing of the 16S rDNA gene

DNA sequencing was carried out by Wolfson Institute for Biomedical Research (University College London) using a Beckman Coulter CEQ2000XL Sequencer. 12µl of plasmid obtained from the mini-preps at a concentration between 50 – 100ng/µl was sequenced using vector specific sequencing primers M13-20 (GTAAAACGACGGCCAG) and M13-R (CAGGAAACAGCTATGAC), both from Invitrogen.

Phylogenetic tree construction for cultured isolates was conducted using software available on the Ribosomal Database Project website (<http://rdp.cme.msu.edu/treebuilder>), which uses the Weighbor weighted neighbor-joining tree building algorithm. Sequence reads from each end of the 16S rDNA gene insert were typically 550bp long, and as such were not able to overlap to generate contig sequences of the insert, which being originally amplified with primers 27F and UN1492R were typically ~1.5kb in length. Therefore, trees were built using sequence reads (trimmed to equal length of ~400bp) that covered the variable regions V7, V8, and V9. A 16S rDNA insert can be ligated into a plasmid vector in either direction, and so each sequence was

assessed to identify the sequence read (M13-20 or M13-R) that covered the correct variable regions. Additionally, sequence data for the closest relatives of the cultured isolates identified from BLASTn were also included in the trees for context, and these, together with the isolate sequences, were aligned using the ClustalW multiple alignment tool (in BioEdit) and trimmed accordingly. Trees generated by RDP were then plotted using the Interactive Tree of Life (Letunic & Bork 2007; Ciccarelli *et al.* 2006).

2.4 Phylogenetic Analysis of the Microbial Community

To obtain a more comprehensive understanding of the microbial community present within a given environment, it is necessary to identify those members of the community that are unable to be isolated through traditional cultivation techniques, especially considering this can constitute >99% of the entire microbial population (Tringe & Rubin 2005; Torsvik *et al.* 1996). One of the most widely employed methods for doing this is the extraction of microbial community DNA directly from the environmental sample itself. Whilst this side-steps the requirement to isolate individual microorganisms, such techniques are not without their pitfalls. In particular, DNA extraction methods are unlikely to successfully obtain genomic DNA from all members of the microbial community, especially where cells adhere to mineral surfaces, or are particularly resistant to lysing. As such, it is important to be aware that whilst environmental DNA extraction is without a doubt an incredibly useful approach, it does not by any means provide a complete picture of microbial diversity.

2.4.1 Genomic DNA extraction from environmental samples

Basaltic lava samples were carefully crushed with a flame sterilized hammer inside multiple layers of sterile Whirlpak bags surrounded by a thick layer of paper tissue ‘padding’ to prevent splitting of the bag upon contact with the hammer (Hirsch *et al.* 1995). Rock fragments were transferred to a fresh Whirlpak bag and a repeat of the above crushing method was carried out if necessary. In general, hyaloclastite lavas were much more friable than pillow basalts and were therefore easier to process. The resulting rock powder was used for DNA extractions, whilst any remaining larger fragments were reserved for culturing. The Powermax soil DNA Isolation kit (MoBio Laboratories) was used to extract total community DNA from pillow lava (ASK009) and hyaloclastite

(ASK004, see Table 2.1 for a brief description of samples). DNA extraction was carried out following the manufacturers instructions. A volume of 15ml Powerbead solution was combined with 5g crushed lava in a PowerMax bead solution tube and vortexed for 1 minute. 1.2ml SDS-based solution (solution C1) was added and the tube vortexed for 30 seconds. The tubes were then attached to the vortex horizontally and vortexed continually for 10 minutes. This was followed by centrifugation at 2500 x g for 3 minutes at room temperature and the supernatant was transferred to a fresh tube. 5ml of solution C2 was added to precipitate non-DNA organic and inorganic material. After 10 minutes incubation at 4°C tubes were centrifuged for 4 minutes at 2500 x g and the supernatant transferred to a fresh collection tube. This step was repeated with solution C3 to remove any residual non-DNA material. 30ml of solution C4 – a high concentration salt solution – was added to the supernatant and the tube inverted twice. The entire solution was centrifuged at 2500 x g for 2 minutes through a spin filter column containing a silica membrane to which the DNA was able to bind. The spin filter containing the now bound DNA was washed by centrifuging through 10ml ethanol solution (solution C5) at 2500 x g for 3 minutes. The spin filter was centrifuged again for 5 minutes to remove any residual ethanol. The spin filter was then placed in a new collection tube and 5ml solution C6 (a sterile elution buffer) added to the silica membrane. This was centrifuged for 3 minutes at 2500 x g, the spin filter discarded and the eluted DNA stored at -20°C.

2.4.2. PCR amplification

As with identification of cultured isolates, PCR is used here for environmental DNA to amplify the 16S rDNA gene. However, whereas PCR for isolate DNA amplifies 16S rDNA from just one organism, environmental DNA is a mix of DNA from all the different members of the community. This difference has several affects. Firstly, the risk of contamination is greater, as the very nature of PCR amplification means even the smallest quantity of contamination can easily be exponentially increased (Wintzingerode *et al.* 1997), and amongst mixed community DNA such contamination could potentially be more difficult to identify. Typical contaminants usually exist as aerosols within pipettes or the lab environment, or occasionally from *Thermus aquaticus* – the microorganism from which the polymerase enzyme used in PCR is obtained. Running a negative

control alongside sample PCRs is a simple way to check for contamination. Secondly, PCR is widely observed to produce an artificial bias towards the more dominant members of the community, reducing diversity, and providing an inaccurate view on microbial community composition. Polz & Cavanaugh (1998) reviewed such issues and demonstrated that significant caution needs to be upheld when conducting a PCR-based ecological study. However, as detailed in their work, such problems can be avoided by reducing the number of PCR cycles, pooling multiple reactions, and increasing the quantity of template DNA. Lastly, whilst such methods may allow the identification of the unculturable community, they are still constrained by what we know from those organisms that have been isolated. This is particularly true of the so-called ‘universal’ primers used to amplify 16S rDNA, which are designed based on what are considered to be conserved regions of the gene (and therefore technically applicable to all Bacteria for example), but are widely believed to miss many members of the community that are perhaps more genetically diverse (Baker *et al.* 2003; Wintzingerode *et al.* 1997). This is especially true for the archaea of which there are significantly less cultured representatives (Kolganova *et al.* 2002)

PCR amplification of the 16S rDNA gene from the community Bacterial and Archaeal genomic DNA was carried out as described in section 2.3.5, using the Bacterial primer pairs 27F and UN1492R, and Archaeal primer pairs Arch21F and UA1492R (Table 2.3). These Bacterial and Archaeal primers span almost the entire length of the 16S rDNA gene, and therefore cover all variable regions (V1 – V9). Reactions were carried out in multiples of three, which were then pooled to firstly help minimise any amplification bias produced during PCR, and secondly to produce a higher yield of PCR product without increasing the number of cycles. PCR products were purified as detailed previously in section 2.3.6.

Table 2.3. Oligonucleotide primer pairs used for amplification of bacterial and archaeal 16S rDNA genes from environmental and isolate DNA.

| Primer pair | Primer sequence 5' – 3' | Target | Position (<i>E.Coli</i>) | Reference |
|---------------------|--|----------|----------------------------|----------------------------|
| 27F UN1492R | AGTTTGATCCTGGCTCAG GGTACCTTGTTACGACTT | Bacteria | 8 – 27 1492 - 1510 | Lane <i>et al.</i> 1991 |
| Arch 21F UN1492R | TTCCGGTTGATCCYGCCGGA GGTACCTTGTTACGACTT | Archaea | 8 – 21 1492 - 1510 | DeLong (1992) |

2.4.3 16S Clone library construction and analysis

Ligation and transformation reactions were carried out as detailed in section 2.3.6, with a total of 8 media plates for each transformation reaction to maximize the number and variability of recombinant clones. Randomly selected white recombinant colonies were picked from the overnight transformation LB agar plates using a sterile pipette tip, and inoculated into 3 ml of LB broth containing 100µg/ml ampicillin. Cultures were incubated overnight with shaking (180rpm) at 37°C. Overnight cultures were checked for growth by visual identification of turbidity, and 2 ml of culture was centrifuged at 13,000 rpm for 10 minutes to pellet cells. The cell pellet was resuspended in 500µl 70% glycerol, of which 450µl went into -80°C stocks and the remaining 50µl was transferred to a sterile 96-well plate (Sterilin), also stored at -80°C. In total, 96 recombinant colonies were picked for each environmental sample in question, for both bacterial and where relevant, archaeal communities.

For sequencing, 50µl of each glycerol stock clone was sent within 96-well plates on dry ice via courier to the NERC Biomolecular Analysis Facility (NBAF) sequencing facility at Edinburgh (<http://genepool.bio.ed.ac.uk/>), where they were sequenced with primers M13-20 and M13-R. Sequence data were edited and aligned using BioEdit (www.mbio.ncsu.edu/BioEdit/bioedit.html), and each sequence was submitted to the CHECK_CHIMERA program of the Ribosomal Database Project (RDP, <http://rdp8.cme.msu.edu/cgis/chimera.cgi?su=SSU>) (Cole *et al.* 2003) for chimeric sequences. For alignment, the ClustalW alignment tool was used to align sequences between 600 – 700bp in length, covering variable regions V1 – V4. Environmental clone sequences were compared with database sequence data deposited in GenBank using the Basic Local Alignment Search Tool (BLAST) (www.ncbi.nlm.nih.gov/blast) to search the nucleotide database nr/nt for highly similar nucleotide sequences using the megablast algorithm (Morgulis *et al.* 2008; Altschul *et al.* 1990), and also the RDP classifier (<http://rdp.cme.msu.edu/classifier/classifier.jsp>, Wang *et al.* 2007) to identify clones, usually at the genus level. Bootstrap cut-off values used were >80% (default), but classification was typically at 100% confidence. Phylogenetic tree construction for clones was conducted using software available on RDP, which uses the Weighbor weighted neighbor-joining tree building algorithm

(<http://rdp.cme.msu.edu/treebuilder>). Trees were drawn using the Interactive Tree of Life version 1.6.1. (Letunic & Bork 2007).

2.5 Analytical Techniques

The following section describes analytical techniques and instrumentation that were used for providing background mineralogical and geochemical context for samples used for both microbiological and experimental work.

2.5.1 Thin Sectioning and petrographic analysis

Standard geological thin sections provide the quickest and simplest way to identify rock mineralogy and rock texture, and these were prepared by Mr. Sean Holding at UCL. Rock samples were sawn to produce a flat surface, which was then attached to a glass slide by epoxy resin and dried for 1 hour. The sample was then sawn further and ground down to a width of 30 microns. The thin sections were left uncovered and diamond polished. Thin section images were taken using a Leica microscope with either 10x, 20x, or 40x objectives using a high quality 35mm exposure film.

2.5.2 Scanning Electron Microscope (SEM)

Scanning electron microscopy allows detailed micron-scale topographic imaging, whereby a beam of electrons interacts directly with the sample. In addition to topographic information, this interaction also results in the generation of x-rays and backscattered electrons, which provide information on elemental composition and relative atomic number respectively. A Jeol Scanning Electron Microscope (JSM-6480LV) with combined Energy Dispersive X-Ray Spectrometer (EDS) and back scatter electron (BSE) detector was used to image and analyse thin sections and rock fragments. Diamond polished thin sections were carbon coated whilst rock fragments/chips were mounted onto an aluminium stub with epoxy resin and silver cement, then gold coated prior to analysis. An accelerating voltage of 15kV was typically used, and EDS elemental analysis was quantified against a cobolt standard.

2.5.3 Raman spectroscopy

Raman spectroscopy was used in Chapter 6 to provide identification of mineralogical species within geological samples. Raman spectroscopy provides

information regarding molecular structure, via the interaction between a focused beam of monochromatic light (laser) at a pre-defined wavelength, and the three-dimensional atomic structure of the material. It is beneficial firstly due to its use on untreated samples, and secondly due to its largely non-destructive nature. Raman spectra were obtained from untreated samples with a Renishaw InVia Raman Spectrometer with a Leica microscope attachment, using either 785nm or 514nm laser wavelengths. Spot size was ~10 μ m using a x50 microscope objective. Typically spectra were gathered from 10 accumulations using an acquisition time of 10 – 20 seconds with laser power ranging between 10 – 100% depending upon fluorescence, sample degradation and clarity of the Raman signal. For identification of mineral species, Raman spectra acquired from the samples were compared against the RRUFF database of Raman spectra (<http://rruff.info/>; Downs 2006).

2.5.4 Inductively coupled plasma atomic emission spectroscopy (ICP-AES)

ICP-AES is used to identify elements and their concentrations, and is used here for water analysis only. Inductively coupled plasma is used to excite atoms within the sample, causing them to emit light, the wavelengths of which are characteristic of particular elements. A Horoba JY Ultima 2C ICP-AES was used in Chapter 5 to identify and quantify the cation concentrations within an experimental water sample. This was conducted at the Wolfson Laboratory for Environmental Geochemistry by Mr. Tony Osborn.

CHAPTER 3

BACTERIAL DIVERSITY OF BASALTIC LAVAS FROM CENTRAL ICELAND

This chapter forms the first of five central chapters documenting the research undertaken during this PhD. This work therefore opens by tackling the first in a series of questions regarding Martian analogue environments on Earth: what life is presently residing there? Here, the uncultured bacterial community is explored in a basaltic lava environment that is considered to be analogous to past volcanic environments on Mars. This was with the aim to explore the three following objectives specifically:

Firstly, the geological context within which the basaltic environments exist is detailed, including the formation of this environment, its physiochemical characteristics, and the local climatic conditions.

The bacterial communities are then explored as a function of lithology. A basaltic subglacial volcanic eruption commonly produces two lava types of contrasting texture and mineralogy, formed from the same initial magma source. These are pillow lavas and hyaloclastite, and the bacterial communities are examined from each of these lithologies individually.

Thirdly, within pillow lava itself there are a number of different components, including the chilled unaltered glassy rind, and the interpillow volcanoclastic deposits, rich in hydrothermal alteration minerals. These two components are also examined individually with regards to their microbial communities.

3.1 Colonisation of basaltic lavas

Basalt is the most widespread geological substrate on both Earth and Mars, often forming as a result of mantle decompression melting, but is also a common feature of hot spot volcanism (Wilson 2009). Pillow lavas especially are thought to be the most common volcanic rock on Earth (Fridleifsson *et al.* 1982), albeit largely within oceanic environments. Lavas can be erupted within a submarine, subglacial, or subaerial environmental setting. This produces a variety of lithologies, which can also vary in their geochemistry. They can be generally characterised based on their varying silica, alkali (Na and K), magnesium, and iron contents. Additionally, basalts subjected to aqueous or hydrothermal processes after emplacement can experience a change in geochemistry, either through the removal of certain chemical species or the deposition of secondary minerals. As a result, basaltic lavas form a vast array of different environments available for microbial colonisation.

Oceanic basaltic lavas exposed at the seafloor have been subject to much investigation regarding their microbiota over the past few decades. Basaltic lavas erupted from mid-ocean ridge systems are widely found to be colonised and altered by a range of bacterial and archaeal chemosynthetic-based microbial communities. These exploit the redox gradients between reduced species (e.g. Fe²⁺) in basalt and oxygenated sea-water (Santelli *et al.* 2008; Mason *et al.* 2007; Lysnes *et al.* 2004; Edwards *et al.* 2003; Thorseth *et al.* 2001). These communities are believed to be actively involved in the dissolution of basaltic glass (McLoughlin *et al.* 2009; Furnes *et al.* 2007 and references therein), potentially down to a depth of 500m (Furnes & Staudigel 1999). Additionally, basaltic lava habitats within the terrestrial deep subsurface have been of great interest in terms of understanding subsurface ecosystems both on Earth and potentially on other planets, such as Mars (McKinley & Stevens 2000; Stevens & McKinley 1995).

However, while the colonisation of subaerial basaltic rocks by lichen communities is well known and relatively well understood (Chen *et al.* 2000), the prokaryotic community inhabiting terrestrial basaltic lavas has been largely unexplored, in basaltic lavas that exist within arctic climates even less so. Previous work identifying a novel colonisation strategy of cryptoendolithic

microorganisms within basaltic lava from Svalbard highlighted the importance of basaltic lavas in providing a habitat for life within hostile environments (Jorge Villar *et al.* 2006). Likewise, recent work by Cockell *et al.* (2009a; 2009b), and Herrera *et al.* (2009) has demonstrated the exploitation of basaltic hyaloclastites as a suitable volcanic habitat for crypto- and chasmoendolithic life. As a result, further exploration of basaltic lavas is needed to identify the microbial communities that inhabit lavas within such harsh environmental settings. Basaltic lavas within arctic environments have often interacted with ice, due to the high latitude and increased elevation of the volcanoes that produce them. As a result, many volcanoes at polar or near-polar locations have been erupted subglacially (Chapman *et al.* 2000). This subglacial volcanism produces lithologies more comparable to those found on the ocean floor than to typical terrestrial lavas. Specifically, pillow basalts and hyaloclastites are commonly formed during basaltic subglacial volcanic eruptions (Smellie 2007).

The aim of this work was to explore the prokaryotic diversity of Arctic subglacial basaltic lavas, with particular emphasis on exploring how microbial diversity and composition changes with lithology. It has been previously shown that bacterial diversity can decline with increased climatic severity within high latitude environments (Yergeau *et al.* 2007), but little work has been conducted regarding geological controls on microbial communities, particularly at high latitudes. Those that have done are typically focused on seafloor environments (e.g. Santelli *et al.* 2008; Inagaki *et al.* 2003), or on basaltic lavas in Hawai'i, where climatic conditions are temperate to tropical (Gomez-Alvarez *et al.* 2007). Specifically, this study centres around the 16S rDNA culture-independent analysis of prokaryotic communities from pillow basalt and hyaloclastite lava from the Askja caldera, Central Iceland.

3.2 The basaltic subglacial lava environment

A subglacial basaltic lava edifice on Earth typically consists of a sequence of pillow basalts and hyaloclastites. Pillow basalt mounds are formed of crystalline spherical – elongate lava pillows, each with its own glassy rind produced by quenching of the magma. In between these pillows are cemented fragments of glass, rock, and hydrothermal mineral deposits, formed via aqueous alteration of the lava by hydrothermal fluids travelling along pillow boundaries (Bloch &

Bischoff 1974). Pillows also contain numerous vesicles, formed by trapped gas within the magma that was unable to escape due to the overlying pressure of the ice (Hoskuldsson & Sparks 2006). In contrast are hyaloclastite lavas. These volcanoclastic rocks consist of fragmentary material – shards of glass and scoria welded together – formed by more explosive eruptions into meltwater beneath the ice (Smellie & Skilling 1994). The glass is thermodynamically unstable, and as a result the smallest glass fragments are quickly altered to palagonite, which generally consists of iron rich phyllosilicates (clay minerals) such as smectite clays (Stroncik & Schmincke 2002; Thorseth *et al.* 1991). This forms a matrix around the surviving glass clasts and lithic fragments, cementing the rock.

These two different lithologies are very different in physical structure and bulk mineralogy, despite having the same initial melt geochemistry (if they erupted from the same magma). Meteoric and hydrothermal fluid pathways exploited by colonising microbes in pillow basalt lavas are predominantly between pillows and through interconnecting vesicles. Hyaloclastites however are clastic rocks, and fluid flow here is confined to grain boundaries, fractures and pore spaces within the rock. It is therefore hypothesised that despite having similar initial bulk chemistries, and experiencing the same external environment, the prokaryotic communities inhabiting these lavas will be different as a result of their differing lithology. Specifically, hyaloclastites may be colonised by a more soil-like community. This is due to hyaloclastites having a higher palagonite content. Indeed, previous studies conducted have observed a similarity between hyaloclastite communities and those of soil. These studies have been carried out on Icelandic subglacial lavas from south Iceland, on both basaltic hyaloclastite (Cockell *et al.* 2009a,b) and rhyolitic obsidian (Herrera *et al.* 2009; 2008). They found a high level of prokaryotic diversity present within the lavas, and represent some of the first studies on subglacially-erupted lavas in Arctic environments. Importantly, the microbial community present within Icelandic hyaloclastite from south Iceland shared no similarity with phylogenetic sequences obtained from seafloor basaltic lavas, and instead found a dominantly heterotrophic community present, with a distinct lack of chemolithotrophic microorganisms (Cockell *et al.* 2009a). As suggested by the authors, this largely reflects the different environmental conditions experienced by Icelandic

terrestrial lavas (aerobic, periodic desiccation, solar radiation) compared to deep sea oceanic environments.

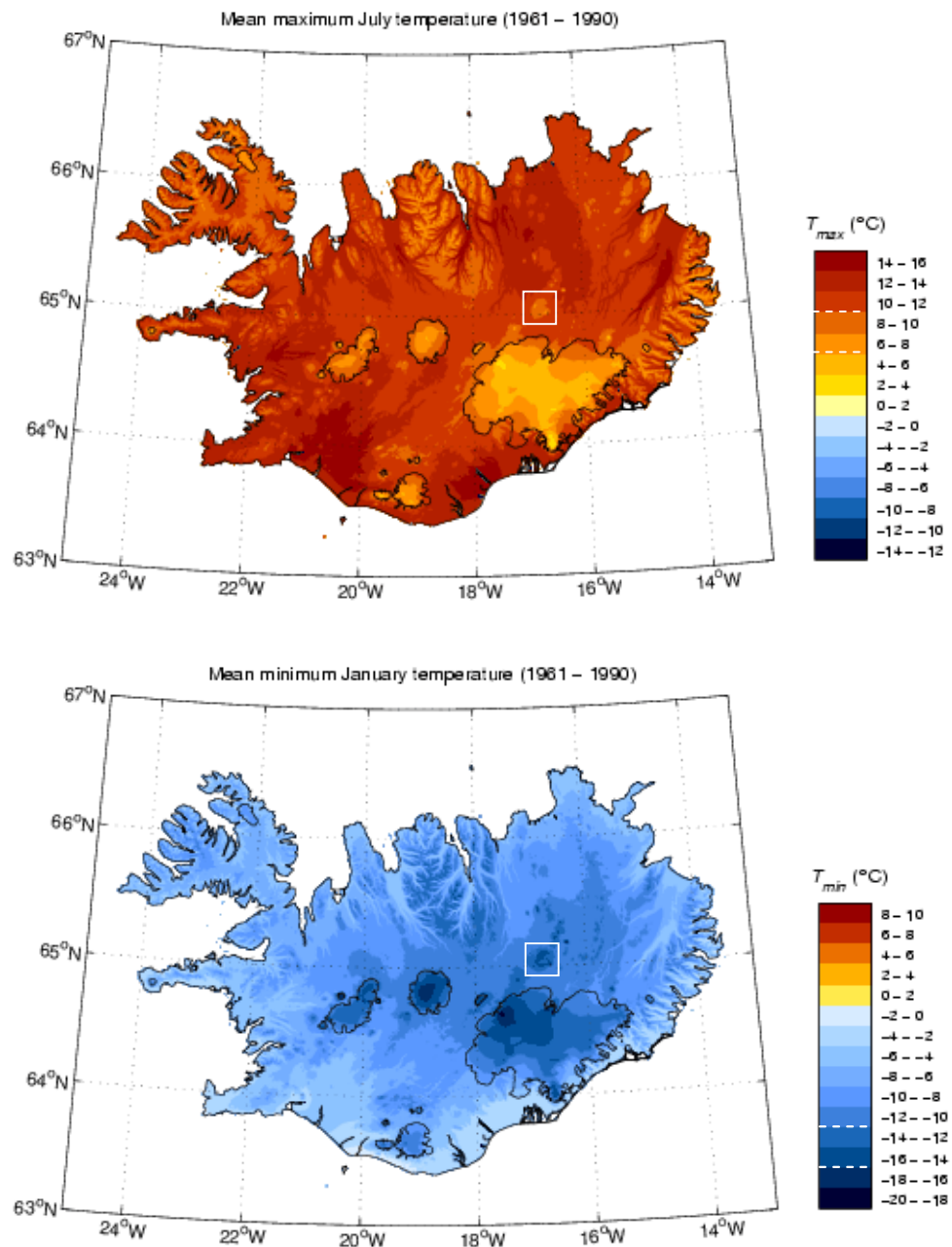
Samples of Pleistocene subglacial lavas were collected in July 2006 from Askja volcano. These lavas have since been exposed by glacial retreat during the last 10,000 years (Sigvaldason 2002). The terrain here is entirely volcanic and consists of stretches of volcanic sand, pumice and more recent subaerially - erupted lavas that surround older subglacially erupted pillow basalts and hyaloclastites. There is no weather station at Askja, but typically the driest areas just north of Vatnajökull receive less than 400mm annual precipitation (Einarsson 1984), and temperatures can range from 4 - 6°C in summer (July), down to as low as -10 to -12°C in winter (January). Additionally, daylight hours vary greatly on a seasonal basis due to the near-polar latitude of Iceland. Whilst Iceland lies just below the Arctic circle, it still experiences almost complete daylight mid-summer, contrasting with only a few hours of daylight during winter. Pillow lava and hyaloclastite were collected from two locations ~3km apart around the Askja caldera rim (Figure 3.1).

Figure 3.1. Aerial view of the Askja caldera eastern rim where sample environments ASK9 and ASK4 are located. Pale grey terrain is loose rhyolitic pumice, whilst the topographically high areas are subglacially-erupted lava flows, which underlie the pumice deposit. To the north is the 1961 basaltic subaerial lava flow, whilst Öskjuvatn (lake) can be seen to the south-west. ASK9 lies in a steep river-cut gorge. NB: illumination from the south.



The lavas here contain little macroscopic plant life. Volcanic sands exist in and around the lava flows and edifices, within which intermittent patches of coarse Marram grass grow. The oldest lavas – those that were subglacially erupted – have been subject to very limited epilithic lichen colonisation, typically on north-facing damp rock surfaces.

Figure 3.2. Map of mean maximum and minimum temperature for July and January respectively (data available from the Icelandic Meteorological Office, <http://en.vedur.is/>). Askja is indicated by the white box on the map, and the representative temperature range is highlighted on the scale.



3.2.1 Pillow lava (ASK9)

This pillow pile (P) is located inside a narrow river-cut gorge, on the south facing slope. It overlies a small section of fine-grained hyalotuff (H) on one corner, surrounded by a steep scree slope and is overlain by a thin lava flow (L) on top (Figure 3.3). The pillows themselves were very glassy and show evidence for hydrothermal alteration along pillow boundaries. This alteration has produced white, red and yellow coloured mineral deposits (see Figure 3.3). Pillows were all a similar size (~50 cm across) and all were elongate in shape. The pillows are fine grained and contain numerous small vesicles, all 0.5 – 2 mm in size, which are evenly distributed throughout the individual pillows. Multiple lava samples were collected from glassy, relatively unweathered regions of pillows. Specifically, samples fall into two broad categories: lava containing quenched glassy rinds; and hydrothermally altered interpillow material typically consisting of fragmented glass, volcanoclastics, and hydrothermal mineral deposits.

Figure 3.3. a) Context field view of pillow basalt outcrop with underlying hyalotuff (H) and overlying subaerial lava flow. Arrow points to person for scale. (Photo credit: Dr. Katie Joy 2007); b) typical pillow morphology; c) alteration between pillows.



Whilst there was a small outcrop of hyalotuff underlying the pillow basalt, it was not sampled for assessing microbial diversity. This outcrop lay particularly close to the water line of the river flowing through the gully. As such, unlike the pillow basalts higher up, it was possible that the hyalotuff was perhaps seasonally affected by the river. Even though the outcrop was sampled during summer when river discharge is generally at it's highest, it was decided that the low-lying position of this outcrop was compromised with regards to assessing microbial diversity from very dry volcanic environments. Additionally, some of the best pillow samples could be accessed by climbing on top of the hyalotuff, and as such the outcrop was no-longer considered 'pristine'.

3.2.2 Hyaloclastite lava (ASK4)

Outcrops of hyaloclastite surround Askja and range from fine grained and well sorted, to unsorted with coarse glass and lithic fragments. The outcrops themselves often display clearly defined depositional banding. Patchy orange–grey colouration can be seen in all outcrops and is a result of low temperature aqueous alteration of glass resulting in palagonite formation. The hyaloclastites collected for this study all came from the same isolated outcrop, and consist of 2 – 4mm sized glass fragments within a palagonite matrix. The hyaloclastite displayed little variation within the outcrop.

Figure 3.4. Context photograph of the hyaloclastite outcrop at Askja (ASK4). Arrow points north. (Rh = Rhyolitic pumice deposit from 1874 eruption; H = hyaloclastite; L = 1961 lava flow). Bag for scale in far right of the photograph.



Representative lava samples from these two sites were selected for physiochemical and microbiological analysis. Bulk geochemistry of the original lava melt (glass) was determined with an Energy Dispersive X-ray System (EDS), and details of structural analysis of the lavas is described in the following section. For phylogenetic analysis, 96 cloned representatives each for pillow lava glass, interpillow, and hyaloclastite were sequenced for taxonomic identification.

3.3 Physical and chemical analysis

3.3.1 Macro texture

Figure 3.5 and 3.6 show hand samples of the hyaloclastite, pillow basalt glass, and interpillow material. Hyaloclastite is considerably more friable than the pillow basalts, due to its phyllosilicate-rich composition and clastic structure. Vesicles in hyaloclastite only exist sealed within the larger glass clasts of the rock, whereas vesicles make up a high proportion of the pillow lavas, even within and near to, the outer glassy rind. The outer surfaces of interpillow and glassy pillow lava samples used in this study were devoid of any macroscopically visible biological colonisation. Glassy rinds of pillows consist of very fresh, unaltered glass, with no evidence of large scale weathering. Additionally, this glass has not been palagonitised indicating limited interaction with water. In contrast, interpillow material shows clear evidence of hydrothermal alteration and aqueous interaction, with the deposition of secondary minerals and subsequent alteration of glass, although there were still areas where significant quantities of fresh unaltered glass remained. Calcite and gypsum deposits are particularly common, together with sulphur and iron-rich mineral alteration products.

Figure 3.5. a) ASK4 hyaloclastite, with glass and scoria clasts surrounded by a palagonite-rich matrix; b) ASK9 Pillow Lava ‘Glass’ sample showing the black unaltered glassy rind; c) ASK9 Pillow Lava ‘Interpillow’ sample showing vesicular fresh glass fragments welded with hydrothermal minerals. Scale bar = 1cm.

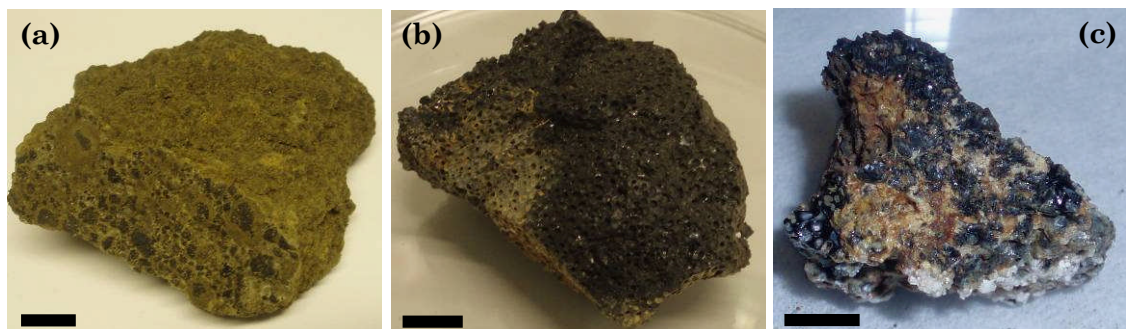
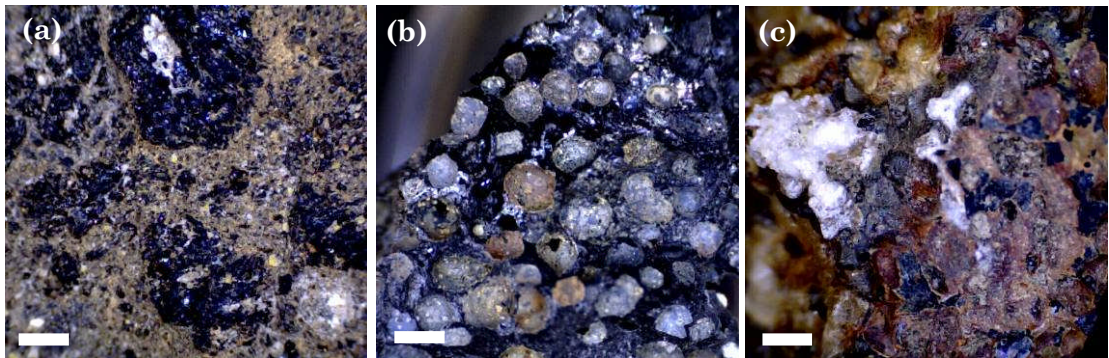


Figure 3.6. Digital microscope images of all three environments highlighting their morphological and mineralogical differences. a) ASK4 hyaloclastite; b) ASK9 pillow basalt glass; c) ASK9 interpillow. Scale bar 1mm.

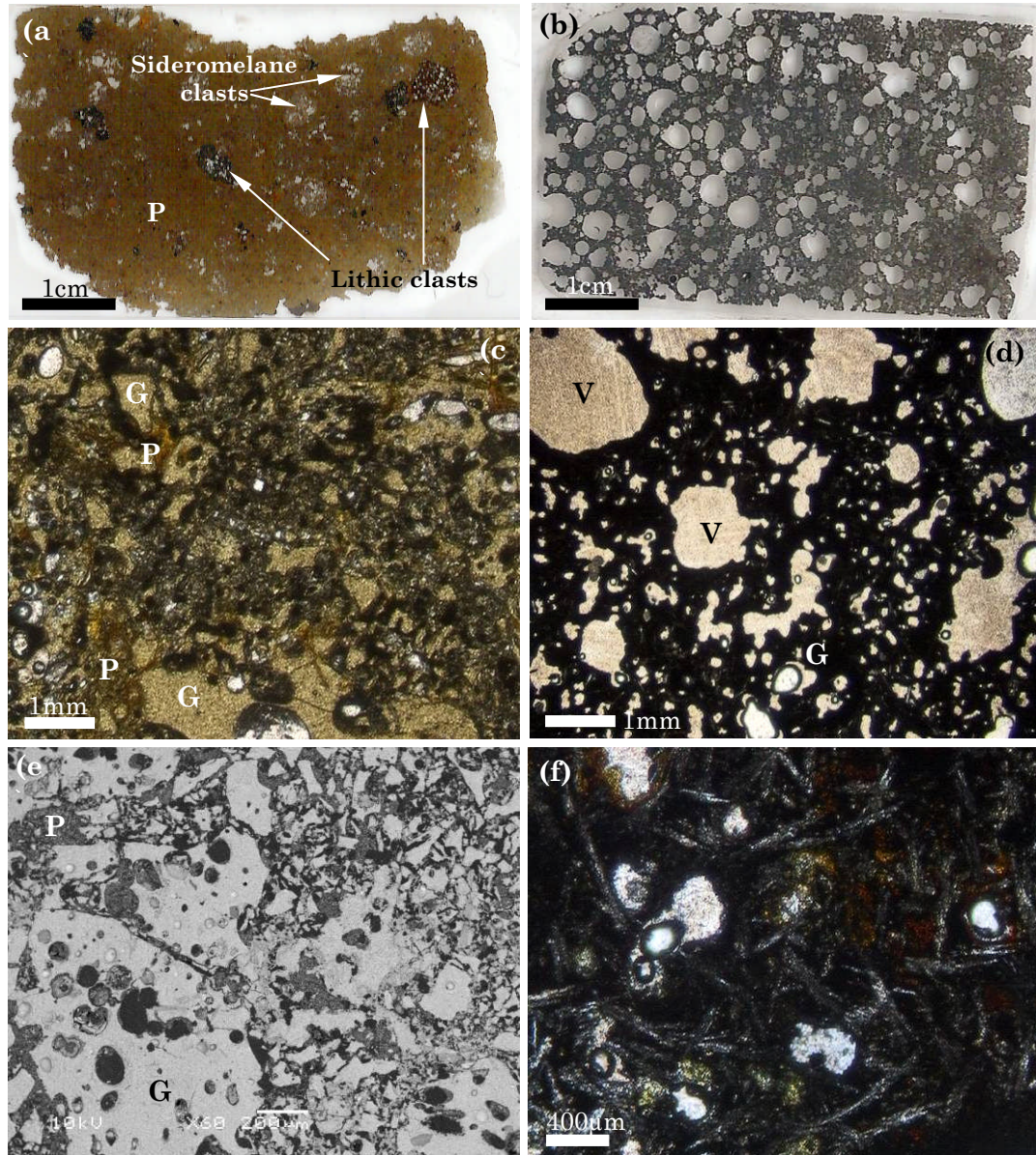


3.3.2 Micro structure

3.3.2.1 Thin section analysis

Petrographic thin sections were made of the ASK9 Pillow Lava and ASK4 Hyaloclastite. Unfortunately, a thin section could not be produced for the ASK9 Interpillow material due to difficulties in making the thin section and limited sample quantity. Petrographic and Back Scatter Electron (BSE) analysis of the lava thin sections show a different mineralogy and texture between the hyaloclastite and pillow basalt. ASK4 hyaloclastite has coarse 1 – 5 mm sized lithic fragments (fine grained lava and scoria) and numerous angular to sub-angular sideromelane (basaltic glass) clasts >1mm cemented by a fine yellow – orange – brown coloured palagonite matrix. Under BSE it can be seen that the larger of these sideromelane clasts are very vesicular, all with nearly-spherical vesicles (Figure 3.7). ASK9 pillow lava is highly vesicular, with numerous rounded to irregular vesicles across a range of sizes (typically >4mm). The pillow lava itself consists of an incredibly fine-grained matrix, containing small plagioclase laths (70%), and occasional small anhedral olivines and pyroxenes, all indicative of rapid cooling of the lava. There are no phenocrysts present. Lastly, despite the widespread occurrence of bioalteration textures in oceanic basaltic lavas (see Chapter 1, Section 1.4.3), none were identified in these pillow lavas and hyaloclastites. All palagonite-glass alteration boundaries were smooth and consistently banded, typical of abiotic aqueous alteration (Furnes *et al.* 2007). Likewise, textural studies of hyaloclastites from southern Iceland revealed a distinctive lack of tubular bioalteration textures emanating from glass/palagonite boundaries, although ‘pitted’ bioalteration weathering textures have been identified (Cockell *et al.* 2009a; Thorseth *et al.* 1992).

Figure 3.7. Petrographic (a, b, c, d, f) and BSE (e) thin section images of lavas ASK4 (left-hand side) and ASK9 (right-hand side). ASK4 hyaloclastite containing angular to sub-rounded vesicular basaltic glass (sideromelane) clasts ‘G’, lithic clasts, all surrounded by palagonite ‘P’; ASK9 pillow basalt showing numerous vesicles ‘V’; surrounded by a black, very fine-grained groundmass ‘GM’. In (f) the groundmass can be seen to consist of many small, randomly orientated plagioclase feldspar laths.



3.3.2.2 Porosity

The amount and nature of porosity of the lavas also varied. Estimates of porosity were undertaken utilising two simple methods. A saturation-based method was carried out whereby the lava sample was submerged in 20ml water for 36 hours with regular agitation to release trapped air and allow full saturation of the lava with water. The remaining water was then removed and measured, and used to calculate porosity (see Appendix B, Equation 1).

Following this, the saturated sample was weighed, and the difference between saturated and dry weight was used to calculate porosity based on sample volume. Values obtained via this method are likely to represent the minimum porosity, as water from surface vesicles is easily lost. In addition, estimated 2D porosity was done digitally using lava thin section images from three scales: x1 (scanned thin section), x4 (petrographic light microscope image), and x60 (BSE image). Digital images were processed using ImageJ software (<http://rsbweb.nih.gov/ij/>) which calculated the percentage of area consisting of vesicles within the rock thin section. Due to the 30 μ m thickness of the thin section, any pore spaces <30 μ m will not be accounted for. Vesicles in hyaloclastite only exist sealed within the larger glass and lithic clasts of the rock, whereas pillow basalt and interpillow material remain highly vesicular throughout, with vesicles commonly up to 3mm in size. Porosity measurements of the lavas are shown in Table 3.1. Overall, ASK9 pillow basalt has a slightly higher interconnected porosity (24.9% (\pm 0.17) for the pillow lava, 24.4% (\pm 0.47) for interpillow material) in comparison to ASK4 hyaloclastite (22.7% \pm 0.36), as determined by 3D saturation and evaporation tests. Porosity estimations by 2D digital image analysis give a greater percentage of porosity for ASK9 pillow basalt (31.9% (\pm 4.0)) compared to the 3D estimation. This can be related to the fact that the digital analysis accounts for all pore spaces, including those that are entirely sealed and therefore not interconnected. Conversely, the digital image analysis of ASK4 hyaloclastite gives a considerably lower porosity value, as the majority of pore spaces within the lava are too small to be identified digitally, existing as numerous fine fracture and crystal boundary networks within the lava. This difference in internal structure and porosity of the lavas may play a role in influencing the colonising prokaryotic community.

Water is one of the most important constituents of an environment. As such, the moisture content of lavas ASK4 and ASK9 was determined gravimetrically. Representative samples were weighed, dried at 50°C until constant weight was achieved (after 4 days), then weighed again to determine water loss through evaporation. It was found that ASK4 hyaloclastite had more than twice the moisture content than ASK9 pillow lava. ASK9 had a moisture content of 0.65% (ASK9 Interpillow 0.71%), compared with 1.94% for ASK4. This is perhaps unsurprising when considering the far greater clay content of the hyaloclastite.

When exposed to the atmosphere, smectite clays are able to adsorb or lose water, depending upon the localised humidity, leading to expansion and shrinkage of the rock. Repeated over time, this expansion and shrinkage produces surface cracks and flaking of the rock, allowing more water to enter the lava (Bell 2000). Due to the seasonal extremes experienced by lavas in Central Iceland, it is likely seasonal shrinkage and expansion plays an important role in shaping the physical microenvironment inside the lavas. During winter months here, water saturation will be highest as a result of constant snow cover, and evaporation greatest during late spring-early summer. The moisture contents are very low, and are comparable to the moisture contents of Antarctic Dry Valley soils (Fell *et al.* 2006; Cowan *et al.* 2002). This is largely due to the fact that these environments are solid rocks, not unconsolidated soils, which due to their greater surface area have the ability to hold and adsorb more water. This is an important factor when considering the conditions that exist within these extreme microenvironments.

Table 3.1. Porosity estimates based on 3D experimental and 2D digital quantification; and moisture content determined gravimetrically. Error is standard deviation.

| Lava | Porosity (%) 3D Measurement (Saturation) | Porosity (%) 2D measurements | | Moisture content (%) |
|-----------------------|---|------------------------------|------|----------------------|
| | | Scale | % | |
| ASK4 hyaloclastite | 22.3 | x 1 | 3* | 1.94 |
| | 22.8 | x 4 | 1.2* | |
| | 23 | x 60 | 2.1* | |
| <i>Mean</i> | <i>22.7 (±0.36)</i> | <i>2.1 (±0.9)</i> | | |
| ASK9 pillow basalt | 25 | x 1 | 36 | 0.65 |
| | 25 | x 4 | 28 | |
| | 24.7 | x 60 | 31.7 | |
| <i>Mean</i> | <i>24.9 (±0.17)</i> | <i>31.9 (±4.0)</i> | | |
| ASK9 Interpillow | 24.9 | N/A | | 0.71 |
| | 24 | | | |
| | 24.2 | | | |
| <i>Mean</i> | <i>24.4 (±0.47)</i> | N/A | | |

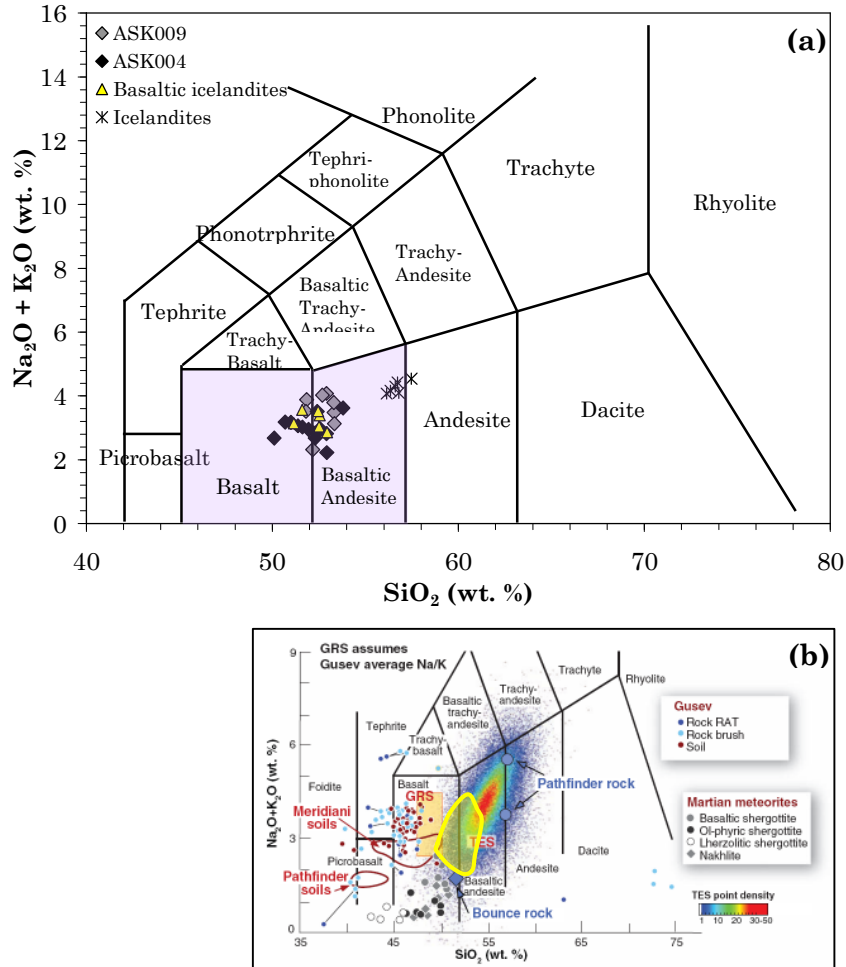
*Digital porosity measurements for ASK4 is believed to be inaccurate due to numerous small pore spaces (<30µm) that are indistinguishable from the surrounding matrix in thin section.

3.3.3 Geochemistry

The melt geochemistry of the pillow basalt (ASK9) and hyaloclastite (ASK4) is broadly the same, with little distinction between the two. Both the lavas can be classified as basaltic andesites on a Total Alkali – Silica (TAS) plot (Figure 3.8),

which is typical of basaltic ‘Icelandite’ (Jonasson 2005). Additionally, both lie on the line between tholeiitic and calc-alkalic lavas. For a table of all measurements see Table 1 in Appendix A.

Figure 3.8. a) TAS classification diagram (Le Bas *et al.* 1986) showing the composition of ASK4 and ASK9 lavas (normalised oxide wt.%). Both lavas lie between basalt and basaltic andesite compositions, consistent with Basaltic Icelandite. Data is also shown for typical Basaltic Icelandite and Icelandic lavas (Jonasson 2005); b) Field plot of the Askja lavas (in yellow) on a TAS of Martian rock composition (McSween *et al.* 2009) for comparison (for a larger version of this plot see Chapter 1, Figure 1.1.)



Pore water pH was measured by adding 2.5ml $d\text{H}_2\text{O}$ to 1g of crushed rock, and measuring the pH of this slurry (Brady & Weil 2002). This yielded pH values of 8.35 (± 0.35) and 7.65 (± 0.07) for the pillow lava and interpillow material respectively, and a pH of 7.35 (± 0.05) for the hyaloclastite. The pore-water aqueous environment that may transiently exist within the lavas therefore is neutral – slightly alkaline. It is likely that such aqueous conditions exist during initial snow melt influx into the lavas following the winter months, and also during snow-free seasons when rainfall occurs throughout summer and autumn.

3.4 Phylogenetic Analysis

Molecular taxonomic assessment was conducted using genomic DNA extracted directly from 5g of each of the lavas (see Chapter 2, section 2.4). Analysis of the communities present shows there to be a significant difference regarding bacterial diversity. Archaeal diversity was also investigated for all three lavas, and only appeared to exist within the hyaloclastite, but the number of clones was limited for reasons explained in the following section (3.4.1). For the bacteria, 290 individual environmental 16S rDNA clones were sequenced in total, (96 clones per lava) yielding sequences ~700bp long. Sequences trimmed to equal length and covering variable regions V1 – V4 were used to construct phylogenetic trees, and identify the dominant phylotypes within the lava community. Of all these sequences, 273 could be identified (using BLASTn) as similarly uncultivated microorganisms from a variety of environments, most of which are either Antarctic, lithic, or hot spring environments. However, many of these (57) shared less than 95% similarity, and some even as low as 86 – 88%. Likewise, comparison with isolated microorganisms showed low percentages, typically between 80 – 95%. Overall, 9 different bacterial phyla (including four subdivisions of the Proteobacteria) were identified from the bacterial community within both types of lava. These are all shown in a phylogenetic tree in Figure 3.9, along with their closest environmental and cultured relatives. Individual clone IDs are for the different lava lithologies as follows: bacterial clones from ASK4 hyaloclastite are prefixed with ‘ASK4B-’ followed by a number, clones from ASK9 pillow basalt are prefixed with ‘ASK9G-’ or ‘ASK9IP-’ for the glassy component of the lava and interpillow material respectively, again followed by a number. Additionally, a small number of archaeal clones were sequenced for the ASK4 hyaloclastite, and these are prefixed with ‘ASK4A-’ followed by a number.

Collectively, the phylogenetic tree shows the basaltic lava environment of central Iceland to be diverse, particularly considering the cold and dry nature of the environment. Clones that could not be identified at the phylum level using the RDP taxonomy classifier appear to broadly fall within the Chloriflexus and Firmicutes groups when displayed in a tree (Figure 3.9). These groups can be seen more clearly in the relevant lava-specific trees detailed further on in this chapter. The exception to this is two clones from the ASK9 Interpillow material (ASK9IP 48 and 84), which exist as a small clade of their own, falling closest to

3.4.1 Bacterial diversity of ASK4 hyaloclastite

Environmental clones identified from the hyaloclastite lava show the highest level of phylogenetic diversity of the three lava environments. As previously found in basaltic lava environments, Actinobacteria dominate, and make up 32% of the total community. Other dominant phyla contribute to the community in fairly equal portions, consisting of Bacteroidetes (13%), Acidobacteria (10%), Cyanobacteria (5%), Planctomycetes (9%), and Verrucomicrobia (9%). Notably, an additional 10% consisted of unclassified Bacteria that could not be identified at the phylum taxonomic level using the RDP classifier. Lastly, the remaining 12% consist of α - β - δ - and γ -Proteobacteria (between 1 – 3% each), Deinococcus-Thermus (2%), and one clone in the candidate phylum TM7 (1%), of which there are no cultured representatives. This top-level composition is highly comparable to that identified for hyaloclastite lava from the south of Iceland, which were also dominated by Actinobacteria (33%), Bacteroidetes (12%), Proteobacteria (28%), Acidobacteria (14%) and Verrucomicrobia (5%) (Cockell *et al.* 2009b).

Figure 3.10 shows a plot of the number of ASK4B hyaloclastite clones against the environment from which their most similar relatives were identified from, using BLASTn. Individual environments are displayed here in distinctive environmental groups. It is apparent that the majority of these closest relatives, all of which are also uncultured, come from cold and dry environments. In particular is the prevalence of Antarctic and Arctic environments, the individuals of which match 21 and 13 of the ASK4B clones respectively. As mentioned, phylotypes from the hyaloclastite are comparable to those identified from hyaloclastite in South Iceland by Cockell *et al.* (2009a,b), and this is also indicated here, with nine ASK4B clones having closest similarity to uncultured individuals from 'Terrestrial basaltic lavas, Iceland'. For details of the closest environmental relative for each and every clone, see Table 2 in Appendix A. Also shown in this plot are the number of phyla represented by these different individuals within the environment types. The plot shows the number of phyla covered by the ASK4B clones and their environmental relatives, which in some cases is as high as 4 or 5 different phyla, signifying a similarity in phylotype composition between the ASK4B community and those residing in other cold or arid environments. However, it is noted that such interpretation is heavily

reliant upon where such previous studies have been conducted (for example, a closer relative may exist in an as-yet unexplored environment).

Figure 3.10. Representative environments of BLASTn closest relatives of the ASK4B Hyaloclastite bacterial clones. Where clones from environmental types span more than one phylum, this is indicated by [#], which also gives the number of phyla.

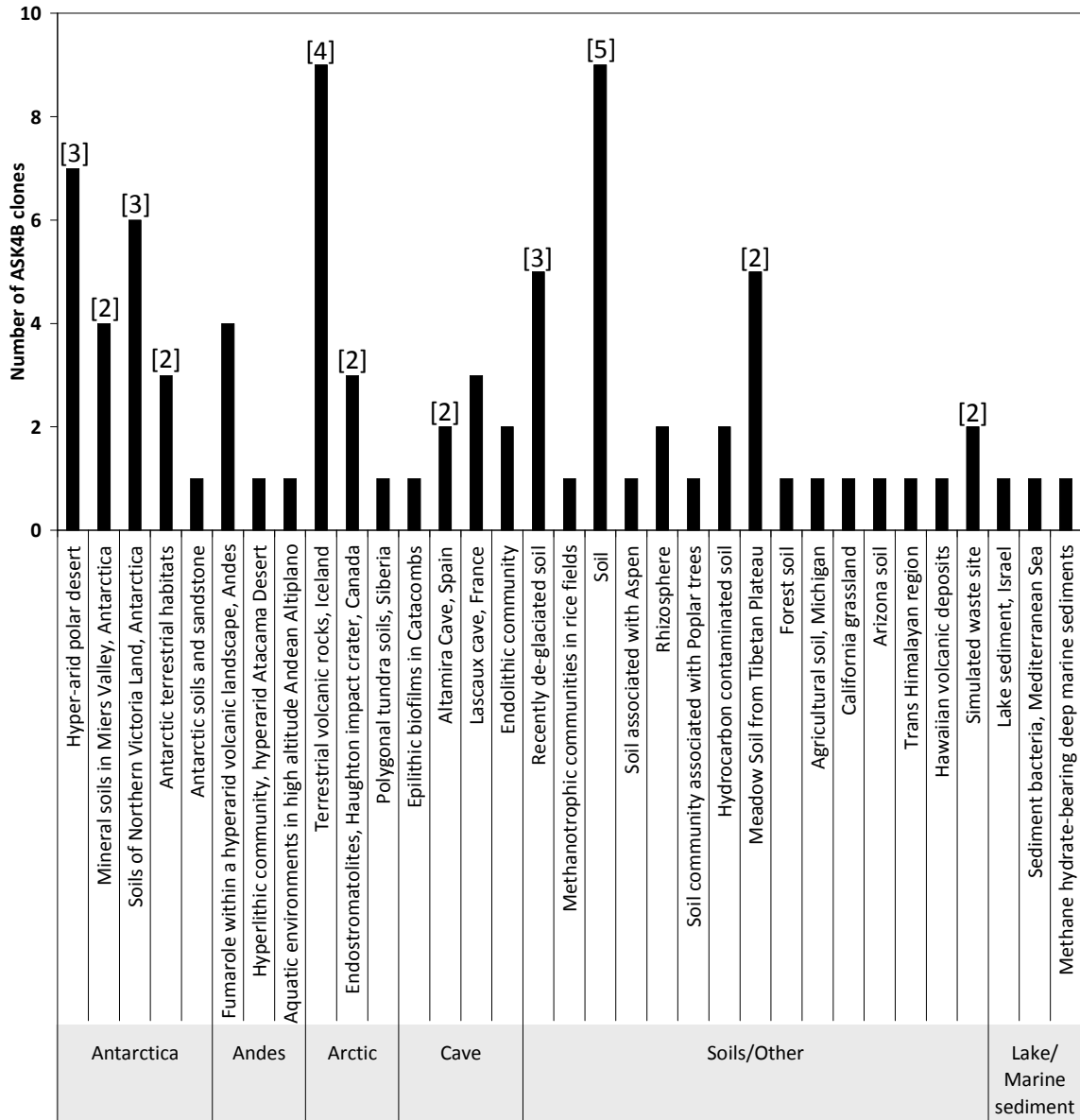


Table 3.2 below gives a representative sample of the ASK4B clones and details of their closest relatives. For a full list of all clones and their closest relatives, see Table 2 in Appendix A. Similarity percentages between the clones and known cultured species is typically low, with the highest similarity between clone ASK4B_16 and the cyanobacterium *Nostoc calcicola* (97%), and the lowest similarity between clone ASK4B_84 and δ -proteobacterium *Desulfovibrio vulgaris* (80%).

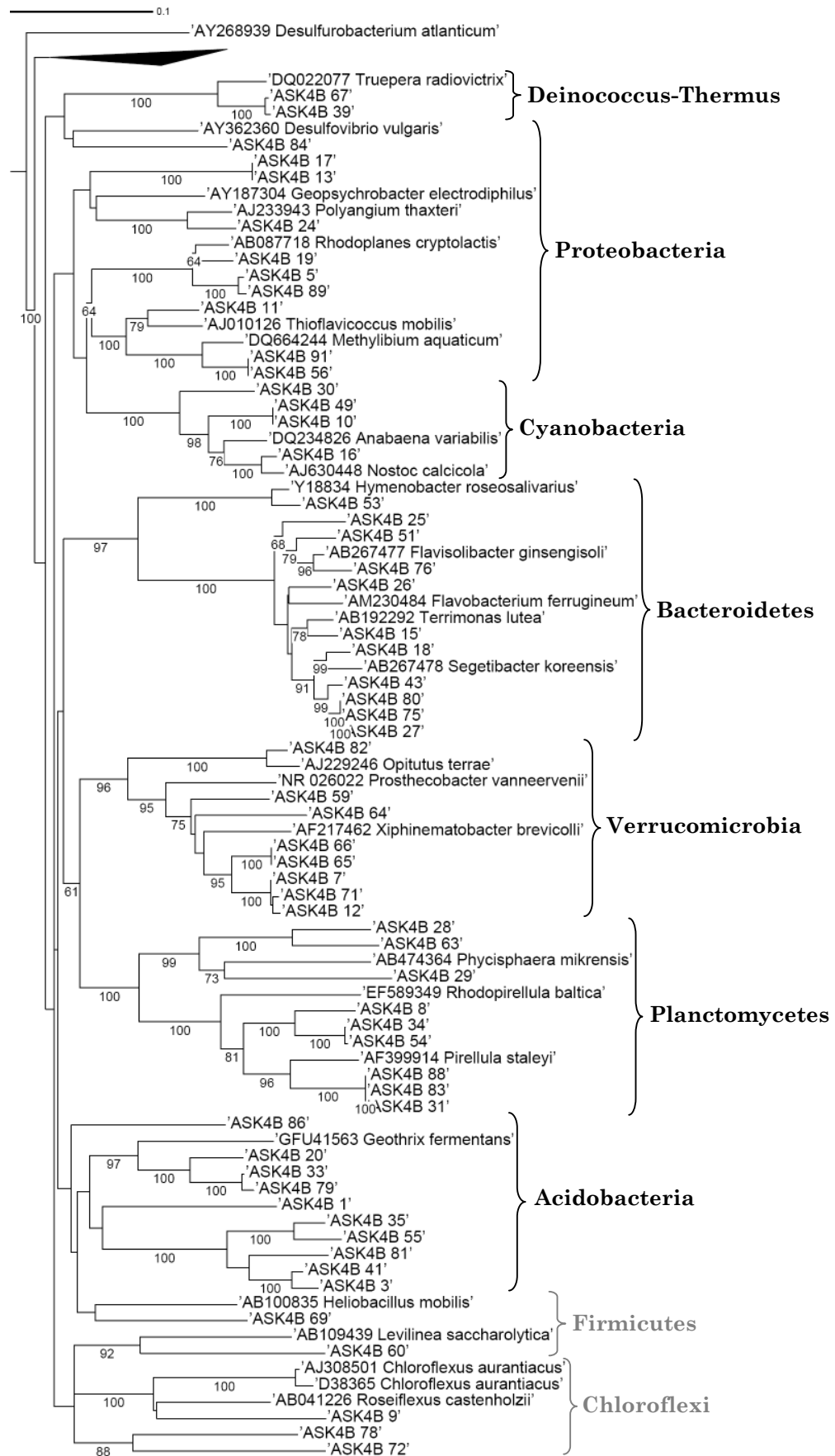
Table 3.2. Selected BLAST database closest environmental isolate/clone relatives and closest species based on 16S rDNA similarity (%) with the ASK4B Hyaloclastite environmental clones. For a full list of all clones see Appendix A.

| Closest relative | | | Closest cultured species relative | |
|----------------------------|-----|---|---|-----|
| ID (Accession #) | (%) | Sampling environment | ID (Accession #) | (%) |
| Actinobacteria | | | | |
| Uncultured (EU883162) | 96 | Endostromatolites, Haughton impact crater, Devon Island, Canada | Actinomadura glomerata (AJ293704) | 85 |
| Uncultured (FJ592818) | 99 | Fumarole within a hyperarid, high-elevation landscape on Socompa Volcano, Andes | Sporichthya polymorpha (X72377) | 92 |
| Bacteroidetes | | | | |
| Uncultured (EU335841) | 96 | Mineral soils in Miers Valley, Antarctica | Flavobacterium ferrugineum (AM230484) | 88 |
| Uncultured (FJ895072) | 98 | Hyper-arid polar desert | Segetibacter koreensis (AB267478) | 94 |
| Proteobacteria | | | | |
| Uncultured (GQ128065) | 99 | Meadow Soil from Tibetan Plateau | Rhodoplanes cryptolactis (AB087718) | 95 |
| Uncultured (EU373912) | 92 | Sediment bacteria, Mediterranean Sea | Geopsychrobacter electrophilus (AY187304) | 82 |
| Deinococcus-Thermus | | | | |
| Uncultured (FJ895086) | 99 | Hyper-arid polar desert | Truepera radiovictrix (DQ022077) | 91 |
| Acidobacteria | | | | |
| Uncultured (EF464954) | 96 | Soils of Northern Victoria Land, Antarctica | Chloracidobacterium thermophilum (EF531339) | 93 |
| Uncultured (GQ495424) | 99 | Terrestrial volcanic rocks, Iceland | Chloracidobacterium thermophilum (EF531339) | 81 |
| Verrucomicrobia | | | | |
| Uncultured (AB374368) | 97 | Endolithic community, 'White rock' Switzerland | Prostheco bacter vanneervanii (AJ966883) | 84 |
| Uncultured (GQ495404) | 98 | Terrestrial volcanic rocks, Iceland | Xiphinematobacter brevicolli (AF217462) | 86 |
| Cyanobacteria | | | | |
| Uncultured (FJ891015) | 98 | Hyperlithic community in quartz, hyper-arid core of the Atacama Desert | Arthrospira platensis (EF432320) | 90 |
| Planctomycetes | | | | |
| Uncultured (EF464902) | 98 | Soils of Northern Victoria Land, Antarctica | Pirellula staleyii (AF399914) | 90 |
| Uncultured (GQ396898) | 99 | Recently de-glaciated soil | Pirellula staleyii (AF399914) | 84 |
| Unclassified | | | | |
| Uncultured (EU644222) | 100 | Terrestrial volcanic rocks, Iceland | Gloeobacter violaceus (BA000045) | 79 |
| Uncultured (EF632950) | 93 | Aquatic environments in high altitude Andean Altiplano | Phycisphaera mikrensis (AB474364) | 81 |

With regards to evolutionary relationships, the phylogenetic tree in Figure 3.11 shows many of the ASK4B clones to be either deeply branching or distantly related to many known species of Bacteria. Particularly interesting are those clones that appear most closely related to representative species of the Firmicutes and Chloroflexi groups. These clones could not be classified at the phylum level by the RDP classifier, and their closest species relatives have a low level of similarity, between 80 – 82%. The tree is particularly useful in identifying clones that are highly similar with little to no genetic variation, and as such are likely to be multiple representatives of the same species within the hyaloclastite environment. The level of diversity is relatively high, and typically no more than two or three clones share this level of similarity. Examples of those that do can be found within nearly all phyla, including the Bacteroidetes (ASK4B_80, _27, and _75), Cyanobacteria (ASK4B_10 and _49), Planctomycetes (e.g. ASK4B_88, _31, and _83), and Proteobacteria (e.g. ASK4B_13 and _17).

Whilst there are many clades of ASK4B clones that appear phylogenetically distinct from known species and genera, there are at least some which can be closely associated with cultivated bacteria, the physiology of which is often well known. Clone ASK4B_16 for example shares high similarity (97%) with the cyanobacterium *Nostoc calcicola*. Cyanobacteria species within the genus *Nostoc* are distinctive in their ability to remain desiccated for months or even years, with full metabolic recovery following re-hydration (Dodds *et al.* 1995). In addition, they are able to withstand repeated freeze-thaw cycles, and can fix atmospheric nitrogen (Dodds *et al.* 1995). As such they are found in polar environments (e.g. Jungblut *et al.* 2009; Hawes *et al.* 1992), and are clearly well adapted to the Icelandic hyaloclastite lava environment. The species with the next highest similarity is the Proteobacterium *Rhodoplanes cryptolactis*, which is the closest cultured match for three of the ASK4B clones (ASK4B_19, _5, _89), at 94 – 95%. Interestingly this species is a type of photolithotrophic thermotolerant purple non-sulphur bacteria common to hot spring environments (Okamura *et al.* 2007). Therefore this particular species would not necessarily be expected to inhabit the cold and dry basaltic lava environment. Reasons for this are discussed further on in this chapter. The remaining closest cultured relatives had a similarity typically of 90% or less, and as such these species are unlikely to be representative of their corresponding species indentified in the hyaloclastite.

Figure 3.11. Phylogenetic tree of ASK4 hyaloclastite bacterial clones (ASK4B) and closest relatives. Collapsed branch represents Actinobacteria (shown in Figure 3.17). Clones within Chloroflexi and Firmicutes (in grey) were not classified by RDP Taxonomy. Scale bar represents number of nucleotide position changes, and bootstrap values >60 are shown. *Desulfurobacterium atlanticum* is used as the outgroup.

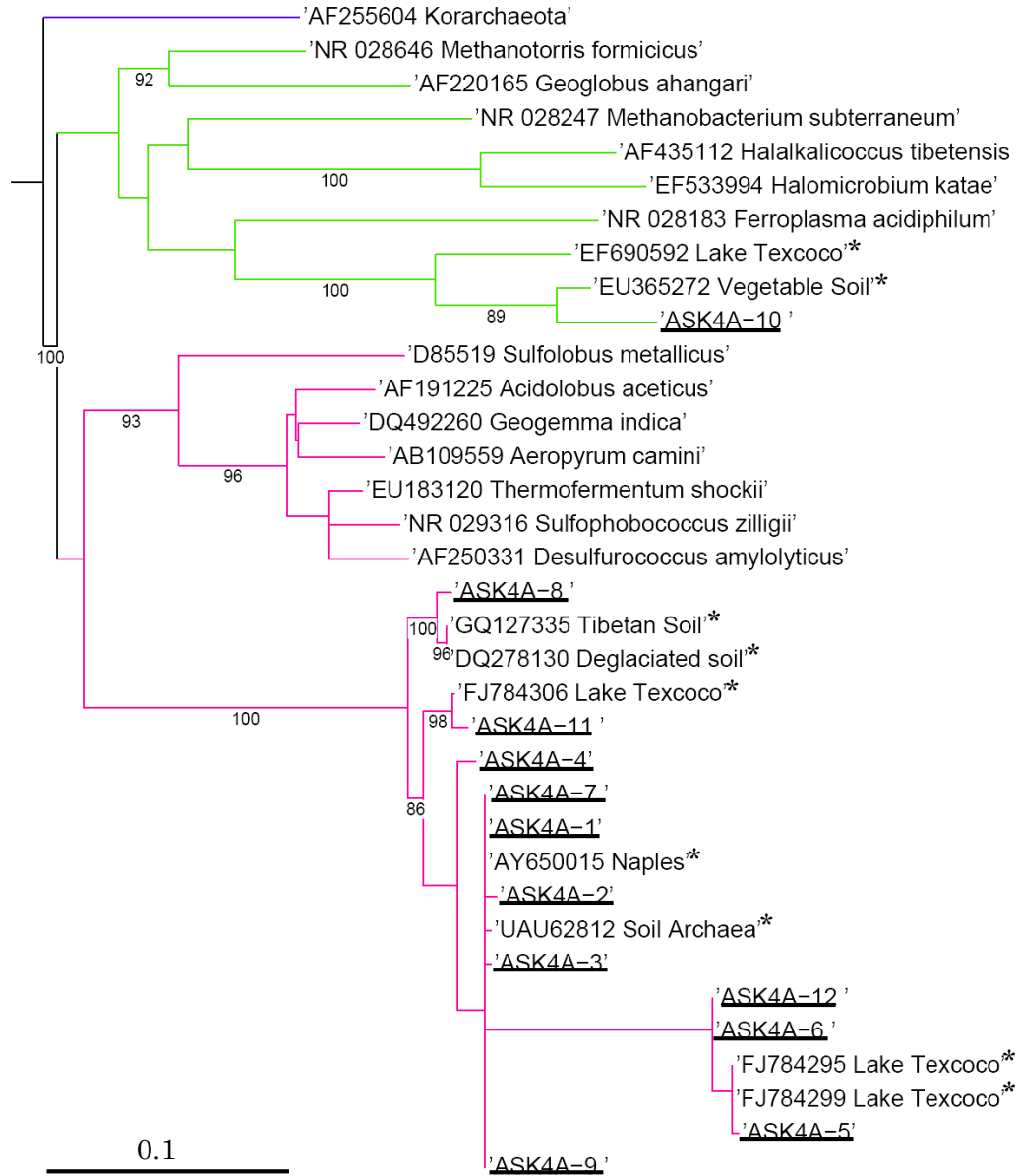


In addition to the bacterial diversity, PCR amplification of ASK4 genomic DNA with Archaeal-specific primers resulted in a PCR product, suggesting the presence of an archaeal component to the prokaryotic microbial community. Archaeal PCR products however were not amplified from either the ASK9 Pillow Basalt glass or interpillow material. Assuming the PCR amplification procedure worked well, this may imply the Archaea are only present within the hyaloclastite, however further PCR reactions using different primer pairs and conditions would need to be conducted in order to verify this. Unfortunately, multiple problems arising during transformation reactions in particular have meant the assessment of this hyaloclastite archaeal community was limited to a handful of clones. Therefore results are summarised here from the limited number (12) of environmental clones obtained for this lava. All but one of the clones fall into the Crenarchaeota, and there is little genetic variation between these, with all having a closest species match to candidate species *Nitrososphaera gargensis* (EU281336), with similarity ranging from 89 – 94%. The other lies within the phylum Euryarchaeota, with a closest species match (81%) to the methanogenic archaeon *Methanogenium thermophilum* (MEERR16S). These clones and their closest environmental and cultured species representatives are given in Table 3.3, and are plotted as a phylogenetic tree in Figure 3.12. Despite the similarity between the ASK4A crenarchaeota clones, individually they are most similar to environmental clones from four different environments. These include drained alkaline saline soil, hot springs, and meadow soil from the Tibetan plateau.

Table 3.3 Archaeal community members from ASK4 hyaloclastite (ASK4A). Sequence lengths are between 500 – 600bp.

| RDP Phylum and Genus | No. of Clones | BLASTn closest relative and similarity (%) | | |
|----------------------------------|---------------|--|--|-----|
| | | Accession number | Environment | (%) |
| Crenarchaeota; (Thermoprotei) | 4 | FJ784299 | Drained alkaline saline soil from the former Lake Texcoco (Mexico) | 99 |
| | 1 | FJ784306 | | |
| | 4 | AY650015 | Non-thermophilic Crenarchaeota from an acidic, 80°C hot spring in Pisciarelli, Italy | 100 |
| | 1 | GQ127335 | Meadow soil from Mount Mila in the Tibetan Plateau. | 99 |
| | 1 | EU281336 | Moderately thermophilic ammonia-oxidizing crenarchaeote from a hot spring | 93 |
| Euryarchaeota | 1 | EF690592 | Vegetable soil | 95 |

Figure 3.12. Phylogenetic tree of the 12 archaeal environmental clones from ASK4 hyaloclastite (ASK4A), along with their closest relatives identified with BLASTn (indicated by an asterisk; see Table 3.3 for details), and representative strains of archaea from GenBank. Branch colour corresponds to phylum, with blue for Korarchaeota (also the outgroup), green Euryarchaeota, and pink Crenarchaeota. Bootstrap values >80 are shown, whilst the scale bar represents number of nucleotide position changes.



3.4.2 Bacterial diversity of ASK9 pillow basalt

The pillow basalt glass and interpillow material have broad similarities regarding their phylogenetic composition. Again there is a significant abundance of Actinobacteria species, which constitute 62% and 57% for the glass and interpillow material respectively, whilst Bacteroidetes contributes to 20% and 18% of the respective communities. Both environments share the same phyla, but the interpillow material has a slightly higher level of diversity than the

glass, with two additional phyla: β -Proteobacteria and Acidobacteria. In relation to the lithic Arctic environment, the communities within the pillow lava are dominated by known radiation and desiccation resistant taxa, such as those in the phylum Deinococcus-Thermus, and in particular the numerous (22 for ASK9 glass; 18 for ASK9 Interpillow) clones that were classed as genus *Rubrobacter*. The prevalence of these particular taxonomic groups reflects the cold and desiccating nature of the basaltic lava environment.

3.4.2.1 ASK9 Pillow Basalt ‘glass’ (ASK9G)

Figure 3.13 shows a plot of the number of ASK9G clones against the environment from which their most similar relatives were identified from, as identified using BLASTn. It is apparent that the ASK9G clone relatives are most commonly from extremely cold and/or dry environments, such as a hyper-arid polar desert (31 clones), McMurdo dry valleys (10 clones), and ancient wall paintings (11 clones). In comparison with the ASK4B hyaloclastite clones, there are significantly fewer ‘closest relatives’ from soil environments, which represent 5 clones in total. Representative ASK9G clones and their closest relatives are given in Table 3.4. The ASK9G clones have the highest number of representatives from the McMurdo dry valleys than either of the other two lava environments. These 10 ASK9G clones share 97 – 99% similarity with three clones from a cryptoendolithic sandstone environment from these dry valleys, the majority of which are Actinobacteria. This dry valley environment is typified by -60°C to +3°C temperatures and extremely desiccating conditions (de la Torre *et al.* 2003). However, whilst the ASK9G clones are dominated by Actinobacteria species, the Antarctic cryptoendolith environment is dominated by cyanobacterial and lichen communities, with Actinobacteria making up only 4% of the bacterial community (de la Torre *et al.* 2003).

Unique for the ASK9G clones are the 9 that are similar (92 – 96%) to uncultured isolates from ‘natural asphalts of the Rancho La Brea Tar pits’. The majority (6) of these clones were not identified at the phylum level by the RDP classifier, whilst the remaining 3 were all classified as Actinobacteria. All were related to environmental tar pit clones from the same sample pit, out of two investigated in the study (Kim & Crowley 2007). This pit consisted of asphalt-permeated soil, and was found to be alkaline with a high concentration of salts and metals (Kim

& Crowley 2007). The closest cultured relatives for these clones were *Sphaerobacter thermophilus* (78 – 84%) and *Ferrithrix thermotolerans* (86%) respectively. Originally classified as the deepest branching member of the Actinobacteria, *Sphaerobacter thermophilus* has since been reclassified within the Chloroflexi class *Thermomicrobia* (Hugenholtz & Stackebrandt (2004), and is characterised as an aerobic thermophile. Likewise, *Ferrithrix thermotolerans* is thermophilic and also extremely acidophilic, although this does lie within the Actinobacterium phylum (Johnson *et al.* 2009).

Figure 3.13. Representative environments of BLASTn closest relatives to the ASK9 Pillow Basalt ‘glass’ bacterial clones (ASK9G). Where clones from environmental types span more than one phylum, this is indicated by [#], which also gives the number of phyla.

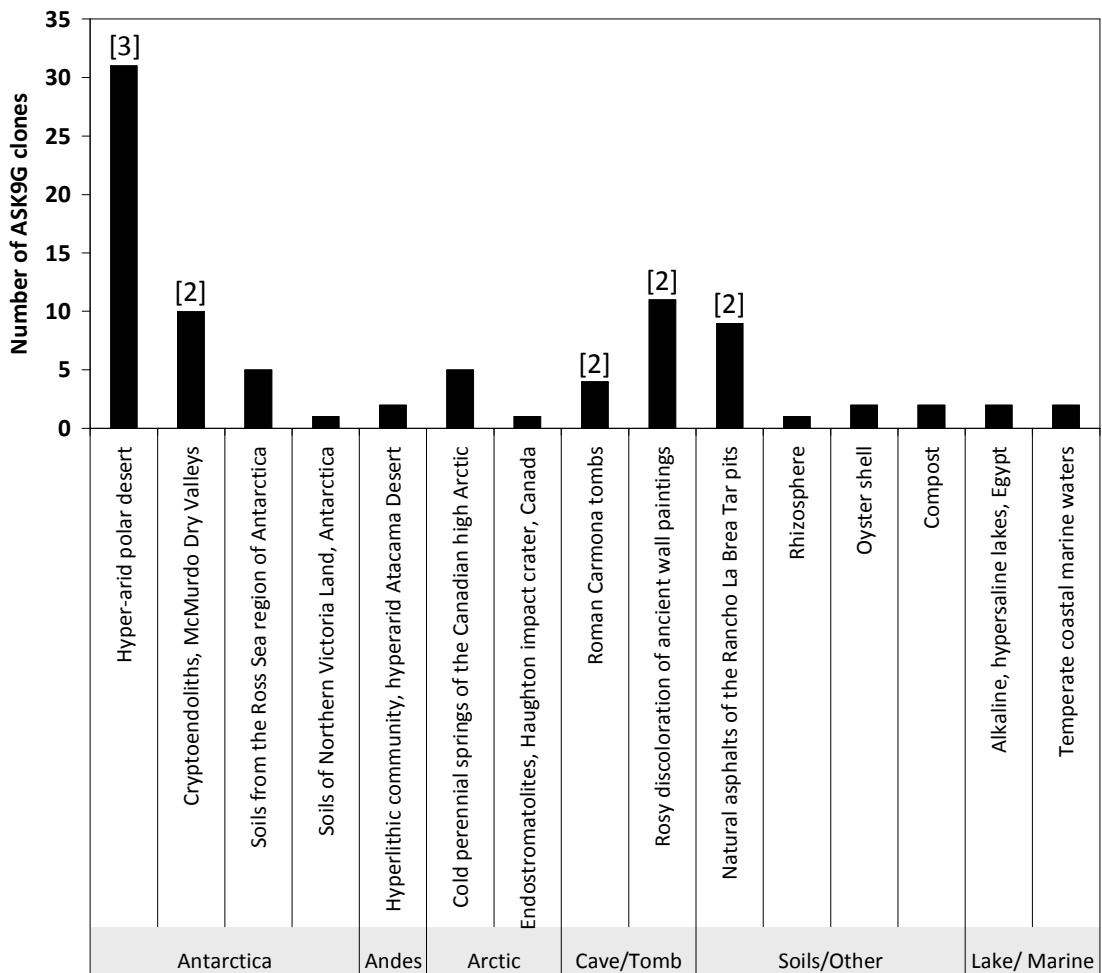


Table 3.4. Selected BLAST database closest environmental isolate relatives and closest cultured species based on 16S rDNA similarity (%) with the ASK9 Pillow Lava ‘glass’ environmental clones. For a full list of all clones see Appendix A.

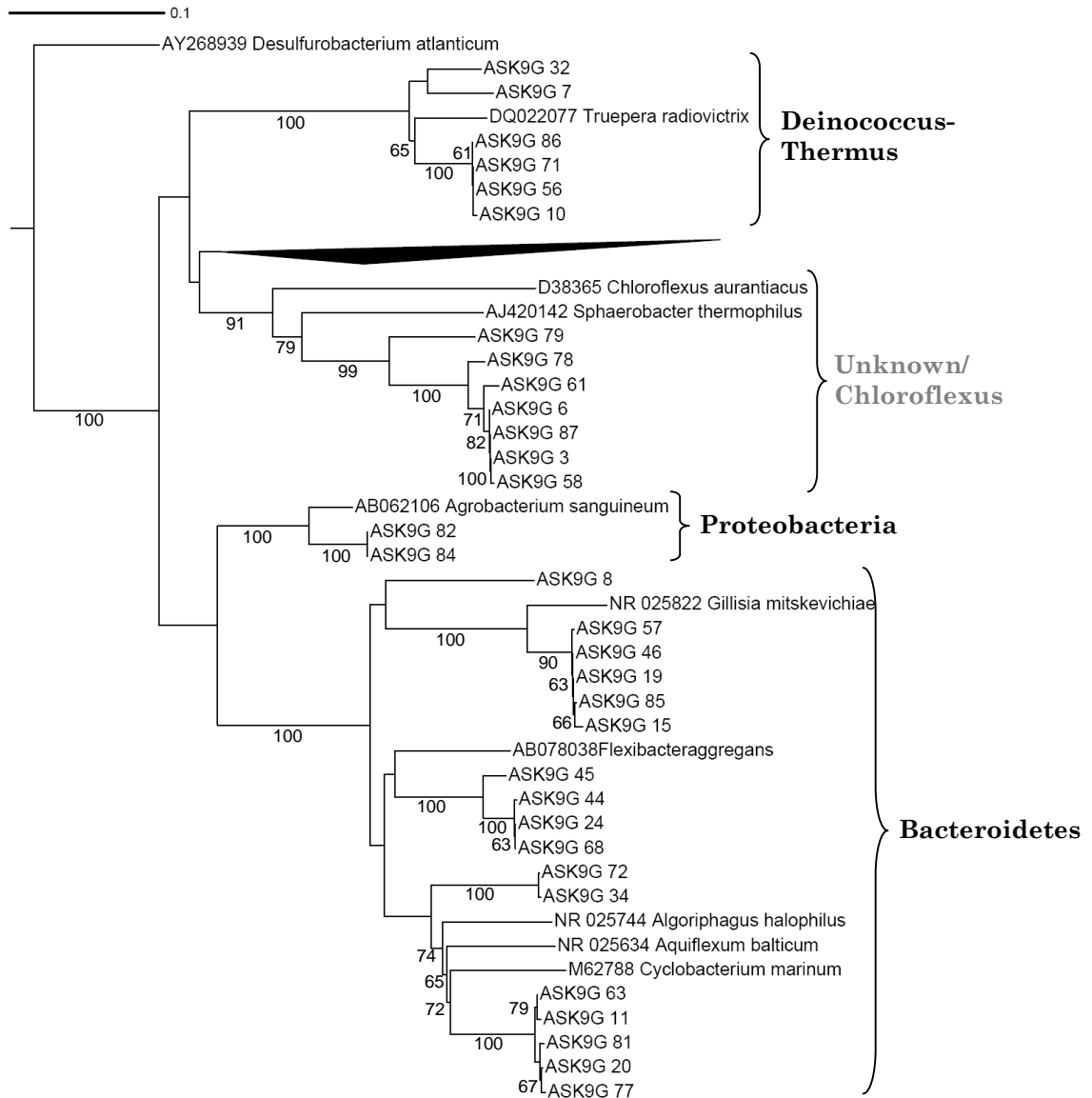
| Closest novel isolate relative | | | Closest cultured species relative | |
|--------------------------------|-----|---|---------------------------------------|-----|
| ID (Accession #) | (%) | Sampling environment | ID (Accession #) | (%) |
| Actinobacteria | | | | |
| Uncultured (AM746696) | 99 | Rosy discoloration of ancient wall paintings | Solirubrobacter soli (AB245334) | 91 |
| Uncultured (FJ895053) | 99 | Hyper-arid polar desert | Ornithinococcus hortensis (AB098587) | 97 |
| Uncultured (AY250873) | 98 | Cryptoendolithic communities, McMurdo Dry Valleys, Antarctica | Rubrobacter radiotolerans (AJ243870) | 93 |
| Uncultured (FN297994) | 93 | Roman Carmona tombs | Nitriliruptor alkaliphilus (EF422408) | 88 |
| Uncultured (FJ895056) | 99 | Hyper-arid polar desert | Patulibacter americanus (AJ871305) | 92 |
| Uncultured (FJ891029) | 95 | Hyperlithic community, hyperarid Atacama Desert | Marmoricola aurantiacus (NR_026507) | 95 |
| Bacteroidetes | | | | |
| Uncultured (EU196299) | 95 | Cold perennial springs of the Canadian high Arctic | Gillisia mitskevichiae (NR_025822) | 92 |
| Uncultured (GQ454873) | 93 | Soils from the Ross Sea region of Antarctica | Cyclobacterium marinum (FLERRDB) | 88 |
| Uncultured (DQ432304) | 87 | Alkaline, hypersaline lakes, Egypt | Flexibacter aggregans (AB078038) | 87 |
| Uncultured (DQ346479) | 88 | Compost | Algoriphagus halophilus (NR_025744) | 86 |
| Proteobacteria | | | | |
| Uncultured (EF215739) | 98 | Temperate coastal marine waters | Agrobacterium sanguineum (AB062106) | 94 |
| Deinococcus-Thermus | | | | |
| Uncultured (FJ895047) | 95 | Hyper-arid polar desert | Truepera radiovictrix (DQ022077) | 93 |
| Uncultured (EU883205) | 98 | Endostromatolites, Haughton impact crater, Devon Island, Canada | Truepera radiovictrix (DQ022077) | 91 |
| Unclassified | | | | |
| Uncultured (EF157190) | 98 | Natural asphalts of the Rancho La Brea Tar pits | Sphaerobacter thermophilus (AJ420142) | 84 |
| Uncultured (EF157223) | 96 | Natural asphalts of the Rancho La Brea Tar pits | Ferrithrix thermotolerans (AY140237) | 86 |
| Uncultured (EU979018) | 88 | Rhizosphere | Phycisphaera mikrensis (AB474364) | 80 |

The phylogenetic tree for ASK9 Pillow Basalt ‘Glass’ (Figure 3.14) shows a clear grouping between highly similar clones, with typically 4 or 5 clones in each group, demonstrating the low level of diversity within this environment. Whilst the majority of clones are grouped in this way, the small clades they form are often a significant distance from their closest cultured species relatives, and therefore likely to be representative of new species.

The closest species match to an ASK9G clone is the actinobacterium *Ornithinococcus hortensis* at 97%, which is the closest species match for three individual clones. In contrast to the typically more extremophilic phylotypes prevalent within this environment, this species is found in temperate garden soil environments (Groth *et al.* 1999), and the particular isolate that shares this 97% similarity to the ASK9G clones was isolated from compost soil (accession number AB098587). However, considerably more common to this environment are the 22 clones whose closest species match is the Actinobacterium *Rubrobacter radiotolerans*, with similarity ranging from 91 – 95%. This species has exceptionally high resistance to both radiation and desiccation (Kausar *et al.* 1997). Likewise, 6 ASK9G clones shared 91 – 93% similarity with the Deinococcus-Thermus species *Truepera radiovictrix*, a chemoorganotrophic radiation resistant strain originally isolated from a 70°C hot spring (Albuquerque *et al.* 2005).

Bacteroidetes constitute the second highest proportion of ASK9G clones, with 17 clones classified within this phylum. However despite this, similarity between these ASK9G clones with both uncultured environmental clones and known species is typically low. As before, closest uncultured relatives are nearly all from cold environments, including cold springs in the Canadian high Arctic (5 clones), and Antarctic soils (5 clones). In contrast to the ASK9G clones in the Actinobacteria, which have high similarities to uncultured environmental clones, those from the Bacteroidetes have similarities of 87 – 95%. With regard to closest cultured relatives, similarities range between 86 – 92%, with the closest Bacteroidetes species match being *Gillisia mitskevichiae* (92%), a marine, heterotrophic bacterium with a wide temperature range for growth of 4 – 31°C (Nedashkovskaya *et al.* 2005).

Figure 3.14 Phylogenetic tree of ASK9 pillow basalt ‘glass’ bacterial clones (ASK9G) and their closest species relatives. The collapsed branch represents the Actinobacteria, which are shown in more detail in Figure 3.17. Clones within the Unknown/Chloroflexi group (in grey) were not classified by RDP Taxonomy. Scale bar represents number of nucleotide position changes, and bootstrap values >60 are shown. *Desulfurobacterium atlanticum* is used as the outgroup.



3.4.2.2 ASK9 Pillow Basalt ‘interpillow’ (ASK9IP)

Regarding the ASK9IP lava, the clones from this environment are, as expected, largely similar to those from ASK9G. The most notable difference is the slightly higher level of diversity, with an additional two phyla represented: Planctomycetes and Acidobacteria. Figure 3.15 shows a plot of the number of ASK9IP clones against the environment from which their most similar relatives were identified from, using BLASTn. As with the ASK9 Glass environmental clones, many of these cover Antarctic and cold soil environments. However, in

this case, the ASK9 interpillow lava clones are clearly dominated by those most similar to clones from a ‘Hyper arid polar desert’, with 47 clones covering 13 different accession ID’s and 5 different phyla. This is by far the highest (for all the above) of the 3 lavas, and suggests this bacterial assemblage may be comparable to that from the lithic environments from that particular study, despite the large geographical separation. There are a higher number of ASK9IP clones with closest relatives from soil environments (9 clones) in comparison to the ASK9G clones. Table 3.5 gives representative closest species and environmental relatives for the ASK9IP clones.

Figure 3.15. Representative environments of BLASTn closest relatives to the ASK9 Pillow basalt ‘interpillow material’ bacterial clones. Where clones from environmental types span more than one phylum, this is indicated by [#], which also gives the number of phyla.

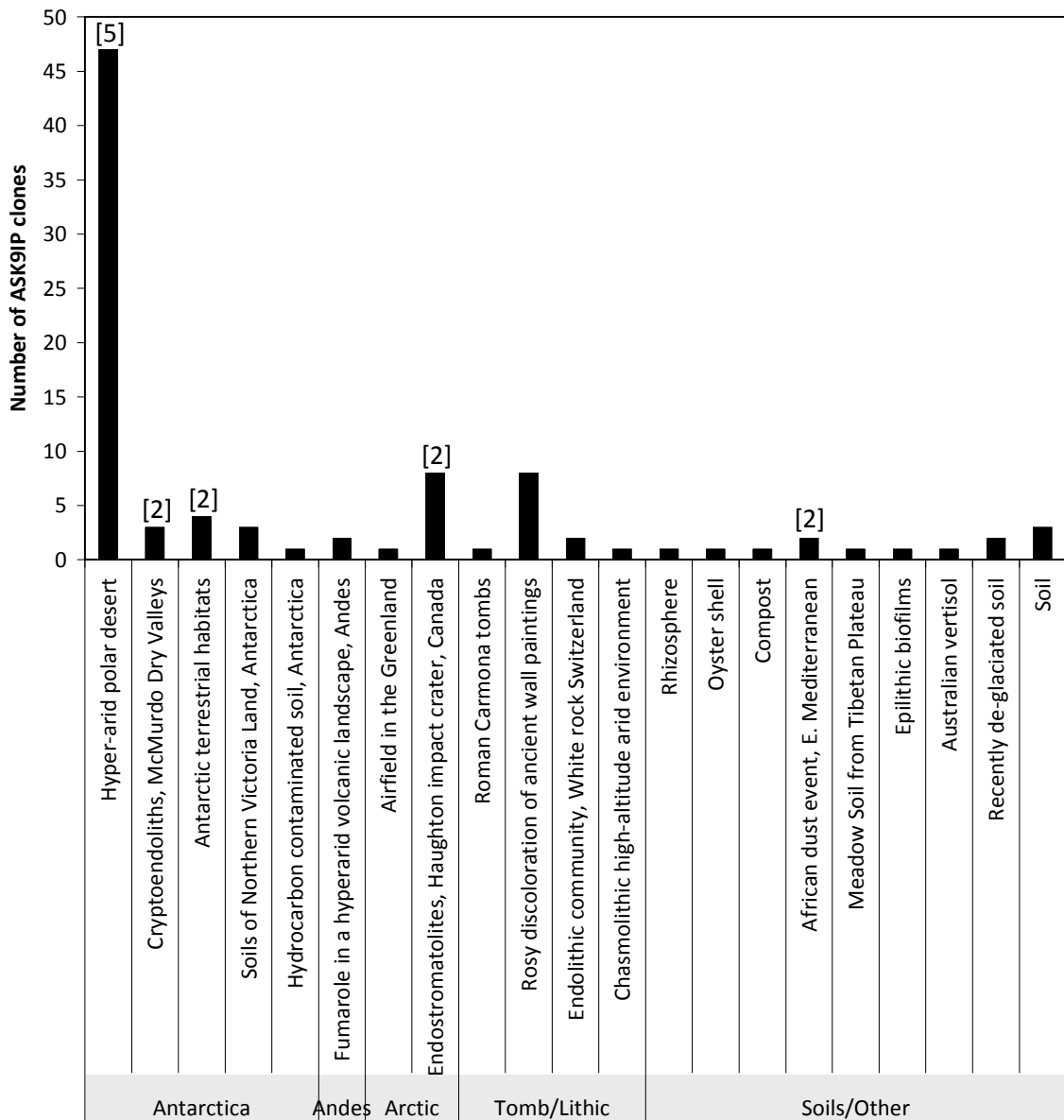


Table 3.5. Selected BLAST database closest environmental isolate relatives and closest cultured species based on 16S rDNA similarity (%) with the ASK9 Pillow Lava ‘interpillow’ environmental clones. For a full list of all clones see Appendix A.

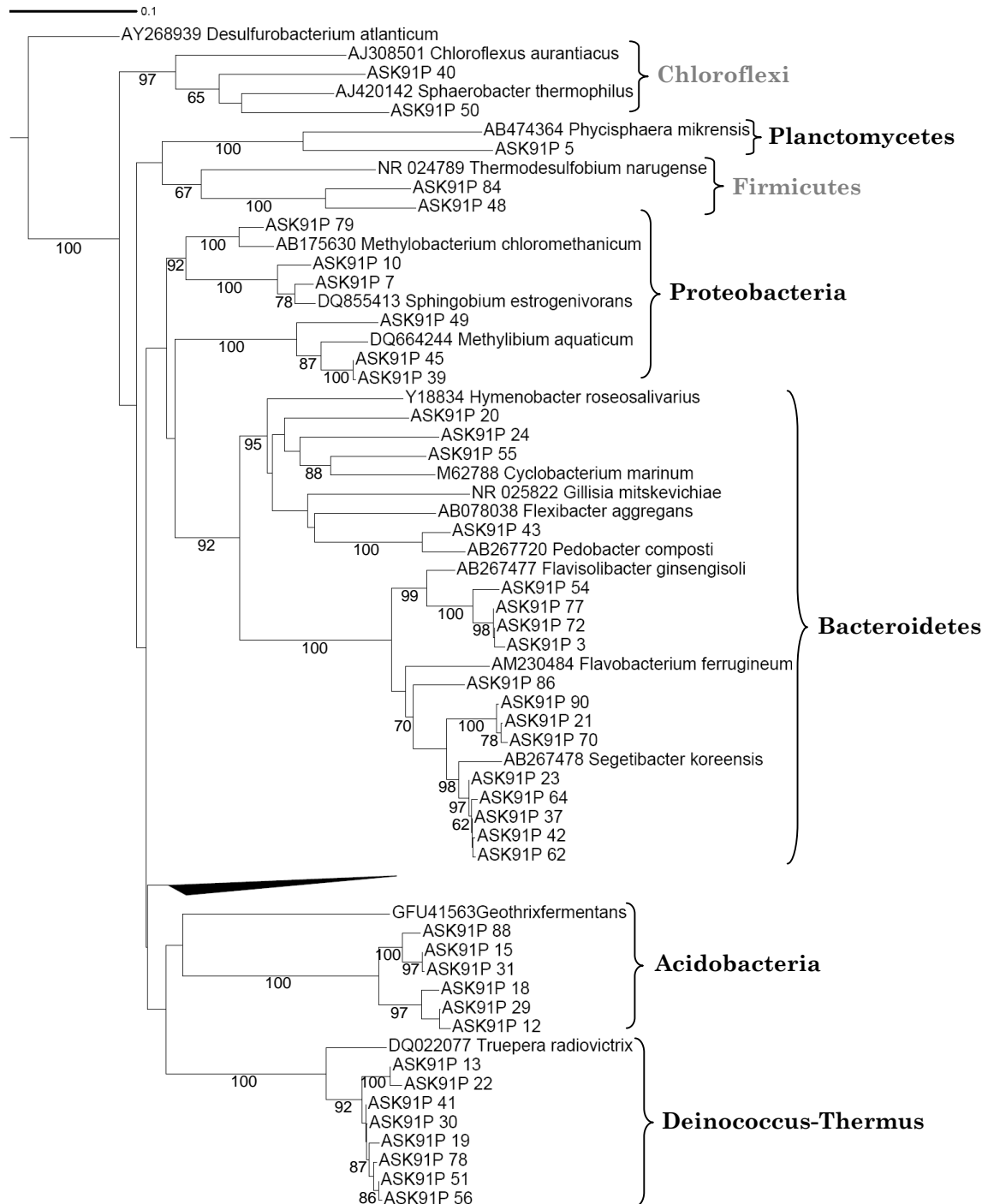
| Closest novel isolate relative | | | Closest cultured species relative | |
|--|-----|---|---|-----|
| ID (Accession #) | (%) | Sampling environment | ID (Accession #) | (%) |
| Actinobacteria | | | | |
| Uncultured (FJ895074) | 99 | Hyper-arid polar desert | Rubrobacter radiotolerans (AJ243870) | 95 |
| Uncultured (EU883196) | 97 | Endostromatolites, Haughton impact crater, Devon Island, Canada | Conexibacter woesei (NR_028979) | 91 |
| Uncultured (AM746696) | 99 | Rosy discoloration of ancient wall paintings | Solirubrobacter soli (AB245334) | 90 |
| Uncultured (GQ396849) | 96 | Recently de-glaciated soil | Ferrimicrobium acidiphilum (AF251436) | 87 |
| Uncultured (FJ895062) | 99 | Hyper-arid polar desert | Nocardioides jensenii (AF005006) | 93 |
| Uncultured (EF465010) | 96 | Soils of Northern Victoria Land, Antarctica | Kribbella ginsengisoli (AB245391) | 92 |
| Bacteroidetes | | | | |
| Uncultured (FJ895060) | 99 | Hyper-arid polar desert | Flavisolibacter ginsengisoli (AB267477) | 91 |
| Uncultured (FJ490252) | 95 | Hyper-arid polar desert | Segetibacter koreensis (AB267478) | 95 |
| Proteobacteria | | | | |
| Uncultured (EU440412) | 95 | Endostromatolites, Haughton impact crater, Devon Island, Canada | Sphingopyxis alaskensis (CP000356) | 93 |
| Variovorax sp. enrichment clone (FJ828944) | 97 | Airfield in the Greenland | Variovorax paradoxus (EU979529) | 95 |
| Deinococcus-Thermus | | | | |
| Uncultured (AB374369) | 97 | Endolithic community, White rock Switzerland | Truepera radiovictrix (DQ022077) | 92 |
| Uncultured (AY250871) | 100 | Cryptoendolithic communities, McMurdo Dry Valleys, Antarctica | Truepera radiovictrix (DQ022077) | 91 |
| Acidobacteria | | | | |
| Uncultured (FJ592780) | 99 | Fumarole within a hyperarid, high-elevation landscape on Socompa Volcano, Andes | Chloracidobacterium thermophilum (EF531339) | 81 |
| Planctomycetes | | | | |
| Uncultured (EF651250) | 93 | Australian vertisol | Phycisphaera mikrensis (AB474364) | 77 |
| Unclassified | | | | |
| Uncultured (FJ895048) | 91 | Hyper-arid polar desert | Leifsonia antarctica (AM931710) | 76 |
| Uncultured (FJ490245) | 99 | Hyper-arid polar desert | Thermodesulfoibium narugense (NR_024789) | 77 |

Figure 3.16 shows a phylogenetic tree of the ASK9 interpillow bacterial clones (ASK9IP). Closest and most abundant cultured relatives are again *Rubrobacter radiotolerans*, between 92 – 95%, but also *Segetibacter koreensis* (93 – 95%) within the Bacteroidetes, accounting for 8 ASK9IP clones. This species was originally isolated from a Ginseng field in South Korea, and is characterised as an aerobic chemoheterotroph (An *et al.* 2007). Radiation resistant *Truepera radiovictrix* is again the closest species relative (90 – 92%) to all clones identified as Deinococcus-Thermus (8 clones).

There is a larger diversity of both Proteobacteria and Bacteroidetes within the interpillow material than the glassy rind, as represented by the higher number of OTUs. Conversely, there are fewer clones within the ‘Unknown/Chloroflexi’ group than the pillow basalt glass, with only 2 ASK9IP clones falling within this clade, compared to 7 ASK9G clones.

The closest environmental relative within the Acidobacteria is one from a fumarole located within the hyper-arid and high elevation Socompa Volcano in the Andes, with 99% similarity. The closest species relative to all Acidobacteria clones was the candidate species *Chloracidobacterium thermophilum*. This species is believed to be an aerobic photoheterotroph, which was originally isolated from hot springs in Yellowstone National Park, USA (Bryant *et al.* 2007). However, similarity between the clones and this species is low, between 81 – 82%.

Figure 3.16. Phylogenetic tree of ASK9 pillow basalt ‘interpillow’ bacterial clones (ASK9IP) and their closest species relatives. The collapsed branch represents the Actinobacteria, which are shown in more detail in Figure 3.17. Clones within the Chloroflexi/Firmicutes group (in grey) were not classified by RDP Taxonomy. Scale bar represents number of nucleotide position changes, and bootstrap values >60 are shown. *Desulfurobacterium atlanticum* is used as the outgroup.

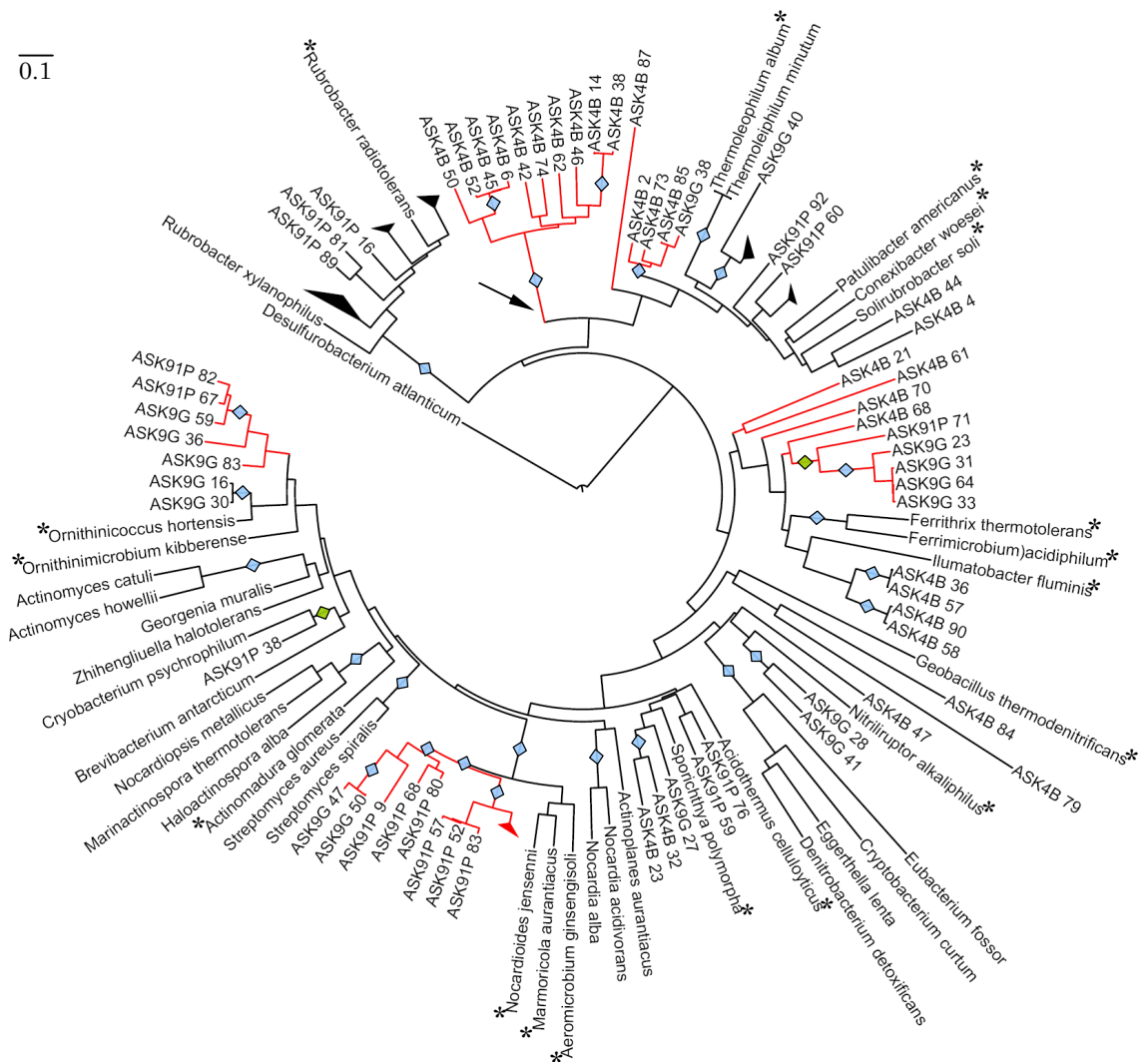


3.4.3 Actinobacteria in the Askja lavas

Actinobacteria are particularly prevalent in both the hyaloclastite and pillow lava lithologies. As such, this phylum is explored here for all lava environments collectively. A phylogenetic tree of clones that fall within the Actinobacteria,

together with closest cultured relatives and representative species is given in Figure 3.17. Many of these clones grouped to form phylogenetically distinct clades of their own, some of which contain clones from all three lava environments, whilst others were closest related to known Actinobacteria species. Those species that had a high similarity to the Askja clones were *Rubrobacter radiotolerans*, *Solirubrobacter soli*, *Patulibacter americanus*, and *Ornithinicoccus hortensis*. Many of the genetically distinct clades are supported by high bootstrap values, with two particularly deep branching clades having bootstrap values of 100.

Figure 3.17. Phylogenetic tree of clones within the phylum Actinobacteria and representative species. Closest relative species are indicated by an asterisk. Where four or more clones have a branch length <0.01, the clade is collapsed. Branches in red indicate clades distantly related to known species of Actinobacteria, one of which is particularly deep branching (indicated by an arrow). Bootstrap values >98 are indicated with a blue diamond; values 75 – 90 are indicated with a green diamond. NB: GenBank accession numbers have been removed for clarity, but for closest relatives these numbers are the same as in Figure 3.9. *Desulfurobacterium atlanticum* is used as the outgroup



A significant proportion of clones from all three lava environments lie within *Rubrobacter*, and vary in similarity between *Rubrobacter xylanophilus* and *Rubrobacter radiotolerans*. However, most clones form well defined and often deep rooted clades distantly related to well known environmental Actinobacteria. These are highlighted in red in the phylogenetic tree. Actinobacteria are often found to dominate in dry mineral soil environments (e.g. Babalola *et al.* 2009), and their predominance within the bacterial communities of these three lavas might be expected. Likewise, a large number of Actinobacteria were identified in lavas from South Iceland (Cockell *et al.* 2009b), and it has been suggested that the ability to form branching hyphae make Actinomycetes particularly suitable for colonising rock substrates (Cockell *et al.* 2009b). Further investigation into the potentially high Actinobacterial diversity within unexplored environments such as these basaltic lavas may reveal an array of distinct evolutionary groups within this phylum. This highlights the importance of investigations into extreme and hostile environments which can contribute to the growing understanding of microbial life on Earth, as well as being applicable to possible life on Mars.

3.5 Variation in Community Composition and Diversity

This study has revealed the Arctic basaltic lava environment at Askja to sustain a microbial community that is diverse and also well adapted, as suggested by clone similarity to a wide range of comparable cold and dry environments.

3.5.1 Phylum composition within the lavas

To provide the phylogenetic context for the bacterial communities within the lavas, the phylum composition of the lava environments collectively are briefly described below, along with broad characteristics of each respective phylum.

Acidobacteria (ASK4B; ASK9IP): This relatively new phylum contains few cultured representatives but are believed to be ubiquitous in a number of soil environments (Quaiser *et al.* 2003). The ecological characteristics are poorly understood, although a clear relationship has been identified between pH and abundance of acidobacteria (Jones 2009).

Bacteroidetes (ASK4B; ASK9G; ASK9IP): Bacteria of this phylum are, like the Proteobacteria, believed to be prevalent in the natural environment, especially those that are aquatic (O’Sullivan *et al.* 2006; Stevens *et al.* 2005). However, they have also been identified in Arctic environments, such as tundra soil (Nemergut *et al.* 2005), where they can dominate the population (Mannisto *et al.* 2009) .

Cyanobacteria (ASK4B): Members of the photosynthetic Cyanobacteria are well known for their proposed importance in the early evolution of life on Earth, and are found in a vast array of environments. These range from both extreme niches in Antarctica (Cowan 2009), to producing expansive algal blooms in temperature lakes (Kolmonen *et al.* 2004). This phylum was found only within the hyaloclastite, representing an important phototrophic component to the microbial community.

Deinococcus-Thermus (ASK4B; ASK9G; ASK9IP): Bacteria within the group *Deinococcus* are well known for their high resistance to ionizing radiation, ultraviolet radiation, oxidizing agents, and desiccating conditions (Griffiths & Gupta 2007). Existing within all three lava types, they were particularly prevalent in the ASK9 pillow lava.

Planctomycetes (ASK4B; ASK9IP): Species within this phylum represent one of the main lines of descent in the Bacterial domain. Originally believed to only exist in aquatic environments, *Planctomycetes* have since been identified in numerous environments, including tundra soils (Buckley *et al.* 2006).

Proteobacteria (ASK4B; ASK9G; ASK9IP): The phylum Proteobacteria presently comprises the largest and most diverse group of Bacteria, with representatives displaying a huge range of physiology (Dworkin & Falkow). As such, it is unsurprising this group was present in all three lava environments. However, despite the prevalence of Proteobacteria within the biosphere, they still only constituted a small component of the community, ranging between 2 – 9%.

TM7 (ASK4B): Candidate phylum TM7 is characterised purely by sequence data alone, as there are currently no cultured representatives, and was proposed after studies of forest soil and reactor sludge (Hugenholtz *et al.* 2001).

Verrucomicrobia (ASK4B): Members of this phylum are widely distributed in soil and aquatic habitats, and are thought to form a close evolutionary relationship with the Planctomycetes and Chlamydiae, (Lee *et al.* 2009).

3.5.1 Comparison of communities between the different lava lithologies

Figure 3.18 and Table 3.6 summarise the composition and diversity indices between the different lava lithologies. It is apparent from this study that the ASK4 hyaloclastite lava supports a markedly more diverse bacterial community than the pillow basalt, despite the common external environment. This is reflected in firstly the number of OTUs (>97% similarity), and secondly the diversity indices for each of the lavas (given in Table 3.6). Shannon’s diversity index values corroborate well with the graph in Figure 3.18 below and also the number of OTUs, whereby the index is highest for the ASK4 hyaloclastite (4.07) and lowest for the ASK9 Pillow lava glass (2.99). In comparison the Simpson Index values give the impression of incredibly high diversity for all the lavas, with little difference between the three environments. However, it is worth bearing in mind the true species richness of the pillow lava may not be fully represented if other phylotypes exist at especially low numbers.

Figure 3.18. Stacked bar charts showing the distribution of Bacterial phylotypes between the three lava environments. ASK9G = ASK9 Glass; ASK9IP = ASK9 Interpillow; ASK4B = ASK4 Hyaloclastite (n=92 for ASK9G, n=93 for ASK9IP and n=88 for ASK4B).

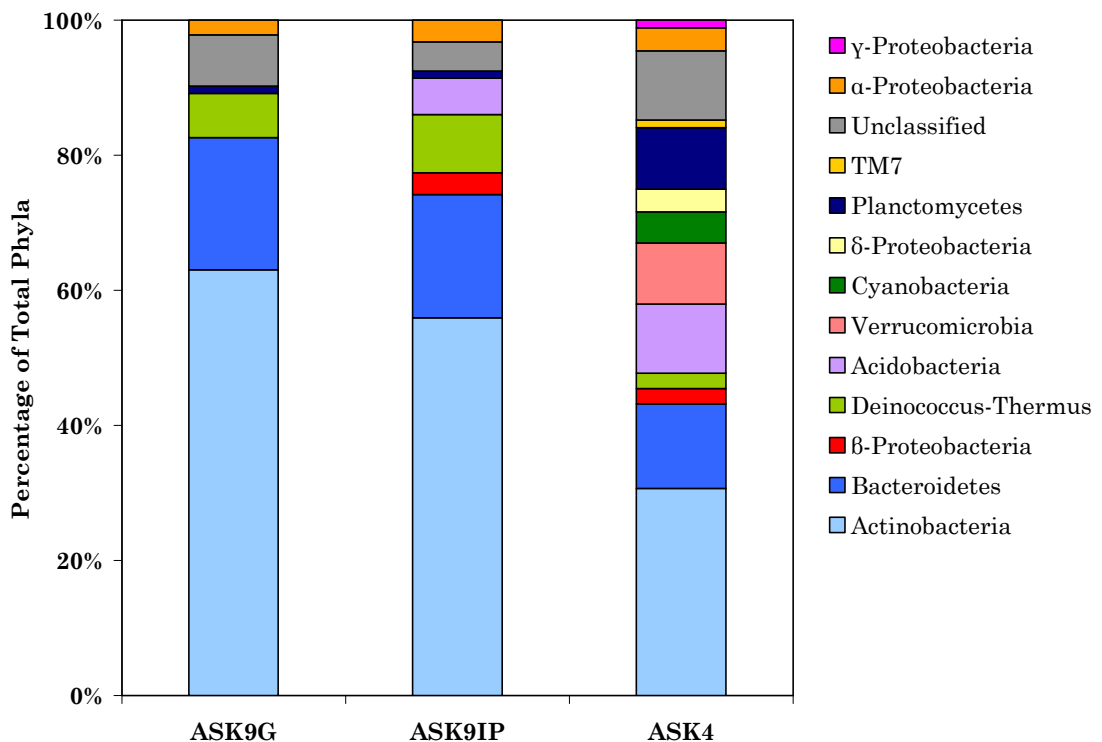


Table 3.6. Phylogenetic distribution of genotypes between the different lavas. OTUs and diversity indices (for diversity indices see Equations 2 and 3 in the Appendix B) were calculated using MOTHUR (Schloss & Handelsman 2005) at a cut-off value of 97%.

| | ASK9 Pillow Basalt | | ASK4B Hyaloclastite |
|--------------------------------|--------------------|-------------------------|------------------------|
| | Glass (ASK9G) | Interpillow (ASK9IP) | |
| Number of OTUs >97% similarity | 30 | 41 | 64 |
| Alpha diversity index | | | |
| Shannon's index | 2.99 | 3.42 | 4.07 |
| Simpson's index (1-D) | 0.94 | 0.97 | 0.99 |
| Phylum Distribution | | | |
| Actinobacteria | 58 | 52 | 27 |
| Bacteroidetes | 18 | 17 | 11 |
| β -Proteobacteria | 0 | 3 | 2 |
| Deinococcus-Thermus | 6 | 8 | 2 |
| Acidobacteria | 0 | 5 | 9 |
| Verrucomicrobia | 0 | 0 | 8 |
| Cyanobacteria | 0 | 0 | 4 |
| δ -Proteobacteria | 0 | 0 | 3 |
| Planctomycetes | 1 | 1 | 8 |
| TM7 | 0 | 0 | 1 |
| α -Proteobacteria | 2 | 3 | 3 |
| γ -Proteobacteria | 0 | 0 | 1 |
| Unclassified | 7 | 4 | 9 |
| <i>Total no. phyla</i> | <i>5</i> | <i>7</i> | <i>12</i> |
| Total no. clones | 92 | 93 | 88 |

One particularly interesting find is the identification of Cyanobacteria within the hyaloclastite and its complete absence from both the pillow basalt glass and interpillow material. Cyanobacteria are known to be found in extreme and often desiccating environments, such as the Antarctic Dry Valleys. It has previously been suggested that Cyanobacteria can act as opportunists in such extreme environments, producing a temporary population during optimum colonisation conditions (Pointing *et al.* 2009). This has been suggested for observed cyanobacterial populations from a hyper-arid polar desert in Antarctica (Pointing *et al.* 2009), and it is also noted that many of the Askja environmental clones have closest genetic similarity with clones from this particular study (see Figures 3.10, 3.13, and 3.15). As such, this result suggests the potential lithological control on phototrophic colonisation.

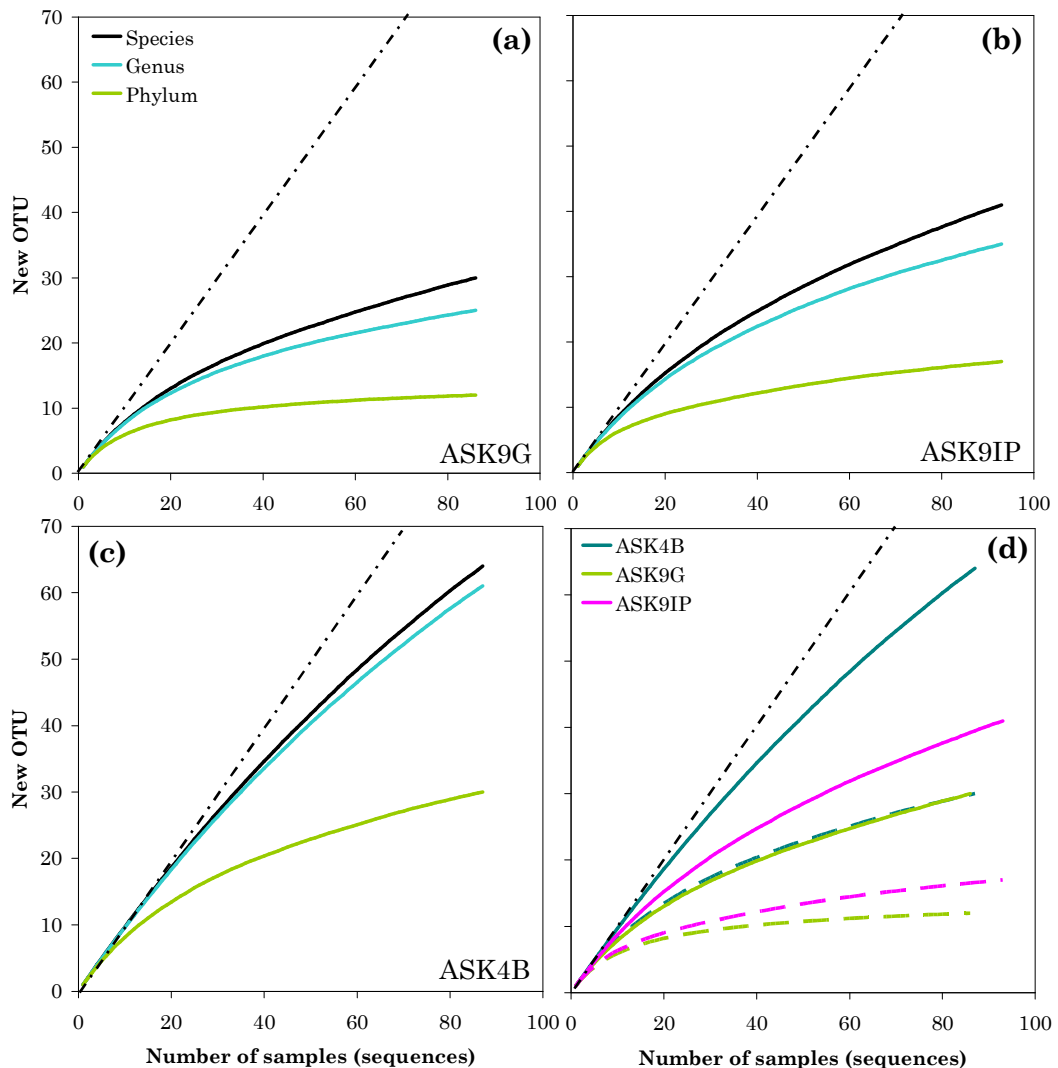
In relation to this is the often high level of similarity between the ASK9 pillow basalt clones to those from cryptoendolithic communities from the Antarctic dry valleys. However, the high-level structure of these two environments is very

different. The cryptoendolith communities from the dry valleys were highly dominated by phototrophs, both lichen and cyanobacterial (de la Torre *et al.* 2003), although it is noted this may, in part, reflect sampling bias towards observable ‘green bands’ within the sandstone. In contrast the ASK9 pillow basalt glass and interpillow lavas were dominated by Actinobacteria, and no cyanobacterial groups were identified. Five bacterial phyla are believed to contain members capable of chlorophyll-based phototrophy: Cyanobacteria, Proteobacteria, Chloroflexi, Firmicutes, and Chlorobi (Bryant *et al.* 2007; Bryant & Frigaard 2006). A small number of α -proteobacteria were found in these lavas (and the ASK4 hyaloclastite), but this group constituted only 2 – 3% of all clones. This group encompasses many phototrophic genera, but the lack of classification to any species or genera means it is not possible to confidently infer these clones to represent phototrophic bacteria. Additionally, the majority were classified with the RDP classifier as Spingomonadales, members of which are chemoheterotrophs, not phototrophs (Dworkin & Falkow). It has been previously suggested that photosynthesis is potentially the main (or even only) source of primary productivity in such Antarctic cryptoendolith environments (Nienow & Friedmann 1993). Despite the similarity in environmental conditions (i.e. cold, desiccating, lithic), the absence of any bacteria clearly capable of photosynthesis suggests the communities within the pillow lava environment do not solely rely on phototrophic primary production. Likewise, whilst the ASK4 hyaloclastite did contain cyanobacteria, these only constituted 5% of the total community.

To estimate the level to which the environmental clones had represented the true bacterial diversity of the three lava environments, rarefaction curves were calculated using MOTHUR (Schloss & Handelsman 2005), and are given in Figure 3.19. These curves show the number of new OTUs (at any given sequence similarity/taxonomic level) that are found with increased sampling of that particular community. The more diverse the community, the more sampling required to identify new individuals. These curves were calculated for each of the lavas, using OTUs defined at three levels of sequence similarity (cut-off values), whereby >97% represents species, >95% represents genus, and >80% represents phylum (Schloss & Handelsman 2005; Stackebrandt & Goebel 1994). It can be seen from these plots that the bacterial community in the ASK4B hyaloclastite lava displays a much higher level of diversity than the ASK9 pillow lava. For

both the ‘glass’ and ‘interpillow’ components of the ASK9 pillow lava environment, diversity at the phylum level (>80%) largely plateaus off at around at sample number of ~30 (Figures 3.19a and b), suggesting the phylum composition of these lavas has been well represented by the number of clones sampled. For all three lava environments, diversity of OTUs with >97% similarity appears diverse, and implies that further sampling would be beneficial towards revealing the composition and diversity of all these environments. This is especially true for the ASK4 hyaloclastite, which at a cut-off level of >97%, lies closest to the theoretical maximum out of all three lava environments (Figure 3.19c).

Figure 3.19. Rarefaction curves for the three lava environments calculated using the MOTHUR program (Schloss & Handelsman 2005) for three cut-off values of sequence similarity which roughly correlate to taxonomic classification: >97% (species), >95% (genus), and >80% (phylum). Appearance of new OTUs is plotted against number of individual sample sequences (clones). Plots (a-c) also show the line for the theoretical maximum (dashed line), whereby each new sample (clone) represents one new OTU. Plot (d) shows all lavas for comparison, for the cut-off of >97% (solid line) and >80% (dashed) .



Regarding sources of inoculum, there are several pathways by which Bacteria and Archaea can colonise these lavas. The most prevalent of these is likely to be wind transportation, as the open expanse of the volcanic desert in this region enables airflow across significant distances with little interruption or redirection, and the surrounding terrain to the north and south a relatively rich in vegetation and geothermal biomass. An additional source lies within snow, which covers the lavas for much of the winter. The subsequent snowmelt runoff could provide a mechanism of transporting microorganisms or their spores between proximally located environments. A particularly interesting find is the identification of the Askja clones as most related to a number of thermophiles and other species that are typical of hot spring environments. There were multiple cases of this from all three environments, with 14 clones in total being most similar to cultured species found in hot springs, 8 of which are from the ASK4 Hyaloclastite (ASK4B). These species are *Thermoleophilum album* (3 clones), *Chloroflexus aurantiacus* (1 clone), *Rhodoplanes cryptolactis* (2 clones), *Ferrithrix thermotolerans* (6 clones), *Acidothermus cellulolyticus* (1 clone), and *Thermodesulfobium narugense* (1 clone). This association is surprising, as whilst hot spring environments are often considered ‘extreme’, the abundance of liquid water and warm-hot temperatures is conflicting to the cold and dry environment within the basaltic lava. A potential explanation may lie with the existence of hydrothermal activity in and around the Askja volcanic complex. Particularly around the caldera lake and within the explosion crater ‘Viti’ (~3 – 5km away) there are several high temperature fumaroles and hot springs that are a potential source of microorganisms that get inadvertently transported to the surrounding lava flows. Such species adapted to warm springs would perhaps not be expected to survive the lava environment, but whilst these bacteria are the closest cultured relatives to the relevant clones, their similarity is low, typically 84 – 86%.

The exception to this are the 2 ASK4B clones which share 94 and 95% similarity to the Proteobacterium *Rhodoplanes cryptolactis*. This species is a thermotolerant phototrophic purple nonsulfur bacteria, originally isolated from hot springs in Japan (Okamura *et al.* 2007). With the exception of this species, the broadly low level of genetic similarity between the clones and these hot spring species suggests one of two possibilities. Firstly that these microorganisms find themselves within a

different environment, and so adapt according to environmental selection pressures, evolving into new, genetically distinctive bacteria. Alternatively, these clones represent as yet undiscovered genera or species that may be closely related to hot spring microorganisms, but are completely unconnected to the hot spring environments around Askja, with the existence of both merely due to coincidence. Conducting further phylogenetic surveys would perhaps shed light on this issue. Specifically, identification of the communities within the nearby Askja hot springs would identify any potential source bacteria, along with temporal sampling of the lavas to ascertain the long-term inhabitants of the lavas.

3.5.3 Lithological controls on colonisation

There are several possible environmental factors that could affect the differing microbial diversities of the hyaloclastite and pillow basalt. As seen in section 3.3, the lavas have very different textures, and vary in moisture content. In addition, they are likely to be subject to differing micro-climate variations with regards to sunlight, rainfall, and temperature. Any combination of these could contribute to the observed differences in microbial colonisation of these rocks. However, although no data is available or was collected for the individual lava localities, it is likely that differences in the external environment of these lavas is small, and it is proposed that it is the lithology that forms the dominant control over bacterial colonisation and population development. Despite the lavas having the same melt major geochemistry from which they formed (basaltic Icelandite), they have evolved into texturally and mineralogically different rocks fitting with their respective lava lithologies. As a result, their mineralogy, like their structure, is likely to be a controlling factor on the inhabiting microbial community.

With regards to habitability, the hyaloclastite lava appears to support a wider range of microbial life than the pillow lava, based on the diversity of phylotypes and additional identification of Archaea. Hyaloclastite is commonly the most porous and least dense rock amongst volcanoclastic rocks, depending on the extent of lithification (Frolova 2008). Their unconsolidated nature in comparison to other volcanoclastic lithologies results may be an important factor in their overall habitability and accessibility for colonising microorganisms. Additionally, this particular hyaloclastite sample had a moisture content almost 3 times

higher than that of the pillow lava, which may make this lithology more conducive to habitation. As identified by Cockell *et al.* (2009a), microorganisms would perhaps extract essential nutrients more easily from palagonite than from a solid crystalline matrix. The large surface area of the smectite clays making up the palagonite will provide more reactive surfaces from which microorganisms can obtain energy and vital nutrients. Additionally, the lack of strong Si – O bonds within clays means the breakdown of the mineralogical structure is far easier than it is for larger more structured crystals (Cockell *et al.* 2009a). Likewise, the amorphous nature of volcanic glass has been previously suggested as a positive factor in the leaching of nutrients by microorganisms, in comparison to crystalline lava.

Interestingly within the ASK9 pillow lava, the interpillow material was more diverse than the pillow glassy rind. There was little difference between these two with regards to moisture content, but the pore water pH of the interpillow material was more neutral (pH 7.67), similar to the hyaloclastite pore water pH. However, the interpillow is more mineralogically diverse than the glass, through the deposition of secondary hydrothermal minerals. This would potentially widen the range of substrates available for microbial growth. It is widely known that the essential ‘building blocks’ of life consist of a small group of major elements – the so-called CHONPS (Carbon, Hydrogen, Oxygen, Nitrogen, Phosphorous, Sulphur) elements (Da Silva & Williams 2001). In addition however are other elements that make up a small but essential part of a bacterial cell: Potassium, Magnesium, Calcium and Iron (Da Silva & Williams 2001). Sulphur, Calcium, and Iron are common to hydrothermally-deposited minerals, such as gypsum (CaSO_4), calcite (CaCO_3), iron oxide (Fe_2O_3), whilst Magnesium is a common constituent of smectite clays. As such, the lack of diverse mineralogical species within the pillow lava glass may be a significant contributor to the reduced bacterial diversity within the ASK9 pillow basalt glass. The work detailed here therefore would benefit from extensive characterisation of the mineralogy of all three lava environments (especially the hyaloclastite and interpillow), to establish the mineralogical (and associated elemental) differences between these environments.

3.6 CONCLUSIONS

This work sought to identify the prokaryotic composition and diversity within basaltic lavas of contrasting lithology. In doing so the following were revealed:

- Basaltic pillow lava and hyaloclastites from the cold and dry volcanic highlands of Central Iceland host a bacterial community that is highly comparable to those previously found within other comparable extreme environments, such as the Antarctic dry valleys, polar deserts, and ancient wall paintings.
- A significantly more diverse bacterial community was found to inhabit the hyaloclastite lava than the pillow lava. Within the pillow lava itself, the interpillow material had a marginally more diverse community than that of the glassy rind.
- Actinobacteria dominated the bacterial community for all three lava environments, particularly within the pillow basalt.
- A limited number of archaea were identified within the hyaloclastite but not the pillow lava. Future work should explore this archaeal community further.

CHAPTER 4

BIOALTERATION IN CONTINENTAL ANTARCTIC BASALTIC LAVAS

As shown, basaltic lavas can be a habitat for a diverse prokaryotic community. In relation to understanding Earth environments as a proxy for life detection on Mars, it is just as important to recognise how the inhabitants of such basaltic environments leave behind evidence of their previous or current existence in the rock record through the production of biosignatures. These biosignatures, being indirect evidence for life, need to be well understood if they are to be used as support for the existence of life on another planetary body, in terms of their generation, preservation, potential for contamination, and external controls. This chapter will present results relating to a putative biosignature that is widespread in basaltic lava environments, so-called 'bioalteration textures' found in basaltic volcanic glass. The work described here is divided into two principle sections:

Firstly, bioalteration textures from terrestrial Antarctic lavas are described and classified based on their ichnotaxonomy. This is the first identification of these biosignatures within Antarctic lavas, and is also one of the few from continental environments specifically (as opposed to oceanic).

Secondly, the unique environmental conditions that these lavas were subjected to meant that the effect of alteration fluid source and composition (in this case marine vs. freshwater) had on the generation of these biosignatures could, for the first time, be identified.

4.1 Bioalteration and Detection of Life on Mars

Bioalteration textures in basaltic lavas have been identified in numerous seafloor environments, and have been widely advocated in their use as a suitable biosignature for Mars (Banerjee *et al.* 2006; 2004a,b; Fisk *et al.* 2006; Fisk and Giovannoni 1999a,b) and the early Earth rock record (e.g. Banerjee *et al.* 2006), and as a result much of the research has focused on proving the biogenic origin of these structures (see Chapter 1, section 1.4.3). However, little is known regarding the formation, environmental controls, and distribution of these biosignatures. These are fundamental parameters, and need to be understood if bioalteration is to be used as a reliable biosignature in Martian exploration. This lack of understanding is partly due to the limited environments that have been explored. Even though bioalteration textures have been extensively identified and described, work has been restricted almost entirely to basaltic lavas from the sea floor, or ophiolite lavas preserved in the rock record (Staudigel *et al.* 2008; Furnes *et al.* 2007). However, extensive aqueous alteration of basalt also occurs in continental freshwater environments, such as those created through subglacial volcanism. Such continental lavas have received little attention, but are important if we are to understand the potential of bioalteration as a biosignature in Martian exploration. This is particularly relevant as subglacial volcanism is a process widely believed to have occurred on Mars (see Chapter 1, section 1.2.2). This work therefore is focused on the identification of bioalteration within continental glaciovolcanic basaltic lavas from Antarctica. These lavas are not only an ideal geological analogue to Martian lavas, due to their subglacial origin, but the Antarctic climate today is widely perceived to be an excellent environmental analogue to conditions on Mars. Here, bioalteration textures in Antarctic lavas are described, and the importance of environmental controls on the formation and occurrence of these biosignatures is demonstrated.

4.1.1 Controls on the formation of bioalteration

The environmental controls on the formation of bioalteration textures are poorly understood. Changes in fluid flux, nutrient supply and local temperature are all believed to be important controls on bioalteration in sea floor lavas (Furnes *et al.* 2007; Furnes *et al.* 2001a), as are the salinity and nutrient content of the circulating fluids (McLoughlin *et al.* 2007). The next step in the study of biomediated processes is to understand better the environmental controls that

affect the distribution and occurrence of bioalteration. The freshwater environment in particular has been overlooked, as typically found in subglacial volcanic settings. Alteration fluids forming as a result of subglacial eruptions will differ significantly from those in an oceanic setting, whilst the basaltic host lithologies remain essentially the same (i.e. basaltic hyaloclastites and pillow lava). It is therefore important to identify whether or not bioalteration textures always reliably form in basaltic glasses that exist within any type of aqueous environmental setting, or if there is in fact any fundamental environmental control on their formation.

4.1.2 Utilising a transitional subglacial – marine environment

This work contains the first petrographic description of bioalteration textures within Antarctic hyaloclastites, and aims to provide an insight into how the local environment affects the occurrence of bioalteration textures within basaltic sequences that have experienced both freshwater (subglacial) and marine conditions. Basaltic subglacial eruptions result in similar lithologies to those erupted on the sea-floor at mid-ocean ridges, due to similar processes of rapid lava quenching upon contact with cold water or ice and the subsequent formation of abundant glass (Staudigel and Schmincke 1984; Jones 1969). As a result, subglacial and marine volcanic sequences have the potential to host comparable microbial activity. In this study, a sequence of Antarctic lava-fed deltas erupted under well-constrained environmental conditions (Smellie *et al.* 2008; Smellie 2006) was studied to identify the major environmental controls on any bioalteration textures found.

These Antarctic sequences from James Ross Island (see Figure 1.7, Chapter 1) were initially erupted subglacially, but some have been interpreted to be later affected by percolating marine water as sea level fluctuated (Johnson and Smellie 2007). In this study, the authors used Na, K, and Ca concentrations to identify the presence of marine alteration of zeolites (phillipsite and chabazite), and therefore sea-water percolation through that particular hyaloclastite delta. By identifying and quantifying the bioalteration in a series of lavas from the same volcanic province under these well-known, but variable, environmental conditions, the major controls that determine the distribution and abundance of endolithic microbial activity in basaltic glass can be more confidently identified.

4.2 Description of Bioalteration in James Ross Island Hyaloclastites

These results for James Ross Island hyaloclastites are the first evidence for bioalteration textures in basaltic glass from Antarctic lavas, and they are also the largest dataset obtained for a subglacial lava sequence anywhere.

4.2.1 Morphology and Ichnotaxonomy

54 thin sections of hyaloclastite from five lava-fed deltas selected from the James Ross Island Volcanic Group (JRIVG) were analysed petrographically with a transmission light microscope and by scanning electron microscopy (SEM), to identify bioalteration textures that were comparable to those previously described from oceanic basalts. Morphological and textural data were used to firstly identify the ichnotaxa present within the Antarctic lavas based on taxonomic nomenclature from McLoughlin *et al.* (2009), and secondly to establish the biogenicity of these microborings based on the biogenicity criteria proposed by McLoughlin *et al.* (2007).

The bioalteration textures in the lavas are almost entirely tubular, consistent with a relatively low temperature alteration environment (Furnes *et al.* 2007). Granular alteration is consistently uncommon (but present), although it is the most widespread form of bioalteration in oceanic lavas, even at low temperatures. Textural identification of bioalteration was based on comparisons with published examples of characteristic features of biologically mediated dissolution of glass (Staudigel *et al.* 2008; Furnes *et al.* 2007 and references therein). It is noted in particular the restriction of bioalteration to glass boundaries, cracks and vesicles (i.e. places where liquid water can circulate); the association with palagonite formation (and therefore water); and most importantly, the characteristic ‘tubular’ appearance and other distinctive morphological features (segmentation, bifurcation, irregular pathways, constant microtubule width of ~2–20µm) of the bioalteration tubules, which closely resemble previously published examples from sea-floor lavas and are thought to be indicative of biological behaviour (Staudigel *et al.* 2006). Examples are shown in Figure 4.1. When viewed under SEM, the edges of glass clasts and fractures also display irregular pitting and etching patterns (see Figure 4.2a) which are

clearly distinguishable from the smooth alteration boundary that characterised ‘normal’ abiotic alteration.

Figure 4.1. Examples of bioalteration textures (a, c, d, e and f) and abiotic alteration (b) seen in the JRIVG hyaloclastites (M = microborings, F = fresh glass, P = palagonite, Z = zeolite). Arrows in photograph (c) indicate bifurcation.

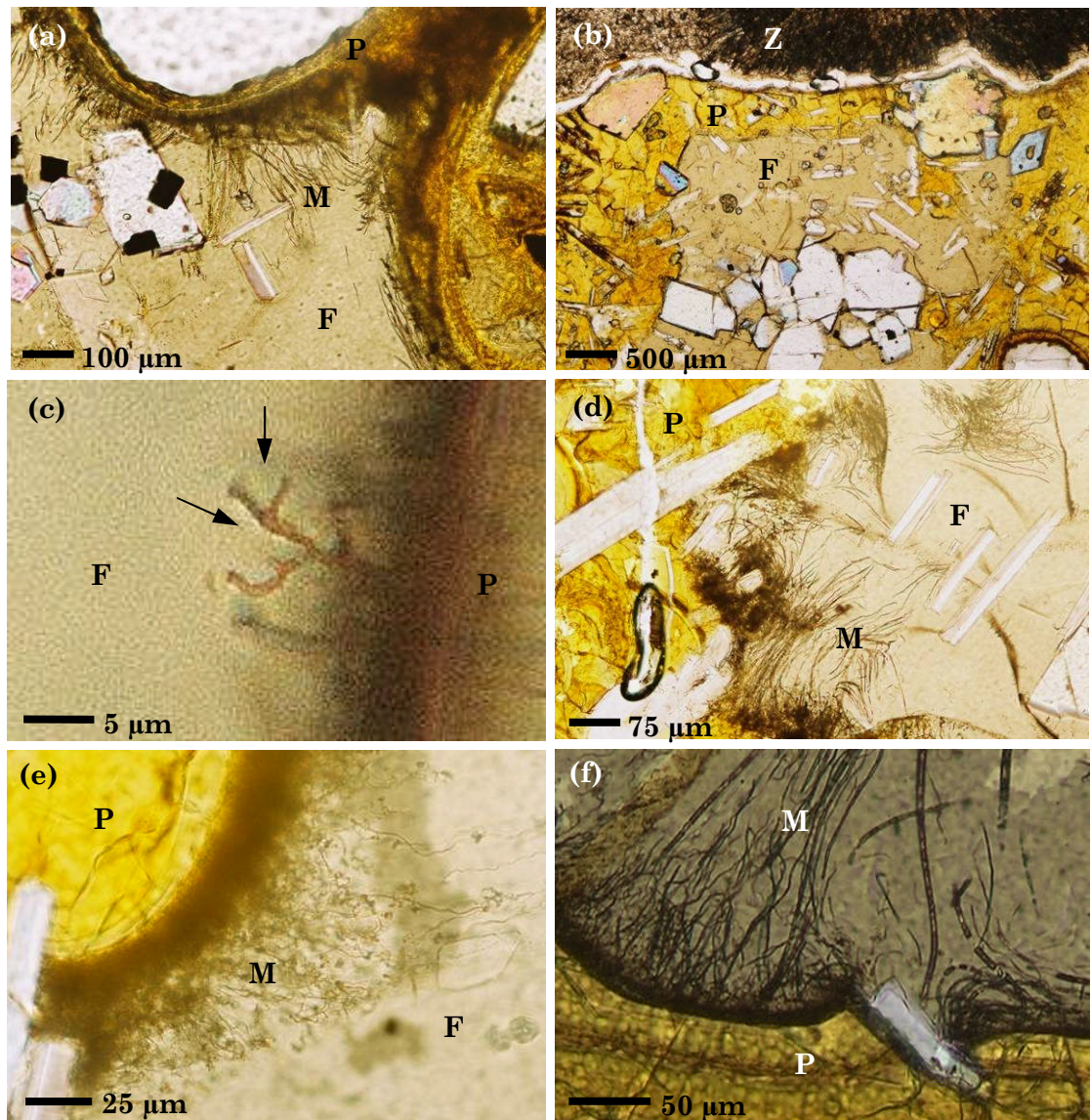
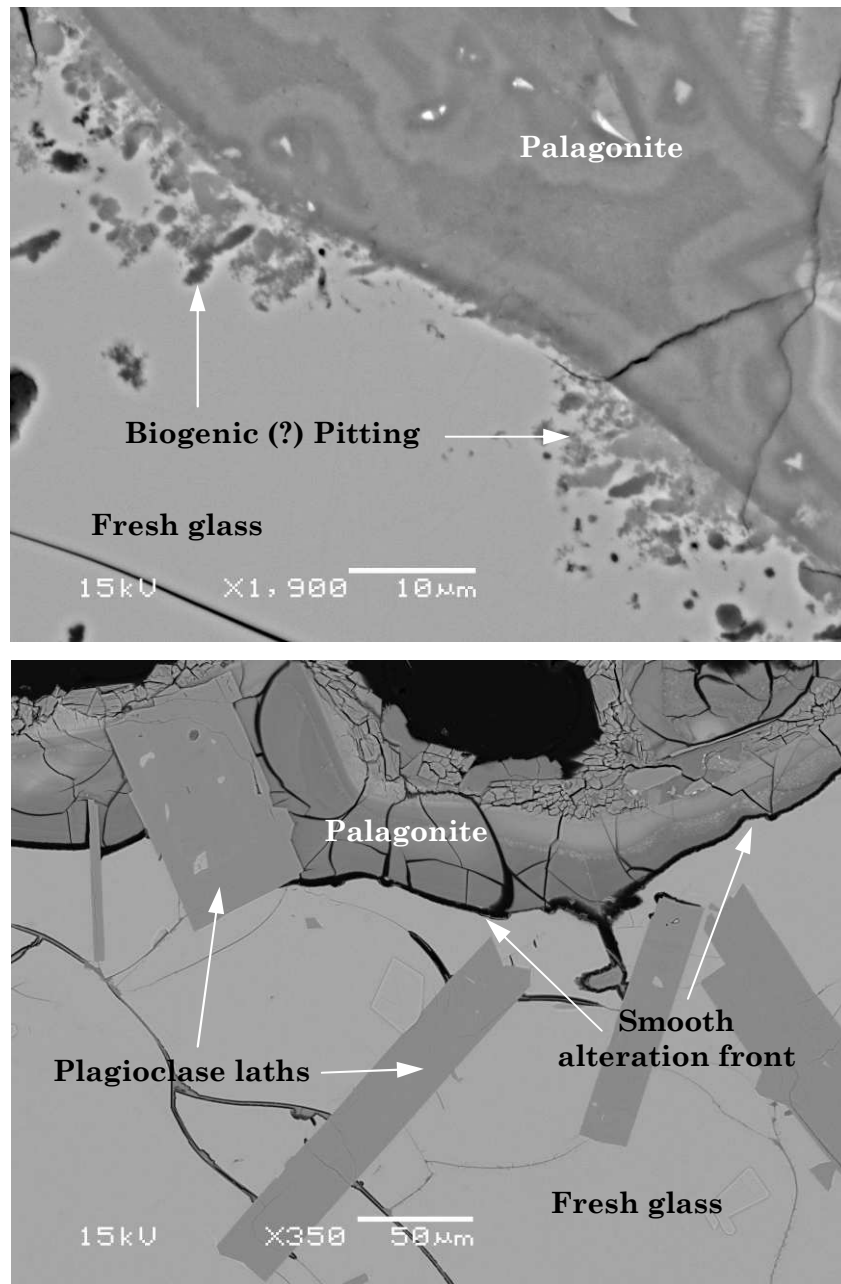


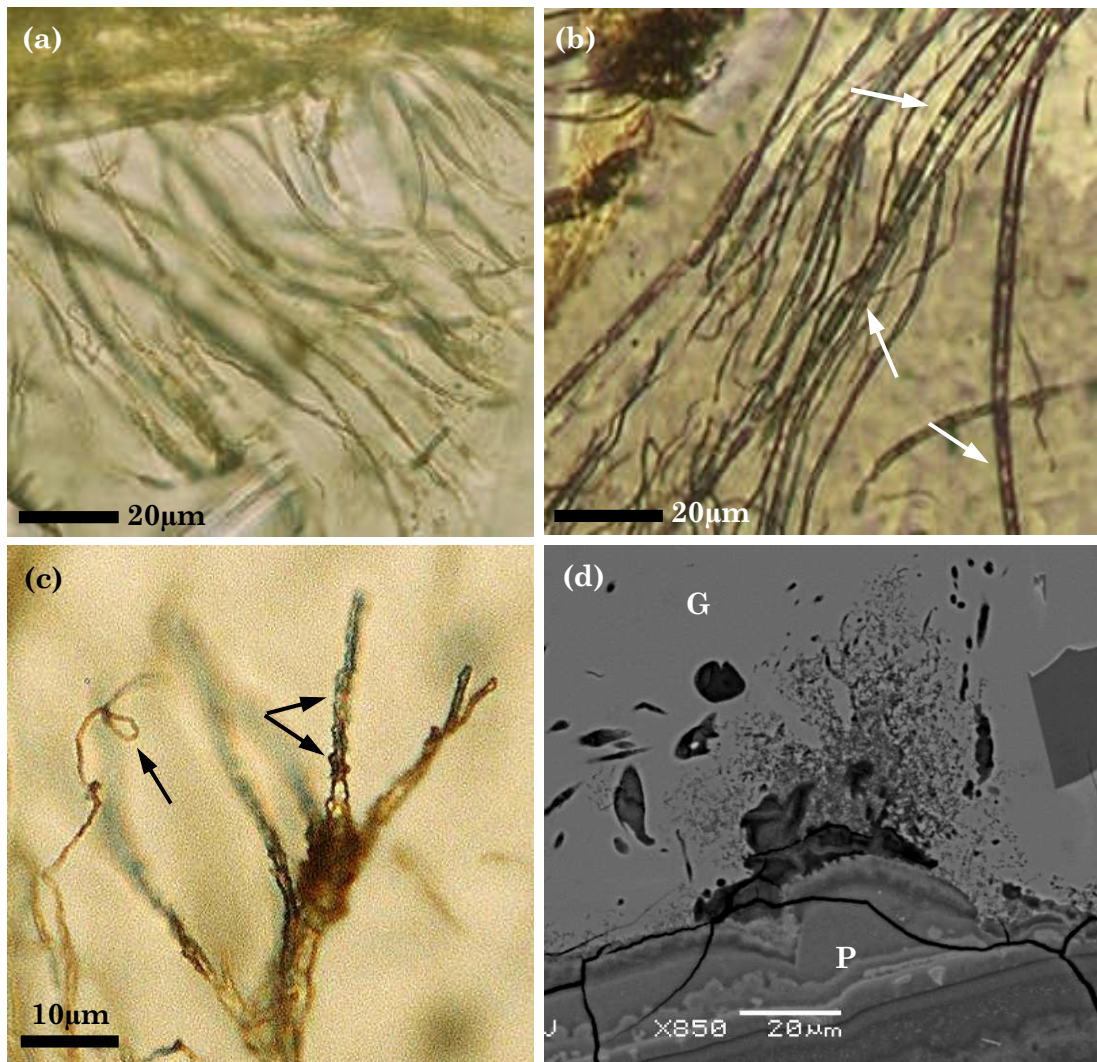
Figure 4.2. a) Bioalteration ‘pitting’ and ‘etching’ into glass boundaries under SEM. These features clearly extend from the fracture into the adjacent glass; b) abiotic alteration for comparison.



Based on the observed bioalteration textures in the James Ross Island lavas, four ichnospecies can be identified, three from the ichnogenera *Tubulohyalichnus*, and one from the ichnogenera *Granulohyalichnus*. All three ichnospecies belonging to *Tubulohyalichnus* were unambiguously identified according to the taxonomic criteria outlined by McLoughlin *et al.* (2009). The first, *Tubulohyalichnus simplex*, is by far the most common, and is characterised by simple tubular structures that extend into the glass away from fractures,

vesicle walls, and the margins of the glass clasts. These tubules nearly always occur in dense clusters, and form pathways that range from gently curvilinear to highly irregular (Figures 4.3a and 4.1e respectively). These ichnofossils are highly comparable to those seen in oceanic lavas, and it is also noted *Tubulohyalichnus simplus* is also the most abundant ichnofossil species of this ichnogenera within previously described lavas (McLoughlin *et al.* 2009). Secondly identified is the ichnofossil *Tubulohyalichnus annularis*. This ichnofossil species is not seen in all the Antarctic lava samples, but it is by no means identified as an isolated case. These tubular structures are similar to *Tubulohyalichnus simplus* in terms of basic morphology and distribution, but they have the addition of clear segmented structures along the length of the tubule (Figure 4.3b). The final ichnospecies within the *Tubulohyalichnus* genera is *Tubulohyalichnus stipes* (Figures 4.3c and 4.1c). This ichnospecies is defined by the branching structure of the tubules, where the branch diameters are the same as the tubule they are originating from. Their overall morphology and mineralogical relationship to the glass/palagonite is identical to that of *Tubulohyalichnus simplus*, although as with *Tubulohyalichnus stipes*, this ichnospecies is much less abundant. Lastly, *Granulohyalichnus vulgaris* was identified in only a few lavas, and was the least abundant of all the ichnospecies. In oceanic lavas this ichnofossil is especially common, much more so than any ichnofossils from the *Tubulohyalichnus* genera, but this does not appear to be the case in any of the James Ross Island hyaloclastite lavas. Where *Granulohyalichnus vulgaris* does appear, it is poorly developed and occurs only in very sporadic and isolated patches along fractures within glass clasts. Individual pits here however are fairly regular, with the majority being 0.5 - 1µm in size (Figure 4.3d). This size range is consistent with the size range attributed to this particular ichnofossil species, and furthermore is comparable to their oceanic counterparts where the most common pit size is ~0.5µm (Furnes *et al.* 2007).

Figure 4.3. Transmission light microscope (a-c) and back-scatter electron (d) images depicting the ichnofossil taxonomic classifications identified in the JRIVG subglacial hyaloclastites, a) *Tubulohyalichnus simplex*; b) *Tubulohyalichnus annularis*, arrows show segmentation within tubules; c) Tubular bioalteration classified as *Tubulohyalichnus stipes* for its branching structure, and the individual branches as *Tubulohyalichnus annularis*, where arrows show annulations along the length of the tubule. Also noted in this image is an example of *Tubulohyalichnus simplex* exhibiting a looped structure; d) *Granulohyalichnus vulgaris*, showing granular pitting extending out from the palagonite (P) into the glass (G).



4.2.2 Biogenicity

The bioalteration textures observed in the James Ross Island hyaloclastites fulfil two out of three biogenicity criteria described by McLoughlin *et al.* (2007):

1. “a geological context that demonstrates the syngenicity and antiquity of the putative biological remains”. The hyaloclastite bioalteration textures are restricted to areas previously exposed to external water. They are associated exclusively with vesicles, fractures and sideromelane clast boundaries.
2. “evidence of biogenic morphology and behaviour”. The hyaloclastite bioalteration textures display evidence of branching, segmentation, spiral pathways and a consistent tubule width. These morphological features can also be confidently identified using established ichnotaxa.

Additionally, evidence for a biological origin of such tubular bioalteration textures, based on morphology, is evaluated by Walton (2008). Here, Walton discusses and refutes the possible abiotic alternatives for these bioalteration textures, such as skeletal crystals, healed fractures and ambient inclusion trails.

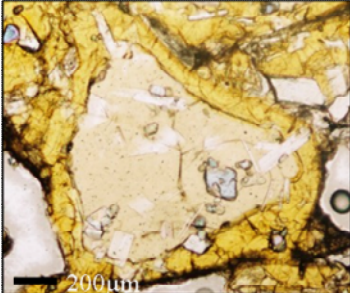
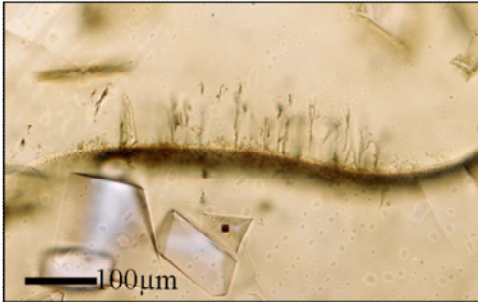
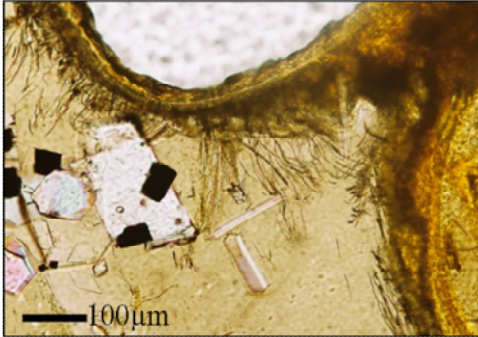
The third biogenicity criteria that was not fulfilled: “Geochemical evidence for biological processing”, was due to unknown collection and storage conditions of these samples. The lavas were originally collected by Prof. John Smellie for volcanological purposes, before being loaned for this work, and as such were not collected or stored in a way conducive for biologically-focused geochemical analysis. Many of the most convincing proofs for a biogenic origin of bioalteration textures are from lavas collected in-situ from oceanic crust. These studies combine geochemical analysis with DNA staining to demonstrate the presence of biological activity within these textures (e.g. Torsvik *et al.* 1998), and some studies even collected the samples aseptically (e.g. Fisk *et al.* 2003). Therefore, as the James Ross Island lava thin sections were not collected under controlled and documented conditions, it was decided any biogeochemical observations would not be reliable, particularly if they were to be used in proving the biogenicity of morphological features. Additionally, the thin sections had already been carbon coated for previous work by Prof. Smellie, and any naturally occurring biological carbon signal within these structures would already be compromised. However, the morphological, behaviourable, and contextual evidence show a high degree of

consistency with published examples, and are therefore interpreted here to be genuine bioalteration textures.

4.3 Bioalteration vs. Environment

To estimate the modal percentage of microborings, a semi-quantitative method was devised whereby the fraction of microborings that have affected the available alteration boundaries (grain boundaries, cracks and vesicles) was visually estimated for suitable basaltic glass clasts (sideromelane clasts) in each thin section. Results are recorded as numbers varying from 0 (absent) to 10 (all boundaries affected), which are termed here 'bioalteration values'. Example thin section images of bioalteration values 0, 5 and 10 are shown in Table 4.1. A typical thin section contains between 35 and 50 suitable clasts. Any clasts that were completely palagonitised were omitted from the assessment, as it has been widely reported that such microborings are not observed within palagonite itself, possibly because they have been destroyed by the alteration process (Furnes and Staudigel 1999). Of all these lavas (53), 20 of the samples are from marine-altered hyaloclastite; the remainder are believed to have only experienced freshwater (i.e. glacial meltwater) conditions. In total, over 2500 individual measurements were made. For each thin section, the mean bioalteration value was calculated from all sideromelane clasts analysed within the thin section. To avoid bias in the results, thin sections were analysed blind and in a random order. Additionally, a random selection of thin sections were later analysed a second time, and results compared to verify the initial estimation. Results of these mean bioalteration values for each thin section are presented in Table 4.2.

Table 4.1. Example bioalteration values used to determine the extent of bioalteration within the JRIVG hyaloclastites. A bioalteration value represents the visually estimated fraction of all alteration boundaries within a sideromelane clast that shows textural evidence of bioalteration. Bioalteration values range from 0 to 10, and examples of values 0, 5, and 10 are shown.

| Bioalteration Value | Description | Example thin section image |
|----------------------------|---|--|
| 0 | Any textural evidence of bioalteration is entirely absent from the sideromelane clast. Aqueous alteration is purely abiotic, producing a typical palagonite alteration boundary. |  |
| 5 | Textural evidence of bioalteration is present in ~50% of the available sideromelane boundaries within a clast. This image shows a fracture within a sideromelane clast, partially affected by bioalteration. |  |
| 10 | All boundaries (cracks, fissures, vesicles) within and around the sideromelane clast have undergone bioalteration. This image shows numerous microborings extending along the entire boundary of a vesicle within a sideromelane clast. |  |

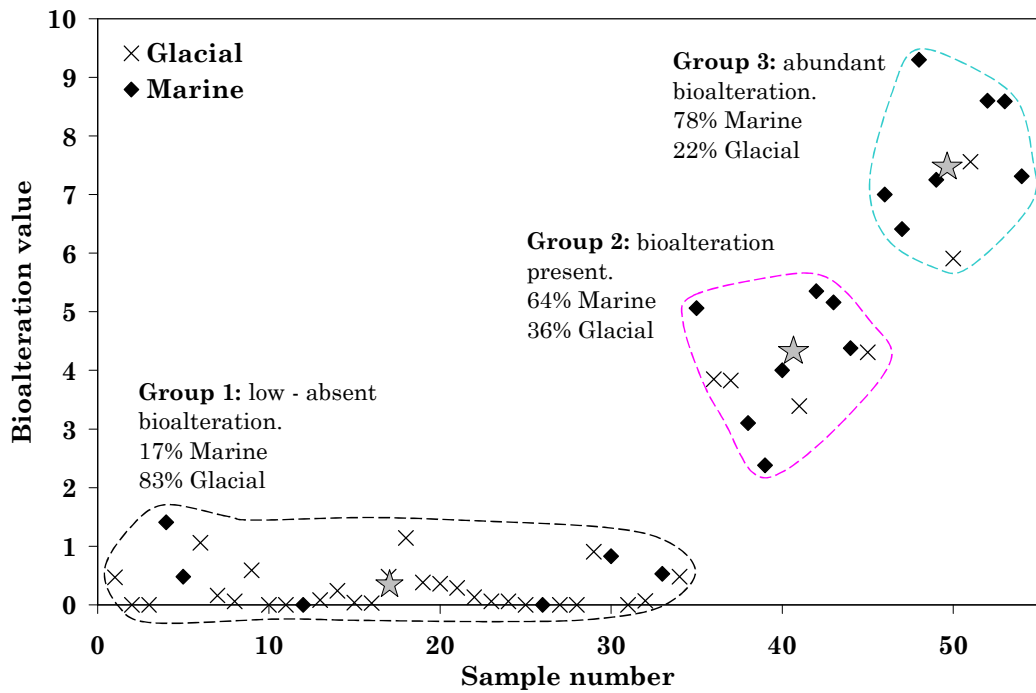
4.3.1 Bioalteration vs. aqueous environment

Mean bioalteration values for all the thin sections were processed using a K-means clustering algorithm using 3 clusters to divide the data into absent, present, and abundant bioalteration values. A K-means algorithm aims to cluster data into groups (of a pre-defined number) whilst minimising intra-cluster variance. The percentage of these individual clusters that consisted of marine and glacially-altered lavas was used to identify any correlation between bioalteration and alteration environment (Figure 4.4). The value of using statistical cluster analysis of large geobiological data sets of this nature is discussed in Storrie-Lombardi & Fisk (2004).

The individual lava deltas analysed (see Chapter 1, Figure 1.7 for names) range from entirely subglacial, subglacially erupted followed by marine alteration, and entirely marine. One delta (Dobson Dome; delta names after Smellie *et al.* 2008) experienced only freshwater conditions whilst a second (Lachman Crags main) was probably wholly marine emplaced. Another three deltas (Forster Cliffs, Patalamon Mesa main and Tumbledown Cliffs) were initially emplaced in a glacial setting (i.e. freshwater alteration) but subsequently were affected by marine incursions (Johnson and Smellie 2007). The Dobson and Lachman deltas were selected to act as possible controls (or ‘end-members’) to help interpret the deltas that experienced both freshwater and marine conditions. The deltas range in age from < 80 ka to 5.15 Ma, thus giving the potential to identify any age-related effects on bioalteration. Much of the alteration probably took place shortly after initial emplacement, while the permeable hyaloclastite pile was cooling and the pore fluids were still relatively warm, but the marine alteration may have taken place at somewhat cooler temperatures, long after volcanic activity (Johnson & Smellie 2007).

Figure 4.4 shows the clustering of the data as revealed by K-means analysis. A clear division between the three groups can be seen, and is taken to be representative of differing levels of bioalteration: ‘absent/low’, ‘present’ and ‘abundant’. The percentage of the two different environments (marine and glacial) for each group clearly shows a strong trend of increasing bioalteration with a marine environment, and decreasing bioalteration with a glacial environment. The overall trend is that bioalteration is typically higher in hyaloclastite samples that experienced marine conditions than those that simply experienced freshwater (meltwater) conditions. Additionally, a t-test value (a test of whether the means of two groups are statistically different from each other) of $p < 0.0001$ was calculated for the data, strongly suggesting this observed pattern is not simply a result of chance.

Figure 4.4. Plot of K-means clustering of the mean bioalteration values obtained on samples from James Ross Island hyaloclastite. The algorithm shows three distinct clusters representative of increasing bioalteration values. Filled symbols are for samples that experienced marine conditions. Crosses only experienced freshwater conditions. Grey stars represent the centroid for each cluster. Dark blue, pink and black represent the different clusters assigned by the algorithm – the dashed field line has been added to clearly show the parameters of these clusters. The ‘abundant bioalteration’ group is dominated by marine altered hyaloclastites, whereas the ‘low - absent bioalteration’ group is dominated by hyaloclastites altered by freshwater (glacial meltwater). The middle group ‘bioalteration present’ is represented almost equally by both environments.



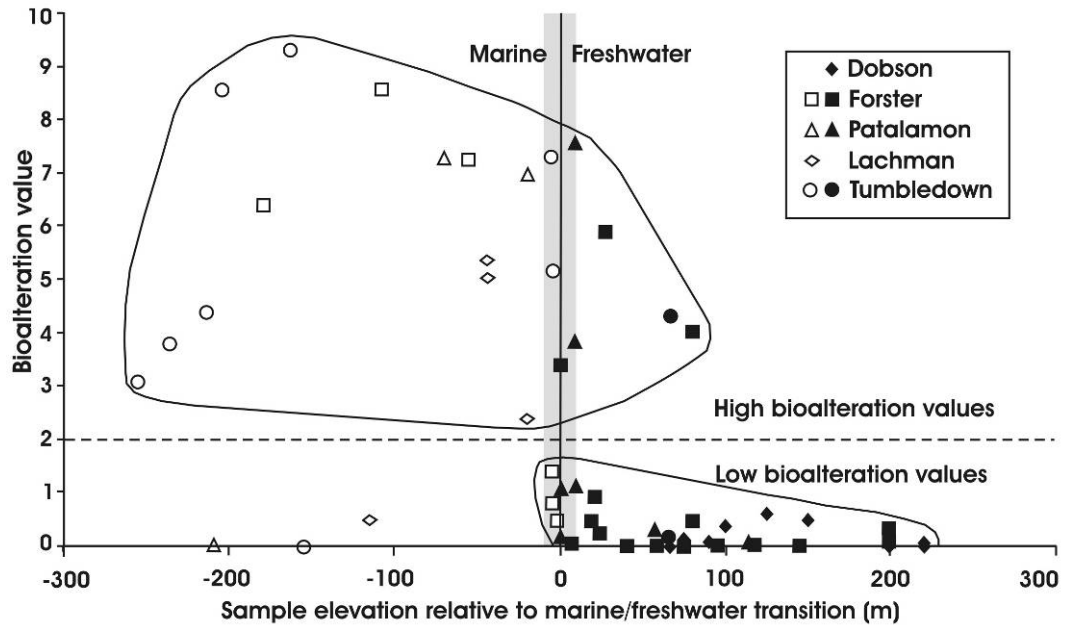
The semi-quantitative analysis demonstrates a relationship between bioalteration extent and alteration fluid source: seawater-affected samples generally show a much higher level of bioalteration compared with samples affected only by freshwater (glacial meltwater). The latter are characterised by extremely low bioalteration values. If bioalteration values <1 are taken to represent no bioalteration present at all, then 76% of glacial hyaloclastite can be interpreted as lacking in bioalteration. In comparison, only 26% of marine-altered hyaloclastites have values <1 . Thus, glacially-derived meltwater does not appear to strongly promote bioalteration. Conversely, there appears to be no difference between the types of microbial textures found in either freshwater or marine altered lavas, pointing towards a common method by which the microbes dissolve or etch the glass, regardless of alteration fluid.

There are three main factors that could possibly explain the relationship between alteration fluid composition and the abundance of microborings. Firstly, the microbial biomass of seawater is significantly higher than that of glacial meltwater. During a subglacial eruption, the primary source of microbes is the overlying glacial ice. As a lava-fed delta eruption progresses, microbes might enter via meltwater pathways, fractures in the ice and from subaerial exposure of the delta top. Other (non-delta-forming) glaciovolcanic eruptions may remain entirely subglacial (e.g. eruptions that cease at the pillow volcano or tindar-forming stages (Smellie 2007). Secondly, seawater is more nutrient rich than glacial meltwater, and combined with the basaltic glass substrate, may provide ideal conditions for microboring formation.

4.3.2 Bioalteration vs. elevation and age

Parameters such as elevation and age may be directly related to the alteration environment, since the lava-fed deltas on James Ross Island are known to have undergone a history of initial freshwater alteration followed by marine alteration (Johnson and Smellie 2007) and they vary in age by up to 6 Myrs (Smellie *et al.* 2008), thus giving the deltas varying time to be altered by percolating fluids. Samples were normalised relative to the elevation of the surfaces that separate marine from freshwater alteration (identified by Johnson and Smellie (2007) for each delta). These normalised elevations are given in Table 4.2. In addition, one delta (Dobson) only experienced freshwater conditions, whilst another (Lachman main) was probably marine emplaced; these two deltas were used as controls for distinguishing marine from freshwater bioalteration effects. There is a relatively strong correlation between those samples with low bioalteration values (<2) that were affected only by freshwater, and marine-affected samples showing significantly higher values (Figure 4.6), with only 15 % of samples contradicting this observation. Note that the marine—freshwater transition may be a *zone* several metres thick rather than a precise elevation. The elevations used here (from Johnson and Smellie 2007) may only be accurate to within ± 5 -10 m, and the presence of “marine-affected” samples with apparently anomalous values close to the transition surface may be simply an artefact of the artificially “precise” elevation used in the calculations (e.g. three supposedly marine-affected samples from the Forster Cliffs delta showing low bioalteration values; Figure 4.5).

Figure 4.5. Plot showing sample elevation and bioalteration values, for James Ross Island hyaloclastites. Elevation is sample height (in metres) relative to the upper surface reached by seawater during later marine influxes (shown as vertical line at 0 m; surface identified by Johnson and Smellie 2007). Samples below that surface experienced marine conditions after an initial freshwater environment, whilst higher samples experienced only freshwater conditions. The elevation of the marine surface is not precisely determined in all deltas (John Smellie, pers. comm.), an uncertainty indicated here schematically by the grey band. Outside of the grey band only 6 samples out of 53 (11 %) plot “anomalously”, and the dataset shows clearly that marine samples typically have significantly higher bioalteration values compared with those at higher elevations that experienced only freshwater conditions.

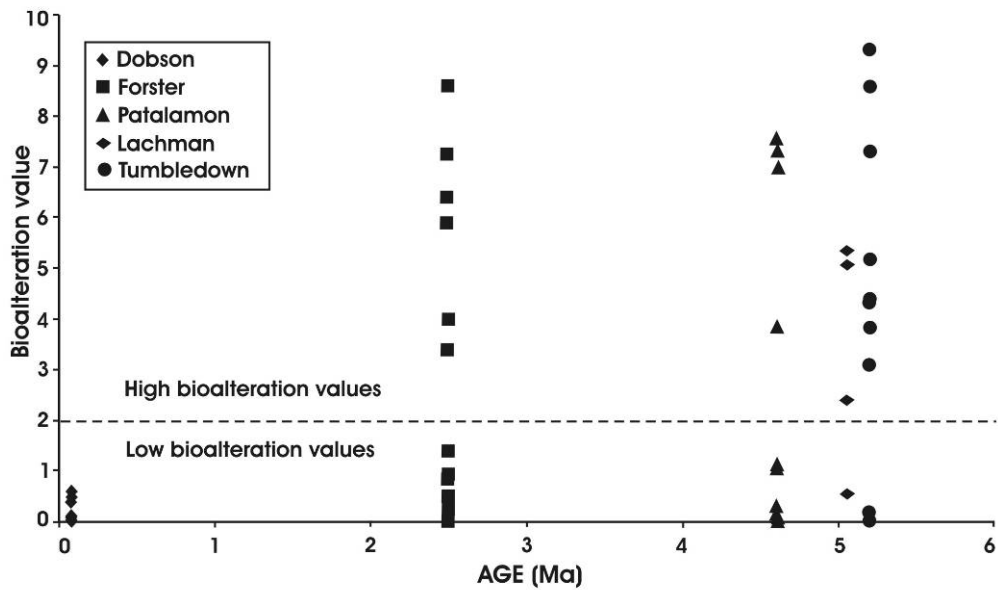


Depth is thought to be one of the most important controls of bioalteration in oceanic lavas, whereby bioalteration decreases with depth due to elevated temperatures and lack of fluids (Furnes *et al.* 2001a; Fisk *et al.* 2003; Furnes and Staudigel 1999). The greater intensity of bioalteration in the JRIVG hyaloclastites occurs in the marine-affected samples, which probably took place at lower temperatures. However, our results suggest that the frequency of microborings in our samples is predominantly controlled by the type of alteration fluid.

Intuitively, hyaloclastites that are older have had a longer residence time and thus might have had more time or opportunities to be altered by endolithic microorganisms. However, there appears to be no obvious relationship between delta age and intensity of bioalteration. Figure 4.6 shows bioalteration values plotted against delta age. Only the youngest delta (Dobson; < 80 ka) shows the least effects of bioalteration so the possibility that insufficient time has elapsed

for bioalteration to occur cannot be completely discounted in this case, but it is also noted that this delta has also only existed within a glacial environment. All the other deltas however show similar, widely varying levels of bioalteration values.

Figure 4.6. Plot of bioalteration values against age (i.e. emplacement age of the host lava-fed delta; ages from Smellie *et al.* 2008). Although the youngest delta (Dobson Dome) shows very limited signs of bioalteration, there is overall no obvious relationship between bioalteration intensity and sample age.



It is possible that it is simply the intensity of aqueous (abiotic) alteration experienced by the glass that promotes the development of bioalteration textures. If the thickness of palagonite rims on glass fragments and amount of zeolite formation within the hyaloclastite are interpreted as a measure of the intensity of aqueous alteration, then comparison of the datasets for the two different environments suggests that there is no correlation with intensity of bioalteration and extent of palagonitisation. The marine altered samples do not contain more secondary minerals than the glacially (freshwater) altered lavas. This observation is consistent with that of Johnson and Smellie (2007), who suggested that the majority of the alteration (of original glass and filling pore spaces) took place relatively soon after delta emplacement under freshwater conditions, with subsequent marine conditions mainly simply modifying the zeolite (and palagonite) compositions and filling any remaining pore spaces and fractures. This further implies the formation of bioalteration textures in this volcanic province is controlled largely by the aqueous chemistry and origin of the

alteration fluids. Alternatively, it is always a possibility that these bioalteration textures are not in fact biogenic, and are an entirely, but as yet unrecognised, type of abiotic alteration, although this latter option is unlikely considering the evidence presented by previous researchers that suggests otherwise (e.g. McLoughlin *et al.* 2009).

Figure 4.7 shows a schematic sequence of events that could potentially explain the observations of freshwater versus seawater bioalteration intensity and sample elevation. Hyaloclastite is initially altered by glacial meltwater, probably soon after emplacement when the volcanic pile is still warm. The hyaloclastite is a coarse-grained lithofacies relatively free of material finer than coarse sand, which facilitates the entry and circulation of freshwater (glacial meltwater). The results suggest that only minor bioalteration takes place at this stage. During interglacial periods, the ice retreats and seawater penetrates the hyaloclastite, probably along fractures, grain boundaries and any unfilled pore spaces (Johnson and Smellie 2007). This is probably when the bulk of the microbial community was introduced, with a consequent increase in intensity of microboring activity.

Figure 4.7. Diagram of a simplified James Ross Island subglacial lava sequence showing different stages of fluid alteration and microboring production.

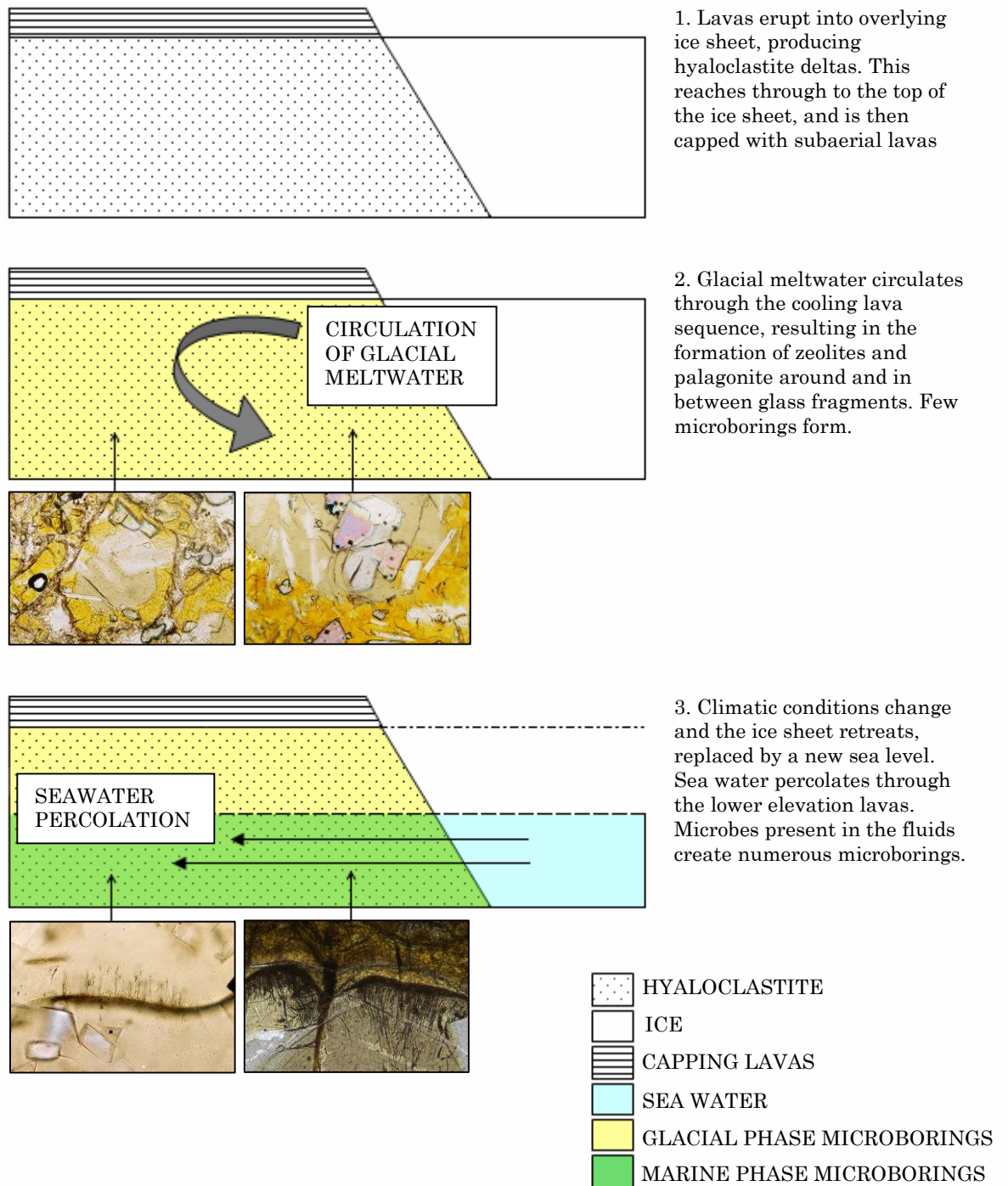


Table 4.2. Mean bioalteration values for hyaloclastites from James Ross Island. Random re-test means values are also shown. Elevation data is normalised to marine-freshwater transition zone (value=0)

| Sample | Age ^(a) (Ma. unless stated) | Environment ^(b) | Elevation ^(c) | Number of glass clasts | Mean fraction of bioalteration (out of 10) ^(d) | Standard deviation of mean bioalteration value | Notes and re-test values |
|--|---|-------------------------------|-----------------------------|------------------------------|--|--|---|
| Dobson Dome | | | | | | | |
| DJ.1733.2 | <80 ka | Freshwater | 220 | 40 | 0 | 0 | |
| DJ.1733.2 | <80 ka | Freshwater | 220 | 27 | 0.07 | 0.27 | |
| DJ.2103.1 | <80 ka | Freshwater | 199 | 48 | 0.03 | 0.18 | |
| DJ.2103.2 | <80 ka | Freshwater | 150 | 31 | 0.48 | 1 | |
| DJ.2103.3 | <80 ka | Freshwater | 125 | 38 | 0.59 | 0.87 | Re-test mean=0.34 |
| DJ.2103.4a | <80 ka | Freshwater | 100 | 32 | 0.38 | 0.91 | |
| DJ.2103.6 | <80 ka | Freshwater | 90 | 32 | 0.06 | 0.25 | |
| DJ.2103.7 | <80 ka | Freshwater | 75 | 26 | 0.08 | 0.27 | |
| DJ.2103.8 | <80 ka | Freshwater | 66 | 53 | 0 | 0 | Re-test mean =0 |
| Forster Cliffs | | | | | | | |
| DJ.1745.6 | 2.50 | Freshwater | 0 | 35 | 3.39 | 2.46 | On marine-freshwater transition |
| DJ.1752.2 | 2.50 | Freshwater | 199 | 28 | 0.36 | 0.91 | |
| DJ.1753.1 | 2.50 | Freshwater | 95 | 45 | 0 | 0 | |
| DJ.2056.1 | 2.50 | Freshwater | 75 | 47 | 0 | 0 | |
| DJ.2056.2 | 2.50 | Freshwater | 7 | 36 | 0.04 | 0.19 | |
| DJ.2056.5 | 2.50 | Freshwater | 199 | 40 | 0.13 | 0.34 | |
| DJ.2056.6 | 2.50 | Freshwater | 119 | 35 | 0.06 | 0.25 | |
| DJ.2056.7 | 2.50 | Freshwater | 145 | 40 | 0 | 0 | |
| DJ.2056.8 | 2.50 | Freshwater | 59 | 35 | 0 | 0 | |
| DJ.2102.3 | 2.50 | Freshwater | 21 | 39 | 0.91 | 1.25 | |
| DJ.2102.4 | 2.50 | Freshwater | 27 | 35 | 5.91 | 2.01 | Re-test mean=4.8 |
| DJ.2102.6 | 2.50 | Freshwater | 19 | 29 | 0.48 | 0.69 | |
| DJ.2102.7 | 2.50 | Freshwater | 24 | 29 | 0.24 | 0.51 | Re-test mean=0.44 |
| DJ.2102.8 | 2.50 | Freshwater | 40 | 50 | 0 | 0 | |
| DJ.1754.8 | 2.50 | Marine | -180 | 42 | 6.41 | 1.36 | |
| DJ.1755.9 | 2.50 | Marine | N/A | 20 | 8.6 | 1.14 | |
| DJ.2056.4 | 2.50 | Marine | -1 | 41 | 0.48 | 1.03 | Just below marine-freshwater transition |
| DJ.2102.1 | 2.50 | Marine | -5 | 30 | 1.41 | 1.04 | Just below marine-freshwater transition |
| DJ.2102.2 | 2.50 | Marine | -4 | 45 | 0.83 | 1.56 | Just below marine-freshwater transition |
| St. Rita Point (=Forster Cliffs?) | | | | | | | |
| DJ.1961.2 | 2.50 | Freshwater | 80 | 37 | 0.47 | 0.76 | |
| DJ.1965.5 | 2.50 | Freshwater | 80 | 40 | 4 | 2.72 | |
| DJ.2001.2 | 2.50 | Freshwater | 116 | 24 | 0 | 0 | |
| DJ.2004.1 | 2.50 | Marine | N/A | 48 | 7.25 | 1.88 | Re-test mean=7.12 |
| Palamon Mesa main | | | | | | | |
| DJ.2073.1 | 4.16 | Freshwater | 1 | 33 | 1.06 | 1.31 | Just above marine-freshwater transition |
| DJ.2073.9 | 4.16 | Freshwater | 114 | 40 | 0.06 | 0.25 | |
| DJ.2083.1 | 4.16 | Freshwater | 57 | 24 | 0.29 | 0.46 | |
| DJ.2083.3 | 4.16 | Freshwater | 0 | 55 | 0.16 | 0.37 | On marine-freshwater transition |
| DJ.2090.1 | 4.16 | Freshwater | 10 | 26 | 7.56 | 1.81 | |
| DJ.2091.1 | 4.16 | Freshwater | 10 | 28 | 1.14 | 1.63 | Re-test mean=0.85 |
| DJ.2090.3 | 4.16 | Freshwater | 10 | 27 | 3.85 | 2.4 | |
| DJ.2982.3 | 4.16 | Marine | -20 | 30 | 7 | 1.54 | Re-test mean=6.7 |
| DJ.2093.5 | 4.16 | Marine | -210 | 40 | 0 | 0 | Re-test mean=0 |
| Lachman Crags main | | | | | | | |
| DJ.1714.4 | 5.06 | Marine | -43 | 32 | 5.06 | 2.53 | |
| DJ.1714.4 | 5.06 | Marine | -43 | 34 | 5.35 | 2.68 | |
| DJ.1715.5 | 5.06 | Marine | -115 | 35 | 0.53 | 1.07 | |
| DJ.1724.1 | 5.06 | Marine | -20 | 45 | 2.38 | 2.46 | |
| Tumbledown Cliffs | | | | | | | |
| DJ.2132.1 | 5.15 | Freshwater | N/A | 32 | 4.31 | 2.22 | |
| DJ.2079.3 | 5.15 | Marine | -255 | 39 | 3.1 | 1.87 | |
| DJ.2086.6 | 5.15 | Marine | -5 | 32 | 7.31 | 2.62 | |
| DJ.2113.1 | 5.15 | Marine | -155 | 28 | 0 | 0 | |
| DJ.2115.1 | 5.15 | Marine | -205 | 41 | 8.59 | 1.37 | Re-test mean=8.98 |
| DJ.2116.1 | 5.15 | Marine | -215 | 29 | 4.38 | 3.28 | |
| DJ.2117.1 | 5.15 | Marine | -162 | 43 | 9.3 | 0.72 | |
| DJ.2136.1 | 5.15 | Marine | -5 | 31 | 5.16 | 3 | |

^aFrom Smellie et al. (2008)

^bFrom Johnson & Smellie (2007); samples listed as marine have also previously experienced freshwater alteration

^cPers.comm. John Smellie (2008)

^dSee test for details of method

4.4 Implications for Using Bioalteration as a Martian Biosignature

The principle aim of this study was to firstly expand the range of environments within which bioalteration is currently explored, and secondly utilise this new knowledge to infer the suitability of bioalteration as a biosignature for Mars. The results appear to show that bioalteration is consistently absent from lavas that have been exposed only to freshwater environments. Whilst there have been very few bioalteration studies on lavas that have experienced non-marine alteration conditions, it is apparent that bioalteration textures are largely restricted to lavas in marine environments. As highlighted in Chapter 3, subglacially erupted basaltic lavas from Iceland also show a distinct lack of bioalteration textures, despite evidence for widespread aqueous alteration and development of palagonite alteration fronts. Putative bioalteration textures have been identified in Icelandic hyaloclastites by Cockell *et al.* (2008), but these are far from the tubular morphologies seen in seafloor lavas and the marine-altered James Ross Island hyaloclastites. Whilst more studies of this nature clearly need to be done, the potential for finding bioalteration textures within Martian basalts that have undergone aqueous alteration is perhaps reduced by this finding. The terrestrial biosphere is rich and extensive, yet this does not always result in the formation of biosignatures in terrestrial rocks. As a result, the presence of a widespread basaltic-lava hosted Martian biosphere may evade detection if the surrounding aqueous environment is not conducive to the formation of bioalteration textures. This is particularly relevant when considering putative subglacially erupted volcanic constructs on Mars (e.g. Chapman 1994; Chapman and Tanaka 2001; Ghatan and Head 2002; Head and Wilson 2002; Chapman and Smellie 2007) as astrobiological targets.

4.5 Conclusions and Future work

The study of the bioalteration of volcanic glass has almost exclusively focused on lavas in an oceanic setting, either associated with spreading ridges or oceanic plateaux. In contrast this study contributes to the knowledge of bioalteration in a terrestrial subaqueous setting. The principal conclusions are:

- The JRIVG hyaloclastites show numerous examples of bioalteration, particularly the formation of microtubules, which display characteristic bioalteration texture biogenic features (McLoughlin *et al.* 2007).
- Semi-quantitative analysis of the intensity of bioalteration shows that there is much greater presence of bioalteration in samples that experienced marine conditions. Indeed, bioalteration is minor and is often absent in samples that were only affected by freshwater. This shows that, additionally to eruptive setting, the composition of the alteration fluids exerts an important control on the intensity of bioalteration textures.
- Variables that affect alteration fluids derived from different sources include microbial biomass, nutrient supply and aqueous chemistry. One or a combination of these could be the cause of the observed bias of microboring formation towards marine-affected samples.
- The main limitation of this work is its reliance on the assumption that the work by Johnson and Smellie (2007) identifying the aqueous environment within which the hyaloclastite has been subjected to is in fact correct. Should this particular study be proved wrong, the apparent dichotomy observed between the presence of bioalteration in marine and freshwater altered hyaloclastite may come under question.
- Finally, this study shows that it is important to characterise bioalteration textures in environments other than seafloor lavas to gain a fuller understanding of their distribution and formation, particularly if such morphological features are to be used as Martian biosignatures. For example, if glacial meltwater is generally very poor in microbes, the chances of detecting exobiology in subglacially erupted Mars glassy rocks are significantly reduced.

Future work should focus on the collection and interpretation of geochemical data associated with these biosignatures. Geochemical differences have often been used for establishing biogenicity (McLoughlin *et al.* 2007), and may shed some light as to why there appears to be a marine – freshwater dichotomy. Likewise, running long-term (e.g. 1 year or longer) incubation experiments whereby pristine basaltic glass is incubated within fresh- and marine-water based media enrichments may reveal a preference towards one environment or another for the generation of bioalteration textures.

CHAPTER 5

THE VIABILITY OF A SUBGLACIAL VOLCANIC HABITAT ON MARS: AN EXPERIMENTAL AND CULTURE - BASED TEST

The preceding chapters have explored environments formed through the interaction of basaltic volcanism and glacial ice, in terms of their present-day microbial diversity (Chapter 3), and the potential for biosignature formation (Chapter 4). This chapter describes experimental work testing subglacial volcanism as an appropriate Martian analogue environment, with regard to providing adequate protection from the inhospitable Martian surface, whilst supplying the key ingredients for life, such as liquid water. This was conducted along two lines of enquiry.

Firstly, a Mars environment simulation chamber was utilised to replicate as close as possible the present day Martian environment, including atmospheric pressure and composition, temperature, and UV flux. A self-contained simplified subglacial volcanic microcosm was incubated under these environmental conditions, with the aim to test for bacterial survivability using culture-based techniques.

Secondly, through the culture-based assessment of bacterial survivability, the culturable microbial diversity of Icelandic subglacial lava was investigated using molecular-based methods of identification. This data is used to identify those isolates that do and don't survive the Martian environment simulation, and also to compare the cultured microbes here to those isolated from other similar cold temperature oligotrophic environments.

5.1 Testing a Martian analogue environment

Subglacial volcanism is a process thought to have occurred on Mars in many different locations and during all three major epochs (see Chapter 1, section 1.2.2). The resulting combination of a liquid water source, geothermal heat, and protection from surface extremes renders these environments potentially viable habitats. As such, the deposits of these environments left in the geological record – such as subglacially erupted lavas, Jökulhlaup sediments, and subglacial lake sediments – could be suitable targets for future life detection missions.

Many previous simulation experiments suggest life on Mars has the greatest chance of survivability if it resides within the subsurface (see Chapter 1, section 1.4.2), or where there is adequate shielding from UV radiation, such as rock crevices. However, whilst this eliminates one problem, the issues of liquid water, energy supply, and nutrient availability remain. Therefore, it is important to investigate and test environments where these requirements are potentially met, such as the conditions created through subglacial volcanism. The aim of this work was to test the hypothesis that subglacial volcanic environments are indeed habitable under simulated Martian conditions. In this experiment, the main environmental factors of present day Mars were implemented: high UV flux, low atmospheric pressure, CO₂ dominated atmosphere, and subzero temperatures. It was hypothesised that the microbial community indigenous to the subglacial lava would be sufficiently protected against the above mentioned Martian conditions by the presence of a constant heat source from below and an overlying ice layer.

This was an entirely culture-based study, for two reasons. Firstly, culturing provides a simple, rapid assessment of the viable microbial community within an environment, so direct comparisons between the simulated environment and the associated untreated sample and negative control could be taken as an indication of survivability. Secondly, identifying the culturable diversity of subglacial basaltic lavas is complementary to the purely molecular analysis detailed in Chapter 3. For this purpose, pillow basalt samples from the same locality (ASK9) were used in these experiments. The natural bacterial communities present within these Arctic basalts are considered here as suitable model organisms

firstly for their adaption to oligotrophic lava habitats, and also for their ability to thrive in cold, dry and highly seasonal environments.

5.2 Experimental Set up and Sample Processing

A subglacial volcanic microcosm (SVM) was devised that aimed to recreate the aspects of a subglacial volcanic environment that were identified as being conducive to the habitability of these systems. This included a heat source (from below) and water-ice (above). The aim was to create a Martian environment that was as realistic as possible. However, the absence of any detectable *active* subglacial volcanic systems on Mars today means there are no measured physical and chemical parameters from which to base this simulated environment upon. However, the presence of widespread subglacial volcanic activity on Earth has resulted in numerous studies on both extinct and active systems, and it is these upon which the experimental set up here is based. More detail on subglacial volcanic environments can be found in Chapter 1, section 1.2.1).

5.2.1 Experimental set-up

Subglacially erupted pillow lava from Askja was used for this study. To minimise any effect of contamination, the subglacial volcanic microcosm (SVM) and its components were confined within a sterilised Nalgene container (Figure 5.1). The only thing not sterilised prior to the experiment assembly was the lava sample (~5cm x 3cm) and its indigenous microbial community. The lava was submerged and frozen into the base of simulated glacial ice, made from sterile distilled and deionised water, inside the container. Prior to freezing, the lava was gently agitated to aid the removal of air bubbles trapped within lava vesicles, so not to interfere with the controlled Martian conditions. It was hypothesised that the temperature difference between the underlying heat pad and overlying ice would result in an intermediate layer of liquid meltwater around the lava, and temperature measurements were taken from this region throughout the experiment. Figure 5.1 shows the presence of a thermocouple at the lava-ice-heat pad interface. As the only way to measure the temperature here was to place a thermocouple directly into the experiment, the thermocouple was also sterilised by autoclaving. The temperature here was recorded every 10 minutes.

To ascertain the importance of heat + ice for the creation of a habitable environment, an additional ‘negative control’ was run. This used a comparable sample of subglacial lava (collected from the same outcrop), and this was completely exposed to the same Martian conditions, without the presence of heat and ice. This was not expected to show significant, or indeed any, signs of survival. Finally, untreated lava provided the original culturable community from which the results of the subglacial volcanic microcosm (SVM) and negative control could be compared. This untreated lava sample was not exposed to any Martian conditions, and the microorganisms that were cultured were taken to represent the natural cultivable indigenous community. It is noted that whilst using an entire microbial community in a microcosm/environmental simulation is more realistic, natural spatial variation of bacterial species between multiple samples of lava will undoubtedly exist. However, all lava samples used were collected at the same time, stored under the same conditions, and processed in the same manner to help avoid any sampling bias. Additionally, the phylogenetic analysis of the ASK9 Pillow Lava (Chapter 3, section 3.4.2) provides the broad taxonomic context for the bacteria isolated for this study, and it is likely that two similar samples of ASK9 Pillow Lava from the same outcrop will be inhabited by a bacterial community of a similar phylogenetic composition, particularly at the phylum level.

Simulation of Martian conditions was achieved with a Mars environmental chamber situated at the Planetary and Space Sciences Research Institute, Open University. The chamber was set up to maintain a pressure of 8 mbar, a Martian atmosphere composition, and UV radiation at -30°C. For UV, a xenon-arc lamp (Muller 450 W lamp, model XBO450W) was used, and generated light with wavelengths >350nm. The Martian atmosphere consisted of Carbon Dioxide with 2.7% Nitrogen, 1.6% Argon, 0.13% Oxygen, and 0.07% Carbon Monoxide, and this was flushed through the chamber before depressurisation. Due to the presence of water ice in the subglacial volcanic environment simulation, humidity was effectively uncontrolled due to effects of sublimation throughout the experiment, which was observed to result in small crystals of ice forming on the inside wall of the chamber. The chamber was connected to a temperature controller, which was able to maintain a constant temperature of the heat pads at around 40°C. The heat pads could not be sterilised so were placed externally

at the base of the Nalgene container. The experiment was incubated in the these Martian analogue conditions for 7 days.

Figure 5.1. Experimental set up of the SVM within the Martian environmental chamber with hypothesised meltwater accumulation at the base of the ice. For the negative control, the same set up was used but without the addition of ice and a heat source. Red circles indicate those parts of the experiment/chamber that the temperature could be measured from. The internal diameter of the chamber is ~12 cm.

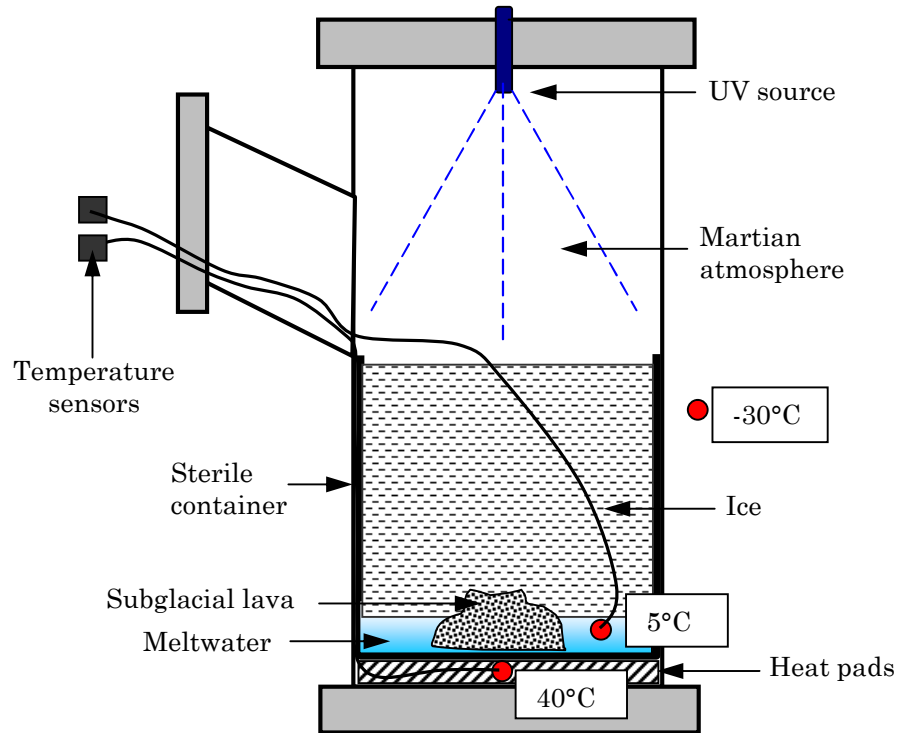


Figure 5.2. Photograph of the Mars chamber used for this experiment, showing all environmental parameters.

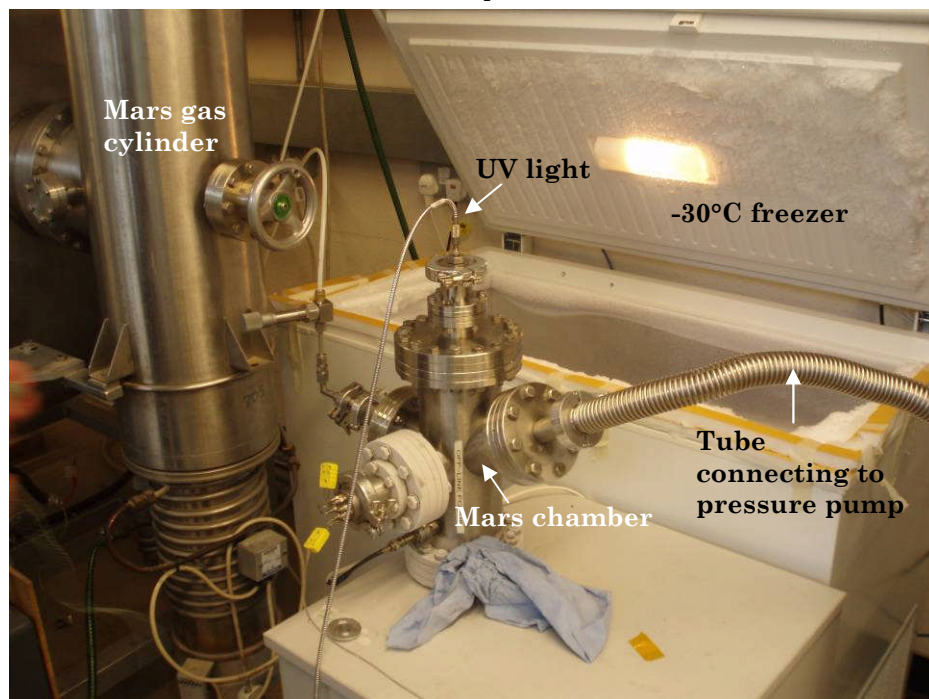


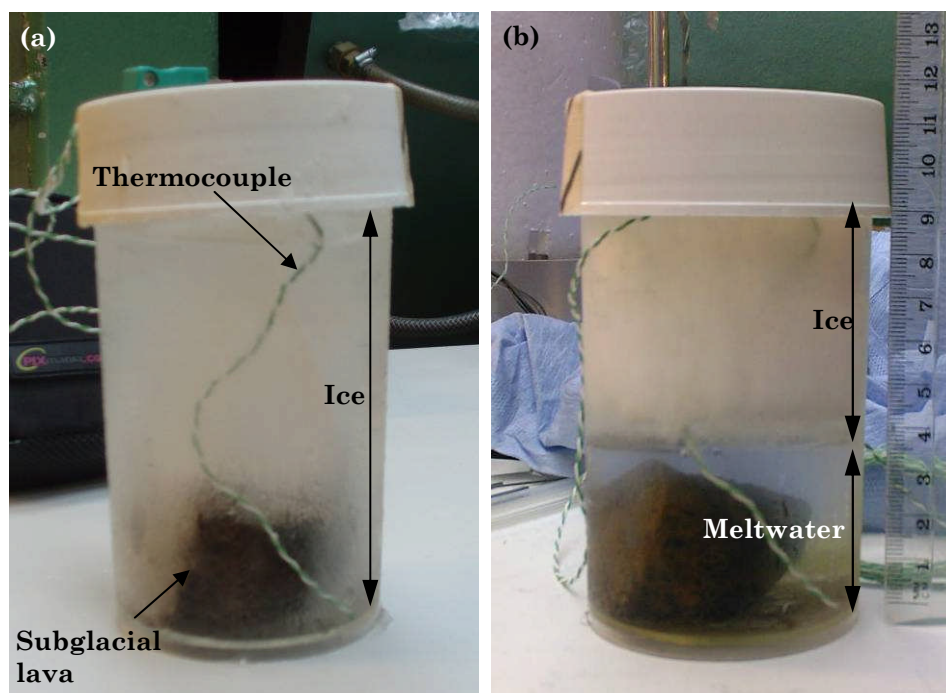
Table 5.1. Environmental conditions in the Mars chamber and on the surface of present day Mars (adapted from Hansen *et al.* 2009).

| Parameter | Mars Chamber | Present-day Mars |
|----------------------------|--------------|------------------|
| Temperature °C | -30 | -123 to +25 |
| Pressure (mbar) | ~8 | 6.7 – 9.9 |
| UV radiation | >350nm | >200nm |
| <i>Gas composition (%)</i> | | |
| CO ₂ | 95.5 | 95.3 |
| N ₂ | 2.7 | 2.7 |
| Ar | 1.6 | 1.6 |
| O ₂ | 0.13 | 0.13 |
| H ₂ O | Unknown | 0.02 |
| CO | 0.07 | 0.07 |

5.2.2 Sample processing and test for survivability

After incubation, the experiment (still within the container) was removed from the chamber, packed in ice and immediately transported back to UCL. Due to the steep thermal gradient created from -30°C (freezer) to +40°C (heat pads), a 3.5cm layer of meltwater existed at the heat – ice interface, within which was the lava, and subsequently the overlying ice layer had been reduced to a thickness of 5.5cm (see Figure 5.3). A core was made through the ice layer using a flame sterilised and heated metal spatula, through which the meltwater was pipetted into six 10ml aliquots. The overlying ice layer was removed by lifting it out using the embedded thermocouple.

Figure 5.3. Subglacial Volcanic Microcosm a) before; and b) after Mars incubation. NB: Lid was on for transport only.



The test for habitability of the SVM was based on the ability to culture organisms from the pillow basalt sample after exposure to the above defined Martian environmental conditions, and also from the meltwater created during the experiment. The lava sample was homogenized for culturing (as described in Chapter 2, section 2.3.3), but this unfortunately meant any spatial heterogeneities in survivability of the microbial community within the sample were lost. Culturing was carried out on two different types of solid media – Pillow Basalt Agar (PBA), and ½ strength Czapek-Dox Agar agar (½ CZD). Low-nutrient media were used to encourage the growth of slower growing organisms, and also to encourage a higher level of diversity (Hirsch *et al.* 1995). PBA was used in an attempt to simulate the oligotrophic basaltic environment as much as possible, and details of this medium are described in Chapter 2, section 2.3.1. It is noted that agar itself can provide additional nutrients that the basaltic component may be lacking, particularly organic carbon. CZD media is used for the cultivation of organisms that can utilise inorganic nitrogen (in the form of sodium nitrate) as their nitrogen source. In particular, actinomycetes are effectively isolated using this medium. Actinomycetes are common to soil environments where water availability is reduced, and as such would be expected to exist in the Icelandic lava environment. Indeed, the work detailed in Chapter 3 showed Actinobacteria to form a dominant part of the prokaryotic community in pillow lava from Askja, and this is consistent with previous work by Cockell *et al.* (2009b). Additionally, the presence of nitrate can prevent the growth of the more rapidly growing bacteria, therefore allowing a wider diversity of slower growing bacteria to grow.

Lava fragments were used to directly inoculate the plates (Cockell *et al.* 2009b) in order to limit any artificial selection against any organisms through aqueous buffer dilution techniques, particularly exopolymer-forming organisms (Hirsch *et al.* 1995). Approximately 50 – 100mg of crushed lava was used per plate, with fragments >2 mm in size. Lava fragments were scattered onto freshly made agar surfaces, as the thin film of water present provides an aqueous contact between the media and lava surface (Hirsch *et al.* 1995), although bias may be introduced if there are lava surfaces that remain completely unconnected from the agar surface or associated water film. Colonies from the SVM, negative control, and untreated lava typically took between 1 – 6 weeks to grow at ~20°C. For isolates

from the pillow lava, data is quantified as colony forming units (CFU) as a function of the number of lava fragments used to inoculate each media plate. This is because the number of colonies that grow are, in part, dependant upon the number of individual lava fragments present, which invariably differs from plate to plate. More fragments lead to an increased surface area of lava from which colonies can emerge, as such the data is quantified as the number of CFU per 100 fragments of lava (i.e. the percentage of lava fragments that exhibit colony growth). It is important to be aware however that the inoculation bias introduced through using lava fragments means ultimately whilst the enumerations are expressed in a seemingly ‘quantitative’ way, the results are largely qualitative, as the number of faces of lava in contact with the agar is variable. The meltwater samples however, being aqueous, were simply quantified as CFU per 100 μ l.

Pure isolates were obtained by repeatedly picking and re-streaking individual colonies onto fresh media plates. For taxonomic identification, DNA was extracted from these isolates (see Chapter 2, section 2.3.4) and the 16S rDNA amplified via PCR using universal Bacterial primers 27F and UN1492R (for reaction conditions see Chapter 2, section 2.3.5). PCR products were then cloned and sequenced (see Chapter 2, section 2.3.6 and 2.3.7). Isolates are named according to the conditions that the lava from which they were cultured was subjected to. As the lava came from Askja volcano, the untreated lava isolates are prefixed with ‘ASK’, whilst isolates from the experimental Mars chamber environment are prefixed with either ‘MCASK’ for lava isolates, ‘MCMW’ for meltwater isolates, and ‘MCEX’ for isolates from the negative control exposed lava.

5.3 Physical and Chemical Properties

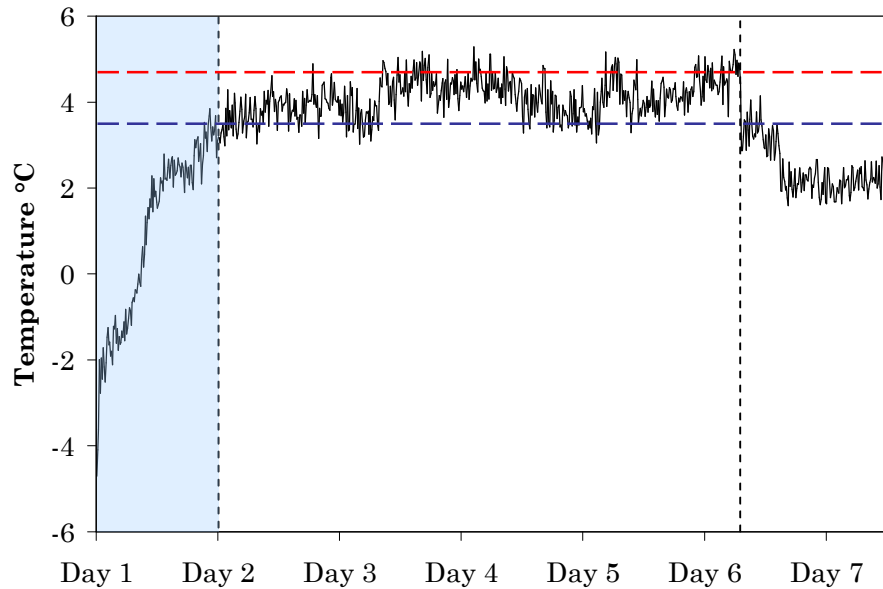
Physiochemical properties (temperature, pH, and dissolved elemental composition) of the Subglacial Volcanic Microcosm (SVM) were measured before, during, and/or after incubation. Physiochemical properties relating to the basaltic lava itself (porosity, geochemistry etc.) have already been detailed in Chapter 3 (section 3.3), and therefore are not repeated here.

5.3.1 Temperature

Thermal conditions within the SVM changed throughout the duration of the experiment within the chamber (Figure 5.4). The temperature of the solid ice and outside the chamber was maintained at a steady -30°C throughout the experiment, whilst the temperature of the meltwater varied between 3 and 5.3°C during the middle four days of the incubation. During the first day of the incubation, heating (and eventually melting) at the base of the ice layer can be seen, controlled by cyclic heating of the underlying heat pads which were maintained at $\sim 40^{\circ}\text{C}$. This produced a steady rise in temperature from -5°C at the start of the incubation to a relatively stable average temperature of $+3.9^{\circ}\text{C}$ ($\pm 0.7^{\circ}\text{C}$) for the next four days. During the last 36 hours, the temperature suddenly drops and is sustained at $\sim 2^{\circ}\text{C}$ lower than before. This change coincided with the replacement of the UV light, which had been temporarily removed for several hours, and is most likely due to a minor unidentified technical fault as the UV lamp was re-connected. It is noted that at the Martian surface, and in many other previous Mars simulation experiments, daily freeze-thaw temperature fluctuations are present. These cycles have been previously shown to have an effect on survivability (Hansen *et al.* 2009; Hawrylewicz *et al.* 1965), but unfortunately the technological ability to implement this was not available for this experiment. However, the meltwater temperature during the majority of the SVM experiment run does lie within the temperature range measured for Skaftá subglacial caldera lake in Iceland (Figure 5.4), which was found to be 4.7°C in the top 90 m of the water column, underlain by 10 m thick water mass with a temperature of $\sim 3.5^{\circ}\text{C}$ (Johannesson *et al.* 2007). As such, where temperature is concerned the environmental conditions created within this Martian analogue microcosm are comparable to those measured from the equivalent terrestrial environment that the microcosm was designed to imitate.

Figure 5.4. Real-time temperature graph of the meltwater layer within the Subglacial Volcanic Microcosm (SVM). Temperature was measured every 10 minutes for the full 7 day incubation. For comparison, the red and blue dashed lines indicate the upper (4.7°C) and lower (3.7°C) temperatures measured from Skaftá caldera lake (Johannesson *et al.*

2007). Black dashed lines indicate the beginning and end of this relatively stable temperature duration, whilst the blue shaded region indicates the steady melting at the base of the ice layer before reaching a stable average of 3.9°C.



5.3.2 Chemistry

After 7 days of incubation the pH of the meltwater had increased in acidity, changing from the starting pH of 7.7 to pH 5.3. As with the temperature measurements, this is very similar to the pH of naturally occurring subglacial caldera lakes beneath Vatnajökull, Iceland, which have a measured pH of between 4.8 – 5.3 (Stefansson *et al.* 2008; Johannesson *et al.* 2007; Gaidos *et al.* 2004). This change in the SVM can be attributed to the low temperature leaching of pillow lava constituents within the meltwater layer during the 1 week incubation, since a measurable increase or introduction of dissolved elements is observed (Table 5.2). The initial starting ‘glacial ice’ water, being sterilised dH_2O , was very pure, with little to no measurable dissolved elements present. After 1 week incubation, the meltwater showed a clear increase (in order of highest concentration) of Na^+ , Ca^{2+} , SO_4^{2-} , Mg^{2+} , Si^{4+} , K^+ and Al^{3+} dissolved cations. Fe and P were also measured but these were not identified in either the starting ‘glacial’ water or the resulting meltwater layer. Elements that have a high degree of mobility during water-rock interactions, such as Na, Ca and Mg show some of the highest enrichments compared to the dH_2O (Figure 5.5). These elements are sourced from the dominant mineralogy of the pillow lava, notably

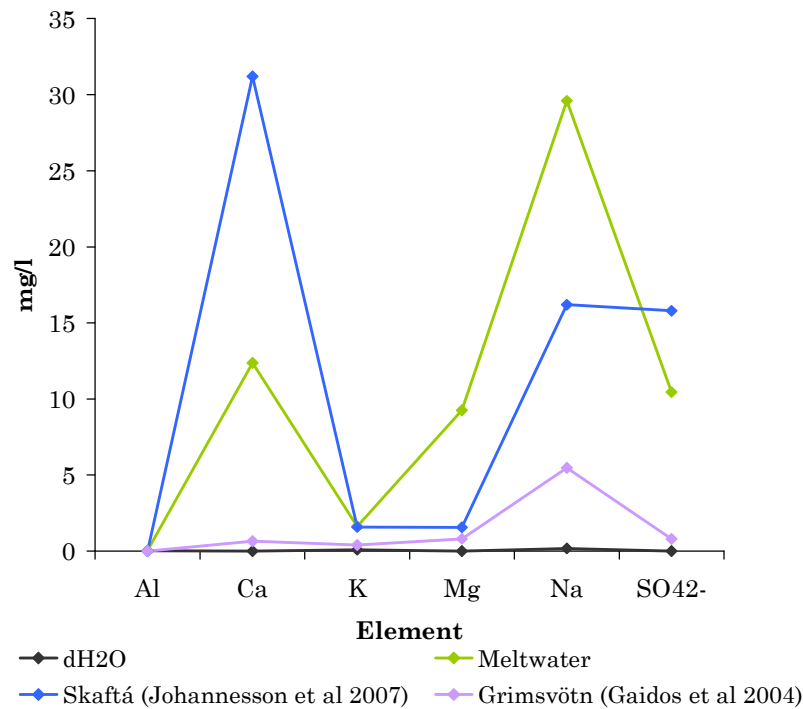
feldspars, pyroxenes and olivines, and as a result they also constitute a large percentage of the lavas geochemistry.

As with the pH and temperature measurements for the meltwater, the chemical composition of the meltwater is comparable with that measured for natural subglacial caldera lakes, with the exception of Si concentration. Skaftá caldera lake is again the most similar, with elevated levels of Na, Ca and SO_4^{2-} and small concentrations of K in the water. Low levels of K commonly exist within low temperature fluids due to the ubiquitous formation of K-rich clays from the hydrous weathering of feldspars. Figure 5.5 shows the similar pattern of elemental concentrations between the SVM meltwater and both Skaftá and Grimsvotn subglacial caldera lakes. The most notable difference is the significantly high level of Si in Skaftá lake compared with the low level of Si in the experimental simulation (Table 5.2). The solubility of Si is strongly dependent upon the temperature of the solution, whereby increasing temperature increases Si in the solution. The low Si concentration (4.32 mg/l) of the meltwater from the SVM is likely to be due to the constantly low temperature of this meltwater throughout incubation (2 – 5°C) and the lack of hydrothermal input present within natural systems, that can introduce warmer, silica-charged fluids into the lake system. Grimsvotn caldera lake chemistry is similar regarding elevated Na levels, but on the whole this lake is very low in dissolved ions. It is noted that Si is not included in the plot in Figure 5.5, firstly due to the large quantity of Si in Skaftá lake which obscures the relative similarity of the other element concentrations when plotted on such a graph, and secondly because no dissolved Si values are available for Grimsvotn lake.

Table 5.2. Measured pH (mean), temperature (mean), and dissolved element concentration (in mg/l) from the *dH₂O* ‘glacial’ water and meltwater after 1 week incubation. For comparison, data is given for Skaftá lake (Johannesson *et al.* 2007). *pH was measured at room temperature.

| | ‘Glacial’ ice | Meltwater layer | Skaftá |
|-------------------------------|---------------|-----------------|-----------|
| pH | 7.7* | 5.3* | 5.22 |
| Temp (°C) | -5.0 | 3.9 (±0.7) | 3.5 - 4.7 |
| Al | 0.02 | 0.05 | - |
| Ca | 0 | 12.37 | 31.2 |
| Fe | 0 | 0 | - |
| K | 0.09 | 1.63 | 1.59 |
| Mg | 0 | 9.26 | 1.57 |
| Na | 0.18 | 29.6 | 16.2 |
| P | 0 | 0 | - |
| SO ₄ ²⁻ | 0 | 10.46 | 15.79 |
| Si | 0.05 | 4.32 | 60.49 |

Figure 5.5. Dissolved element composition of the *dH₂O* ‘glacial’ water, SVM meltwater, and Skaftá and Grimsvötn caldera lake. NB: Silica has been excluded for clarity.



5.4 Simulated Martian Conditions and Survivability

After the experiments, bacteria were cultured from basaltic pillow lava that had experienced two differing conditions: a subglacial volcanic microcosm (SVM), and full exposure to present day Martian conditions (negative control). The colony numbers reflect these conditions, and broadly demonstrate the increased microbial survivability (and therefore environment habitability) in subglacial

volcanic systems in comparison to the negative control. Table 5.3 gives specific details regarding the basaltic lava colony growths following incubation in the Mars chamber, and also from the original lava prior to any experimentation (untreated), on the two different types of media. Whilst the terms ‘colony’ and ‘CFU’ are used here, the method of inoculation (using lava fragments directly on the agar surface) means they aren’t necessarily ‘colonies’ by the traditional definition, whereby a colony has arisen from a single bacterial cell. Also given are the number of lava fragments used to inoculate the media plates, as the CFU enumeration was unsurprisingly found to increase with the number of lava fragments (Figure 5.6). As such, the enumeration of CFU and survivability is presented here as a function of lava fragments, and these results are also given in Table 5.3.

Figure 5.6. Number of CFU plotted against number of lava fragments for each test: Untreated, Subglacial Volcanic Microcosm (SVM) and Negative control, for both media types combined. Linear trendlines are shown and the respective R^2 values are given.

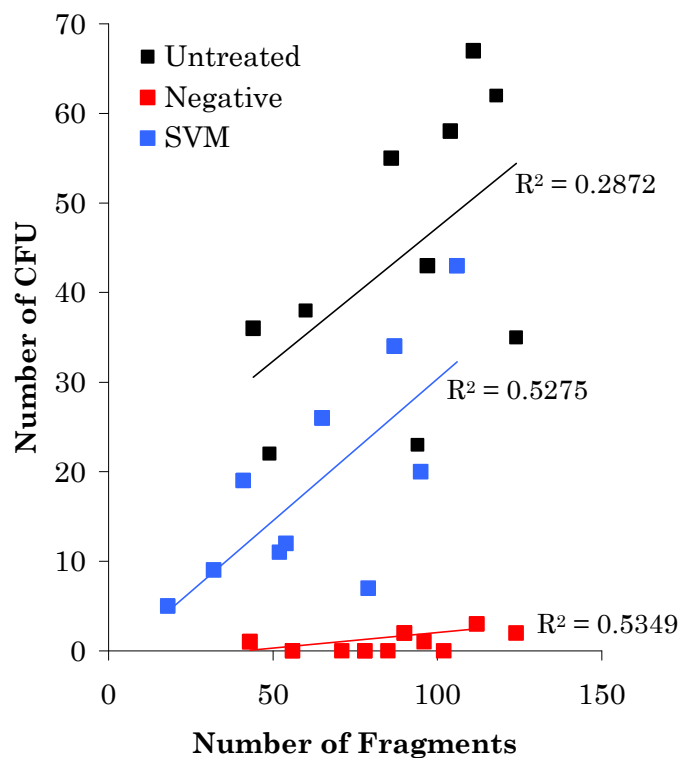


Table 5.3. Colony growths on media plates inoculated with lava or meltwater after 30 days incubation at 20°C. Shown are the total number of CFU (*C*) and lava fragments (*F*) from each plate, and the Mean and Standard Deviation (σ) calculated from these numbers. Numbers in bold are used to assess survivability, detailed in Table 5.4 below.

| PLATE # | | PBA (nutrient poor) | | | $\frac{1}{2}$ CZD (nutrient rich) | | | | |
|------------------|------|--|-------------|-------------|-----------------------------------|---|-------------|----------|-------------|
| | | Description of colonies | <i>F</i> | <i>C</i> | $(C/F)*100$ | Description of colonies | <i>F</i> | <i>C</i> | $(C/F)*100$ |
| Untreated | 1 | Numerous pink, green, brown, orange, yellow and white small flat colonies, all emerging from lava fragments | 118 | 62 | 52.5 | Flat brown and white colonies extending 2-4mm out from lava fragments, solid yellow colonies, cream coloured gloopy colonies. Pale pink-orange, white 'fungal' | 86 | 55 | 63.9 |
| | 2 | | 124 | 35 | 28.2 | | 104 | 58 | 55.8 |
| | 3 | | 60 | 38 | 63.3 | | 44 | 36 | 81.9 |
| | 4 | | 49 | 22 | 44.9 | | 97 | 43 | 44.3 |
| | 5 | | 94 | 23 | 24.5 | | 111 | 67 | 60.4 |
| | Mean | 89 | 36 | 42.7 | 88.4 | 51.8 | 61.2 | | |
| σ | 33.7 | 16.2 | 16.4 | 26.5 | 12.3 | 13.7 | | | |
| SVM: Lava | 1 | Many small, pale grey – white flat colonies surrounding lava fragments. Significantly less variation in colour and morphology than the equivalent plates from the untreated lava | 32 | 9 | 28.1 | Large (>5mm) gloopy cream and orange colonies surrounding lava fragments. Smaller, pale pink – brown flat colonies. | 65 | 26 | 40 |
| | 2 | | 54 | 12 | 22.2 | | 41 | 19 | 46.3 |
| | 3 | | 79 | 7 | 8.86 | | 18 | 8 | 44.4 |
| | 4 | | 95 | 20 | 21.1 | | 87 | 34 | 39.1 |
| | 5 | | 52 | 11 | 21.2 | | 106 | 43 | 40.6 |
| | Mean | 62.4 | 11.8 | 11.8 | 63.4 | 26 | 42.1 | | |
| σ | 24.7 | 5.0 | 4.9 | 35.1 | 13.5 | 3.1 | | | |
| SVM: Meltwater | 1 | Limited colony growth, those colonies that do grow are pale and small. | NA* | 0 | 0 | Numerous small (1mm) firm green-grey colonies on all plates, plus a few cream colonies. Bright pink and orange colonies on most plates. All colonies are small (1-2mm). | NA* | 61 | 61 |
| | 2 | | | 0 | 0 | | | 12 | 12 |
| | 3 | | | 0 | 0 | | | 48 | 48 |
| | 4 | | | 13 | 13 | | | 42 | 42 |
| | 5 | | | 7 | 7 | | | 5 | 5 |
| | Mean | NA* | 4 | 4 | NA* | 33.6 | 33.6 | | |
| σ | | 5.9 | 5.9 | | 2.4 | 2.4 | | | |
| Negative control | 1 | No colony growth across all but two plates, which have 1 - 2 small white colonies extending from lava. | 124 | 2 | 1.61 | Low colony counts, with two plates lacking any growth. Colonies appear to be either cream or bright orange-pink, all are small (~1mm). | 43 | 1 | 2.3 |
| | 2 | | 96 | 1 | 1.04 | | 112 | 3 | 2.7 |
| | 3 | | 85 | 0 | 0 | | 78 | 0 | 0 |
| | 4 | | 102 | 0 | 0 | | 56 | 0 | 0 |
| | 5 | | 71 | 0 | 0 | | 90 | 2 | 2.2 |
| | Mean | 95.6 | 0.6 | 0.53 | 75.8 | 1.2 | 1.44 | | |
| σ | 19.8 | 0.9 | 0.75 | 27.3 | 1.3 | 1.33 | | | |

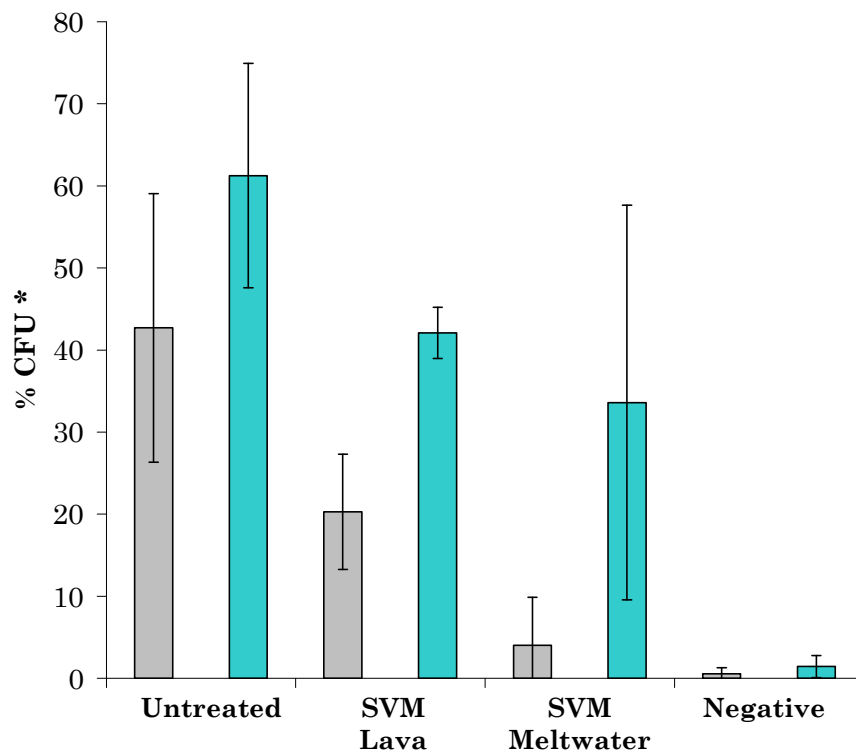
*SVM meltwater plates were inoculated with 100µl of meltwater from the experiment

Table 5.4. Mean CFU expressed as a % of growth per 100 lava fragments or 100µl of meltwater (see Table 5.3 for raw data). Survivability is calculated as the percentage of the total mean CFU % from the untreated lava (taken to represent 100%) from both media plates combined.

| Experiment | Agar media | Mean CFU % (both media) | Survivability % |
|-----------------------|------------|-------------------------|-----------------|
| Untreated | BA | 52 | 100 |
| | ½ CZD | | |
| SVM Lava | BA | 31.2 | 60 |
| | ½ CZD | | |
| SVM Meltwater | BA | 18.8 | 36.2 |
| | ½ CZD | | |
| Negative Control Lava | BA | 0.98 | 1.9 |
| | ½ CZD | | |

Figure 5.7 plots the mean CFU % given in Table 5.4 above for both types of media individually, calculated as a percentage of growth per 100 lava fragments of 100µl of meltwater (relevant to the SVM experiment only). In all cases there are more CFU from the more nutrient-rich ½ CZD media plates than the BA plates.

Figure 5.7. Mean (n=5) CFU from each of the untreated lava, simulated subglacial volcanic system (SVM), and negative control. Values are specific to the different agar mediums used: PBA (grey) and ½ CZD (blue). Error bars represent standard deviation. *CFU % is the number of CFU as a function of the number of lava fragments, expressed as a percentage, or in the case of ‘SVM Meltwater’, the number of CFU per 100µl.



When looking at survivability percentage, it is evident that lava incorporated into a simulated subglacial volcanic microcosm (SVM) is considerably more habitable than lava that has been fully exposed to Martian environmental conditions (the negative control). Here, the number of colonies grown amounts to just 1.9% of those grown from the original untreated lava. In contrast, the lava from the SVM is markedly higher, with CFU count equating to 60% of the original untreated lava colonies. In addition, bacteria were found to be present in the SVM meltwater component of the environmental simulation, although the number of colonies cultured here are almost half that from the lava itself, and potentially signifies the passive movement of microorganisms from the lava into the meltwater layer. In the following sections, the type and number of colony growths from each experiment are described and discussed in more detail.

5.4.1 Isolates from untreated lava

Many bacterial colonies were cultured from the untreated pillow lava on both $\frac{1}{2}$ CZD and PBA. These could be seen emanating from individual rock fragments across the surface of the agar plate (see Figure 5.8). Individual colonies ranged from white, green, pink, yellow and orange in colour (Figure 5.8 and 5.9). A greater diversity of slow-growing microorganisms were cultured from PBA, but some of these were impossible to sub-culture. Colonies grew much faster on $\frac{1}{2}$ CZD agar and were easy to sub-culture onto fresh plates, but their morphological diversity was much lower.

Figure 5.8. Untreated lava ‘colonies’ on PBA after 40 days growth. Scale bar = 2mm

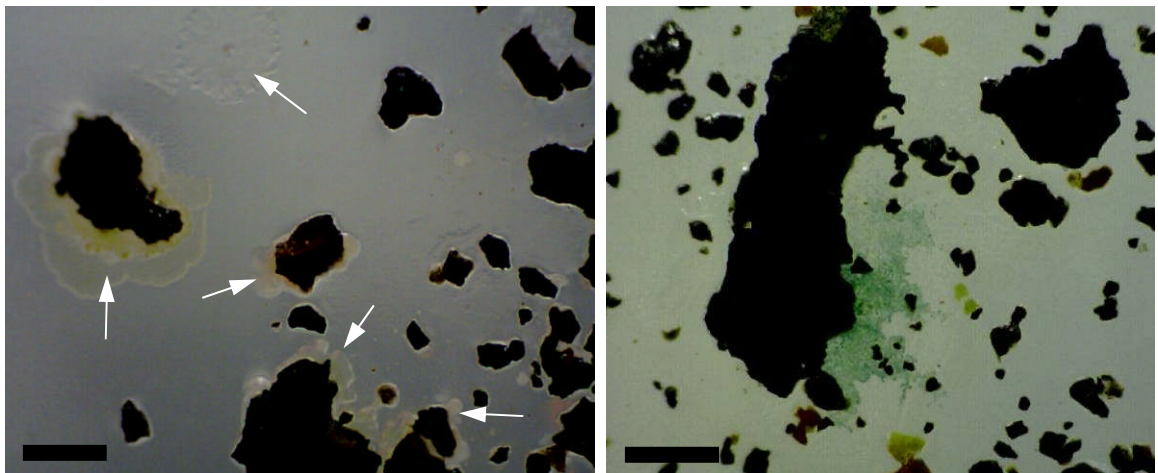
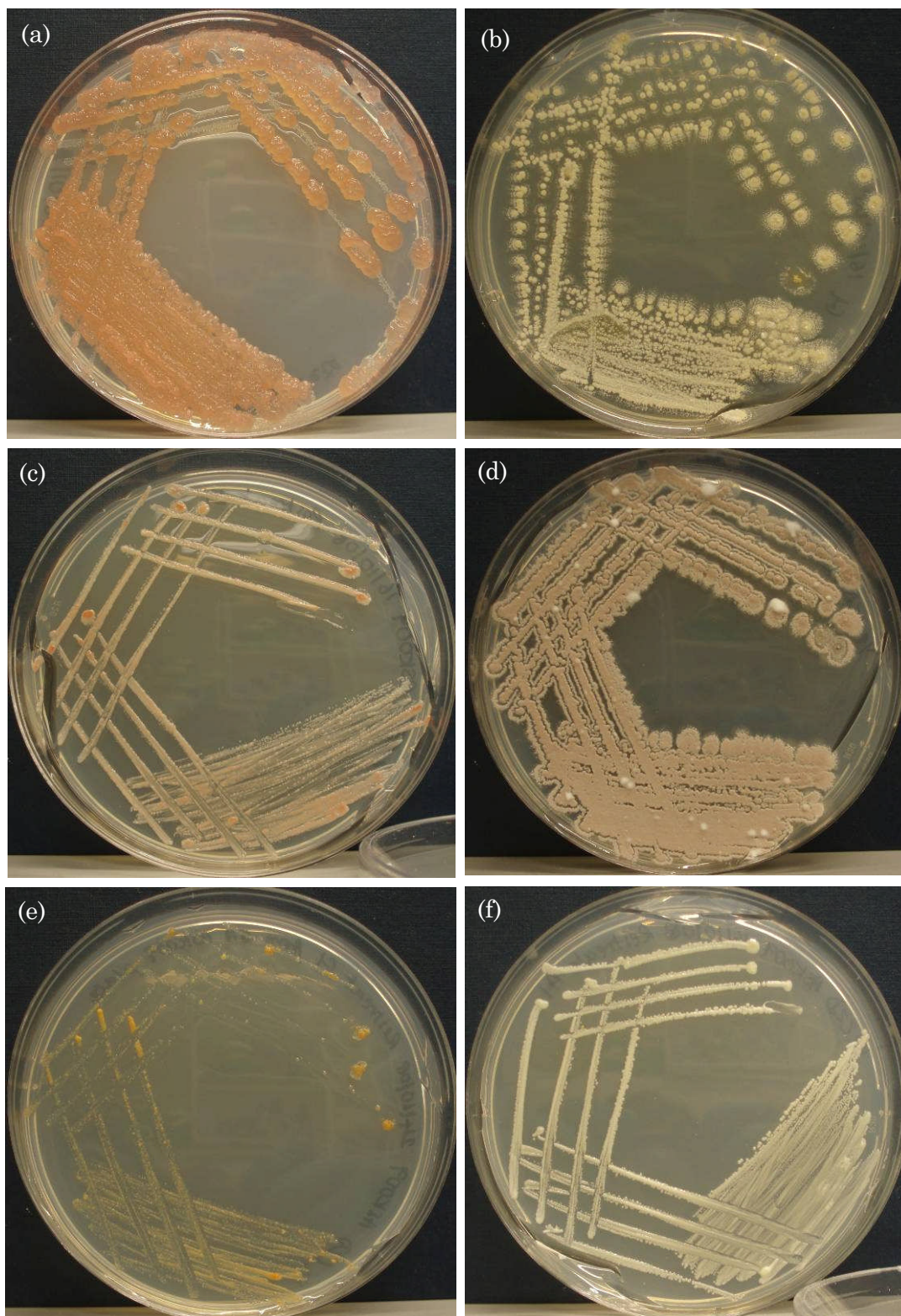


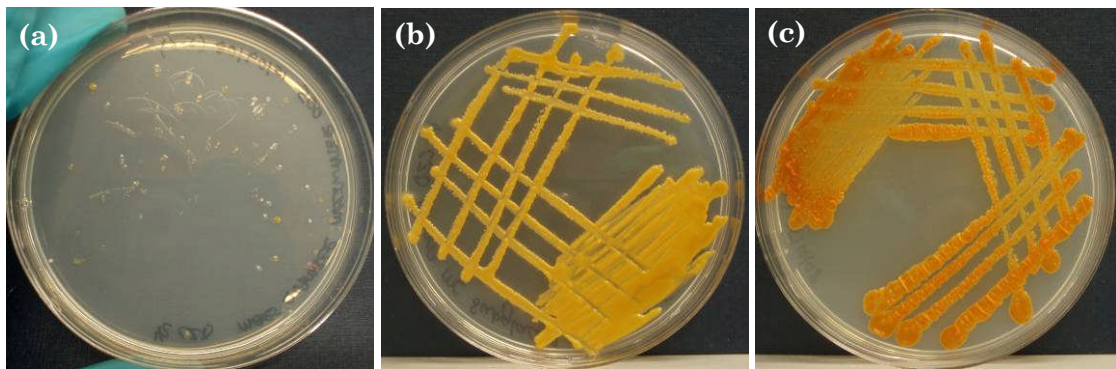
Figure 5.9. Pure isolates from untreated lava plates; a) ASK9-F; b) ASK9-K; c) ASK9-G; d) ASK9-E; e) ASK9-C; f) ASK9-L. All are isolated from $\frac{1}{2}$ CZD media, with the exception of (e) which was isolated from PBA.



5.4.2 Isolates from the Subglacial Volcanic Microcosm (SVM)

After 10 days, extensive colony growths were seen growing from the pillow lava fragments inoculating $\frac{1}{2}$ CZD agar. These included large orange, pink, white and yellow bacterial colonies (Figure 5.10). On the PBA colonies were much smaller and appeared to be of just one type, typically creamy white in colour and all extending out from the individual rock fragments. The first visible colonies appeared on two out of the 5 meltwater plates after 1 week of incubation on $\frac{1}{2}$ CZD agar. Colonies were all <1mm in size and appeared to be of the same type, all a pale green-grey colour. After 20 days incubation small pale pink colonies appeared.

Figure 5.10. Cultures on $\frac{1}{2}$ CZD media from subglacial pillow basalt from the Subglacial Volcanic Microcosm; a) meltwater after 40 days incubation; b) isolate MCASK9-D; c) isolate MCASK9-E.

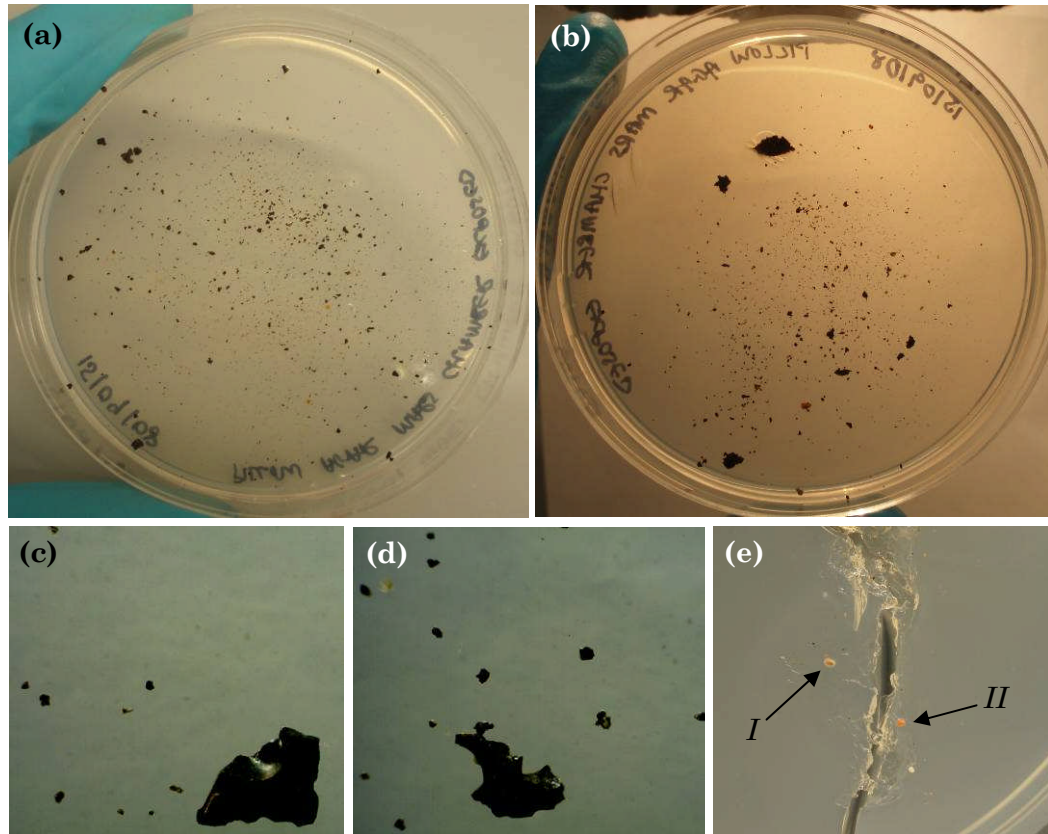


5.4.3 Isolates from the exposed Martian environment

It was hypothesised that the negative control would not be conducive to the survivability of microorganisms after exposure to Martian conditions. Inoculation of both PBA and $\frac{1}{2}$ CZD agar plates with pillow lava fragments failed to produce any colony growths after 20 days. However, after 30 days a few isolated colonies had grown on 2 out of 6 plates (Figure 5.11). This is lower than the original number of isolates, and those that survived the Subglacial Volcanic Microcosm. The pillow lava used for these experiments has many vesicles and cracks, and it is possible that the surviving microbes were those that existed within micro-shelters and managed to survive temporary Martian exposure. It is noted that the presence of an overlying layer of rock, even a few millimetres, can sufficiently protect from UV radiation (Cockell *et al.* 2005). This will be particularly relevant to those microbes residing within the vesicles, cracks and other pore spaces within the rock. However, it is possible that if the lava was left

in there longer, the combination of low pressure and a Martian atmosphere would eventually sterilise the rock, and demonstrates the need for longer duration experiments to test this.

Figure 5.11. PBA (a – c) and $\frac{1}{2}$ CZD (d – e) media inoculated with negative control pillow basalt a) after 38 days incubation; b) after 17 days incubation; c) close up images of lava fragments showing a distinct lack of colony growths. Arrows indicate the few isolated culture growths: *I* = MCEX-A, *II* = MCEX-B



5.5 Identification of Cultures

A total of 23 aerobic isolates were identified from their partial 16S rDNA sequence from the untreated lava, Subglacial Volcanic Microcosm, and negative control combined. Of these, 10 could be identified as a particular species ($\geq 99\%$ similarity), whilst others shared genetic similarity to uncultured environmental clones, many of which are originally cultured from cold, dry environments. Details of identification at the genus level are given in Table 5.5. Typically, partial sequences of ~ 550 bp were used, as due to the large size of the insert (~ 1500), forward and reverse end sequences did not overlap.

Table 5.5. Identification of isolates as determined by RDP taxonomic classification, using sequences covering variable regions V7, V8, and V9. All taxonomic identifications have a bootstrap cut-off value >80% (default setting). Taxonomic identification at the family or order level are given in brackets where genus identification was not possible. Isolates from PBA media are highlighted with an asterisk, and ½CZD with †.

| Experiment | Isolate | Sequence Length (bp) | Phylum; Genus |
|-------------------------------|----------|----------------------|----------------------------------|
| Untreated Lava | ASK-A* | 660 | Bacteroidetes; Hymenobacter |
| | ASK-B† | 576 | γ-Proteobacteria; Pseudomonas |
| | ASK-C* | 590 | β-Proteobacteria; Herbaspirillum |
| | ASK-D* | 528 | Bacteroidetes; Hymenobacter |
| | ASK-E† | 579 | Actinobacteria; Streptomyces |
| | ASK-F* | 569 | Bacteroidetes; Hymenobacter |
| | ASK-G† | 508 | Actinobacteria; Arthrobacter |
| | ASK-H* | 628 | Actinobacteria; Aeromicrobium |
| | ASK-I† | 480 | α-Proteobacteria; Roseomonas |
| | ASK-J* | 577 | Actinobacteria; Arthrobacter |
| | ASK-K† | 628 | Actinobacteria; Streptomyces |
| | ASK-L† | 548 | Actinobacteria; Arthrobacter |
| | ASK-M* | 558 | Firmicutes; Paenibacillus |
| Subglacial Volcanic Microcosm | MCASK-A† | 588 | β-Proteobacteria; Massilia |
| | MCASK-C† | 548 | α-Proteobacteria; Rhizobium |
| | MCASK-D† | 467 | β-Proteobacteria; Herbaspirillum |
| | MCASK-E† | 567 | Bacteroidetes; Hymenobacter |
| | MCMW-B† | 530 | β-Proteobacteria; Massilia |
| | MCMW-C† | 578 | α-Proteobacteria; Roseomonas |
| | MCMW-D† | 577 | β-Proteobacteria; Massilia |
| | MCMW-E† | 569 | β-Proteobacteria; Massilia |
| Negative control | MCEX-A† | 568 | β-Proteobacteria; Massilia |
| | MCEX-B† | 606 | Actinobacteria; Rubrobacter |

5.5.1 Untreated lava isolates

Of the colonies observed on the ½ CZD and BA plates combined, 13 of these were successfully sub-cultured and isolated for 16S rDNA identification, and represent 4 different phyla: *Actinobacteria* (6 isolates), *Bacteroidetes* (3 isolates), *Proteobacteria* (3 isolates), and *Firmicutes* (1 isolate). Nearly all were comparable to bacteria previously isolated from cold environments, and are consistent with the phyla identified in the pillow lava in Chapter 3.

Of the six *Actinobacteria*, isolates were found based on their partial 16S rDNA sequence to be closely related to a variety of species, with 99 – 100% similarity. Two isolates were most closely related to a species of *Streptomyces* (100% and 99%). The first isolate displayed a 100% similarity with one that had been identified from soil in Antarctica. Specifically, the closest cultured relative of this isolate is *Streptomyces himgiriensis* (100%), a novel species isolated from the cold

desert of the Himalayas (Singla *et al.* 2003). The second *Streptomyces* isolate (99%) is most closely related to one identified in agricultural soil (Wirth & Ulrich 2002), and whose closest cultured species relative is *Streptomyces bottropensis* (99%), a bacterium known to be a pathogen of potato plants (Takeuchi *et al.* 1996). Three isolates were identified as *Arthrobacter tecti* (98 – 99%), a gram-positive bacterium originally isolated from ancient deteriorated mural paintings (Heyrman *et al.* 2005). Lastly, the final *Actinobacteria* isolate had the highest similarity (94%) to an uncultured clone from a Rocky Mountain endolithic microbial ecosystem (Walker & Pace 2007), and the closest cultured match was that of gram positive bacterium *Aeromicrobium alkaliterrae* (96%), a novel species first isolated from alkaline (pH 10.0) soil (Yoon *et al.* 2005). Actinobacteria are common to soil environments, particularly in environments where water availability is limited, and this is demonstrated in the nature of the environments where the closest matches for the Askja pillow lava isolates have been cultured or identified from. Notably Actinobacteria have also been previously identified in basaltic hyaloclastite lavas from South Iceland (Cockell *et al.* 2009a), and dominated the pillow lava bacterial community detailed in Chapter 3.

Three isolates belong to the phylum *Bacteroidetes*, all of which are *Hymenobacter* species (class *Sphingobacteria*). Isolates belonging to the genus *Hymenobacter* have been previously isolated from a wide range of environments, many of which could be considered extreme or oligotrophic. They are gram negative obligate aerobic chemoheterotrophic bacteria, often observed to have red – yellow colony colouration due to carotenoid pigments (Dworkin & Falkow 2006). This is consistent with the colony colour of the three isolates which ranged from dark orange (ASK9-A), to bright orange (ASK9-D), to bright pink (ASK9-F, see Figure 5.8a). Of these three isolates, one had a closest match (99%) at the species level as gram-negative bacterium *Hymenobacter gelipurpurascens* (Buczolits *et al.* 2006), whilst the other two isolates were most closely identified (98%) with unclassified *Hymenobacter* species from Arctic sea water (Zeng *et al.* 2007). In particular, it is noted *Hymenobacter gelipurpurascens* grows optimally at low temperatures, with growth observed at 4°C, but not 37°C (Buczolits *et al.* 2006). Other species of *Hymenobacter* have been isolated from the continental Antarctic soils and irradiated pork (Dworkin & Falkow 2006).

Three isolates were *Proteobacteria*, one from the γ -*Proteobacteria*, which matched most closely (99%) to the species *Pseudomonas stutzeri* isolated from deep sea sediment in the South Pacific. The bacterium *Pseudomonas stutzeri* has been described as a gram negative heterotrophic species, which utilises denitrification as a respiratory pathway in anaerobic conditions (Yu *et al.* 2009). It has however been reported to have a wide range of growth temperatures, ranging from 4 – 45°C, and likewise exhibits a huge physiological and biochemical diversity. As such, this species has been found in a large variety of natural environments (Lalucat *et al.* 2006). With relevance to this work, *Pseudomonas stutzeri* is known to produce siderophores, which are required to utilise otherwise insoluble Fe³⁺ from basaltic substrates (Dr. Karen Olsson-Francis, pers. comm.). The second isolated *Proteobacteria* falls within the β -*Proteobacteria*, and was identified (98%) as an uncultured species belonging to the *Herbaspirillum* genus that had been identified during a genetic inventory of the NASA Mars Science Laboratory (MSL) spacecraft assembly clean room (Le Duc *et al.* 2009). The closest cultured species match for this isolate is *Aquaspirillum autotrophicum* (96%). This species is interesting within the context of this work as it's facultatively chemolithoautotrophic, characterised by its ability to oxidize hydrogen utilising CO₂ as its sole carbon source (Arango & Schlegel 1978), and as such could be considered to be one of the more applicable model organisms out of those isolated from the Askja pillow lava to assess the habitability of Martian environments. Lastly, the third isolate belongs to the α -*Proteobacteria*, and matched most closely in species to *Roseomonas aquaticica*. It has been previously noted that *Roseomonas* species occur in a vast range of environments, and this particular species is so-called due to its isolation from drinking water in Spain (Gallego *et al.* 2006).

Finally, one Firmicutes species was isolated, and shared most similarity (97%) to *Paenibacillus borealis*, a nitrogen fixing, facultative anaerobic bacterium that stains gram negative and also spore forming (Elo *et al.* 2005). However, *Paenibacillus* is closely related to *Bacillus* species, and as such are in fact gram positive.

Overall, the isolates from the untreated pillow lava from Askja, central Iceland, largely reflect the cold, oligotrophic nature of this environment, as seen in the

predominance of *Actinobacteria* and *Hymenobacter* species, which constitute 77% of the species identified. Additionally, even with such a small proportion of the microbial community identified, it is possible to infer potential microbial ecological functions within the basaltic lava. For example, *Paenibacillus borealis* has the capability to fix nitrogen into the system, providing a source of organic nitrogen to microorganisms, and therefore in turn a supply of ammonium, and lastly nitrate, that can be utilised by denitrifiers like *Pseudomonas stutzeri*. Likewise, siderophore production by *Pseudomonas stutzeri* could potentially release bioavailable iron into the near surroundings. Another point to note is the dominance of chemotrophic metabolic pathways – there is a complete lack of phototrophic species identified, despite the almost constant day light hours during summer months in Iceland. This potentially reflects the harsh conditions that exist externally at the lava surface, highlighting the preference for a chasmo- or endolithic lifestyle within these environments. Likewise, the 16S rDNA phylogenetic survey (Chapter 3) revealed a lack of likely phototrophs within the pillow lava (Chapter 3, section 3.4.2). These observations are in contrast to the 16S rDNA metagenomic study by Herrera *et al.* (2009) and Cockell *et al.* (2009a,b) which identified phototrophic microorganisms from both hyaloclastite lavas and rhyolitic lavas from Iceland. However, they only constituted a minor proportion (6 – 7%) of the entire community. Additionally, the lavas from both these previous studies were from south-west of Iceland, where the external environment is typically less extreme than the Icelandic interior, due to the influence of the Gulf Stream bringing warmer temperatures and significantly more rainfall than that experienced by the lavas at Askja (see Chapter 3: section 3.1 for a more detailed environmental description), and as such could be a controlling factor in this observed difference.

5.5.2 Isolates from the Subglacial Volcanic Microcosm (SVM)

Of the 16 colonies cultured from both the meltwater and lava components of the microcosm, only 8 were able to be isolated for identification (4 lava, 4 meltwater). These are detailed in Table 5.5. Of these, only one (MCASK-E) belonged to the phylum *Bacteroidetes*, and is closely related to a *Hymenobacter chitinivorans* (99% similarity), species isolates from the Antarctic Dry Valleys (Hirsch *et al.* 1998). As with *Hymenobacter gelipurpurascens*, this species is strongly pigmented (Buczolits *et al.* 2006), and the deep orange pigmentation of this

isolate can be clearly seen in Figure 5.9c. *Hymenobacter* species were also isolated from the untreated lava, and is one of two genera that were identified from both the untreated lava and experimental simulation.

Three of the SVM lava and meltwater isolates were identified broadly as β -*Proteobacteria Massilia* species, all of which had a common isolation environment of environmental sands and sediments (Table 5.6). A fourth *Massilia* species identified from a genetic inventory of the NASA Phoenix mission clean assembly rooms was isolated, potentially signifying the preferential selection of more hardy microorganisms through the environment simulation. Likewise, a fifth *Massilia* species isolate most closely matches to that isolated from anaerobic petroleum contaminated soils (Kasai *et al.* 2005), even though the isolate was cultured in anaerobic conditions.

Roseomonas aquatica was isolated from the meltwater component of the SVM (100% similarity match), and also represents one of the few isolates common to the untreated lava isolates. These pale pink microorganisms are strictly aerobic (Gallego *et al.* 2006), and their survivability could be due to dissolved oxygen that may have been present within the ice, or any remaining air trapped within the vesicular lava. Although care was taken to thoroughly saturate the lava with the dH_2O prior to freezing at the beginning of the experiment, the porous nature of this lava could result in small pockets of air entering the experiment.

Lastly, a *Rhizobium* species was isolated from the lava component of the SVM. This isolate shares 100% similarity with *Rhizobium giardinii*, an aerobic, nitrogen fixing bacterium. The isolation of this particular species from the SVM lava is somewhat unexpected, as *Rhizobium* species are well known to form an endosymbiotic nitrogen fixing relationship with legumes (Amarger *et al.* 1997), and as such would not be expected from an environment that is characteristically dry, cold, and generally free of macroscopic vegetation. Therefore, this particular isolate may represent a potential contaminant. This could be from the environment itself (e.g. wind-blown from its natural environment), during experimental set up, or lab contamination.

5.5.3 Isolates from the negative control

Out of the 4 colonies that grew from the negative control lava on the ½ CZD media, 2 of these were able to be sub-cultured into pure isolates for identification. Both are distantly related, representing two different phyla – *Proteobacteria* (MCEX-A) and *Actinobacteria* (MCEX-B) – but both share similar attributes as regards to their ability to withstand harsh environments. The closest relative of MCEX-A is an uncultured *Massilia* species identified from a genetic inventory carried out on the spacecraft assembly clean room for the NASA Phoenix lander (Le Duc *et al.* 2009). This bacterium was able to survive the simulated Martian conditions for one week within its natural habitat of basaltic lava. This would potentially have implications regarding the issue of planetary protection for Mars, for two reasons. Firstly because the Phoenix mission landed at a site that required the mission to be classed as a Category IVc (Smith *et al.* 2008), the highest planetary protection category for a mission not returning samples to Earth, and secondly because Phoenix identified evidence of water ice deposits at the near surface (Smith *et al.* 2009). However, it should be noted that whilst conditions within the Mars chamber were designed to be as realistic as possible, -30°C is at the upper limit of the Martian surface temperatures measured at the Phoenix landing site, where the temperature ranged between -80°C in the early morning to a maximum of -30°C in the afternoon. This difference in temperature may have an effect on the survivability of this bacterium.

Isolate MCEX-B was identified as having a 97% match to *Rubrobacter radiotolerans*, an extremely radiation tolerant gram positive bacterium (Kausar *et al.* 1997). This suggests why this particular organism was one of the few that survived exposed conditions during the Mars chamber incubation, as one of the more destructive environmental factors within this environment is the UV radiation. This organism was also widely identified during the 16S rDNA phylogenetic survey of ASK009 pillow lava (Chapter 3). It has also been previously shown that radiation resistance is a consequence of desiccation resistance (Mattimore & Battista 1996), an attribute that would also have been extremely beneficial within the Mars chamber where atmospheric pressure was lowered to 8mbar. Despite exhibiting high radiotolerance, *Rubrobacter radiotolerans* is not phylogenetically closely related to *Deinococaceae*, members of

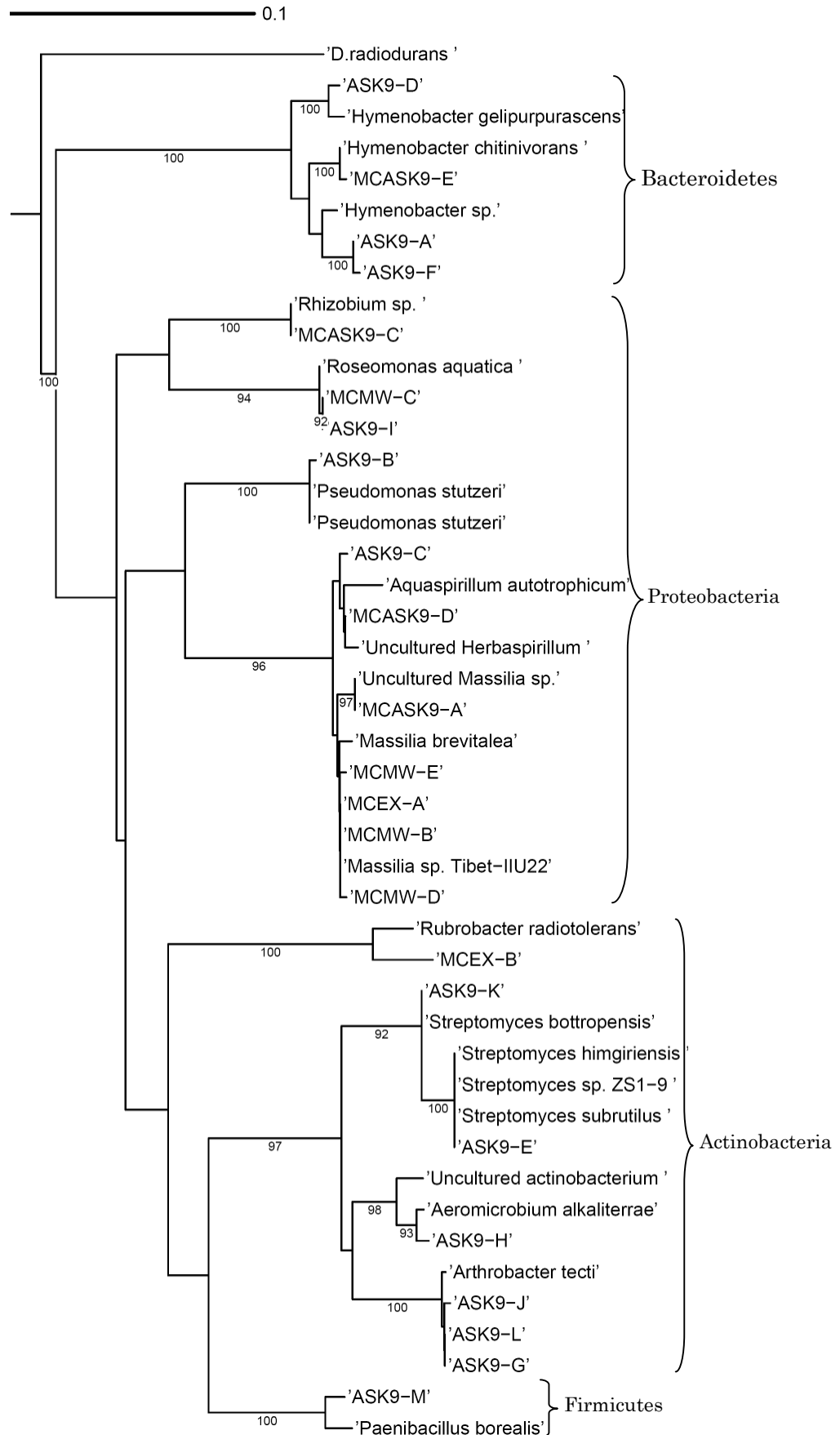
which, such as *Deinococcus radiodurans*, also exhibit radiotolerance and have often been used as model organisms in previous Mars simulation studies (Diaz & Schulze-Makuch 2006).

Phylogenetic trees of all the isolates and their closest relatives are shown in Figure 5.12. The trees were plotted (see Chapter 2, section 2.3.7 for program details) using equal length trimmed sequences of ~400bp encompassing the 16S rDNA variable and hyper-variable regions V7, V8 and V9, which correspond to *E.coli* positions of 1116 – 1155, 1241 – 1293, and 1433 – 1464 respectively (Baker *et al.* 2003). It is clear from this that the *Actinobacteria* and *β -proteobacteria* phyla are considerably more dominant within isolates from all experiments combined, and specifically that the *β -proteobacteria* largely include isolates from the SVM, whilst the *Actinobacteria* are almost entirely represented by the untreated lava isolates. It can be seen in Figure 5.12 that many isolates exhibit little genetic variation, such as SVM isolates MCMW-B, -D and -E, and untreated lava isolates ASK9-G, -J, and -L. Therefore it is likely they represent the multiple isolates of the same species, despite the fact they were morphologically dissimilar enough to warrant individual sub-culturing. This is noticeable in Figure 5.9 where isolate ASK9-G exhibits pink colouration (Figure 5.9c), whilst ASK9-L is distinctively white (Figure 5.9f), although they do both exhibit the same ‘gloopy’ texture.

Table 5.6. BLAST database closest environmental isolate relatives and closest cultured species based on 16S rDNA similarity (%) with the ASK009 and Mars Chamber isolates.

| Isolate | Closest relative (BLASTn) | | | Closest cultured species relative (BLASTn) | |
|---------|--|-----|---|---|-----|
| | ID (Accession #) | (%) | Sampling environment | ID (Accession #) | (%) |
| ASK-A | <i>Hymenobacter</i> sp. BSw20462 (EF639389) | 98 | Arctic Sea Water | <i>Hymenobacter chitinivorans</i> (Y18837) | 97 |
| ASK-B | <i>Pseudomonas stutzeri</i> strain hyss62 (FJ613315) | 99 | Deep sea sediment of the southwest Pacific | <i>Pseudomonas stutzeri</i> (FJ613315) | 99 |
| ASK-C | Uncultured <i>Herbaspirillum</i> sp. (GQ129875) | 98 | 'JPL-SAF' spacecraft assembly clean room during MSL mission | <i>Aquaspirillum autotrophicum</i> (AB074524) | 96 |
| ASK-D | <i>Hymenobacter gelipurpurascens</i> (Y18836) | 99 | Antartica soils and sandstone | <i>Hymenobacter gelipurpurascens</i> (Y18836) | 99 |
| ASK-E | <i>Streptomyces</i> sp. ZS1-9 (FJ842685) | 100 | Antarctica | <i>Streptomyces himgiriensis</i> (AY370772.1) | 100 |
| ASK-F | <i>Hymenobacter</i> sp. BSw20462 (EF639389) | 98 | Arctic Sea Water | <i>Hymenobacter chitinivorans</i> (Y18837) | 97 |
| ASK-G | <i>Arthrobacter tecti</i> (AJ639829) | 99 | Deteriorated mural paintings | <i>Arthrobacter tecti</i> (AJ639829) | 99 |
| ASK-H | Uncultured actinobacterium clone EPLS012 (EF522201) | 96 | A Rocky Mountain endolithic microbial ecosystem | <i>Aeromicrobium alkaliterrae</i> (AY822044) | 96 |
| ASK-I | Uncultured alpha proteobacterium FL10C12 (AY145635) | 99 | Vents at Mammoth Hot Springs, Yellowstone National Park | <i>Roseomonas aquatica</i> (AM231587) | 99 |
| ASK-J | <i>Arthrobacter tecti</i> (AJ639829) | 98 | Deteriorated mural paintings | <i>Arthrobacter tecti</i> (AJ639829) | 98 |
| ASK-K | <i>Streptomyces</i> sp. So10 (AJ308575) | 99 | Agricultural soil | <i>Streptomyces bottropensis</i> (GQ258687) | 99 |
| ASK-L | <i>Arthrobacter tecti</i> (AJ639829) | 99 | Deteriorated mural paintings | <i>Arthrobacter tecti</i> (AJ639829) | 99 |
| ASK-M | <i>Paenibacillus borealis</i> (AJ011321) | 97 | Norwegian humus | <i>Paenibacillus borealis</i> (AJ011321) | 97 |
| MCASK-A | Uncultured <i>Massilia</i> sp. (FJ191781) | 99 | Genetic inventory of 'KSC-PHSF' spacecraft assembly clean room during Phoenix mission | <i>Massilia timonae</i> (NR_026014) | 99 |
| MCASK-C | <i>Rhizobium</i> sp. (DQ499515) | 100 | Illinois prairie | <i>Rhizobium giardinii</i> (EU288739) | 100 |
| MCASK-D | Uncultured bacterium (AB161315) | 99 | Unsaturated, anaerobic, petroleum contaminated soil | <i>Massilia timonae</i> (EU274637) | 99 |
| MCASK-E | <i>Hymenobacter chitinivorans</i> (Y18837) | 99 | Antartica soils and sandstone | <i>Hymenobacter chitinivorans</i> (Y18837) | 99 |
| MCMW-B | Uncultured bacterium (AY527790) | 98 | Subsurface sediment contaminated with uranium and nitrate | <i>Massilia brevitalea</i> (EF546777) | 98 |
| MCMW-C | <i>Roseomonas aquatica</i> (AM231587) | 100 | Drinking water | <i>Roseomonas aquatica</i> (AM231587) | 100 |
| MCMW-D | Uncultured bacterium (FM209301) | 98 | Negev Desert sand | <i>Massilia brevitalea</i> (EF546777) | 98 |
| MCMW-E | Uncultured bacterium (GQ340264) | 98 | Marathonas Reservoir, Greece | <i>Massilia brevitalea</i> (EF546777) | 97 |
| MCEX-A | Uncultured <i>Massilia</i> sp. (FJ192248) | 98 | 'KSC-PHSF' spacecraft assembly clean room during Phoenix mission | <i>Massilia timonae</i> (NR_026014) | 98 |
| MCEX-B | Uncultured bacterium (AM746686) | 99 | Rosy discoloration of ancient wall paintings | <i>Rubrobacter radiotolerans</i> (U65647) | 97 |

Figure 5.12. Phylogenetic tree for all isolates, along with their closest relatives. *D. radiodurans* is used as the outgroup. Bootstrap values >80 are shown. Scale bar: estimated number of substitutions per nucleotide position



5.6 Factors Affecting Survivability

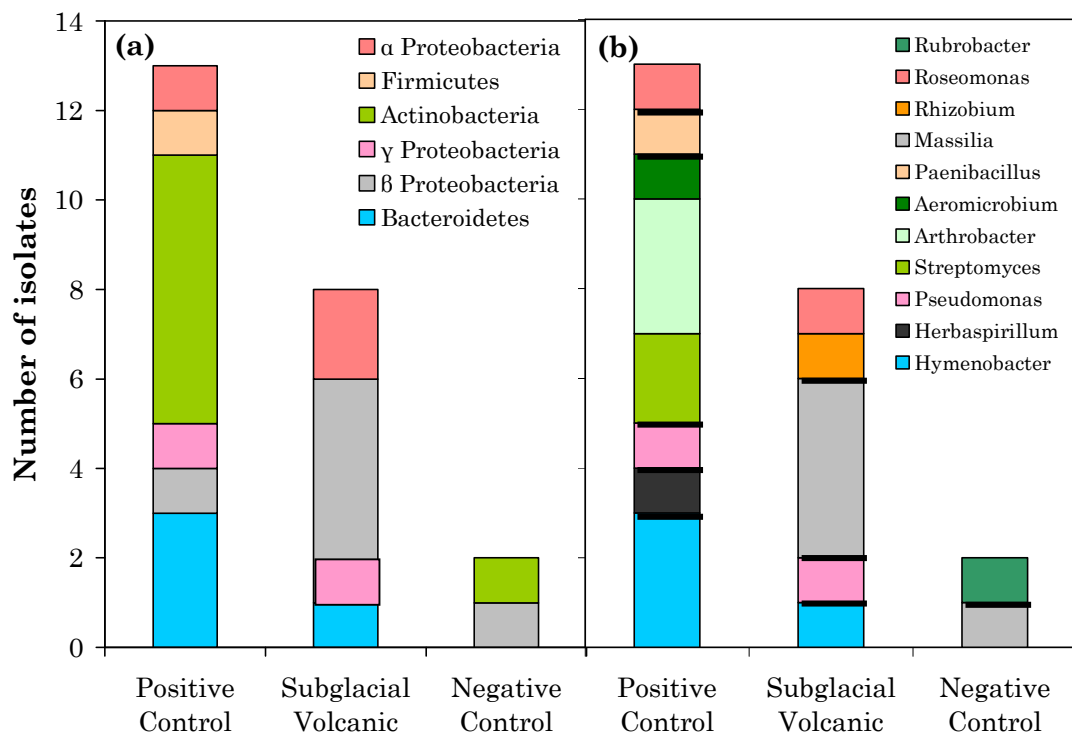
5.6.1 Survivability vs. phylotype

The stacked bar chart in Figure 5.13 shows the composition of the phyla and genera for the microorganisms isolated from the untreated lava, SVM, and negative control. Firstly, it is clearly evident that the decrease in the number of isolates from each experiment is accompanied by a decrease in diversity for both phyla and genera. The β -*Proteobacteria* are the only phyla to be cultured from all three experiments (notably all isolates are similar to those identified in NASA spacecraft clean rooms), whilst *Bacteroidetes*, γ - and α -*proteobacteria* were present in the untreated lava and the SVM only. Interestingly, the *Actinobacteria* were present in the untreated lava and negative control, but not the SVM. *Actinobacteria* are relatively resistant to desiccating environments, and their absence from the SVM could be a result of the aqueous nature of the environment, which may have allowed other bacteria to dominate. Likewise, *Paenibacillus* species are sporulating, and therefore suited to long-term survival in adverse conditions, but this isolate was only cultured from the untreated lava. *Hymenobacter*, *Roseomonas*, and *Massilia* were the only genera present in both the SVM and the untreated lava. As such, there is a lack of consistency within the culturable isolates between the SVM and untreated lava and negative control, which highlights the disadvantage in utilising a solely culture based study as opposed to a more thorough molecular-based approach. However, whilst DNA and/or lipid biomarker based taxonomic analysis would provide a more thorough investigation of species-specific survival, the persistence of these biomolecules in the environment after the death of a microorganism would not provide any clear evidence on species viability.

Another additional factor that may lead to an inconsistency in isolate genera between the untreated lava and Mars chamber incubations is that of potential contamination. For example, it would perhaps be expected that if *Rubrobacter radiotolerans* was isolated from the negative control lava, it should theoretically be isolated from the untreated lava as well, but the results clearly show this not to be the case, and therefore one might suspect that such isolates are contamination if they were not part of the original culturable community. As with any biological-based experiment there is the potential for contamination at all stages, whether in the components of the experiment themselves, whilst in the

Mars chamber, or during microbial isolation. As such, throughout the experiment every care was taken to avoid the introduction of contaminants, including appropriate sterilisation of all non-biological components, placing sterile repeat agar media plates amongst those inoculated with lava or meltwater to check for air-borne contamination, and the final assessment of the isolate 16S rDNA identity that may point to potential contaminants. Notably the most likely laboratory contaminants do not appear to be present, such as *E.coli*, or *Staphylococcus*, and airborne contaminants can probably be ruled out due the lack of growth on the control sterile agar plates, and the observation that bacterial growth on the inoculated plates is restricted to lava fragments only. Similarly the use of low-nutrient culture media (as opposed to more common nutrient-rich media such as LB or Nutrient Broth) will also limit the growth of potential contaminants such as *E.coli*. The phylogenetic assessment of the isolates suggest they are genuine environmental isolates. Firstly, the vast majority are comparable with microorganisms cultured from similarly cold, dry, or otherwise extreme environments. Secondly, the cultured isolates are consistent with bacteria isolated from hyaloclastite lava from south Iceland, some of which are also identifiable as *Streptomyces*, *Firmicutes*, and *Paenibacillus* (Cockell *et al.* 2009b).

Figure 5.13. Stacked bar chart showing a) the isolate phyla; and b) the isolate genera from all three experiments. Genus colour coding corresponds to that for phyla, with thicker lines forming boundaries between genera.



Interestingly, all of the bacteria cultured from the SVM were gram-negative, and not gram-positive as is usually found from Mars simulation studies (Hansen *et al.* 2009) and has often been attributed to the tolerance of gram-positive bacteria to desiccation and radiation (Miyamoto-Shinohara *et al.* 2000; Nicholson *et al.* 2000). For comparison, the untreated lava isolates consisted of both gram-negative and gram-positive bacteria in largely equal measure, potentially suggesting an environmental selection for gram-negative bacteria within the SVM, although given the relatively small number of isolates this could be entirely coincidental. This absence of gram-positive bacteria here is related to the absence of Actinobacteria from the SVM isolates, especially given their prevalence in the untreated lava. The two isolates identified from the negative control are, like the untreated lava, representative of both gram negative and gram positive equally. Nevertheless, it has previously been noted that the survivability of gram-negative bacteria under Martian conditions has so far been largely overlooked, and as such needs more attention in future studies (Hansen *et al.* 2009).

5.6.2 Survivability and the lava environment

The results of this series of experiments demonstrate the suitability of subglacial volcanic environments as a theoretical haven for life on Mars. The protection from the harsh surface conditions by the ice layer, and perhaps most crucially the presence of a meltwater layer at the rock-ice interface creates suitable conditions for the survival of a naturally existing microbial population. Additionally the lava itself is likely to have provided some degree of protection, through the existence of numerous cavities and vesicles. The near-arctic environment of the original microbial community also suggests much of the microbial population would have resided within these cavities as a means of protection against the cold, dry Icelandic environment. This natural preference to the rock interior (as opposed to dependence on surface conditions) may also have played a role in the survivability of this community under Martian conditions, both as part of a Subglacial Volcanic Microcosm, but also the fully exposed negative control experiment.

It was hypothesised that the negative control lava would emerge from the Mars chamber completely sterilised, showing the benefit of having heat and ice as part

of the volcanic environment. However, two isolates were cultured from the fully exposed lava. This is still much lower than both the original number of isolates and those that survived the subglacial volcanic environment, and can most likely be attributed to the duration of exposure to Mars conditions. However, it is most likely that if the lava was left in there longer, the combination of low pressure and a Martian atmosphere would eventually sterilise the rock completely.

5.7 Conclusions and Future Work

The key factor in the experiment carried out here was to test the combined effect of heat and ice on the survivability of an indigenous basaltic bacterial community, the result of which showed that subglacial volcanic environments on Mars could potentially be viable systems. As such, the geological deposits from such volcanic environments could be fruitful targets for astrobiological missions such as ExoMars, and this is explored in detail later in Chapter 8.

With regards to limitations of this experimental work, there are a number of changes/additions that could be implemented to improve the validity of the results. In particular, the addition of more control experiments would provide further context for CFU quantification. These could include a SVM under Earth conditions, and also a truly ‘negative’ control whereby a pillow lava sample would be sterilised (by autoclaving and UV sterilisation), and tested for growth. With regards to isolation of bacteria from the lava, increased sample size or multiple experimental runs would allow for the employment of other isolation techniques. Such suitable techniques include the use of liquid media, and extraction of bacteria from the lava into an aqueous buffer, which could then be plated onto solid media. Likewise, increased sample size would also allow for the use of a wider variety of media types, maximising the diversity of bacterial phylotypes. Finally, devising a method of colony enumeration that would produce truly quantitative colony enumerations (such as extracting bacteria from the lava into an aqueous buffer, of which serial dilutions could then be made) would further validate and constrain (or potentially disprove, though unlikely given the clear trends in survivability) the results.

There are a multitude of experiments that could follow on from the initial experiment described here, incorporating and controlling new and existing

variables, whilst still retaining the focus on a subglacial volcanic environment. These are briefly described below:

- An important factor is that of organics within these environments. In natural subglacial volcanic systems organic material would be introduced to the subsurface system via subaerial in-fall and subsequent incorporation into the ice (Gaidos *et al.* 2004). In the experiment described in this chapter, the source of organics would have been solely from the pillow basalt and its resident microbial community. Using snow melt or actual glacial ice would introduce a second source of organics into the system, which would benefit the heterotrophic members of the population. Likewise, measuring total and dissolved organic carbon from the lava and meltwater respectively would provide another level of characterising these environmental simulations.
- Regarding the detection of life from such environments, it is necessary to test biosignature survival under Martian conditions. In particular, experiments would be conducted to assess the degradation of biomolecules such as lipids and DNA in subglacial volcanic deposits that may be preserved in the geological record, including lavas (hyaloclastite and pillow basalt), Jokulhlaup sediments, and subglacial caldera lake sediments.
- Lastly, as mentioned previously, longer duration incubations would provide a clearer picture regarding not just survivability of a microbial community, but also how this community develops over time, regarding environmental selection of particular groups of microorganisms, and a preference of particular metabolic pathways. Ideally, multiple experiments that can be assessed over time, together with duplicates to validate particular findings, would greatly enhance microcosm experiments such as these.

CHAPTER 6

DEVELOPMENT AND TESTING OF THE GEOLOGICAL FILTERS ON THE EXOMARS PANCAM INSTRUMENT

Following on from the previous chapters which centred around characterising a volcanic Martian analogue environment (specifically, subglacial volcanism) in terms of microbial diversity, biosignatures, and habitability, the next two chapters will focus on the detection of these environments (and others) on Mars using rover instrumentation. In particular, the PanCam instrument is currently in development for inclusion on the European Space Agency ExoMars mission, and the work described here contributes to the development of this instrument.

Firstly, several alternative geological filter sets were designed to replace the set currently planned for the ExoMars PanCam instrument – that adopted from the Beagle2 PanCam. This was conducted with the aim to detect past habitable environments in the Martian geological record, a primary goal of the ExoMars mission.

Secondly, laboratory testing of these new filter sets were conducted under controlled conditions on a selection of predominantly volcanic Martian analogue material from Iceland, with the primary focus being the detection of hydrated mineral deposits (and therefore evidence of liquid water) and biosignatures (evidence of life) likely to be present in geological Martian analogue samples. These criteria were used to identify the advantages of the new filter sets.

Thirdly, the addition of a UV illumination source is currently being considered for inclusion on PanCam. Here, initial testing was conducted along side the laboratory testing of filters on Martian analogue samples, to assess the benefit of a UV illumination source in the detection of astrobiological targets.

6.1 Formulating a new Geological Filter set for the ExoMars PanCam Instrument

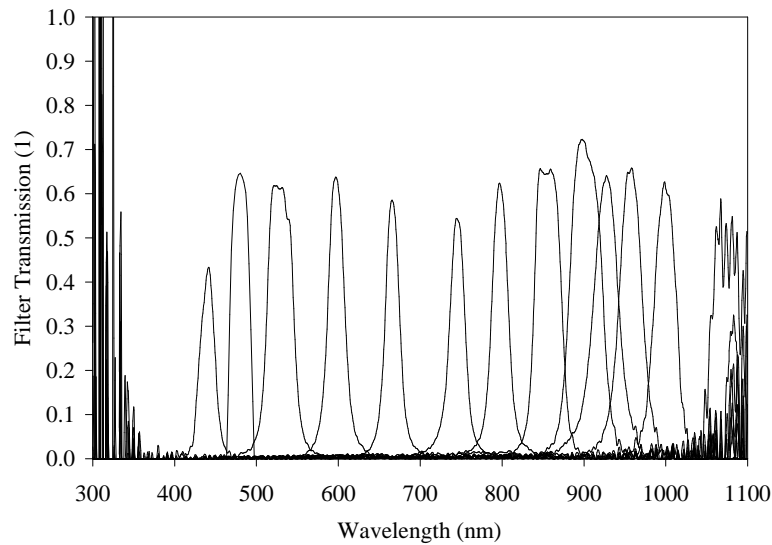
6.1.1 An astrobiological objective

The ability to detect environments on Mars that may have once been habitable is fundamental to any astrobiologically-focused mission. This is highlighted in the scientific objectives of both the NASA Mars Science Laboratory mission (launch due 2013), and the European Space Agency (ESA) ExoMars mission (launch due 2018). ExoMars aims, primarily, to find evidence for past or present life on Mars via a drill that can reach depths of 2m into the subsurface. Prime astrobiological targets will be those that display evidence for the existence of past liquid water in the geological record. As such, hydrated minerals on Mars therefore are of particular interest to the ExoMars mission, as they are essential in establishing the history of liquid water on the planet, which in turn is directly related to the search for past or present Martian life. Minerals with OH or H₂O as part of their chemical structure require aqueous conditions to form, but do not necessarily need liquid water to remain stable in their current environment after formation (Bishop 2005). It is this knowledge that has driven the need to explore terrains rich in hydrated minerals, with the aim of identifying evidence for habitable environments on Mars.

6.1.2 Selection of new geological filter wavelengths

As the PanCam multispectral imaging capability is largely dependent upon a suitable set of 12 pre-selected ‘geological’ filters, the wavelengths of these individual filters needs to be chosen to fit the objectives of the ExoMars mission. The geological filter wavelengths for the PanCam are required to fall in the 440 – 1000nm range, with a minimum of 12 (and possibly up to 14) filter spaces available. A notional set of filter wavelengths has already been allocated for this PanCam, however this filter set was inherited from Beagle2 (Figure 6.1), which in turn was adopted from Mars Pathfinder.

Figure 6.1. Filter wavelengths used in the Beagle2 camera, originally adopted from Pathfinder. Points below 400nm and above 1000nm are noise signals.



Filters for the Imager for Mars Pathfinder (IMP) device were selected with two main objectives in mind. Firstly, to identify ferric oxides and oxyhydroxides, and secondly to determine the silicate mineralogy present, particularly pyroxenes (Smith *et al.* 1997). More recently, this filter set has been largely adopted for the MER PanCam, again focusing on the detection of iron-bearing silicates, iron oxides and oxyhydroxides, and also to provide a direct comparison to the IMP results (Bell *et al.* 2003). ExoMars on the other hand has a distinct astrobiological focus, and may encounter an extensive range of hydrated mineral-bearing lithologies. As a consequence, the notional filter set for the PanCam needs to be revised.

The ability to detect regions or outcrops of interest remotely is a fundamental aspect of planetary rover exploration, as the selection of high priority targets proximal to the rover is essential to maximise the science output of the operation during finite rover operations. However, whilst multispectral imaging at optical to near-infrared wavelengths (400 – 1000nm) can tell us a lot about mineralogy and chemistry, the majority of distinguishing spectral features occur in the infrared, and therefore out of the PanCam range of detection. As a result, the combination of reflectance spectra with other instrumental analysis can enhance the ability of the PanCam in identifying mineralogy and lithology. The MicrOmega instrument can provide additional detailed spectral information in the 0.85 – 2.6 μ m region, helping to confirm many of the mineralogical features identified with PanCam. Additionally, the Raman instrument will be able to

provide accurate mineral identification (Wiens *et al.* 2005), and will provide vital data to complement the PanCam’s multispectral capabilities. However, these instruments are currently envisaged to work on the micro-scale as contact instruments for drill samples, and as such are not remote surveying tools, therefore target selection will be based solely upon PanCam image and spectral data.

Reflectance spectra between the region 440 – 1000nm of hydrated minerals from the publically available USGS spectral library splib06a (Clark *et al.* 2007) and splib04 (Clark *et al.* 2003) were used to select potential new geology filter wavelengths for the ExoMars PanCam. Minerals were chosen based on the identification of hydrated mineral groups on Mars, and are shown in Table 6.1. These alternative filter sets, plus the Beagle2 (B2) filter set (which is currently selected for the PanCam) were tested on their ability firstly to successfully discriminate between multiple spectra from hydrated mineral groups, and secondly, detect hydrated minerals present in untreated Martian analogue rocks from Iceland.

For statistical filter selection (described below), the USGS spectra were required to have evenly spaced spectral points, and as such the raw spectral data were re-binned to produce data points every 10nm. It is noted the samples used by Clark *et al.* (2007; 2003) to generate their mineral spectra are not compositionally 100% pure, and often have other minor mineral fractions present. As such, these powdered mineral reflectance spectra are taken as an ideal *spectrally* pure ‘end member’. Another important factor is the variation between one sample spectrum to another within the database, for example the spectra for different samples of jarosite will vary slightly. Ideally, multiple sample spectra would be utilised in the formulation of the new filter set to eliminate any bias towards one arbitrarily chosen sample. However, there is a lack of consistency within the sample spectra available for any given mineral, e.g. there are 9 samples available for jarosite but just 2 for gypsum available. Therefore, a single representative sample spectrum was used for each mineral (specified in the text) to use in the generation of a new filter set to prevent any skew towards a particular mineral. Sample spectra were chosen based on the purity of the sample and lack of noise. An alternative method – whereby data is averaged

from all the available samples for a particular mineral – was also considered. However, it was decided that using a genuine mineral spectrum was better than using a modelled spectrum for the selection of filters.

Table 6.1. Hydrated mineral reflectance spectra used for PanCam filter selection.

| Mineral group | Mineral (USGS Sample Reference) | Proposed time period on Mars (from Bibring <i>et al.</i> 2006 and Milliken <i>et al.</i> 2008) |
|-----------------|---|--|
| Phyllosilicates | Nontronite (SWa-1.a) Montmorillonite (CM27) | Early – mid Noachian |
| Sulphates | Gypsum (SU2202) Kieserite (KIEDE1) Jarosite (JR2501) Alunite (HS295) | Late Noachian - Hesperian |
| Hydrated silica | Opaline silica (TM8896) | Late Hesperian, possibly Amazonian |

The three new filter sets were devised as follows:

Filter set F1-12: Firstly, 12 optimal wavelengths that most accurately reproduced a specific mineral spectrum were calculated for all the selected hydrated minerals individually (e.g. the best 12 points for jarosite, the best 12 for gypsum, and so on). This filter selection used a brute force approach to search through the possible wavelength selections between 440 and 1000nm, using 10nm increments. Additionally, Two of these 12 wavelengths were always fixed at 440 and 1000nm. The suitability of a wavelength selection was calculated firstly by interpolating the points between the 12 randomly chosen wavelengths to obtain a full set of data (i.e. a complete spectrum). Then, the absolute difference in reflectance (residual) was calculated between the actual spectrum of the mineral (R_a), and the spectrum estimated (R_e) using the current wavelength selection at each respective 10nm spaced point (λ). The summation of these absolute distances is then used as the ‘error score’ for that particular wavelength selection and mineral (σ_m):

$$\sigma_m = \sum_{\lambda=440}^{1000} |R_a(\lambda) - R_e(\lambda)|$$

where λ increments in steps of 10nm. The lower the error score, the better the wavelength selection, producing the optimal set of 12 wavelength points for each mineral. In addition, spectral features were visually identified from all available USGS spectra for each hydrated mineral in question – such as ferrous and ferric iron absorption bands, and O-H or H₂O absorption bands (Figure 6.2a). These data combined were then used to subjectively decide on a suitable filter set, named ‘F1-12’.

Filter set F2-12: 12 optimal wavelengths were calculated for the selected minerals collectively (all normalised to the same starting value, shown in Figure 6.2b). This used the same computational method described above, but calculated the 12 best wavelengths for all minerals together (rather than individually). To find the best wavelength selection for this mineral set, the error scores for each mineral were summed into an overall error score (σ) for each combination of wavelengths assessed:

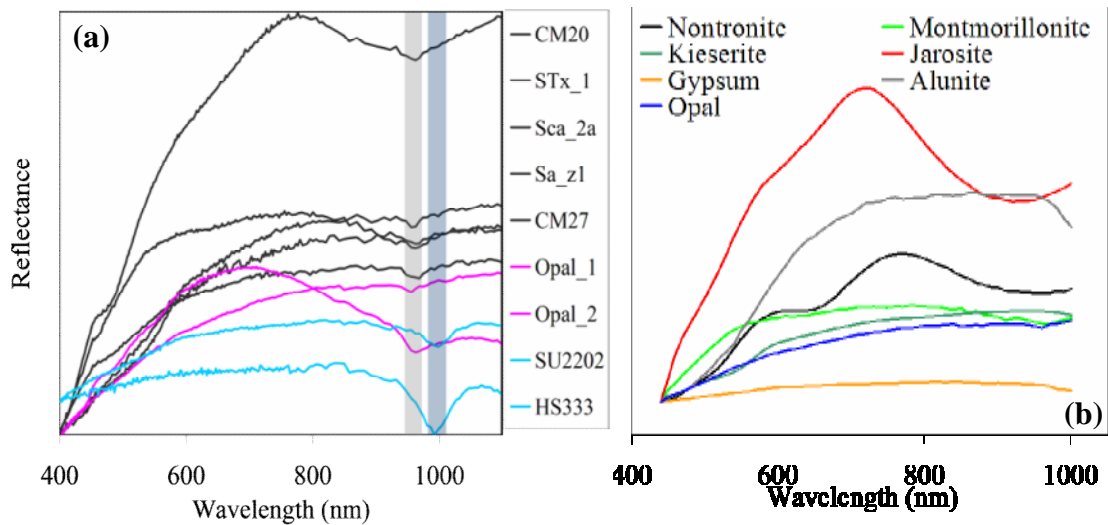
$$\sigma = \sum_{m=1}^M \sigma_m$$

This generated filter set ‘F2-12’ and was not adjusted further.

Filter set F3-12: The third filter set created had evenly spaced filters every 50nm (with the exception of the first two filters, which have 60nm spacing) and was not biased towards any pre-determined set of minerals.

These three new filter sets, and the original Beagle2 (B2) filters, were principally tested on Martian analogue samples, to evaluate their suitability in the detection of hydrated minerals on Mars. One of these filter sets was then selected for field testing in Svalbard during AMASE, described in the following chapter.

Figure 6.2. a) Spectra of montmorillonite (CM20 – CM27), opal, and gypsum (SU2202 and HS333) with OH and H₂O absorption bands at 950 and 1000nm respectively; b) USGS spectra (Clark *et al.* 2007) of the minerals used to statistically calculate new filter selections for ‘F1-12’ and ‘F2-12’. For specific USGS sample numbers, see Table 6.1.



6.1.3 Description of the new geological filter sets

The new filter sets differ principally to the B2 filters in that they lack a concentration of filters towards the NIR end of the spectrum, with a broader range of filters within the visible. Filter set F1-12 was chosen, in part, subjectively based on the ability to detect a variety of hydrated minerals known to exist at the Martian surface, but also iron oxides and oxyhydroxides, which have previously been shown to also be of astrobiological interest (Bishop *et al.* 1998). The spectral region between 440-1000nm is dominated by Fe excitational and charge transfer bands (Bishop 2005a), and therefore is particularly sensitive to iron-bearing mineralogy (Farrand *et al.* 2008). As a result, distinctive spectral features are particularly evident in Fe-bearing hydrated minerals such as jarosite and nontronite, as well as silicates pyroxene and olivine and a range of iron oxides such as haematite and goethite. Ferric absorption bands exist at 480nm, 650nm and 950nm, whilst a ferrous absorption band also in the 950nm region can often obscure that produced by ferric iron (Stewart *et al.* 2006). Whilst nontronite and jarosite share these similar Fe-absorption bands, nontronite has a distinctive kink around 650nm that is not present in the jarosite spectrum. For these reasons, filters within this filter set were placed so as to be sensitive to such diagnostic features. In addition, estimated filter bandpasses were also accounted for. For the B2 filters, bandpasses had already been previously assigned (Griffiths *et al.* 2006), and these were used in the re-sampling of sample

data based on the full-width-at-half-maximum (FWHM) values. For the new filter sets, estimated bandpasses were assigned, based on those chosen for the B2 filters. These are shown in Table 6.2. Multispectral data was averaged within the range covered by the FWHM bandpass for each filter.

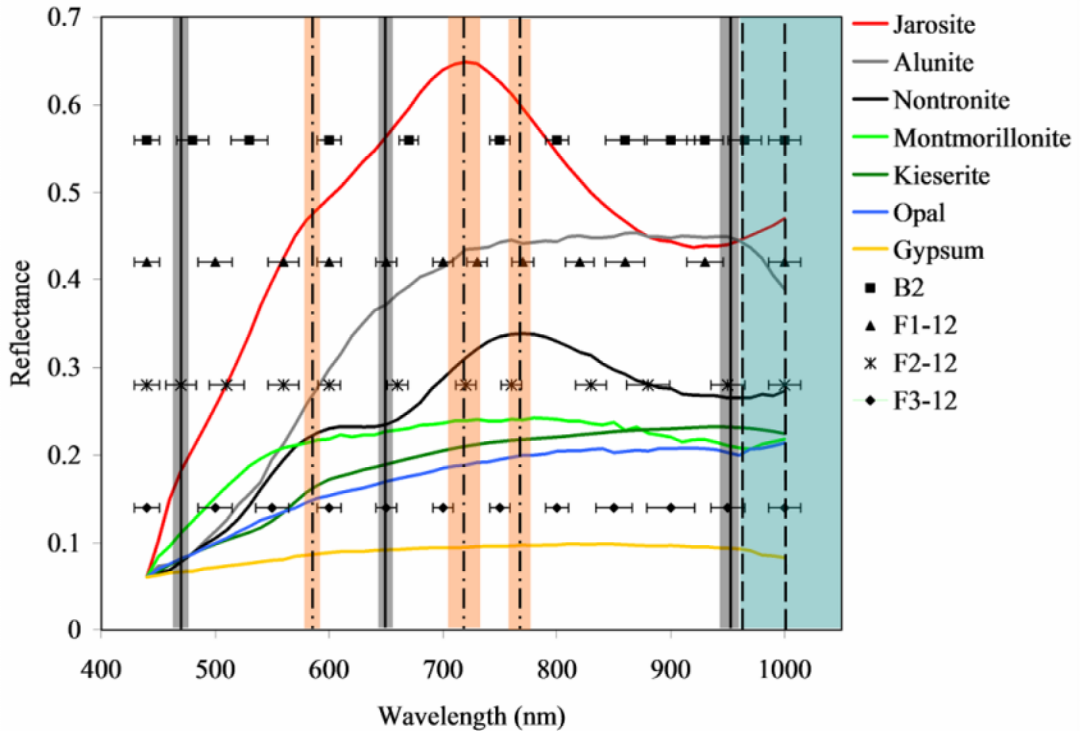
Table 6.2. Filter centre wavelengths (λ) and estimated filter bandpasses at FWHM for B2 and the proposed filter sets. The ‘B2’ filter set is a duplicate of that from the Beagle2 PanCam (Griffiths *et al.* 2006); ‘F1-12’ was subjectively formulated; F2-12 was calculated statistically; and F3-12 has filters regularly spaced every 50nm. All data are in nm.

| B2 | | F1-12 | | F2-12 | | F3-12 | |
|-----------|----------|--------------|----------|--------------|----------|--------------|----------|
| λ | Bandpass | λ | Bandpass | λ | Bandpass | λ | Bandpass |
| 440 | 22 | 440 | 22 | 440 | 22 | 440 | 22 |
| 480 | 28 | 500 | 30 | 470 | 26 | 500 | 30 |
| 530 | 32 | 560 | 27 | 510 | 30 | 550 | 29 |
| 600 | 21 | 600 | 21 | 560 | 27 | 600 | 21 |
| 670 | 17 | 650 | 18 | 600 | 21 | 650 | 18 |
| 750 | 18 | 700 | 17 | 660 | 18 | 700 | 17 |
| 800 | 20 | 730 | 18 | 720 | 17 | 750 | 18 |
| 860 | 34 | 770 | 19 | 760 | 18 | 800 | 20 |
| 900 | 42 | 820 | 25 | 830 | 27 | 850 | 32 |
| 930 | 32 | 860 | 34 | 880 | 38 | 900 | 42 |
| 965 | 29 | 930 | 32 | 950 | 30 | 950 | 30 |
| 1000 | 28 | 1000 | 28 | 1000 | 28 | 1000 | 28 |

The filter centre wavelengths and their estimated bandpasses at FWHM are shown in Figure 6.3, together with the position of iron and water/hydroxyl bands that are common to the hydrated minerals used in this study. Note the lateral extent of these bands is estimated. It can be seen that the B2 filters miss a Fe^{3+} absorption band at 650nm, and the jarosite and nontronite emission bands at 720 and 760nm. Overall, five of the B2 filters fall directly (i.e. their centre wavelength, 2 filters) or partially (i.e. coverage by their bandpass, 3 filters) within these spectral bands. Likewise, only five of the F3-12 filters fall within the spectral bands (three of these by their centre wavelength). In comparison, six of the new F1-12 filters fall within the spectral bands (three of these by their centre wavelength), whilst computer-generated filter set F2-12 is best with seven filters falling within the spectral absorption/emission bands (four by their centre wavelength). We also note that although the new filter sets are primarily based on hydrated mineral spectra, the distribution of filter wavelengths are still well placed to detect spectral features that the original Pathfinder/Beagle2 filters were designed to detect. For example, the near-UV to visible ferric absorption edge from 440 – 750nm is now covered by 6 filters with F1-12 and F3-12 (1 more

than the Pathfinder/B2 set), and 7 filters with F2-12. Additionally, the wavelengths diagnostic of different pyroxene compositions (930 and 1000nm) are still covered by all the new filter sets.

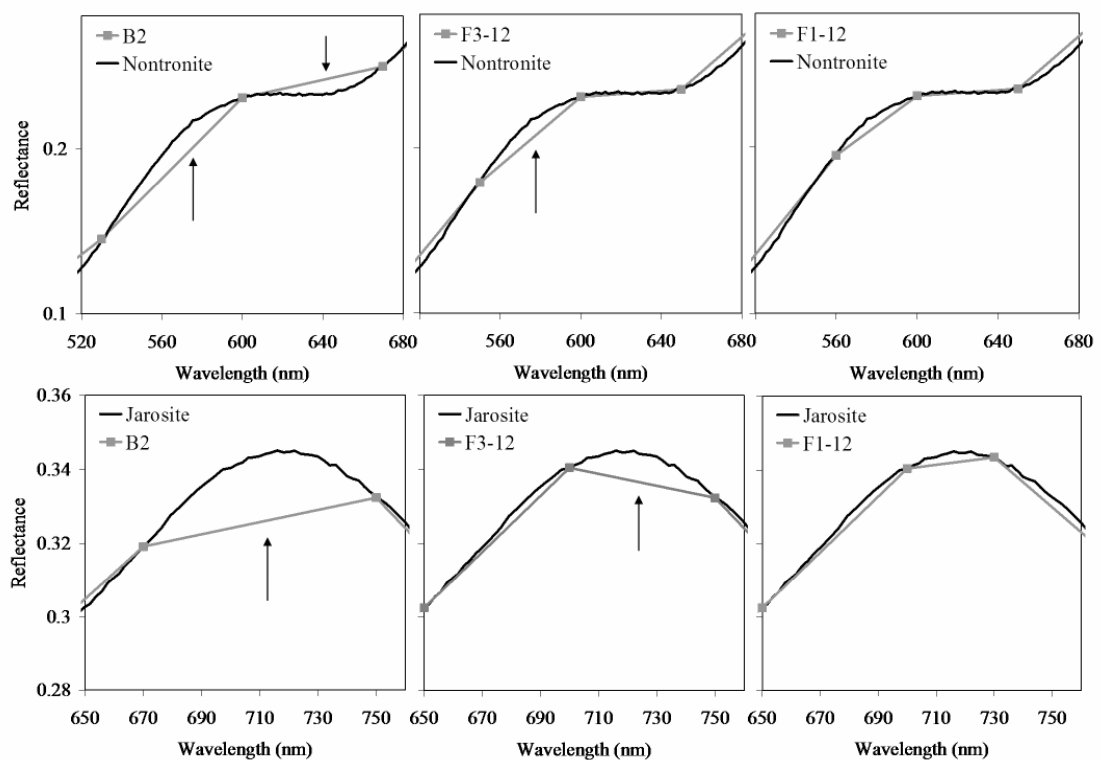
Figure 6.3. Plot of filters and estimated filter bandpasses for Beagle2 (B2) and new filter sets, together with the absorption bands for ferric or ferrous iron (grey, solid line) and water (blue, dashed line), and also the emission peaks for nontronite and jarosite around 700nm (pink, dash-dot line). Also shown are the hydrated mineral spectra used to calculate filter set F1-12 and F2-12.



The effect different filter wavelengths can have on an observed PanCam spectrum is demonstrated using the USGS spectra for nontronite and jarosite. Figure 6.4 shows a close up of particularly diagnostic spectral features for nontronite and jarosite, sub-sampled to three of the filter sets (B2, F1-12 and F3-12). Here, it can be seen that the B2 filter set does not fully represent key diagnostic spectral points for the mineral nontronite, where the Fe^{3+} absorption feature at 650nm falls between B2 filters 600nm and 670nm. Likewise, the main peak at $\sim 700\text{nm}$ for jarosite is missed by the B2 filters. Additionally, having filters spaced at regular intervals (filter set F3-12) can miss these points. In both minerals, filter set F1-12 more closely represents the original mineral spectrum, especially for jarosite. In either case, filter sets F1-12 and F3-12 both outperform B2. For nontronite, the difference between F1-12 and F3-12 is relatively small, with filter set F1-12 producing a slightly better match than F3-12. In this

example, the key difference between the two sets is the filter at 560nm for F1-12, and 550nm for F3-12. The other filter wavelengths in the range under observation (520 – 680nm) are the same. For jarosite the difference is particularly evident, as the current B2 filters completely miss a significant peak at ~710nm, whilst filter set F3-12 partially misses it. Filter set F1-12 however closely matches the spectrum.

Figure 6.4. Reflectance spectra of nontronite (SWa-1.a) and jarosite (JR2501) showing the effect of the different filter sets on diagnostic features. Filter sets shown are the existing ‘B2’ filters, compared with ‘F1-12’ and ‘F3-12’ filter sets. Arrows highlight spectral features that are missed by particular filters.



6.2 Detection of Astrobiological Targets in Martian

Analogue Samples

Establishing and understanding the spectra of Martian analogue material was conducted with the aim to conduct realistic testing of the PanCam filter sets, and also for ground-truthing. For this work, a variety of Martian analogue samples that were believed to encompass hydrated minerals were used to test the new geological filters. These samples are from environments that are directly related to volcanic activity.

6.2.1 Martian analogue rocks

Geological samples from Iceland were used to test the old Beagle 2 (B2) and new filter sets. Table 6.3 provides more detail on the location and nature of the samples used in this study, and Figure 6.5 shows images of some of these samples. These included subglacial basaltic lavas, subaerial basaltic flows, hydrothermally altered lavas, and hot spring precipitates. These Martian analogue samples were used in their natural state, in contrast to comparable studies that use homogenised, powdered mineral fractions (Bishop *et al.* 2004a; Bishop *et al.* 2004b). The benefit of using raw samples has been highlighted by Harloff & Arnold (2001). Previous to that, Yon & Pieters (1988) noted the most appropriate analogue to outcropping rock on a planetary surface is not a powdered sample, but a rough bulk sample surface. As such, raw geological samples are used for this work, to best simulate the nature of geological outcrops that may be encountered during the ExoMars mission. Contextual information was also gathered on mineralogy, chemistry, and morphological features using Raman spectroscopy, Scanning Electron Microscopy (SEM) and Energy Dispersive X-Ray Spectrometer (EDS) analysis (see Chapter 2, section 2.5 for details).

Figure 6.5. Martian analogue samples used for testing different filter sets. a) GY2 – silicified biomat; b) GY1 – silica sinter; c) KH – hyaloclastite with opaline silica coating; d) NAL – acid fumarole weathered lava; e) HH – hyaloclastite; f) NBO – acid weathered lava. Scale bar = 1cm. A description of samples is given in Table 6.3 below.

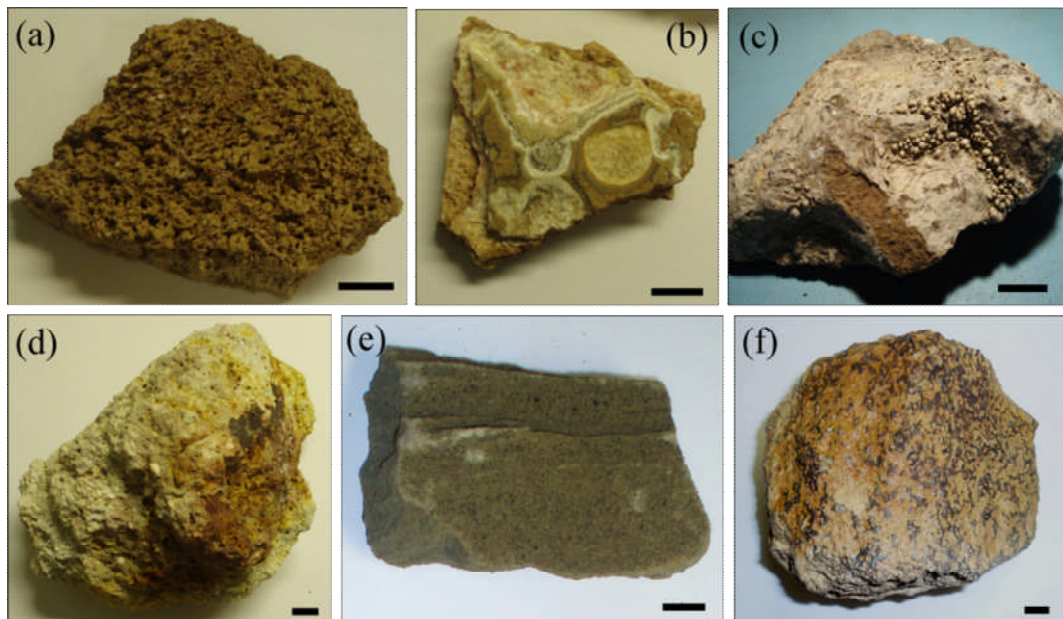


Table 6.3. Description and original location of the samples used in this study.

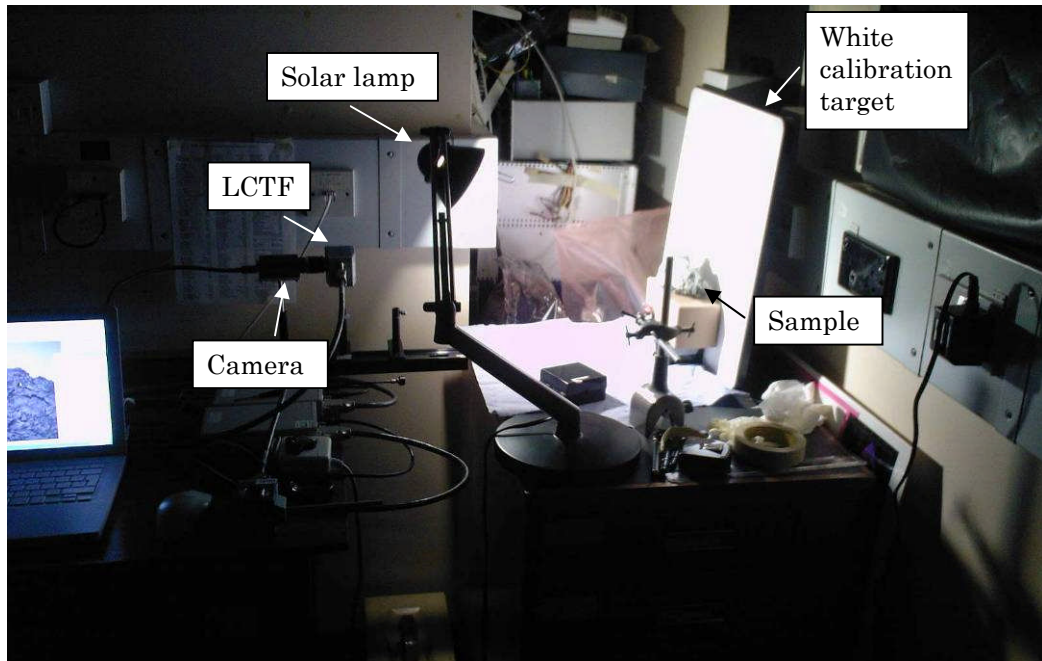
| Sample | Location | Description |
|--------|-----------------------------|---|
| NBO | Namafjall solfatarara field | A weathered Holocene basalt lava that has undergone solfataric interaction with acidic fumaroles and hydrothermal fluids, leaving behind dark orange coloured mineral deposits inside vesicles and depressions in the rock surface. |
| NAL | | A Holocene basaltic lava that has undergone extensive high temperature solfataric alteration via fumaroles, producing white, grey, yellow and red mineral deposits on the surface. |
| HH | Helgafell | A Pleistocene subglacially erupted basaltic hyaloclastite with 0.5 – 3mm sized glass fragments in a palagonite-rich matrix. |
| KH | Krysuvik | A Pleistocene subglacially erupted basaltic hyaloclastite with 1 – 10mm sized glass and scoria fragments in a fine palagonite matrix. This hyaloclastite has interacted with hot spring fluids, which have deposited a 1 – 4mm thick opaline silica crust on the surface of the lava. |
| GY1 | Geysir | Silica sinter deposit ‘geyserite’ exhibiting different coloured 1 – 2 mm thick layers of black, red and yellow coloured deposits. |
| GY2 | | Silicified biological material, including a silicified microbial hot spring biomat that still retains its clear fibrous structure and silicified macroscopic biological material. |
| KV007 | Kverkfjoll | A Pleistocene subglacially erupted highly vesicular pillow basalt lava. |
| LL | Myvatn | A Holocene subaerial lava with extensive epilithic lichen colonisation. |

6.2.2 Multispectral imaging

For multispectral imaging, all samples were illuminated with a Solex solar lamp at an average distance of 60 cm, although this varied slightly depending on the size of the sample. Still-capture imaging was carried out at a distance of 1 meter from the sample, at the Mullard Space Science Laboratory, by a Foculus FO432SB camera (1.4Mpixels, 8- bits/pixle greyscale, 15° field of view lens, exposure time 1 ms to 65 s). As with the ExoMars PanCam, this camera has a 1024 x 1024 pixel CCD which responds to wavelengths between 400 – 1000nm. The camera was interfaced with one of two CRI Varispec liquid crystal tunable filters (LCTF) – one covering the visible (wavelength range of 400 – 750nm; bandpass of 20nm) and the other covering the near infrared (wavelength range of

650 – 1100nm; bandpass of 10nm). Images were taken with the filters every 10nm. Figure 6.6 shows an example experimental set up and all the components.

Figure 6.6. Experimental set up for PanCam – style multispectral imaging.



For testing the ability of the proposed UV laser addition (Storrie Lombardi *et al.* 2009; 2008; Muller *et al.* 2009; Griffiths *et al.* 2008) to the PanCam instrument in detecting astrobiological targets, samples were also imaged with the Foculus camera interfaced with the flight-spare Beagle2 filter wheel. UV illumination was achieved using either a 365nm Nichia single LED (NSHU590B) or a 375nm Nichia laser diode (NDU1113E). Colour images of fluorescence were taken with a commercial digital camera. The LED working distance illumination ranged from 10cm to 30cm, whilst laser working distance illumination was fixed at 2.6m. Figure 6.7 shows example experimental set ups for UV illumination and imaging.

Images were processed with ImageJ software (<http://rsbweb.nih.gov/ij/>), and an example multispectral image is shown in Figure 6.8. Relative reflectance spectra (T/C) were calculated by dividing the brightness values measured for the target (T) sample/region of interest by that measured from a white calibration target (C) in the background of each image. The size of the regions from which spectra were extracted varied from 10 x 10 pixels to 200 x 200 pixels, depending upon the size of the feature in question. The new geological filter sets were used to

produce 12-point spectra for Martian analogue samples by re-sampling the multispectral data to match the proposed filter wavelengths

Figure 6.7. Experimental set up for UV illumination using a) LED+Foculus+B2 filter wheel; b) Laser+Digital camera. In (b), the laser is housed at the top of a 2m long tube, channelling the laser down.

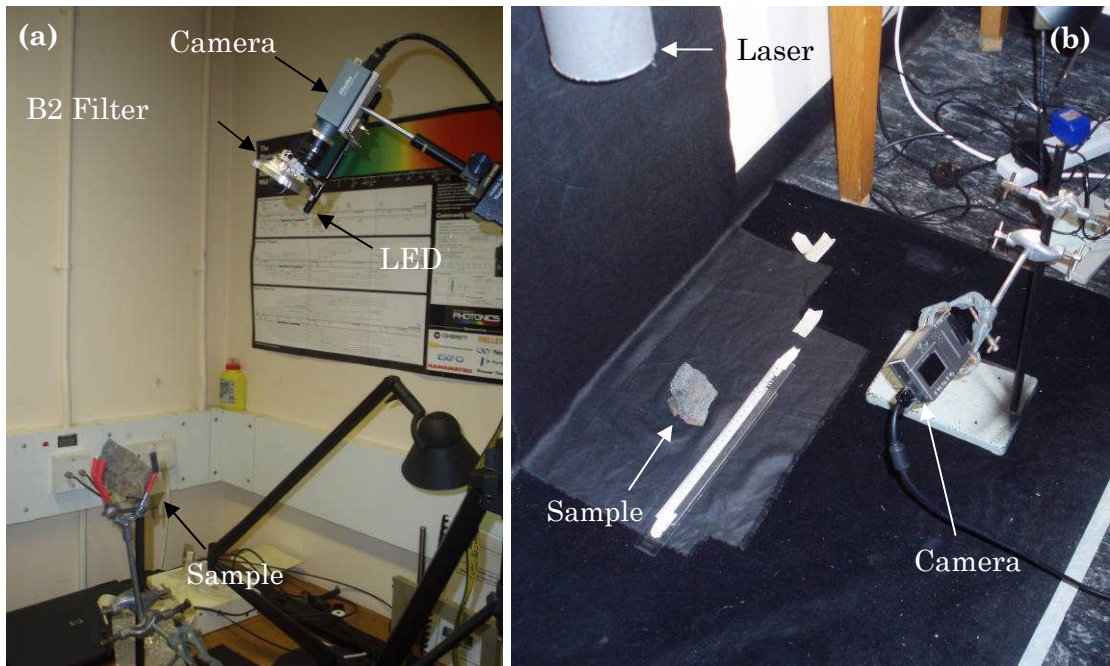
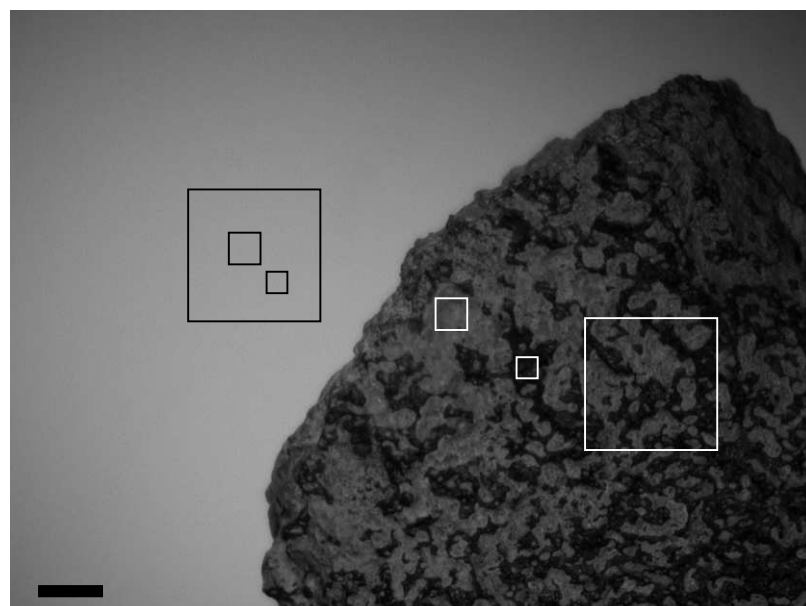


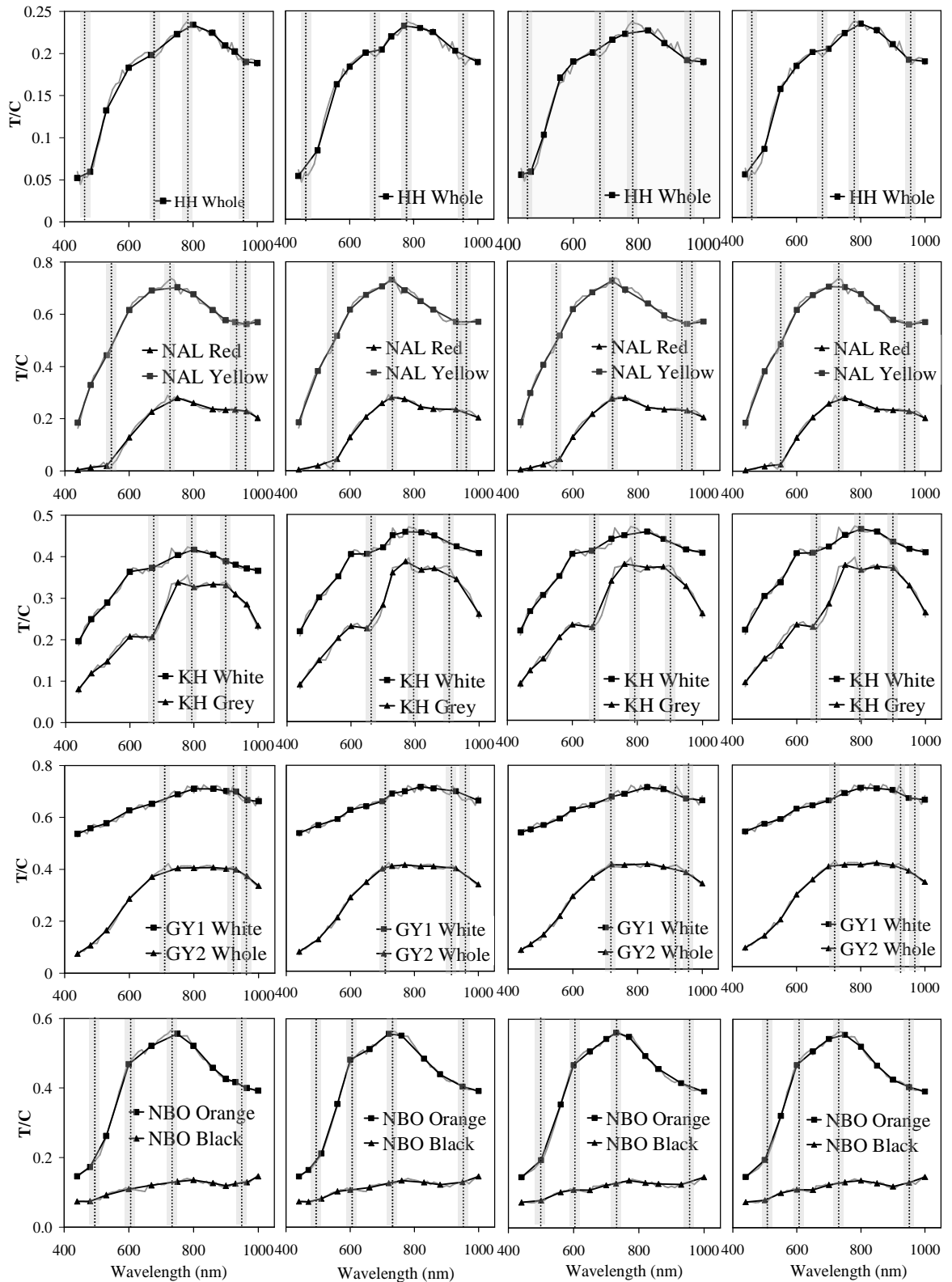
Figure 6.8. Example image of sample NBO as seen with a 590nm filter. In the background is the white calibration target. White squares indicate the regions where reflectance values are measured, e.g. the altered lava (pale grey), unaltered lava (dark grey), and 'whole' measurement (incorporating both components). These are calibrated using reflectance from the white calibration target (indicated by the black squares). Scale bar = 1cm.



6.2.3 Martian analogue PanCam reflectance spectra

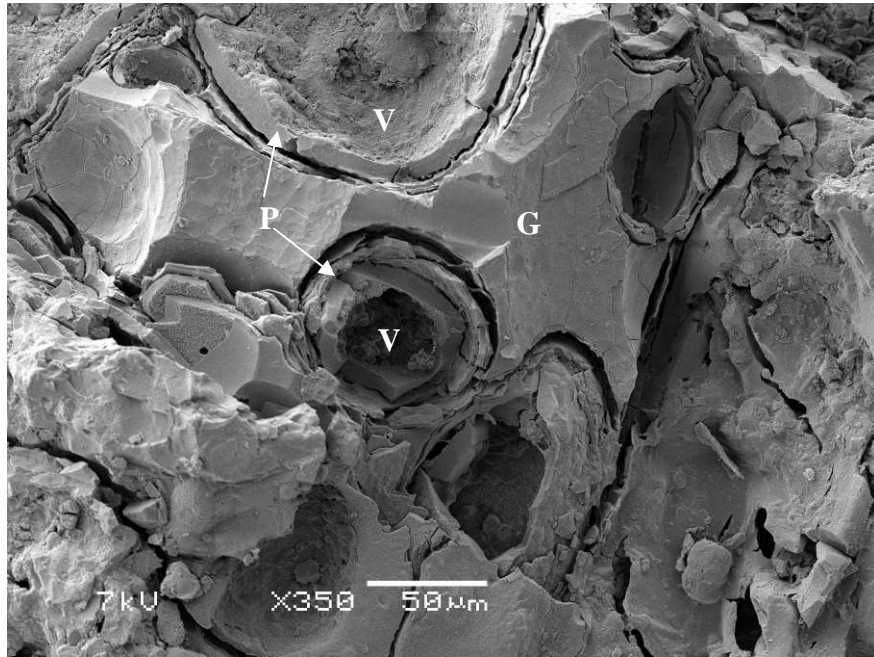
The new filter sets were used to model 12-point spectra for Martian analogue samples by re-sampling the multispectral data to match the proposed filter wavelengths. In addition, the data were averaged within the range covered by the FWHM bandpass for each filter. The filter sets were tested on whether or not they were able to capture spectral features that could potentially lead to the identification of particular mineral species or assemblages within the rocks. Spectral parameters, such as those used to identify spectral variability within MER PanCam multispectral images (e.g. Farrand *et al.* 2008; 2006), were also used to investigate the suitability of particular filter sets. Different filter sets will have different filter wavelengths covering a particular spectral feature, such as the 440 – 700nm absorption edge, or the 900nm absorption band. Where there is not a filter centred at the specific band in question, the nearest filter is used, and so is representative of how spectral parameter data will appear with the different filter sets. Six geological samples were tested (Table 6.3), and the spectra for each respective filter set for these samples are shown in Figure 6.9. Where relevant, spectra for different coloured regions (and therefore potentially different mineralogy) on the rock are shown, highlighting the spectral variation across a naturally heterogeneous geological sample. Filter sets were tested on their ability to either detect, or miss, key spectral features present within the complete rock spectrum, the results of which are detailed in Table 6.4 and discussed for individual samples in more detail below. In particular, the detection of different hydrated minerals (including phyllosilicates, sulphates, and opaline silica) is the primary focus. Overall, all the filter sets were able to detect hydrated minerals and other spectral features in at least 4 out of the 6 samples, and the specific samples varied with the different filter sets.

Figure 6.9. Martian analogue sample spectra modelled for: column (A) Beagle2; (B) F1-12; (C) F2-12; (D) F3-12 filter sets. Spectra are either for the whole sample, or specific coloured regions, as indicated on individual plots. The full spectrum (grey) underlies the modelled ‘PanCam’ spectrum (black). Grey bands overlying the spectra highlight spectral features (e.g. absorption bands, reflectance peaks/plateaus) that correspond to those in Table 6.4. Larger versions of these plots, together with their relevant mineral spectra, are given in Appendix C.



Hyaloclastite sample HH is rich in phyllosilicates, which exist as palagonite alteration rinds around basaltic glass clasts. The spectral features of this rock suggest a significant nontronite component, with characteristic Fe absorption features at 480, 680, and 950nm. The absorption features observed at ~460nm and ~950nm can be attributed to the presence of Fe³⁺, whilst the shifting of the absorption from 650nm (more typical for nontronite) to 680nm is indicative of a change from Fe³⁺ to Fe²⁺ (Stewart *et al.* 2006). Of the four filter sets, this sample spectrum is best reproduced by sets B2 and F3-12, in terms of the number of spectral features covered (Table 6.4). The new filter set F1-12 misses two spectral features: 480nm and 950nm, whilst F2-12 misses features at 680nm and 800nm. However, although the B2 filters only miss one spectral feature (the kink at 680nm), this absorption is a key distinguishing feature of the nontronite spectrum. A notable difference observed between the HH and a typical nontronite spectrum (e.g. SWa – 1) is the reduced reflectance peak at ~800nm in the HH spectrum. This could be due to the reflectance being measured from the rough surfaces of raw samples, which has been shown to decrease band depths in comparison to homogenised particulate sample spectra (Harloff & Arnold 2001). Additionally, the regions from which the spectra were extracted will exhibit small-scale mineralogical heterogeneities, which will all contribute to the spectral profile. Like nontronite, montmorillonite is a common constituent of palagonite, and linear mixing of 40% nontronite with 60% montmorillonite decreases the peak at 800nm, and therefore is a possible contributor to the bulk mineralogy, although without confirmatory mineralogical data this is purely speculative at this stage. Under SEM, a typical texture can be seen for the hyaloclastite, consisting of angular glass fragments with palagonite rinds around areas of aqueous alteration – in this case, vesicles within the glass clast (Figure 6.10). The main constituents of palagonite are Fe-rich smectite clays, and where aqueous alteration is extensive, as in hyaloclastite lavas, palagonite forms a significant constituent of the lava. As a result, the spectrum of the rock will be dominated by clays such as montmorillonite and nontronite. The detection of phyllosilicates is highly relevant for an astrobiologically mission. Phyllosilicate terrains on Mars are thought to represent the most habitable past environments, and therefore are most likely to hold clues to the planet's biological history (Bibring *et al.* 2006). As a result, the ability of the ExoMars PanCam to identify such phyllosilicate minerals is imperative to the mission objectives.

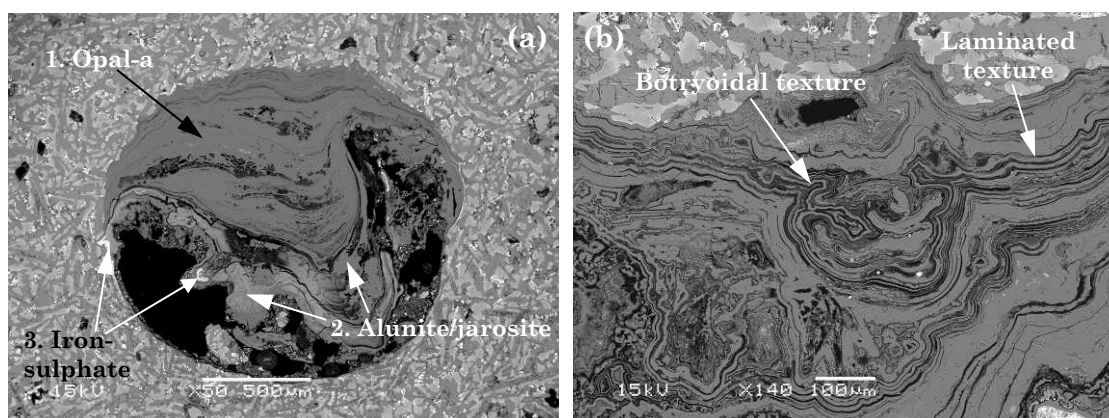
Figure 6.10. SEM image of the hyaloclastite (P = palagonite; G = glass; V = vesicle).



Sample NAL is a subaerial basaltic lava that is covered in extensive sulphur-rich alteration products due to acid-fumarole weathering, producing distinctively different colour regions on the rock surface. The spectra of the different regions on this rock are suggestive of the iron sulphate jarosite ($\text{KFe}_3(\text{SO}_4)_2(\text{OH})_6$), and the aluminium sulphate alunite ($\text{KAl}_3(\text{SO}_4)_2(\text{OH})_6$), for 'Yellow' and 'Red' regions respectively (Figure 6.9). The 'Yellow' region produces a spectrum that has a steep ferric absorption edge between 440 – 700nm, culminating in a peak at 710nm. This is followed by a broad absorption centred around 950nm, which is characteristic of Fe^{3+} . The 'Red' region has spectral features synonymous with those often seen for alunite, including a steep gradient between 440-700nm, and particularly an absorption feature at 950nm – 1000nm. Pure alunite is typically white (Hunt *et al.* 1971), but in this case it exists as red deposits on the surface of the lava. This red colouration is due to the partial replacement of Al^{3+} with Fe^{3+} (Hunt *et al.* 1971), which is represented by the broad absorption feature between 800 and 900nm. The spectrum also has a well defined absorption feature between 950 – 1000nm which can be attributed to OH stretching vibrations that exist further into the NIR, the first band existing at 1010nm (Hunt *et al.* 1971). Although jarosite is also a hydrated sulphate, it doesn't exhibit any OH bands until further into the infra-red spectrum (Clark 1990). All these spectral features for both the 'Yellow' and 'Red' regions were best captured with the new filter sets

F1-12 and F2-12, whilst both the B2 and F3-12 filter sets miss the peak at 710nm in the ‘Yellow’ spectrum (Figure 6.9). BSE analysis of NAL in thin section (Figure 6.11) demonstrate the high degree of alteration this lava has experienced. Mineral deposits can be seen inside lava vesicles, and these are typically a mix of iron and aluminium sulphates, but also amorphous (opal-a) silica. This silica component was not detected through multispectral imaging, potentially due to its confinement within vesicles and resulting absence from the rock surface. Silica deposits are characterised firstly by their elemental chemistry, and secondly their intricate botryoidal features and laminations within the deposits (Figure 6.11b). Iron-rich regions can also be found distributed throughout the lava, identified by it’s bright white appearance in BSE.

Figure 6.11. BSE images of a) mineral-filled vesicle and b) botryoidal amorphous silica deposits in sample NAL. Table below displays representative values as oxide wt.%.



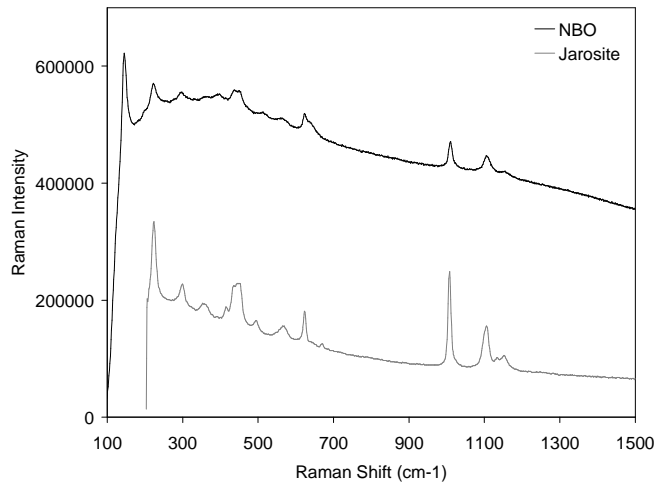
| | SiO ₂ | FeO | Al ₂ O ₃ | SO ₃ | CaO | K ₂ O | Total* |
|---------------------|------------------|------|--------------------------------|-----------------|-----|------------------|--------|
| 1. Opal-a | 92.7 | - | - | - | - | - | 92.67 |
| 2. Alunite/Jarosite | 31.7 | 29.5 | 16.4 | 1.9 | 0.5 | 1.4 | 81.48 |
| 3. Iron oxide | 6.3 | 72.4 | - | 1.5 | - | - | 80.22 |

*Low total values likely to be a result of water content, sample porosity, or both

Sample NBO, like sample NAL, is an acid-weathered basaltic lava, with orange coloured deposits filling the vesicles that are surrounded by unaltered basalt. The spectrum of these ‘Orange’ deposits is highly similar to the ‘Yellow’ mineral deposit in sample NAL, exhibiting a main peak at 720nm, and absorption features at 480 and 950nm (Figure 6.9). As with the NAL deposits, these features imply the presence of jarosite, which is entirely consistent with the geological setting of this lava. This is confirmed with Raman analysis (Figure 6.12, below). Unlike the deposits in sample NAL, all filter sets appear to represent this spectrum fully, although the B2 and F3-12 filter sets only

partially capture the 720nm peak. The ‘Black’ spectrum corresponds with the unaltered basalt component of the lava surface, and as such exhibits a relatively low-albedo spectrum. There is a small absorption band in an otherwise flat and featureless spectrum at 900nm, which is representative of the presence of low-Ca pyroxene (Farrand *et al.* 2008), and this is detected by all four filter sets.

Figure 6.12. Raman spectrum of the orange deposits on sample NBO, and jarosite for comparison.

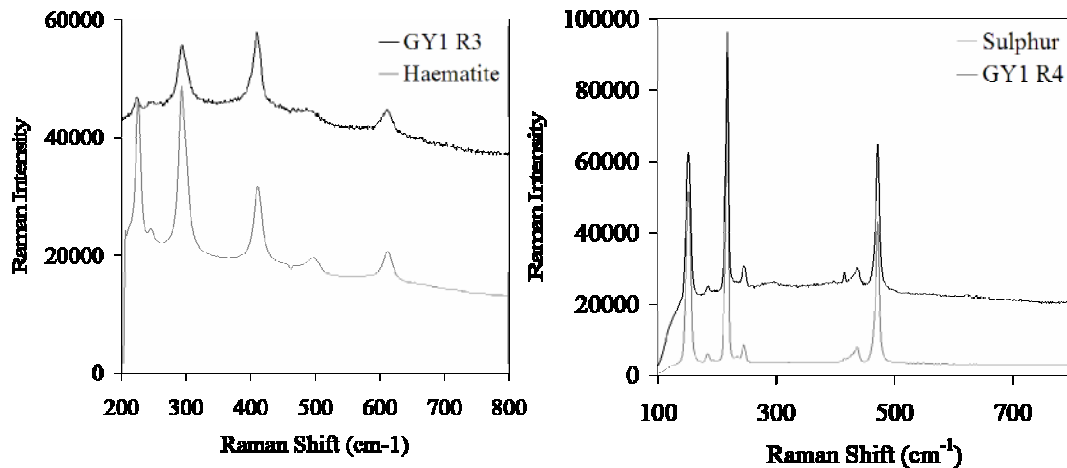


Sample KH is a hyaloclastite lava with a hot-spring deposited opaline silica crust (1 – 4mm thick) on the surface. Additionally, this crust is inhabited by chasmolithic lichen communities, and as such have an influence on the observed spectrum. The spectra of this white crust is consistent with that of opal, exhibiting a smooth arcing spectrum, although the hydration feature at 950nm is not present (Figure 6.9). The additional presence of the lichens has the effect of creating a slight absorption feature at 670nm, indicative of chlorophyll *a* (Bishop *et al.* 2004b). This feature is particularly strong in the ‘Lichen’ spectrum, along with a steep H₂O absorption between 900 – 1000nm. All the filter sets represented these spectral features, from both the ‘White’ and ‘Lichen’ regions (Table 6.4).

Samples GY1 and GY2 are both hot spring silica sinters. GY1 is characterised by several different coloured layered regions, ranging from black, red, yellow, and white (Figure 6.5b), with these components ranging from 1 – 10mm in size. The spectrum of the ‘White’ region has a generally flat morphology, with a small absorption at 950nm, comparable to the spectral features of opal-CT, where the 950nm absorption feature can be attributed to OH⁻. This 950nm absorption is

captured by all the filter sets except F1-12 (Table 6.4). The spectra of the other coloured regions of sample GY1 however are less indicative of its true mineralogy. Raman analysis of the ‘Red’ and ‘Yellow’ sinter components identifies these regions as haematite and sulphur respectively (Figure 6.13), yet this is not revealed by multispectral imaging.

Figure 6.13. Raman spectra for GY1 R3 and GY1 R4 showing the presence of haematite and sulphur respectively



These mineral components are 1 – 2mm in size, and are therefore well within the limits of the Foculus camera resolution (100 – 200 $\mu\text{m}/\text{pixel}$). Figure 6.13 shows the F2-12 filter spectra for these two regions. The spectral features are more consistent with those for the sulphate alunite (Figure 6.14). These two spectra exhibit differences in features that suggest perhaps a minor influence of their true mineralogy, such as the flatter profile of ‘GY1 Yellow’ between 600 – 830nm (sulphur has a flat profile between 500 – 1000nm), and the absorption between 440 - 560nm which is a feature typically seen for haematite. However, these features are by no means diagnostic, and highlight potential problems of remotely identifying small mineralogical targets within an otherwise heterogeneous rock sample.

Like GY1, sample GY2 also formed as part of a silica sinter, but it exhibits a different spectral profile to that seen for the white region of GY1. GY2 is a silicified biomat with a dominantly Si composition (as determined by EDS), yet this is not represented within the spectral features, which exhibit a steep gradient between 440-700nm, followed by a plateau between 700-950nm, and an absorption feature between 950 – 1000nm. As with the small sulphur and

haematite mineral deposits in GY1, these spectral features are suggestive of alunite, despite their silica-rich composition. This alunite component most likely exists as a fine particulate coating on the surface of the sinter deposit (discernable from hand specimen), therefore preventing the silica mineralogy from influencing the observed spectrum. Likewise, the biological origin of this deposit appears to have no impact on the observed spectra, even though morphological microfossils can be easily identified as a significant structural component (Figure 6.15).

Figure 6.14. F2-12 spectra for GY1 regions 'Red' and 'Yellow', which have a Raman spectrum of haematite and sulphur respectively. Alunite is also shown for comparison.

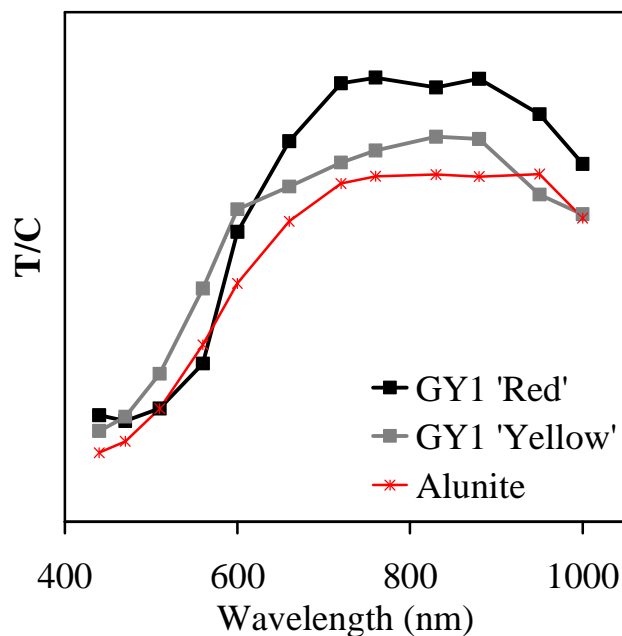
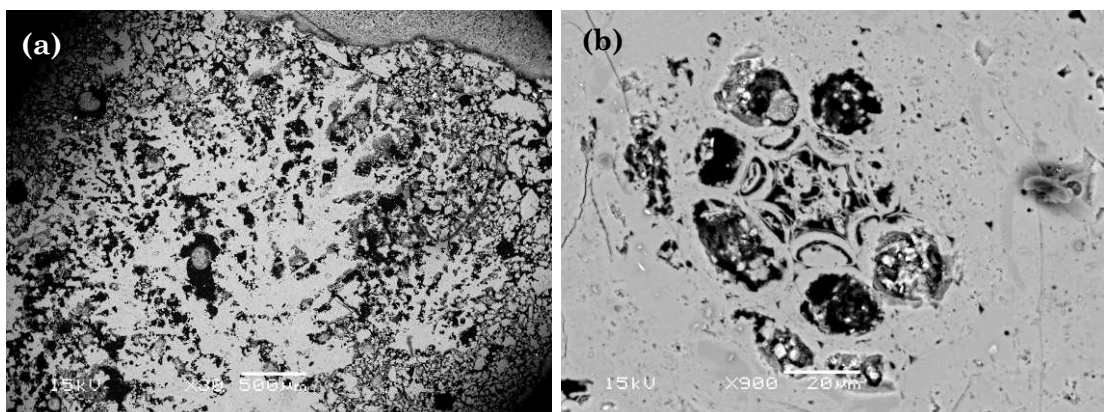


Figure 6.15. BSE image of GY2 silica sinters, showing preserved biological structures within the silica matrix, a) silicification of branching dendritic structures that extend up vertically from the base of the sinter; b) detailed cellular structures.



Opaline silica deposits have the potential to provide information on past life on Mars, but the reflectance spectra of the silica sinter samples from Geysir provided little evidence of their hot-spring origin. As with sample KH, all filter sets included the key spectral morphologies of the GY2 spectrum.

Table 6.4. Ability of the Beagle2 and new filter sets to detect specific spectral features in the Martian analogue rock spectra, displayed in Figure 6.9. Detection is classed as either positive (+) or negative (-).

| Sample and description | Colour Region | Feature (nm) | B2 | F1-12 | F2-12 | F3-12 |
|--------------------------------------|---------------|--|-----------|-----------|-----------|-----------|
| HH Hyaloclastite | Whole sample | 440 – 700 (Ferric absorption edge) | + | + | + | + |
| | | 470 (Fe ³⁺) | + | - | + | - |
| | | 680 (Fe ²⁺) | - | + | - | + |
| | | 950 (Fe ³⁺) | + | - | + | + |
| | | 800 (Peak) | + | + | - | + |
| NAL Acid weathered basalt | Yellow | 440 – 700 (Ferric absorption edge) | + | + | + | + |
| | | 510 (Fe) | + | + | + | + |
| | | 710 (Peak) | - | + | + | - |
| | | 950 (Fe ³⁺) | + | + | + | + |
| | Red | 440 – 700 (Ferric absorption edge) | + | + | + | + |
| | | 750 (Peak) | + | + | + | + |
| | | 850 (Fe ³⁺) | + | + | + | + |
| | | 950 - 1000 (OH ⁻) | + | + | + | + |
| KH Silica encrusted hyaloclastite | White | 670 (Chlorophyll) | + | + | + | + |
| | | 800 (Peak) | + | + | + | + |
| | Lichen | 670 (Chlorophyll) | + | + | + | + |
| | | 900 – 1000 (H ₂ O) | + | + | + | + |
| GY1 Geysirite | White | 950 (OH ⁻) | + | - | + | + |
| GY2 Silicified biomat | Whole | 700 (spectral plateau) | - | + | + | + |
| | | 950 - 1000 (OH ⁻) | + | + | + | + |
| NBO Acid weathered basalt | Orange | 440 – 700 (Ferric absorption edge) | + | + | + | + |
| | | 480 (Fe ³⁺) | + | + | + | + |
| | | 600 (Start of Fe ³⁺ absorption) | + | + | + | + |
| | | 750 (Peak) | + | + | + | + |
| | | 950 (Fe ³⁺) | + | + | + | + |
| | | 900 (Low-Ca pyroxene) | + | + | + | + |
| POSITIVE | | | 22 | 22 | 23 | 23 |
| NEGATIVE | | | 3 | 3 | 2 | 2 |

Finally, spectral parameter plots were used to group Martian analogue spectra into spectral groups based on particular spectral features, such as the steepness of an absorption slope, or the depth of an absorption band (listed in Table 6.5). These plots are often used to define spectral variability within Martian rocks, and therefore potential lithological variability (Farrand *et al.* 2008; 2006). Likewise, such plots can be used to identify the distribution of a particular mineralogical feature across a Martian scene (Rice *et al.* In Press). Therefore, the selection of particular filter wavelengths may affect the ability of PanCam to correctly identify different lithologies/mineral species.

Table 6.5. Spectral parameters used to assess the different filter sets (adapted from Farrand *et al.* 2006). All data are in nm; ‘R’ denotes reflectance.

| Parameter | Filter Set | Representative filter wavelengths | Description |
|------------------|------------|-----------------------------------|--|
| 440 – 700 Slope | B2 | 440 – 670 | $(R_{670} - R_{440})/(670 - 440)$ |
| | F1-12 | 440 – 700 | $(R_{700} - R_{440})/(700 - 440)$ |
| | F2-12 | 440 – 660 | $(R_{660} - R_{440})/(660 - 440)$ |
| | F3-12 | 440 – 700 | $(R_{700} - R_{440})/(670 - 440)$ |
| 920 – 1000 Slope | B2 | 930 – 1000 | $(R_{1000} - R_{930})/(1000 - 930)$ |
| | F1-12 | 940 – 1000 | $(R_{1000} - R_{940})/(1000 - 940)$ |
| | F2-12 | 950 – 1000 | $(R_{1000} - R_{950})/(1000 - 950)$ |
| | F3-12 | 950 – 1000 | $(R_{1000} - R_{950})/(1000 - 950)$ |
| 900 Band Depth | B2 | 900 | $1 - (R_{900}/[(0.429 * R_{860}) + (0.571 * R_{930})])$ |
| | F1-12 | 930 | $1 - (R_{930}/[(0.500 * R_{860}) + (0.500 * R_{1000})])$ |
| | F2-12 | 880 | $1 - (R_{880}/[(0.583 * R_{830}) + (0.417 * R_{950})])$ |
| | F3-12 | 900 | $1 - (R_{900}/[(0.500 * R_{850}) + (0.500 * R_{950})])$ |
| 470 Band Depth | B2 | 480 | $1 - (R_{480}/[(0.556 * R_{440}) + (0.444 * R_{530})])$ |
| | F1-12 | 500 | $1 - (R_{500}/[(0.500 * R_{440}) + (0.500 * R_{560})])$ |
| | F2-12 | 470 | $1 - (R_{470}/[(0.571 * R_{440}) + (0.429 * R_{510})])$ |
| | F3-12 | 500 | $1 - (R_{500}/[(0.455 * R_{440}) + (0.545 * R_{550})])$ |

Figure 6.16 highlights the dependence of spectral parameter values on the filter wavelengths. Two outliers are evident in this plot, one for NAL Red and one for GY2 rock spectra. These are both spectral parameter values produced by the F1-12 filter set, highlighting the influence filter wavelengths have on the observed parameter values, and subsequent interpretation. In this case, the variation lies within the 900nm band depth values, and most likely signifies the lack of a filter at 900nm (filters lie either side at 860nm and 930nm). The remaining filters for each of the rocks tend to cluster within the same region, particularly for NBO Orange. NBO Black has the highest band depth at 900nm, and could be

interpreted as the presence of low-Ca pyroxene in the unaltered basalt lava. NAL Yellow and NBO Orange have the next highest 900nm band depths, coupled with particularly steep 440 – 700nm gradients, both indicators of iron-bearing mineralogies, such as the jarosite known to be in NBO Orange.

Figure 6.16. Spectral parameter plot of 900nm* band depth vs. 440 – 700nm slope for the Martian analogue rock spectra. *Band depth is represented by different filter wavelengths dependant upon the filter set, detailed in Table 6.5.

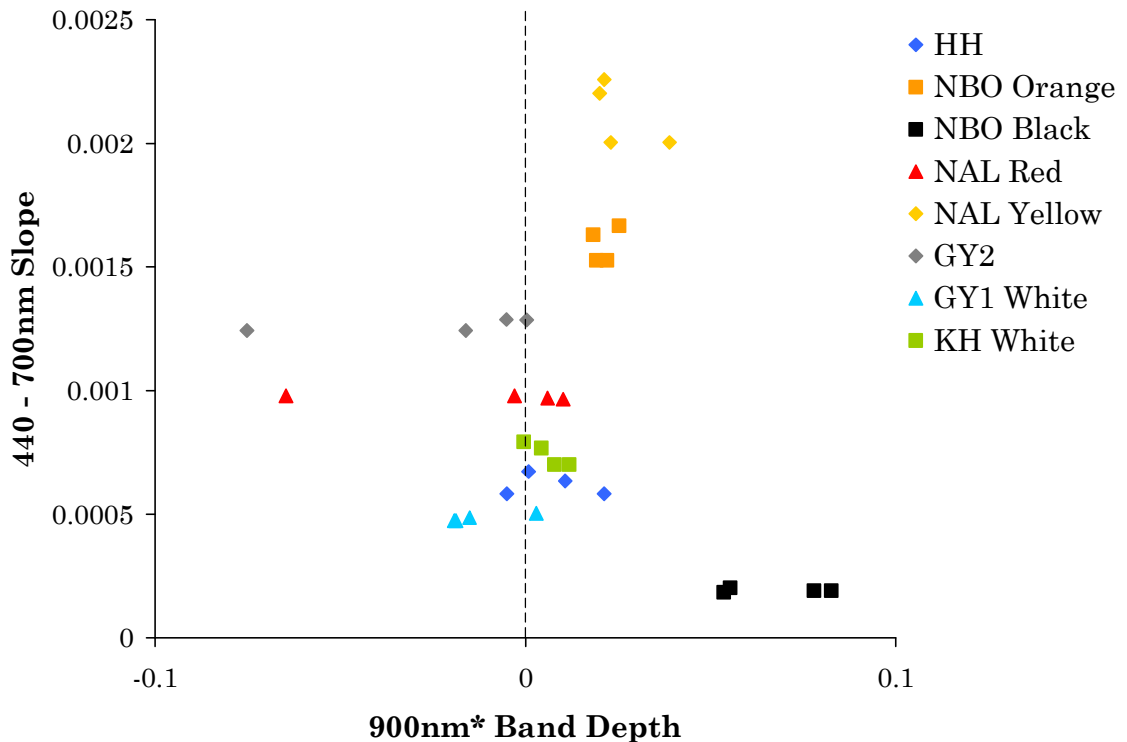
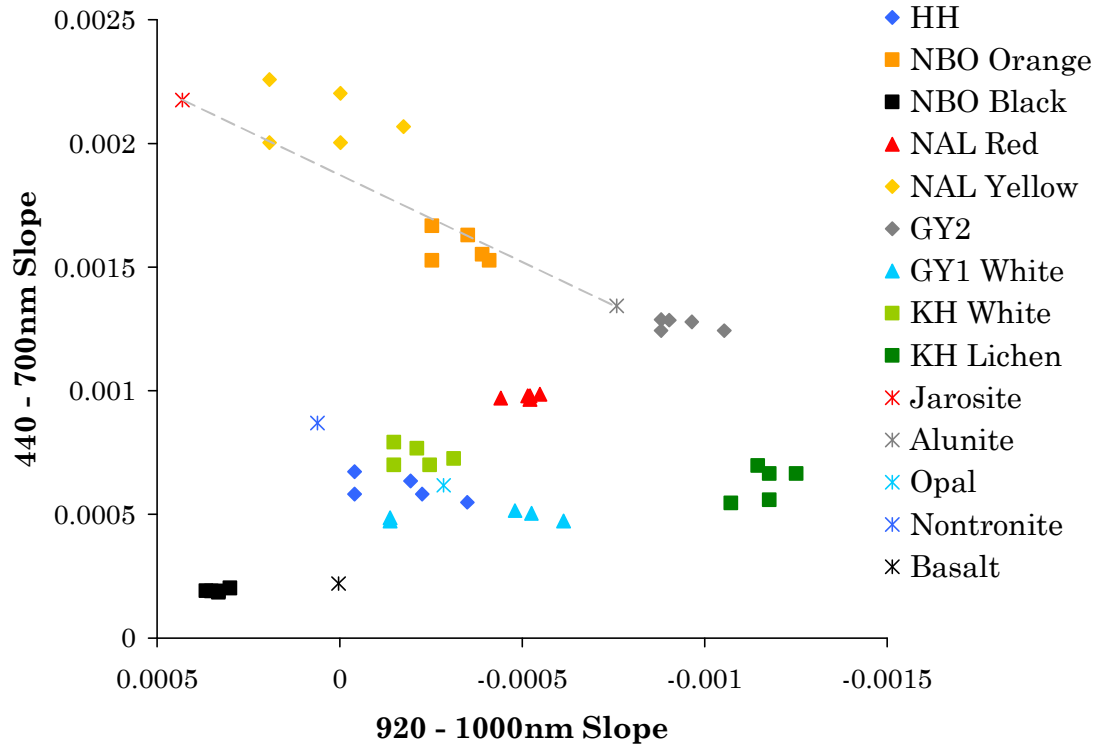


Figure 6.17 plots the slope between 440 – 700nm against that for 920 – 1000nm. The rock spectra are well defined in this plot, which plots iron content (steepness of the 440 – 700nm slope) against water content (920 – 1000nm slope). Representative minerals from the USGS spectral database are also plotted for comparison. A linear mixing line between minerals jarosite and alunite is shown, and it can be seen that samples NAL Yellow, NBO Orange, and GY2 lie either at the end, or along this line. Unsurprisingly, the water-rich KH Lichen has the steepest 920 – 1000nm spectral slope, followed by the GY2 spectra which is dominated by spectral features consistent with alunite, as described previously. There is little difference between the spectra for samples KH White, GY1 White, and HH, which cluster in a similar region to Opaline silica, consistent for KH White and GY1 White, but not HH. The exception to this is the division between

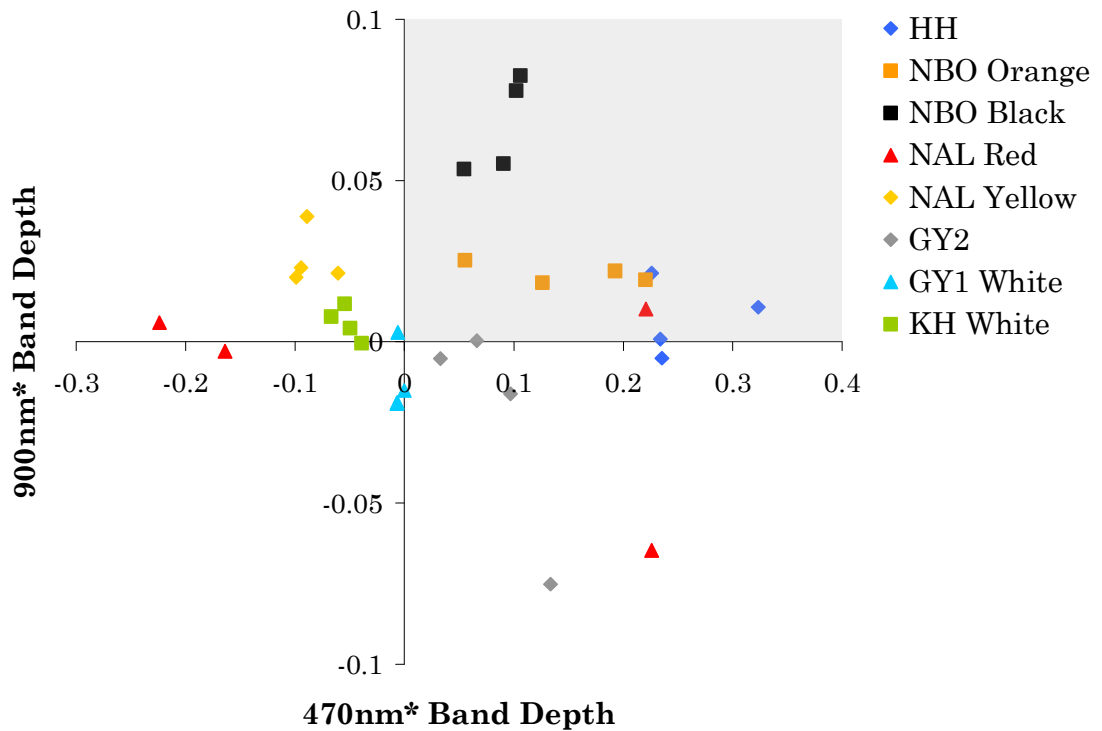
the four filter sets for GY1 White into two distinct groups, with one group (filter sets F2-12 and F3-12) plotting close to the values for both opaline silica and KH White, and the other group (F1-12 and B2) plotting outside this cluster with a significantly steeper 920 – 1000nm absorption.

Figure 6.17. Spectral parameter plot of 920 – 1000nm slope vs. 440 – 700nm slope for the Martian analogue rock spectra. The dashed line represents the path of a linear mix between jarosite and alunite.



In Figure 6.18, both the absorption bands at 470nm and 900nm are indicators of the presence of iron-bearing mineralogies, and those rock spectra that exhibit absorptions at both these wavelengths fall into the grey shaded region of the plot. Unlike the plots in Figures 6.16 and 6.17, sample HH plots in a different region to samples KH White and GY1 White, indicating the different mineralogical composition of this rock.

Figure 6.18. Spectral parameter plot of 470nm* band depth vs. 900nm* band depth for the Martian analogue rock spectra. The shaded area represents spectra that have both a 470nm and 900nm absorption. *Band depth is represented by different filter wavelengths dependant upon the filter set, detailed in Table 6.5.



This study was conducted with two aims: firstly to produce several alternate geological filter sets to replace the current Beagle2/Pathfinder filter wavelengths, and secondly to present initial results from the testing of these putative filter sets on raw, Martian analogue rock samples. It is apparent that a concentration of filters towards the NIR end of the spectrum, as with the B2 filter set, is not beneficial in the detection hydrated minerals by PanCam, either in pure form, or as a component in heterogeneous rock samples. As a result, the new proposed filter sets F1-12 and F2-12 have more filters in the visible (see Table 6.2). The third new filter set also explored - 'F3-12' - has filters spaced at regular intervals every 50nm. The benefit of this filter set is that the even spread of spectral points is not biased towards any particular group of minerals, and so theoretically makes the PanCam equally suited to detecting any given mineral or lithology it comes across. However, whilst much is still unknown as regards to the lithology and mineralogy of the Martian surface, ExoMars will be focused particularly on regions where hydrated minerals are likely to predominate. The aim of positioning these points so that they favour certain mineral groups is to

enhance the detection of these specific minerals in keeping with the mission objectives. The effectiveness of this can be seen in Figure 6.4.

The filter set that was generated statistically (F2-12) based on a set of seven different hydrated minerals, proved one of the most effective filter sets at identifying hydrated minerals in the Martian analogue rocks, and also from the mineral data set from the USGS spectral database. This suggests that this particular method of filter wavelength assignment is successful at selecting a suitable set of geological filters. As such, there is the potential to utilise this method using a much wider set of mineral spectral data before the PanCam filter wavelengths are finalised. It is noted that several USGS spectra often exist for one mineral, some of which exhibit slightly different spectral profiles. For this work just one representative sample spectrum of each of the hydrated minerals was used for the filter selection, and it is important to be aware that the selection of different examples of mineral spectra (e.g. montmorillonite) may have an effect on the filter wavelengths chosen. Additionally, our knowledge of the mineralogical diversity of the Martian surface is increasing, and as such, future PanCam geological filter selection and testing will need to incorporate a much wider range of minerals and analogue samples. Another factor is the mineralogy of the selected ExoMars landing site (still to be finalised). The availability of CRISM and OMEGA data allows the characterisation of the bulk mineralogy of a potential landing site, and as such could be used to heavily influence the PanCam filter wavelengths. For example, if such orbital spectrometer data showed there to be extensive and rover accessible clay-bearing geological units, the PanCam filters may be more useful if they were optimised to detect phyllosilicate minerals only. Such focused target selection would benefit from potentially more diagnostic PanCam spectra, but may significantly reduce the ability of PanCam to undertake perhaps more opportunistic science and any subsequent unexpected discoveries. The generation of a range of filter sets, each biased towards a specific mineral group or spectral feature(s), could be tested in their ability to fulfil their function (e.g. unambiguously detect phyllosilicates), and also how detrimental they may be in the detection of other mineral assemblages.

The need to expand on spectral ground-truthing data sets was recently highlighted by Poulet *et al.* (2009). As with natural outcrops that are likely to be encountered on Mars, these rock samples display large and small scale mineralogical/lithological heterogeneities, only some which were clearly distinguished with PanCam-style 12-point spectra, as in sample NBO where the spectral data was clearly able to distinguish between the ‘Orange’ jarosite component from that of the surrounding unaltered basalt (Figure 6.9). Likewise, the lichens in sample KH were spectrally distinct from the surrounding silica crust. However, detecting heterogeneity was a problem for the silica sinter samples – deposits that would have a particular astrobiological relevance. Opaline silica deposits have the potential to provide information on past life on Mars, but the reflectance spectra of the silica sinter samples from Geysir provided little evidence of their hot-spring origin. If similar silica deposits formed through hot spring sinter development on Mars - a process so commonly seen in volcanically active regions on Earth - there is a possibility for the discovery of morphological, mineralogical and chemical biosignatures within these precipitates (e.g. Preston *et al.* 2008; Schulze-Makuch *et al.* 2007; Goryniuk *et al.* 2004). As a result, identifying spectral features that may hinder the remote detection of such deposits is an important step in identifying astrobiological targets at the Martian surface. This is also true of the small mineralogical variations within sample GY1, the spectra of which did not correspond to the presence of haematite or sulphur as detected by Raman. Haematite has been previously documented to be an effective inorganic barrier to UV radiation (Clark 1998), and has also been shown to be present at the Martian surface by the MER Opportunity (Klingelhofer *et al.* 2004), and as such is one of the many minerals that could be expected to be found around the ExoMars landing site.

6.3 UV Detection of Astrobiological Targets

UV illumination was tested as a potential addition to the ExoMars PanCam, with the aim to assess the feasibility of UV illumination in the detection of astrobiological targets through an epifluorescence response that could be detected with PanCam imaging. Previous field testing has shown UV illumination and imaging to be useful in the detection of life in extreme environments (Weinstein *et al.* 2008). UV illumination of Martian analogue samples is shown here to be useful, and sometimes essential, in detecting both

hydrated mineralogy and extant photosynthetic communities within lavas, the results of which are detailed in the following sections.

6.3.1 Detection of gypsum

UV illumination of a basaltic lava successfully led to the detection the calcium sulphate gypsum ($\text{CaSO}_4 \cdot 2\text{H}_2\text{O}$), occurring as hydrothermal deposits within a subglacially-erupted pillow basalt (sample KV007). Small gypsum deposits were detected by UV induced epifluorescence emanating from vesicles inside the lava. Illumination of the outside lava surface failed to show any presence of surface fluorescence. This activity was bright blue-green-white and confined within the boundaries of individual small depressions in the basalt. Figures 6.19 a+b show the visible fluorescence when excited by the 365nm LED penlight at a working distance of 10 cm. Foculus-captured images at a distance of 2m through the flight-spare Beagle2 green filter were obtained with both Solex illumination (Figure 6.20a) and with 375nm laser illumination (Figure 6.20b) with 150 second total exposure time for the fluorescence image. Fluorescence and Solex images are combined in Figure 6.20c to show the position of the fluorescence within the lava vesicles, which are clearly distinguishable from the surrounding lava matrix. Figure 6.21 shows the detailed morphology of the gypsum precipitations inside the vesicles. Raman spectroscopic analysis (785 nm excitation) shows the deposits are attributed to gypsum (Figure 6.22). VIS-NIR (440 – 1000nm) multispectral imaging of KV007 however produces a reflectance spectrum that bears similarities with that of USGS gypsum reflectance (sample SU2202). The main distinguishing feature is the slightly increased albedo of the gypsum deposits in comparison with the surrounding basaltic lava matrix, but is by no means diagnostic. In contrast, the UV epifluorescence response is significantly clearer.

Figure 6.19. a + b) Digital camera captured image of sample KV007 under natural light (a) and showing the native epifluorescence emitted from gypsum deposits (b) when excited with 375nm laser illumination at a distance of 10 cm; c + d) Foculus captured image of the epifluorescence produced by 365nm illumination as seen through a 530nm filter with 75s exposure (c) and 440nm filter with 100s total exposure (d). Scale bar 1cm.

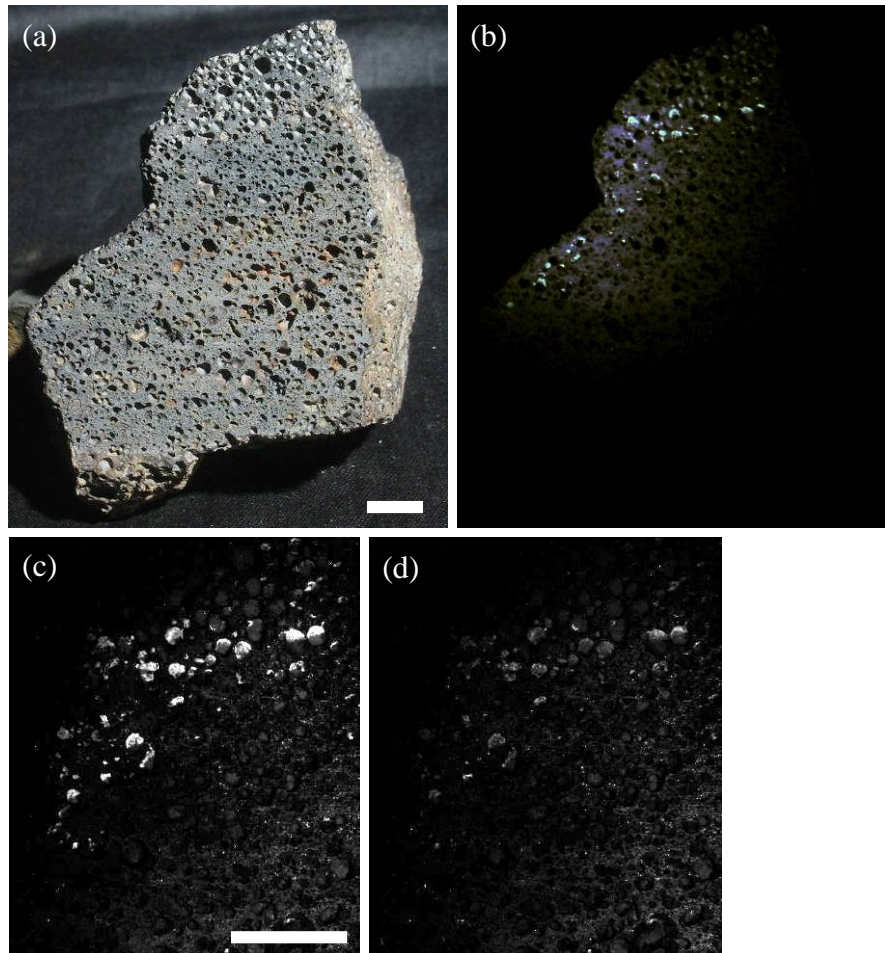


Figure 6.20. Magnified Foculus captured image of KV007 epifluorescence at a distance of 2m through the green filter. a) with Solex illumination; b) with 375nm laser illumination and 150s total exposure; c) images 'a' and 'b' combined to show the position of the fluorescence within the lava vesicles. Scale bar 1cm.



Figure 6.21. KV007 gypsum epifluorescence, (a + b) close up natural light images of the gypsum (G) deposits inside the vesicles of the lava; c) green – blue fluorescence under 365nm illumination of the area highlighted in (a). Scale bar 1mm.

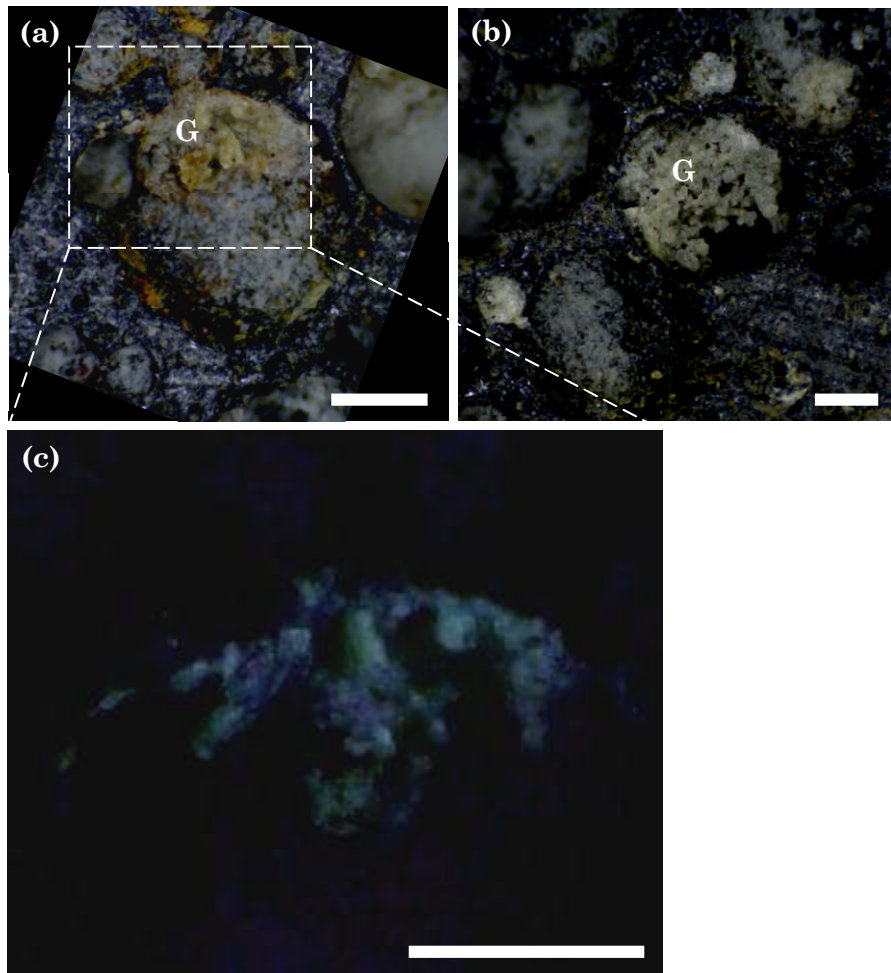
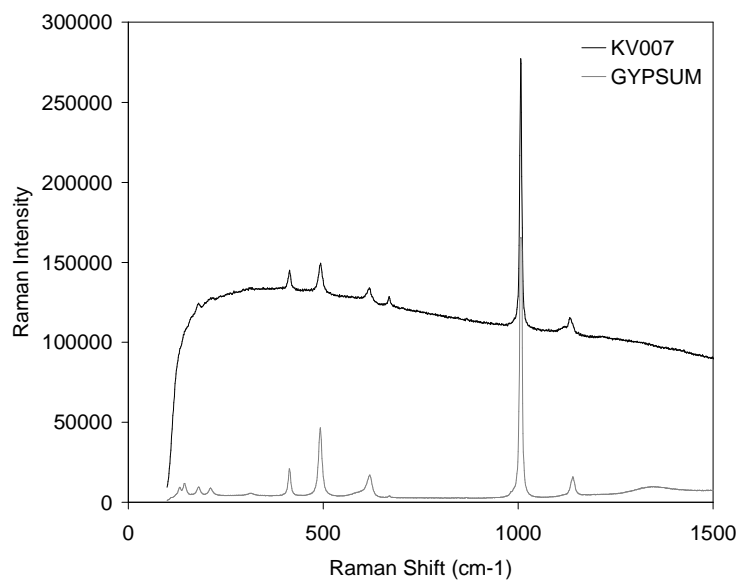


Figure 6.22. Raman spectrum of KV007 vesicle deposits using 785nm laser excitation. All peaks are diagnostic of gypsum.



The individual deposits are small (1-3 mm in size), and restricted to the upper inside surfaces of vesicles in the top 14mm of lava (Figures 6.19 and 6.20). Their presence shows these lavas experienced aqueous alteration, most likely when the lavas were still warm and recently erupted beneath a glacier. Central Iceland, north of Vatnajökull, is characterized by an expansive volcanic desert consisting predominantly of basaltic lava flows and basaltic sands. As a result, the lavas evaluated here have undergone little weathering and biological colonization since their time of eruption during the Pleistocene. Hence, the gypsum deposits in this sample provide evidence of previous hydrothermal alteration that originally deposited this hydrated mineral. Uncovering evidence of past aqueous activity such as this will be one of the primary aims of the ExoMars rover. Discovery of a gypsum deposit similar to this sample would document evidence of liquid water *within* a lava, a finding that opens up the possibility of endolithic subsurface micro-habitats on Mars where life might once have survived.

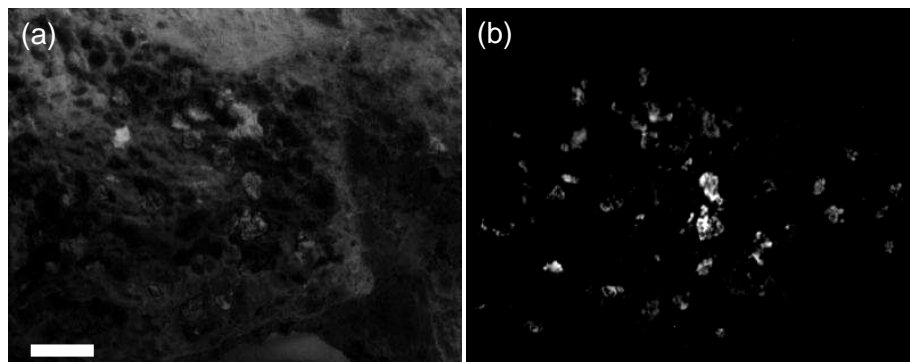
The detection of in-situ gypsum on Mars would be important for both astrobiology (identifying past aqueous environments) and Martian geology (understanding hydrothermal alteration), and the addition of UV illumination facilitates this process. Gypsum not only provides evidence of past aqueous activity, but also acts as an extremophile habitat in itself. Gypsum deposits at the Haughton Impact crater in the Canadian High Arctic, have been found to contain endolithic cyanobacteria communities residing within cleavage planes of gypsum crystals as a way of protecting themselves against desiccation and UV radiation (Parnell *et al.* 2004). Likewise, fungal and cyanobacteria endolithic communities were found inhabiting gypsum crusts on the surface of sandstone boulders on the Antarctic Peninsula, again providing protection against UV radiation, desiccation and low temperatures (Hughes & Lawley 2003). The fact that this survival strategy has been identified in both polar regions on Earth points towards a commonly exploited microhabitat in environments that are cold, desiccating, and subjected to high UV flux. Similar survival strategies could have evolved on Mars in the past. During exploration of the Mars regolith rapid location of such gypsum deposits using UV epifluorescent imaging would enhance mission control sample selection capability and facilitate close analysis of these samples by other ExoMars organic experiments. Due to the relative brightness of the fluorescence emitted by the gypsum compared to the non-

fluorescing host rock, deposits only millimetres in size were detectable from a distance of ~2 meters (Figure 6.20b). The reflectance spectrum of gypsum is dominated by spectral features attributed to water – a key component of the gypsum crystal structure (Hunt *et al.* 1971). However, these features exist predominantly in the NIR, the first beginning just after 1000nm. As a result, as with other hydrated minerals, these water bands are out of the PanCam spectral range. In this respect, the detection of gypsum in the vesicles of subglacial pillow lava (KV007) was initially reliant upon UV illumination to produce the observed fluorescence signal in the visible, before confirmation with Raman spectroscopy. It has been previously suggested that sulphate minerals such as gypsum should be key astrobiological targets on Mars (Rothschild 1990; Parnell *et al.* 2004; Aubrey *et al.* 2005; Aubrey *et al.* 2006; Parnell *et al.* 2007; Schulze-Makuch *et al.* 2007). They have been shown to preserve organic compounds, such as amino acids, for geologically significant periods of time. These amino acids and their degradation products are thought to have been preserved at the time of gypsum deposition as part of the original evaporite. It has been postulated that such organic matter could be preserved within the resulting geobiological assemblage for billions of years in Mars basalts (Aubrey *et al.* 2006).

6.3.2 Detection of photosynthetic communities

Lastly, UV illumination of extant lichen communities produced biological epifluorescence in the visible (Figures 6.23 and 6.24). Basalt sample LL was extensively colonized by multiple lichen communities exhibiting significant differences in visible wavelength coloration (Figure 6.24). Likewise, chasmolithic lichens produced a similarly bright response under UV illumination.

Figure 6.23. KH chasmolithic lichens illuminated with a) solar lamp and b) 365nm fluorescence, both seen through a 560nm filter. Lichen colonies stand out from the surrounding silica much more clearly when their fluorescence is imaged. Scale bar = 1cm.

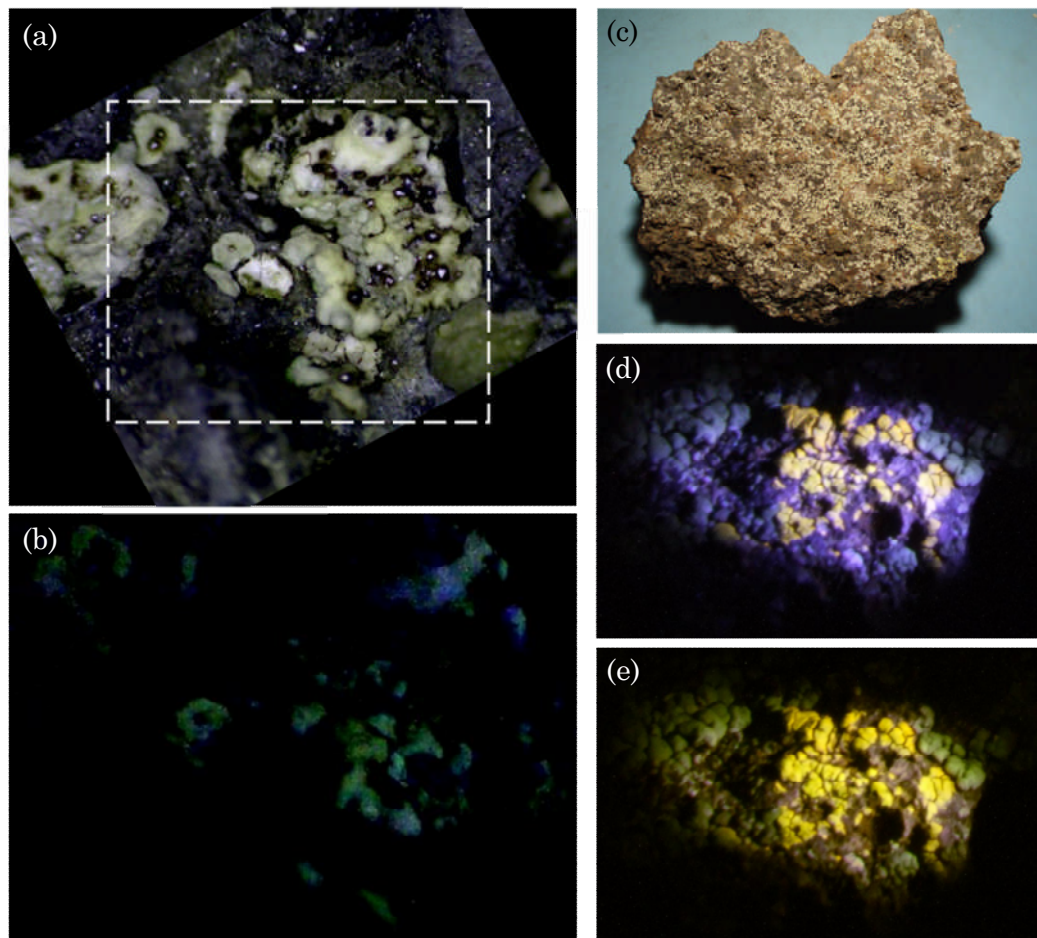


These lichens experience seasonal freeze-thaw cycles and extensive light loss during wintertime snow coverage followed by excessive summertime UV exposure. The samples collected all produced strong, easily detectible yellow – green epifluorescence signals against the non-fluorescing basalt surface when illuminated with 365 nm light (Figure 6.24). Digital extraction of the blue channel data in the original image permits rapid visual discrimination of yellow and yellow-green fluorescence signals of distinct microbial consortia against the non-fluorescing rock surface (Figure 6.24e). Epilithic lichen communities including those inhabiting Arctic and Antarctic polar environments are often comprised of a fungal host and a resident cyanobacteria or algal photosynthetic symbiote (Sun and Friedmann 1999; Friedmann and Sun 2005; Sun and Friedmann 2005). These complex microbial consortia contain a wide variety of photosynthetic and UV-screening pigments that, when excited as individual molecular species, are known to fluoresce following near-UV illumination. However, pigments that provide UV screening for the lichen community produce a significant absorption feature for both the incoming excitation light and any fluorescence response. As a result, lichen communities exhibit wide variation in intensity and coloration of a reflectance or fluorescence signal.

The inclusion of UV illumination in standard multi-spectral imaging provides an additional means of remote spot targeting on nearby rock outcrops, as well as providing a simple survey tool for material obtained by the ExoMars drill. In particular, the combination of such a light source with all the PanCam cameras provide not only multispectral detection, but also high resolution colour imaging of the fluorescence response using the HRC. The rapid, non-destructive, and simple nature of this method makes it an advantageous search tool to be used in conjunction with PanCam multispectral imaging and potentially other instruments on board ExoMars, such as MIMA infra-red mapping of targets, or remote Raman-LIBS (if included in the final payload). Raman-LIBS analysis however, is carried out as a spot analysis on a predetermined region of the rock, meaning any spatial heterogeneities across the rock surface may be missed. As a result, while PanCam multispectral imaging does not provide the same level of precise data acquisition, it plays a crucial role in the selection of these specific target areas. This is demonstrated with the UV detection of gypsum deposits within sample KV007 (Figures 6.19 and 6.20). An additional benefit is that if

UV illumination is to be incorporated into the PanCam instrument, a wider range of filters in the visible will be advantageous to the detection of the fluorescence from organic and inorganic material.

Figure 6.24. a + b) Image of KH chasmothic lichens under normal light (a) and the area in the white box as seen under 365nm illumination (b) NB: blue in the image is not fluorescence but reflectance of the 365nm LED penlight off the sample (image 6cm across). c – e) Image of LL epilithic lichens under normal light (c) and under 365nm illumination (d). Image e) shows image (d) with the blue channel removed to show just the fluorescence signal. Scale bar 1cm. In both cases the lichens exhibited a detectable fluorescence against the non-fluorescing rock substrate they colonise.



6.4 Conclusions and Future Work

The work described in this chapter has shown that there are many considerations that need to be accounted for when optimising instrument hardware for an astrobiologically-focused mission such as ExoMars. Significantly more work is needed however in firstly the testing of potential new geological filters, and secondly the collection of Martian analogue spectral data, for the purposes of ground truthing Martian data in the years to come. Further work

and suggested improvements are detailed here, in relation to the conclusions that can be drawn from this work.

Whilst more extensive testing of the new filter sets is needed on a much wider range of samples, it is apparent from this initial study that filter set F2-12 appears more suitable for the detection of astrobiological targets than the other filter sets explored, particularly B2 and F1-12. This filter set was created by testing a novel filter selection methodology that was based entirely on the spectral properties of relevant minerals, and had no subjective input. This method could be easily expanded to incorporate firstly a wider assemblage of mineral spectra, especially the inclusion of carbonate minerals, and secondly multiple spectral data of the same mineral. This particular filter set was selected for field-testing in Svalbard, the details of which are documented in the next chapter.

Future imaging of Martian analogue rocks should incorporate a wider range of realistic analogue samples. In particular, once the landing site for ExoMars has been selected, the focus should be predominantly on rocks that are the closest analogues to those expected to be encountered on the mission. Imperative to this future testing is the additional collection of contextual data to fully characterise the mineralogical and textural features of each sample in question. For the work described here this utilised Raman spectroscopy, SEM, and EDS analysis, but more extensive work should also include X-ray diffraction and measured reflectance spectra (using a spectrometer). Lastly, this work would also be greatly improved through the detailed characterisation of the sample surface, such as quantifying mineral heterogeneity and surface roughness.

The addition of a UV laser to the PanCam instrument has so far proven to be useful in identifying features of interest that may otherwise be missed by normal PanCam imaging, and likewise further testing this using more samples will again show more conclusively whether or not this is the case.

As well as collecting and interpreting PanCam data from Martian analogue rock samples, the issue of dust cover remains a major problem for the remote identification of rock mineralogy. Previous studies (e.g. Mustard & Hays 1997;

Johnson *et al.* 2002) have attempted to tackle this issue, but mostly with regard to basaltic lava with dust coatings. Therefore, PanCam studies involving a wider variety of rock targets with carefully controlled dust coatings will help the future interpretation of Martian PanCam data. Such studies can be used in conjunction with spectral mixing models to identify the spectral end members within a heterogeneous, dust-covered rock (Parente *et al.* 2009; Poulet *et al.* 2007) . Linear mixing can be used to model spectra, which can then be coupled with actual laboratory data to validate the suitability of such models in the interpretation of PanCam data.

Finally, in contrast to the MER mission, where the rovers were designed to be ‘field geologists’, ExoMars has a highly specific scientific objective, and the question of whether instruments such as PanCam should be finely tuned to meet this objective at the expense of making unexpected discoveries is one that needs to be carefully explored.

CHAPTER 7

TESTING FILTER SET ‘F2-12’ ON MARTIAN ANALOGUE TARGETS IN SVALVARD

After testing new filter wavelengths on samples within controlled laboratory conditions (Chapter 6), one of these filter sets – F2-12 – was tested in the field combined with a simulated PanCam instrument mast and camera in Svalbard during the 2009 AMASE (Arctic Mars Analogue Svalbard Expedition) field campaign. AMASE is a joint NASA – ESA funded annual expedition to Svalbard which aims to provide planetary scientists with an ideal Martian analogue environment for field testing rover instrumentation, and also sample collecting and astrobiologically-focused research. This field deployment allowed for the in-situ testing of the new selected filter set on a range of Martian analogue environments, with the overall aim to establish the suitability of this filter set for the ExoMars mission. This testing was carried out with the following objectives:

Firstly, to deploy the PanCam at a range of field localities that have particular astrobiological significance, and acquire a full data set of multispectral images of geological and biological targets within a natural setting and with mission-realistic protocols. Biological targets included both extant and fossilized life, whilst geological targets ranged from sites with a large lithological and mineralogical diversity, to those that are highly analogous to Martian terrains.

Secondly, following the acquisition of the PanCam field data sets, they are processed and interpreted with the view to assess the ability of PanCam to identify evidence of past or present environment habitability, and also any biosignatures that may be present.

7.1 Instrument Specifications and Operation

For the 2009 expedition, ExoMars instruments selected to attend AMASE were PanCam, MicrOmega (IR spectrometer), RAMAN (Raman spectrometer), and WISDOM (ground penetrating radar). This was the first time the PanCam instrument had multispectral capability during AMASE based testing of PanCam, and this was used to provide colour panoramic shots, as well as multispectral imaging of specific targets for the generation of reflection spectra. Filter set F2-12 was selected for testing during AMASE due to its ability to detect relevant minerals in laboratory samples. The PanCam used during AMASE was designed to be as close as possible to the current specifications for the ExoMars PanCam, consisting of two Wide Angle Cameras (WACs) separated by distance of 50cm between their optical axes. Between these is the High Resolution Camera (HRC). The PanCam mast and its individual components is shown in Figure 7.1 below. The left and right WAC filter wheels together contained 12 narrowband (10nm bandpass) geology filters (centre wavelengths from filter set F2-12) and 6 wideband (100nm bandpass) Red, Green and Blue filters, for multispectral and colour stereo imaging respectively, making a total of 18 filters (Table 7.1).

Figure 7.1. The PanCam instrument used for field testing in Svalbard during AMASE. The whole instrument consists of 2 x wide angle cameras (WAC), 2 filter wheels (FW), and 1 high resolution camera (HRC). The HRC also has RGB external filters (not shown).

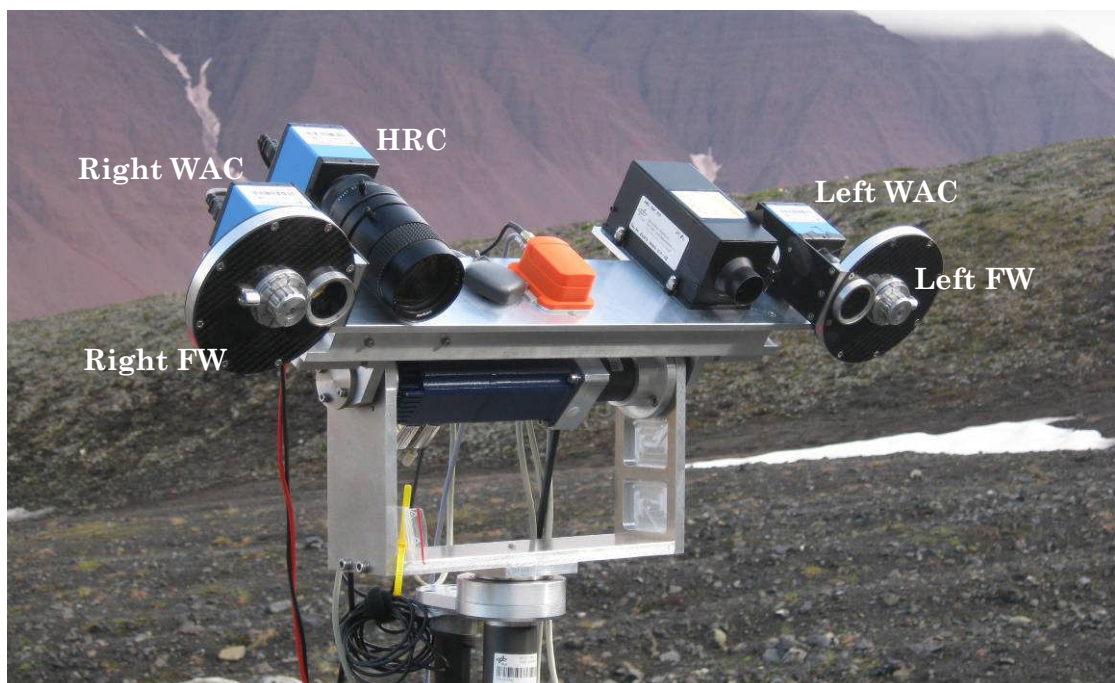


Table 7.1. Filter characteristics for the AMASE camera filters

| Filter Position | Centre Wavelength (nm) | Band pass (nm) | Filter category |
|------------------------|-------------------------------|-----------------------|------------------------|
| Left 1 | 460 | ~ 100 | Colour - Blue |
| Left 2 | 550 | | Colour - Green |
| Left 3 | 660 | | Colour - Red |
| Left 4 | 440 | 10 - 40 | Geology (VIS) |
| Left 5 | 470 | | |
| Left 6 | 510 | | |
| Left 7 | 560 | | |
| Left 8 | 600 | | |
| Left 9 | 660 | | |
| Right 1 | 460 | ~ 100 | Colour - Blue |
| Right 2 | 550 | | Colour - Green |
| Right 3 | 660 | | Colour - Red |
| Right 4 | 720 | 10 - 40 | Geology (NIR) |
| Right 5 | 760 | | |
| Right 6 | 830 | | |
| Right 7 | 880 | | |
| Right 8 | 950 | | |
| Right 9 | 1000 | | |

The filter wheels were manufactured and interfaced with the WACs at Aberyswyth University, whilst the PanCam PanTilt unit and HRC were constructed at the Deutsches Zentrum für Luft- und Raumfahrt (German Aerospace Centre). The WACs used for this field testing are two commercial monochrome cameras, and simulated the ExoMars PanCam WAC specifications. The HRC allows for magnification and increased resolution of selected targets identified in WAC Images. A commercial monochrome camera with the correct payload optical specifications was used. The specifications for the AMASE WACs and HRC are given in Table 7.2.

The principal aim of this work was to test the ability of the new geological filter set (F2-12) for the detection of astrobiological targets in a field Martian analogue terrain, as part of a realistic instrument set up and field deployment in an essentially uncontrolled environment. It is noted that this filter testing was carried out in conjunction with technical testing of the WACs and HRC, details of which are not described here unless relevant. Four field localities in Svalbard were selected by AMASE leaders (Dr. Andrew Steele and Dr. Hans Amundsun) based on their relevance to astrobiological field testing. These sites are described individually for context in the following sections.

Table 7.2. AMASE PanCam WAC and HRC demonstrator specifications.

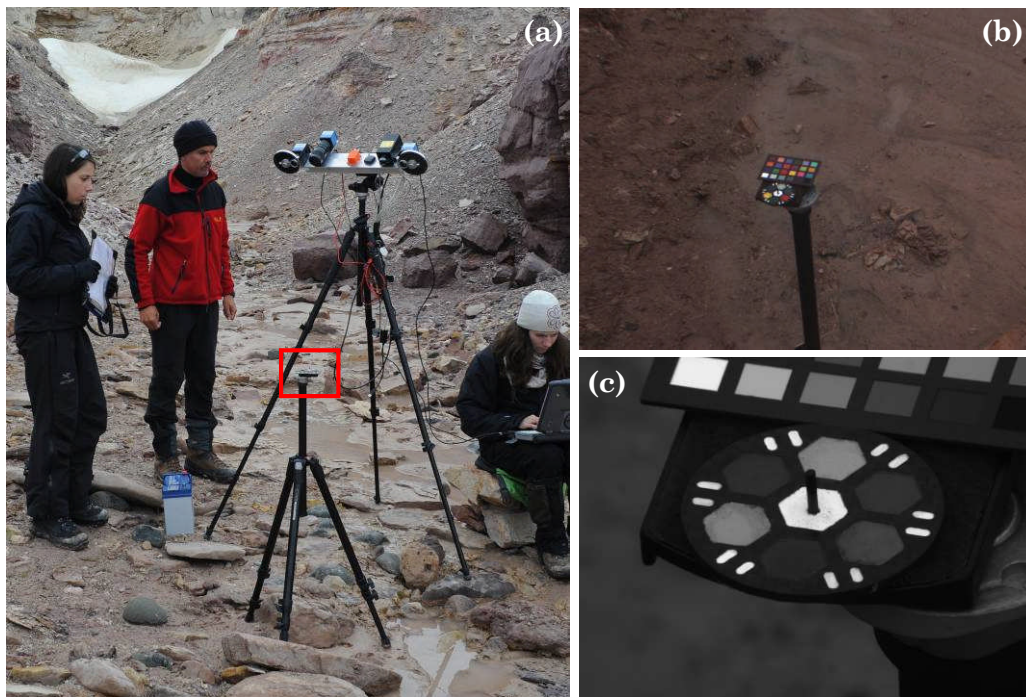
| Parameter | WAC demonstrators |
|-------------------------|---|
| Pixels | 1024 x 768 (horizontal x vertical) |
| Focal Length | 8mm |
| FoV | 34° x 26° |
| Aperture | f/4 |
| Focus | Fixed (optimised for 2.4m), with a range of 1.2m – infinity |
| Filters | 6 RGB (3 per eye) and 12 geological filters (6 per eye) |
| HRC demonstrator | |
| Pixels | 1280 x 960 |
| Focal Length | 70mm |
| FoV | 5° x 4° |
| Focus | Manual, with range 0.9m - infinity |
| Filters | RGB (external to the camera) |

Calibration of multispectral images was achieved using a payload-design PanCam Calibration Target (PCT), courtesy of Dr. Dave Barnes at Aberystwyth University. The calibration target is 5cm in diameter, and consists of red, green, blue, yellow and two greyscale calibration targets for colour imaging, and a central white target for calibrating multispectral data. Central to the whole target is a 10mm high gnomon, although this was not used in any part of the PanCam testing. The PCT was positioned with a tripod so to represent the current placement on the rover top deck (Figure 7.2). Calibration of multispectral images used for the generation of geological spectra was carried out using two methods. The first was done by placing a larger version (~10cm in width) of the PCT in the actual scene being imaged by PanCam, providing direct normalisation of each filter where the white calibration is subject to the same localised illumination conditions and exposure time as the targets within the image. Normalisation here is the same as was done with the laboratory set up (Chapter 6, section 6.2.2). Although not realistic to true rover instrument operation, it produced a reliable method of normalisation whilst saving time, or in some instances, where the ground was too unstable to place the PCT at the required distance and height using the tripod. The second method was realistic to actual PanCam operations, whereby the PCT was imaged prior to imaging of the surrounding scene or outcrop. The downside of this method is that the exposure times and local illumination conditions are slightly different to those experienced by the imaged targets. Whilst nothing can be done about different illumination, the exposure time can be accounted for by calculating the measured brightness per millisecond (ms) for both the PCT and target of interest, i.e.

dividing the brightness values by exposure time (in ms). Image processing and the calculation of PanCam spectra was again carried out with ImageJ (details in Chapter 6, section 6.2.2). Error bars on the following plots within this chapter represent the standard deviation of the mean for all the pixels averaged within the defined region from which the target spectra were calculated.

The following sections describe the science results from PanCam imaging at several different sites visited during AMASE. The four sites include geological and biological material, and range from volcanic to sedimentary deposits, and both extinct and extant life. Typically, one site/target scene would take 1 day to acquire a complete PanCam image set for both the WAC and HRC science objectives.

Figure 7.2. a) Position of the PanCam Calibration Target (PCT) to represent the currently proposed position on the rover top deck ~1.2m from the WACs; b) WAC RGB composite image of the PCT (beneath Macbeth Colour Checker); c) HRC monochrome (green filter) image of the PCT, from the same set up as (b).



7.2 PanCam Analysis of Astrobiological Targets

Science results are described within the context of the field sites individually, as different sites were suitable for different objectives, summarised in Table 7.3. It is noted that the interpretation of PanCam spectra from heterogeneous rock targets is often a challenging task, as there are multiple effects that can impact

on the overall spectral morphology. These include the effect of light interaction between one mineral grain and another, weathering state, roughness of the rock surface, grain size, degree of heterogeneity, shadowing effects, composition, and surface particulates. As such, PanCam spectra can not always be clearly matched with that from a pure mineral spectral library (such as the USGS spectral library and the JPL spectral library). IMP and Pancam data from the Mars Pathfinder and MER missions respectively have led to significant advancement in deciphering PanCam spectra, including direct matching of spectral features (i.e. spectral profile) with mineral library spectra (e.g. Rice *et al.* In Press; Bibring *et al.* 2007; Bishop *et al.* 2004), experimental petrology (Singletary & Grove 2008), and computerised spectral unmixing and clustering to identify spectral end-members (e.g. Parente *et al.* 2009; Farrand *et al.* 2008; 2006). Likewise, the availability of CRISM and OMEGA hyperspectral data has led to similar methods of interpretation, where linear spectral mixing models are used to infer mineral composition and dust contamination (e.g. Poulet *et al.* 2007). Such algorithm-based analysis is beyond the scope of this chapter, therefore the interpretation of PanCam spectra here is limited solely to matching diagnostic spectral features. One of the major issues, as well as those variables mentioned above, is that strong spectral features largely occur well into the infra-red, and outside the range detected by the PanCam, meaning spectral features are often subtle, or heavily dominated by those minerals that do have strong spectral features within the Vis-NIR region. Little to no work has so far been conducted on the interpretation of PanCam data for the ExoMars mission, particularly for geological multispectral data, and as such this work represents the initial study in this area.

Table 7.3. Summary of the four PanCam test sites during AMASE field deployment. For a map of these sites see Chapter 1, Figure 1.9)

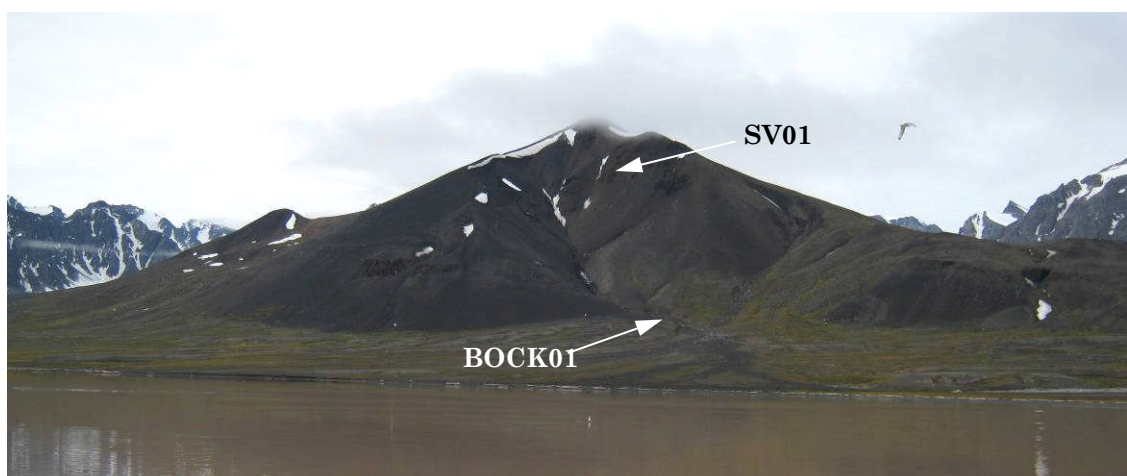
| Site | Description | Science focus | Data set |
|-----------------|---|---|--------------------|
| Sverrefjell | Basaltic volcano with hydrothermal alteration | Detection of lithological diversity and past habitability | WAC/filters HRC |
| Jotun Springs | Carbonate springs with biomats | Detection of extant and extinct biosignatures | WAC/filters |
| Troll Springs | Carbonate springs with large terraces | | WAC/filters |
| Wahlenbergfjord | Iron-rich quartz sandstones | Detection of iron oxide mineralogy | WAC/filters HRC |

7.2.1 Sverrefjell: lithological diversity and past habitability

Sverrefjell volcano is a basaltic subglacially-erupted volcano typified by large pillow lavas overlain by glass and palagonite rich hyaloclastite and volcanic breccia. This volcano is unique in the world for its significant mineralogical similarity to Martian geology, with olivine rich primitive basaltic lava containing later hydrothermal deposits of carbonate and phyllosilicate minerals (see Introduction for more detail). There were two main objectives for PanCam imaging at this locality. The first was to test the PanCam in the identification of this mineralogical and lithological diversity, and the second was to identify evidence suggestive of past environmental habitability.

Two sites at Sverrefjell were utilized for PanCam imaging of volcanic terrains (Figure 7.3) The first (BOCK01) is an outwash deposit consisting of a number of boulders and rocks that have been sourced from the volcano above. In addition to volcanic material, the outwash deposit also contains lithologies from surrounding terrains. Such a site is typical of one that would be suitable for rover exploration, and provides easy access to otherwise unreachable outcrops further up the volcano. The second site (SV01) is focused on an outcrop located a few hundred meters up the volcano, and provides in-situ outcrop imaging to complement that carried out at the outwash plain below.

Figure 7.3. Sverrefjell Volcano in Bockfjord. The outwash plain (BOCK01) and the in-situ outcrop (SV01) are indicated.



At BOCK01, imaging was undertaken on an outwash deposit which consisted of a number of loose boulders and rocks of diverse lithology. Such a site is typical of

that suitable for rover exploration (i.e. low angle slopes, multiple approach routes to target boulders), and provides easy access to representative lithologies of otherwise unreachable outcrops further up the volcano. Rocks consist of basaltic lava sourced from the volcano, basement metamorphic rocks through which the volcano erupted, and glacial till deposits consisting of exotic rocks from further away. These rocks are randomly distributed. Notable is the large compositional diversity between the rocks, which range from ultramafic (mantle xenoliths) to felsic silica rich rocks (gneiss), with a variety of secondary alteration minerals present from both hydrothermal deposition and mineral weathering. A reconnaissance survey of the outwash deposit led to the identification of the following targets of interest (identified in Figure 7.4 below):

Basaltic lava (X): a very fine-grained, vesicular lava containing large (4 – 10cm diameter) bright green olivine-rich mantle derived xenoliths, often of lherzolitic composition (Skjelkvåle *et al.* 1989).

Weathered xenolith (S): mantle xenolith, such as those from the Basaltic lava described above, that has been since weathered out of the lava and undergone mild serpentinisation, turning the once green xenolith into a pale green-white rock.

Magnesite (M): bright white – pale yellow carbonate deposit. Specifically, the carbonate is magnesite from hydrothermal alteration of the ultramafic rocks (Treiman *et al.* 2002).

Altered basalt lava (FeB): small, angular lava fragment with a hard, dark red surface coating indicative of oxidized iron-rich mineralogy.

Weathered basalt (SiB): small, angular highly vesicular lava fragment with a hard pale grey – white surface coating. Likely to be a silica crust where the mafic minerals have been stripped away by weathering, as opposed to hydrothermal deposition as the vesicles remain empty throughout the lava and through the crust.

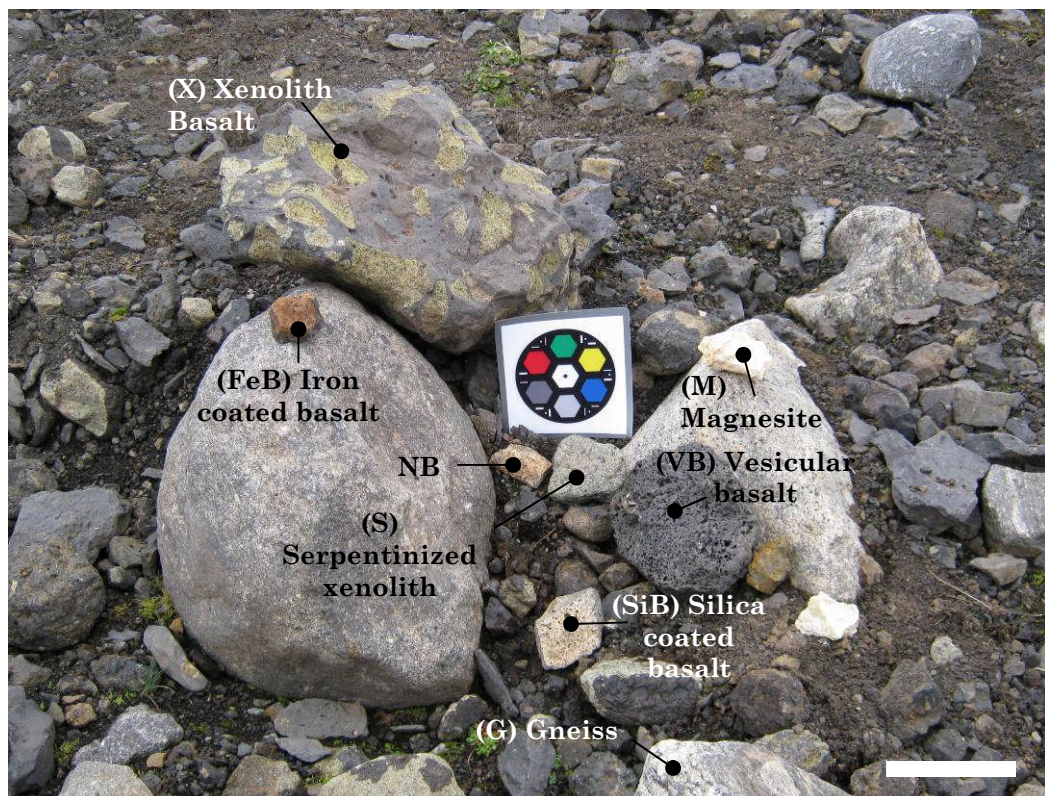
Vesicular basalt (VB): Highly vesicular lava free of any visible mantle xenoliths. The vesicles themselves are round, ~5mm in diameter, and exist as a clear ‘swirling’ flow-banding texture.

Gneiss (G): Quartz and plagioclase feldspar rich gneiss with clear compositional segregation from darker hornblende and mica rich regions. Sourced from the basement rocks through which Sverrefjell volcano itself erupted. Similar

gneissose and granulitic rocks occur as xenoliths within the Sverrefjell lava flows, sometimes alongside mantle xenoliths such as those described in the basaltic lava target ‘X’ above.

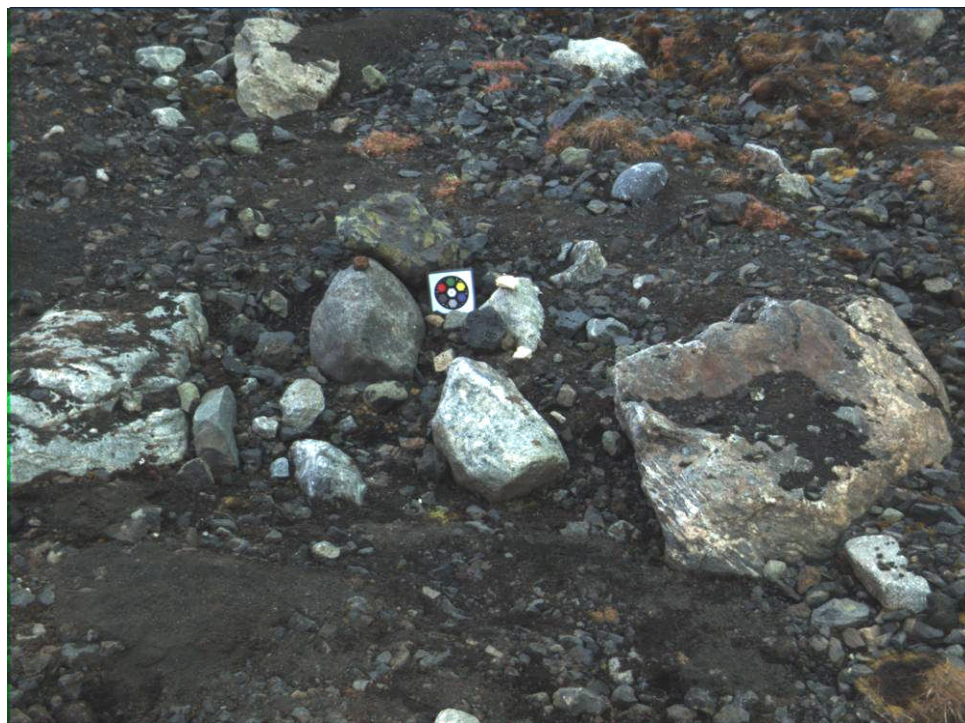
For initial testing of PanCam’s multispectral capabilities with the new filter set F2-12, these rocks were arranged into a representative scene within the WACs field of view (single frame). As a positive control, sample ‘NBO’ was also incorporated into the scene. This rock is a basaltic lava with jarosite deposits within the vesicles and on the surface (for more details see Chapter 6, section 6.2.1), and was used for this first test site to identify any anomalous filter or camera behavior. The PanCam was positioned at a distance of 4.70m from the center of the target scene, and images were taken using the stereo RGB filters and geology multispectral filters (18 images in total). For the generation of PanCam spectra, the calibration target placed within the rock scene was used. A WAC colour composite image using the RGB colour filters is shown in Figure 7.5.

Figure 7.4. Digital photograph of rock targets, and positive control sample ‘NBO’. Shortened identification labels for the targets are shown in brackets. Scale bar = 10cm.



Colour data from the RGB composite (Figure 7.5) allows the clear distinction of broadly different rock types within the scene, and it is evident a contrast in rock composition exists between the dark and light rocks. Particularly notable is the unusual green colouration of the clasts present within the xenolith basalt, which are absent from the other rocks. Mineralogical distinction between the lighter colour rocks is not possible at this stage, although clear compositional segregation characteristic of gneiss can be seen, suggesting this rock is rich in quartz and feldspar. One particularly noticeable anomaly can be seen with the red colour grass. Whilst the majority of chlorophyll reflectance in the visible is between 500 – 600nm, between 700 – 750nm the reflectance increases 5 fold (the vegetation ‘red edge’), and this is partially detected by the Red colour filter which, due to it’s bandpass and centre wavelength, has a coverage of 610 – 710nm. Such high reflectance, even if partially detected, appears to mask the true visible green reflectance, leading to incorrect colour representation.

Figure 7.5. Left WAC RGB colour composite image of the BOCK01 rock targets at a distance of 4.70m from the WAC optical axis.

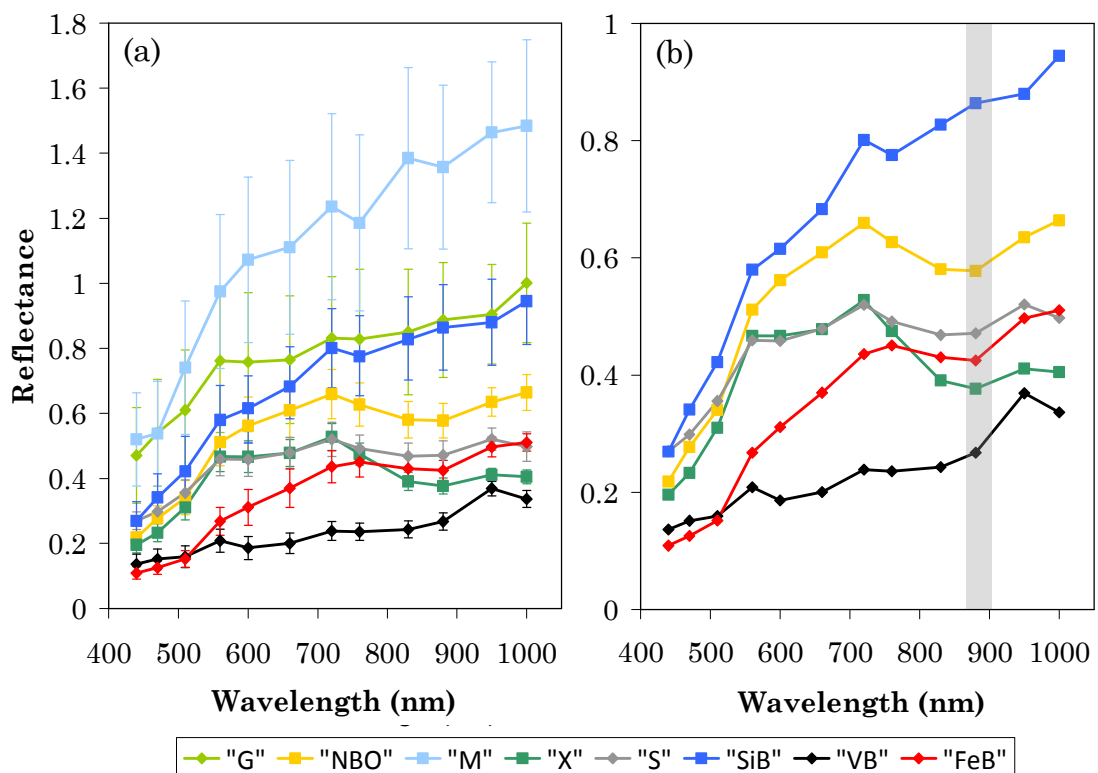


The addition of multispectral imaging using the F2-12 geology filters provides clarity between the more similar coloured rocks, and also provides initial compositional and mineralogical identification for particular targets. PanCam reflectance spectra were obtained for the above rocks from the 12 multispectral

images. Figure 7.6a below shows the PanCam spectra of these targets. Spectral variability can be related to lithological diversity (Farrand *et al.* 2006), and it is apparent from the overall morphology of the different target spectra that this terrain hosts a number of different rock types. When only the basaltic rock spectra are shown (Figure 7.6b), the 880nm absorption band is present in all spectra except one – target SiB. This particular target, although basaltic lava, has a silica-rich crust, which lacks the Fe³⁺ absorption at 880nm.

The positive control sample “NBO” spectrum correctly shows the spectral features of jarosite, exhibiting a step ferric absorption edge between 440 – 720nm, a large absorption at 880nm, and a peak at 720nm. No anomalous features are present. Similar to the “NBO” spectrum is the “FeB” spectrum – a weathered basaltic lava that has a red-orange crust visible on the surface. The dark red colour in the RGB composite suggests this crust is most likely rich in iron oxide, and the subsequent multispectral data reveals this to have the spectral features of haematite, with absorptions at 510 and 880nm, and reflectance peaks at 720 and 950 – 100nm.

Figure 7.6. a) PanCam spectra of all the target and control rocks from the scene at 4.70 m, error bars represent standard deviation; b) PanCam spectra of just the basaltic rocks, with error bars removed for clarity. The 880nm absorption band is shown in grey.



The ‘S’ (serpentinite) and ‘X’ (xenolith) have almost identical spectra until after 760nm, where the dunite has a much increased absorption compared to the serpentinite. The shallower absorption at 880nm in the serpentinite suggests a loss of iron. In addition, the serpentinite has a possible absorption at 1000nm which is potentially the beginning of a hydration feature further into the infrared, although this feature is not seen in a pure serpentine USGS mineral spectrum. Figure 7.7. shows the PanCam spectra of ‘S’ and ‘X’ together with the spectra (sub-sampled to F2-12 filter wavelengths) for the minerals diopside, augite, olivine, serpentine (USGS spectral library), and the rock pyroxenite (JPL spectral library). These minerals are all commonly found in mantle xenoliths such as these, yet at first glance there appears to be little similarity between these mineral spectra and that of the ‘S’ and ‘X’ targets. The rock targets exhibit well defined spectral features including the inflection at 560nm, peak at 720nm, and absorption at 880nm, which are highlighted by grey bands in the plot. The USGS and JPL spectra that share these particular characteristics are pyroxenite and augite, but their spectra do not match consistently between 440 – 1000nm.

Figure 7.7. PanCam spectra of BOCK01 targets ‘X’ and ‘S’, plus library spectra re-sampled to PanCam filter wavelengths of minerals and rocks analogous to the targets.

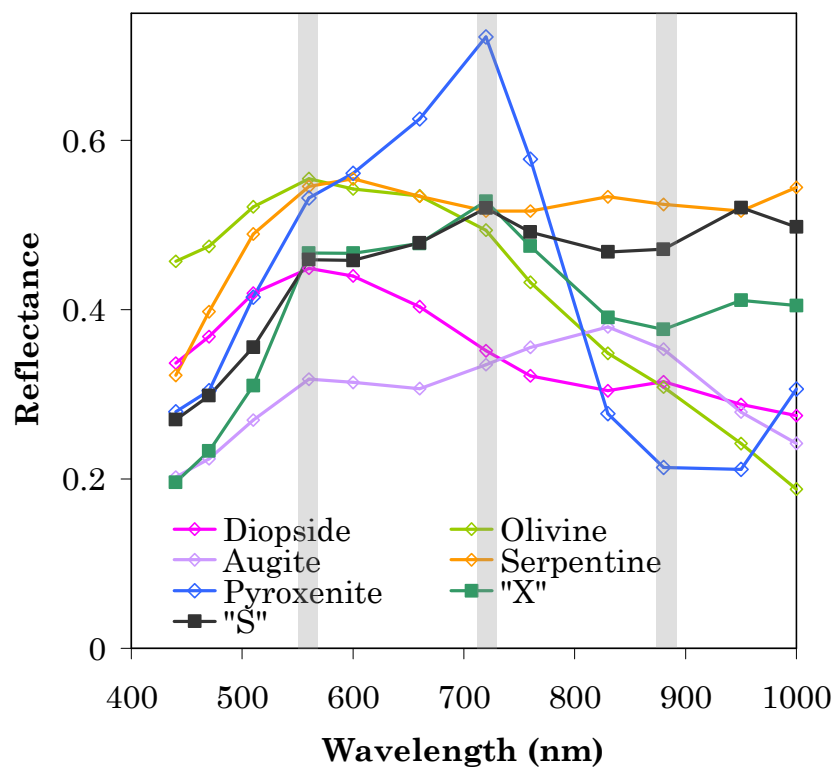
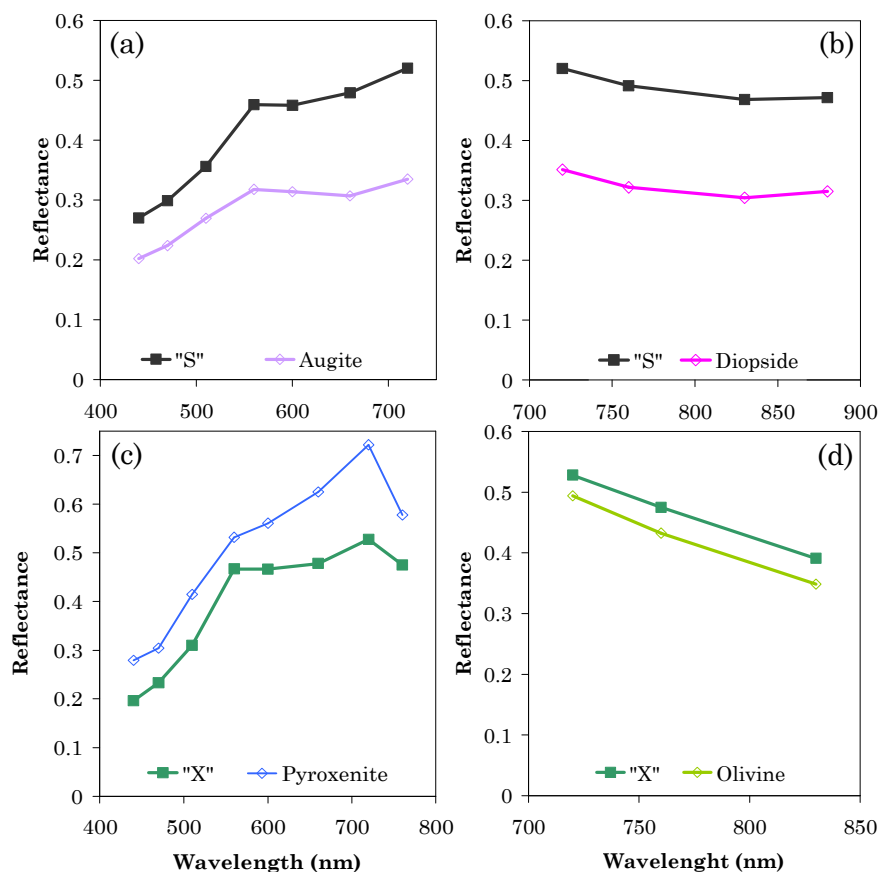


Figure 7.8 shows the spectra of ‘S’ and ‘X’ that, in particular wavelengths, have spectral profiles that are highly similar to those minerals mentioned above. Target ‘S’ especially is clearly characteristic of the pyroxene augite between the region of 440 – 720nm (Figure 7.8a), yet between 720 – 880nm the spectrum is consistent with diopside (Figure 7.8b). Linear mixing between these two minerals does not however produce any satisfactory spectral model that matches target ‘S’. The situation is similar for target ‘X’ (Figure 7.8c), where the spectrum between 440 – 760nm is comparable to that measured for the rock pyroxenite (JPL spectral library), but the same as for olivine (USGS spectral library) between 720 – 830nm (although it is noted this particular match is only between 3 wavelengths). Hand specimen analysis of these particular xenoliths show them to comprise ~75% olivine, ~15% augite and ~10% diopside, and so the bias of the PanCam spectrum towards pyroxene minerals could be due to their stronger spectral features (particularly augite) dominating the overall spectrum, masking the olivine signal.

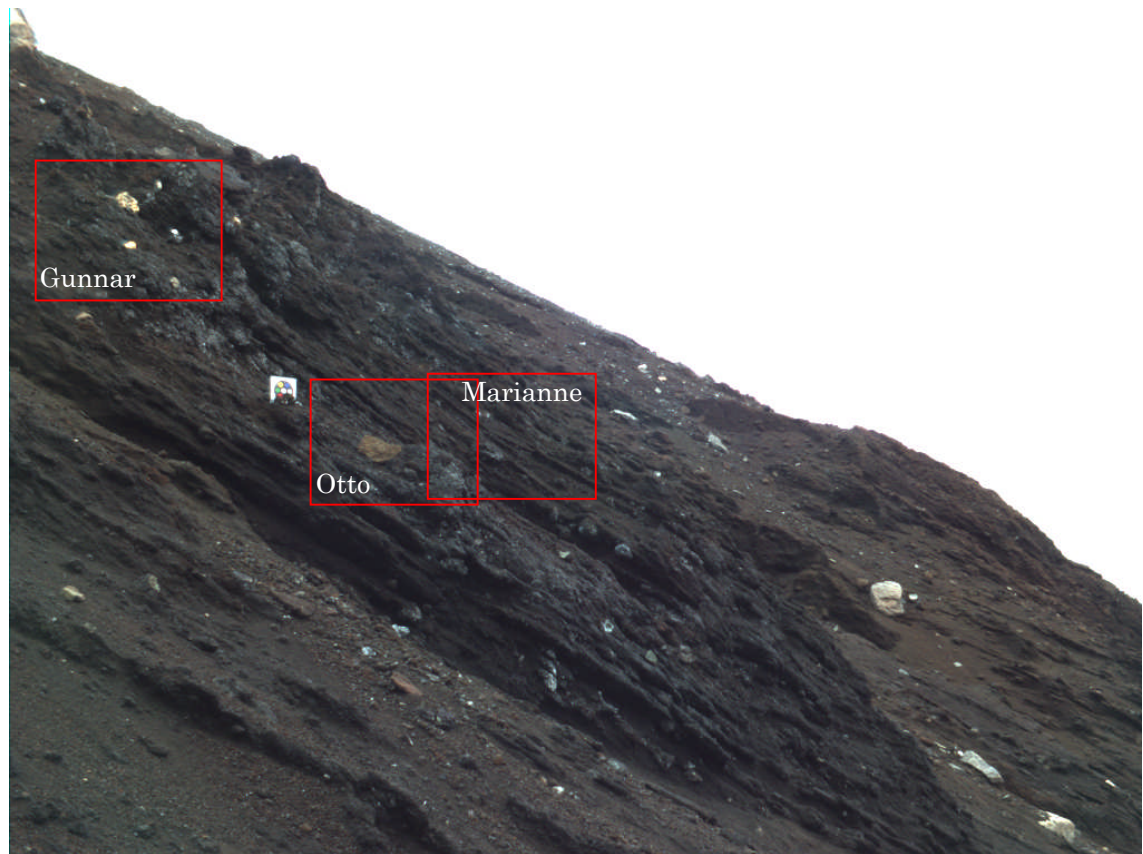
Figure 7.8. Partial PanCam spectra of BOCK01 targets ‘S’ and ‘X’ that match mineral library spectra (re-sampled to PanCam filter wavelengths): a) 440 – 720nm match between ‘S’ and Augite; b) 720 – 880nm match between ‘S’ and Diopside; c) 440 – 760nm match between ‘X’ and Pyroxenite; d) 720 – 830nm match between ‘X’ and Olivine.



The ‘SiB’ basalt has a silica rich crust where the mafic minerals have been stripped away by weathering processes. The spectrum of this crust is consistent with silica, and shares spectral similarities to the quartz rich gneiss, particularly in the infra-red (720 – 1000nm). In the visible the ‘SiB’ spectrum has a higher absorbance than target ‘G’, which is consistent with that observed for USGS spectral of minerals opal and quartz, suggesting the silica rich crust on target SiB is to some degree structurally amorphous, compared to the entirely crystalline silica in the quartz-rich gneiss (G). This thin (1 – 2mm) crust on SiB also masks any spectral signature of the basaltic lava underneath, highlighting the limitation of PanCam multispectral data to the very surface of the target. Similar to the SiB target spectra is that for the carbonate target ‘M’, which differs spectrally only in that it has a steeper slope between 440 – 600nm than SiB, a difference which is consistent for magnesite and opal respectively. Finally, the spectrum of rock target “VB” (vesicular basalt) shares spectral features in the visible with Ca-rich pyroxene augite, such as the reflectance peak captured by the 560nm filter.

At the second site SV01 (Figure 7.3), PanCam imaging focused on an in situ outcrop of a basaltic volcanoclastic breccia. This outcrop site is complementary to the PanCam work carried out at site BOCK01, an outwash plain at the base of the volcano, which consists of loose rocks brought down from the outcrops situated at higher elevations at the volcano, such as this one. The outcrop itself contains a few xenoliths like the ones at BOCK01, but these are typically more weathered. In addition, loose rocks were present on the outcrop, which is also surrounded by scree, and it is presumed these loose rocks are sourced from further up the volcano. The WAC RGB colour composite (Figure 7.9) reveals a consistently dark, predominantly mafic composition outcrop, with isolated loose boulders of white – grey rocks and the occasional light brown rock. Particularly clear is the unidirectional fabric dipping at nearly 45°, which is potentially consistent with deposition of volcanoclastic sediments either in liquid water, a process common to subglacial basaltic volcanism, or alternatively as pyroclastic flows. The similarity between the angle of dip and the slope of the volcano suggests the outcrop was deposited in-situ and hasn’t been subjected to any later disturbance except localised weathering. Additionally the profile shape of the outcrop follows the trend of both the internal fabric and slope of the volcano.

Figure 7.9. WAC RGB colour composite of the outcrop at Sverrefjell volcano, at a distance of 3 – 5 m. HRC target[†] footprints are also shown.

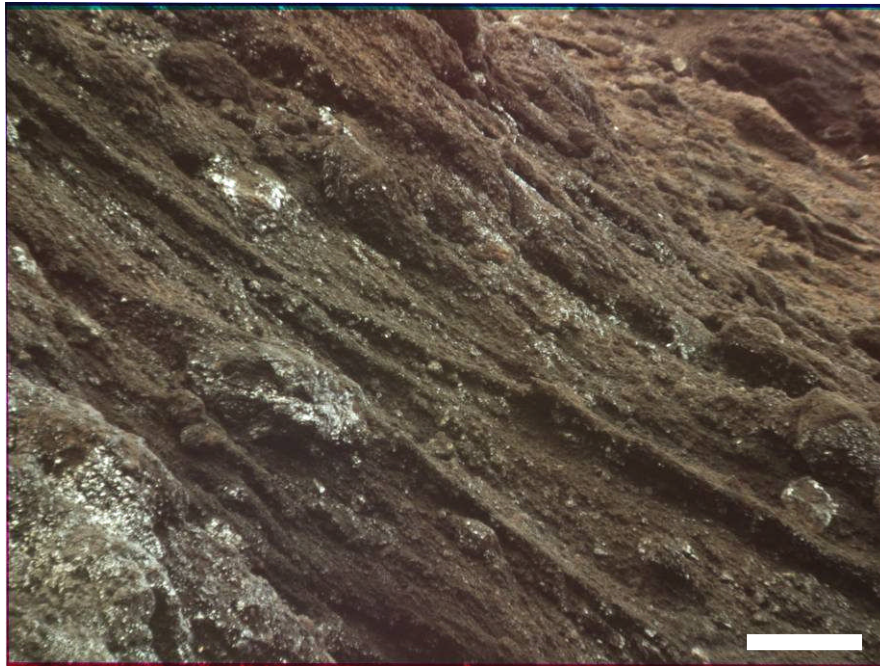


[†]Targets in outcrop SV01 were named in the field after crew members on board R/V Lance

The WAC images themselves are not able to resolve any small scale lithological structure or mineralogical variation that might be present within the loose boulders/larger clasts that exist in an around the outcrop. Some of these rocks are clearly compositionally different to the main volcanoclastic outcrop due to their significantly higher albedo and light colour. The initial WAC colour data suggest either silica, carbonate, or perhaps even sulphate rich lithologies. High resolution imaging of targets within the WAC field of view enables a significantly higher level of scientific interpretation than that possible from just the WAC data alone. With regards to assessing the habitability, the HRC colour data allows for the preliminary identification of fine-scale mineralogy and lithology, and as such an initial interpretation of the deposition environment. Figure 7.10 is an HRC image of target Marianne[†], and both confirms and resolves the sedimentary fabric seen in the WAC RGB image. These layered structures within this volcanoclastic deposit are likely depositional structures, and potentially (but by no means conclusive) evidence of deposition within a body liquid water. Figure 7.11 shows HRC images of the targets Gunnar[†] and Otto[†],

with magnified images of the target rocks themselves inset. It is apparent from these images that both target rocks are also volcanoclastic like the main outcrop, and display dark, basaltic clasts surrounded by a mineral matrix. Both rocks lack any discernable internal structure, such as layering or sorting, and as such can be classified as massive, unsorted sedimentary rocks.

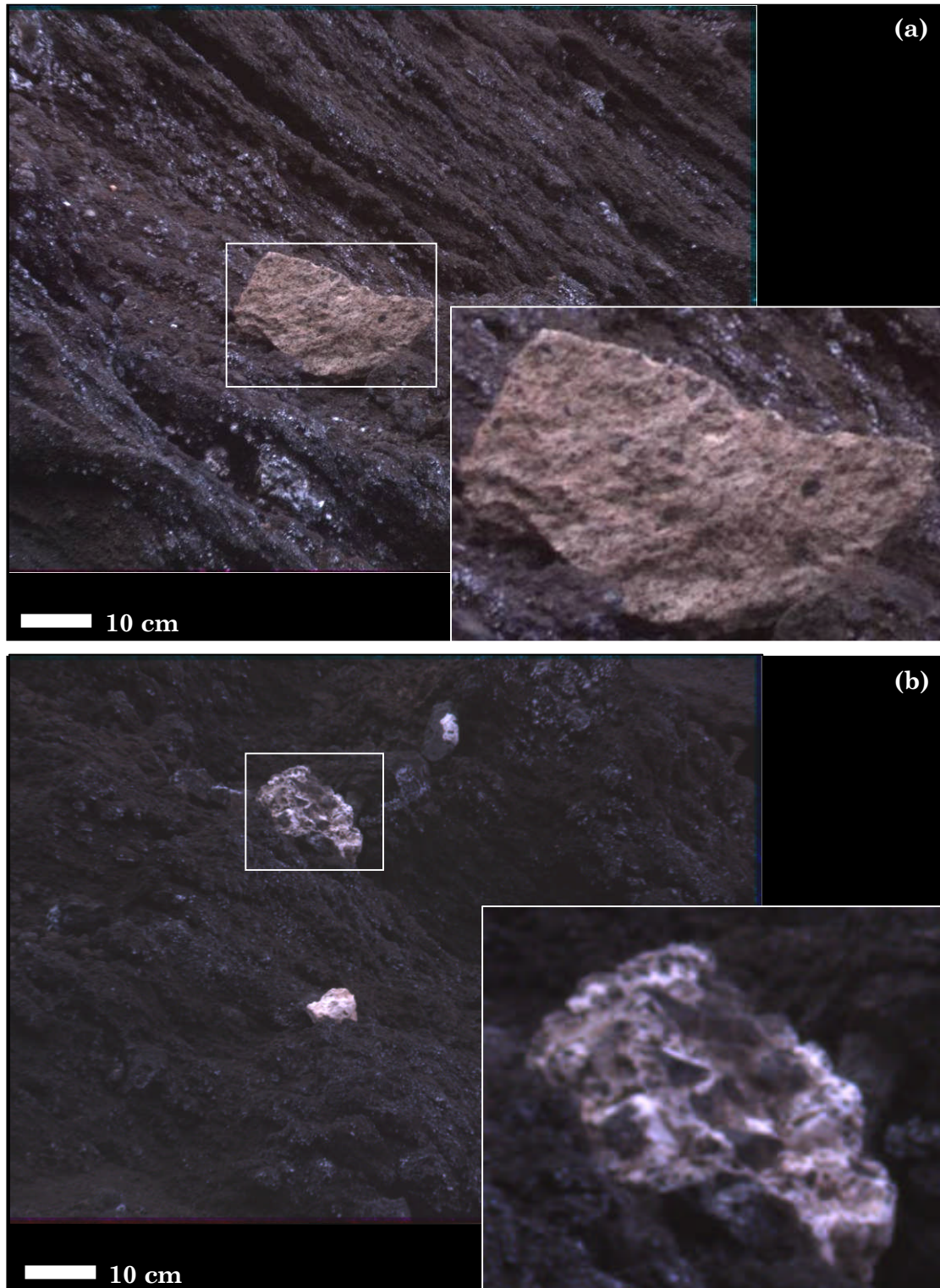
Figure 7.10. ‘Marianne’ HRC image of layering structures within the outcrop. NB – image has been brightened to clearly display structure. Scale bar = 10cm.



As shown in Figure 7.11a, these basaltic clasts are small, ranging in size from 1-10mm, and are surrounded by a pale orange-brown fine-grained matrix. Such lithological features are consistent with a phyllosilicate-rich volcanic breccia, such as hyaloclastite, where basaltic glass has altered to palagonite through the interaction with low temperature hydrothermal fluids. Palagonite is commonly rich in smectite clays such as nontronite and montmorillonite. It is also noted that the massive nature of this clastic rock is not consistent with the surrounding outcrop, which show a clear depositional fabric in the HRC image, suggesting this rock is either a large xenolith entrained during deposition, or a loose rock sourced from a different part of the volcano. Figure 7.11b differs from the example in Figure 7.11a in that the clasts are significantly larger, suggesting the clasts are crystalline basalt, as opposed to basaltic glass. The white mineral deposits, which appear to be cementing the basaltic clasts together, could be

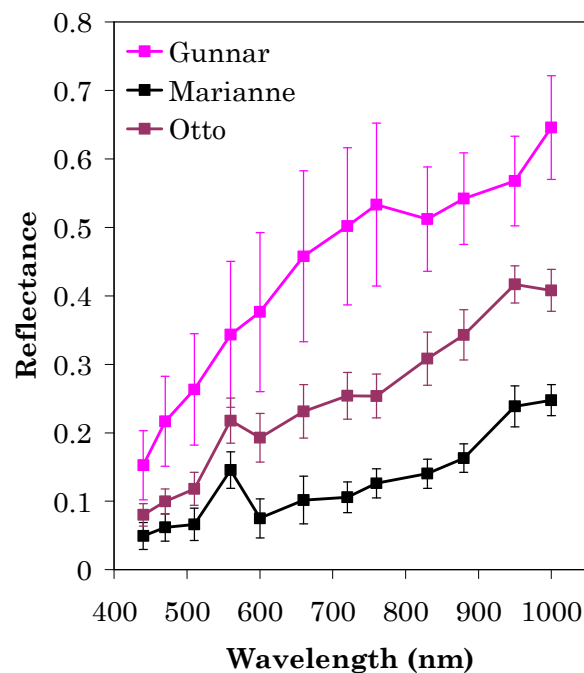
either carbonate or silica rich (or both), and again likely to be the result of hydrothermal alteration.

Figure 7.11. HRC target images showing two different lithologies. a) ‘Otto’ - small dark clasts supported by a finer pale orange-brown matrix; b) ‘Gunnar’ - large angular dark clasts cemented by a pale mineral matrix. Scale bar is for the main HRC image.



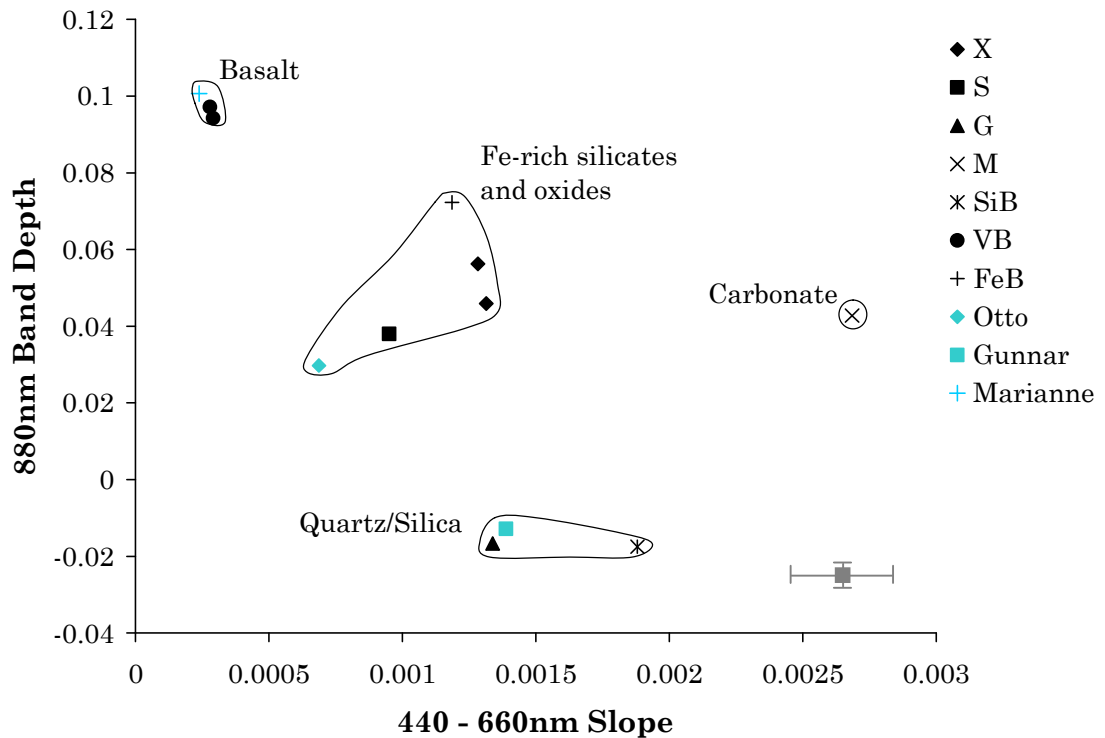
Multispectral analysis of these targets supports many of the inferences made using the WAC and HRC images. Figure 7.12 shows PanCam spectra of targets Gunnar, Otto, and Marianne. It is evident that Marianne has a spectrum highly similar to that of target ‘VB’ at site BOCK01 (vesicular basaltic lava), and this is in agreement with the WAC and HRC colour images which both show this target to be almost black in colour and therefore likely to be basaltic in composition. There is a significant reflectance peak at 560nm which is also seen in the ‘VB’ basaltic spectrum (Figure 7.6b). Otto has a spectrum similar in profile to Marianne, but it has an overall higher albedo and has a 440 – 660nm ferric absorption edge nearly 3 times steeper than Marianne, suggesting a higher iron content. This is consistent with the dark orange colour of this target, clearly seen in the HRC image (Figure 7.10a). Lastly, Gunnar was identified in the HRC images as a volcanic breccia cemented by either carbonate or silica. Multispectral analysis of Gunnar is consistent with this observation, although due to a lack of spectral features it is difficult to say which out of the two is more likely. Opaline silica does exhibit an absorption in the NIR followed by the beginning of a reflectance at 950 – 1000nm, both features which are seen in the Gunnar spectrum, suggesting that at the very least opaline silica may be present within this rock. However this by no means rules out the possibility of carbonate being present as well.

Figure 7.12. PanCam spectra of SV01 targets (shown in Figure 7.9).



Multispectral data acquisition at Sverrefjell volcano using the F2-12 filter set has correctly identified the wide range of lithological diversity at BOCK01 and SV01. Spectral parameters can be used to define spectrally-distinct groups, which can be used to infer broad lithological diversity (Farrand *et al.* 2006). As filters within the PanCam spectral range are most sensitive to Fe oxide absorption bands, spectral parameters that relate to these features are used here. Figure 7.13 shows 440 – 660nm slope plotted against 880nm band depth (relative to adjacent filters) for all targets at BOCK01 and SV01. It can be seen that these targets fall into four broadly distinct groups, which can be classified (based on field/hand specimen identification) into basalt, Fe-rich silicates/oxides, carbonate, and quartz/silica rich groups. It is noted these spectral parameters cannot be used to identify specific mineralogical species per se, but simply provide a way to distinguish between those targets that are spectrally distinct and those that are spectrally similar. However, such information is potentially useful in the selection of remote targets for the ExoMars rover to approach for analysis with contact instrumentation (e.g. Raman, IR). With limited rover lifetime and resources, it might be of more scientific value to select one target from each of the four groups, and so get a more representative view of the lithological diversity, and therefore ultimately past environments and geological processes at that site. It is evident from the plot that the targets from BOCK01 and SV01 mostly correspond well to each other, with Marianne plotting with the Basalt (VB) from BOCK01, suggesting the volcanoclastic outcrop at SV01 is indeed broadly basaltic in composition with little evidence for secondary mineral deposition or extensive weathering. Otto plots most closely to the iron-rich silicates and oxides from BOCK01, and, together with the HRC image data, this suggests this rock is potentially rich in smectite clays. Gunnar plots closest to the silica-rich BOCK01 targets ‘G’ and ‘SiB’, and not the carbonate ‘M’, which could lead to the conclusion that the basaltic clasts in Gunnar are cemented by silica, not carbonate. However, field analysis of Gunnar show the white mineral cement to be predominantly carbonate, highlighting the potential for PanCam spectral data to be misleading in the absence of contextual or more conclusive information. The inclusion of a remote Raman-LIBS system, as opposed to just a contact Raman, would be one such way of clarifying the mineralogy.

Figure 7.13. 440 – 660nm slope vs. 880nm band depth spectral parameter plot for PanCam targets for BOCK01 (black points) and SV01 (blue points) at Sverrefjell volcano. Mean error bars are shown bottom right hand corner.



One major issue with the PanCam analysis of the targets at Sverrefjell is the lack of multiple data sets from any one target. Targets vary greatly in size, and some targets are only big enough to obtain one measurement, such as the target ‘M’ at BOCK01, or target Gunnar at SV01. This will also be true of PanCam analysis of Martian terrains, and the acquisition of extensive multiple data sets from the MER rovers Spirit and Opportunity has been accomplished through the steady gathering of multispectral images across entire traverses (e.g. Farrand et al. 2007; 2006) with over 60,000 (as of 2006) PanCam images having been acquired since the rovers’ landing in January 2004 (Bell *et al.* 2006). This data set has allowed for a thorough statistical analysis of the PanCam spectra acquired (Farrand et al. 2008). Clearly gathering a similarly extensive data-set was not possible during the Svalbard testing of PanCam, and is one particular objective that could be easily achieved through short-term deployment at any lithologically diverse site (Martian analogue or otherwise) and should be a focus of future PanCam testing.

With regards to the detection and assessment of past environmental habitability at Sverrefjell, PanCam data has detected, through both multispectral data and

colour imaging, a number of features that could be interpreted as evidence for a past habitable environment which could be approached for more extensive rover investigation. A particular example is the detection of potentially hydrothermally-deposited carbonate and silica. Hydrothermal systems are widely known to be firstly a likely occurrence on Mars in the past (e.g. Abramov & Kring 2005; Rathbun & Squyres 2002; Gulick 1998; Griffith & Shock 1995), and secondly a high priority environment within which to search for evidence of past life (Newson *et al.* 2001; Farmer & Des Marais 1999; Walter & Des Marais 1993). Additionally, hydrothermal carbonate and silica deposits on Earth commonly preserve morphological fossils (Konhauser *et al.* 2001; Allen *et al.* 2000; Hofmann & Farmer 2000; Cady & Farmer 1996), organic compounds (Preston *et al.* 2008; Zhang *et al.* 2004; Westall *et al.* 2000), and geochemical biosignatures (Oehler *et al.* 2006). Such targets would be significant finds on Mars and would no doubt be a clear priority for the ExoMars mission. Although PanCam spectral data were not able to clearly identify the white minerals as either silica or carbonate, both minerals have important implications for past habitability. Carbonates especially are thought to indicate more clement conditions, with neutral – alkaline pH and a steady supply of liquid water (Ehlmann *et al.* 2008a). Silica also could be indicative of a neutral-alkaline (in this case, silica depositing) aqueous environment (Wang *et al.* 2008; Yen *et al.* 2008), such as that seen at Geysir, Iceland. However, it could also be the result of highly acidic gases weathering the basaltic lava (McAdam *et al.* 2009; Squyres *et al.* 2008; Schiffman *et al.* 2006), an environment that may not be considered as favorable to life. This particular issue currently surrounds the interpretation of the silica deposits identified on Mars by the rover Spirit, the answer of which could potentially have a significant effect on the past habitability of the area around Gusev Crater (Squyres *et al.* 2008; Yen *et al.* 2008).

In addition to the carbonate and/or silica deposits, the suggestion of possible smectite clays suggest past aqueous activity at this outcrop. As with carbonate minerals, phyllosilicates are suggestive of habitable conditions with the presence of long term liquid water and neutral – alkaline pH values (Poulet *et al.* 2009; Poulet *et al.* 2005), and phyllosilicate terrains in particular are recognised as priority targets for missions ExoMars and MSL. One notable result of the multispectral data is the lack of clear hydration features for any of the targets

(e.g. Figure 7.6), even those likely to be hydrated minerals, such as opaline silica or carbonate. The hydration feature is a small, but distinctive indicator of past liquid water activity, and it would be highly advantageous for an astrobiology mission such as ExoMars to have the ability to detect it. The laboratory testing detailed in the previous chapter (Chapter 6) demonstrated the filter wavelengths in F2-12 were suitable for the detection of this hydration feature in a number of Martian analogue samples (GY2, GY1), yet it is not detected at either BOCK01 or SV01.

In addition to the mineralogical indications of habitability, there is also evidence of depositional bedding structures within the volcanoclastic sediments at SV01. For such depositional structures to occur, these sediments would have needed to have flowed unidirectionally. Within the volcanic context of Sverrefjell, this is likely to be either as a pyroclastic deposit, or through deposition within a body of liquid water (hydroclastic). It is clear that at least part of the eruption at Sverrefjell was influenced by liquid water, as large pillow basalt lavas outcrop mid-way up the volcano. Therefore it is entirely possible that the volcanic breccia, and particularly the phyllosilicate – rich target ‘Otto’, were erupted in close association with a significant source of liquid water. Likewise, the alternative scenario – a pyroclastic flow – would require some degree of explosivity. Such deposits are fairly typical for intermediate – acidic composition volcanoes, or where volatiles such as water are able to interact with the lava. Either way, such a basaltic breccia is indicative of the presence of liquid water.

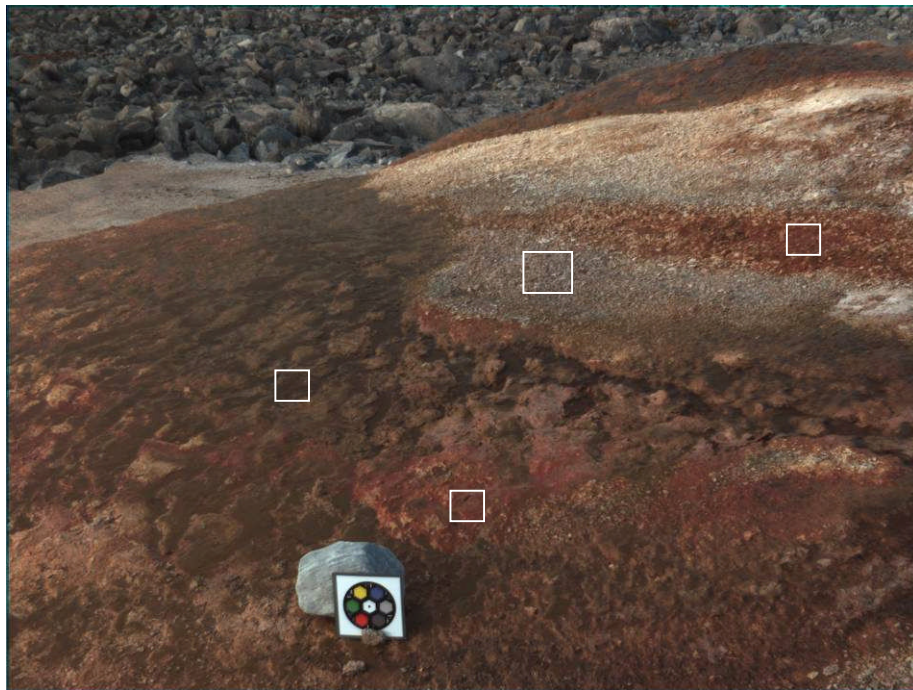
7.2.2 Jotun and Troll Springs: detection of biosignatures

Two warm, carbonate depositing springs were used to test the PanCam detection of biosignatures. The first, Jotun Springs (Chapter 2, Figure 2.4), consists of warm springs containing extensive photosynthetic microbial mats which follow the path of the spring over shallow (1 – 3cm deep) carbonate terraces. The second, Troll Springs, has large (20 – 50cm deep) well developed terraces, many with extinct, mineralized biomats on the surface, providing a contrast to the extant life at Jotun.

At Jotun Springs, imaging was carried out at the main spring and associated run-off over shallow carbonate terraces deposited by the spring water.

Distinctive colour variations can be seen between both the different biomat communities (principally green and pink) and also the mineral precipitates (white and orange). The objective at this site was to utilise PanCam multispectral imaging of bacterial biomats growing on the surface of carbonate terraces to distinguish between a variety of photosynthetic pigments known to be present within these different biomats. In the following section, all photosynthetic pigment absorption wavelengths come from Viscarra Rossel *et al.* (2006). In addition, the clear lateral distribution of the pigmented biomats made this a suitable site for utilising 2D spectral mapping. A RGB colour composite image from the right WAC is shown in Figure 7.14. Regions from which spectra are measured are also indicated.

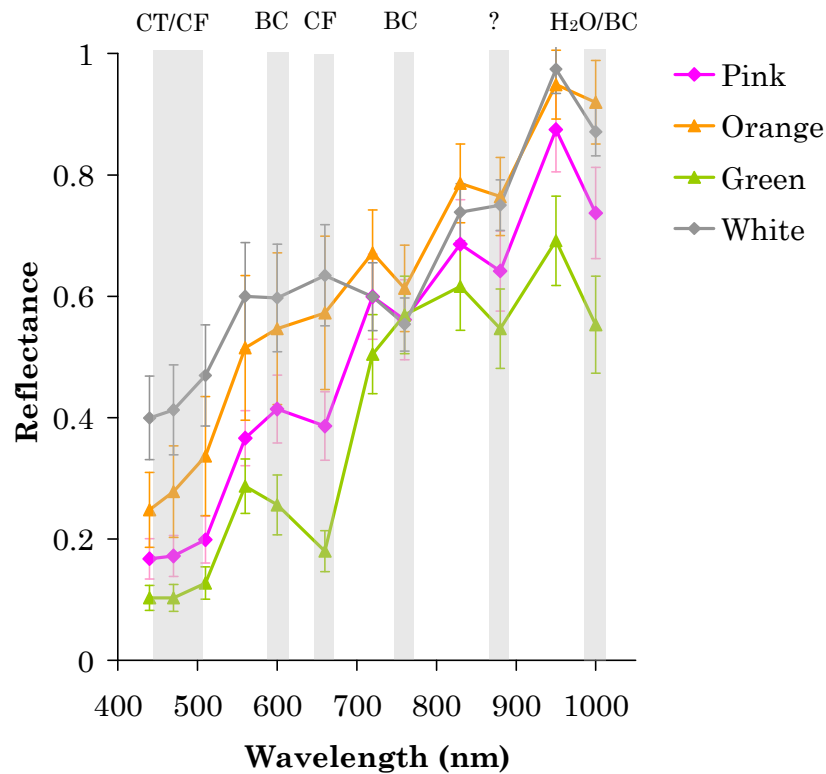
Figure 7.14. Right WAC RGB colour composite image of Jotun Springs. The regions from which multispectral measurements are made are shown.



The PanCam spectra (Figure 7.15) of both the pigment rich biomats and mineral precipitate crusts show distinctive spectral absorption features relating to both photosynthetic features and mineral chemistry. The green biomat shows strong absorptions for both carotenoid pigments (400 – 500nm, detected with filters 440, 470, and 510nm) and especially the 670nm chlorophyll absorption feature which is detected by the 660nm filter. These absorption features are also present in the pink biomat spectrum, although they are not as pronounced. There are two

distinct bacteriochlorophyll *a* absorption bands at 800nm and 860nm, but these fall between filters 760, 830, and 880nm, and so there is a possibility these pigments would not be detected by PanCam. However, the PanCam spectra for the green and pink biomats in particular show a strong absorption at the 880nm filter, which may be due to the influence of this pigment (highlighted with a '?'). The mineral precipitate/crust spectra are broadly representative of carbonate, but are interspersed with shallow absorptions which correspond to photosynthetic pigments, such as between filters 440 – 510nm, and at 600nm (white crust only), and again at 880nm (currently unknown cause). This detection of photosynthetic pigments is potentially representative of biomats that exist either beneath the mineral crust or in between mineral grains, as such photosynthetic pigments would easily affect an otherwise featureless carbonate spectra. Although if this indeed the case it is anomalous that the strong chlorophyll absorption at 660nm is not present, in either the orange or white mineral crust. One particularly notable feature in the white crust exists at 760nm. This sharp absorption is not present in either the extant green or pink biomats, but does appear in the orange mineral crust. This absorption, together with the shallow feature at 600nm in the white crust, is suggestive of the pigment bacteriochlorophyll *a*, which absorbs at both these wavelengths, principally at 760nm. Lastly, there is a strong absorption in all spectra at 1000nm, which could either be water, or bacteriochlorophyll *b* which absorbs at 1020nm. Although the geological filters were able to detect a number of photosynthetic pigments within the extant biomats at Jotun Springs, they are not well placed to distinguish between different photosynthetic pigments within a pigment group – for example between chlorophyll *a* and chlorophyll *b*.

Figure 7.15. PanCam spectra from Jotun Springs. Individual spectra have been offset for clarity by 0.05 increments. Grey bands show absorption of photosynthetic pigments. CT = Carotenoids; CF = Chlorophyll a & b; BC = Bacteriochlorophyll. The beginning of either an H₂O, or Bacteriochlorophyll *b* absorption can also be seen.



Simple 2D spectral mapping was carried out to test how PanCam multispectral imaging could be used to show the spatial distribution of a target of interest. This was calculated using MATLAB, and worked on the principle of highlighting only those pixels that represented a particular spectral feature characteristic of the target. To calculate this, first the image was normalized relative to the white calibration target. This involved adjusting the image threshold to remove all pixels with a brightness value greater than that of the white calibration target mean value, then renormalizing all the remaining pixel values by dividing them by the mean calibration target value (i.e. the same value used to normalize the PanCam spectra). This converted the pixel values so that they matched the values used to plot the target PanCam spectra. Of these remaining pixels, only those with brightness values that are equal to the value in the PanCam target spectrum, or within the region bound by the average standard deviation, remain. This is done for three images of the relevant filters that depict the spectral feature of interest, and only those pixels that match the values of the spectrum all three images remain.

Figure 7.16. Spectral mapping of targets at Jotun Springs: a) 560nm WAC image; b) map showing distribution of ‘Green’ and ‘Pink’ biomats and ‘White’ precipitate; c) WAC RGB composite, arrows depict similar coloured regions distinguished by spectral mapping (see text for detail); d) ‘White’ distribution; e) ‘Pink’ distribution; f) ‘Green’ distribution.

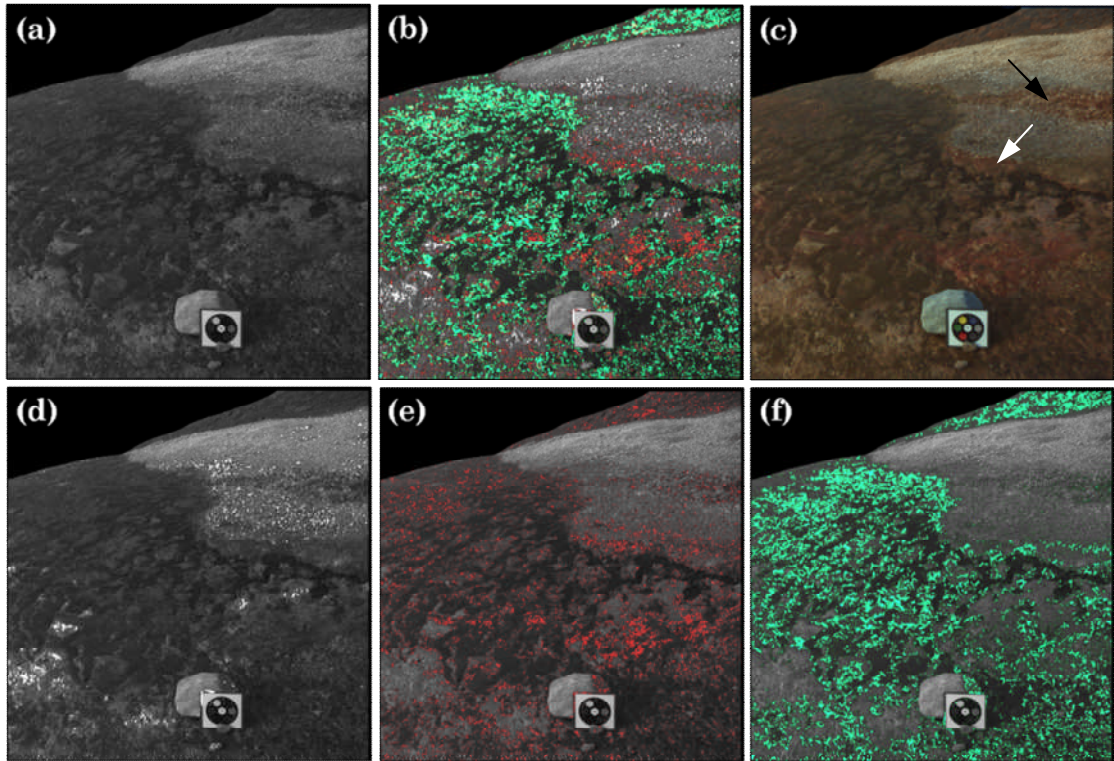
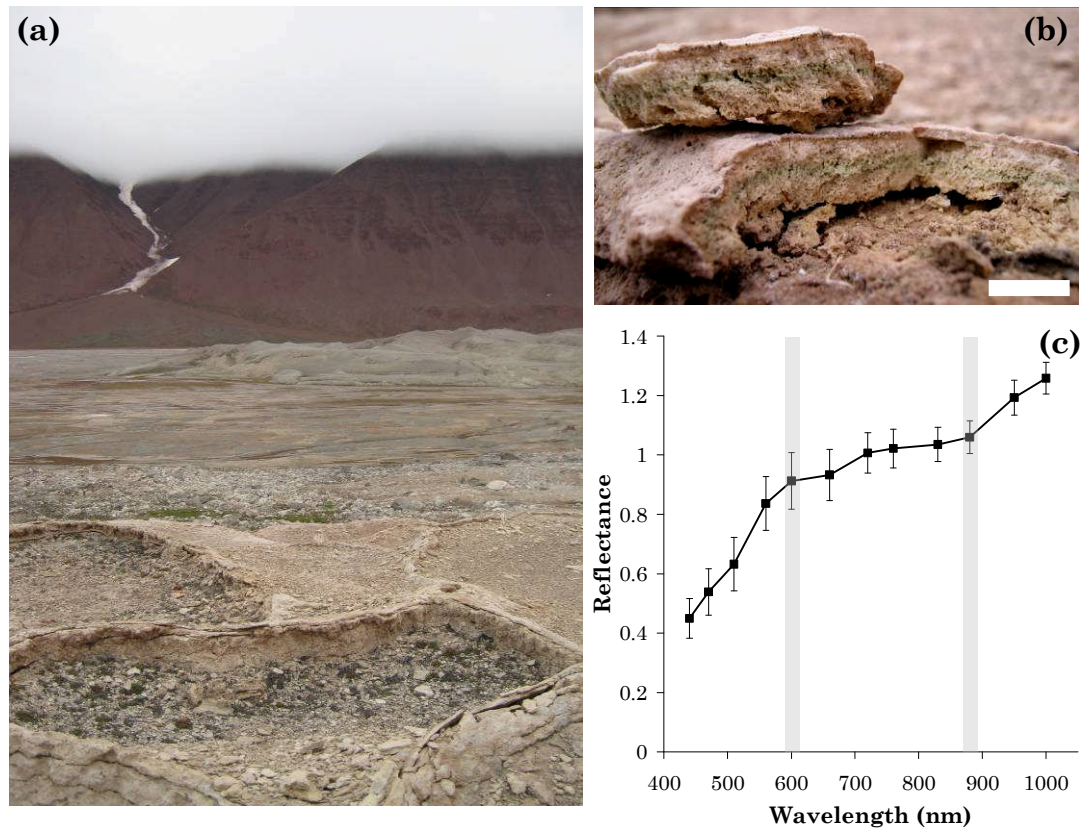


Figure 7.16 shows the spatial surface distribution of the spectrum that distinguishes the green and pink biomats, and the white carbonate precipitate. It is evident the green biomat dominates the spring, and on the whole is confined to the running spring water (7.16f). The pink biomat is less widespread, but contrary to the green biomat this is restricted to regions that lie just above the water line of the spring (7.16e). Where the spectral maps are particularly useful is the distinction between areas of similar colour but different composition, for example, the pink biomat and the orange mineral precipitate. In the RGB composite (7.16c) this orange precipitate appears as a streak across the otherwise white-grey carbonate deposit (marked with a black arrow). Just below this however is a pink-orange region (marked with a white arrow), which from the colour image alone is difficult to identify as either the pink biomat or the orange precipitate. The spectral mapping however shows this to be predominantly the pink biomat. In comparison to the biomats, the white mineral precipitate is less well represented in these spectral maps, being limited to isolated groups of pixels or small ‘islands’ within the spring.

One problem with this method of spectral mapping is that it relies on pixel matching between the different filter images. This was an issue with the data-set acquired with the instrument set up used for this field testing, as the filter wheel was designed to be manually turned between each image. This manual switching of filters meant unavoidable small changes in position were made to the PanCam, and as such single-camera images are not perfectly matched. Therefore, individual images need to be translated so to align pixels. A far bigger problem is if a spectral feature falls across filters between the left and right WAC, as the separation between these two cameras results in each camera viewing the target at a different angle, meaning it is not possible to match pixels even through translation. For the targets mapped in Figure 7.16 above, the respective defining spectral features were produced by the filters on the left WAC only, so in this instance, this problem did not arise. It is also noted that this method relies on the absolute brightness values for each pixel, and so regions in the image that do contain the target, but for some reason (e.g. they are in shadow) have a lower or higher albedo (outside of the allowed error) will not be recognised.

Troll Springs, like Jotun, is a carbonate depositing spring, but here there are extensive and well developed very large carbonate terraces consisting of both currently forming terraces and old carbonate terrace deposits. Warm spring water feeds a large shallow pool, from which small side streams and run-off flows branch off, depositing the terraces downslope. Thick green and green-yellow biomats fill the pools that form in the terraces. Where old spring flows used to run there are dried out and/or mineralised biomat structures encrusted on the outside walls of the terraces where the spring water used to flow. Additionally to the extant biomats in the terrace pools, endolithic cyanobacteria exist within the dried out carbonate terraces themselves, occupying pore spaces within the carbonate. The objective at this site was to identify any multispectral signature of firstly the carbonate mineralogy, secondly the extinct fossilized life on the terrace surfaces, and lastly the cryptoendolithic cyanobacteria.

Figure 7.17. a) Troll Spring carbonate terraces in the foreground (~1m in width); b) cryptoendolithic cyanobacteria colonising the carbonate (scale bar = 1cm); c) PanCam spectrum of the carbonate terrace, with spectral features consistent with those for the carbonate magnesite.



The PanCam spectrum of the carbonate terrace at Troll Springs (Figure 7.17c) is consistent with that of the carbonate magnesite, with spectral kinks at 600 and 880nm, but contains no evidence of either active photosynthetic pigments from the cryptoendolithic cyanobacteria, or the fossilised biomats. Without any active biological pigmentation present, the detection of these fossils with PanCam spectra alone was not possible. This is consistent with the multispectral imaging of sample GY2 in Chapter 6, section 6.2.3), which showed that silicified biomats (in contrast to the calcified biomats at Troll Springs) had no impact on the PanCam spectra. Likewise, even though cryptoendolithic life is present millimeters below the surface of the carbonate terrace, this is still too deep to have any impact on the observed remote spectrum. Cryptoendolithic life in particular has often been used as an analogue for survival strategies for life on Mars (Hughes & Lawley 2003; Fike *et al.* 2003; Walker & Pace 2007; Wynn-Williams & Edwards 2000; McKay *et al.* 1992), particularly where a rock thickness of only a few millimeters has been demonstrated to be a highly

effective barrier against UV radiation (Cockell *et al.* 2005). This PanCam deployment at Troll springs therefore has shown that the PanCam instrument alone should not be used as a reliable life-detection system. However, the unambiguous detection of carbonate, coupled with the characteristic terrace morphology of the deposits, provides clear evidence of a past habitable environment that should be approached for further rover investigation.

7.2.3. Wahlenbergfjord: detection of iron oxide deposits

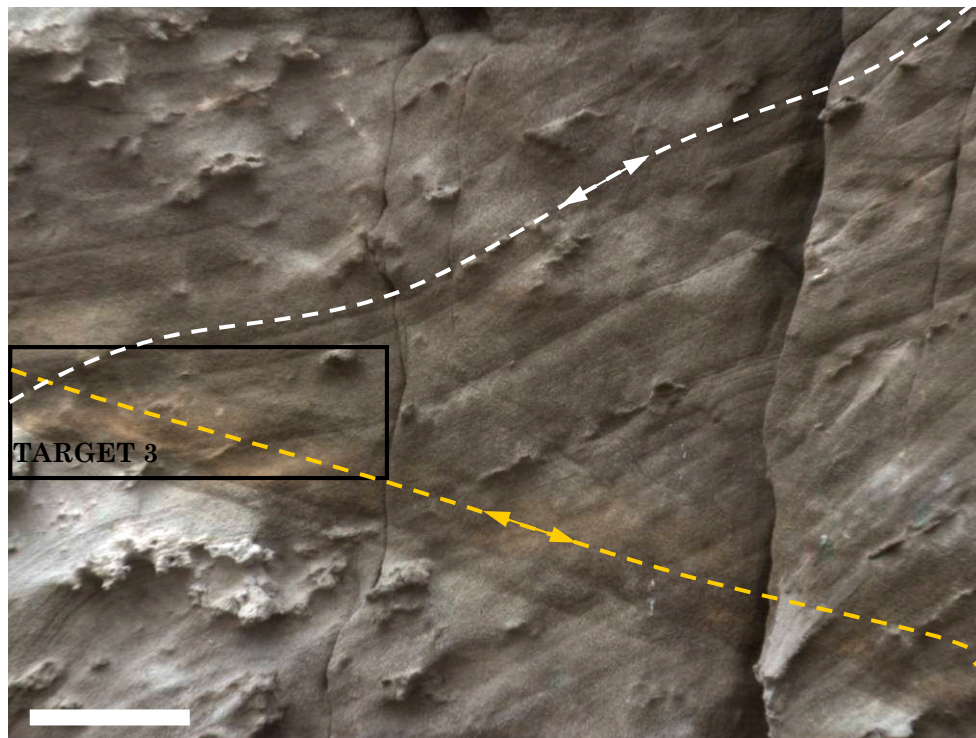
Iron oxide is an abundant constituent of the Martian regolith (Chevrier & Mathé 2007; Morris *et al.* 2006), and as such it was imperative that the PanCam was tested at a site that contained iron oxide mineralogy. At Wahlenbergfjorden, there are extensive outcrops of quartz sandstone with later goethite mineral deposition, producing a distinctive red – yellow – pink colouration of the sandstone, although there are regions that have remained unaffected, which are typically paler in colour. The outcrops occasionally display clear cross bedding features, which are often cross-cut by bands of iron oxide deposits, indicating these deposits occurred post deposition. The objectives at this site were to identify the iron oxides present within these rocks, and to use PanCam to quantify the relative distribution of goethite/iron oxide throughout the outcrop stratigraphy.

The WAC RGB colour composite image in Figure 7.18 below shows clearly the red – pink – grey – beige colouration of the outcrop. In addition, cross bedding features are also easily identified in the lower portion of the outcrop, whilst distinctive weathering textures in the top half of the outcrop can also be seen. It is difficult to infer from the WAC image alone whether the colour variations correspond with structural or depositional units, although a HRC image of the outcrop region around Target 3 (Figure 7.19) confirms one region of colour variation to clearly cross-cut the other structures present in the outcrop. Little is known about the formation and deposition environment of this outcrop (*pers. comm.* Dr. Andrew Steele), therefore without any reliable palaeoenvironment contextual information, the interpretation of the PanCam images is focused solely on the detection of iron oxide within this outcrop, and not to formulate any ideas regarding the past environmental habitability of this site.

Figure 7.18. Right WAC RGB composite of the outcrop and the target areas that spectra are calculated from (white boxes). Cross bedding can be seen in the outcrop below the dashed line. The yellow box shows the area a stratigraphic section (Figure 7.21) is taken, and the blue box shows the footprint of the HRC image shown in Figure 7.19.

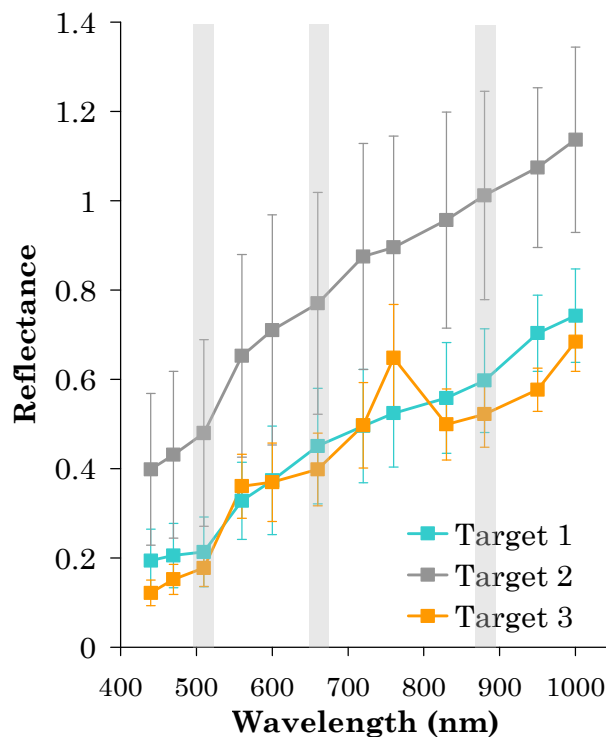


Figure 7.19. HRC image of Target 3 (indicated by black box) and surrounding outcrop, showing the yellow goethite deposits (general lineation trend highlighted by yellow dashed line and arrow) cross-cutting the underlying rock structure (lineation trend highlighted by white dashed line and arrow). Scale bar = 10cm.



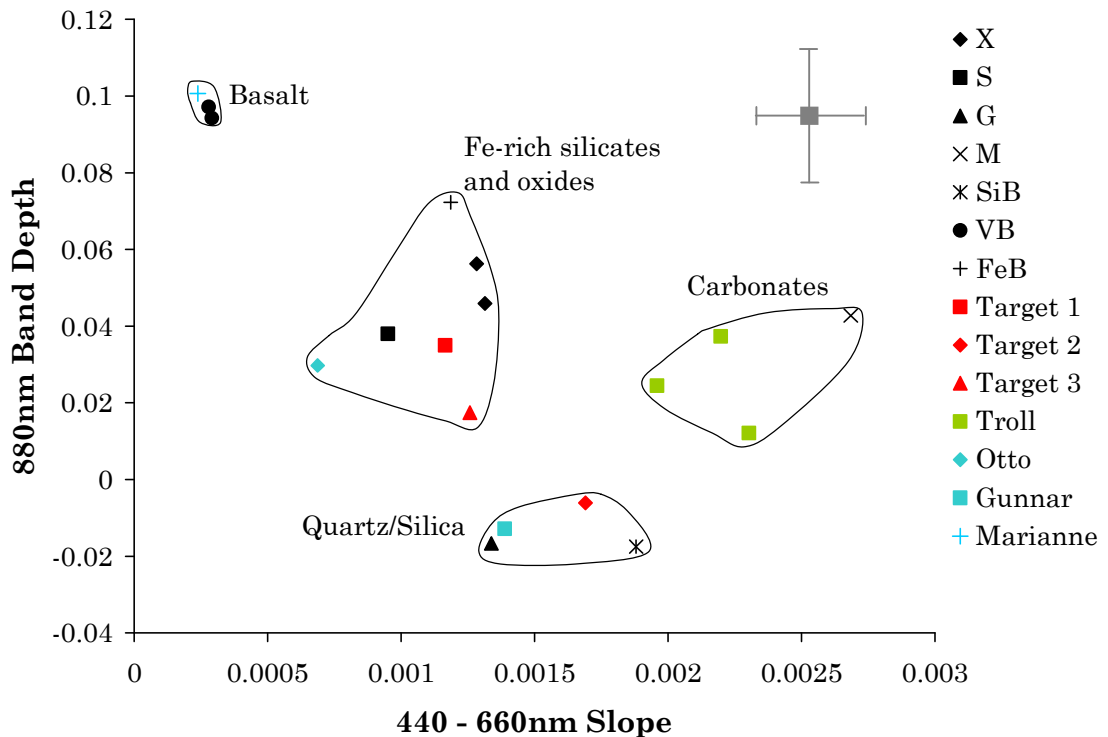
The PanCam spectra of three targets (shown in Figure 7.20) are representative of the mineralogy present in the outcrop. The target 1 and target 2 spectra are consistent with quartz – the dominant mineralogy of the sandstone outcrop. Target 3 on the other hand is representative of goethite (an iron oxide), with absorptions between 440 – 510nm, at 660nm, and between 800 – 950nm, and a pronounced peak at 760nm. The 440 – 510nm absorption can be also seen in the Target 1 spectrum. This is in agreement with field observations and the RGB colour composite image (Figure 7.18), where it is apparent that the Target 2 region is considerably paler in colour (white – grey) and lacking in any of the red-pink colouration seen in the rest of the outcrop, and as such it produces a purely quartz spectrum.

Figure 7.20. PanCam spectra of targets shown in Figure 7.18, showing a Fe²⁺ absorption band at 500nm and Fe³⁺ absorption bands at 650 and 880nm. The reflectance peak at 760nm is also characteristic of goethite.



When these targets are plotted onto the spectral parameter plot (Figure 7.21) previously shown for the Sverrefjell targets, they also plot in similar regions relating to their mineralogy and composition. Target 2, the region of sandstone lacking any visible deposition of goethite, plots closest to the quartz/silica group

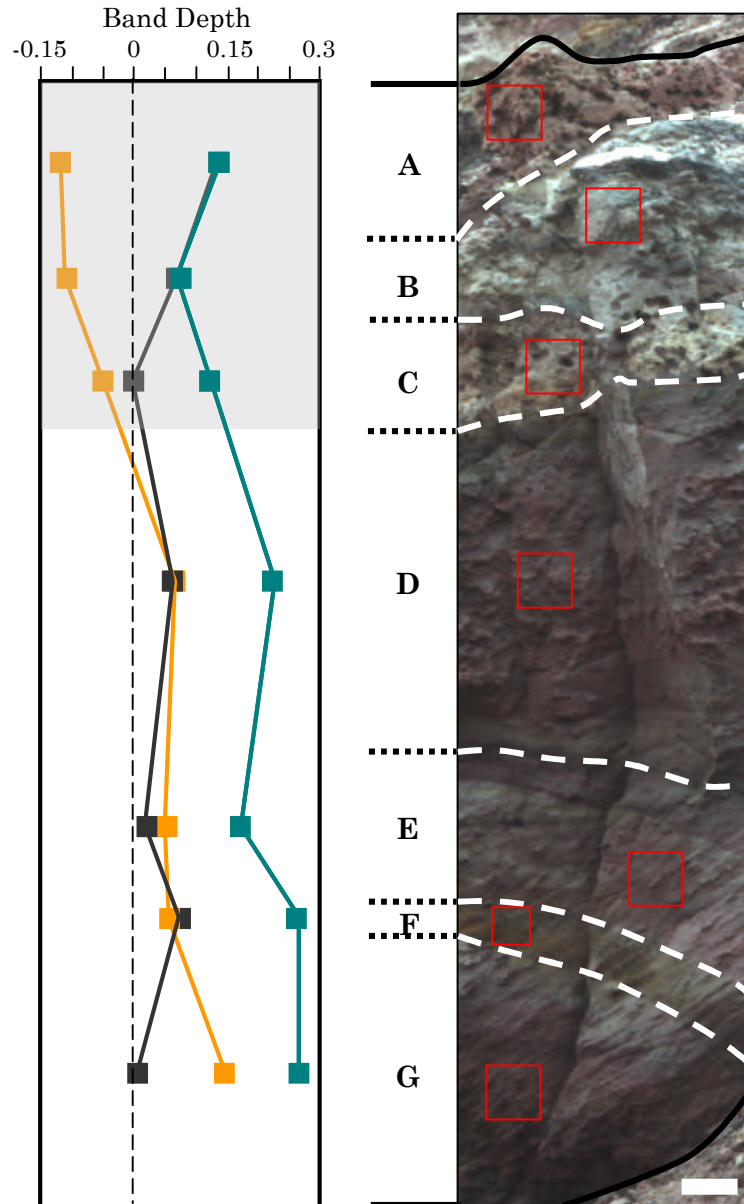
Figure 7.21. 440 – 660nm slope vs. 880nm band depth spectral parameter plot for geological targets: Black = BOCK01, Blue = SV01, Red = Wahlenbergfjorden, Green = Troll Springs. Mean error bars are shown top right hand corner.



The stratigraphic section and associated band depth plots in Figure 7.22 can be used to give an indicator of how iron oxide content varies throughout the outcrop. The 880nm band depth can be used as an indicator of iron oxide (Farrand *et al.* 2006), with increasing band depth correlating with increasing iron oxide content. The initial spectral analysis of the outcrop (Targets 1, 2, and 3; Figure 7.20) suggest the presence of goethite in particular, with goethite spectral features varying in intensity from strong (Target 3), to weak (Target 1), to almost non-existent (Target 2), as shown in Figure 7.19. Therefore, the band depths of the features that are particularly strong for goethite (510nm and 660nm) are used here as an indicator of specifically goethite distribution throughout the outcrop. It is evident from the RGB WAC image alone that the red colouration (and therefore possibly iron oxide concentration) of the outcrop varies from dark red/purple – to yellow – to grey. From the 880nm band depth profile, it can be seen that the band depth gradually increases with depth down the outcrop. In particular, the top three units A, B, and C, have no absorption at this filter wavelength at all, potentially suggesting no to little iron oxide content. This is further implied by the lack of red colouration within these units, which are

typically grey – beige in colour, especially units B and C. The 510nm band depth measurements also display this overall trend, with the lowest band depths also occurring within these top three units. The biggest 510nm band depth occurs at unit F, a yellow band that cross-cuts the cross bedding in units E and G (also the same region that contains Target 3 – see Figure 7.19), suggesting this yellow band has relatively higher levels of goethite. Goethite is considered a mineralogical marker for aqueous alteration on Mars due to the presence of hydroxide within its mineral structure (Morris *et al.* 2008). Notably, goethite forms part of a complex mineral assemblage identified by Spirit at Columbia Hills, and one which has been interpreted to represent acidic aqueous processes resulting in extensive alteration (Ming *et al.* 2006). As such, iron oxide minerals such as goethite can be used as clear indicators of past environmental conditions.

Figure 7.22. Stratigraphic section through the outcrop at Wahlenbergfjord, showing individual units distinguished based on colour and/or texture, bound top and bottom by the solid black line. Dashed white lines mark boundaries between the different units, and red boxes indicate regions spectral measurements are made. Spectral band depths indicative of iron oxide mineralogy are plotted on the left (Yellow = 880nm; Grey = 660nm; Blue = 510nm). All band depths above the black dashed line (at zero) have an absorption at the respective wavelengths, and therefore are likely to contain iron oxide. Scale bar = 10cm.



7.3 Conclusions and Future Work

The results of this field test show that PanCam multispectral imaging can be used successfully to identify targets of astrobiological interest, and as such will play a key role during the ExoMars mission. In addition to mineral deposits, PanCam was also able to detect a variety of extant life via the identification of

different photosynthetic pigments, although morphological fossils and cryptoendolithic communities within carbonate deposits had no observable effect on the reflectance spectra obtained. This demonstrates the limitation of the astrobiological application of PanCam to principally the detection of past habitable environments, and not for use as a reliable life detection tool in itself.

Field-testing rover instrumentation undoubtedly has numerous drawbacks: lighting conditions are uncontrolled and variable, targets are unexpected, and data collection is often slowed by difficult environmental conditions or instrument failure. However, the uncontrolled nature of field testing allows for a much more rigorous investigation on the suitability of the instrument components, such as the geological filters, both in terms of instrument operations and interpretation of PanCam data.

Perhaps the most unrealistic aspect of this field testing in Svalbard is the lack of a homogenous dust (i.e. Martian regolith) coating rock surfaces and collecting within rock crevices. Whilst the lithology and mineralogy of the outcrops imaged with the PanCam may be highly analogous to Martian geology, the presence of Martian dust would no doubt obscure and alter many of the key spectral features produced by the outcrops. It was this Martian dust which led to inclusion of the Rock Abrasion Tool (RAT) on the MER rovers (Squires *et al.* 2003). However, it is not particularly practical to place a Martian analogue dust coating on large field outcrops, particularly where lithologies are type localities or rarely found worldwide, an issue not uncommon in Svalbard. Therefore, this aspect of ground truthing and instrument testing is purely restricted to the laboratory.

Lastly, such field testing will help to develop PanCam surface operations. For example, the issue of how spectral resolution (i.e. how accurately or clearly the spectrum represents a particular mineral/lithology) varies with distance from an outcrop needs to be carefully explored. Constraining the number of pixels need to produce an accurate spectrum from a mineralogically distinct area of an outcrop needs to be tested, so to quantifiably determine the limits of the PanCam's capability when it comes to remote target selection. Such tests do not need to be conducted in Svalbard, and could be easily carried out in numerous UK localities with good outcrop exposures and limited vegetation.

CHAPTER 8

DISCUSSION

This final chapter discusses the research documented in the previous chapters, and explores the implications of these findings within the wider context. Additionally, data leading to the generation of ideas that were considered too speculative to include in the core chapters of this thesis are detailed here. The aim of this PhD was to utilise Martian analogue environments that existed geographically at high latitudes, to further our understanding of the possibility for life to have existed on Mars, and the potential for finding evidence of such life. Through understanding the microbiology, biosignatures, and geology of selected environments it is hoped this goal has, in part, been achieved.

First, the core theme of this PhD is assessed – utilising volcanic environments at high latitudes for astrobiological research. The wide range of environments and habitats that exist in these settings is summarised as a whole.

Secondly, subglacial volcanic environments are discussed in detail with regards to their habitability. The previous chapters demonstrated such systems to be highly viable and to contain diverse prokaryotic communities. Therefore, such environments on Mars are discussed, exploring issues relating to their colonisation, ability to support metabolic pathways, and potential for biosignature preservation.

Thirdly, implications of this work for the ESA ExoMars mission are reviewed, with reference to the work conducted towards the development of the ExoMars PanCam instrument in particular.

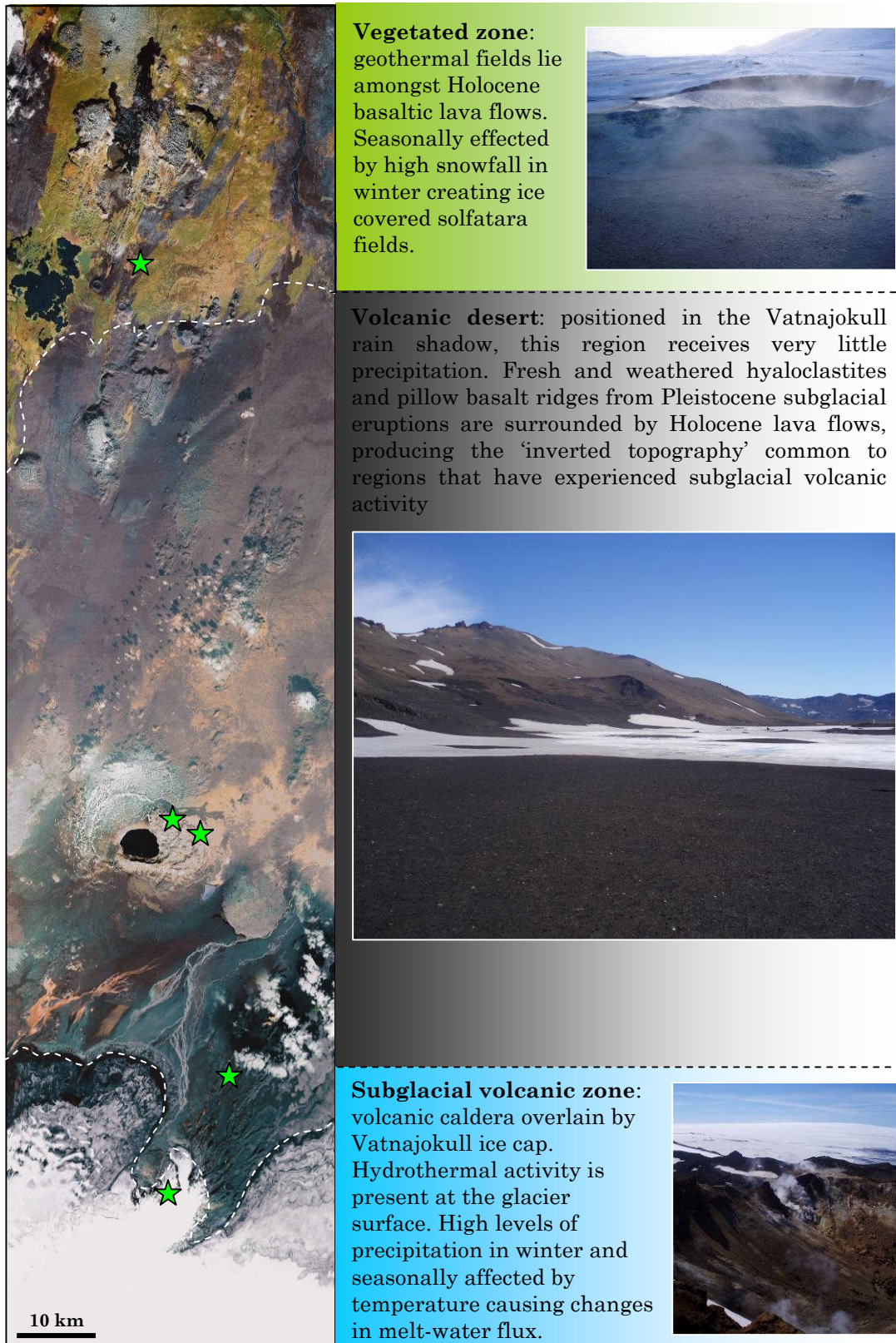
Lastly, the final section of this chapter outlines areas favoured for further research – in particular focusing on astrobiologically relevant studies of active subglacial volcanic systems in Iceland.

8.1 High Latitude Volcanic Environments

The primary focus of this research has been the utilisation of basaltic volcanic environments at high latitude, as a suitable analogue for Martian environments, both in the past and at this present day. A wide variety of such volcanic environments were sampled for both geological and biological investigation. The samples analysed from these environments have helped in the development of the ExoMars PanCam instrument, identified an environmental control on biosignature development in basaltic volcanic glass, and shown that basaltic lavas in cold and dry environments provide a habitat for a diverse array of prokaryotic communities, and, finally, that these communities may be able to survive in putative subglacial volcanic environments on Mars.

Many of these environments are specific to Iceland, where sampling took place. These environments are displayed in Figure 8.1, and demonstrate the range of conditions that exist within active and extinct volcanic terrains at high latitude. The unique Arctic climate means these environments are all affected and modified by seasonal extremes, with near constant sub-zero temperatures, combined with snow cover during winter months. Each environment is typified by its own specialised physiochemical regime. The work in this thesis demonstrates such terrains can play an important role in Martian analogue research. In particular, the study of bacterial diversity within basaltic subglacially-erupted lavas revealed the community to be highly comparable to those residing in well-known and previously studied analogues, such as the Antarctic dry valleys. Many of these earlier studies have been in relation to quartz sandstone or marble lithologies, which are not currently believed to exist on Mars due to lack of tectonic activity. The basaltic lava environment of central Iceland however is directly comparable to Mars in the geological sense. Therefore, there is a huge potential for these environments, and their microbial communities, to be utilised more extensively as a proxy for Martian research. These environments are also significantly easier to access and sample than their counterparts in Antarctica, meaning more time and money can be devoted to the research itself as opposed to complicated logistics. As such, these Icelandic environments should be exploited for future work in the field of astrobiology, both for biologically and geologically focused research.

Figure 8.1. Google Earth areal view of the different environments sampled (localities shown by stars) in north Iceland for this work. A simplified diagrammatic cross section of these environments is given in Chapter 1 (Figure 1.6).



8.2 Subglacial Volcanic Environments on Mars

It is evident that subglacial volcanic environments on Earth are conducive to life, be it subglacial caldera lakes (Gaidos *et al.* 2004) or subglacially erupted lavas (Chapter 3), and that potential sites of volcano – ice interaction have been widely identified on Mars. As a result the habitability of such a system within a Martian setting needs to be considered, and the question of whether or not indigenous microbial communities could survive such conditions was tested experimentally (Chapter 5). This research, like others (see Chapter 1, section 1.4.2), has demonstrated increased survivability of a microbial community within a subsurface environment on Mars.

However, there are a number of other factors relating to the long-term habitability of these environments on Mars, including the availability of these systems for colonisation (can life access these systems?), the potential for metabolic pathways to occur (can life be sustained in these systems?) and the duration of this habitat (does the environment exist long enough to allow a community to flourish?). Therefore these issues are briefly discussed here, with the aim to put the habitability of subglacial volcanic systems into context, in particular focusing on the key differences likely to exist between terrestrial and putative Martian systems.

8.2.1 Availability of liquid meltwater

An active volcano – ice system theoretically can provide all the necessary ingredients for life. The continual release of geothermal heat into an overlying glacier can sustain a subsurface meltwater environment, whilst the release of volcanic gases could sustain a variety of chemosynthetic metabolisms. The presence of this heat flow will also mean a continual convective system will create a cycling of material through the different environments, removing waste products from some niches whilst delivering nutrients to others. It is clear that the presence of liquid meltwater is key to volcano – ice systems being suitable for life. On Mars, the melting efficiency of water – ice is much reduced due to the low initial temperature of the ice (Hovius *et al.* 2008), which perhaps suggests volcano – ice systems on Mars are not as viable as those on Earth. Indeed there are locations on Mars interpreted to be the result of subglacial volcanism that display a distinct lack of evidence for meltwater. Such places include the

proposed subglacial lava flows at Ascræus Mons, where rapid re-freezing of a cold-based glacier would prevent any significant basal melting (Kadish *et al.* 2008). However, it has been suggested that the temperature of the meltwater is highly influential on the formation of Jökulhlaups, in terms of higher heat flow enabling the enlargement of subglacial drainage tunnels (Gudmundsson *et al.* 1997). The occurrence of Jökulhlaup-like deposits and flows on Mars therefore suggests subglacial eruptions can potentially produce meltwater temperatures that are favourable to life.

8.2.2 Initial colonisation

Whilst habitable environments potentially may exist in this subglacial volcanic setting on Mars, they are most likely to be transient and isolated. On Earth, any new body of liquid water will be rapidly colonised due to the widespread and globally connected biosphere (Cockell & Lim 2005). Whilst it remains possible for pockets of Martian life to exist, as yet there is no evidence for a similarly extensive biosphere. As a result, the delivering of Martian life to these environments remains a problem. It can be seen that features indicative of subglacial volcanic activity often occur in clusters (e.g. Alfaro *et al.* 2007). This suggests that their localised habitable environments exist within a close enough proximity to allow transport of microorganisms between individual environments. This perhaps is one of the major advantages of a volcano-based system. On Earth, regions of anomalously high heat flow are rarely isolated to just one volcano within a volcanic system. This can be clearly seen in Iceland where Vatnajökull (glacier) overlies 7 individual volcanic centres (see Chapter 1, Figure 1.5), all of which have formed as a result of either the local lithospheric rifting or their proximal position to the Icelandic hotspot, or both. As a result, it is possible to envisage such subglacial systems to be connected via fractures and channels within the ice, where meltwater (and any microbial life it may carry) can circulate, distributing microorganisms from one system to another. It has been observed that rapid vertical transport of hydrothermal fluid occurs beneath Mýrdalsjökull via faults (Björnsson 2002). This to some extent could potentially solve the problem of colonisation, in terms of delivering microorganisms to a newly-formed system from an older one.

8.2.3 Potential for photosynthesis and chemosynthesis

The vast majority of the terrestrial biosphere is dependant upon photosynthesis, either directly or indirectly (Varnes *et al.* 2003). Photosynthesis on Mars however is hindered by the exposure to UV radiation and by the increased distance to the Sun, reducing photosynthetically active radiation (PAR) to ~55% that of those experienced on Earth (Cockell & Raven 2004). If photosynthetic communities were to exist within a subglacial volcanic system, they would be limited to the near-surface ice and specifically use blue and green wavelengths due to the high absorbance of red light within ice (Hawes & Schwarz 2000). Cockell & Raven (2004) have experimentally shown that the maximum depth within snow-pack at which the minimum level of PAR can penetrate is 24cm. Additionally, work on ice-covered lakes in Antarctica has shown there to be benthic photosynthetic communities residing at ~16m water depth beneath 3.5 – 5m of ice cover (Vopel & Hawes 2006), which is still far below the depths of many subglacial volcanic systems, which are typically beneath several hundred meters of overlying ice (Wilson & Head 2002). At depths of 100m within glacial ice, PAR is entirely absent (Warren *et al.* 2002). However, if a volcanic system breaks through the overlying ice, it is entirely possible a photosynthetic community could thrive in the surrounding meltwater lake in an early Martian setting, if atmospheric pressures were high enough to allow liquid water to remain stable at the surface. After this time however, with the exception of communities that may reside within the top ~10 – 20m of the glacial surface, subglacial volcanic environments are not conducive to a photosynthesis-based community. This limits the primary producers of this environmental setting to chemosynthetic pathways.

On Earth, chemoautotrophs are major contributors for communities residing within dark, extreme environments, such as deep sea vents (McCollom & Shock 1997). Specifically to Mars, anaerobic chemolithoautotrophs can potentially inhabit subglacial volcanic environments, through the oxidation of inorganic compounds and fixation of carbon dioxide as the carbon source (Boston *et al.* 1992). Numerous chemosynthetic pathways could potentially be exploited due to the disequilibrium and reduced chemical species that result from the mixing of high- and low-temperature fluids (Gaidos & Marion 2003). On Earth, the majority of the chemosynthetic microbial communities residing in present-day hydrothermal systems are indirectly dependant on photosynthetically produced

O₂. However, ~ 1 – 2% of these communities obtain chemical energy from redox reactions that are completely independent of photosynthesis (Varnes *et al.* 2003), and it is these microorganisms and their metabolic pathways that are potentially suitable for survivability on Mars, particularly with subglacial hydrothermal systems. Methanogens ($\text{CO}_2 + 4\text{H}_2 \rightarrow \text{CH}_4 + 2\text{H}_2\text{O}$), sulphate reducers ($\text{SO}_4^{2-} + 2\text{H}^+ + 4\text{H}_2 \rightarrow \text{H}_2\text{S} + 4\text{H}_2\text{O}$), sulphur reducers ($\text{S}^0 + \text{H}_2 \rightarrow \text{H}_2\text{S}$) and iron reducers ($2\text{Fe}^{3+} + \text{H}_2 \rightarrow 2\text{Fe}^{2+} + 2\text{H}^+$) are typical examples of anaerobic chemosynthetic microorganisms (Boston *et al.* 1992; McCollom & Shock 1997; Van Dover 2000).

8.2.4 Habitat duration

Important to the habitability of the volcano – ice system is its ability to be sustained long enough for life to make use of the variety of environments that arise, and to be spatially recurrent frequently enough for life to be sustained or migrated. Under this context, the identification of tuyas and flat topped ridges holds importance for the duration of such environments. In Iceland, it is thought that the formation of subglacial tuyas with a subaerial lava cap require repeated eruptions of magma into the overlying glacier (Gudmundsson *et al.* 1997), in order to build up such a sized edifice. This is in contrast to the short-term, monogenetic eruptions that produce smaller hyaloclastite ridges that remain entirely subglacial throughout their emplacement. The sustained and localised heat flow this requires can potentially be achieved on Mars, where the lack of plate tectonics has resulted in prolonged periods of hot-spot activity in the same location. Of interest here are the interior layered deposits in the Valles Marineris region. It has been suggested that the exceptionally large dimensions of these Martian features in comparison with the much smaller terrestrial subglacial edifices are a consequence of long-lived polygenetic subglacial volcanism (Chapman & Smellie 2007). As stated by Chapman & Smellie (2007) these types of volcanoes would construct a large edifice through a long-lived thick ice sheet, again demonstrating the potential longevity of these systems.

8.2.5 Biosignatures

After identifying habitable environments on Mars it is important to ascertain how life inhabiting such an environment will be recognised or preserved in the rock record for possible discovery during future exploration. Hydrothermal systems are noted for their ability to preserve detailed microbial fossils,

particularly within silica and carbonate systems (Preston *et al.* 2008). However, this relies on the deposition of mineralised or solute-rich fluids and the subsequent precipitation of the mineral phases and preservation through fossilisation of the in situ microbial community. Examples include siliceous sinter deposits and the fossilisation of microbial biomats forming stromatolite-like structures (E.g. Konhauser *et al.* 2001). As seen at Sverrefjell volcano in Svalbard, PanCam imaging can be used to identify evidence of hydrothermal mineral deposition, including carbonate and silica, within subglacial lava lithologies (Chapter 7, section 7.2.1). Identification of such deposits with the ExoMars rover could therefore be possible, leading to the potential detection of organics that may be preserved.

An additional possibility is the formation of trace fossils in basaltic glass. These are widely believed to be formed by the activities of euendolithic microbes to produce distinctive textures at the glass – palagonite interface (Furnes *et al.* 2007 and references therein), and it has been previously suggested that such microfossils would make suitable biosignatures when looking for life on Mars (Banerjee *et al.* 2006). However, an abundance of such textures is yet to be found in pillow lavas and hyaloclastites of a subglacial origin. As shown in Chapter 4, these biosignatures appear to form readily within an oceanic environment, but are almost absent when lava flows of the same origin exist only in a subglacial freshwater setting. Additionally, analysis of hyaloclastite thin sections from Askja and Helgafell also revealed a distinct lack of these bioalteration textures, despite the similarity in lithology and aqueous alteration conditions to their seafloor counterparts. This is, in part, consistent with work carried out by Cockell *et al.* (2009), which also concluded that long, filamentous tubular textures typical of oceanic bioalteration were not found in Icelandic basaltic or rhyolitic obsidian glass, but that bioweathering instead formed pitted textures at the edge of glass clasts.

Lastly, evidence for life in volcano – ice systems may be recorded via the presence of biomolecules within subglacial lavas and Jökulhlaup deposits. Data from the OMEGA instrument on the Mars Express shows the presence of phyllosilicate minerals at the Martian surface, and clay minerals such as montmorillonite and nontronite have been identified (Poulet *et al.* 2005). It has

been proposed that clay-rich deposits may be suitable sites of organic preservation on Mars (Ehlmann *et al.* 2008b). Such minerals are ubiquitous amongst subglacially erupted basaltic lavas, due to the widespread breakdown of volcanic glass to palagonite through contact with liquid water. If such deposits coincide with volcano – ice interaction terrains on Mars, these could be prime geological formations to search for evidence of life.

8.3 Implications for the ExoMars Mission

One of the overarching aims of Martian analogue research should be the application to actual astrobiology-focused missions. This can either take the form of laying the groundwork for site selection, providing ground-truthing datasets to interpret Martian data, or by directly influencing the design of the mission instrumentation itself. The latter principally was tackled by the work conducted for this PhD thesis, whereby focused scientific experimental techniques and testing were utilised to contribute to the design of the ExoMars PanCam instrument for the first time in its development.

8.3.1 Developing PanCam for an astrobiology mission

Martian analogue geological and hydrothermal samples proved invaluable in testing the new geology filter wavelengths devised for the PanCam instrument. Whilst the new filters were selected based on their ability to detect hydrated minerals (Chapter 6, section 6.1.2), it was through multispectral imaging of Martian analogue rocks using these filters that gave the real indication of the capabilities of PanCam (Chapters 6 and 7). The minerals and biosignatures that were used to test the ability of the PanCam instrument to be applied to an astrobiology mission are summarised in Table 8.1. More minerals were positively identified during laboratory testing than field testing, and is likely due to the controlled environment and data acquisition within the laboratory. Svalbard field testing in particular showed the importance of utilising both image and multispectral data combined to identify mineralogy and lithology. Field testing results often led to ambiguous identification of minerals, and demonstrates the limitation in relying on visual and coarse VIS-NIR reflectance data alone to direct the rover to sites consistent with past habitability. Further focused development, and especially data acquisition, is required to maximise the scientific value of the PanCam instrument for an astrobiology mission such as

ExoMars. This is particularly important if instrumentation such as Raman-LIBS and the Mars Infrared Mapper (MIMA) are to be limited to contact analysis only, or removed from the mission entirely.

Table 8.1. All minerals and biosignatures used to aid design and testing of the ExoMars PanCam instrument. Those that were positively detected (+), not detected (-), or ambiguously detected (~) by PanCam data alone are as indicated. Those that were only used for testing UV epifluorescence are indicated by (UV).

| Filter Selection | Laboratory testing | Field testing |
|---|---|--|
| Nontronite | Nontronite*(~) | Olivine (~) |
| Montmorillonite | Montmorillonite*(-) | Pyroxene: augite/diopside (+) |
| Opaline Silica | Opaline Silica (+) | Serpentine* (-) |
| Kieserite | Gypsum (UV) (+) | Haematite*(+) |
| Gypsum | Alunite* (+) | Goethite (+) |
| Alunite | Jarosite (+) | Magnesite (+) |
| Jarosite | Sulphur (-) | Quartz (~) |
| | Haematite (-) | Opaline Silica (~) |
| | Fossilised life (-) | Calcite(~) |
| | Photosynthetic pigments (UV) (+) | Photosynthetic pigments (+) |
| | | Fossilised life (-) |
| Spectral data from the USGS spectral database | Mineral components or deposits within untreated Martian analogue samples from Iceland | Mineral components or deposits within in-situ field outcrops in Svalbard |

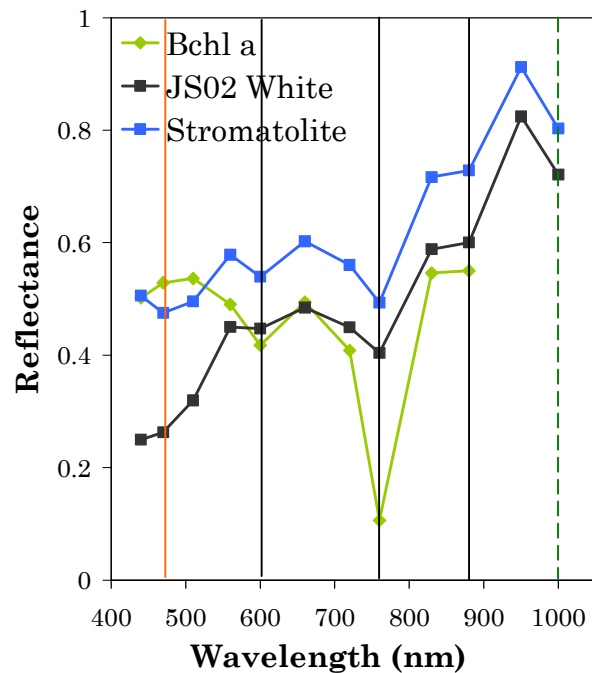
*Unconfirmed minerals. The rest have been confirmed by Raman spectroscopy or EDS analysis, thin section petrography, hand specimen, or previously published work.

Additionally, it was found that PanCam multispectral imaging was unable to detect extinct biosignatures or extant cryptoendolithic life within rocks. This has implications regarding remote site and target selection for rover operations, and is particularly dependant on whether the intention is to search for extinct or extant life. For example, cryptoendolithic life may not necessarily inhabit lithologies that are indicative of past habitability. So faced with the option of two separate sites, one containing a phyllosilicates rich lithology, and the other rich in a translucent mineral crust such as gypsum or silica, PanCam data alone could not be relied upon to indicate any preference towards one site or another.

There may be one exception to this conclusion. PanCam imaging at Jotun Springs revealed spectral characteristics consistent with a variety of photosynthetic pigments, firstly in the well developed microbial mats, and secondly in the carbonate precipitate around the edge of the spring, which exhibited a large absorption at 760nm (Chapter 7, Figure 7.15). This absorption is consistent with that for bacteriochlorophyll *a* (Bchl *a*), and, being surrounded

by extant microbial biomats, it was inferred that this absorption was caused by actively photosynthesising communities either in between the unconsolidated carbonate precipitate grains, or perhaps just below the surface. PanCam was also used for imaging fossil Precambrian (750 – 800Ma) stromatolite structures for a mission simulation activity undertaken by the whole AMASE team, results of which have not been described here in this thesis. The PanCam spectrum exhibited by these stromatolites bears striking similarity to the carbonate precipitate at Jotun Springs (Figure 8.2). In particular, many of the absorption features of these two spectra are typical for photosynthetic pigments, especially the large absorption at 760nm, which is characteristic of Bchl *a* (absorption lines shown on Figure 8.2).

Figure 8.2. PanCam spectra of Precambrian stromatolites ('Stromatolite') and the carbonate precipitate at Jotun Springs ('JS02 White'). Also shown is the spectrum for Bchl *a* (Viscarra Rossel *et al.* 2006), and absorption lines are shown for Bchl *a* (black), Bchl *e* (orange), and Bchl *b* (dashed green), NB: absorption wavelength for Bchl *b* is ~1020 – 1040nm, just outside the PanCam spectral range, indicated with a dashed line.



Whereas the carbonate precipitate at Jotun Springs was surrounded by extant photosynthesising communities, the stromatolites have, since their formation, been silicified (Knoll 1984) and tectonically overturned by ~90° (pers. comm. Dr. Andrew Steele), destroying all presence of the active microbial communities that made them. Therefore, assuming the PanCam spectrum does indeed signify the

presence of Bchl *a*, there are two potential explanations: Firstly, that this pigment is simply present within epilithic communities living on the surface of the stromatolite unit, or secondly that the pigment is a vestige of the photosynthetic communities that originally existed within the stromatolite during formation.

With regards to the first possible cause of this feature, the cold and dry Arctic environment results in little vegetation or lichens, and inspection of the stromatolite deposits in the field reveals that there is no significant macroscopic life on the stromatolites themselves, neither on the surface nor within cracks/depressions within the rocks. Additionally, if this were the cause, it would be more likely for the spectrum to have absorption features typical of Chlorophyll pigments, such as the large Chl *a* absorption at 660nm. In fact, the spectrum exhibits a reflectance peak at this wavelength, consistent with Bchl *a*. Likewise, this spectral feature was not present during imaging of any other rock targets from the other PanCam testing sites in Svalbard.

A more exciting, but currently entirely speculative possibility, is that Bacteriochlorophyll pigments have been preserved within the fossilised stromatolites. Green sulphur and purple bacteria are a common constituents of the stromatolite phototrophic microbial community (Konhauser 2007), and contain bacteriochlorophylls *c*, *d*, and *e*, and bacteriochlorophylls *a* and *b* respectively (Le Olson *et al.* 2007). The stromatolite formation imaged by PanCam contains numerous black phosphorite nodules 1 – 4mm in size (Knoll 1984). Such nodules are known to preserve organic matter from the original microbial community (Konhauser 2007), and these could be the cause of the strong absorption features seen in the outcrop spectrum. Although these nodules are small, they are distributed all over the surface of the outcrop, and their contrast to the otherwise pale grey outcrop may emphasize their spectral features, particularly as neither silica or carbonate have strong spectral features of their own in this wavelength range. Controlled spectral analysis and identification of organics from samples of this stromatolite outcrop could potentially shed light on this issue.

8.3.2 Application to future astrobiology missions

Whilst the work conducted here was in relation to the ExoMars mission specifically, the results and novel methods employed also have relevance to other planned astrobiology missions. Most notable of these is the NASA Mars Science Laboratory (MSL) rover ‘Curiosity’, which, like ExoMars, has a clearly defined life-detection objective. This rover has a stereo camera – the ‘Mastcam’ – which is also equipped with a filter wheel (Malin *et al.* (2005). The filter wavelengths for the ‘geology’ filters are mostly identical to those selected for the MER Pancam (Bell *et al.* (2003), and in turn the Imager for Mars Pathfinder (Smith *et al.* (1997). Details of filter wavelengths for comparable missions are given in Table 5 in Appendix A. As such, there appears to be no attempt (so far) by the MSL team to maximise the filter selection for specific astrobiological science objectives, such as the identification of hydrated mineral terrains. Instead, the Mastcam is still optimised to detect and distinguish iron oxide mineralogy, as originally implemented in the Pathfinder mission (Smith *et al.* 1997). However, in relation to this it is noted that the MSL rover is equipped with additional instruments for remote target analysis, including the ChemCam (Wiens *et al.* 2008) which provides both elemental data and close-up imaging from remote targets. As such, the Mastcam is not solely relied upon to provide remote target selection, as may be the case with the ExoMars mission.

8.4 Future Work

During this work, it became apparent that the microbiology of both extinct and active subglacial volcanic environments is still largely unexplored, yet exhibits huge potential in relation to understanding of volcanic terrestrial habitats, and also in the wider context of the existence and evolution of life elsewhere. One particular locality was identified somewhat serendipitously during fieldwork in Iceland in July 2007. However, due to time and equipment constraints, only limited sampling and data collection was undertaken at the time, and as such this locality has not formed a main part of this thesis. Here in this section, this field site is described, and details of potential future work are outlined.

8.4.1 The Kverkfjöll subglacial caldera

Kverkfjöll is a partially subglacial central volcano, on the northern margin of Vatnajökull. It consists of two calderas, of which the northernmost caldera is only partially covered by the glacier (Hoskuldsson *et al.* 2006). This volcano is located almost directly above the Icelandic hot spot (Sigvaldason *et al.* 1974), which coupled with its position in the neo-volcanic zone, results in very high heat flow and intensive thermal activity (Olafsson *et al.* 2000). During fieldwork in July 2007, the summit of the Kverkfjöll subglacial caldera was visited with the aim to collect hydrothermal samples from the surface environment of an active subglacial volcanic system. This environment is geographically isolated, and the main inputs are from the melting overlying glacial ice and volcanic gases emitted from the underlying volcanic system, coupled with seasonal snowfall.

Figure 8.3 Map showing the locations of Kverkfjöll sample sites KV004 and KV006. Dotted line indicates the estimated position of the northern caldera rim.



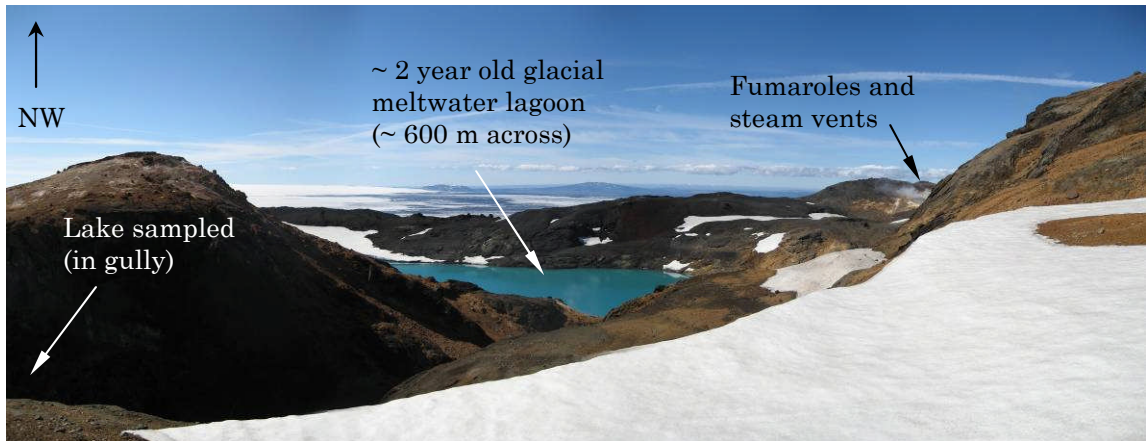
Four glacial meltwater pools were identified on the western rim of the Kverkfjöll subglacial northern caldera. This area consists of three geothermal fields, which going south to north are: 'Hveradalur', 'Hveraskál' and 'Hveratagl'. Of these, two were sampled, Hveradalur and Hveratagl, and the location of these is shown in Figure 8.3. These environments have formed as a result of high heat flow at Kverkfjöll, which in isolated pockets has melted the glacier and resulted in

hydrothermal activity. At Hveradalur, one pool was sampled that was isolated from active volcanic input (such as fumaroles), and resided in an area previously affected by hydrothermal activity. At Hveratagl, several pools were situated amongst active fumaroles, vents and springs. These two geothermal sites are described below in more detail, together with environmental data that was collected at the time.

8.4.2 Hveradalur

This geothermal field sits near the summit of the Kverkfjöll region and consists of numerous steep and very active solfataritic gorges surrounded by ice and altered hyaloclastites. Nearby to the SE of this area are two large glacial meltwater lakes. Of these, one has been forming since 1953 where it began as a small, steaming depression within the ice (Thórarinnsson 1953). Since then, another one just to the north has formed more recently, within the last 2 or so years. These lakes were inaccessible at the time, and so a nearby meltwater pool of a similar nature was sampled. This was likely to be a product of seasonal summer melting of the glacier.

Figure 8.4. Contextual photograph of the area around Hveradalur. The blue meltwater lagoon shown can be seen in Figure 8.3 (northern most lake). (Photo credit Dr. Katie Joy)



The pool sampled was ~12m in length and situated in a ground hollow surrounded by heavily altered hyaloclastite, basalt and other volcanics. The pool was bordered on all sides by lavas, and was being fed by a small meltwater stream originating from a section of ice lying 3-4 meters away. On the bottom and the margins of the lake were fine to sandy heterogeneous sediments of an orange – brown colour. These sediments are most likely a combination of

weathered basaltic lavas and hydrothermal soils. Loose rocks within and surrounding the pool consisted of heavily altered scoriaceous lava. The pH of this pool was measured to be 6.5, with a temperature of 9.1°C.

8.4.3 Hveratagl

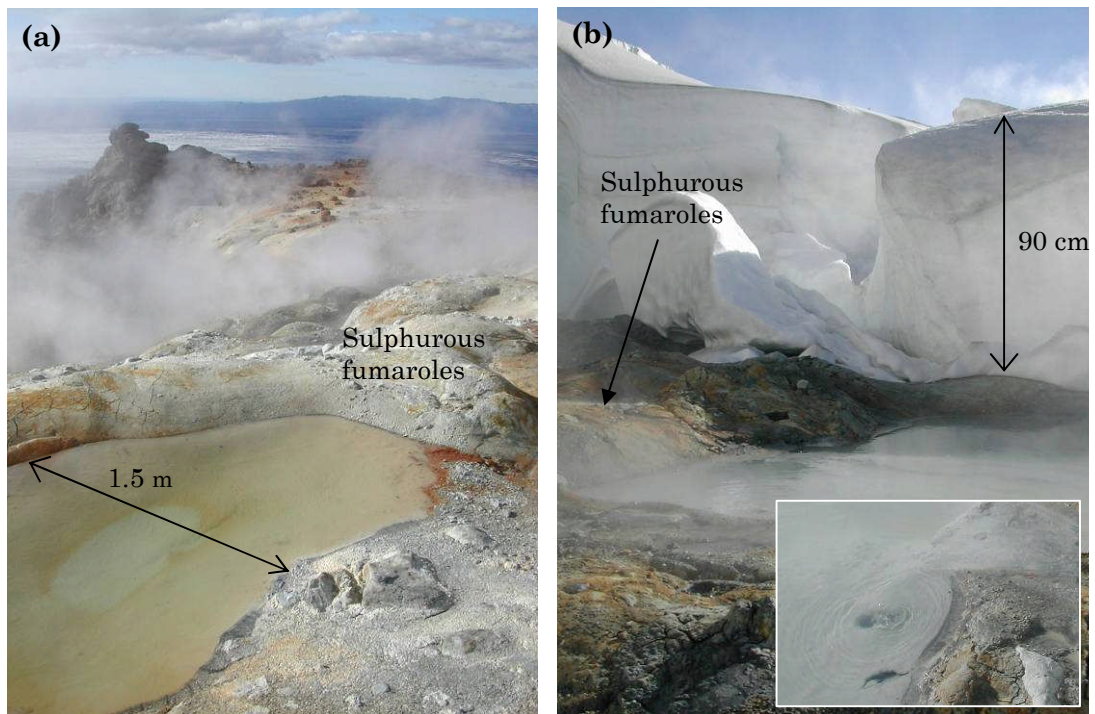
This site lies to the north of Hveradalur and is a single solfatara field bordered by thick ice on one margin and a steep break in slope on the other. The field consists of numerous sulphurous fumaroles, iron-rich springs, boiling mud pots and glacial meltwater pools. Geochemical monitoring work at Kverkjöll has shown fumarole gases in the Hveratagl geothermal field to be dominantly rich in CO₂, H₂S and H₂ (Ólafsson *et al.* 2000). The glacial meltwater forms a shallow braided river which emerges from a collapsed ice cave and runs through one half of the field. Nearby, glacial meltwater also forms two isolated small pools, which were the focus of the sampling in this locality. Like the meltwater pools sampled at Hveradalur, these pools are likely to be a result of seasonal melting of the glacier. The formation of soft sediments at the bottom of these pools suggests these pools form annually in the same location. Both pools were of similar size, ~ 1.5m x 80cm, and like the larger ponds described in the upper geothermal field are lined with a layer of sediment of undetermined thickness along the bottom. Numerous sulphur depositing fumaroles bordered both pools, and whilst one was fed with meltwater from nearby ice (Figure 8.5a), the other lay adjacent to the glacier itself (Figure 8.5b).

8.4.4 Initial Environmental Data

Environmental data collected at these sites consisted of pH, temperature and redox potential (ORP). These three parameters were chosen because pH and temperature have a huge effect on an organisms function and so play a major role in limiting what can live in a particular range of conditions. Redox potential was chosen due to the fact that areas of hydrothermal activity often have large differences in oxidation/reduction states and are very chemically and physically active. Both pools were acidic, with pH ranging between 3.50 (± 0.04) and 3.75 (± 0.13), and temperatures were warm, between 20.6°C (± 0.47) and 11.1°C (± 0.81). However, there was a large difference in oxidation state. The first pool (Figure 8.5a) was oxidizing, as indicated by an ORP measurement of +375mV (± 3.13). This was additionally verified by the field observation of oxidized iron

deposits in and around the pool. Conversely, the second pool was very reducing with a measurement of -291mV (± 2.34), indicating a completely anoxic environment, potentially a result of the continuous stream of volcanic gas bubbles emerging from the floor of the pool. Due to this difference in redox state, two very different microbial communities would be expected to inhabit these two pools, despite their close proximity.

Figure 8.5. Hydrothermal pools at Hveratagl (a) acidic and oxidising, and (b) acidic and reducing, possibly caused by volcanic gas input (inset).



Based on the initial observations taken during sampling, it can be seen that solfatara systems that reside within glaciers or ice caps are extremely isolated. Surface observations suggest the primary inputs into this system are the overlying glacier, in the form of meltwater, and volcanic gasses emitted via numerous fumaroles and fissures in the ground. Additionally, surface water in the form of the pools sampled is continually interacting with the underlying hydrothermally altered volcanic sediments. There has yet to be any extensive investigation into solfatara environments within glacial settings and their associated microbial communities and phylogenetic diversity. Those that have been conducted include studies at Tramway Ridge, Antarctica (Soo *et al.* 2009) and fumaroles in the hyperarid region of the Andes (Costello *et al.* 2009).

Therefore it is believed that future studies at the Kverkfjoll geothermal field will build on these past studies.

8.5 Final Conclusions

The search for life on other planetary bodies must, in part, begin on Earth, utilising the combination of planetary analogue environments and their interaction with terrestrial life. This multidisciplinary work has been wide-ranging, utilising a variety of biomolecular, experimental, and analytical techniques, but with the overarching focus of contributing to the astrobiological exploration of Mars. Here, the results of this work are summarised into the following conclusions:

- Multidisciplinary research centred around a focused objective can expand our knowledge regarding the search for life on Mars. In particular, such investigations link traditionally unrelated techniques and lines of enquiry, and demonstrates the necessity to approach astrobiology research from different angles.
- Basaltic hyaloclastite and pillow lava provides a habitat for prokaryotic communities, many of which are chemoheterotrophic, and are genetically similar to species that are radiation and desiccation resistant. Notably, hyaloclastite was found to support a more diverse microbial community, which demonstrates the importance of lithology on the habitability of an environment.
- The indigenous bacterial communities inhabiting basaltic pillow lava are able to survive present day Martian conditions for one week, whilst within a simulated subglacial volcanic environment. In comparison, when this community was fully exposed to the same Martian conditions, survivability was low.
- *Rubrobacter radiotolerans* was identified within basaltic lava through a 16S phylogenetic survey, and was also found to survive exposure to Martian conditions whilst within the basaltic lava environment. As such,

this strain could be used as a model organism for future Martian astrobiology research.

- Whilst bioalteration textures within glass-rich basaltic lavas from the seafloor are widespread, the same cannot be said of their subglacially-erupted continental counterparts. This shows for the first time that the generation of such putative biosignatures is strongly controlled by the environmental setting. As such, it cannot be assumed that bioalteration textures will form in basaltic glass merely in the presence of hydrous alteration.
- Utilising Martian analogue geological samples and environments from Iceland and Svalbard proved effective at furthering the development and testing of the ExoMars Panoramic Camera instrument. In particular, the need to update the technology to meet the requirement to remotely identify evidence of habitability was addressed. Specifically, this involved accounting for the many hydrated minerals now known to be present within the Martian crust.

It is hoped that the findings from the work conducted for this PhD thesis will contribute on some level to the ongoing search for life on Mars, and that this work can be explored further through future research.

REFERENCES

- Abramov, O., Kring, D. A. (2005) Impact-induced hydrothermal activity on early Mars. *Journal of Geophysical Research* 110, E12S09.
- Albuquerque, L., Simoes, C., Nobre, M. F., Pino, N. M., Battista, J. R., Silva, M. T., Rainey, F. A., da Costa, M. S. (2005) *Truepera radiovictrix* gen. nov., sp. nov., a new radiation resistant species and the proposal of *Trueperaceae* fam. nov. *FEMS Microbiology Letters* 247, 161 – 169.
- Alfaro, R., Brandsdottir, B., Rowlands, D. P., White, R. S. and Gudmundsson, M. T. (2007) Structure of the Grimsvötn central volcano under the Vatnajökull icecap, Iceland. *Geophysical Journal International* 168, 863 – 876.
- Allen, C. G. (1979) Volcano-ice interactions on Mars. *Journal of Geophysical Research* 84, 8048 – 8059.
- Allen, C. C., Albert, F. G., Chafetz, H. S., Combie, J., Graham, C. R., Kieft, T. L., Kivett, S. J., McKay, D. S., Steele, A., Taunton, A. E., Taylor, M. R., Thomas-Keprta, K. L., Westall, F. (2000) Microscopic Physical Biomarkers in Carbonate Hot Springs : Implications in the Search for Life on Mars. *Icarus* 147, 49 – 67.
- Altschul, S. F., Gish, W., Miller, W., Myers, E. W. & Lipman, D. J. (1990) Basic local alignment search tool. *Journal of Molecular Biology* 215, 403 – 410.
- Amann, R. I., Ludwig, W., Schleifer, K-H. (1995) Phylogenetic Identification and In Situ Detection of Individual Microbial Cells without Cultivation. *Microbiological Reviews* 59, 143 – 169.
- Amils, R., Gonza lez-Toril, E., Fernandez-Remolar, D., Gomez, F. Aguilera, A., Rodriguez, N., Malki, M., Garcia-Moyano, A., Fairen, A. G., de la Fuente, V., Sanz, J. L. (2007) Extreme environments as Mars terrestrial analogs: The Rio Tinto case. *Planetary and Space Science* 55, 370 – 381.
- An, D-S., Lee, H-G., Im, W-T., Liu, Q-M., Lee, S-T. (2007) *Segetibacter koreensis* gen. nov., sp. nov., a novel member of the phylum *Bacteroidetes*, isolated from the soil of a ginseng field in South Korea. *International Journal of Systematic and Evolutionary Microbiology* 57, 1828 – 1833.
- Aragno, M., Schlegel, H. G. (1978) *Aquaspirillum autotrophicum*, a New Species of Hydrogen Oxidizing, Facultatively Autotrophic Bacteria. *International Journal of Systematic Bacteriology* 28, 112 – 116.
- Aubrey, A., Cleaves, H. J., Chalmers, J. H., Skelley, A. M., Mathies, R. A., Grunthaner, F., Ehrenfreund, P. and Bada, J. L. (2006) Sulfate minerals and organic compounds on Mars. *Geology* 34, 357 – 360.

- Aubrey, A., Cleaves, H. J., Chalmers, J. H. and Bada, J. L. (2005) Sulfate minerals as targets for biomolecule detection on Mars. *Geochemica et Cosmochimica Acta* 69 (10): A533.
- Bailey, M. J. (1995) Extraction of DNA from the phyllosphere. In *Nucleic Acids in the Environment: Methods and Applications*, pp. 89-109. Edited by J. T. Trevors & J. D. Elsas. Berlin: Springer-Verlag.
- Baker, G. C., Smith, J. J., Cowan, D. A. (2003) Review and re-analysis of domain-specific 16S primers. *Journal of Microbiological Methods* 55, 541– 555
- Baker, V. R., Strom, R. G., Gulick, V. C., Kargel, J. S., Komatsu, G., Kale, V. S. (1991) Ancient oceans, ice sheets and the hydrological cycle on Mars. *Nature* 352, 589 – 594.
- Bandfield, J. L., Glotch, T. D., Christensen, P. R. (2003) Spectroscopic identification of carbonate minerals in the Martian dust. *Science* 301, 1084 – 1087.
- Banerjee, N. R., Muehlenbachs, K., Furnes, H., Staudigel, H., de Wit, M. (2004a) Potential for early life hosted in basaltic glass on a wet Mars. In: Proceedings of the Second Conference on Early Mars, Jackson Hole, WY, October 11–15. Lunar Planetary Institute (Abstract 8048).
- Banerjee, N. R., Furnes, H., Muehlenbachs, K., Staudigel, H. (2004b) Microbial alteration of volcanic glass in modern and ancient oceanic crust as a proxy for studies of extraterrestrial material. In: Proceedings of the Lunar and Planetary Science Conference, XXXV, LPI Contribution No. 1197, abstract 1248.
- Banerjee, N. R., Furnes, H., Simonetti, A., Muehlenbachs, K., Staudigel, H., deWit, M., Van Kranendonk, M. (2006) Ancient microbial alteration of oceanic crust on two early Archean Cratons and the search for extraterrestrial life. In: Proceedings of the Lunar and Planetary Science Conference, XXXVII, Abstract 2156.
- Banks, D., Siewers, U., Sletten, R. S., Haldorsen, S., Dale, B., Heim, M., Swensen, B. (1999) The thermal springs of Bockfjorden, Svalbard: II: selected aspects of trace element hydrochemistry. *Geothermics* 28, 713 – 728.
- Babalola, O. O., Kirby, B. M., Le Roes-Hill, M., Cook, A. E., Cary, S. C. Burton, S. G., Cowan, D. A. (2009) Phylogenetic analysis of actinobacterial populations associated with Antarctic Dry Valley mineral soils. *Environmental Microbiology* 11, 566 – 576.
- Bazalgette Courrèges-Lacoste, G., Ahlers, B., Rull Pérez, F. (2007) Combined Raman spectrometer laser-induced breakdown spectrometer for the next ESA mission to Mars. *Spectrochim. Acta, Part A*, 68, 1023 – 1028.
- Bell, F. G. *Engineering Properties of Rocks and Soils* (Fourth Edition). Blackwell Publishers (2000).

Bell, J. F., J. R. Joseph, J. Sohl-Dickstein, H. Arneson, M. Johnson, M. Lemmon, and D. Savransky. (2006) In-Flight Calibration of the Mars Exploration Rover Panoramic Camera Instrument. *J. Geophys. Res.* 111 (E02S03).

Bell, J. F., Squyres, S. W., Herkenhoff, K. E., Maki, J. N., Arneson, H. M., Brown, D., Collins, S. A., Dingizian, A., Elliot, S. T., Hagerott, E. C., Hayes, A. G., Johnson, M. J., Johnson, J. R., Joseph, J., Kinch, K., Lemmon, M. T., Morris, R. V., Scherr, L., Schwochert, M., Shepard, M. K., Smith, G. H., Sohl-Dickstein, J. N., Sullivan, R. J., Sullivan, W. T., Wadsworth, M. (2003). Mars Exploration Rover Athena Panoramic Camera (Pancam) investigation. *Journal of Geophysical Research* 108 (E12), 8063.

Bell, J. F., Squyres, S. W., Arvidson, R. E., Arneson, H. M., Bass, D., Blaney, D., Cabrol, N., Calvin, W., Farmer, J., Farrand, W. H., Goetz, W., Golombek, M., Grant, J. A., Greeley, R., Guinness, E., Hayes, A. G., Hubbard, M. Y. H., Herkenhoff, K. E., Johnson, M. J., Johnson, J. R., Joseph, J., Kinch, K. M., Lemmon, M. T., Li, R., Madsen, M. B., Maki, J. N., Malin, M., McCartney, E., McLennan, S., McSween Jr., H. Y., Ming, D. W., Moersch, J. E., Morris, R. V., Noe Dobrea, E. Z., Parker, T. J., Proton, J., Rice Jr., J. W., Seelos, F., Soderblom, J., Soderblom, L. A., Sohl-Dickstein, J. N., Sullivan, R. J., Wolff, M. J., Wang, A. (2004) Pancam Multispectral Imaging Results from the Spirit Rover at Gusev Crater. *Science* 305, 800 – 806.

Bibring, J.-P., Arvidson, R. E., Gendrin, A., Gondet, B., Langevin, Y., Le Mouelic, S., Mangold, N., Morris, R. V., Mustard, J. F., Poulet, F., Quantin, C., Sotin, C. (2007) Coupled Ferric Oxides and Sulfates on the Martian Surface. *Science* 317, 1206 – 1210.

Bibring, J.-P., Y. Langevin, J. F. Mustard, F. Poulet, R. Arvidson, A. Gendrin, B. Gondet, N. Mangold, P. Pinet, and F. Forget (2006) Global mineralogical and aqueous Mars history derived from the OMEGA/Mars Express data, *Science* 312, 400 – 404.

Bibring, J.-P., Langevin, Y., Gendrin, A., Gondet, B., Poulet, F., Berthe, M., Soufflot, A., Arvidson, R., Mangold, N., Mustard, J., Drossart, P. and the OMEGA team. (2005) Mars Surface Diversity as Revealed by the OMEGA/Mars Express Observations. *Science* 307, 1576 – 1581.

Bishop, J. L., Dobrea, E. Z. D., McKeown, N., K., Parente, M., Ehlmann, B. L., Michalski, J. R., Milliken, R. E., Poulet, D., Swayze, G. A., Mustard, J. F., Murchie, S. L., Bibring, J.-P. (2008) Phyllosilicate Diversity and Past Aqueous Activity Revealed at Mawrth Vallis, Mars. *Science* 321, 830 – 833.

Bishop (2005a) Hydrated Minerals on Mars. In: Water on Mars and Life, Tetsuya Tokano (ed.), Adv. Astrobiol. Biogeophys., pp. 65-96.

Bishop, J. L., Dyar, M. D., Lane, M. D. and Banfield, J. F. (2004a). Spectral identification of hydrated sulfates on Mars and comparison with acidic environments on Earth. *International Journal of Astrobiology* 3, 275 – 285.

Bishop, J. L., Murad, E., Lane, M., Mancinelli, R. L. (2004b) Multiple techniques for mineral identification on Mars: a study of hydrothermal rocks as potential analogues for astrobiology sites on Mars. *Icarus* 169, 311 – 323.

Bishop, J. L., H. Fröschl, and R. L. Mancinelli (1998) Alteration processes in volcanic soils and identification of exobiologically important weathering products on Mars using remote sensing. *Journal of Geophysical Research* 103, 31457–31476.

Björnsson, H. (2002) Subglacial lakes and Jökulhlaups in Iceland. *Global and Planetary Change* 35, 255 – 271.

Bloch, S., Bischoff, J. L. (1979) The effect of low-temperature alteration of basalt on the oceanic budget of potassium. *Geology* 7, 193 – 196.

Boston, P. J., Ivanov, M. V., McKay, C. P. (1992) On the Possibility of Chemosynthetic Ecosystems in Subsurface Habitats on Mars. *Icarus* 95, 300 – 308.

Bourgeois, O., Dauteuil, O., Van Vliet-Lanoe, B. (1998) Pleistocene subglacial volcanism in Iceland: tectonic implications. *Earth and Planetary Science Letters* 164, 165 –178.

Brady, N.C. and Weil, R.R. (2002) *The Nature and Properties of Soils*, Prentice Hall, Upper Saddle River, NJ.

Bryant, D. A., Garcia Costas, A. M., Maresca, J. A., Chew, A. G. M., Klatt, C. G., Bateson, M. M., Tallon, L. J., Hostetler, J., Nelson, W. V., Heidelberg, J. F., Ward, D. M. (2007) *Candidatus* Chloroacidobacterium thermophilum: An Aerobic Phototrophic Acidobacterium. *Science* 317, 523 – 526.

Bryant, D. A., Frigaard, N. U. (2006) Prokaryotic photosynthesis and phototrophy illuminated. *Trends in Microbiology* 14, 488 – 496.

Buckley, D. H., Huangyutitham, V., Nelson, T. A., Rumberger, A. and Thies, J. E. (2006) Diversity of Planctomycetes in Soil in Relation to Soil History and Environmental Heterogeneity. *Applied and Environmental Microbiology* 72, 4522 – 4531.

Buczolits, S., E. B. M. Denner, P. Kämpfer, and H.-J. Busse. (2006) Proposal of *Hymenobacter norwichensis* sp. nov., classification of ‘*Taxeobacter ocellatus*’, ‘*Taxeobacter gelipurpurascens*’ and ‘*Taxeobacter chitinivorans*’ as *Hymenobacter ocellatus* sp. nov., *Hymenobacter gelipurpurascens* sp. nov. and *Hymenobacter chitinivorans* sp. nov., respectively, and emended description of the genus *Hymenobacter* Hirsch et al. 1999. *International Journal of Systematic and Evolutionary Microbiology* 56, 2071 – 2078

Cady, S.L., Farmer, J.D., (1996) Fossilisation processes in siliceous thermal springs: Trends in preservation along thermal gradients. In: Evolution of Hydrothermal Systems on Earth (and Mars?). In: Ciba Foundation Symposium, vol. 202. Wiley, Chichester, pp. 105 –173.

Carr, M. H., Head, J. W (2003) Basal melting of snow on early Mars: A possible origin of some valley networks. *Geophysical Research Letters*, 30, 2245.

Carr, M. H. (1996) Channels and valleys on Mars: cold climate features formed as a result of a thickening cryosphere. *Planetary and Space Science* 44, 1411 – 1423.

Carr, M. H. (1987) Water on Mars. *Nature* 326, 30-35.

Cavicchioli, R. (2002) Extremophiles and the Search for Extraterrestrial Life. *Astrobiology* 2, 281 – 292.

Chapman, M. G., Smellie, J. L. (2007) Mars interior layered deposits and terrestrial sub-ice volcanoes compared: observations and interpretations of similar geomorphic characteristics. In *The Geology of Mars: Evidence from Earth-Based Analog*, edited by M. G. Chapman. Published by Cambridge University Press, Cambridge, UK, 2007, p.178.

Chapman, M. G. (2003) Sub-ice volcanoes and ancient oceans/lakes: a Martian challenge. *Global and Planetary Change* 35, 185 – 198.

Chapman, M. G., Gudmundsson, M. T., Russell, A. J., Hare, T. M. (2003) Possible Juventae Chasma subice volcanic eruptions and Maja Valles ice outburst floods on Mars: Implications of Mars Global Surveyor crater densities, geomorphology, and topography. *Journal of Geophysical Research* 108, 5113.

Chapman, M. G., Tanaka, K. L. (2002) Related Magma–Ice Interactions: Possible Origins of Chasmata, Chaos, and Surface Materials in Xanthe, Margaritifer, and Meridiani Terrae, Mars. *Icarus* 155, 324 – 339.

Chapman, M.G., Tanaka, K.L. (2001) Interior trough deposits on Mars: Subice volcanoes? *Journal of Geophysical Research* 106, 10087 – 10100.

Chapman, M. G., Allen, C. C., Gudmundsson, M. T., Gulick, V. C., Jakobsson, S. P., Lucchitta, B. K., Skilling, I. P., Waitt, R. B. (2000) in *Environmental Effects on Volcanic Eruptions: From Deep Oceans to Deep Space*, Edited by Zimbelman and Gregg, Kluwer Academic/Plenum Publishers, New York, 2000.

Chapman, M.G. (1994) Evidence, age, and thickness of a frozen paleolake in Utopia Planitia, Mars. *Icarus*, 109, 393 – 406.

Chen, J., Blume, H-P., Beyer, L. (2000) Weathering of rocks induced by lichen colonization - a review. *Catena* 39, 121–146.

Chevrier, V., Mathe, P. E. (2007) Mineralogy and evolution of the surface of Mars: A review. *Planetary and Space Science* 55, 289 – 314.

Clark B. C. (1998) Surviving the limits to life at the surface of Mars. *Journal of Geophysical Research:Planets* 103, 445 – 455.

Clark, R. N., Swayze, G. A., Wise, R., Livo, E., Hoefen, T., Kokaly, R., Sutley, S.J., (2007) USGS digital spectral library splib06a: U.S. Geological Survey, Digital Data Series 231.

Clark, R. N., Swayze, G. A., Gallagher, A. G., King, T. V. V. and Calvin, W. M. (1993) The U. S. Geological Survey, Digital Spectral Library: Version 1: 0.2 to 3.0 microns, U.S. Geological Survey Open File Report 93 – 592.

Clifford, S. M. (1993) A model for the hydrologic and climatic behaviour of water on Mars. *Journal of Geophysical Research* 98, 10973-11016.

Cockell, C. S., Olsson-Francis, K., Herrera, A., and Meunier, A. (2009a) Alteration textures in terrestrial volcanic glass and the associated bacterial community. *Geobiology* 7, 50 -65.

Cockell, C. S., Olsson, K., Knowles, F., Kelly, L., Herrera, A., Thorsteinsson, T., Marteinson, V. (2009b) Bacteria in Weathered Basaltic Glass, Iceland. *Geomicrobiology Journal* 26, 491 – 507.

Cockell, C. S., Schuerger, A. C., Billi, D., Friedmann, E. I. and Panitz, C. (2005) Effects of a Simulated Martian UV Flux on the Cyanobacterium, *Chroococcidiopsis* sp. 029. *Astrobiology* 5, 127 – 140.

Cole J. R, Chai B, Marsh T. L, Farris R. J, Wang Q, Kulam S. A, Chandra S, McGarrell D. M, Schmidt T. M, Garrity G. M, Tiedje J. M. The Ribosomal Database Project (RDP-II): previewing a new autoaligner that allows regular updates and the new prokaryotic taxonomy. *Nucleic Acids Research* 31, 442 – 443.

Costello, E. K., Halloy, S. R. P., Reed, S. C., Sowell, P. Schmidt, S. K. (2009) Fumarole-Supported Islands of Biodiversity within a Hyperarid, High-Elevation Landscape on Socoma Volcano, Puna de Atacama, Andes. *Applied Environmental Microbiology* 75, 735 – 747.

Cowan, D. A. (2009) Cryptic microbial communities in Antarctic deserts. *PNAS* 106, 19749 – 19750.

Cowan, D. A., Russell, N. J., Mamais, A., Sheppard, D. M. (2002) Antarctic Dry Valley mineral soils contain unexpectedly high levels of microbial biomass. *Extremophiles* 6, 431 – 436.

Da Silva, J. J. R. F., Williams, R. J. P. (2001) The biological chemistry of the elements – The inorganic chemistry of life. Second edition. Oxford University Press.

Diaz, B. and Schulze-Makuch (2006) Microbial Survival Rates of *Escherichia coli* and *Deinococcus radiodurans* Under Low Temperature, Low Pressure, and UV-Irradiation Conditions, and Their Relevance to Possible Martian Life. *Astrobiology* 6, 332 – 347.

Dodds, W. K., Gudder, D. A., Mollenhauer, D. (1995) The Ecology of *Nostoc*. *Journal of Phycology* 31, 2 – 18.

Downs, R. T. (2006) The RRUFF Project: an integrated study of the chemistry, crystallography, Raman and infrared spectroscopy of minerals. Program and Abstracts of the 19th General Meeting of the International Mineralogical Association in Kobe, Japan. 003-13

Dworkin, M. and Falkow, S. (2006) *The prokaryotes: a handbook on the biology of bacteria*. Volume 7, Edition 3. Springer.

Edwards, H. G. M., Russell, N. C., Wynn-Williams, D. D. (1997) Fourier Transform Raman Spectroscopic and Scanning Electron Microscopic Study of Cryptoendolithic Lichens from Antarctica. *Journal of Raman Spectroscopy* 28, 685 – 690.

Edwards, H. G. M., Mohsin, M. A., Sadooni, F. N., Nik Hassan, N. F. Munshi, T. (2006) Life in the sabkha: Raman spectroscopy of halotrophic extremophiles of relevance to planetary exploration. *Analytical and Bioanalytical Chemistry* 385, 46 – 56.

Edwards, K. J., Rogers, D. R., Wirsen, C. O., McCollom, T. M. (2003) Isolation and characterization of novel psychrophilic, neutrophilic, Fe-oxidizing, chemolithoautotrophic alpha- and gamma-Proteobacteria from the deep sea. *Applied and Environmental Microbiology* 69, 2906 – 2913.

Edwards, B. R., Russell, J. K., Anderson R. G. (2002) Subglacial, phonolitic volcanism at Hoodoo Mountain volcano, northern Canadian Cordillera. *Bulletin of Volcanology* 64, 254 – 272.

Ehlmann, B. L., Mustard, J. F., Murchie, S. L., Poulet, F., Bishop, J. L., Brown, A. J., Calvin, W. M., Clark, R. N., Des Marais, D. J., Milliken, R. E., Roach, L. H., Roush, T. L., Swayze, G. A., Wray, J. J. (2008a) Orbital Identification of Carbonate-Bearing Rocks on Mars. *Science* 322, 1828 – 1832.

Ehlmann, B. L., Mustard, J. F., Fassett, C. I., Schon, S. C., Head, J. W., Des Marais, D. J., Grant, J. A., Murchie, S. L. (2008b) Clay minerals in delta deposits and organic preservation potential on Mars. *Nature Geoscience* 1, 355 – 358.

Ellery, A., Wynn-Williams, D. (2003) Why Raman Spectroscopy on Mars? – A Case of the Right Tool for the Right Job. *Astrobiology* 3, 565 – 579.

Elo, S., Suiminen, I., Kampfer, P., Juhanoja, J., Salkinoja-Salonen, M., Haahtela, K. (2001) *Paenibacillus borealis* sp. nov., a nitrogen-fixing species isolated from spruce forest humus in Finland. *International Journal of Systematic and Evolutionary Microbiology* 51, 535 – 545.

Einarsson, Markús Á.: Climate of Iceland, in H. van Loon (editor): *World Survey of Climatology: 15: Climates of the Oceans*. Elsevier, Amsterdam, 1984, pp 673-697.

Evans, D. L., Adams, J. B. (1979) Comparison of Viking Lander multispectral images and laboratory reflectance spectra of terrestrial samples (1979). In: Lunar and Planetary Science Conference, 10th, Houston, Tex., March 19-23,

1979, Proceedings. Volume 2. (A80-23617 08-91) New York, Pergamon Press, Inc., 1979, p. 1829-1834.

Fagents, S. A., Lanagan, P., Greely, R. (2002). Rootless cones on Mars: a consequence of lava-ground interaction. From Smellie, J. L. & Chapman, M. G. (eds) 2002. *Volcano – Ice Interaction on Earth and Mars*. Geological Society, London, Special Publications, 202, 295 – 317.

Fagents, S. A., Thordarson, T. (2007) Rootless volcanic cones in Iceland and on Mars. In *The Geology of Mars: Evidence from Earth-Based Analog* edited by M. G. Chapman Published by Cambridge University Press, Cambridge, UK.

Farmer, J. D. (1996) Hydrothermal systems on Mars: an assessment of present evidence. *Evolution of hydrothermal ecosystems on Earth (and Mars?)*. Wiley, Chichester (Ciba Foundation Symposium 202), 273 – 299.

Farmer, J. D., Des Marais, D. J. (1999) Exploring for a record of ancient Martian life. *Journal of Geophysical Research* 104, 26977 – 26995

Farrand, W. H., J. F. Bell III, J. R. Johnson, R. E. Arvidson, L. S. Crumpler, J. A. Hurowitz, and C. Schröder (2008), Rock spectral classes observed by the Spirit Rover's Pancam on the Gusev Crater Plains and in the Columbia Hills, *J. Geophys. Res.*, 113, E12S38

Farrand, W.H., J.F. Bell III, J.R. Johnson, B.L. Joliff, A.H. Knoll, S.M. McLennan, S.W. Squyres, W.M. Calvin, J.P. Grotzinger, R.V. Morris, J. Soderblom, S.D. Thompson, W.A. Watters, and A.S. Yen (2007) Visible and near-infrared multispectral analysis of rocks at Meridiani Planum, Mars by the Mars Exploration Rover Opportunity, *J. Geophys Res.:Planets*, 112, E06S02, 10.1029/2006JE002773.

Farrand, W.H., J.F. Bell III, J.R. Johnson, S.W. Squyres, J. Soderblom, D.W. Ming (2006) Spectral variability among rocks in visible and near infrared multispectral Pancam data collected at Gusev Crater: Examinations using spectral mixture analysis and related techniques. *J. Geophys. Res.: Planets*, 111, E02S15.

Fassett, C. I., Head, J. W. (2007) Valley formation on martian volcanoes in the Hesperian: Evidence for melting of summit snowpack, caldera lake formation, drainage and erosion on Ceraunius Tholus. *Icarus* 189, 118 – 135.

Fell, J. W., Scorzetti, G., Connell, L., Craig, S. (2006) Biodiversity of micro-eukaryotes in Antarctic Dry Valley soils with <5% soil moisture. *Soil Biology and Biochemistry* 38, 3107 – 3119.

Felsenstein, J. 2005. PHYLIP (Phylogeny Inference Package) version 3.6. Distributed by the author. Department of Genome Sciences, University of Washington, Seattle.

Fisk, M. R., Popa, R., Mason, O. U., Storrie-Lombardi, M. C., Vicenzi, E.P. (2006) Iron-magnesium silicate bioweathering on earth (and Mars?) *Astrobiology*, 6, 48–68.

Fisk, M. R., Storrie-Lombardi, M. C., Douglas, S., Popa, R., McDonald, G., Di Meo-Savoie, C. (2003) Evidence of biological activity in Hawaiian subsurface basalts. *Geochem. Geophys. Geosyst.*, 4, 2003GC000387.

Fisk, M. R., Giovannoni, S. J. (1999a) Microbial weathering of igneous rocks: a tool for locating past life on Mars [abstract 199]. In 30th Lunar and Planetary Science Conference Abstracts, LPI Contribution No. 964, Lunar and Planetary Institute, Houston, pp. 1903.

Fisk, M.R., Giovannoni, S.J. 1999b, Sources of nutrients and energy for a deep biosphere on Mars. *Journal of Geophysical Research* 104, 11805–11815.

Fisk, M. R., Giovannoni, S. J., Thorseth, I. H. (1998) Alteration of oceanic volcanic glass: textural evidence of microbial activity. *Science* 281, 978 – 979.

Foster, T. L., Winans L. JR., Casey, R. C., Kirschner, L. E. (1978) Response of Terrestrial Microorganisms to a Simulated Martian Environment. *Applied and Environmental Microbiology* 35, 730 – 737.

Fridleifsson, I. B., Furnes, H., Atkins, F. B. (1982) Subglacial volcanics – on the control of magma chemistry on pillow dimensions. *Journal of Volcanology and Geothermal Research* 13, 103 – 117.

Friedmann, E.I., Sun, H.J. (2005) Communities adjust their temperature optima by shifting producer-to-consumer ratio, shown in lichens as models: I. Hypothesis. *Microbial Ecology* 49(4): 523 – 527.

Friedmann, E. I. (1982) Endolithic Microorganisms in the Antarctic Cold Desert. *Science* 215, 1045 – 1053.

Frolova, Y. V. (2008) Specific features in the composition, structure, and properties of volcanoclastic rocks. *Vestnik Moskovskogo Universiteta. Geologiya* 1, 30 – 38.

Furnes, H., Banerjee, N. R., Staudigel, H., Muehlenbachs, K., McLoughlin, N., de Wit, M., Van Kranendonk, M. V. (2007) Comparing petrographic signatures of bioalteration in recent to Mesoarchean pillow lavas: Tracing subsurface life in oceanic igneous rocks. *Precambrian Research* 158, 156–176.

Furnes, H., Banerjee, N.R., Muehlenbachs, K., Kontinen, A. (2005) Preservation of biosignatures in the metaglassy volcanic rocks from the Jormua ophiolite complex, Finland. *Precambrian Research* 136, 125–137.

Furnes, H., Banerjee, N.R., Muehlenbachs, K., Staudigel, H., de Wit, M. (2004) Early life recorded in Archaean pillow lavas. *Science* 304, 578–581.

Furnes, H., Thorseth, I.H., Torsvik, T., Muehlenbachs, K., Staudigel, H. Tumyr, O. (2002a) Identifying bio-interaction with basaltic glass in oceanic crust and implications for estimating the depth of the oceanic biosphere: a review. In Special Publication 202: Volcano-Ice Interactions on Earth and Mars, edited by

- J.L. Smellie and M.G. Chapman, Geological Society of London, London, pp. 407–421.
- Furnes, H., Muehlenbachs, K., Torsvik, T., Tumyr, O., Shi, L. (2002b) Biosignatures in metabasaltic glass of a Caledonian ophiolite West Norway. *Geol. Mag.*, 139, 601–608.
- Furnes, H., Staudigel, H., Thorseth, I.H., Torsvik, T., Muehlenbachs, K., Tumyr, O. (2001a) Bioalteration of basaltic glass in the oceanic crust. *Geochem. Geophys. Geosyst.*, 2, 2000GC000150.
- Furnes, H., Muehlenbachs, K., Tumyr, O., Torsvik, T., Xenophontos, C. (2001b) Biogenic alteration of volcanic glass from the Troodos ophiolite, Cyprus. *Journal of the Geological Society London* 158, 75–84.
- Furnes, H., Staudigel, H. (1999) Biological mediation in ocean crust alteration: how deep is the deep biosphere? *Earth and Planetary Science Letters*. 166, 97–103.
- Furnes, H., Thorseth, I.H., Tumyr, O., Torsvik, T., Fisk, M.R. (1996) Microbial activity in the alteration of glass from pillow lavas from Hole 896A. In Proceedings Ocean Drilling Program, Scientific Results 148, edited by J.C. Alt, H. Kinoshita, L.B. Stokking, and J.P. Michael, Ocean Drilling Program, College Station, TX, pp. 191–206.
- Gaidos, E., Mareinsson, V., Thorsteinsson, T., Johannesson, T., Runarsson, A. R., Stefansson, A., Glazer, B., Lanoil, B., Skidmore, M., Han, S., Miller, M., Rusch, A., Foo, W. (2008) An oligarchic microbial assemblage in the anoxic bottom waters of a volcanic subglacial lake. *ISME Journal*. 3, 486 – 497.
- Gaidos, E., Lanoil, B., Thorsteinsson, T., Graham, A., Skidmore, M., Han, S., Rust, T., Popp, B. (2004) A Viable Microbial Community in a Subglacial Volcanic Crater Lake, Iceland. *Astrobiology* 4, 327 – 344.
- Gaidos, E., Marion, G. (2003) Geological and geochemical legacy of a cold early Mars. *Journal of Geophysical Research*, 108(E6).
- Gallego, V., Sanchez-Porro, C., Garcia, M. T., Venosa, A. (2006) *Roseomonas aquatica* sp. nov., isolated from drinking water. *International Journal of Systematic and Evolutionary Microbiology* 56, 2291 – 2295.
- Garvin, J. B., Sakimoto, S. E. H., Frawley, J. J., Schnetzler, C. C., Wright, H. M. (2000) Topographic Evidence for Geologically Recent Near-Polar Volcanism on Mars. *Icarus* 145, 648 – 652.
- Gendrin, A., Mangold, N., Bibring, J-P., Langevin, Y., Gondet, B., Poulet, F., Bonello, G., Quantin, C., Mustard, J., Arvidson, R., LeMouelic, S. (2005) Sulfates in Martian Layered Terrains: The OMEGA/Mars Express View. *Science* 307, 1587 – 1591.

Ghatan, G. J. and Head, J. W. (2002) Candidate subglacial volcanoes in the south polar region of Mars: Morphology, morphometry, and eruption conditions. *Journal of Geophysical Research* 107, pp. 2.1-2.19.

Ghatan, G. J., Head, J. W., and Pratt, S. (2003) Cavi Angusti, Mars: Characterization and assessment of possible formation mechanisms. *Journal of Geophysical Research* 108, pp. 11.1-11.19

Gilichinsky, D. A., Wilson, G. S., Friedmann, E. I., Mckay, C. P., Sletten, R. S., Rivkina, E. M., Vishnivetskaya, T. A., Erokhina, L. G., Ivanushkina, N. E., Kochkina, G. A., Shcherbakova, V. A., Soina, V. S., Spirina, E. V., Vorobyova, E. A., Fyodorov-Davydov, D. G., Hallet, B., Ozerskaya, S. M., Sorokovikov, V. A. Laurinavichyus, K. S., Shatilovich, A. V., Chanton, J. P., Ostroumov, V. E., Tiedje, J. M. (2007) Microbial Populations in Antarctic Permafrost: Biodiversity, State, Age, and Implication for Astrobiology. *Astrobiology* 7, 275 – 311.

Giovannoni, S.J., Fisk, M.R., Mullins, T.D., Furnes, H. (1996) Genetic evidence for endolithic microbial life colonizing basaltic glass/seawater interfaces. In: Alt, J.C., Kinoshita, H., Stokking, L.B., Michael, P.J. (Eds.), Proceedings of the Ocean Drilling Program, Sci. Results 148. College Station, TX (Ocean Drilling Program), pp. 207 – 214.

Golubic, S., Friedmann, I., Schneider, J. (1981) The lithobiontic ecological niche, with special reference to microorganisms. *Journal of Sedimentary Petrology* 51, 475 – 478.

Gomez-Alvarez, V., King, G. M., Nusslein, K. (2007) Comparative bacterial diversity in recent Hawaiian volcanic deposits of different ages. *FEMS Microbial Ecology* 60, 60 – 73.

Goryniuk, M. C., Rivard, B. A. and Jones, B. (2004) The reflectance spectra of opal-A (0.5–25 Mm) from the Taupo Volcanic Zone: Spectra that may identify hydrothermal systems on planetary surfaces. *Geophysical Research Letters*, 31, L24701.

Grasby, S. E., Allen, C. C., Longazo, T. G., Lisle, J. T., Griffin, D. W. and Beauchamp, B. (2003) Supraglacial Sulfur Springs and Associated Biological Activity in the Canadian High Arctic—Signs of Life Beneath the Ice. *Astrobiology* 3, 583 – 596.

Green, R.H., Taylor, D.M., Gustan, E.A., Fraser, S.J., and Olson, R.L. (1971) Survival of microorganisms in a simulated martian environment. *Space Life Sci.* 3, 12 – 24.

Griffiths, E., Gupta, R. S. (2007) Identification of signature proteins that are distinctive of *Deinococcus-Thermus* phylum. *International Microbiology* 10, 201 – 208.

Griffiths, A. D., Coates, A. J., Jaumann, R., Michaelis, H., Paar, G., Barnes, D., Josset, J-L. and the PanCam Team. (2006) Context for the ESA ExoMars rover: the Panoramic Camera (PanCam) instrument. *International Journal of Astrobiology* 5, 269 – 275.

Griffith, L. L., Shock, E. L. (1995) A geochemical model for the formation of hydrothermal carbonates on Mars. *Nature* 377, 406 – 408.

Groth, I., Schumann, P., Martin, K., Schuetze, B., Augsten, K., Kramer, I., Stackebrandt, E. (1999) *Ornithinococcus hortensis* gen. nov., sp. Nov., a soil actinomycete which contains L-ornithine. *International Journal of Systematic Bacteriology* 49, 1717 – 1724.

Gudmundsson, M. T., Sigmundsson, F., Björnsson, H. (1997) Ice–volcano interaction of the 1996 Gjalp subglacial eruption, Vatnajökull, Iceland. *Nature* 389, 954 – 957.

Gulick, V. C. (1998) Magmatic intrusions and a hydrothermal origin for fluvial valleys on Mars. *Journal of Geophysical Research* 103, 19365–19387.

Hammer, O., Jamtveit, B., Benning, L. G., Dysthe, D. K. (2005) Evolution of fluid chemistry during travertine formation in the Troll thermal springs, Svalbard, Norway. *Geofluids* 5, 140 – 150.

Hansen, A. A., Jensen, L. L., Kristoffersen, T., Mikkelsen, K., Merrison, J., Finster, K. W., Lomsterin, B. A. (2009) Effects of Long-Term Simulated Martian Conditions on a Freeze-Dried and Homogenized Bacterial Permafrost Community. *Astrobiology* 9, 229 – 240.

Hansen, A. A., Merrison, J., Nørnberg, P., Lomstein, B.A., Finster, K. (2005) Activity and stability of a complex bacterial soil community under simulated martian conditions. *International Journal of Astrobiology* 4, 135 – 144.

Hausrath, E. M., Treiman, A. H., Vicenzi, E., Bish, D. L., Blake, D., Sarrazin, P., Hoehler, T., Midtkandal, I., Steele, A., Brantley, S. L. (2008) Short- and Long-Term Olivine Weathering in Svalbard: Implications for Mars. *Astrobiology* 8, 1079 – 1092.

Hawes, I., Howard-Williams, C., Vincent, W. F. (1992) Dessication and recovery of Antarctic cyanobacterial mats. *Polar Biology* 12, 587 – 594.

Hawrylewicz, E., Gowdy, B., Ehrlich, R. (1962) Microorganisms under a Simulated Martian Environment. *Nature*, 497 – 503.

Hawes, I., Schwarz, A-M. J. (2000) Absorption and utilization of irradiance by cyanobacterial mats in two ice-covered Antarctic lakes with contrasting light climates. *Journal of Phycology* 37, 5 – 15.

Head, J. W., Wilson, L. (2002) Mars: a review and synthesis of general environments and geological settings of magma-H₂O interactions. From Smellie, J. L. & Chapman, M. G. (eds) 2002. *Volcano – Ice Interaction on Earth and Mars*. Geological Society, London, Special Publications 202, 27 – 57.

Head, J. W. and Wilson, L. (2007) Heat transfer in volcano–ice interactions on Mars: synthesis of environments and implications for processes and landforms. *Annals of Glaciology* 45, 1 – 13.

Hennerberger, R. M., Walter, M. R., Anitori, R. P. (2006) Extraction of DNA from Acidic, Hydrothermally Modified Volcanic Soils. *Environmental Chemistry* 3, 100 – 104.

Herrera, A, Cockell, C. S (2007) Exploring microbial diversity in volcanic environments – a review of methods in DNA extraction. *Journal of Microbiological Methods* 70, 1–12.

Herrera, A., Cockell, C. S., Self, S., Blaxter, M., Reitner, J., Arp, G., Dröse, W., Thorsteinsson, T. and Tindle, A. G. (2008) Bacterial Colonization and Weathering of Terrestrial Obsidian in Iceland, *Geomicrobiology Journal*, 25, 25 – 37.

Herrera, A. Cockell, C. S., Self, S., Blaxter, M., Reitner, J., Thorsteinsson, T., Arp, G., Drose, W., Tindle, A. G. (2009) A Cryptoendolithic Community in Volcanic Glass. *Astrobiology* 9, 369 – 381.

Heyrman, J., Verbeeren, J., Schumann, P., Swings, J., De Vos, P. (2005) Six novel *Arthrobacter* species isolated from deteriorated mural paintings. *International Journal of Systematic and Evolutionary Microbiology* 55, 1457 – 1464.

Hiesinger, H. & Head, J. W. III Characteristics and origin of polygonal terrain in southern Utopia Planitia, Mars: results from Mars Orbiter Laser Altimeter and Mars Orbiter Camera data. *Journal of Geophysical Research* 105, 11999 –12022 (2000).

Hirsch, P., Ludwig, W., Hethke, C., Sittig, M., Hoffmann, B., Gallikowski, C. A. (1998). *Hymenobacter roseosalivarius* gen. nov., sp. nov. from continental Antarctica soils and sandstone: bacteria of the *Cytophaga/Flavobacterium/Bacteroides* line of phylogenetic descent. *Systematic and Applied Microbiology* 21, 374 – 383.

Hirsh, P., Eckhardt, F. E. W., Palmer, R. J. (1995) Methods for the study of rock-inhabiting microorganisms – A review. *Journal of Microbiological Methods* 23, 143 – 167.

Hofmann, B. A., Farmer, J. D. (2000) Filamentous fabrics in low-temperature mineral assemblages: are they fossil biomarkers? Implications for the search for a subsurface fossil record on the early Earth and Mars. *Planetary and Space Science* 48, 1077 – 1086.

Horneck, G. (2000) The microbial world and the case for Mars. *Planetary and Space Science* 48, 1053 –1063.

Horowitz, N.H., Hobby, G.L. and Hubbard, J.S. (1977) Viking on Mars: The carbon assimilation experiments. *Journal of Geophysical Research* 82, 4659 – 4662.

- Hoshino, Y. T., Matsumoto, N. (2005) Skim Milk Drastically Improves the Efficacy of DNA Extraction from Andisol, a Volcanic Ash Soil. *JARQ* 39, 2476 – 252.
- Hoshino, Y. T., Matsumoto, N. (2004) An Improved DNA Extraction Method Using Skim Milk from Soils That Strongly Adsorb DNA. *Microbes Environ.* 19, 13 – 19.
- Höskuldsson, A., Sparks, R. S. J (1997) Thermodynamics and fluid dynamics of effusive subglacial eruptions. *Bulletin of Volcanology* 59, 219 – 230.
- Höskuldsson, A. and Sparks, R. S. J (2006) Constraints on the dynamics of subglacial basalt eruptions from geological and geochemical observations at Kverkfjöll, NE-Iceland. *Bulletin of Volcanology* 68, 689 – 701.
- Hovius, N., Lea-Cox, A. and Turowski, J. M. (2008) Recent volcano–ice interaction and outburst flooding in a Mars polar cap re-entrant. *Icarus* 197, 24–38.
- Howari, F. M. (2006) Spectral analyses of sabkha sediments with implications for remote sensing on Mars. *International Journal of Astrobiology* 5, 47 – 56.
- Hugenholtz, P., Stackebrandt, E. (2004) Reclassification of *Spraerobacter thermophilus* from the subclass *Sphaerobacteridae* in the phylum *Actinobacteria* to the class *Thermomicrobia* (emended description) in the phylum *Chloroflexi* (emended description). *International Journal of Systematic and Evolutionary Microbiology* 54, 2049 – 2051.
- Hugenholtz, P., Tyson, G. W., Webb, R. I., Wagner, A. M., Blackall, L. L. (2001) Investigation of Candidate Division TM7, a Recently Recognized Major Lineage of the Domain *Bacteria* with No Known Pure-Culture Representatives. *Applied and Environmental Microbiology* 67, 411 – 419.
- Hughes, K.A. and Lawley, B. (2003) A novel Antarctic microbial endolithic community within gypsum crusts. *Environmental Microbiology* 5, 555–565.
- Humlum, O. (1992) Observations on rock moisture variability in gneiss and basalt under natural, arctic conditions. *Geogr. Ann.* 74 A (2-3), 197 – 205.
- Hunt, G. R., Salisbury, J. W. and Lenhoff, C. J. (1971). Visible and Near-infrared spectra of minerals and rocks: IV. Sulphides and sulphates. *Modern Geology* 3, 1–14.
- Hvidberg, C. S. (2005). Polar Caps. In: Water on Mars and Life, Tetsuya Tokano (ed.), Adv. Astrobiol. Biogeophys. pp.129 – 152.
- Inagaki, F., Suzuki, M., Takai, K., Oida, H., Sakamoto, T., Aoki, K., Nealson, K., Horikoshi, K. (2003) Microbial Communities Associated with Geological Horizons in Coastal Subseafloor Sediments from the Sea of Okhotsk. *Applied and Environmental Microbiology* 69, 7224 – 7235.

Izawa, M. R. M., Banerjee, N. R., Flemming, R. L., Bridge, N. J., Schultz, C. (In Press). Basaltic glass as a habitat for microbial life: Implications for astrobiology and planetary exploration. *Planetary and Space Science*. xxx

Jakosky, B. M. and Phillips, R. J. (2001) Mars' volatile and climate history. *Nature* 412, 237 – 244.

Jamtveit, B., Hammer, Ø., Anderson, C., Dysthe, D.K., Heldmann, J., & Vogel, M. (2006) Travertines from the Troll thermal springs, Svalbard. *Norwegian Journal of Geology* 86, 387-395.

Johannesson, T., Thorsteinsson, T., Stefansson, A., Gaidos, E. J., Einarsson, B. (2007) Circulation and thermodynamics in a subglacial geothermal lake under the Western Skafta cauldron of the Vatnajökull ice cap, Iceland. *Geophysical Research Letters* 34, L19502.

Johnson, D. B., Bacelar-Nicolau, P., Okibe, N., Thomas, A., Hallberg, K. B. (2009) *Ferrimicrobium acidophilum* gen. nov., sp. nov. and *Ferrithrix thermotolerans* gen. nov., sp. nov.: heterotrophic, iron-oxidizing, extremely acidophilic actinobacteria. *International Journal of Systematic and Evolutionary Microbiology* 59, 1082 – 1089.

Johnson, J. S., Smellie, J. L. 2007, Zeolite compositions as proxies for eruptive paleoenvironment. *Geochem. Geophys. Geosyst.*, 8, doi:10.1029/2006GC001450.

Jonasson, K. (2005) Magmatic evolution of the Heiðarspordur ridge, NE-Iceland. *Journal of Volcanology and Geothermal Research* 147, 109 – 124.

Jones, R. T., Robeson, M. S., Lauber, C. L., Hamady, M., Knight, R., Fierer, N. (2009) A comprehensive survey of soil acidobacterial diversity using pyrosequencing and clone library analyses. *The ISME Journal* 3, 442 – 453.

Jones, J. G. 1969, Intraglacial volcanoes of the Laugarvatn region, south-west Iceland – I. *Quarterly Journal of the Geological Society, London*, 124, 197-211.

Jorge Villar, S. E., Edwards, H. G. M., Worland, M. R. (2005) Comparative evaluation of Raman spectroscopy at different wavelengths for extremophile exemplars. *Origins of Life and Evolution of Biospheres* 35, 489 – 506.

Jorge Villar, S. E., Edwards, H. G. M., Benning, L. G. (2006) Raman spectroscopic and scanning electron microscopic analysis of a novel biological colonisation of volcanic rocks. *Icarus* 184, 158 – 169.

Joseph, S. J., Hugenholtz, P., Sangwan, P., Osborne, C. A., Janssen, P. H. (2003) Laboratory Cultivation of Widespread and Previously Uncultured Soil Bacteria. *Applied and Environmental Microbiology* 69, 7210 – 7215.

Jungblut, A. D., Lovejoy, C., Vincent, W. F. (2009) Global distribution of cyanobacterial ecotypes in the cold biosphere. *The ISME Journal*, xx (online ahead of print)

- Kadish, S. J., Head, J. W., Parsons, R. L. and Marchant, D. R. (2008) The Ascræus Mons fan-shaped deposit: Volcano–ice interactions and the climatic implications of cold-based tropical mountain glaciation. *Icarus* 197, 84 – 109.
- Kasai, Y., Takahata, Y., Hoaki, T. and Watanabe, K. (2005) Physiological and molecular characterization of a microbial community established in unsaturated, petroleum-contaminated soil. *Environmental Microbiology* 7, 806-818.
- Kauser, J., Ohyama, Y., Terato, H., Ide, J., Yamamoto, O. (1997) 16s rRNA Gene Sequence of *Rubrobacter radiotolerans* and Its Phylogenetic Alignment with Members of the Genus *Arthrobacter*, Gram-Positive Bacteria, and Members of the Family *Deinococcaceae*. *International Journal of Systematic Bacteriology* 47, 684 – 686.
- Kelly, D.S., Baross, J.A. and Delaney, J.R. (2002) Volcanoes, fluids, and life at mid-ocean ridge spreading centers. *Annual Review of Earth and Planetary Sciences* 30, 385–491.
- Keszthelyi, L., Thordarson, T., McEwen, A., Haack, H., Guilbaud, M., Self, S. and Rossi, M. J. (2004) Icelandic analogs to Martian flood lavas. *Geochem. Geophys. Geosyst.*, 5.
- Kim, J-S., Crowley, D. E. (2007) Microbial Diversity in Natural Asphalts of the Rancho La Brea Tar Pits. *Applied and Environmental Microbiology* 73, 4579 – 4591.
- Kirk, J. L., Beaudette, L. A., Hart, M., Montoglis, P., Klironomos, J. N., Lee, H., Trevors, J. T. (2004) Methods of studying soil microbial diversity. *Journal of Microbiological Methods* 58, 169 – 188.
- Klein, H.P. (1977) The Viking biological investigation: General aspects. *Journal of Geophysical Research* 82: 4677 – 4680.
- Klein, H. P., Lederberg, J., Rich, A., Horowitz, N. H., Oyama, V. I. and Levin, G. V. (1976) Viking mission search for life on Mars. *Nature* 262, 24 – 27.
- Klingelhofer, G., Morris, R. V., Bernhardt, B., Schroder, C., Rodionov, D. S., de Souza Jr., A., Yen, A., Gellert, R., Evlanov, E. N., Zubkov, B., Foh, J., Bonnes, U., Kankeleit, E., Gutlich, P., Ming, D. W., Renz, F., Wdowiak, T., Squyres, S. W., Arvidson, R. E. (2004) Jarosite and Hematite at Meridiani Planum from Opportunity's Mossbauer Spectrometer. *Science* 306, 1740 – 1745.
- Knoll, A. H. (1984) Microbiotas of the late Precambrian Hunnberg Formation, Nordaustlandet, Svalbard. *Journal of Paleontology* 58, 131 – 162.
- Kolganova, T. V., Kuznetsov, B. B., Tourova, T. P. (2002) Designing and Testing Oligonucleotide Primers for Amplification and Sequencing of Archaeal 16S rRNA Genes. *Microbiology* 71, 283 – 286.
- Kolmonen, E., Sivonen, K., Rapala, J., Haukka, K. (2004) Diversity of cyanobacteria and heterotrophic bacteria in cyanobacterial blooms in Lake Joutikas, Finland. *Aquatic Microbial Ecology* 36, 201 – 211.

Konhauser, K. O., Pheonix, V. R., Bottrell, S. H., Adams, D. G. and Head, I. M. (2001) Microbial-silica interactions in Icelandic hot spring sinter: possible analogues for some Precambrian siliceous stromatolites. *Sedimentology* 48, 415-433.

Konhauser, K. O. (2007). Introduction to Geomicrobiology. Blackwell Publishing.

Korenaga, J. (2004). Mantle mixing and continental breakup magmatism. *Earth and Planetary Science Letters* 218, 463 – 473.

Kuzmin, R. O. (2005) Ground Ice in the Martian Regolith. In: Water on Mars and Life, Tetsuya Tokano (ed.), Adv. Astrobiol. Biogeophys., pp. 155 – 189.

Le Bas, M. J., R. W. Le Maitre, A. Streckeisen, and B. Zanettin (1986), A chemical classification of volcanic rocks based on the total alkali-silica diagram, *Journal of Petrology* 27, 745–750.

La Duc, M. T., Osman, S., Vaishampayan, P., Piceno, Y., Andersen, G., Spry, J. A., Venkateswaran, K. (2009). Comprehensive Census of Bacteria in Clean Rooms by Using DNA Microarray and Cloning Methods. *Applied and Environmental Microbiology* 75, 6559 – 6567.

Lalucat, J., Bennasar, A., Bosch, R., Garcia-Valdes, E., Palleroni, N. J. (2006) Biology of *Pseudomonas stutzeri*. *Microbiology and Molecular Biology Reviews* 70, 510 – 547.

Lane D J. 16S/23S rRNA sequencing. In: Stackebrandt E, Goodfellow M, editors; Stackebrandt E, Goodfellow M, editors. Nucleic acid techniques in bacterial systematics. Chichester, United Kingdom: John Wiley & Sons; 1991. pp. 115–175.

Lane, M. D., Dyar, M. D. and Bishop, J. L. (2004) Spectroscopic evidence for hydrous iron sulfate in the Martian soil. *Geophysical Research Letters*, 31, L19702

Leask, H. J., Wilson, L. and Mitchell, K. L (2006) Formation of Aromatum Chaos, Mars: Morphological development as a result of volcano-ice interactions. *Journal of Geophysical Research*, 111.

Lee, K-C., Webb, R. I., Jansse, P. H., Sangwan, P., Romeo, T., Staley, J. T., Fuerst, J. A. (2009) Phylum *Verrucomicrobia* representatives share a compartmentalized cell plan with members of bacterial phylum *Planctomycetes*. *BMC Microbiology* 9: 5.

Le Olson, T., van de Meene, A. M. L., Francis, J. N., Pierson, B. K., Blankenship, R. E. (2007) Pigment Analysis of “*Candidatus Chlorothrix halophila*,” a Green Filamentous Anoxygenic Phototrophic Bacterium. *Journal of Bacteriology* 189, 4187 – 4195.

Letunic I and Bork P (2007) Interactive Tree Of Life (iTOL): an online tool for phylogenetic tree display and annotation. *Bioinformatics* 23, 127 - 128

- Link, L. S., Jakosky, B. M. and Thyne, G. D. (2005) Biological potential of low-temperature aqueous environments on Mars. *International Journal of Astrobiology* 4, 155 – 164.
- Loizeau, D., Mangold, N., Poulet, F., Bibring, J.-P., Gendrin, A., Ansan, V., Gomez, C., Gondet, B., Langevin, Y., Masson, P. and Neukum, G. (2007) Phyllosilicates in the Mawrth Vallis region of Mars. *Journal of Geophysical Research* 12, E08S08.
- Lysnes, K., Thorseth, I. H., Steinsbu, B. O., Øvreas, L., Torsvik, T., and Pedersen, R. B. (2004) Microbial community diversity in seafloor basalt from the Arctic spreading ridges. *FEMS Microbial Ecology* 50, 213 – 230.
- Malin, M. C., Bell, J. F., Cameron, J., Dietrich, W. W., Edgett, K. S., Hallet, B., Herkenhoff, K. E., Lemmon, M. T., Parker, T. J., Sullivan, R. J., Sumner, D. Y., Thomas, P. C., Wohl, E. E., Ravine, M. A., Caplinger, M. A., Maki, J. N. (2005) The mast cameras and Mars decent imager (MARDI) for the 2009 Mars Science Laboratory. Lunar and Planetary Science XXXVI. Abstract number 1214.
- McKay, C. P., Freidmann, E. I., Wharton, R. A., Davies, W. L (1992) History of water on Mars: A biological perspective. *Adv. Space Res.* 12, 231 – 238.
- Mancinelli, R. L., Fahlen, T. F., Landheim, R., Klovstad, M. R. (2004) Brines and evaporites: analogs for Martian life. *Advances in Space Research* 33, 1244 – 1246.
- Mancinelli, R.L. and Klovstad, M. (2000) Martian soil and UV radiation: microbial viability assessment on spacecraft surfaces. *Planetary and Space Science* 48:1093–1097.
- Mannisto, M. K., Tirola, M., Haggblom, M. M. (2009) Effect of Freeze-Thaw Cycles on Bacterial Communities of Arctic Tundra Soil. *Microbial Ecology* 58, 621 – 631.
- Martinez-Frias, J., Amaral, G., (2006) Astrobiological significance of minerals on Mars surface environment. *Reviews in Environmental Science and Biotechnology* 4, 219 – 231.
- Mason, O. U., Stingl, U., Wilhelm, L. J., Moeseneder, M. M., Di Meo-Savoie, C. A., Fisk, M. R., Giovannoni, S. J. (2007) The phylogeny of endolithic microbes associated with marine basalts. *Environmental Microbiology* 9, 2539 – 2550.
- Mattimore, V., Battista, J. R. (1996) Radioresistance of *Deinococcus radiodurans*: functions necessary to survive ionizing radiation are also necessary to survive prolonged desiccation. *Journal of Bacteriology* 178, 633 – 637.
- McAdam, A. C., Zolotov, M. Y., Mironenko, M. V., Sharp, T. G. (2009) Formation of silica by low-temperature acid alteration of Martian rocks: Physical-chemical constraints. *Journal of Geophysical Research* 113, E08003.

- McCollom, T. M. and Shock, E. L. (1997) Geochemical constraints on chemolithoautotrophic metabolism by microorganisms in seafloor hydrothermal systems. *Geochimica et Cosmochimica Acta* 61, 4375 – 4391.
- McKay, C. P., Stoker, C. R. (1989) The early environment and its evolution on Mars: Implications for life. *Reviews of Geophysics* 27, 189 – 214.
- McKinley, J. P., Stevens, T. O. (2000) Microfossils and Paleoenvironments in Deep Subsurface Basalt Samples. *Geomicrobiology Journal*, 17, 43 – 54.
- McLoughlin, N., Furnes, H., Banerjee, N. R., Muehlenbachs, K., Staudigel, H. (2009) Ichnotaxonomy of microbial trace fossils in volcanic glass. *Journal of the Geological Society* 166, 159 – 169.
- McLoughlin, N., Brasier, M. D., Wacey, D., Green, O. R., Perry, R. S. (2007) On Biogenicity Criteria for Endolithic Microborings on Early Earth and Beyond. *Astrobiology* 7, 10 – 26.
- McSween, H. Y., Taylor, G. J., Wyatt, M. B. (2009) Elemental Composition of the Martian Crust. *Science* 324, 736 – 739.
- Mellon, M. T., R. E. Arvidson, J. J. Marlow, R. J. Phillips, and E. Asphaug (2008a), Periglacial landforms at the Phoenix landing site and the northern plains of Mars, *Journal of Geophysical Research* 113, E00A23.
- Mellon, M. T., Boynton, W. V., Feldman, W. C., Arvidson, R. E., Titus, T. N., Bandfield, J. L., Putzig, N. E., Sizemore, H. G. (2008b) A prelanding assessment of the ice table depth and ground ice characteristics in Martian permafrost at the Phoenix landing site, *Journal of Geophysical Research*. 113, E00A25.
- Mileikowsky, C., Cucinotta, F., Wilson, J.W., Gladman, B., Horneck, G., Lindegren, L., Melosh, J., Rickman, H., Valtonen, M., and Zheng, J.Q. (2000) Natural transfer of viable microbes in space. 1. From Mars to Earth and Earth to Mars. *Icarus* 145, 391 – 427.
- Milliken, R. E., Swayze, G. G., Arvidson, R. E., Bishop, J. L., Clark, R. N., Ehlmann, B. L., Green, R. O., Grotzinger, J. P. (2008) Opaline silica in young deposits on Mars. *Geology* 36, 847 – 850.
- Ming, D. W., et al. (2006), Geochemical and mineralogical indicators for aqueous processes in the Columbia Hills of Gusev crater, Mars, *Journal of Geophysical Research*. 111, E02S12.
- Mitrofanov, I. G. (2005) Global Distribution of Subsurface Water Measured by Mars Odyssey. In : *Water on Mars and Life*, Tetsuya Tokano (ed.), Adv. Astrobiol. Biogeophys., 99 – 128.
- Miyamoto-Shinohara, Y., Imaizumi, T., Sukenobe, J., Murakami, Y., Kawamura, S., and Komatsu, Y. (2000) Survival rate of microbes after freeze-drying and long-term storage. *Cryobiology* 41, 251–255.

- Morgulis A, Coulouris G, Raytselis Y, Madden TL, Agarwala R, & Schäffer AA. (2008) Database indexing for production MegaBLAST searches. *Bioinformatics* 15, 1757-1764
- Morozova, D., Möhlmann, D. and Wagner, D. (2007) Survival of Methanogenic Archaea from Siberian Permafrost under Simulated Martian Thermal Conditions. *Origins of Life and Evolution of the Biosphere* 37, 189 – 200.
- Morris, R. V., et al. (2008), Iron mineralogy and aqueous alteration from Husband Hill through Home Plate at Gusev Crater, Mars: Results from the Mossbauer instrument on the Spirit Mars Exploration Rover. *Journal of Geophysical Research* 113, E12S42.
- Morris, R. V., Klingelhofer, G., Schroder, C., Rodionov, D. S., Yen, A., Ming, D. W., de Souza Jr., P. A., Fleischer, I., Wdowiak, T., Gellert, R., Bernhardt, B., Evlanov, E. N., Zubkov, B., Foh, J., Bonnes, U., Kankeleit, E., Gutlich, P., Renz, F., Squyres, S. W., Arvidson, R. E. (2006). Mossbauer mineralogy of rock, soil, and dust at Gusev crater, Mars: Spirit's journey through weakly altered olivine basalt on the Plains and pervasively altered basalt in the Columbia Hills. *Journal of Geophysical Research*. 111 (E02S13).
- Mouginis-Mars, J. J. (1990) Recent Water Release in the Tharsis Region of Mars *Icarus* 84, 362—373.
- Mouginis-Mark, J. J. (1985) Volcano/Ground Ice Interactions in Elysium Planitia, Mars. *Icarus* 64, 265-284.
- Mustard, J. F., Murchie, S. L., Pelkey, S. M., Ehlmann, B. L., Milliken, R. E., Grant, J. A., Bibring, J.-P., Poulet, F., Bishop, J., Noe Dobrea, E. N., Roach, L., Seelos, F., Arvidson, R. E., Wiseman, S., Green, R., Hash, C., Humm, D., Malaret, E., McGovern, J. A., Seelos, K., Clancy, T., Clark, R., Marais, D. D., Izenberg, N., Knudson, A., Langevin, Y., Martin, T., McGuire, P., Morris, R., Robinson, M., Roush, T., Smith, M., Swayze, G., Taylor, H., Titus, T. and Wolff, M. (2008) Hydrated silicate minerals on Mars observed by the Mars Reconnaissance Orbiter CRISM instrument. *Nature* 454, 305 – 309.
- Navarro-Gonzalez, R., Rainey, F. A., Molina, P., Bagaley, D. R., Hollen, B. J., de la Rosa, J., Small, A. M., Quinn, R. C., Grunthaner, F. J., Ca'ceres, L., Gomez-Silva, B. and McKay, C. P. (2003) Mars-Like Soils in the Atacama Desert, Chile, and the Dry Limit of Microbial Life. *Science* 302, 1018 – 1021.
- Nicholson, W.L., Munakata, N., Horneck, G., Melosh, H.J., and Setlow, P. (2000) Resistance of Bacillus endospores to extreme terrestrial and extraterrestrial environments. *Microbiology and Molecular Biology Reviews* 64, 548–572.
- Nienow, J. A., McKay, C. P. and Friedmann, E. I. (1988) The Cryptoendolithic Microbial Environment in the Ross Desert of Antarctica: Light in the Photosynthetically Active Region. *Microbial Ecology* 16, 271 – 289.
- Nedashkovskaya, O. I., Kim, S. B., Lee, K. H., Mikhailov, V. V., Bae, K. S. (2005) *Gillisia mitskevichiae* sp. nov., a novel bacterium of the family *Flavobacteriaceae*,

isolated from sea water. *International Journal of Systematic and Evolutionary Microbiology* 55, 321 – 323.

Nelson, P. H. H. (1975) The James Ross Island volcanic group of north-east Graham Land, *British Antarctic Survey Science Report* 54, pp. 62.

Nemergut, D. R., Costello, E. K., Meyer, A. F., Pescador, M. Y., Weintraub, M. N., Schmidt, S. K. (2005) Structure and function of alpine and arctic soil microbial communities. *Research in Microbiology* 156, 775 – 784.

Newsom, H. E., Hagerty, J. J., Thorsos, I. E. (2001) Location and Sampling of Aqueous and Hydrothermal Deposits in Martian Impact Craters. *Astrobiology* 1, 71 – 88.

Nienow, J. A., and E. I. Friedmann. 1993. Terrestrial lithophytic rock communities, p. 343–412. In E. I. Friedmann (ed.), *Antarctic microbiology*. Wiley-Liss, New York, N.Y.

Oehler, D. Z., Robert, F., Mostefaoui, S., Meibom, A., Selo, M., McKay, D. S (2006) Chemical Mapping of Proterozoic Organic Matter at Submicron Spatial Resolution. *Astrobiology* 6, 838 – 850.

Okamura, K., Hisada, T., Hiraishi, A. (2007) Characterization of thermotolerant purple nonsulfur bacteria isolated from hot-spring Chloroflexus mats and the reclassification of “Rhodopseudomonas cryptolactis” Stadtwald-Demchick *et al.* 1990 as Rhodoplanes cryptolactis nom. rev., comb. nov. *Journal of General and Applied Microbiology* 53, 357–361.

Ólafsson, M., Torfason, H., and Grönvold, K. (2000) Surface exploration and monitoring of geothermal activity in the Kverkfjöll geothermal area, central Iceland. Proceedings World Geothermal Congress 2000.

Omelon, C. R., Pollard, W. H., Ferris, F. G. (2007) Inorganic Species Distribution and Microbial Diversity within High Arctic Cryptoendolithic Habitats. *Microbial Ecology* 54, 740–752.

O’Sullivan, L. A., Rinna, J., Humphreys, G., Weightman, A. J., Fry, J. C. (2006) Culturable phylogenetic diversity of the phylum ‘Bacteroidetes’ from river epilithon and coastal water and description of novel members of the family *Flavobacteriaceae*: *Epilithonimonas tenax* gen. nov., sp. Nov. and *Persicivirga xylanidelens* gen. nov., sp. nov. *International Journal of Systematic and Evolutionary Microbiology* 56, 169 – 180.

Pace, N. R. (1997) A Molecular View of Microbial Diversity and the Biosphere. *Science* 276, 734-740.

Parente, M., Bishop, J. L., Bell, J. F. (2009) Spectral unmixing for mineral identification in pancam images of soils in Gusev crater, Mars. *Icarus* 203, 421 – 436.

Parnell, J., Cullen, D., Sims, M.R., Bowden, S., Cockell, C.S., Court, R., Ehrenfreund, P., Gaubert, F., Grant, W., Parro, V., Rohmer, M., Sephton, M.,

Stan-Lotter, H., Steele, A., Toporski, J. Vago, J. (2007) Searching for life on mars: Selection of molecular targets for ESA's aurora ExoMars mission. *Astrobiology* 7, 578 – 604.

Parnell, J., Lee, P., Cockell, C. S., Osinski, G. R. (2004) Microbial colonization in impact-generated hydrothermal sulphate deposits, Haughton impact structure, and implications for sulphates on Mars. *International Journal of Astrobiology* 3, 247 – 256.

Payne, M. C., Farmer, J. D. (2001) Volcano-Ice Interactions and the Exploration for Extant Martian Life. American Geophysical Union, Fall Meeting 2001, abstract #P22B-0549.

Payne, M. C., Farmer, J. D. (2002) Looking Through the Ice: Searching for Past and Present Habitable Zones in the Martian North Polar Region Using MOLA DEMs. American Geophysical Union, Fall Meeting 2002, abstract #U61B-05.

Payne, M. C., Farmer, J. D. (2003) Using Mars orbiter laser altimeter data to detect subglacial features at the residual north polar ice cap. Third International Conference on Mars Polar Science and Exploration, October 13-17 2003, Alberta, Canada, abstract no.8002.

Peckmann, J., Back, W., Behrens, K., Reitner, J. (2008) Putative cryptoendolithic life in Devonian pillow basalt, Rheinisches Schiefergebirge, Germany. *Geobiology*, 6, 125 – 135.

Pederson, K. (2000) Exploration of deep intraterrestrial microbial life: current perspectives. *FEMS Microbiology Letters* 185, 9 – 16.

Pirajno, F., and Van Kranendonk, M.J. (2005) Review of hydrothermal processes and systems on Earth and implications for Martian analogues. *Australian Journal of Earth Science* 52, 329 – 351.

Pointing, S. B., Chan, Y., Lacap, D. C., Lau, M. C. Y., Jurgens, J. A., Farrell, R. L. (2009) Highly specialized microbial diversity in hyper-arid polar desert. *PNAS* 106, 19964 – 19969.

Polz, M. F., Cavanaugh, C. M. (1998) Bias in Template-to-Product Ratios in Multitemplate PCR. *Applied and Environmental Microbiology* 64, 3724 – 3730.

Pope, K. O., Kieffer, S. W. and Ames, D. E. (2006) Impact melt sheet formation on Mars and its implication for hydrothermal systems and exobiology. *Icarus* 183, 1-9.

Poulet, F., Beaty, D. W., Bibring, J-P., Bish, D., Bishop, J. L., Dobreá, E. N., Mustard, J. F., Petit, S., Roach, L. H. (2009). Key Scientific Questions and Key Investigations from the First International Conference on Martian Phyllosilicates. *Astrobiology* 9, 257 – 267.

Poulet, F., Gomez, C., Bibring, J.-P., Langevin, Y., Gondet, B., Pinet, P., Belluci, G., Mustard, J. (2007) Martian surface mineralogy from OMEGA/MEx: Global mineral maps. *Journal of Geophysical Research* 112, E08S02.

- Poulet, F., Bibring, J-P., Mustard, J. F., Gendrin, A., Mangold, N., Langevin, Y., R. E. Arvidson, R. E., Gondet, B., Gomez, C., & the Omega Team. (2005) Phyllosilicates on Mars and implications for early martian climate. *Nature* 438, 623 – 627.
- Preston, L. J., Benedix, G. K., Genge, M. J., Sephton, M. A. (2008) A multidisciplinary study of silica sinter deposits with applications to silica identification and detection of fossil life on Mars. *Icarus* 198, 331 – 350.
- Priscu, J.C., Christner, B. C. (2004) Earth's icy biosphere, pp. 130-145, In "Microbial Diversity and Bioprospecting", A. Bull (editor). Chap 13. ASM Press, Washington, D.C.
- Prosser (2008) <http://www.dcs.qmul.ac.uk/~bryan/>
- Pullan, D., Westall, F., Hofmann, B. A., Parnell, J., Cockell, C. S., Edwards, H. G. M., Jorge Villar, S. E., Schroder, C., Cressey, G., Marinangeli, L., Richter, L. and Klingelhofer, G. (2008) Identification of Morphological Biosignatures in Martian Analogue Field Specimens Using *In Situ* Planetary Instrumentation. *Astrobiology* 8, 119 – 156.
- Quaiser, A., Ochsenreiter, T., Lanz, C., Schuster, S. C., Treusch, A. H., Eck, J., Schleper, C. (2003) Acidobacteria form a coherent but highly diverse group within the bacterial domain: evidence from environmental genomics. *Molecular Microbiology* 50, 563 – 575.
- Rathbun, J. A., Squyres, S. W. (2002) Hydrothermal Systems Associated with Martian Impact Craters. *Icarus* 157, 362 – 372.
- Rice, M. S., Bell, J. F., Wang, A, Cloutis, E. A. (2008) VIS-NIR spectral characterization of Si-rich deposits at Gusev Crater, Mars. Lunar and Planetary Science XXXIX.
- Rice, M. S., Bell, J. F., Cloutis, E. A., Wang, A., Ruff, S. W. Craig, M. A., Bailey, D. R., Johnson, J. R., de Souza Jr., P. A., Farrand, W. H. (2010) Silica-rich deposits and hydrated minerals at Gusev Crater, Mars: Vis-NIR spectral characterization and regional mapping. *Icarus* 205, 375-395.
- Rieder, R., Gellert, R., Anderson, R. C., Bruckner, J., Clark, B. C., Dreibus, G., Economou, T., Kingelhofer, G., Lugmair, G. W., Ming, D. W., Squyres, S. W., d'Uston, C., Wanke, H., Yen, A., Zipfel, J. (2004) Chemistry of Rocks and Soils at Meridiani Planum from the Alpha Particle X-ray Spectrometer. *Science* 306, 1746 – 1749.
- Ross, K. A., Fisher, R. V. (1986) Biogenic grooving on glass shards. *Science* 14, 571 – 573.
- Rothschild, L. J. (1990) Earth Analogs for Martian Life. Microbes in Evaporites, a New Model System for Life on Mars. *Icarus* 88, 246 – 260.

- Rull Pérez, F., Martínez Frias, J (2006) Raman spectroscopy goes to Mars. *Spectroscopy Europe* 18, 18 – 21.
- Rushmer, E.L. (2006) Sedimentological and geomorphological impacts of the jökulhlaup (glacial outburst flood) in January 2002 at Kverkfjöll, northern Iceland. *Geogr. Ann.* 88 A (1), 43 – 53.
- Santelli, C. M., Orcutt, B. N., Banning, E., Bach, W., Moyer, C. L., Sogin, M. L., Staudigel, H., Edwards, K. J. (2008) Abundance and diversity of microbial life in ocean crust. *Nature* 453, 653 – 657.
- Schiffman, P., Zierenberg, R., Marks, N., Bishop, J. L., Dyar, M. D. (2006) Acid-fog deposition at Kilauea volcano: A possible mechanism for the formation of siliceous-sulfate rock coatings on Mars. *Geology* 34, 921 – 924.
- Schloss, P.D. and Handelsman, J. (2005) Introducing DOTUR, a computer program for defining operational taxonomic units and estimating species richness. *Applied Environmental Microbiology* 71, 1501–1506.
- Schulze-Makuch, D, Dohm, J. M., Fan, C., Fairen, A. G., Rodrigues, J. A. P., Baker, V. R., Fink, W. (2007) Exploration of hydrothermal targets on Mars. *Icarus* 189, 308–324.
- Sharma, S. K., Misra, A. K., Lucey, P. G., Wiens, R. C., Clegg, S. M. (2007) Combined remote LIBS and Raman spectroscopy at 8.6m of sulfur-containing minerals, and minerals coated with hematite or covered with basaltic dust. *Spectrochimica Acta Part A* 68, 1036–1045.
- Sigmundsson, F., Sæmundsson, K. (2008) Iceland: a window on North-Atlantic divergent plate tectonics and geologic processes. *Episodes* 31, 92 – 97.
- Sigvaldason, G. E. (2002) Volcanic and tectonic processes coinciding with glaciation and crustal rebound: an early Holocene rhyolitic eruption in the Dyngjufjöll volcanic centre and the formation of the Askja caldera, north Iceland. *Bulletin of Volcanology* 64, 192 – 205.
- Sigvaldason, G. E., Steinthorsson, S, Oskarsson, N., Imsland, P. (1974) Compositional variation in recent Icelandic tholeiites and the Kverkfjöll hotspot. *Nature* 251, 579-582.
- Singletary, S.J., Grove, T.L. (2003) Early petrologic processes on the ureilite parent body. *Meteoritics Planet. Sci.*, 38, 1, 95-108.
- Skjelkvale, B-L., Amundsen, H. E. F., O'Reilly, S. Y., Griffin, W. L., Gjelsvik, T. (1989) A Primitive Alkali Basaltic Stratovolcano and Associated Eruptive Centres, Northwestern Spitsbergen: Volcanology and Tectonic Significance. *Journal of Volcanology and Geothermal Research* 37, 1 – 19.
- Skilling, I.P. (2002) Basaltic pahoehoe lava-fed deltas: large-scale characteristics, clast generation, emplacement processes and environmental discrimination. *Volcano—Ice Interaction on Earth and Mars*. J. L. Smellie, M. G. Chapman. Geological Society, London, Special Publications 202, pp. 91-114.

Smellie, J. L., Skilling, I. P. (1994) Products of subglacial volcanic eruptions under different ice thicknesses: two examples from Antarctica. *Sedimentary Geology* 91, 115 – 129.

Smellie, J. L. (1999) Lithostratigraphy of Miocene-Recent, alkaline volcanic fields in the Antarctic Peninsula and eastern Ellsworth Land. *Antarctic Science* 11, 362 – 378.

Smellie, J. L. (2006) The relative importance of supraglacial versus subglacial meltwater escape in basaltic subglacial tuya eruptions: an important unresolved conundrum. *Earth-Science Reviews* 74, 241 –268.

Smellie, J. L. (2007) Quaternary volcanism: subglacial landforms. Encyclopedia of Quaternary Sciences. S.A.Elias. Elsevier, Amsterdam, pp. 784-798.

Smellie, J. L., McArthur, J.M., McIntosh, W.C., Esser, R. (2006) Late Neogene interglacial events in the James Ross Island region, northern Antarctic Peninsula, dated by Ar/Ar and Sr-isotope stratigraphy. *Palaeogeography, Palaeoclimatology, Palaeoecology* 242, 169 – 187.

Smellie, J. L., Johnson, J. S., McIntosh, W. C., Esser, R., Gudmundsson, M. T., Hambrey, M. J., van Wyk de Vries, B. (2008) Six million years of glacial history recorded in the James Ross Island Volcanic Group, Antarctic Peninsula. *Palaeogeography, Palaeoclimatology, Palaeoecology* 260, 122 – 148.

Smellie, J. L., Haywood, A. M., Hillenbrand, C-D., Lunt, D. J., Valdes, P. J. (Submitted) Nature of the Antarctic Peninsula Ice Sheet during the Pliocene: geological evidence & modelling compared. *Earth-Science Reviews*.

Smith, D. J., Schuerger, A. C., Davidson, M. M., Pacala, S. W., Bakermans, C., Onstott, T. C. (2009) Survivability of *Psychrobacter cryohalolentis* K5 Under Simulated Martian Surface Conditions. *Astrobiology* 9, 221 – 228.

Smith, P. H., Tamppari, L. K., Arvidson, R. E., Bass, D., Blaney, D., Boynton, W. V., Carswell, A., Catling, D. C., Clark, B. C., Duck, T., DeJong, E., Fisher, D., Goetz, W., Gunnlaugsson, H. P., Hecht, M. H., Hipkin, V., Hoffman, J., Hviid, S. F., Keller, H. U., Kounaves, S. P., Lange, C. F., Lemmon, M. T., Madsen, M. B., Markiewicz, W. J., Marshall, J., McKay, C. P., Mellon, M. T., Ming, D. W., Morris, R. V., Pike, W. T., Renno, N., Staufer, U., Stoker, C., Taylor, P., Whiteway, J. A., Zent, A. P. (2009) H₂O at the Phoenix Landing Site. *Science* 325, 58 – 61.

Smith, P. H., Tamppari, L. K., Arvidson, R. E., Bass, D., Blaney, D., Boynton, W. V., Carswell, A., Catling, D. C., Clark, B. C., Duck, T., DeJong, E., Fisher, D., Goetz, W., Gunnlaugsson, H. P., Hecht, M. H., Hipkin, V., Hoffman, J., Hviid, S. F., Keller, H. U., Kounaves, S. P., Lange, C. F., Lemmon, M. T., Madsen, M. B., Markiewicz, W. J., Marshall, J., McKay, C. P., Mellon, M. T., Ming, D. W., Morris, R. V., Pike, W. T., Renno, N., Staufer, U., Stoker, C., Taylor, P., Whiteway, J. A., Zent, A. P. (2008) Introduction to special section on the Phoenix Mission: Landing Site Characterization Experiments, Mission Overviews and Expected Science. *Journal of Geophysical Research* 113, E00A18.

- Smith, P. H., Tomasko, M. G., Britt, D., Crowe, D. G., Reid, R., Keller, H. U., Thomas, N., Gliem, F., Rueffer, P., Sullivan, R., Greely, R., Knudsen, J. M., Madsen, B., Gunnlaugsson, H. P., Hviid, S. F., Goetz, W., Soderblom, L. A. Gaddis, L., Kirk, R. (1997) The imager for Mars Pathfinder experiment. *Journal of Geophysical Research* 102, 4003 – 4025.
- Soo, R. M., Wood, S. A., Grzymiski, J. J. McDonald, I. R., Cary, S. C. (2009) Microbial biodiversity of thermophilic communities in hot mineral soils of Tramway Ridge, Mount Erebus, Antarctica. *Environmental Microbiology* 11, 715 – 728.
- Squyres, S. W., Wilhelms, D. E. and Moosman, A. C. (1987) Large-Scale Volcano-Ground Ice Interactions on Mars. *Icarus* 70, 385 – 408.
- Squyres, S. W., Arvidson, R. E., Baumgartner, E. T., Bell, J. F., Christensen, P. R., Gorevan, S., Herkenhoff, K. E., Klingelhofer, G., Madsen, M. B., Morris, R. V., Rieder, R., Romero, R. A (2003) Athena Mars rover science investigation. *Journal of Geophysical Research* 108, 8062.
- Squyres, S. W., Arvidson, R. E., Ruff, S., Gellert, R., Morris, R. V., Ming, D. W., Crumpler, L., Farmer, J. D., Des Marais, D. J., Yen, A., McLennan, S. M., Calvin, W., Bell, J. F., Clark, B. C., Wang, A., McCoy, T. J., Schmidt, M. E., de Souza, P. A. (2008) Detection of Si-rich Deposits on Mars. *Science* 320, 1063 – 1067.
- Stackebrandt, E. and Goebel, B.M. (1994) Taxonomic note: a place for DNA-DNA reassociation and 16S rRNA sequence analysis in the present species definition in bacteriology. *International Journal of Systematic Bacteriology* 44, 846–849.
- Staudigel, H., Furnes, McLoughlin, N., Banerjee, N. R., Connell, L. B., Templeton, A. (2008). 3.5 billion years of glass bioalteration: Volcanic rocks as a basis for microbial life? *Earth-Science Reviews* 89, 156 – 176.
- Staudigel, H., Furnes, H., Banerjee, N. R., Dilek, Y., Muehlenbachs, K. (2006) Microbes and volcanoes: A tale from the oceans, ophiolites, and greenstone belts. *GSA Today* 16, 4 – 10.
- Staudigel, H., Schmincke, H-U. (1984) The Pliocene Seamount Series of La Palma/Canary Islands. *Journal of Geophysical Research* 89,11195 – 11215.
- Steffan, R. J., Atlas, R. M. (1991) Polymerase Chain Reaction: Applications in Environmental Microbiology. *Annual Review of Microbiology* 45, 137 – 161.
- Stefansson, A., Thorsteinsson, T., Johannesson, T., Einarsson, B., Gaidos, E. J. and Marteinson, V. (2008) Circulation, chemistry, thermodynamics and biology of the Skaftarkatlar subglacial geothermal lakes, Vatnajokull ice cap, Iceland. Abstract IAVCEI 2008.
- Stevens, H., Stubner, M., Simon, M., Brinkhoff, T. (2005) Phylogeny of Proteobacteria and Bacteroidetes from oxic habitats in a tidal flat ecosystem. *FEMS Microbial Ecology* 54, 351 – 65.

Stevens, T. O., McKinley, J. P. (1995) Lithoautotrophic microbial ecosystems in deep basalt aquifers. *Science* 270, 450–454.

Stewart, L., Cloutis, E., Bishop, J., Craig, M., Kaletzke, L., and McCormack, K. (2006). Classification of iron bearing phyllosilicates based on ferric and ferrous iron absorption bands in the 400 – 1300nm region. Lunar and Planetary Science XXXVII.

Stroncik, N. A., Schmincke, H-U. (2002) Palagonite – a review. *International Journal of Earth Science* 91, 680 – 697.

Storrie-Lombardi, M. C., Fisk, M. (2004) Elemental abundance distributions in sub-oceanic basalt glass: evidence of biogenic alteration. *Geochem. Geophys. Geosys.* 5, 1-15, Q10005.

Storrie-Lombardi, M. C. (2005) Post-Bayesian Strategies to Optimize Astrobiology Instrument Suites: Lessons from Antarctica and the Pilbara. Astrobiology and Planetary Missions, R. B. Hoover, G. V. Levin, A. Y. Rozanov, Bellingham, WA, SPIE 5906, 288 – 301.

Storrie-Lombardi, M. C., Muller, J. P., Fisk, M. R., Griffiths, A. D., Coates, A. J. (2008) Potential for non-destructive astrochemistry using the ExoMars PanCam. *Geophysical Research Letters*, 35, L12201.

Takeuchi, R., Sawada, H., Tanaka, F., Matsuda, I. (1996) Phylogenetic Analysis of *Streptomyces* spp. Causing Potato Scab Based on 16S rRNA Sequences. *International Journal of Systematic Bacteriology* 46, 476 – 479.

Thorseth, I.H., Pederson, R.B., Christie, D.D. (2003) Microbial alteration of 0–30 Ma seafloor and subseafloor basaltic glass from the Australian Antarctic Discord. *Earth and Planetary Science Letters*. 215, 237–247.

Thorseth, I.H., Torsvik, T., Torsvik, K., Daae, F.L., Pederson, R.B., the Keldysh-98 Scientific Party. (2001a) Diversity of life in ocean floor basalt. *Earth and Planetary Science Letters*., 194, 31–37.

Thorseth, I.H., Furnes, H., Tumyr, O. (1995) Textural and chemical effects of bacterial activity on basaltic glass: an experimental approach. *Chemical Geology* 119, 139 –160.

Thorseth, I. H., Furnes, H., Heldal, M. (1992) The importance of microbiological activity in the alteration of natural basaltic glass. *Geochemica et Cosmochimica Acta* 56, 845 – 850.

Thorseth, I. H., Furnes, H., Tumyr, O. (1991) A textural and chemical study of Icelandic palagonite of varied composition and its bearing on the mechanism of the glass-palagonite transformation. *Geochemica et Cosmochimica Acta* 55, 731 – 749.

- Torsvik, T., Furnes, H., Muehlenbachs, K., Thorseth, I.H., Tumyr, O. (1998) Evidence for microbial activity at the glass-alteration interface in oceanic basalts. *Earth and Planetary Science Letters* 162, 165–176.
- Torsvik, V., Sorheim, R., Goksoyr, J., (1996) Total bacterial diversity in soil and sediment communities - a review. *Journal of Industrial Microbiology* 17, 170–178.
- Travis, B. J. (2004) Early Mars, Hydrothermal convection plumes, and ‘columns of life’ Second Conference on Early Mars.
- Travis, B. J., Rosenberg, N. D. and Cuzzi, J. N. (2003) On the role of widespread subsurface convection in bringing liquid water close to Mars’ surface. *Journal of Geophysical Research*, 108, 8040.
- Treiman, A. H., Amundsen, H. E. F., Blake, D. F., Bunch, T. (2002) Hydrothermal origin for carbonate globules in Martian meteorite ALH84001: a terrestrial analogue from Spitsbergen (Norway). *Earth and Planetary Science Letters* 204, 323 – 332.
- Tringe, S. G., Rubin, E. M. (2005) Metagenomics: DNA sequencing of environmental samples. *Nature Reviews (Genetics)* 6, 805 – 814.
- Vago, J.L. (2005). ExoMars Science Management Plan, EXM-MS-PLESA-00002.
- Van Dover, C. L. (2000) *The Ecology of Deep-Sea Hydrothermal Vents* (Princeton Univ. Press, Princeton, NJ).
- Varnes, E. S., Jakosky, B. M. and McCollom, T. M. (2003) Biological Potential of Martian Hydrothermal Systems. *Astrobiology* 3, 407 – 414.
- Viscarra Rossel, R.A., R.N. McGlynn and A.B. McBratney. (2006) Determining the composition of mineral-organic mixes using UV–vis–NIR diffuse reflectance spectroscopy. *Geoderma* 137, 70 – 82
- Villar, S. E. J., Edwards, H. G. M., Wynn-Williams, D. D., Worland, M. R. 2003, FT-Raman spectroscopic analysis of an Antarctic endolith. *International Journal of Astrobiology* 1, 349 – 355.
- Vopel, K. and Hawes, I. (2006) Photosynthetic performance of benthic microbial mats in Lake Hoare, Antarctica. *Limnology and oceanography* 51, 1801 – 1812.
- Walker, J. J. and Pace, N. R. (2007) Endolithic Microbial Ecosystems. *Annual Review of Microbiology* 61, 331 – 347.
- Walker, J. J., and Pace, N. R., (2007) Phylogenetic Composition of Rocky Mountain Endolithic Microbial Ecosystems. *Applied and Environmental Microbiology* 73, 3497 – 3504.
- Walton, A. W. (2008) Microtubules in basalt glass from Hawaii Scientific Driling Project #2 phase 1 core and Hilina slope, Hawaii: evidence of the occurrence and behavior of endolithic microorganisms. *Geobiology* 6, 351 – 364.

Walter, M. R., Des Marais, D. J. (1993) Preservation of Biological Information in Thermal Spring Deposits: Developing a Strategy for the Search for Fossil Life on Mars. *Icarus* 101, 129 – 143.

Wang, A., Bell, J. F., Li, R., Johnson, J. R., Farrand, W. H., Cloutis, E. A., Arvidson, R. E., Crumpler, L., Squyres, S. W., McLennan, S. M., Herkenhoff, K. E., Ruff, S. W., Knudson, A. T. Chen, W., Greenberger, R. (2008) Light-toned salty soils and coexisting Si-rich species discovered by the Mars Exploration Rover Spirit in Columbia Hills, *Journal of Geophysical Research* 113, E12S40.

Wang, Q, G. M. Garrity, J. M. Tiedje, and J. R. Cole. 2007. Naïve Bayesian Classifier for Rapid Assignment of rRNA Sequences into the New Bacterial Taxonomy. *Appl Environ Microbiol.* 73(16):5261-7.

Warren, S.G., Brandt, R.E., Grenfell, T.C., and McKay, C.P. (2002) Snowball Earth: Ice thickness on the tropical ocean. *Journal of Geophysical Research* 107
Westall, F. Brack, A., Hofmann, B., Horneck, G., Kurat, G., Maxwell, J, Ori, G. G., Pillinger, C., Raulin, F., Thomas, N., Fitton, B., Clancy, P., Prieur, D., Vassaux, D. (2000) An ESA study for the search for life on Mars. *Planetary and Space Science* 48, 181 – 202.

Weinstein, S., Pane, D., Ernst, L. A., Warre-Rhodes, K., Dohm, J. M., Hock, A. N., Piatek, J. L., Emani, S., Lanni, F., Wagner, M., Fisher, G. W., Minkley, E., Dansey, L. E., Smith, T., Grin, E. A., Stubbs, K., Thomas, G., Cockell, C. S., Marinangeli, L., Ori, G. G., Heys, S., Teza, J. P., Moersch, J. E., Coppin, P., Diaz, G. C., Wettergreen, D. S., Cabrol, N. A., Wagoner, A. S. (2008) Application of pulsed-excitation fluorescence imager for daylight detection of sparse life in tests in the Atacama Desert. *Journal of Geophysical Research* 113, G01S90.

Westall, F., Steele, A., Toporski, J. Walsh, M., Allen, C., Guidry, S., Gibson, E., Mckay, D., Chafetz, H. (2000). Polymeric substances and biofilms as biomarkers in terrestrial materials: Implications for extraterrestrial samples. *J. Geophys. Res. Planets*, 105, 24,511-24,527.

Whitman, W.B., Coleman, D.C. and Wiebe, W.J. (1998) Prokaryotes: the unseen majority. *Proc. Natl. Acad. Sci. USA* 95, 6578–6583.

Wierzchos, J., Sancho, L. G and Ascaso, C. (2005) Biomineralization of endolithic microbes in rocks from the McMurdo Dry Valleys of Antarctica: implications for microbial fossil formation and their detection. *Environmental Microbiology* 7, 566-575.

Wiens, R. C., Clegg, S., Barefield, J., Vaniman, D., Lanza, N., Newsom, H., Herkenhoff, K., Bridges, N., Blaney, D., Maurice, S., Gasnault, O., Blank, J., Dyar, M. D., Milliken, R., Grotzinger, J., Crisp, J. and the ChemCam and MSL teams. ChemCam remote analyses and imaging on the Mars Science Laboratory 2007 ‘Slow motion’ field test. *Lunar and Planetary Science XXXIX* (2008) Abstract 1500.

Wilson, L. and Head, J. W. (2002) Heat transfer and melting in subglacial basaltic volcanic eruptions: implications for volcanic deposit morphology and meltwater volumes. From Smellie, J. L. & Chapman, M. G. (eds) 2002. *Volcano –*

Ice Interaction on Earth and Mars. Geological Society, London, Special Publications, 202, 5 – 26.

Wilson, L., Head, J. W. (2007) Heat transfer in volcano–ice interactions on Earth. *Annals of Glaciology* 45, 83 – 86.

Wilson, L. (2009) Volcanism in the Solar System. *Nature Geoscience* 2, 389 – 397.

Wintzingerode, F. v, Gobel, U. B., Stackebrandt, E. (1997) Determination of microbial diversity in environmental samples: pitfalls of PCR-based rRNA analysis. *FEMS Microbiology Reviews* 21, 213 – 229.

Wirth and Ulrich (2002) Cellulose-Degrading Potentials and Phylogenetic Classification of Carboxymethyl-cellulose Decomposing Bacteria Isolated from Soil. *Systematic and Applied Microbiology* 25, 584 – 591.

Wyatt, H. M. B., McSween, Jr. Y., Christensen, P. R., Head, J. W. (2003) Basalt, altered basalt, and andesite on the Martian surface: observations, interpretations and outstanding questions. Sixth International Conference on Mars, July 20-25 2003, Pasadena, California, abstract no.3271.

Wynn-Williams, D. D. & Edwards, H. G. M. (2000) Proximal Analysis of Regolith Habitats and Protective Biomolecules *in Situ* by Laser Raman Spectroscopy: Overview of Terrestrial Antarctic Habitats and Mars Analogs. *Icarus* 144, 486 – 503.

Yen, A. S., Morris, R. V., Clark, B. C., Gellert, R., Knudson, A. T., Squyres, S., Mittlefehldt, D. W., Ming, D. W., Arvidson, R., McCoy, T., Schmidt, M., Hurowitz, J., Li, R., Johnson, J. R. (2008) Hydrothermal processes at Gusev Crater: An evaluation of Paso Robles class soils. *Journal of Geophysical Research* 113, E06S10.

Yergeau, E., Newsham, K. K., Pearce, D. A., Kowalchuk, G. A. (2007) Patterns of bacterial diversity across a range of Antarctic terrestrial habitats. *Environmental Microbiology* 9, 2670 – 2682.

Yoon, J-H., Lee, C-H., Oh, T-K. (2005) *Aeromicrobium alkaliterrae* sp. Nov., isolated from an alkaline soil, and emended description of the genus *Aeromicrobium*. *International Journal of Systematic and Evolutionary Microbiology* 55, 2171 – 2175.

Zhang, C. L., Fouke, B. W., Bonheyo, G. T., Peacock, A. D., White, D. C., Huang, Y., Romanek, C. S. (2004). Lipid biomarkers and carbon-isotopes of modern travertine deposits (Yellowstone National Park, USA): Implications for biogeochemical dynamics in hot-spring systems. *Geochimica et Cosmochimica Acta* 68, 3157 – 3169.

APPENDIX

A) Data Tables

Table 1. EDS measurements (as oxide wt.%) from glassy regions of ASK004 hyaloclastite and ASK009 pillow basalt. For Figure 3.8 all sample values are normalised to 100%.

| Sample | Na ₂ O | MgO | Al ₂ O ₃ | SiO ₂ | K ₂ O | CaO | TiO ₂ | FeO | TOTAL | |
|--------|-------------------|-----|--------------------------------|------------------|------------------|-----|------------------|------|-------|-------|
| ASK004 | 1 | 2.6 | 4.8 | 10.8 | 48.6 | 0.0 | 9.8 | 2.2 | 12.9 | 91.8 |
| | 2 | 2.3 | 4.8 | 11.5 | 48.0 | 0.7 | 9.7 | 2.6 | 14.5 | 94.1 |
| | 3 | 1.6 | 3.7 | 9.4 | 40.5 | 0.5 | 9.3 | 2.5 | 13.4 | 80.9 |
| | 4 | 2.8 | 5.0 | 12.1 | 49.1 | 0.0 | 9.3 | 2.6 | 13.6 | 94.5 |
| | 5 | 2.3 | 5.1 | 11.6 | 48.0 | 0.5 | 9.9 | 2.6 | 12.9 | 93.0 |
| | 6 | 3.1 | 5.7 | 12.8 | 53.8 | 0.5 | 9.9 | 2.4 | 13.5 | 101.8 |
| | 7 | 2.0 | 4.6 | 11.3 | 47.6 | 0.0 | 9.3 | 2.3 | 12.8 | 90.0 |
| | 8 | 2.2 | 4.3 | 10.3 | 43.5 | 0.6 | 9.2 | 2.2 | 13.6 | 85.9 |
| | 9 | 3.1 | 6.0 | 12.5 | 52.2 | 0.4 | 10.1 | 2.5 | 12.8 | 99.7 |
| | 10 | 2.2 | 5.0 | 10.7 | 46.6 | 0.6 | 9.8 | 2.5 | 13.3 | 90.7 |
| | 11 | 2.6 | 5.5 | 12.9 | 51.2 | 0.0 | 9.8 | 2.2 | 13.8 | 98.0 |
| | 12 | 2.3 | 5.0 | 11.9 | 49.6 | 0.5 | 9.2 | 2.1 | 13.8 | 94.4 |
| Mean | 2.4 | 5.0 | 11.5 | 48.2 | 0.4 | 9.6 | 2.4 | 13.4 | 92.9 | |
| SD | 0.4 | 0.6 | 1.0 | 3.5 | 0.3 | 0.3 | 0.2 | 0.5 | 5.5 | |
| ASK009 | 1 | 2.9 | 4.0 | 11.4 | 47.5 | 0.8 | 8.8 | 2.0 | 12.3 | 89.7 |
| | 2 | 3.0 | 4.2 | 12.6 | 48.8 | 0.7 | 8.8 | 2.9 | 13.2 | 94.1 |
| | 3 | 2.7 | 3.7 | 10.7 | 46.9 | 0.9 | 8.6 | 2.6 | 12.9 | 88.9 |
| | 4 | 2.5 | 3.8 | 11.2 | 46.7 | 0.5 | 8.4 | 2.3 | 12.2 | 87.6 |
| | 5 | 2.7 | 3.7 | 13.1 | 46.5 | 0.0 | 9.5 | 2.0 | 9.6 | 87.2 |
| | 6 | 2.7 | 3.7 | 11.3 | 46.9 | 0.6 | 8.1 | 2.7 | 12.0 | 88.1 |
| | 7 | 2.8 | 4.5 | 11.2 | 47.4 | 0.5 | 8.8 | 2.7 | 13.8 | 91.6 |
| | 8 | 2.1 | 4.5 | 10.8 | 46.1 | 0.0 | 9.3 | 2.6 | 13.0 | 88.4 |
| | 9 | 2.6 | 5.5 | 12.1 | 47.2 | 0.0 | 10.3 | 1.9 | 10.8 | 90.4 |
| Mean | 2.7 | 4.2 | 11.6 | 47.1 | 0.4 | 8.9 | 2.4 | 12.2 | 89.6 | |
| SD | 0.3 | 0.6 | 0.8 | 0.8 | 0.4 | 0.6 | 0.3 | 1.3 | 2.2 | |

Table 2. Exhaustive list of all closest novel relatives and species relatives for the ASK4B environmental clones based on BLASTn 16s rDNA similarity

| ASK4B Clones | Closest novel relative | | | Closest genus and/or species | |
|----------------|------------------------------------|----|--|--|----|
| | ID | % | Sampling environment | ID | % |
| Actinobacteria | | | | | |
| ASK4B_2 | Uncultured (FJ592854) | 99 | Fumarole within a hyperarid, high-elevation landscape, Andes | <i>Patulibacter americanus</i> (AJ871305) | 92 |
| ASK4B_4 | Uncultured (EU979046) | 97 | Rhizosphere | <i>Conexibacter woesei</i> (NR_028979) | 88 |
| ASK4B_6 | Uncultured (EU790374) | 97 | Lascaux cave, France | <i>Patulibacter americanus</i> (AJ871305) | 84 |
| ASK4B_14 | Uncultured (GQ495408) | 97 | Terrestrial volcanic rocks, Iceland | <i>Patulibacter americanus</i> (AJ871305) | 84 |
| ASK4B_38 | Uncultured (GQ495408) | 97 | Terrestrial volcanic rocks, Iceland | <i>Patulibacter americanus</i> (AJ871305) | 84 |
| ASK4B_21 | Uncultured (EU883162) | 96 | Endostromatolites, Haughton impact crater, Canada | <i>Actinomadura glomerata</i> (AJ293704) | 85 |
| ASK4B_22 | Uncultured (FJ895062) | 99 | Hyper-arid polar desert | <i>Aeromicrobium ginsengisoli</i> (AB245394) | 92 |
| ASK4B_23 | Uncultured (FJ592818) | 94 | Fumarole within a hyperarid, high-elevation landscape, Andes | <i>Sporichthya polymorpha</i> (X72377) | 91 |
| ASK4B_32 | Uncultured (FJ592818) | 99 | Fumarole within a hyperarid, high-elevation landscape, Andes | <i>Sporichthya polymorpha</i> (X72377) | 92 |
| ASK4B_36 | Uncultured (GQ396916) | 90 | Recently de-glaciated soil | <i>Ferritrix thermotolerans</i> (AY140237) | 86 |
| ASK4B_42 | Uncultured (AJ863185) | 97 | Soil community associated with Poplar trees | <i>Thermoleophilum album</i> (NR_025543) | 85 |
| ASK4B_44 | Uncultured (AM935529) | 95 | Hydrocarbon contaminated soil | <i>Conexibacter woesei</i> (NR_028979) | 89 |
| ASK4B_45 | Uncultured (EU790374) | 97 | Lascaux cave, France | <i>Patulibacter americanus</i> (AJ871305) | 85 |
| ASK4B_46 | Uncultured (EU883154) | 97 | Endostromatolites, Haughton impact crater, Canada | <i>Thermoleophilum album</i> (NR_025543) | 85 |
| ASK4B_47 | Uncultured (AY093463) | 94 | Methane hydrate-bearing deep marine sediments | <i>Acidothermus cellulolyticus</i> (AJ007290) | 86 |
| ASK4B_50 | Uncultured (GQ396948) | 97 | Recently de-glaciated soil | <i>Patulibacter americanus</i> (AJ871305) | 84 |
| ASK4B_52 | Uncultured (EU790374) | 97 | Lascaux cave, France | <i>Patulibacter americanus</i> (AJ871305) | 85 |
| ASK4B_57 | Uncultured (EU133006) | 92 | Recently de-glaciated soil | <i>Ferritrix thermotolerans</i> (AY140237) | 86 |
| ASK4B_58 | Uncultured (EU133006) | 97 | Soil | <i>Ilumatobacter fluminis</i> (AB360343) | 90 |
| ASK4B_61 | Uncultured (FM209057) | 86 | Hydrocarbon contaminated soil | <i>Blastococcus saxosidens</i> (AJ296064) | 84 |
| ASK4B_68 | Uncultured (GQ495419) | 98 | Terrestrial volcanic rocks, Iceland | <i>Ferrimicrobium acidiphilum</i> (AF251436) | 88 |
| ASK4B_70 | Uncultured (EU132977) | 98 | Soil | <i>Ferrimicrobium acidiphilum</i> (AF251436) | 86 |
| ASK4B_73 | Uncultured (FJ592851) | 98 | Fumarole within a hyperarid, high-elevation landscape, Andes | <i>Patulibacter minatonensis</i> (AB193261) | 93 |
| ASK4B_74 | Uncultured (GQ263179) | 99 | Simulated waste site | <i>Thermoleophilum album</i> (NR_025543) | 85 |
| ASK4B_79 | Uncultured (EU979046) | 96 | Rhizosphere | <i>Conexibacter woesei</i> (NR_028979) | 88 |
| ASK4B_85 | Uncultured (FJ895056) | 99 | Hyper-arid polar desert | <i>Patulibacter americanus</i> (AJ871305) | 92 |
| ASK4B_90 | Uncultured (EF220440) | 92 | Antarctic terrestrial habitats | <i>Ilumatobacter fluminis</i> (AB360343) | 89 |
| Bacteroidetes | | | | | |
| ASK4B_15 | Uncultured (GQ396974) | 96 | Recently de-glaciated soil | <i>Terrimonas lutea</i> (AB192292) | 93 |
| ASK4B_18 | Uncultured (FJ490252) | 93 | Hyper-arid polar desert | <i>Segetibacter korensis</i> (AB267478) | 93 |
| ASK4B_25 | Uncultured (EU335841) | 96 | Mineral soils in Miers Valley, Antarctica | <i>Flavobacterium ferrugineum</i> (AM230484) | 88 |
| ASK4B_26 | Uncultured (FJ490262) | 96 | Hyper-arid polar desert | <i>Flavobacterium ferrugineum</i> (AM230484) | 90 |
| ASK4B_27 | Uncultured (GQ128159) | 97 | Meadow Soil from Tibetan Plateau | <i>Segetibacter korensis</i> (AB267478) | 92 |
| ASK4B_43 | Uncultured (FJ895072) | 98 | Hyper-arid polar desert | <i>Segetibacter korensis</i> (AB267478) | 94 |
| ASK4B_51 | Uncultured (AM168126) | 94 | Trans himalayan region | <i>Flavisolibacter ginsengisoli</i> (AB267477) | 94 |
| ASK4B_53 | <i>H. roseosalivarius</i> (Y18834) | 94 | Antartica soils and sandstone | <i>Hymenobacter roseosalivarius</i> (Y18834) | 94 |
| ASK4B_76 | Uncultured (GQ128159) | 97 | Meadow Soil from Tibetan Plateau | <i>Segetibacter korensis</i> (AB267478) | 92 |

Appendix

| | | | | | |
|----------------------------|-----------------------|----|--|--|-----|
| ASK4B_78 | Uncultured (EF605799) | 99 | Soil | <i>Flavisolibacter ginsengiterrae</i> (AB267476) | 94 |
| ASK4B_80 | Uncultured (GQ128159) | 97 | Meadow Soil from Tibetan Plateau | <i>Segetibacter koreensis</i> (AB267478) | 92 |
| ASK4B_75 | Uncultured (GQ128159) | 95 | Meadow Soil from Tibetan Plateau | <i>Segetibacter koreensis</i> (AB267478) | 92 |
| Proteobacteria | | | | | |
| ASK4B_5 | Uncultured (GQ128065) | 98 | Meadow Soil from Tibetan Plateau | <i>Rhodoplanes cryptolactis</i> (AB087718) | 94 |
| ASK4B_11 | Uncultured (AM409805) | 93 | Lake sediment, Israel | <i>Thioflavicoccus mobilis</i> (AJ010126) | 93 |
| ASK4B_13 | Uncultured (EU373912) | 92 | Sediment bacteria, Mediterranean Sea | <i>Geopsychrobacter electrodiphilus</i> (AY187304) | 82 |
| ASK4B_17 | Uncultured (EU373912) | 92 | Sediment bacteria, Mediterranean Sea | <i>Geopsychrobacter electrodiphilus</i> (AY187304) | 82 |
| ASK4B_19 | Uncultured (EU881166) | 97 | Forest soil | <i>Rhodoplanes cryptolactis</i> (AB087718) | 95 |
| ASK4B_24 | Uncultured (AM909934) | 94 | Methanotrophic communities in rice fields | <i>Polyangium thaxteri</i> (AJ233943) | 92 |
| ASK4B_56 | Uncultured (DQ643704) | 98 | Soil | <i>Methylibium aquaticum</i> (DQ664244) | 93 |
| ASK4B_89 | Uncultured (GQ128065) | 99 | Meadow Soil from Tibetan Plateau | <i>Rhodoplanes cryptolactis</i> (AB087718) | 95 |
| ASK4B_91 | Uncultured (DQ643704) | 98 | Soil | <i>Methylibium aquaticum</i> (DQ664244) | 93 |
| Deinococcus-Thermus | | | | | |
| ASK4B_39 | Uncultured (FJ895086) | 98 | Hyper-arid polar desert | <i>Truepera radiovictrix</i> (DQ022077) | 91 |
| ASK4B_67 | Uncultured (FJ895086) | 99 | | | |
| Acidobacteria | | | | | |
| ASK4B_1 | Uncultured (DQ139452) | 95 | Epilithic biofilms in Catacombs | <i>Solibacter usitatus</i> (AY234728) | 91 |
| ASK4B_3 | Uncultured (EF464879) | 97 | Soils of Northern Victoria Land, Antarctica | <i>Chloracidobacterium thermophilum</i> (EF531339) | 93 |
| ASK4B_9 | Uncultured (EU335850) | 95 | Mineral soils in Miers Valley, Antarctica | <i>Chloroflexus aurantiacus</i> (AJ308501)* | 81 |
| ASK4B_20 | Uncultured (EF188386) | 94 | Altamira Cave, Spain | <i>Geothrix fermentans</i> (GFU41563) | 81 |
| ASK4B_33 | Uncultured (EU122856) | 99 | Soil | <i>Geothrix fermentans</i> (GFU41563) | 83 |
| ASK4B_35 | Uncultured (EU335868) | 94 | Mineral soils in Miers Valley, Antarctica | <i>Acidobacteriaceae bacterium</i> (AB245338) | 84 |
| ASK4B_41 | Uncultured (EF464954) | 96 | Soils of Northern Victoria Land, Antarctica | <i>Chloracidobacterium thermophilum</i> (EF531339) | 93 |
| ASK4B_55 | Uncultured (EU335868) | 95 | Mineral soils in Miers Valley, Antarctica | <i>Acidobacteriaceae bacterium</i> (AB245338) | 83 |
| ASK4B_69 | Uncultured (GQ262975) | 99 | Simulated waste site | <i>Heliobacillus mobilis</i> (AB100835)* | 82 |
| ASK4B_81 | Uncultured (EU122856) | 98 | Soil | <i>Geothrix fermentans</i> (GFU41563) | 82 |
| ASK4B_86 | Uncultured (GQ495424) | 99 | Terrestrial volcanic rocks, Iceland | <i>Chloracidobacterium thermophilum</i> (EF531339) | 81 |
| Verrucomicrobia | | | | | |
| ASK4B_7 | Uncultured (GQ495404) | 99 | Terrestrial volcanic rocks, Iceland | <i>Xiphinematobacter brevicolli</i> (AF217462) | 87 |
| ASK4B_12 | Uncultured (GQ495404) | 97 | Terrestrial volcanic rocks, Iceland | <i>Xiphinematobacter brevicolli</i> (AF217462) | 86 |
| ASK4B_59 | Uncultured (EF188458) | 89 | Altamira Cave, Spain | <i>Rubritalea sabuli</i> (AB353310) | 84 |
| ASK4B_64 | Uncultured (EF664102) | 97 | Agricultural soil, Michigan | <i>Prostheco bacter vanneervanii</i> (AJ966883) | 81 |
| ASK4B_65 | Uncultured (AB374368) | 96 | Endolithic community, White rock Switzerland | <i>Prostheco bacter vanneervanii</i> (AJ966883) | 84 |
| ASK4B_66 | Uncultured (AB374368) | 97 | Endolithic community, White rock Switzerland | <i>Prostheco bacter vanneervanii</i> (AJ966883) | 84 |
| ASK4B_71 | Uncultured (GQ495404) | 98 | Terrestrial volcanic rocks, Iceland | <i>Xiphinematobacter brevicolli</i> (AF217462) | 86 |
| ASK4B_82 | Uncultured (EU280630) | 96 | California grassland | <i>Opiritatus terrae</i> (AJ229246) | 92 |
| Cyanobacteria | | | | | |
| ASK4B_10 | Uncultured (EF220798) | 97 | Antarctic terrestrial habitats | <i>Chroococciopsis</i> sp. (DQ914863) | 92 |
| ASK4B_16 | Nostoc sp. (EF174228) | 97 | Pannaria aff. leproloma cyanobiont | <i>Nostoc calcicola</i> (AJ630448) | 97 |
| ASK4B_30 | Uncultured (FJ891015) | 98 | Hyperlithic community in quartz, hyperarid core of the Atacama | <i>Arthrospira platensis</i> (EF432320) | 90 |
| # | Chloroplast | / | / | / | N/A |
| ASK4B_49 | Uncultured (EF220798) | 98 | Antarctic terrestrial habitats | <i>Anabaena variabilis</i> (DQ234826) | 91 |

Appendix

| # | Chloroplast | / | / | / | / |
|----------------|-----------------------|-----|--|--|----|
| # | Chloroplast | / | / | / | / |
| Planctomycetes | | | | | |
| ASK4B_8 | Uncultured (EF020083) | 96 | Soil associated with Aspen | <i>Rhodopirellula baltica</i> (EF589349) | 83 |
| ASK4B_31 | Uncultured (EF464902) | 98 | Soils of Northern Victoria Land, Antarctica | | 89 |
| ASK4B_34 | Uncultured (GQ396898) | 99 | Recently de-glaciated soil | <i>Pirellula staleyi</i> (AF399914) | 84 |
| ASK4B_54 | Uncultured (GQ396898) | 99 | Recently de-glaciated soil | | 84 |
| ASK4B_83 | Uncultured (EF464902) | 98 | Soils of Northern Victoria Land, Antarctica | <i>Rhodopirellula baltica</i> (EF589349) | 90 |
| ASK4B_88 | Uncultured (EF464902) | 98 | Soils of Northern Victoria Land, Antarctica | | 90 |
| RDP Unknown | | | | | |
| ASK4B_28 | Uncultured (EF465024) | 98 | Soils of Northern Victoria Land, Antarctica | <i>Phycisphaera mikrensis</i> (AB474364) | 82 |
| ASK4B_29 | Uncultured (EF632950) | 93 | Aquatic environments in high altitude Andean Altiplano | <i>Phycisphaera mikrensis</i> (AB474364) | 81 |
| ASK4B_60 | Uncultured (AF507691) | 98 | Arizona soil | <i>Levilinea saccharolytica</i> (AB109439) | 80 |
| ASK4B_62 | Uncultured (GQ495408) | 94 | Terrestrial volcanic rocks, Iceland | <i>Thermoleophilum album</i> (NR_025543) | 84 |
| ASK4B_63 | Uncultured (EU644222) | 92 | Polygonal tundra soils, Siberia | <i>Phycisphaera mikrensis</i> (AB474364) | 82 |
| ASK4B_72 | Uncultured (GQ495395) | 100 | Terrestrial volcanic rocks, Iceland | <i>Gloeobacter violaceus</i> (BA000045) | 79 |
| ASK4B_84 | Uncultured (EU134889) | 93 | Soil | <i>Desulfovibrio vulgaris</i> (AY362360) | 80 |

Table 3. Exhaustive list of all closest novel relatives and species relatives for the ASK9G environmental clones based on BLASTn 16s rDNA similarity.

| ASK9G Clones | Closest novel relative | | | Closest genus and/or species | |
|----------------|------------------------|----|---|---|----|
| | ID | % | Sampling environment | ID | % |
| Actinobacteria | | | | | |
| ASK9G_1 | Uncultured (FJ895046) | 98 | Hyper-arid polar desert | <i>Conexibacter woesei</i> (NR_028979) | 92 |
| ASK9G_2 | Uncultured (FJ895046) | 98 | Hyper-arid polar desert | <i>Solirubrobacter soli</i> (AB245334) | 91 |
| ASK9G_9 | Uncultured (FJ895046) | 98 | Hyper-arid polar desert | <i>Solirubrobacter soli</i> (AB245334) | 91 |
| ASK9G_12 | Uncultured (FJ895046) | 98 | Hyper-arid polar desert | <i>Solirubrobacter soli</i> (AB245334) | 91 |
| ASK9G_13 | Uncultured (FJ895051) | 99 | Hyper-arid polar desert | <i>Rubrobacter radiotolerans</i> (AJ243870) | 94 |
| ASK9G_14 | Uncultured (FJ895046) | 98 | Hyper-arid polar desert | <i>Solirubrobacter soli</i> (AB245334) | 90 |
| ASK9G_16 | Uncultured (FJ895053) | 99 | Hyper-arid polar desert | <i>Ornithinococcus hortensis</i> (AB098587) | 97 |
| ASK9G_17 | Uncultured (FJ895051) | 98 | Hyper-arid polar desert | <i>Rubrobacter radiotolerans</i> (AJ243870) | 93 |
| ASK9G_18 | Uncultured (AY250873) | 97 | Cryptoendolithic communities, McMurdo Dry Valleys, Antarctica | <i>Rubrobacter radiotolerans</i> (AJ243870) | 92 |
| ASK9G_21 | Uncultured (FJ895051) | 98 | Hyper-arid polar desert | <i>Rubrobacter radiotolerans</i> (AJ243870) | 92 |
| ASK9G_22 | Uncultured (FJ895046) | 98 | Hyper-arid polar desert | <i>Solirubrobacter soli</i> (AB245334) | 91 |
| ASK9G_25 | Uncultured (FJ895051) | 99 | Hyper-arid polar desert | <i>Rubrobacter radiotolerans</i> (AJ243870) | 95 |
| ASK9G_26 | Uncultured (FJ895046) | 98 | Hyper-arid polar desert | <i>Solirubrobacter soli</i> (AB245334) | 90 |
| ASK9G_27 | Uncultured (AY250865) | 99 | Cryptoendolithic communities, McMurdo Dry Valleys, Antarctica | <i>Sporichthya polymorpha</i> (X72377) | 94 |
| ASK9G_28 | Uncultured (FN297993) | 93 | Roman Carmona tombs | <i>Acidotherrmus cellulolyticus</i> (AJ007290) | 86 |
| ASK9G_29 | Uncultured (AY250873) | 98 | Cryptoendolithic communities, McMurdo Dry Valleys, Antarctica | <i>Rubrobacter radiotolerans</i> (AJ243870) | 93 |
| ASK9G_30 | Uncultured (FJ895053) | 98 | Hyper-arid polar desert | <i>Ornithinococcus hortensis</i> (AB098587) | 97 |
| ASK9G_31 | Uncultured (EF157223) | 95 | Natural asphalts of the Rancho La Brea Tar pits | <i>Ferrithrix thermotolerans</i> (AY140237) | 86 |
| ASK9G_33 | Uncultured (EF157223) | 96 | Natural asphalts of the Rancho La Brea Tar pits | <i>Ferrithrix thermotolerans</i> (AY140237) | 86 |
| ASK9G_35 | Uncultured (AM746696) | 98 | Rosy discoloration of ancient wall paintings | <i>Solirubrobacter soli</i> (AB245334) | 91 |
| ASK9G_36 | Uncultured (AM746693) | 93 | Rosy discoloration of ancient wall paintings | <i>Ornithinimicrobium kibberense</i> (AY636111) | 93 |
| ASK9G_37 | Uncultured (FJ895046) | 99 | Hyper-arid polar desert | <i>Solirubrobacter soli</i> (AB245334) | 91 |
| ASK9G_38 | Uncultured (FJ895056) | 99 | Hyper-arid polar desert | <i>Patulibacter americanus</i> (AJ871305) | 92 |
| ASK9G_39 | Uncultured (AM746696) | 99 | Rosy discoloration of ancient wall paintings | <i>Solirubrobacter soli</i> (AB245334) | 91 |
| ASK9G_40 | Uncultured (FJ895046) | 94 | Hyper-arid polar desert | <i>Solirubrobacter soli</i> (AB245334) | 88 |
| ASK9G_41 | Uncultured (FN297994) | 93 | Roman Carmona tombs | <i>Nitriliruptor alkaliphilus</i> (EF422408) | 88 |
| ASK9G_42 | Uncultured (FJ895046) | 99 | Hyper-arid polar desert | <i>Solirubrobacter soli</i> (AB245334) | 91 |
| ASK9G_43 | Uncultured (AY250873) | 98 | Cryptoendolithic communities, McMurdo Dry Valleys, Antarctica | <i>Rubrobacter radiotolerans</i> (AJ243870) | 93 |
| ASK9G_47 | Uncultured (FJ891029) | 94 | Hyperlithic community, hyperarid Atacama Desert | <i>Marmoricola aurantiacus</i> (NR_026507) | 95 |
| ASK9G_48 | Uncultured (FJ895046) | 99 | Hyper-arid polar desert | <i>Solirubrobacter soli</i> (AB245334) | 91 |
| ASK9G_49 | Uncultured (EF464818) | 96 | Soils of Northern Victoria Land, Antarctica | <i>Rubrobacter radiotolerans</i> (NR_029191) | 93 |
| ASK9G_50 | Uncultured (FJ891029) | 95 | Hyperlithic community, hyperarid Atacama Desert | <i>Marmoricola aurantiacus</i> (NR_026507) | 95 |
| ASK9G_51 | Uncultured (AM746685) | 98 | Rosy discoloration of ancient wall paintings | <i>Rubrobacter radiotolerans</i> (NR_029191) | 91 |
| ASK9G_52 | Uncultured (FJ895046) | 98 | Hyper-arid polar desert | <i>Solirubrobacter soli</i> (AB245334) | 90 |
| ASK9G_53 | Uncultured (FJ895051) | 99 | Hyper-arid polar desert | <i>Rubrobacter radiotolerans</i> (NR_029191) | 95 |
| ASK9G_54 | Uncultured (AM746685) | 98 | Rosy discoloration of ancient wall paintings | <i>Rubrobacter radiotolerans</i> (NR_029191) | 92 |
| ASK9G_55 | Uncultured (FJ895046) | 98 | Hyper-arid polar desert | <i>Solirubrobacter soli</i> (AB245334) | 91 |

Appendix

| | | | | | |
|----------------------------|-----------------------|-----|---|---|----|
| ASK9G_59 | Uncultured (AM746693) | 94 | Rosy discoloration of ancient wall paintings | <i>Ornithinimicrobium kibberense</i> (AY636111) | 93 |
| ASK9G_60 | Uncultured (AY250887) | 98 | Cryptoendolithic communities, McMurdo Dry Valleys, Antarctica | <i>Rubrobacter radiotolerans</i> (AJ243870) | 91 |
| ASK9G_62 | Uncultured (AM746681) | 98 | Rosy discoloration of ancient wall paintings | <i>Rubrobacter radiotolerans</i> (AJ243870) | 92 |
| ASK9G_64 | Uncultured (EF157223) | 96 | Natural asphalts of the Rancho La Brea Tar pits | <i>Ferrithrix thermotolerans</i> (AY140237) | 86 |
| ASK9G_65 | Uncultured (AM746681) | 98 | Rosy discoloration of ancient wall paintings | <i>Rubrobacter radiotolerans</i> (NR_029191) | 92 |
| ASK9G_66 | Uncultured (AY250873) | 98 | Cryptoendolithic communities, McMurdo Dry Valleys, Antarctica | <i>Rubrobacter radiotolerans</i> (NR_029191) | 93 |
| ASK9G_67 | Uncultured (AY250873) | 99 | Cryptoendolithic communities, McMurdo Dry Valleys, Antarctica | <i>Rubrobacter radiotolerans</i> (AJ243870) | 93 |
| ASK9G_69 | Uncultured (FJ895051) | 99 | Hyper-arid polar desert | <i>Rubrobacter radiotolerans</i> (AJ243870) | 95 |
| ASK9G_70 | Uncultured (AM746685) | 95 | Rosy discoloration of ancient wall paintings | <i>Rubrobacter radiotolerans</i> (NR_029191) | 94 |
| ASK9G_73 | Uncultured (AY250873) | 98 | Cryptoendolithic communities, McMurdo Dry Valleys, Antarctica | <i>Rubrobacter radiotolerans</i> (NR_029191) | 93 |
| ASK9G_74 | Uncultured (FJ895046) | 99 | Hyper-arid polar desert | <i>Solirubrobacter soli</i> (AB245334) | 91 |
| ASK9G_75 | Uncultured (FJ895051) | 99 | Hyper-arid polar desert | <i>Rubrobacter radiotolerans</i> (AJ243870) | 91 |
| ASK9G_76 | Uncultured (FJ895051) | 100 | Hyper-arid polar desert | <i>Rubrobacter radiotolerans</i> (AJ243870) | 95 |
| ASK9G_80 | Uncultured (AY250873) | 98 | Cryptoendolithic communities, McMurdo Dry Valleys, Antarctica | <i>Rubrobacter radiotolerans</i> (AJ243870) | 93 |
| ASK9G_83 | Uncultured (AM746693) | 97 | Rosy discoloration of ancient wall paintings | <i>Ornithinicoccus hortensis</i> (AB098587) | 93 |
| ASK9G_88 | Uncultured (FJ895046) | 98 | Hyper-arid polar desert | <i>Solirubrobacter soli</i> (AB245334) | 90 |
| Bacteroidetes | | | | | |
| ASK9G_8 | Uncultured (AM746683) | 91 | Rosy discoloration of ancient wall paintings | <i>Flexibacter aggregans</i> (AB078038) | 86 |
| ASK9G_11 | Uncultured (GQ454873) | 93 | Soils from the Ross Sea region of Antarctica | <i>Aquiflexum balticum</i> (NR_025634) | 89 |
| ASK9G_15 | Uncultured (EU196299) | 93 | Cold perennial springs of the Canadian high Arctic | <i>Gillisia mitskevichiae</i> (NR_025822) | 92 |
| ASK9G_19 | Uncultured (EU196299) | 94 | Cold perennial springs of the Canadian high Arctic | <i>Gillisia mitskevichiae</i> (NR_025822) | 92 |
| ASK9G_20 | Uncultured (GQ454873) | 92 | Soils from the Ross Sea region of Antarctica | <i>Cyclobacterium lianum</i> (DQ534063) | 89 |
| ASK9G_24 | Uncultured (DQ346479) | 88 | Compost | <i>Flexibacter aggregans</i> (AB078038) | 87 |
| ASK9G_34 | Uncultured (EU369131) | 91 | Oyster shell | <i>Cyclobacterium lianum</i> (DQ534063) | 89 |
| ASK9G_44 | Uncultured (DQ346479) | 88 | Compost | <i>Flexibacter aggregans</i> (AB078038) | 87 |
| ASK9G_45 | Uncultured (DQ432304) | 88 | Alkaline, hypersaline lakes, Egypt | <i>Algoriphagus halophilus</i> (NR_025744) | 86 |
| ASK9G_46 | Uncultured (EU196299) | 94 | Cold perennial springs of the Canadian high Arctic | <i>Gillisia mitskevichiae</i> (NR_025822) | 92 |
| ASK9G_57 | Uncultured (EU196299) | 95 | Cold perennial springs of the Canadian high Arctic | <i>Gillisia mitskevichiae</i> (NR_025822) | 92 |
| ASK9G_63 | Uncultured (GQ454873) | 93 | Soils from the Ross Sea region of Antarctica | <i>Cyclobacterium lianum</i> (DQ534063) | 89 |
| ASK9G_68 | Uncultured (DQ346479) | 88 | Compost | <i>Flexibacter aggregans</i> (AB078038) | 87 |
| ASK9G_72 | Uncultured (EU369131) | 91 | Oyster shell | <i>Cyclobacterium lianum</i> (DQ534063) | 88 |
| ASK9G_77 | Uncultured (GQ454873) | 93 | Soils from the Ross Sea region of Antarctica | <i>Cyclobacterium marinum</i> (FLERRDB) | 88 |
| ASK9G_81 | Uncultured (GQ454873) | 93 | Soils from the Ross Sea region of Antarctica | <i>Aquiflexum balticum</i> (NR_025634) | 89 |
| ASK9G_85 | Uncultured (EU196299) | 95 | Cold perennial springs of the Canadian high Arctic | <i>Gillisia mitskevichiae</i> (NR_025822) | 92 |
| Proteobacteria | | | | | |
| ASK9G_82 | Uncultured (EF215739) | 98 | Temperate coastal marine waters | <i>Agrobacterium sanguineum</i> (AB062106) | 94 |
| ASK9G_84 | Uncultured (EF215739) | 98 | Temperate coastal marine waters | <i>Agrobacterium sanguineum</i> (AB062106) | 94 |
| Deinococcus-Thermus | | | | | |
| ASK9G_7 | Uncultured (FJ895047) | 94 | Hyper-arid polar desert | <i>Truepera radiovictrix</i> (DQ022077) | 91 |
| ASK9G_32 | Uncultured (EU883205) | 98 | Endostromatolites, Haughton impact crater, Devon Island, Canada | | 91 |
| ASK9G_56 | Uncultured (FJ895047) | 95 | Hyper-arid polar desert | | 93 |
| ASK9G_71 | Uncultured (FJ895047) | 96 | Hyper-arid polar desert | | 92 |

Appendix

| | | | | | |
|-------------|--------------------------|----|---|---|----|
| ASK9G_86 | Uncultured (FJ895047) | 95 | Hyper-arid polar desert | | 92 |
| ASK9G_10 | Uncultured (FJ895047) | 95 | Hyper-arid polar desert | | 92 |
| RDP Unknown | | | | | |
| ASK9G_3 | Uncultured (EF157190) | 92 | Natural asphalts of the Rancho La Brea Tar pits | <i>Sphaerobacter thermophilus</i> (AJ420142) | 83 |
| ASK9G_4 | Uncultured (EU979018) | 88 | Rhizosphere | <i>Phycisphaera mikrensis</i> (AB474364) | 80 |
| ASK9G_5 | Uncultured (EF157268) | 95 | Natural asphalts of the Rancho La Brea Tar pits | <i>Sphaerobacter thermophilus</i> (AJ420142) | 78 |
| ASK9G_6 | Uncultured (FN298047) | 92 | Roman Carmona tombs | <i>Sphaerobacter thermophilus</i> (AJ420142) | 84 |
| ASK9G_23 | Uncultured (EF157223) | 96 | Natural asphalts of the Rancho La Brea Tar pits | <i>Ferrithrix thermotolerans</i> (AY140237) | 86 |
| ASK9G_58 | Uncultured (EF157190) | 92 | Natural asphalts of the Rancho La Brea Tar pits | <i>Sphaerobacter thermophilus</i> (AJ420142) | 84 |
| ASK9G_61 | Uncultured (FN298047) | 91 | Roman Carmona tombs | <i>Sphaerobacter thermophilus</i> (AJ420142) | 83 |
| ASK9G_78 | Uncultured (EF157190) | 93 | Natural asphalts of the Rancho La Brea Tar pits | <i>Sphaerobacter thermophilus</i> (AJ420142) | 84 |
| ASK9G_79 | Uncultured (AY250886) | 97 | Cryptoendolithic communities, McMurdo Dry Valleys, Antarctica | <i>Sphaerobacter thermophilus</i> (AJ420142) | 84 |
| ASK9G_87 | Uncultured (EF157190) | 92 | Natural asphalts of the Rancho La Brea Tar pits | <i>Sphaerobacter thermophilus</i> (AJ420142) | 84 |

Table 4. Exhaustive list of all closest novel relatives and species relatives for the ASK9IP environmental clones based on BLASTn 16s rDNA similarity

| ASK9IP Clone | Closest novel relative | | | Closest genus and/or species | |
|----------------|------------------------|----|---|---|----|
| | ID | % | Sampling environment | ID | % |
| Actinobacteria | | | | | |
| ASK9IP_1 | Uncultured (FJ895074) | 99 | Hyper-arid polar desert | <i>Rubrobacter radiotolerans</i> (AJ243870) | 94 |
| ASK9IP_2 | Uncultured (FJ895062) | 99 | Hyper-arid polar desert | <i>Nocardioides jensenii</i> (AF005006) | 92 |
| ASK9IP_4 | Uncultured (FJ895074) | 99 | Hyper-arid polar desert | <i>Rubrobacter radiotolerans</i> (AJ243870) | 94 |
| ASK9IP_6 | Uncultured (FJ895062) | 99 | Hyper-arid polar desert | <i>Nocardioides jensenii</i> (AF005006) | 93 |
| ASK9IP_8 | Uncultured (FJ895074) | 99 | Hyper-arid polar desert | <i>Rubrobacter radiotolerans</i> (AJ243870) | 95 |
| ASK9IP_9 | Uncultured (EF465010) | 94 | Soils of Northern Victoria Land, Antarctica | <i>Marmoricola aurantiacus</i> (NR_026507) | 92 |
| ASK9IP_11 | Uncultured (EU883196) | 97 | Endostromatolites, Haughton impact crater, Canada | <i>Conexibacter woesei</i> (NR_028979) | 91 |
| ASK9IP_14 | Uncultured (AM746696) | 99 | Rosy discoloration of ancient wall paintings | <i>Solirubrobacter soli</i> (AB245334) | 91 |
| ASK9IP_16 | Uncultured (AY571811) | 99 | Hydrocarbon contaminated soil around Scott Base, Antarctica | <i>Rubrobacter radiotolerans</i> (AJ243870) | 94 |
| ASK9IP_17 | Uncultured (FJ895062) | 99 | Hyper-arid polar desert | <i>Aeromicrobium ginsengisoli</i> (AB245394) | 93 |
| ASK9IP_25 | Uncultured (FJ895074) | 98 | Hyper-arid polar desert | <i>Rubrobacter radiotolerans</i> (AJ243870) | 94 |
| ASK9IP_26 | Uncultured (FJ895051) | 98 | Hyper-arid polar desert | <i>Rubrobacter radiotolerans</i> (AJ243870) | 95 |
| ASK9IP_27 | Uncultured (FJ895046) | 98 | Hyper-arid polar desert | <i>Solirubrobacter soli</i> (AB245334) | 90 |
| ASK9IP_28 | Uncultured (FJ895062) | 99 | Hyper-arid polar desert | <i>Aeromicrobium ginsengisoli</i> (AB245394) | 92 |
| ASK9IP_32 | Uncultured (AM746681) | 98 | Rosy discoloration of ancient wall paintings | <i>Rubrobacter radiotolerans</i> (NR_029191) | 92 |
| ASK9IP_33 | Uncultured (FJ895046) | 98 | Hyper-arid polar desert | <i>Solirubrobacter soli</i> (AB245334) | 90 |
| ASK9IP_34 | Uncultured (AM746696) | 99 | Rosy discoloration of ancient wall paintings | <i>Solirubrobacter soli</i> (AB245334) | 90 |
| ASK9IP_35 | Uncultured (FJ895046) | 98 | Hyper-arid polar desert | <i>Solirubrobacter soli</i> (AB245334) | 89 |
| ASK9IP_36 | Uncultured (FJ895051) | 99 | Hyper-arid polar desert | <i>Rubrobacter radiotolerans</i> (NR_029191) | 95 |
| ASK9IP_38 | Uncultured (AY250880) | 99 | Cryptoendolithic communities, McMurdo Dry Valleys, Antarctica | <i>Actinotalea fermentans</i> (NR_026176) | 93 |
| ASK9IP_44 | Uncultured (EU440405) | 98 | Endostromatolites, Haughton impact crater, Canada | <i>Rubrobacter radiotolerans</i> (AJ243870) | 94 |
| ASK9IP_46 | Uncultured (EU883196) | 97 | Endostromatolites, Haughton impact crater, Canada | <i>Solirubrobacter soli</i> (AB245334) | 92 |
| ASK9IP_47 | Uncultured (EU440491) | 97 | Endostromatolites, Haughton impact crater, Canada | <i>Solirubrobacter soli</i> (AB245334) | 92 |
| ASK9IP_52 | Uncultured (EF220380) | 97 | Cryptoendolithic communities, McMurdo Dry Valleys, Antarctica | <i>Aeromicrobium ginsengisoli</i> (AB245394) | 93 |
| ASK9IP_53 | Uncultured (EU883196) | 97 | Endostromatolites, Haughton impact crater, Canada | <i>Geobacillus thermodenitrificans</i> (AB210956) | 82 |
| ASK9IP_57 | Uncultured (EF220380) | 97 | Antarctic terrestrial habitats | <i>Nocardioides jensenii</i> (AF005006) | 94 |
| ASK9IP_58 | Uncultured (FJ895074) | 98 | Hyper-arid polar desert | <i>Rubrobacter radiotolerans</i> (AJ243870) | 94 |
| ASK9IP_59 | Uncultured (FJ490270) | 96 | Hyper-arid polar desert | <i>Sporichthya polymorpha</i> (X72377) | 93 |
| ASK9IP_60 | Uncultured (EU883196) | 94 | Endostromatolites, Haughton impact crater, Canada | <i>Solirubrobacter soli</i> (AB245334) | 92 |
| ASK9IP_61 | Uncultured (FJ895062) | 99 | Hyper-arid polar desert | <i>Aeromicrobium ginsengisoli</i> (AB245394) | 92 |
| ASK9IP_63 | Uncultured (AM746696) | 99 | Rosy discoloration of ancient wall paintings | <i>Solirubrobacter soli</i> (AB245334) | 91 |
| ASK9IP_65 | Uncultured (AM746696) | 98 | Rosy discoloration of ancient wall paintings | <i>Solirubrobacter soli</i> (AB245334) | 90 |
| ASK9IP_66 | Uncultured (FJ895062) | 99 | Hyper-arid polar desert | <i>Aeromicrobium ginsengisoli</i> (AB245394) | 91 |
| ASK9IP_67 | Uncultured (AM746693) | 94 | Rosy discoloration of ancient wall paintings | <i>Ornithinimicrobium kibberense</i> (AY636111) | 93 |
| ASK9IP_68 | Uncultured (EF465010) | 95 | Soils of Northern Victoria Land, Antarctica | <i>Nocardioides jensenii</i> (AF005006) | 93 |
| ASK9IP_69 | Uncultured (FJ895051) | 99 | Hyper-arid polar desert | <i>Rubrobacter radiotolerans</i> (NR_029191) | 94 |

Appendix

| | | | | | |
|----------------|--|----|---|---|----|
| ASK9IP_71 | Uncultured (GQ396849) | 96 | Recently de-glaciated soil | <i>Ferrimicrobium acidiphilum</i> (AF251436) | 87 |
| ASK9IP_73 | Uncultured (FJ895074) | 98 | Hyper-arid polar desert | <i>Rubrobacter radiotolerans</i> (NR_029191) | 94 |
| ASK9IP_74 | Uncultured (EU440491) | 97 | Endostromatolites, Haughton impact crater, Canada | <i>Solirubrobacter soli</i> (AB245334) | 92 |
| ASK9IP_75 | Uncultured (FJ895051) | 99 | Hyper-arid polar desert | <i>Rubrobacter radiotolerans</i> (AJ243870) | 94 |
| ASK9IP_76 | Uncultured (FJ895042) | 99 | Hyper-arid polar desert | <i>Sporichthya polymorpha</i> (X72377) | 94 |
| ASK9IP_80 | Uncultured (EF465010) | 96 | Soils of Northern Victoria Land, Antarctica | <i>Kribbella ginsengisoli</i> (AB245391) | 92 |
| ASK9IP_81 | Uncultured (EF683038) | 97 | African dust event, E. Mediterranean | <i>Rubrobacter radiotolerans</i> (AJ243870) | 93 |
| ASK9IP_82 | Uncultured (AM746693) | 94 | Rosy discoloration of ancient wall paintings | <i>Ornithinimicrobium kibberense</i> (AY636111) | 92 |
| ASK9IP_83 | Uncultured (EF220380) | 97 | Antarctic terrestrial habitats | <i>Nocardioides jensenii</i> (AF005006) | 94 |
| ASK9IP_85 | Uncultured (FJ895051) | 99 | Hyper-arid polar desert | <i>Rubrobacter radiotolerans</i> (NR_029191) | 94 |
| ASK9IP_86 | Uncultured (GQ128159) | 97 | Meadow Soil from Tibetan Plateau | <i>Rubrobacter radiotolerans</i> (NR_029191) | 94 |
| ASK9IP_87 | Uncultured (FJ895051) | 99 | Hyper-arid polar desert | <i>Rubrobacter radiotolerans</i> (NR_029191) | 95 |
| ASK9IP_89 | Uncultured (FJ790551) | 99 | Chasmo lithic high-altitude arid environment | <i>Rubrobacter radiotolerans</i> (NR_029191) | 93 |
| ASK9IP_91 | Uncultured (FJ895077) | 99 | Hyper-arid polar desert | <i>Aeromicrobium ginsengisoli</i> (AB245394) | 93 |
| ASK9IP_92 | Uncultured (EF220124) | 96 | Antarctic terrestrial habitats | <i>Solirubrobacter soli</i> (AB245334) | 90 |
| ASK9IP_93 | Uncultured (AM746696) | 98 | Rosy discoloration of ancient wall paintings | <i>Solirubrobacter soli</i> (AB245334) | 90 |
| ASK9IP_94 | Uncultured (FJ895046) | 98 | Hyper-arid polar desert | <i>Solirubrobacter soli</i> (AB245334) | 90 |
| Bacteroidetes | | | | | |
| ASK9IP_3 | Uncultured (FJ895060) | 99 | Hyper-arid polar desert | <i>Flavisolibacter ginsengisoli</i> (AB267477) | 91 |
| ASK9IP_20 | Uncultured (DQ346479) | 88 | Compost | <i>Flexibacter aggregans</i> (AB078038) | 87 |
| ASK9IP_21 | Uncultured (FJ895052) | 98 | Hyper-arid polar desert | <i>Segetibacter koreensis</i> (AB267478) | 93 |
| ASK9IP_23 | Uncultured (FJ895052) | 95 | Hyper-arid polar desert | <i>Segetibacter koreensis</i> (AB267478) | 95 |
| ASK9IP_24 | Uncultured (EF683049) | 94 | African dust event, E. Mediterranean | <i>Rhodocytophaga aerolata</i> (EU004198) | 91 |
| ASK9IP_37 | Uncultured (FJ490252) | 95 | Hyper-arid polar desert | <i>Segetibacter koreensis</i> (AB267478) | 95 |
| ASK9IP_42 | Uncultured (FJ490252) | 95 | Hyper-arid polar desert | <i>Segetibacter koreensis</i> (AB267478) | 95 |
| ASK9IP_43 | Uncultured (GQ396844) | 97 | Recently de-glaciated soil | <i>Pedobacter composti</i> (AB267720) | 95 |
| ASK9IP_54 | Uncultured (FJ895060) | 99 | Hyper-arid polar desert | <i>Flavisolibacter ginsengisoli</i> (AB267477) | 93 |
| ASK9IP_55 | Uncultured (EU369131) | 91 | Oyster shell | <i>Cyclobacterium lianum</i> (DQ534063) | 88 |
| ASK9IP_62 | Uncultured (FJ490252) | 95 | Hyper-arid polar desert | <i>Segetibacter koreensis</i> (AB267478) | 95 |
| ASK9IP_64 | Uncultured (FJ490252) | 95 | Hyper-arid polar desert | <i>Segetibacter koreensis</i> (AB267478) | 95 |
| ASK9IP_70 | Uncultured (FJ490252) | 98 | Hyper-arid polar desert | <i>Segetibacter koreensis</i> (AB267478) | 93 |
| ASK9IP_72 | Uncultured (FJ895060) | 96 | Hyper-arid polar desert | <i>Flavisolibacter ginsengisoli</i> (AB267477) | 92 |
| ASK9IP_77 | Uncultured (FJ895060) | 96 | Hyper-arid polar desert | <i>Flavisolibacter ginsengisoli</i> (AB267477) | 92 |
| ASK9IP_90 | Uncultured (FJ490252) | 99 | Hyper-arid polar desert | <i>Segetibacter koreensis</i> (AB267478) | 93 |
| Proteobacteria | | | | | |
| ASK9IP_7 | Uncultured (EF606067) | 97 | Soil | <i>Sphingobium estrogenivorans</i> (DQ855413) | 95 |
| ASK9IP_10 | Uncultured (EU440412) | 95 | Endostromatolites, Haughton impact crater, Canada | <i>Sphingopyxis alaskensis</i> (CP000356) | 93 |
| ASK9IP_39 | Uncultured (DQ643704) | 98 | Soil | <i>Methylibium petroleiphilum</i> (CP000555) | 93 |
| ASK9IP_45 | Uncultured (DQ643704) | 98 | Soil | <i>Methylibium petroleiphilum</i> (CP000555) | 93 |
| ASK9IP_49 | Variovorax sp. enrichment clone (FJ828944) | 97 | Airfield in the Greenland | <i>Variovorax paradoxus</i> (EU979529) | 95 |
| ASK9IP_79 | Uncultured (AM158417) | 97 | Rhizosphere | <i>Methylobacterium chloromethanicum</i> (CP001298) | 95 |

| Deinococcus-Thermus | | | | | |
|---------------------|-----------------------|-----|--|--|----|
| ASK9IP_13 | Uncultured (AB374369) | 97 | Endolithic community, White rock Switzerland | <i>Truepera radiovictrix</i> (DQ022077) | 92 |
| ASK9IP_19 | Uncultured (FJ895086) | 97 | Hyper-arid polar desert | | 90 |
| ASK9IP_22 | Uncultured (AB374369) | 96 | Endolithic community, White rock Switzerland | | 91 |
| ASK9IP_30 | Uncultured (FJ895086) | 99 | Hyper-arid polar desert | | 90 |
| ASK9IP_41 | Uncultured (AY250871) | 100 | Cryptoendoliths, McMurdo Dry Valleys, Antarctica | | 91 |
| ASK9IP_51 | Uncultured (FJ895086) | 98 | Hyper-arid polar desert | | 90 |
| ASK9IP_56 | Uncultured (FJ895086) | 98 | Hyper-arid polar desert | | 90 |
| ASK9IP_78 | Uncultured (FJ895086) | 98 | Hyper-arid polar desert | | 92 |
| Acidobacteria | | | | | |
| ASK9IP_12 | Uncultured (FJ592786) | 97 | Fumarole within a hyperarid, high-elevation landscape, Andes | <i>Chloracidobacterium thermophilum</i> (EF531339) | 81 |
| ASK9IP_15 | Uncultured (FJ895045) | 97 | Hyper-arid polar desert | | 82 |
| ASK9IP_18 | Uncultured (FJ592780) | 99 | Fumarole within a hyperarid, high-elevation landscape, Andes | | 81 |
| ASK9IP_29 | Uncultured (EF220302) | 98 | Antarctic terrestrial habitats | | 82 |
| ASK9IP_31 | Uncultured (FJ028683) | 97 | Epilithic biofilms | | 81 |
| ASK9IP_88 | Uncultured (FJ895045) | 97 | Hyper-arid polar desert | | 82 |
| Planctomycetes | | | | | |
| ASK9IP_5 | Uncultured (EF651250) | 93 | Australian vertisol | <i>Phycisphaera mikrensis</i> (AB474364) | 77 |
| RDP Unknown | | | | | |
| ASK9IP_40 | Uncultured (FN298047) | 87 | Roman Carmona tombs | <i>Sphaerobacter thermophilus</i> (AJ420142) | 82 |
| ASK9IP_48 | Uncultured (FJ895048) | 91 | Hyper-arid polar desert | <i>Leifsonia antarctica</i> (AM931710) | 76 |
| ASK9IP_50 | Uncultured (FJ895083) | 91 | Hyper-arid polar desert | <i>Sphaerobacter thermophilus</i> (AJ420142) | 85 |
| ASK9IP_84 | Uncultured (FJ490245) | 99 | Hyper-arid polar desert | <i>Thermodesulfobium narugense</i> (NR_024789) | 77 |

Table 5. ‘Geology’ Filter wavelengths (in nm) for comparable Mars rover and lander stereo cameras, given in chronological order.

| Viking ^[I] (1976 – 1982) | Pathfinder ^[III] (1997) | Beagle ^[III] (2003, Lost) | MER ^[IV] (2004 – Present) | MSL ^[VI] (Launch 2011) | ‘F2-12’ ^[VII] (ExoMars) (Launch 2018) |
|--|---------------------------------------|---|---|--------------------------------------|--|
| 400 - 500 | 443 | 440 | 432 | 435 | 440 |
| 500 - 600 | 479 | 480 | 482 | 480 | 470 |
| 600 - 700 | 530 | 530 | 535 | 535 | 510 |
| 820 - 920 | 599 | 600 | 601 | 600 | 560 |
| 900 - 940 | 671 | 670 | 673 | 675 | 600 |
| 930 - 1100 | 752 | 750 | 753 | 750 | 660 |
| | 801 | 800 | 803 | 800 | 720 |
| | 858 | 860 | 864 | 865 | 760 |
| | 897 | 900 | 904 | 905 | 830 |
| | 931 | 930 | 934 | 935 | 880 |
| | 966 | 965 | 1009 | 1010 | 950 |
| | 1002 | 1000 | | | 1000 |

^[I] Evans & Adams (1979); ^[III] Smith *et al.* (1997);

^[III] Griffiths *et al.* (2006)

^[IV] Bell *et al.* (2003);

^[VI] Malin *et al.* (2005);

^[VII] Chapter 6, section 6.1.3

B) Equations

Equations for porosity and diversity indices calculated in Chapter 3.

Equation 1. Calculation of porosity as a fraction of the volume of pore spaces over the total volume, where:

V_V = volume of pore space (as measured by fluid saturation)
 V_T = bulk volume of material

$$\phi = \frac{V_V}{V_T} \times 100$$

Equation 2. Shannon Diversity Index as calculated using MOTHUR (Schloss & Handelsman 2005), where:

S = number of OTUs
 n_i = number OTUs with i individuals
 N = Total number of individuals within the community

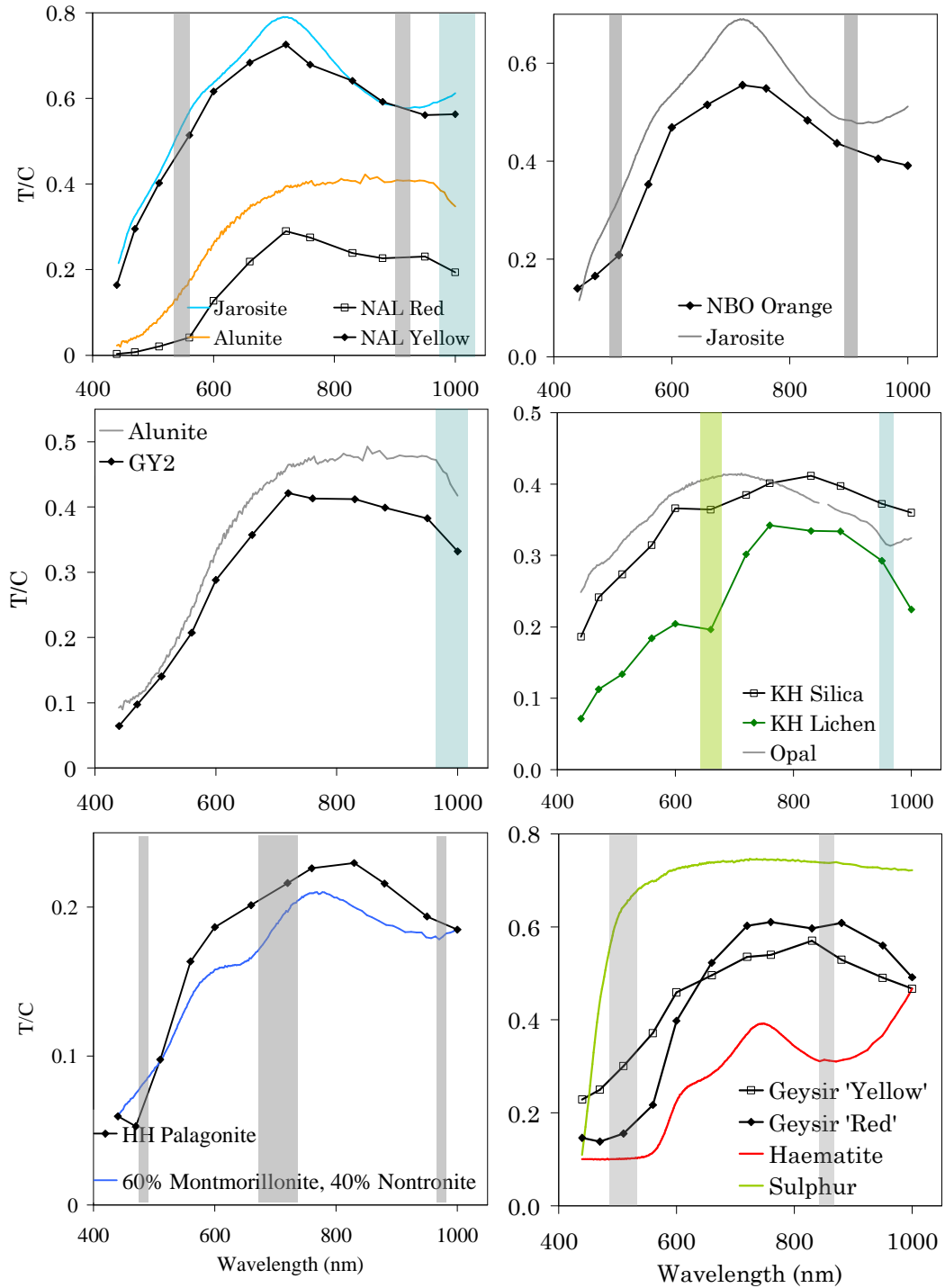
$$H' = -\sum_{i=1}^S \frac{n_i}{N} \ln \frac{n_i}{N}$$

Equation 3. Simpson's diversity index as calculated using MOTHUR (Schloss & Handelsman 2005), where:

S = number of OTUs
 n_i = number OTUs with i individuals
 N = Total number of individuals within the community

$$D = \frac{\sum_{i=1}^S n_i(n_i - 1)}{N(N - 1)}$$

C) 'PanCam' spectra of geological samples used for testing filter sets in Chapter 6, with the relevant mineral spectra from the USGS spectral library (Clark *et al.* 1997) for comparison. Absorption features are indicated as follows: Blue = water; Grey = Iron oxide ($Fe^{2+/3+}$); Green = Chlorophyll *a*.



D) Publications

List of all published conference abstracts and journal papers resulting from the work detailed in this PhD thesis (in chronological order):

1) Storrie-Lombardi, M. C., Muller, J-P., Fisk, M. R., Cousins, C. R., Sattler, B., Griffiths, A. D., Coates, A. J. (2010) “**Laser Induced Fluorescence Emission (L.I.F.E.): Searching for Mars Organics with a UV-Enhanced PanCam**”. *Astrobiology* vol. 9 (10), 953 – 964

2) Cousins, C. R. Griffiths, A. D., Crawford, I. A. (2009) “**Combined PanCam, UV Epifluorescence, and Raman Spectroscopic Identification of Astrobiological Targets: Applications to the ExoMars Mission**”. *Astrobiology Graduate Conference 2009. Astrobiology* vol. 9, (5), pp. 510.

3) Cousins, C. R., Griffiths, A. D., Schmitz, N., Paar, G., Barnes, D., and the AMASE '09 team. (2009) “**Wide Angle Camera testing during the 2009 AMASE expedition for the ExoMars PanCam instrument**”. *EPSC Abstracts, Vol. 4, EPSC2009-813, 2009*

4) Cousins, C. R., Ward, J. M., Crawford, I. A., Towner, M. C., Jones, A. P. (2009) “**Life in subglacial lavas as an analogue for life on Mars**”. *Goldschmidt Conference Abstracts 2009. Geochimica et Cosmochimica Acta* vol. 73, (13), Supplement 1, pp. A248.

5) Storrie-Lombardi, M., Sattler, B., Muller, J-P., Fisk, M., Cousins, C., Dartnell, L. (2009) “**Laser Induced Fluorescence Imaging: Searching for Organics from the Dry Valleys of Queen Maud Land Antarctica to the Regolith and Ices of Mars**”. *Geophysical Research Abstracts* Vol. 11, EGU2009-11088, EGU General Assembly 2009.

6) Cousins, C. R., Smellie, J. L., Jones, A. P., Crawford, I. A. (2009) “**A comparative study of endolithic microborings in basaltic lavas from a transitional subglacial - marine environment**”. *International Journal of Astrobiology* vol. 8 (1), pp. 37 - 49.

